

2008

# Mathematical modelling of hepatopancreatic digestive cell of the blue mussel

McVeigh, Allan

<http://hdl.handle.net/10026.1/1678>

---

<http://dx.doi.org/10.24382/3500>

University of Plymouth

---

*All content in PEARL is protected by copyright law. Author manuscripts are made available in accordance with publisher policies. Please cite only the published version using the details provided on the item record or document. In the absence of an open licence (e.g. Creative Commons), permissions for further reuse of content should be sought from the publisher or author.*

**Mathematical modelling of hepatopancreatic digestive cell of the  
blue mussel**

by

**Allan McVeigh**

A thesis submitted to the University of Plymouth in partial fulfilment  
for the degree of

**Doctor of Philosophy**

School of Computing, Communications & Electronics

Faculty of Technology

In collaboration with Plymouth Marine Laboratory

University of Plymouth Library	
Item No.	9007936735
Shelfmark	THESIS 511.8 MAC

**Allan McVeigh**

**Mathematical modelling of hepatopancreatic digestive cell of the blue mussel**

**Abstract**

The lysosomal system of the hepatopancreatic digestive cell of the mussel (*Mytilus sp.*) is critical in intracellular food degradation, toxic responses and internal cellular turnover. Mathematical and numerical models are developed to simulate the responses of this system to varying conditions, dietary and toxicological. The model evolution encompasses: inclusion of glycogen/lipid storage forms; extrapolation to include nitrogen metabolism; development of rate of endocytosis and food signal; increased functionality of endo/lysosomes; shift to protein/carbohydrate/lipid based model; and the incorporation of the cost of normal function and replacement of damaged components. Control is asserted through control of cytosolic concentrations: the initial assumption of constant carbon concentration is shown to be unacceptable for later models. A control algorithm is developed which regulates cell volume by the ratio of proteinaceous material to energy forms.

Endocytosis is shown to be the main determinant behind routine cellular behaviour. Observed phasic behaviour of the digestive tubules is incorporated into the cellular behavioural pattern. A probability-based model for the rate of endocytosis is developed.



Increased autophagy as the sole response to toxic injury is found to be inadequate to explain observed responses. It is proposed to complement this response with impairment of lysosomal efficiency to explain this inadequacy. Toxic injury is implemented through an increase in the rates of damage to cellular components. Within the lysosome this leads to a reduction in the concentration of digestive enzymes inhibiting lysosomal performance and, in conjunction with the enhanced autophagy due to increased cytosolic damage, invoking the lysosomal swelling commonly observed.

## Table of Contents

Abstract .....	i
Table of Contents .....	iii
List of illustrations and tables .....	vi
Acknowledgements .....	xii
Author's Declaration .....	xiii
Chapter 1 General Introduction .....	1
1.1 Rationale & objectives .....	1
1.2 Mussels & Lysosomal Stability .....	4
1.3 Conceptual Model .....	7
1.4 Endocytosis, recycling and lysosomal transport .....	12
1.5 Autophagy .....	15
1.6 Degradation and exocytosis .....	20
1.7 General metabolic rates .....	23
1.8 Nutrient Storage and Export .....	24
1.9 C:N Ratios & control .....	26
1.10 Damage .....	28
1.11 Contaminants .....	32
1.12 Dietary restriction .....	35
1.13 Hypotheses .....	37
Chapter 2 Carbon Model .....	42
2.1 Objectives .....	42
2.2 Introduction .....	43
2.3 Model development .....	47
2.4 Endosome and cell volume dependent endocytosis: Model 1g .....	51
2.5 Toxicity effect: Model 1h .....	62
Chapter 3 Storage Models .....	83
3.1 Introduction .....	83
3.2 Glycogen store: Model 2a .....	86
3.3 Lipid subsystem: Model 2b .....	98
3.4 Lipid catabolism: Model 2b2 .....	105

3.5 Combined glycogen and lipid system: Model 2c .....	117
3.6 Discussion .....	129
Chapter 4 Carbon and Nitrogen Model .....	135
4.1 Introduction .....	135
4.2 Control conditions: Model 3 .....	139
4.3 Nitrogen control: Model 3a .....	147
4.4 Nitrogen controlled autophagy & digestive efficiency: Model 3b .....	155
4.5 Discussion .....	161
Chapter 5 Endosomal and Lysosomal Models .....	165
5.1 Introduction .....	165
5.2 Delay model: Model 4b .....	167
5.3 Throughput model: Model 4c .....	178
5.4 Discussion .....	189
Chapter 6 Endocytosis .....	193
6.1 Cellular Feeding – Objectives and Hypotheses .....	193
6.2 Mussel and cellular feeding .....	195
6.3 Tubule phase model .....	196
6.4 Spatial tubule and cell model .....	201
6.5 Stochastic model: Model 5a .....	207
6.6 Endocytotic model: Model 5b .....	212
6.7 Partial derivative equation model: Model 5c .....	217
6.8 Variable lumen volume: Model 5d .....	224
6.9 Discussion .....	227
Chapter 7 Macromolecular Model .....	231
7.1 Objectives .....	231
7.2 Introduction .....	232
7.3 Macromolecular model initial set up .....	236
7.4 Initial macromolecular model: Model 6a .....	251
7.5 Glycogen functions: Model 6b .....	259
7.6 Nitrogen control factor: Model 6c .....	263
7.7 Concentrations sensitivity analysis: Model 6d .....	267
7.8 Simple cell division model: Model 6e .....	276
7.9 Annual variable rest of animal signal model: Model 6f .....	281

7.10 Discussion.....	284
Chapter 8 Lipid Metabolism & Starvation Models .....	287
8.1 Introduction .....	287
8.2 Lipid metabolism model: Model 7a .....	288
8.3 Food availability: Model 7b .....	295
8.4 Dietary quality: Model 7b6 .....	306
8.5 Lipid to carbohydrate: Model 7c .....	320
8.6 Sensitivity analysis .....	326
8.7 Discussion.....	330
Chapter 9 Toxicity Models .....	333
9.1 Introduction, Objectives & Hypotheses .....	333
9.2 Experimental Paradigm .....	335
9.3 Theoretical model: Model 8a.....	338
9.4 Contaminant flow: Model 8b.....	344
9.5 Cytosolic contaminant removal and effects: Model 8c.....	358
9.6 Contaminant diffusion: Model 8d .....	367
9.7 Lysosomal damage & release: Model 8e .....	380
9.8 Cellular contaminant defence: Model 8f.....	388
9.9 Contaminant bio-transformation: Model 8g.....	399
9.10 Lipofuscin: Model 8h .....	405
9.11 Discussion.....	411
10 General Discussion .....	415
Appendix A Revised System of ODEs .....	422
Appendix B Analytical solutions to decay equations .....	428
Appendix C Numerical solutions to PDE exact solution.....	432
Appendix D Vesicle sizes .....	441
References.....	442

## List of illustrations and tables

Fig 1.1 Conceptual Cell Model.....	2
Fig 2.1 Schematic for model 1.....	44
Fig 2.2 Division of cell volume- $f_{ev}$ parameter space.....	51
Fig 2.3 Simulation of Model1g with $S_c = 3.6$ .....	54
Fig 2.4 Ten day simulation of Model1g with $S_c = 4.7095$ .....	55
Fig 2.5 Ten day simulation of Model1g with $S_c = 6.0$ .....	57
Fig 2.6 Endosomal concentrations.....	58
Fig 2.7 Health function .....	59
Fig 2.8 Health function with increased digestive efficiency .....	60
Fig 2.9 Smallest possible digestive efficiency .....	61
Fig 2.10 100 day simulation, with autophagy increased twofold from day 50 onwards.....	63
Fig 2.11 100 day simulation, with autophagy doubled and $f_d = 0.625$ for days 50-78.....	65
Fig 2.12 Lysosomal stability .....	66
Fig 2.13 100 day simulation of model 1h, with fivefold increase in autophagic boost and $f_d=0.787$ for days 50-78.....	68
Fig 2.14 100 day capped rate Model 1hb .....	70
Fig 2.15 10 day capped rate Model 1hb tidal simulation .....	73
Fig 2.16 10 day simulation of capped rate/endocytosis switching.....	75
Fig 3.1 Schematic for model 2a with introduction of glycogen store .....	87
Fig 3.2 20 day simulation of Model 2a.....	92
Fig 3.3 Model 2a as detailed for Fig 3.2 but with autophagy boost turned off when glycogen available.....	94
Fig 3.4 Model 2a as detailed for Fig 3.2 but with glycogen concentration increased tenfold.....	95
Fig 3.5 100 day simulation of models 2a.....	96
Fig 3.6 Schematic for lipid subsystem model 2b .....	99
Fig 3.7 10 day simulation for Model 2b .....	102
Fig 3.8 100 day simulation of model 2b lipid model .....	104
Fig 3.9 Schematic of Lipid submodel.....	105
Fig 3.10 300 day simulation for Model 2b2 introducing lipid catabolism.....	106

Fig 3.11 Lipid Food % effect .....	108
Fig 3.12 365 day simulation .....	109
Fig 3.13 Annual simulation for model 2b2 .....	110
Fig 3.14 Annual simulation for model 2b3 .....	112
Fig 3.15 Annual simulations of model 2b3 sensitivity analysis .....	113
Fig 3.16 50 day simulation of Model 2b3 .....	115
Fig 3.17 Schematic for carbon model with glycogen and lipid included .	117
Fig 3.18 100 day simulation of model 2c.....	120
Fig 3.19 100 day simulation of Model 2c2 with new lipid and glycogen control algorithms.....	123
Fig 3.20 Breakdown of available carbon utilisation .....	125
Fig 3.21 Comparison of 10 day simulation of models 2c and 2c2.....	127
Fig 4.1 Nitrogen and carbon model 3 schematic.....	136
Fig 4.2 100 day simulation of model 3 carbon and nitrogen model .....	143
Fig 4.3 Comparison of 100 day simulations of models 2c2 & 3 .....	144
Fig 4.4 100 day simulation of Model 3 .....	146
Fig 4.5 100 day simulation of model 3a, nitrogen constraint.....	147
Fig 4.6 50 day simulation of model 3a.....	148
Fig 4.7 100 day simulation of model 3a.....	152
Fig 4.8 100 day simulations of Model 3a health function.....	154
Fig 4.9 Simulation designed to observe survival of model3b.....	156
Fig 4.10 Simulation designed to observe survival of model3c .....	158
Fig 5.1 1hour simulation of first delay model 4a .....	172
Fig 5.2 Determination of initial endosomal concentrations.....	174
Fig 5.3 6 hour simulation of second delay model 4b .....	177
Fig 5.4 Model 4c degradative organelle scheme.....	180
Fig 5.5 Throughput model comparison .....	182
Fig 5.6 Degradative organelle volumes with periodic feeding .....	184
Fig 5.7 Model 4c1: endosomal and lysosomal relative volume dependent endocytosis and lysosomal traffic suspension.....	187
Fig 6.1 Relative frequency of tubule phase.....	197
Fig 6.2 Spatial models .....	202
Fig 6.3 Spatial dimension variations with cell volume.....	205

Fig 6.4 Stochastic feeding model .....	207
Fig 6.5 Model5a showing flow of particles.....	210
Fig 6.6 Probability model5b1 to determine endocytotic rate .....	214
Fig 6.7 Model5b1 10,000 initial particles, vesicle diameter = 23 $\mu$ m.....	216
Fig 6.8 Initial condition dependence on number of eigenvalues.....	219
Fig 6.9 Particle migration. ....	219
Fig 6.10 Time course development of tubule lumen particle concentration .....	220
Fig 6.12 Parameter determination for exponential approximation.....	222
Fig 6.13 approximation to the time series of particles in the tubule lumen across the B parameter space.....	223
Fig 6.14 Schematic for simplest tubule lumen extension model.....	224
Fig 6.15 Model 6c 100 mins simulation .....	225
Fig 7.1 Model 6 Schematic.....	235
Fig 7.2 Annual C:N ratio .....	236
Fig 7.3 Annual (a) carbon & (b) nitrogen cellular concentrations.....	238
Fig 7.4 Conceptual model of newly synthesised or 'clean' endosome ....	240
Fig 7.5 Decision tree for control of cell behaviour .....	245
Fig 7.6 Annual tubule phase feeding regime setup for model 6a.....	250
Fig 7.7 Annual simulation of Model 6a.....	252
Fig 7.8 Dry weight comparison for Model 6a .....	255
Fig 7.9 Model 6a average export per timestep through annual simulation .....	257
Fig 7.10 Comparison of models 6b, glycogen store functions, and 6a for annual simulation.....	261
Fig 7.11 Total cellular carbon content split.....	265
Fig 7.12 Model 6c1 comparison .....	266
Fig 7.13 Comparison of the effect of amino acid concentration relative to that of bound protein on annual dry weight proportions .....	269
Fig 7.14 Amino acid split comparison on annual dry weight effect .....	271
Fig 7.15 Annual simulation comparison of effect of glycogen concentration relative to free sugar compartment .....	273
Fig 7.16 Annual simulation with cell division .....	277
Fig 7.17 Annual simulation of total cellular dry weight with cell division .....	278

Fig 7.18 Annual simulation of total cellular dry weight with capped cell division .....	279
Fig 7.19 Model 6f annual dry weight comparison .....	283
Fig 8.1 Cellular lipid metabolism schematic.....	291
Fig 8.2 Model 7a Annual cycle .....	293
Fig 8.3 Feeding and resting phases .....	297
Fig 8.4 Model 7b2 exponential decrease in FoodAvailability from day 50 to low at day 365 .....	299
Fig 8.5 Autophagy boost test - Model 7b3.....	301
Fig 8.6 No feeding phase on complete starvation - Model 7b4 .....	303
Fig 8.7 Decreasing food availability Model 7b5.....	305
Fig 8.8 Model 7b6, all protein diet after day 10.....	308
Fig 8.9 All protein diet after day 10 .....	311
Fig 8.10 Model 7b6a 10 days full food, thereafter no nitrogen in diet .....	314
Fig 8.11 Model 7b6b 10 days full food, thereafter no nitrogen in diet.....	317
Fig 8.12 100 day simulation of Model 7b6b 10 days full food, thereafter maximum nitrogen and carbon but no carbohydrate in diet .....	319
Figure 8.13 Schematic of model 7c.....	321
Fig 8.14 30 day simulation of Model 7b6c 10 days full food, thereafter maximum nitrogen and carbon but no carbohydrate in diet .....	322
Fig 8.15 30 day simulation of Model 7b6c 10 days full food, thereafter maximum nitrogen and carbon but no lipid in diet .....	325
Fig 8.16 Sensitivity analysis for food availability and protein content of food.....	326
Fig 8.17 Model 7c showing date of expiry of cell .....	327
Fig 8.18 Model 7c sensitivity analysis .....	329
Fig 9.1 Lysosomal stability .....	336
Fig 9.2 Model 8a1 3 day contaminant exposure simulation .....	339
Fig 9.3 Model 8a2 3 day contaminant exposure 12 day recovery simulation, but unfed throughout .....	341
Fig 9.4 Model 8a2a 3 day contaminant exposure 12 day recovery simulation, but unfed throughout with "dripfeed" .....	343
Fig 9.5 Contaminant model schematic.....	344
Fig 9.6 15 day simulation of toxicity model 8b1 .....	351
Fig 9.7 Model 8b2 toxicity simulation .....	355



Fig 9.8 Model 8c1 reduced autophagy boost otherwise.....	360
Fig 9.9 Model 8c contaminant autophagic factor comparison .....	362
Fig 9.10 Model 8c2 survival across the contaminant autophagic factor and cytosolic damage factor parameter space .....	365
Fig 9.11 Model 8d1 continual exposure diffusion.....	369
Fig 9.12 Recharging tubule lumen model .....	373
Fig 9.13 Recharged lumen tubule models .....	375
Fig 9.14 Model 8d2b starved mussel with maximum resting phase reduced to 150mins.....	377
Fig 9.15 Double contaminant cytosol damage and residency .....	378
Fig 9.16 Increased Lysosomal damage Model 8e .....	382
Fig 9.17 Model 8e1 starved simulation with increased lysosomal damage .....	383
Fig 9.18 Model 8e2 tenfold reduction in lysosomal to residual body contaminant flow .....	385
Fig 9.19 Model 8e3 lysosomal stability.....	386
Fig 9.20 Model 8f varying cytosolic and lysosomal contaminant bases..	392
Fig 9.21 Model 8f1 below base defensive value precludes damage boost	395
Fig 9.22 Model 8f2 as previous model except starved.....	398
Fig 9.23 Bio-transformation Model 8g.....	402
Fig 9.24 Lipofuscin Model 8h1. ....	409
Fig 9.25 as for previous model except extended to 1000 days.....	410
Fig B1 Analytical solutions .....	430
Fig C1 Comparison of approximations .....	439
Fig C2 approximations to the initial conditions using various numbers of eigenvalues and $A = 16000$ , $L1 = 0.4$ , $L = 1$ and $B = 1$ .....	440
Table 2.1 Variables nomenclature and limits .....	43
Table 2.2 Rate processes nomenclature and limits.....	44
Table 3.1 numerical experiments and relevant parameters presented for lipid and glycogen models .....	85
Table 3.2 Nomenclature used for model 2b .....	98
Table 3.3 atomic breakdown of phosphoglyceride.....	101
Table 3.4 Comparison of percentage breakdown of carbon loss from cell .....	126

Table 4.1 Extra variable names for model3 .....	137
Table 4.2 Element composition of relative frequency amino acids.....	150
Table 5.1 Instantaneous rates of entry and exit from the endo/lysosomal system for volumes and carbon/nitrogen content.....	169
Table 6.1 Average values for radial heights during different tubule stages .....	203
Table 7.1 Description of various compartments and nomenclature for Figure 7.1 .....	234
Table 9.1 Experimental tests run for toxicity model.....	334
Table 9.2 Comparison of Model 8c2 and 8d1 .....	370
Table 9.3 Table of model 8g results for various transformation factors...	404
Table D Various results given for size of vesicles.....	441

## **Acknowledgements**

I would like to take this opportunity to thank PML for its financial support and provision of facilities, without which this study could not have been achieved. Also, my thanks go to the School of Mathematics & Statistics, University of Plymouth for the room space provided when on campus.

My thanks to my supervisors for their generous support and assistance: Professor Mike Moore, for his patience with a biological neophyte and unstinting enthusiasm for the project; Icarus Allen, for sharing his modelling acuity and appreciation of cricket; & Professor Phil Dyke, for his timely reviews, suggestions and interest.

### **Author's Declaration**

At no time during the registration for the degree of Doctor of Philosophy has the author been registered for any other University award without prior agreement of the Graduate Committee.

This study was financed with the aid of a studentship from Plymouth Marine Laboratory.

Relevant scientific seminars and conferences were attended at which work was presented; external institutions were visited for consultation purposes and several papers prepared for publication.

#### **Publications:**

1. Allen, J.I. & McVeigh, A. (2004). Towards computational models of cells for environmental toxicology. *J.Mol.Hist.*, **35**, 697-706.
2. McVeigh, A., Allen, J.I., Moore, M.N., Dyke, P. & Noble, D. (2004). A carbon and nitrogen flux model of mussel digestive gland epithelial cells and their simulated response to pollutants. *Mar. Environ. Res.*, **58**, 821-827.
3. Moore, M.N., Allen, J.I. & McVeigh, A. (2004). Ecophysiomics: a systems biology approach to environmental toxico-pathology from the molecular and cellular levels to the ecosystem. *J. Histochem. Cytochem.*, **52**, Suppl. 1, S12.
4. McVeigh, A., Moore, M.N., Allen, J.I. & Dyke, P. (2006). Lysosomal responses to nutritional and contaminant stress in mussel hepatopancreatic digestive cells: a modelling study. *Mar. Environ. Res.*, **62**, Suppl. 1, S433-S438.
5. Moore, M.N., Allen, J.I. & McVeigh, A. (2006). Environmental prognostics: an integrated model supporting lysosomal stress responses as

predictive biomarkers of animal health status. *Mar. Environ. Res.*, **61**, 278-304.

6. Moore, M.N., Allen, J.I., McVeigh, A. & Shaw, J. (2006). Lysosomal and autophagic reactions as diagnostic and predictive indicators of environmental pollutant toxicity in aquatic animals. *Autophagy*, **2**, 2. 20.

7. McVeigh, A & Dyke, P., (submitted), A Simple Computational Model of digestion in the Marine Mussel. *Applied Mathematical Modelling*.

Presentation and Conferences Attended:

Conferences – PRIMO 12, Florida (poster presentation)  
PRIMO 13, Alessandria (oral presentation)

Word count of main body of thesis: 56,785 words.

Signed .....

Date .....

predictive biomarkers of animal health status. *Mar. Environ. Res.*, **61**, 278-304.

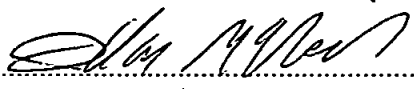
6. Moore, M.N., Allen, J.I., McVeigh, A. & Shaw, J. (2006). Lysosomal and autophagic reactions as diagnostic and predictive indicators of environmental pollutant toxicity in aquatic animals. *Autophagy*, **2**, 217-220.

7. McVeigh, A & Dyke, P., (submitted), A Simple Computational Model of digestion in the Marine Mussel. *Applied Mathematical Modelling*.

Presentation and Conferences Attended:

Conferences – PRIMO 12, Florida (poster presentation)  
PRIMO 13, Alessandria (oral presentation)

Word count of main body of thesis: 56,785 words.

Signed  .....

Date 2/9/2008 .....

## **Chapter 1 General Introduction**

### *1.1 Rationale & objectives*

Environmental toxicology is concerned with the effects that pollutants have on the environment with especial regard to the consequences to ecosystem status and human health. The importance of estuarine and coastal environments as a global resource for food, biological diversity and industrial raw materials combined with the widespread industrial and domestic discharge from nearby human populations makes predicting consequences and monitoring health in these areas especially significant (Depledge *et al.*, 1993; Di Giulio & Benson, 2002; Moore *et al.*, 2004).

Measuring the effect of disturbances or stressors to these systems is a complex task as there is a combination of multiple factors involved, resultant changes are seldom apparent in the short term (Allen & Moore, 2004). Moreover, whilst the focus remains on ecosystem or human health, these are too far removed from the causes to be of use for early detection. Hence, molecular distress signals in sentinel species are used as a measure of environmental health (Moore, 2002; Depledge & Galloway, 2005). In order for this approach to work, the relevant molecular and cellular endpoints have to be associated with higher level ecological consequences. If the stress is a chemical pollutant, then understanding of the uptake, biotransformation, depuration and molecular damage will be necessary.

The ability to predict a distress signal to a pollutant at the cellular level will require integrating information on basal metabolic behaviour and responses to stress drivers into a testable, explanatory framework (Allen & Moore, 2004; Moore *et al.*, 2006a). The progression from conceptual through mathematical to numerical models provides just such an instrument (Allen & Moore, 2004; Noble, 2002). Moreover, composing and testing a conceptual model in order to numerically model a system requires explicit formulation of hypotheses, which highlights knowledge gaps, crystallises grey areas and aids identification of critical processes.

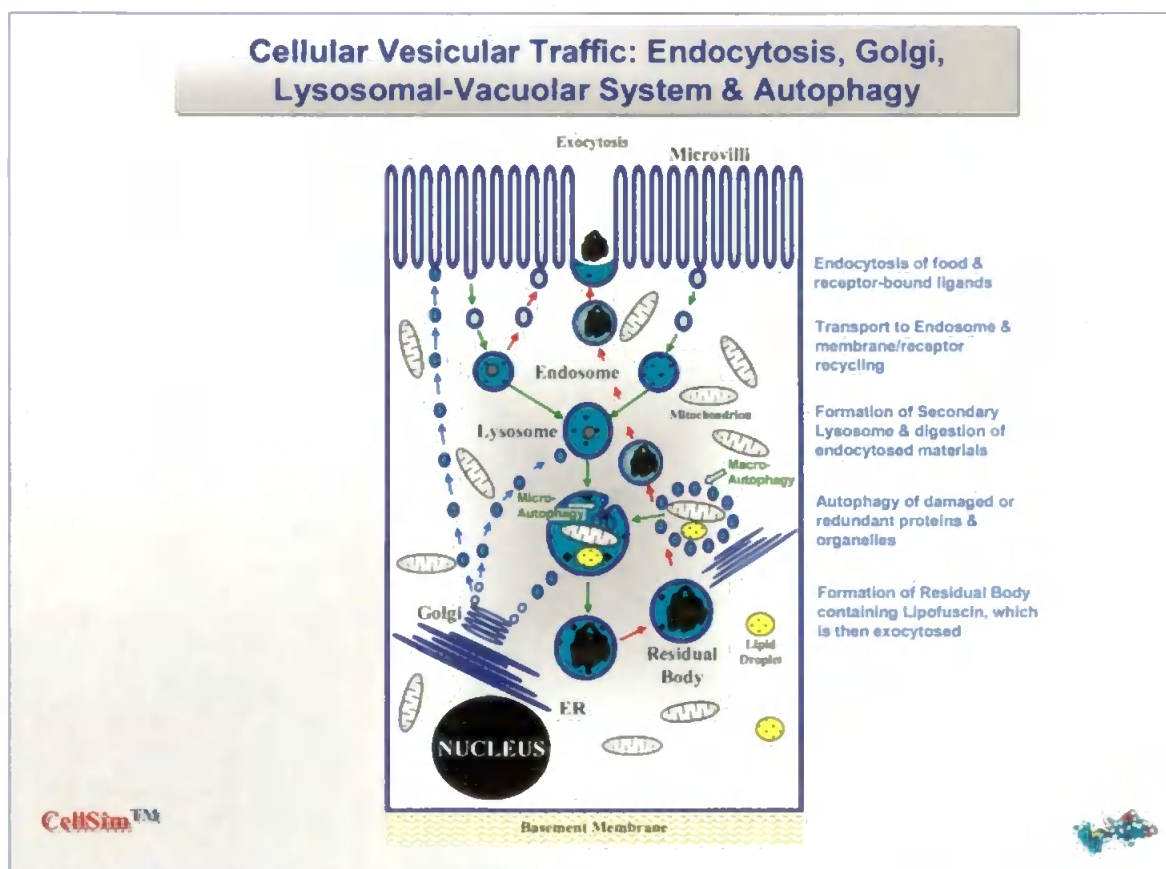


Fig 1.1 Conceptual Cell Model showing endocytotic and autophagic components of vesicular traffic and lysosomal degradation in cell feeding (heterophagy) and organelle/protein turnover (autophagy).



Consequently the aim of this investigation was to develop a generic model of cellular function (Fig. 1.1) that could be used, together with empirical experimentation and observation, to develop a platform for deriving explanatory frameworks for toxicological and pathological reactions to environmental stressors. The specific objectives included the testing of the hypotheses defined below in section 1.13.

## 1.2 Mussels & Lysosomal Stability

Mussels have long been used as sentinel species for environmental monitoring programmes due to a number of attributes: widespread geographical distribution; sedentary; tolerant but not insensitive to a wide range of environmental conditions, including moderately high levels of various contaminants; as suspension feeders they filter a large volume thus exposing themselves to a large proportion of the available environment; bioaccumulate contaminants within tissue which is indicative of how available these contaminants are, not readily apparent from sediment or water analysis; population levels are stable and sufficiently large for long or short term sampling programmes; can be transplanted to different locations; they are an important commercial species (Widdows & Donkin, 1992).

This study has nominally been of a particular species, *Mytilus edulis*, the common blue mussel which has been the subject of intense international and local Plymouth-based investigation for many years. Since the majority of biological functions and organisation at the cellular level can be generalised, and more specifically the evolutionarily conserved hepatopancreas organ, within this genus, a model has been designed so that extrapolation to closely related species is a matter of re-parameterisation rather than comprehensive modifications.

As a widely studied species, a variety of biomarkers have been proposed for *Mytilus edulis* to indicate deleterious effects on the health of the mussel (Cajaraville *et al.*, 2000). The responses of the lysosomal-vacuolar system have been chosen as potential cellular prognostic biomarkers for whole animal health, as perturbations to this system often precede cell and tissue pathology (Fig. 1.1; Moore *et al.*, 2006a). The functional stability of the lysosomal membrane has become the benchmark measure for lysosomal health in response to environmental stressors in both molluscs and fish (Moore, 1976; Moore, 2002; Köhler *et al.*, 2002).

In the mussel, the hepatopancreas or digestive gland has been and remains a common tissue for biomonitoring and contaminant exposure experiments (Cajaraville *et al.*, 2000). This is largely due to its function in uptake of food, which exposes it directly to the external environment. It is directly exposed to water soluble contaminants and, also, due to uptake of food at specific sites (digestive cells located within blind ending tubules) is also at risk from particulate associated contaminants (Owen, 1970). The hepatopancreatic digestive cell is then one of the most dynamic and active cells within the mussel and a major site of intracellular digestion, nutrient absorption, glycogen and lipid storage, as well as contaminant uptake and detoxification. Consequently, injury to this cell type in particular has damaging effects on overall animal health.

Therefore, a numerical model of the digestive cell of the hepatopancreas cell is proposed, which will deliver a prediction of lysosomal stability for various combinations of environmental stresses.

### 1.3 Conceptual Model

Figure 1.1 is a stylised depiction of the major organelles and components of a eukaryotic cell. The first major task of the modelling process was to simplify the cell into a pertinent and tractable form for the proposed investigation. For example, Bassingthwaite (2001) describes the simplest set of requirements for a sustainable cell, where protein metabolism and cell division have been excluded, focussing on the electrophysiological features. In accordance with this focus the postulated conceptual cell model's main features are the ionic pumps and channels which are used to regulate the potentials across membrane divides.

In contrast, the proposed mussel cell model was to be based on energy and protein metabolism, as these are the factors affecting whole animal physiology, including vesicular traffic and lysosomal function. Since the main aim of this model was to predict the lysosomal stability of the cell the focal point was the lysosome. The endo-lysosomal pathway degrades both intracellular and extracellular material and consists of endocytotic vesicles, early and late endosomes, endosomal carrier vesicles and lysosomes (Pillay *et al.*, 2002). The exact nature of the endo-lysosomal system has not been clearly resolved; i.e. questions still remain over the genesis and evolution of the separate components. However, it can be split into two major components, the endosome and lysosome.

The endosome (sic) is primarily concerned with the uptake of exogenous material and the recycling back to the cell membrane of lipid and proteins used in the vesicular transport of this material. The lysosome (sic) degrades both this exogenous material and endogenous material transported through the autophagic pathway. Whilst the dynamics of endosomal/lysosomal synthesis and turnover are undoubtedly important, it was decided to amalgamate all of the endosomes and lysosomes into singular separate compartments. All lysosomes are apparently capable of engaging simultaneously in autophagy and endocytosis (Fengsrud *et al.*, 2004).

Conventional modelling protocol dictated that the conceptual model be as simple as possible to capture the requisite dynamics of the parameter of interest. Hence, the majority of intracellular components (e.g. nucleus, Golgi, endoplasmic reticulum, proteasomes and mitochondria) and activity (e.g. protein transcription, respiration) were excluded or simplified. Thus, the rest of the cell has been combined into one 'cytosol' compartment.

In particular, the mitochondria is responsible for the majority of ATP production and thus their exclusion from a purported 'energy'-based model is possibly the most contentious. Additionally, toxic exposure has been shown to affect them (Viarengo *et al.*, 1981) and the majority of 'basal' ROS generation in cells is a consequence of normal aerobic respiration through the mitochondrial electron transport chain. Equally, damage to their membrane leads to an influx into the cytosol of damaging proteins

which leads to cell death. Finally, there is a proposed scheme detailing the diffusion of the oxyradical  $H_2O_2$  from the mitochondria to the lysosome which may be responsible for some of the generation of lipofuscin (Brunk & Terman, 2002; Winkler *et al.*, 1999). All of these features staked a claim for inclusion of the mitochondria within the model. However, a balance between complexity and practicality needed to be struck. As the dynamics of the 3-body system was unknown at the inception of this study, it was concluded that the exclusion of the mitochondria was reluctantly necessary in order to initiate the model.

It was then necessary to characterise these compartments so that the lysosomal stability can be calculated. As there is a strong positive correlation between the relative lysosomal volume and lysosomal instability, it was expedient to model the volume of each of the three compartments. Additionally, lysosomal stability is directly linked to the turnover of proteins. Hence, some means of characterising these macromolecular forms was necessary. As carbon is the principal identifier of organic compounds, this was a suitable initial choice for a characterising property. The conceptual model characterisation has evolved over the course of this investigation: an initial carbon-based model (chapter 2); an augmented lipid/glycogen carbon model (chapter 3); a nitrogen/carbon model (chapter 4); a protein/lipid/carbohydrate-based model (chapter 7).

The bulk transport of these characterising variables between the three compartments then needed to be identified and subsequently modelled:

- Endocytosis – transfer of exogenous material from the cell surface to the endosome.
- Recycling – transfer of ‘rejected’ material and solute from the endosome to the external environment.
- Lysosomal traffic – movement, by vesicular transport or evolution of endosome to lysosome, of material from the endosome to the lysosome.
- Autophagy – uptake of material from the cytosol to the lysosome.
- Degradation – transfer of successfully degraded material from the lysosome to the cytosol.
- Exocytosis – transfer of waste components from the degradative processes to the external environment.
- Export – transfer of material from this type of cell to the rest of the animal.
- Respiration/Excretion/Secretion – loss of characterising material from cytosol to the external environment due to activity and maintenance of cell.



- Storage/Release – segregation/liberation of characterising material into/from a protected form for utilisation during periods of stress.

There follows a brief introduction to each rate process with regard to this model.

#### *1.4 Endocytosis, recycling and lysosomal transport*

Endocytosis is an all-encompassing term for the internalization of extracellular components by surrounding them with a portion of the plasma membrane, which subsequently detaches to form an endocytotic vesicle. There are many distinctions made between the different types of endocytosis such as pinocytosis (“cell drinking” the bulk internalization of small vesicles) and phagocytosis (uptake of large particles with evidence for 130 nm diameter as minimum size (Desjardins & Griffiths, 2003)), but this model was only concerned with the overall rate of uptake of relevant material.

Once material has entered the cell, via endocytosis, two possible routes are generally considered: either it is sent for further degradation or else recycled back to the cell surface as unwanted material. There is at least one more possible path whereby proteins are sequestered into specialized holding compartments awaiting secretion to the cell surface (Robinson *et al.*, 1996) but this was not considered in this model.

The mechanisms for vesicular transport within the endo-lysosomal pathways are not entirely understood with two basic schemes being proposed, either fusion or “kiss and run” (Ryan, 2003). Under the fusion model there is complete membrane mixing of the vesicle membrane (donor) and that of the destination organelle (acceptor). To ensure the size of the vesicle pool is sustained there must be a subsequent mechanism for

recycling membrane which also provides the opportunity to eject unwanted material and solute. The “kiss and run” model proposes that vesicles fuse temporarily with the acceptor membrane and the vesicle contents are released into the acceptor lumen, then the vesicle pinches off from the acceptor. Additionally a more recent model, “fuse-pinch-linger”, proposes that the fused vesicles remain intact far longer after they initially fuse and a dynamin governed bridge may stop membrane contents from becoming intermixed before the vesicle is released (Ryan, 2003).

Inevitably the presentation of food to the hepatopancreatic cell is inextricably entwined with the feeding activity of the mussel in general. The seasonal variation shown in the different parts of the feeding process (filtration, ingestion, clearance and absorption rates), are not solely due to responses to food availability, but are to some degree self-regulated by the mussel itself (Cranford & Hill, 1999). These authors have speculated that this is due to the combined restraints of the need to maximise net energy gain when food concentration is low and seasonal reproductive energy demand. Furthermore, Hawkins *et al.* (1985) suggest that absorption rates are mainly endogenously regulated to reflect the current phase of reproductive cycle and energy stores, and thus that feeding is governed for time-averaged rather than immediate optimization. If the digestive cell is taken as the final destination in the feeding process, then some of the adaptation will have occurred previously in the digestive tract (extracellular digestion), but whatever the food signal made available to the digestive

tubule, there is still adaptation in how long food stays in the tubule, possibly extracting the maximum amount of nutrient when food quality or quantity is low and maximising the amount of digestive pre-processing done therein.

## 1.5 Autophagy

Autophagic turnover of long lived proteins occurs at a basal level throughout a cell's lifespan. This is rate augmented under various conditions and certain stressors. Increased autophagic activity is observed when the cell is subject to nutritional deprivation, salinity and temperature changes, toxic stress and during certain parts of the cell cycle and cell death (Cuervo, 2004; Lockshin & Zakeri, 2004; Moore *et al.*, 2006b)

Four pathways for endogenous material to be passed to the secondary lysosome have been identified: microautophagy, macroautophagy, crinophagy & chaperone mediated autophagy (Cuervo, 2004). Chaperone mediated has not been demonstrated in non-mammalian cells so is ignored hereafter. Additionally various names abound for particular substrates sequestered by the different methods (e.g. micro/macropexophagy for peroxisomes picked up by micro/macroautophagy (Reggiori & Klionsky, 2002). The entire autophagic process has been broken down into 7 steps as shown below (Levine & Klionsky, 2004):

1. Induction as a response to various signals, either developmentally or nutritionally linked.
2. Cargo selection – generally considered to be non selective (Klionsky & Emr, 2000) but in yeast the Cytoplasm –to–vacuole transport pathway can recognise and package specific material.

3. Vesicle nucleation – the process of vesicle generation is generally regarded as being unclear, but the consensus seems to be that the endoplasmic reticulum is significant (Fengsrud *et al.*, 2004).
4. Vesicle expansion and completion – the deformation/curvature of the sequestering vesicle, normally accomplished by membrane-associated protein components forming a transient coat e.g. clathrin coated vesicles as in endocytotic pathways.
5. Retrieval – recycling of some of the components of autophagy back to the cytoplasm for possible reuse. Most proteins concerned with autophagosome generation are not taken up with the notable exception being Atg8 which is often used as a marker of autophagy.
6. Vesicle targeting, docking and fusion- vesicle docks or fuses outer membrane with the outer membrane of vacuole.
7. Vesicle breakdown – fusion of dual membrane autophagosomes releases inner membrane bound vesicle into vacuole or lysosomal lumen. Vesicle lysis step is unknown.

Under basal metabolic conditions a small proportion of the cytosolic proteins are taken up through the arbitrary microautophagic pathway (Doherty & Mayer, 1992). Upon the introduction of stress, such as nutritional deprivation of amino acids and/or proteins, macroautophagic vacuoles are formed which contain target material for degradation. Dunn (1990) postulates that the vacuoles are originally produced at the ribosome

free areas of the endoplasmic reticulum, while Yamamoto *et al.* (1990) claims that they are synthesised at the post-Golgi region; but generally the source of the vacuoles is considered unknown. The one or more specialized membrane cisternae used to form the vacuoles are called phagophores and are lipid rich and relatively devoid of membrane bound proteins (Fengsrud, *et al.* 2004). The autophagic vacuole generated for macroautophagy is also known as an autophagosome and its contents are homologous to the cytosol (Baba, *et al.*, 1994), containing (mitochondria, ribosomes RER glycogen granules, etc...). In microautophagy it is the lysosomal membrane itself which would fold in on itself to engulf cytosolic material and transfer it to lysosomal lumen (Müller *et al.*, 2000).

Macroautophagy is generally considered non-selective (Baba *et al.*, 1994), but more recently Baba *et al.* (1997) have shown evidence for two pathways by which aminopeptidase I (API) may be targeted to reach the vacuole. Normally API is sent to the vacuole via the cytoplasm to vacuole (Cvt) targeting pathway, but under starvation conditions the macroautophagy instigated either uses the same machinery as Cvt or else they utilise different mechanisms with a sizeable overlapping of molecular machinery (Ishihara *et al.*, 2001). Tuttle & Dunn (1995) observe that changes in the sources of carbon (e.g., from methanol based to ethanol or glucose based), requires the rapid degradation and synthesis of enzymes relevant to each type of metabolism, which is achieved through an upregulation of the autophagic process. It has also been shown (Huang &

Chiang, 1997; Chiang *et al.*, 1996) that fructose-1,6-bisphosphatase (FBPase), an important regulatory enzyme in gluconeogenesis, and peroxisomes are specifically targeted for degradation once extracellular glucose becomes available to previously starved cells. Moreover, an excessive number of peroxisomes are dealt with by specific autophagic sequestration (Klionsky, 2005)

### *Starvation induced autophagy*

Study of the mTOR kinase system (mammalian target of rapomycin) has revealed that under starvation unutilized energy-consuming components are targeted for lysosomal degradation (Klionsky & Emr, 2000). TOR is a kinase which normally coordinates aspects of cell growth, such as transcription, translation ribosome biogenesis. Starvation (or by some other TOR inhibitor) inhibits TOR activity which in turn provokes the cellular response of cell cycle arrest in G<sub>1</sub> phase, inhibition of protein synthesis and autophagy (Klionsky & Emr, 2000). TOR inactivation induces two steps of the autophagic process, whereby various macroautophagic genes are activated & autophagosomes are produced.

By comparing nitrogen excretion rates and composition (Bayne & Scullard, 1977a), and also accounting for changes in ration-related biochemical proportions, during the year have shown that protein also serves as a valuable source of energy for the mussel over an annual cycle. A thirty-fold increase in protein turnover during October relative to May indicates that previous depletion of carbohydrate and lipid energy stores



necessitates the release of energy from structural proteins (Hawkins & Bayne, 1985), which forms another facet to the important role of protein degradation in bivalve molluscs.

Autophagic increase is not solely constrained to stress responses but actively increases during cell differentiation and other developmental processes (de Duve & Wattiaux, 1966). Autophagy also has a role in cell death (Edinger & Thompson, 2004). The model cell was conceived as a mature cell within the hepatopancreatic organ and hence none of these effects were considered pertinent to this study.

## 1.6 Degradation and exocytosis

There are two major sites of intracellular degradation: the dedicated degradative organelle, the lysosome, and the cytosol. Additionally, small rates of protein catabolism have been observed within mitochondria, chloroplasts and the endoplasmic reticulum, which despite their relative importance to the various organelles comprise an insignificant proportion of total cell turnover and are ignored hereafter. The observed differences in the half lives of various proteins and their observed sites of degradation through radioactive pulse and chase techniques leads to the crude maxim that most short lived cytosolic proteins are degraded in the cytosol by proteasomes (Doherty & Mayer, 1992), whilst longer lived proteins tend to be degraded in the lysosome (Chiang *et al.*, 1996), possibly because of the perceived non-selective nature of lysosomal sequestration.

Cytosolic degradation and the proteasomes were not explicitly included in any form of the model, which may be considered an oversight. However, lysosomes have been identified as the probable major site for protein degradation in bivalve molluscs (Hawkins & Day, 1996). Any perturbation which raises the level of oxidatively damaged components over the capability for cytosolic repair leads to up-regulated autophagic uptake into the lysosome. Thus perturbation to the cytosolic protein degradation is seen to be a cause for the observed increase in autophagic lysosomal activity (Cuervo, 2004).

### *Lysosomal protein degradation*

The other major site of protein degradation is the lysosome: these membrane bound vesicles are found in the majority of eukaryotic cells. Two types of lysosome have been proposed (Stinchcombe *et al.*, 2004): secretory and conventional. The secretory lysosomes are primarily present in immune system cells, and are a fusion of a conventional lysosome with a store of inactive secretory products such as perforin and granzymes which can be rapidly mobilized to attack virus infected or tumour cells. The model and following discussion relates only to the ‘conventional’ lysosome.

The lysosome (sic) was first identified by de Duve in 1956. Subsequent research suggests that the lysosome has a number of forms based on the activity it is engaged in. It was commonly supposed that it is first generated as a sac full of inactive hydrolytic enzymes dubbed the “primary lysosome”. This structure then either fuses with another vesicle containing material for degradation or else such material is deposited into the lysosomal lumen, and the optimal conditions for the hydrolytic enzymes is acquired by means of a proton pump to acidify the internal environment; this structure is known as a secondary lysosome (de Duve, 1983). Some doubt now exists as to whether or not this is an accurate picture; instead the lysosome as a component of the endo-lysosomal system is stressed.

Regardless of the specific mechanics of the system, the degradative capacity and competence of the endo-lysosomal system is due to components such as hydrolases, lysosomal associated membrane proteins (LAMPs), H<sup>+</sup>-ATPases and cysteine transporters (Doherty & Mayer, 1992; Eskelinen *et al.*, 2003).

Lumenal acidic conditions are required for a number of reasons: disassociation of ligands from receptors in endosomes; transporters have acidic pH optima; activation of lysosomal hydrolases and once activated many of the hydrolases have acidic pH optima. Current research suggests the lysosomes may be organelles for the storage of hydrolases in an unresponsive form due to their internal environment. Thus when delivered to a late endosome or phagosomes with the correct environment the degradation can occur (Pillay *et al.*, 2002).

Exocytosis properly refers to the bulk transport of material from cells, e.g. excretion of water and secretion of hormones and mucus (Prescott, 1988). However, in this model it refers directly to the excretion of the remnants from lysosomal degradation. Mathers (1972) observed rejected material in the form of excretory spheres in the tubule lumen of the oyster *Ostrea edulis* 90 minutes after the commencement of feeding.

### *1.7 General metabolic rates*

Any rate which contributes to the overall general maintenance of the cell and explicitly loses or gains any significant amount of the model variables needed to be accounted for. The use of energy in the cell is commonly taken to correspond to the rate of respiration, whereby the energy inherent in chemical bonds is released by oxidative (aerobic) processes. Energy is also made available during deamination which is linked to the rate of nitrogen excretion (Bayne & Scullard, 1977b). The cell also routinely secretes proteins to aid extracellular processes and to 'communicate' with other cells.

### *1.8 Nutrient Storage and Export*

The mussel, as a consequence of the variable environment it inhabits, builds up reserves of nutrient derived stores for use in either reproduction or for maintenance during the part of the annual cycle when food availability is low (Thompson *et al.*, 1974). Different parts of the mussel are used as storage facilities. For example, the mantle tissue can at certain parts of the season be composed of up to 90% of storage cells (Lowe & Pipe, 1986); either adipogranular cells, which store lipid and proteinaceous material, or vesicular connective tissue cells which accumulate large reserves of glycogen. Gabbott & Peek (1991) show seasonal changes in the various storage forms with glycogen levels declining over the winter during gametogenesis and then rapidly recovering to 50% of the dry tissue weight within 10 weeks of spawning. As the digestive cell is the primary site for uptake of nutrients, this increase in mantle stores must be a consequence of export from these cells, thus representing an important rate to be incorporated within the cell model.

Additionally, the digestive cell has the ability to store energy in different forms for either short-term (principally glycogen) or long-term (lipid) durations (Thompson *et al.*, 1974). These stores are either released during periods of stress, such as seasonal nutritional deprivation and changes in physical environmental conditions (e.g., temperature and salinity); or else they are transported to the gland and sent to the gonad

during gametogenesis, especially egg formation or vitellogenesis (Gabbott & Bayne, 1973). By measuring an O:N ratio, Bayne (1973a, 1973b) determined the primary organic macromolecular form used for energy throughout the year (see below). Additionally, the effect of body size, temperature and nutritive stress upon the seasonal metabolism (Bayne & Scullard, 1977a) is reflected in the source of energy being used. To summarise, during the summer glycogen, is the main energy source and stress results in increased utilization reflected in higher oxygen consumption. Conversely, in the winter protein is the main energy source and stress results in increased protein catabolism, amino acid deamination and excretion with elevated oxygen consumption.

### *1.9 C:N Ratios & control*

The particular segmentation /compartmentalisation of the candidate model cell was decided and the relevant pathways were identified. In order to proceed further some form of regulation had to be imposed in order to decide how the cell reacted to its state; to reflect the constraint put upon the cell by available energy and metabolic substrates. Initially, then, the carbon concentration of the cytosolic compartment were used, as the variations in cellular carbon were considered to be sufficiently small within this compartment (Moore & Allen, 2002). Recognition that this one element model cannot adequately satisfy the proposed aims of the model led to the search for a second element to add to the model (Chapter 4). Mann (1982) recognised that the flow of carbon/energy within coastal ecosystems can be limited by the lack of the nitrogen, thus predicating a need to model both chemical species in order to reflect the control exerted by the minimum ratio of one to the other. Thus, one of the initial aims of this thesis was to determine a way of incorporating nitrogen into the model.

However, in contrast to this nitrogen limiting view, Hawkins & Bayne (1992) stated that mussels do not require more protein for growth nor maintenance. They report a seasonal C:N ratio for maintenance which ranges from as high as 83:1 in winter to 12:1 during summer, with an average annual value of 16:1. Clearly if the model was to be controlled by nitrogen and carbon concentrations then either an average value needed to



be taken or else an adaptive algorithm developed to decide the control level and how to achieve it. Originally it was assumed that with an annual average cytosolic carbon concentration of 8.3 moles/litre the nitrogen concentration should be 0.5 moles/litre and both should be kept constant accordingly (Moore & Allen, 2002). But Gardner & Thompson (2001) showed C:N whole body ratios of 5-4:1 over 100 days in coastal regimes and slightly less for 70 days under estuarine conditions. Relating this to the model, and the later awareness that to properly imbue the lysosome with properties which reflect observation, led to a final proposed model based upon tracking the flow of the three nutritional major organic macromolecules (protein, lipid and carbohydrates) (McVeigh *et al.*, 2006).

Furthermore, the proposed relative utilisation of different nutrient reserves for energy requirements throughout an annual cycle (Gabbott & Bayne, 1973) subsequently made the constant concentration control conditions untenable. Thus, in later models (Chapters 7, 8 & 9), adaptive systems were used to reflect the seasonal changes in tissue biochemistry. Various control mechanisms were introduced and tested to simulate an annual cycle. However, the sparseness of the data and the extrapolation of one cell to whole organ behaviour serve to compromise the accuracy of the model.

### 1.10 Damage

In order for the model to be useful it first had to be able to simulate lysosomal stability under unstressed conditions and then under stressed conditions.

As has been seen the source material for the lysosome is divided into internal and external material. The amount of endogenous material taken up by the lysosome is driven by the rate of autophagy, which in turn is primarily dependent upon the amount of damage to extant components of the rest of the cell under 'normal' metabolic conditions. The rate of degradation of proteins shows dependence on the extent of oxidation of substrate proteins (Dunlop *et al.*, 2002). For the model, this was assumed to be predominantly oxidative damage to nucleic acids, proteins and lipids.

Most of the molecular oxygen taken up by animals will end up being tetravalently reduced to water coupled to the oxidation of food and the production of energy. Partial reduction leads to various reactive oxygen species (ROS), also known as oxyradicals or oxygen derived species, and comprise both radical (e.g. superoxide  $O_2^-$  and hydroxyl radical  $OH\cdot$ ) and non-radical species (e.g. hydrogen peroxide  $H_2O_2$  and peroxynitrite  $ONOO^-$ , also known as a reactive nitrogen species - RNS). Radicals are highly reactive atomic or molecular species as they have either unpaired electrons or other open shell configuration. These ROS are assumed to be responsible for the oxidative destruction/transformation of biomolecules.

Reactivity and properties of each varies, but the presence of less damaging species can lead through a series of reactions to the more damaging species, principally the short-lived hydroxyl radical (OH•) which is extremely reactive (Livingstone, 2001). Despite the injurious nature of ROS, they are also utilised by cells in maintaining homeostasis and regular cellular function, either as specific signalling molecules, in fighting infection or regulating cell proliferation (Finkel & Holbrook, 2000).

The generation of these species is stimulated by both exogenous and endogenous factors. The majority of ROS generation is a consequence of normal aerobic respiration through the mitochondrial electron transport chain. Most ROS damaged cellular components undergo enzymatic degradation, releasing damaged elements and conserving reusable components (Pacifi & Davies, 1991).

Oxidized proteins are predominantly sent to proteasomes for degradation and, possibly, this occurs without the need for ubiquitin conjugation (Dunlop *et al.*, 2002). There is some evidence that the proteasomal and lysosomal systems work sequentially as well as in parallel – some proteins are catabolised by one or the other or either, and some oxidised proteins are first sent to the proteasome and then subsequently to the lysosome for final degradation (Dunlop *et al.*, 2002). The accumulation of oxidised proteins in ageing cells is a well-established phenomenon and it has been speculated that this is possibly due to changes in catabolism. Proteasome levels are unchanged in older cells but their activity was

reduced, the activity of lysosomal cathepsins was similarly reduced. Moreover old cells have been shown to have no capacity to upregulate proteolytic capability in response to oxidative stress (Cuervo & Dice, 2000; Dunlop *et al.*, 2002).

For the model the cytosolic degradative processes have been disregarded, due to the more strongly observed lysosomal reaction within the types of cell under consideration. To incorporate damaging effects the initial models attempted to up-regulate or ‘boost’ the autophagic rate. Consideration of how this affected subsequent degradative results was given as it was shown to be critical to the survival of the early model cell. Subsequent models attempted to generate damaged pools of material and made autophagy a function of these cytosolic pools. Then the rates of damage themselves were be increased due to, say, contaminant exposure; whilst autophagic increase due to nutritional deprivation sourced intact material for degradation.

Environmental factors can also increase ROS production: these include UV radiation and hypoxia (Livingstone *et al.*, 1990; Livingstone, 2001), but are not used in this model as environmental conditions are considered static to reduce the complexity of the situations under consideration. Rates or amounts of ROS can be increased by the presence of xenobiotics such as quinones, polycyclic aromatic hydrocarbons (PAHs), halogenated hydrocarbons (e.g., PCBs) and metal contaminants. Initially, it was the aim of this study to incorporate the effects of toxic

exposure to the cell model. Subsequently, however, the need to compose a better basis for the basal functioning of the cell has led to less work on this subject matter than originally planned.

### 1.11 Contaminants

Mussels are exposed to a wide variety and mixture of toxic metal and organic contaminants, the latter collectively referred to as xenobiotics, which produce varying degrees of stress (Livingstone & Pipe, 1992; Livingstone *et al.*, 2000a). In order to formulate a model for this stress signal required knowledge of the toxicity and metabolism of the contaminants. Lipophilic organic xenobiotics tend to bioaccumulate above environmental levels within mussel tissue, as they are poorly metabolised or biotransformed (Livingstone *et al.*, 2000a). Common contaminants which have been observed to bioaccumulate in mussel tissues include heavy metals and organic pollutants such as aliphatic hydrocarbons, polycyclic aromatic hydrocarbons (PAHs) and polychlorobiphenyls (PCBs).

The rates of organic xenobiotic metabolism are dependent on the tissue concentration, hence, they are determined by those features which influence their rates of uptake, biotransformation and discharge (Livingstone *et al.*, 2000a).

To predict the transport and effect of a pollutant it was necessary to know its physiochemical state (speciation). Organic compounds can exist in various forms in natural water including gaseous, dissolved, micelle forms, surfaced adsorbed onto particulates, occluded inside particles, associated with lipid films at the air/water interface and incorporated into

biota (Readman *et al.*, 1984). Complexation with dissolved organic matter affects the transport and uptake of such chemicals (McCarthy *et al.*, 1985). Those factors which determine the speciation are primarily the physico-chemical properties of the compounds such as solubility, hydrophobicity and vapour pressure (Readman *et al.*, 1984; Djomo *et al.*, 1996).

Bioaccumulation of most organic xenobiotics tends to follow an initial linear rate of uptake with an eventual attainment of some tissue equilibrium concentration. Most uptake is considered a passive transit from the aqueous to the biotic environment but selective uptake is possible. The most important sites of pollutant uptake in the mussel include the gill and hepatopancreas (Livingstone *et al.*, 2000a). Selective bioaccumulation can occur in subcellular compartments, membranes, macromolecular adducts and specific binding sites and is often related to the tissue lipid levels. Sequestering in lysosomes provokes the higher concentrations seen in hepatopancreatic tissues as a large number of lysosomes present (Moore & Viarengo, 1987) and, additionally, food associated contaminants are transferred to these sites directly.

After 30 days exposure to mixtures of PAHs and PCBs the mussel can bioaccumulate concentrations up to 400 and 22 times respectively over those in control animals (Krishnakumar *et al.*, 1997). However, the ratio of different PAHs in the contaminant mix (phenanthrene, fluoranthene, benzo(a) pyrene) is not reflected in tissue concentrations: this could be

evidence for preferential biotransformation of one compound over another, or else, could imply differing bioaccumulation kinetics for each.

Equally important to understanding of pollutant response is the recovery or detoxification processes. Depuration is also considered a passive process but active excretion for some compounds is observed (Livingstone & Pipe, 1992). Plotting the depuration rate for many xenobiotics reveals an exponential curve. However, the length and level of exposure can radically alter this relationship: short term exposures tend to result in the elimination of all xenobiotic in a rapid manner; long term exposures often result in incomplete and slow removal, with a residual concentration remaining. The chemical structure of the xenobiotic has also been observed to be important in determining the nature of the depuration rate (Livingstone *et al.*, 2000a). Higher molecular weight, less water soluble compounds are often eliminated at a slower rate.

Three basic lysosomal responses to environmental stress (chemical pollution, salinity and/or temperature fluctuations, malnutrition and reproductive stress) have been observed: content variability (hydrolytic enzymes and lipofuscin), changes in fusion events/or changes in lysosomal volume and changes in membrane permeability (Moore *et al.*, 1987; Marigómez & Baybay-Villacorta, 2003). The final model presented in this study attempted to specifically simulate these responses.



### 1.12 Dietary restriction

One particular, surprising, beneficial effect which the model sought to emulate is that of caloric restriction (CR) or diet restriction (DR) which confers protection against stress and ageing with induced autophagy (Moore, 2004; Moore *et al.*, 2006b, 2007). DR has been shown to facilitate recovery of lysosomal membrane stability from toxic injury due to phenanthrene and copper exposure. Exposed to both toxicants and starved there was recovery after a number of days, while with phenanthrene exposure coupled to feeding, there is no recovery in lysosomal stability, whereas with copper exposure and food available there is only partial recovery (Moore, 2004).

Why does caloric restriction increase ability to deal with age-related decline? Reverter-Branchart *et al.* (2004) showed that an oxidative stress on specific proteins is evident in aged cells compared to young cells. Those proteins involved include stress resistance proteins and enzymes involved in glucose metabolism, which if the host organism is subject to a caloric restriction show less damage, less lipofuscin generation and no internal iron build up.

Masoro (2005) has proposed that dietary restriction is a variation on hormesis. This low level stressor, DR, promotes a beneficial action (increased longevity, retarding deterioration of age associated diseases and coping with intense stressors) on the organism. DR has been shown to

enable coping with stressors such as intense heat, inflammatory response and damaging toxic drugs. It is proposed that accumulated damage from endogenous stressors (such as reactive oxygen) and environmental factors (chemical toxins, infectious agents) is decreased by DR (Masoro, 2005; Moore *et al.*, 2007).

### 1.13 Hypotheses

The major hypotheses that the modelling activity encompassed within this thesis has been designed to address are as follow:

*Hypothesis 1.1* The digestive cell can, most simply and adequately for the purposes set out above, be modelled as a temporal-spatial model based on three aggregated compartments: the endosome, the lysosome and remainder (dubbed the cytosol).

Corollary: Lysosomal stability can be determined by the relative lysosomal volume.

Justification: Within the digestive cell the major sites of organelle and long-lived endogenous protein degradation, the lysosomes, are also the final destination of food prior to degradation into usable components for the whole animal. Since the response to toxic insult is to be addressed by the model, the sites of toxin accumulation and effect also need to be included. Diffusion of toxic chemicals into the cytosol leads to enhanced damage to internal components, which augments the process of autophagy by which they are removed to the lysosome. Those toxins which enter attached to food particles are also destined to accumulate within the lysosome (Moore *et al.*, 2004). Under these conditions the lysosome became the pivotal component of the cell model. Consideration of the role of uptake of food and attached pollutants led to the additional inclusion of the endosome.

*Hypothesis 1.2* Increased autophagic rates can explain and simulate the major stress responses seen in the mussel digestive gland cell.

Justification: One observed response to stress is increased autophagy; the evolution of the model seeks to move from an empirical augmentation of this rate in response to derived cellular toxic concentrations and nutritional signals to a functional impetus for augmentation based on model cell state. Reactive oxygen species (ROS) mediated damage to the components of the cell, and the lysosome is the major recipient of damaged material. Hence, if the machinery for basal cytosolic proteolysis is overwhelmed, then the excess damaged material will be targeted for lysosomal degradation. Consequently a subsystem of basal oxidative damage and defence will drive increased autophagy. In the model, increased autophagic responses would then be delivered by increased oxidative damage linked to toxic concentration; and also as a response to nutritional deprivation.

*Hypothesis 1.3* The endocytotic rate can be modelled as a function of food availability and cell feeding capability.

Justification: Before the toxic response was considered, a model that is adaptive to nutritional stress was required as a basis, which could be augmented by other stresses. The primary driver for this system was the endocytotic rate, which needed to be considered with regard to whole animal feeding, digestive gland tubule morphology and observed cycles, seasonal food availability and quality. The cellular feeding capability to

presented food needed to be incorporated to represent restrictions placed by the energetic and functional state of the digestive cell.

*Hypothesis 1.4* In order to develop the explanatory facet of the model, the lysosome and endosome can be modelled as engineering analogues to chemical processing plants; whereby material entering the compartment was subject to a time delay before exiting via one of the prescribed pathways. The division between waste material and successfully processed material was a prime parameter in determining the functional effectiveness of this organelle.

Corollary: Inclusion of lipofuscin within the lysosome gives incoming material a new endpoint which will simulate internal accumulation.

Justification: Modelling the rates of the entry and exit to the degradative organelles as constants cannot hope to simulate the necessary adaptability of the cell to its dynamic environments. Furthermore, modelling these rates as volume dependent would not reflect the functional nature of these two organelles, especially with respect to perturbations to the incoming signals as observed with increased oxidative stress or nutritional deprivation.

Lipofuscin generation and accumulation has been shown to be correlated with various types of induced stress; and provides a reasonable explanation for some of the observed lysosomal swelling and decrease in protein degradation under conditions of stress.

*Hypothesis 1.5* The storage and export responses to nutritional uptake cannot be modelled as being solely dependent upon the state of the cell.

Justification: As the mussel is relatively sedentary it is presented with a variable food signal which necessitates that reserves are built up in times of plenty and utilised during deprivation. Whilst reluctant to impose arbitrary signals from the rest of the animal, seasonal observations of biochemical ratios within the cell show that the form of macromolecular store which is utilised in response to stressors throughout the year is variable.

Furthermore, the whole animal reproductive cycle has been shown to elicit mobilisation of reserves from one part of the animal to another. Therefore, storage and export from the digestive cell needed to be considered as responses to not only the current cellular state, but also as responses to higher level organisation. Moreover, in the later models, rather than arbitrary empirical rates applied at discrete thresholds as in the earlier models, these rates needed to be continually adapted to regulate the biochemical ratios within the cell.



## **Chapter 2 Carbon Model**

### *2.1 Objectives*

In this chapter the carbon based cellular model is introduced. This model was the simplest of those evaluated and established many of the concepts which recur throughout this study. The two major themes which govern the behaviour of all the models were examined: the 'nutritional' intake and feeding patterns which allow the cell to be sustainable; and the effect of toxic stress upon the cell. Finally, the inadequacies of this model were explored and provided the basis for the next model.

Whilst the model underwent a series of evolutionary steps only the two most pertinent sub-models are presented here. The results of the bypassed sub-models are discussed in section 2.3.



## 2.2 Introduction

The preliminary model described by Moore & Allen (2002) was used as a basis for the first carbon model. The conception of the cellular model as a three compartmental system was based on the premise of the centrality of autophagy and the lysosomal response to basal behaviour and the augmentation of these processes due to pollutant exposure, as detailed in Chapter 1. The mathematical model employed was based on the assumption of advective flow between the compartments, which due to their finite nature was determined as being inappropriate. Thus the original ODEs were reformulated to reflect the finite compartmental volumes (Moore & Allen, 2002). The schematic (Fig 2.1), notation and equations derived are presented below.

*Table 2.1 Variables nomenclature and limits*

Variable Name	Variable Description	Values/Limits
$E_v$	Endosomal volume	1-5% $Cell_v$
$L_v$	Lysosomal volume	1-30% $Cell_v$
$C_v$	Cytosolic volume	$2.4 \times 10^{-13}$ - $2.4 \times 10^{-12}$ l
$E_{xc}$	Endosomal carbon content	
$L_{xc}$	Lysosomal carbon content	
$C_{xc}$	Cytosolic carbon content	
$E_c = \frac{E_{xc}}{E_v}$	Endosomal carbon concentration	8.3-12.0 mol l <sup>-1</sup>
$L_c = \frac{L_{xc}}{L_v}$	Lysosomal carbon concentration	8.3-15.0 mol l <sup>-1</sup>
$C_c = \frac{C_{xc}}{C_v}$	Cytosolic carbon concentration	8.3 mol l <sup>-1</sup>
$S_c$	Carbon concentration at cell surface	0-6.0 mol l <sup>-1</sup>

# COMPUTATIONAL SIMULATION MODEL FOR POLLUTANT UPTAKE AND PATHOLOGY: MODEL 1

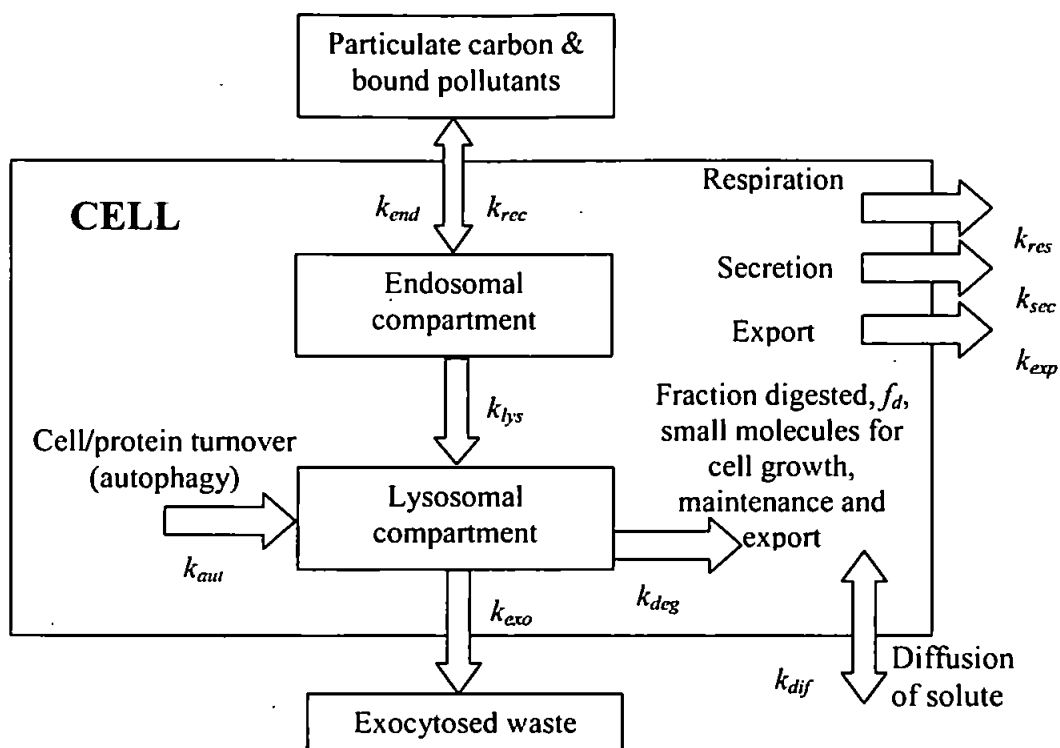


Fig 2.1 Schematic for model 1

Table 2.2 Rate processes nomenclature and limits. \*The rate of diffusion was added later in the model development and its limits are those determined from the model.

Name	Description of process	Values/Limits (litres min <sup>-1</sup> cell <sup>-1</sup> )
$k_{end}$	rate of endocytosis	$6.7 \times 10^{-17}$ - $2.0 \times 10^{-15}$
$k_{rec}$	rate of recycling	
$k_{lys}$	rate of traffic from endosome to lysosome	$0.0$ - $3.5 \times 10^{-16}$
$k_{aut}$	rate of autophagy	$1.7 \times 10^{-16}$ - $1.2 \times 10^{-15}$
$k_{deg}$	rate of successfully degraded material from lysosome to cytosol	$1.0 \times 10^{-16}$ - $1.0 \times 10^{-15}$
$k_{exo}$	rate of exocytosis	$1.0 \times 10^{-16}$ - $1.0 \times 10^{-15}$
$k_{res}$	rate of respiration	$0.0$ - $2.0 \times 10^{-17}$
$k_{sec}$	rate of secretion	$1.4 \times 10^{-19}$ - $2.8 \times 10^{-18}$
$k_{exp}$	rate of export	$0.0$ - $6.0 \times 10^{-16}$
$k_{dif}$	rate of diffusion (solute only)*	$0.0$ - $7.5 \times 10^{-16}$

The following parameters are also used in the text.

### Parameters

$$f_r = \frac{\text{amount of carbon leaving endosome by recycling}}{E_c} \quad \text{fraction of recycled}$$

material

$$f_d = \frac{\text{amount of carbon passed to cytosol}}{\text{amount of carbon out of lysosome}} \quad \text{the fraction of degraded material}$$

$$f_{ev} = \frac{\text{Endosomal volume}}{\text{Total Volume}} = \frac{E_v}{Cell_v} \quad \text{the fraction of endosomal volume}$$

$$f_{lv} = \frac{\text{Lysosomal volume}}{\text{Total Volume}} = \frac{L_v}{Cell_v} \quad \text{the fraction of lysosomal volume}$$

### Compartmental Volume Equations

$$\frac{dE_v}{dt} = k_{end} - k_{rec} - k_{lys} \quad [2.1]$$

$$\frac{dL_v}{dt} = k_{lys} + k_{aut} - k_{deg} - k_{exo} \quad [2.2]$$

$$\frac{dC_v}{dt} = k_{deg} - k_{aut} - k_{exp} - k_{sec} - k_{res} + k_{dif} \quad [2.3]$$

### Compartmental Carbon Content Equations

$$\frac{dE_{xc}}{dt} = k_{end} S_c - (f_r k_{rec} + k_{lys}) E_c \quad [2.4]$$

$$\frac{dL_{xc}}{dt} = k_{lys} E_c + k_{aut} C_c - (k_{deg} + k_{exo}) L_c \quad [2.5]$$

$$\frac{dC_{xc}}{dt} = k_{deg} L_c - (k_{aut} + k_{exp} + k_{sec} + k_{res}) C_c \quad [2.6]$$

### Compartmental Carbon Concentration Equations

$$\frac{dE_c}{dt} = \frac{1}{E_v} (k_{end} (S_c - E_c) + k_{rec} (1 - f_r) E_c) \quad [2.7]$$

$$\frac{dL_c}{dt} = \frac{1}{L_v} (k_{lys}(E_c - L_c) + k_{aut}(C_c - L_c)) \quad [2.8]$$

$$\frac{dC_c}{dt} = \frac{1}{C_v} (k_{deg}(L_c - C_c) - k_{dif}C_c) \quad [2.9]$$

### *2.3 Model development*

Once the system of ODEs had been established the model required only a set of initial values for the variables, the determination of the rate constants and to be supplied with a food regime in order to be able to calculate the value of the variables at any time in the future. Differing schemes for the evaluation of the rates determining the flow of material between the various compartments were attempted and a synopsis of their results is presented below.

Initially the model system was examined to see the effect of using mean values for all the rate constants. This rigid scheme was rejected as it led to rapid violation of most of the prescribed limits of the variables (i.e. cell death was inevitable and irrespective of the amount of nutrient supplied). This reflects the necessity of adaptation to ever changing endogenous or exogenous conditions. Hence various schemes were proposed and tested for adaptive systems of the rate constants.

Model 1a considered the primary cellular control condition – the constant cytosolic carbon concentration. Since material being passed to the cytosol varied in carbon concentration it was necessary to introduce a new diffusion rate which passed solute in and out of the cytosol.

Model 1b introduced the primary means of determining variable rates by making them dependent upon the volume of the compartment from which they issued. One exception to this rule was endocytosis which was

not sourced from any internal compartment and was dependent upon external influences and the status of the whole animal. Endocytosis was therefore considered in later sub models and kept constant as an exploration of the parameter space was made to determine the likely outcome of the model under differing initial conditions and food concentrations. It was found that initial conditions had minimal impact in comparison to the food concentration. Problems discovered included the lack of attainment of maximum cell volume and the exceedance of endosomal and lysosomal upper concentration limits.

It was also at this juncture in the model development that attempts to find analytical solutions were abandoned and numerical methods employed to produce the model results. This was necessary due to the non-linear nature of the concentration ODEs. Three standard numerical methods (Euler, Predictor Corrector and 4<sup>th</sup> level Runge-Kutta) were evaluated to discern their suitability. It was found with a reasonable timestep (0.1 minutes) that the simplest Euler method reproduced the results of the more complex methods. This method was used thereafter to solve all the model systems discussed in this work.

Model 1c adjusted the rate determination algorithm to account for compartmental volumes dropping to below their minimum values. It was found that this adjustment diminished the survival proportion of the parameter space.

Model 1d deferred the export of material away from the cell to the rest of the animal until the maximum cellular volume had been attained. This system was adopted as export was seen to be a major contributory factor to cellular decline. It is possible that there is a less arbitrary decision-making process within the cellular mechanics as the animal would probably demand nutrients to at least recover feeding costs in the rest of the body. The inclusion of this process extended the survival period to a small extent but did not increase the concentration of food necessary for survival.

Model 1e was an attempt to simulate the effects of increased autophagy when the cell is not supplied with sufficient food for maintenance. Unsurprisingly any increase in autophagy, due to the less than perfect degradation process, led to a more rapid decline in volume and consequent expiry of the cell. As the degradation and supply of external material is one of the primary functions of these cells it is possible that their metabolic activity decreases and hence their decline is halted due to decreased relative-demand for metabolites. Hence whilst the autophagic rate may increase in relative terms over that observed when feeding it may not increase in net terms.

Model 1f examined the amount of carbon taken up by the cell. This was achieved by varying both the endocytotic rate and food concentration to determine a survival space. This was done to establish when autophagic enhancement would be triggered. Whilst lower food concentrations may entail greater processing, and hence cost, it was decided that this could be

ignored as the overall carbon intake was probably a better measure of when maintenance conditions were failed than food carbon concentration.



## 2.4 Endosome and cell volume dependent endocytosis: Model 1g

Due to the focus on the uptake of nutrients the model behaviour was strongly dependent on the nature of the uptake of nutrients. It was not only the concentration of available source carbon but also the rate by which it enters, that roughly determined the model behaviour. Consequently, an attempt to put endocytosis on a sturdier footing had to be made. Chapter 6 presents a much more detailed examination of this important process, but in order to develop the earlier models an interim compromise was sought which assuaged some of the problems with using a constant rate. Model 1g was defined by making the rate of endocytosis linearly dependent on cell volume.

$$k_{end}(t) = k_{end\ min} + (k_{end\ max} - k_{end\ min}) \left( \frac{Cell_v(t) - Cell_{v\ min}}{Cell_{v\ max} - Cell_{v\ min}} \right) \quad [2.1]$$

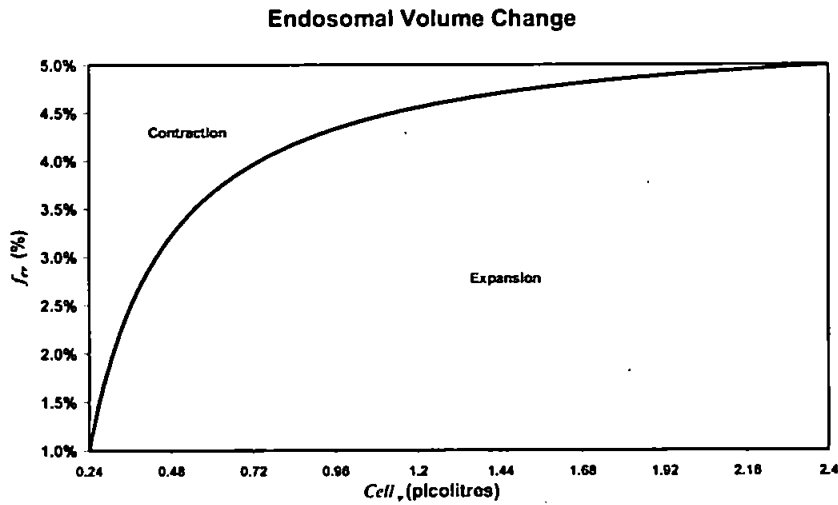


*Fig 2.2 Division of cell volume- $f_{ev}$  parameter space into areas of endosomal expansion and contraction.*

By making endocytosis linearly dependent on cell volume, then the solution of the rate of endosomal growth in equation 2.1 was only dependent on the endosomal relative volume,  $f_{ev}$ , and cell volume. The sign of the right hand side of the endosomal volume ODE is shown in Figure 2.2, the line represents zero endosomal growth, above the line there would be reduction in endosomal volume and below it there would be endosomal volume enhancement. Encouragingly for this specification of the endocytotic rate the parameter space was dominated by growth.

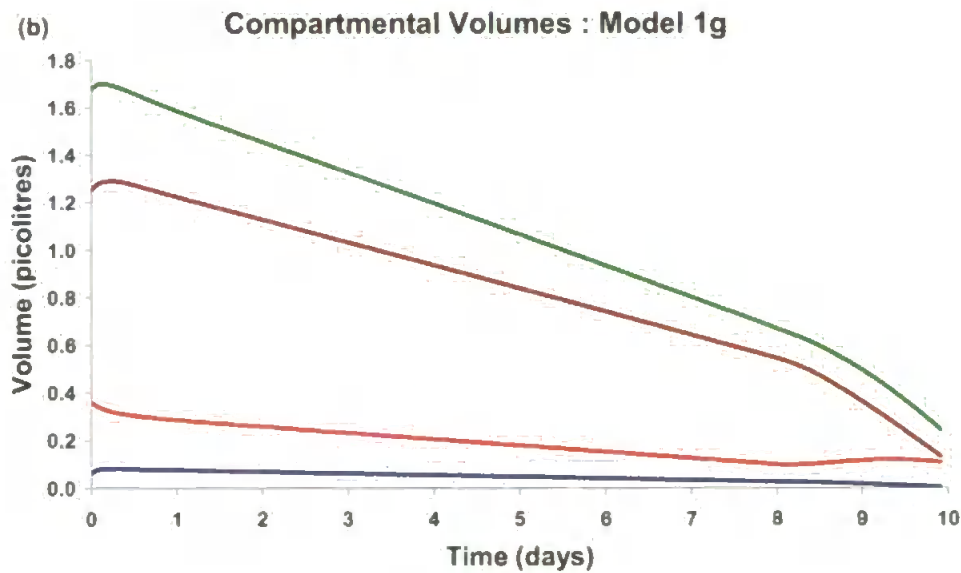
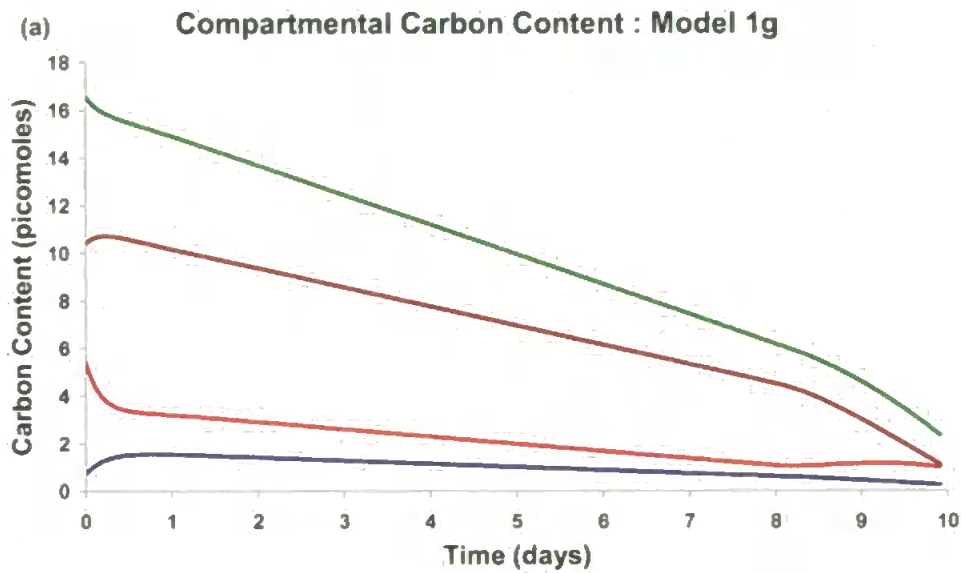
Three types of behaviour emerge for the set of initial conditions used, the food concentration was found to be the decisive factor in which was adopted:

### **(1) Death**

There was a brief initial increase in volume, when both the endosome and cytosol swelled (Fig 2.3b). This was due to the degradation of material, initially in the lysosome, reaching the cytosol (Fig 2.3a) and increasing cytosolic volume through the diffusion rate. Thereafter, there was a steady decrease as the amount of material being degraded was exceeded by the metabolic and autophagic costs. Finally, the cell volume reached a level where autophagy was augmented (Fig 2.3d) precipitating a more rapid decline to expiry. The endocytotic rate declined due to the falling cell volume (Fig 2.3c).

The rates of exocytosis and degradation were indistinguishable, due to possession of the same parameter range and lysosomal volume

dependency. Thus, the efficiency of the lysosomal degradative process was 50% for all these models. This inherent inefficiency was the principal mechanism governing the rate at which cell volume declined when not enough external carbon was supplied.



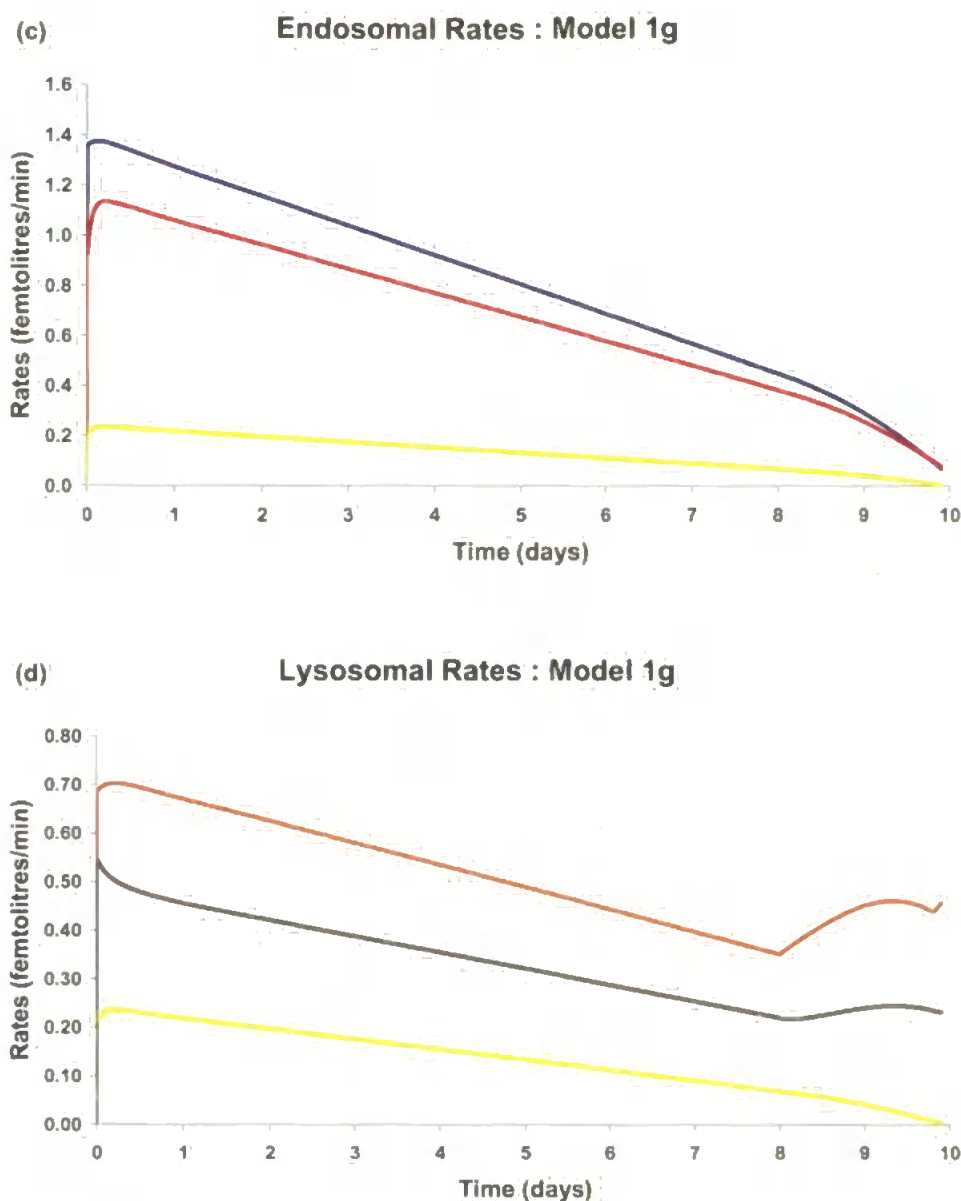
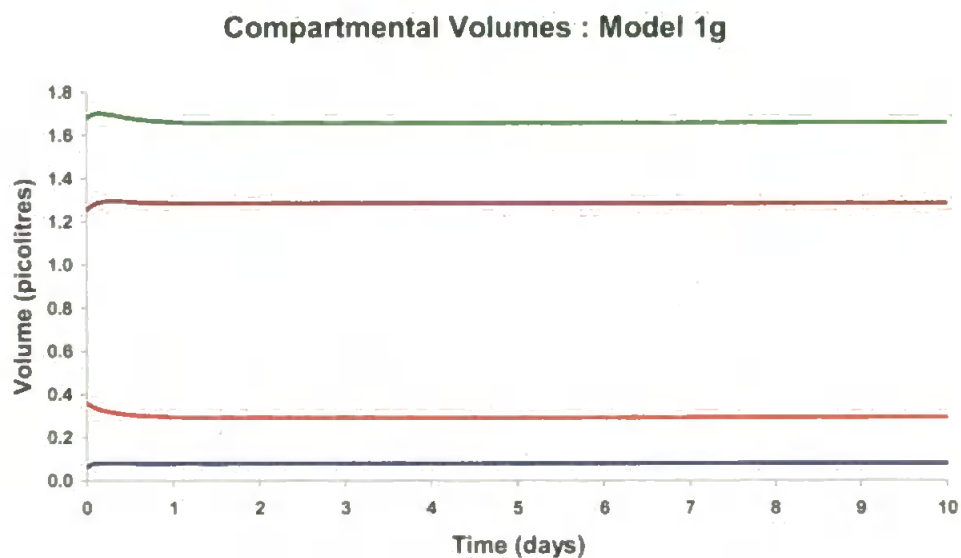


Fig 2.3 Simulation of Model1g with  $S_c = 3.6$  and ICs :  $Cell_v = 1.6764$  picolitres;  $f_{ev} = 3.65\%$ ;  $f_{lv} = 21.55\%$ ;  $E_c = 11.927$ ;  $L_c = 14.978$  &  $f_d \equiv 0.5$ .  
 (a) Compartmental carbon contents  $E_{xc}$  —,  $L_{xc}$  —,  $C_{xc}$  —,  $Cell_{xc}$  — (b) compartmental volumes  $E_v$  —,  $L_v$  —,  $C_v$  —,  $Cell_v$  — (c) endosomal rates  $k_{end}$  —,  $k_{rec}$  —,  $k_{lys}$  — (d) lysosomal rates  $k_{lys}$  —,  $k_{aut}$  —,  $k_{deg}$  —,  $k_{exo}$  —.

## (2) Equilibrium

There was a narrow band of external carbon concentrations at which the model eventually settles into a static state. Once again there was an initial

decrease in lysosomal content and volume (Fig 2.4a), however, the incoming material from the endosome was sufficient to stabilise the flux out of the cell. After the effects of the initial conditions were superseded by the incoming volume, the incoming and outgoing rates into each cell compartment were balanced, resulting in equilibrium in all compartments. The equilibrium state was achieved within 2 days and remained static thereafter.

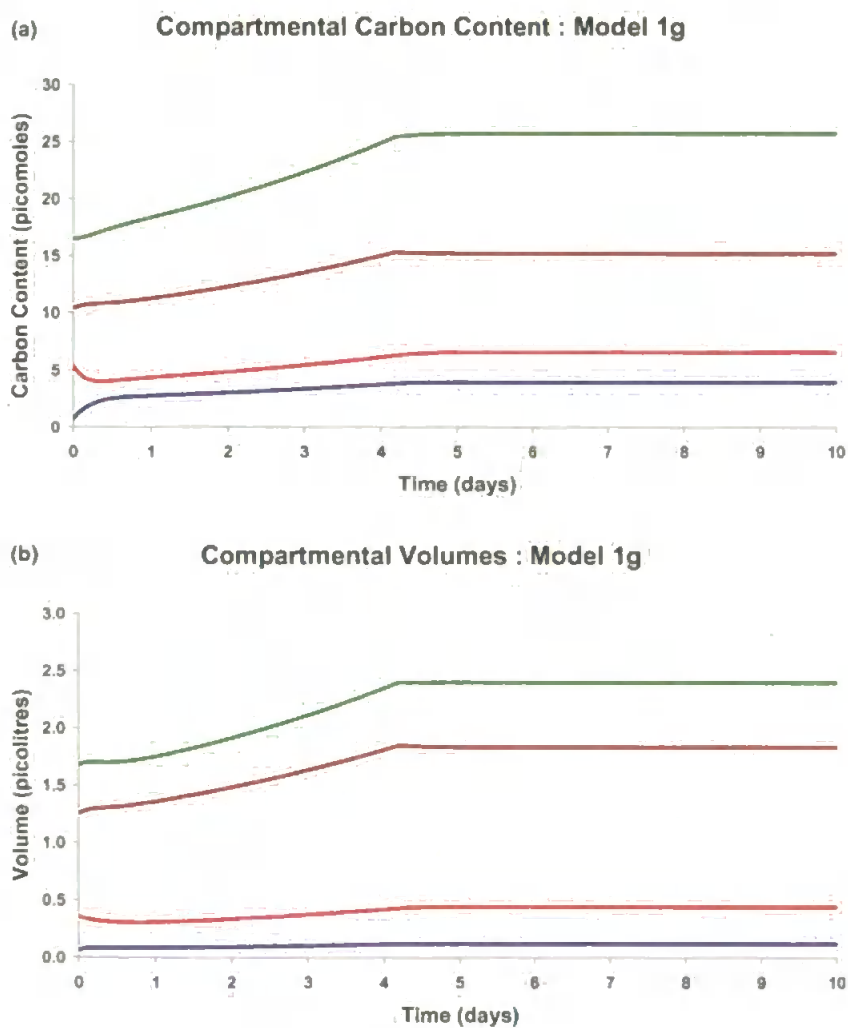


*Fig 2.4 Ten day simulation of Model1g with  $S_c = 4.7095$  and ICs as detailed for Fig 2.3 showing compartmental volumes  $E_v$  —,  $L_v$  —,  $C_v$  —,  $Cell_v$  — attaining a steady state.*

### **(3) Export**

Given a sufficient food concentration the cell showed, once again after an initial amount of redistribution of the initially available resource, an increase in all compartmental contents and volumes (Figs 2.5a,b), until the cell maximum volume was reached. Thereafter, with the export rate

removing excess volume, there was a small (imperceptible in the Figure) amount of oscillation between the compartments as the system sought an equilibrium level. Exporting started after 4.2 days when the cell first reached its maximum volume (Figs 2.5c). After 5.15 days the endosome reached an equilibrium state. The cytosol and lysosome settled into a static state at day 9.64. Thereafter, the cell was in complete equilibrium and exporting material, representing a fully functioning, healthy cell.



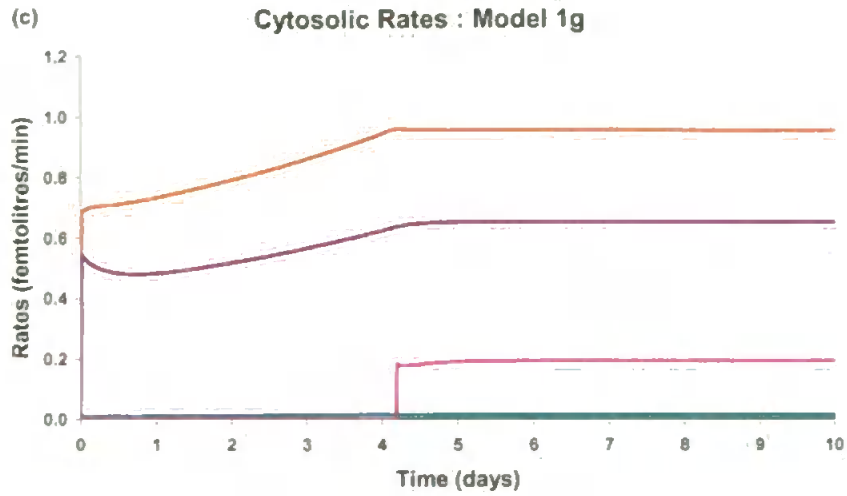


Fig 2.5 Ten day simulation of Model1g with  $S_c = 6.0$  and ICs as detailed for Fig 2.3. (a) Compartmental carbon contents  $E_{xc}$  —,  $L_{xc}$  —,  $C_{xc}$  —,  $Cell_{xc}$  — (b) compartmental volumes  $E_v$  —,  $L_v$  —,  $C_v$  —,  $Cell_v$  — (c) cytosolic rates  $k_{aut}$  —,  $k_{deg}$  —,  $k_{res}$  —,  $k_{sec}$  —,  $k_{exp}$  —.

Unfortunately, in each of the situations described above, the carbon concentration of the endosome rose above the prescribed limit (Fig 2.6). This was due to the recycling fraction parameter that is set at 0.01, so that whilst a less-than-average concentration of material was entering in the endocytosed vesicles, the amount of solvent leaving via recycling overcompensated and hence the ratio of volume to carbon content suffered. This anomaly was left until the work described in Chapter 5 (where the passage of material through the lysosome and endosome is explored with more rigour), as the relative importance of the endosomal variables remaining within their parameter limits was seen as small in comparison to the overall cell behaviour.

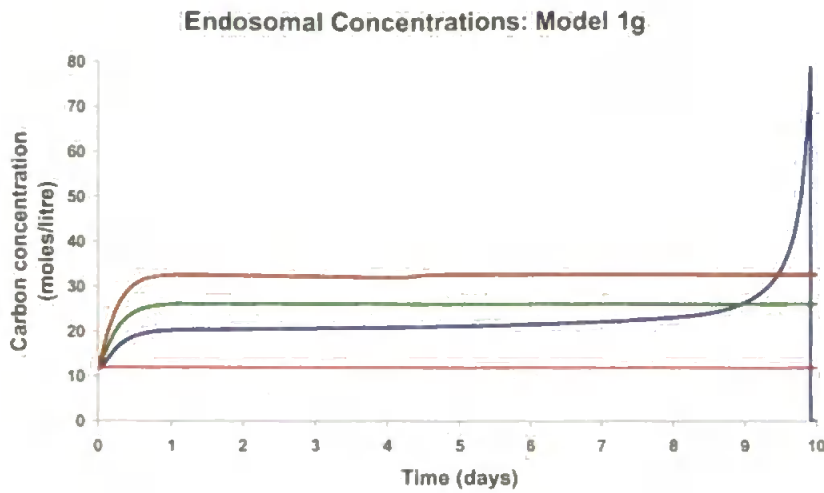


Fig 2.6 Endosomal concentrations in each of the three preceding simulations: — *Death*, — *Export*, — *Equilibrium*, — *Theoretical Maximum*.

In order to better assess the survival of the cell over the parameter space a “cellular health” function was defined:

$$H = \begin{cases} \frac{t_n - \text{MaxTimeofDeath}}{\text{MaxTimeofDeath}} & \text{when cell dies at time } t_n \\ \frac{\text{Cell}_v(t_n) - \text{Cell}_{v \min}}{\text{Cell}_{v \max} - \text{Cell}_{v \min}} & \text{when cell achieves equilibrium at time } t_n \\ \frac{\text{CumulativeExport}(1000\text{days})}{\text{MaxExport}} & \text{when cell exports} \end{cases} \quad [2.2]$$

This health function was used to assess the effect of the initial conditions and food concentration on the cellular behaviour with respect to the three modes detailed above (Fig 2.7). This was accomplished by iterating through the model on a discrete grid.



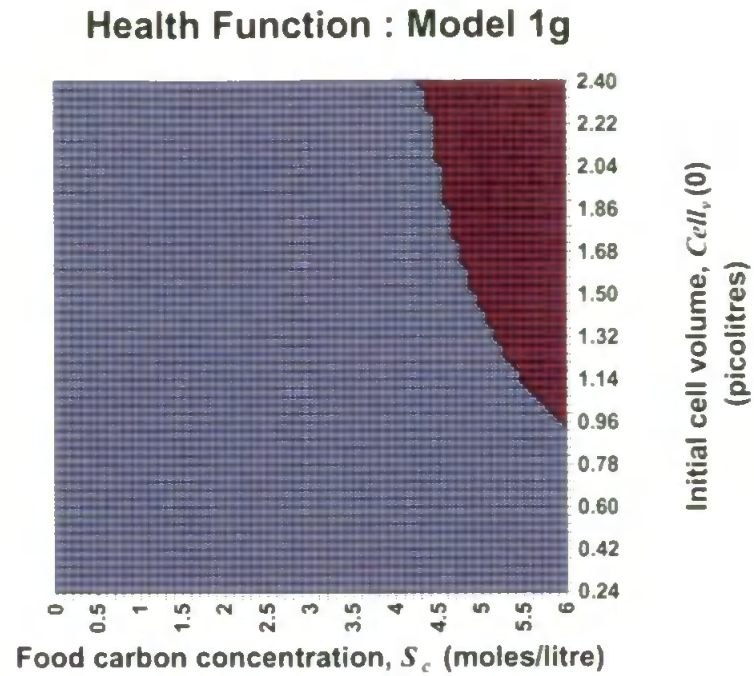


*Fig 2.7 Health function over the food concentration and initial cell volume space with the following initial conditions  $f_{ev}=3\%$ ,  $f_{lv} = 15.5\%$ ,  $E_c=11.927$ ,  $L_c = 14.978$  and  $f_d = 0.5$ . Key: ■=Death, ■=Equilibrium, ■=Export.*

It was determined that the survival space was only a fraction of the entire space (Fig 2.7). Also the equilibrium state, as described above, was not replicated on this grid of the parameter space indicating that it occupied only a thin band between the two other possible states.

The cell's functional efficiency and long term viability was essentially defined by the amount of food entering the lysosome via the endosome, which was then passed on to the cytosol. To ascertain the effect of this efficiency on overall cellular behaviour the exocytosis and degradation rates were altered.  $f_d$  was defined as the ratio of degradation content delivered successfully to the cytosol from the lysosome to the total

lysosomal content loss (i.e. degradation and exocytosis) and was used to weight these two rates accordingly.

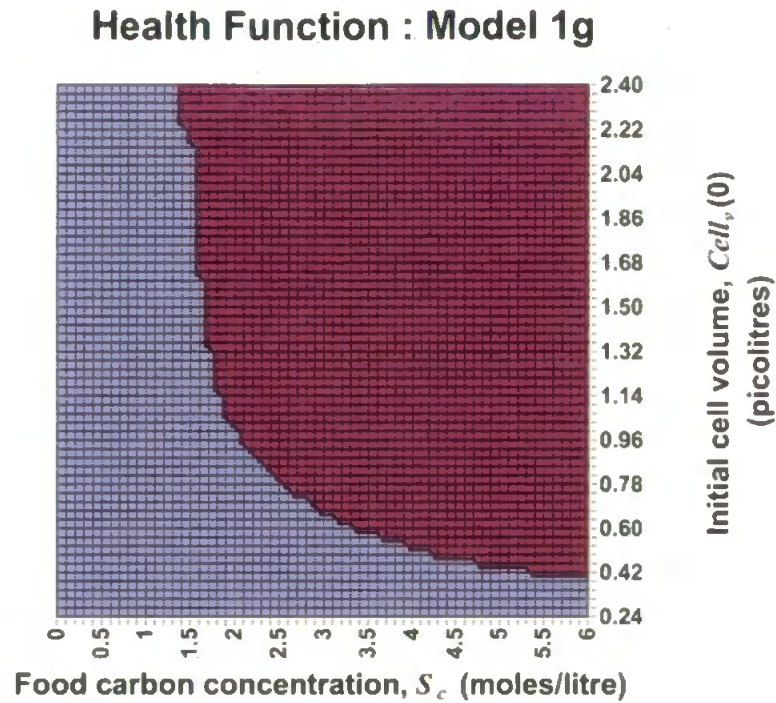


*Fig 2.8 Health function with increased digestive efficiency: ICs as detailed for Fig 2.7 except  $f_d = 0.75$ . Key ■=Death, ■=Equilibrium, ■=Export.*

The survival space became far greater with this greater efficiency, inhabiting 60.12% of the parameter space as opposed to 12.93% with  $f_d = 0.5$  (Fig 2.8). Hence, the maintenance of the cell was dependent on the amount of food not only entering the cell, but passing successfully through the endosomal-lysosomal system to the cytosol. It was also evident from Figure 2.8 that the end state of the cell is more sensitive to the supplied food carbon concentration than initial cell volume.

### Digestive Efficiency Survival Surface : Model 1g

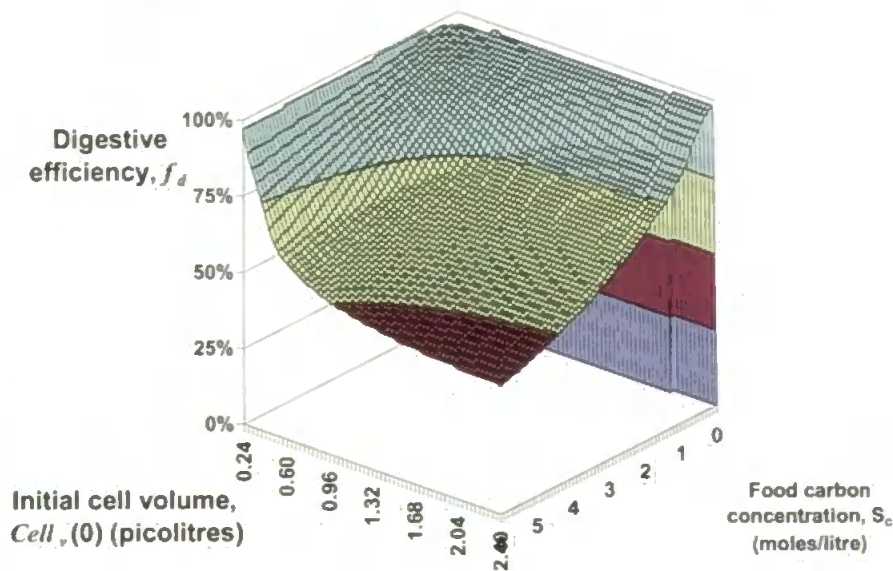


*Fig 2.9 Smallest possible digestive efficiency to ensure survival on initial cell volume and food concentration parameter space*

Figure 2.9 shows a surface across this parameter space at which survival was attained. The volume above this surface was approximately 30% of the total parameter space volume. This indicates that the robustness of this model was probably insufficient at this stage to simulate any real world situation.

Hawkins and Day (1996) demonstrated that improved growth efficiency involved increased lysosomal efficiency, with increased protein breakdown (Hawkins & Bayne, 1991), in mussels. Thus it can be inferred that the efficiency of the lysosome is variable and should be accounted for in the model.

### 2.5 Toxicity effect: Model 1h

It was deemed salutary at this early stage to attempt to mimic the effect of toxic exposure on the model cell, as an example of the procedures which will later be used with more complicated models (see Chapter 9). The basic premise for these models was: the presence of a pollutant within the cytosol of the cell initiates an increase in autophagy. This increase was primarily due to the generation of oxyradicals which damage cellular constituents that must be removed for the cell to function (Cuervo, 2004; Moore *et al.*, 2007). Further effects such as impairment to lysosomal function were considered and will be addressed in Chapter 9.

This preliminary work was only concerned with investigating the effect of increasing autophagy within an otherwise healthy (i.e. well-fed and exporting) cell. The actual increase in autophagy would be dependent upon the concentration and toxicity of pollutants in the cell, but as modelling this would have involved the toxicokinetics of entry and accumulation as well as neutralisation, only the effects of autophagic enhancement were considered at this stage.

Initially the simulation was run for 50 days at the highest food concentration to provide as healthy and stable a cell as possible. Thereafter the rate of calculated autophagy was doubled (Fig 2.10b) for 28 days.

However, the cell attained minimum volume within 10.5 days of the increase in autophagy (Fig 2.10a). It was noted that the food entering the cell declined with cellular volume due to its dependency on this variable.

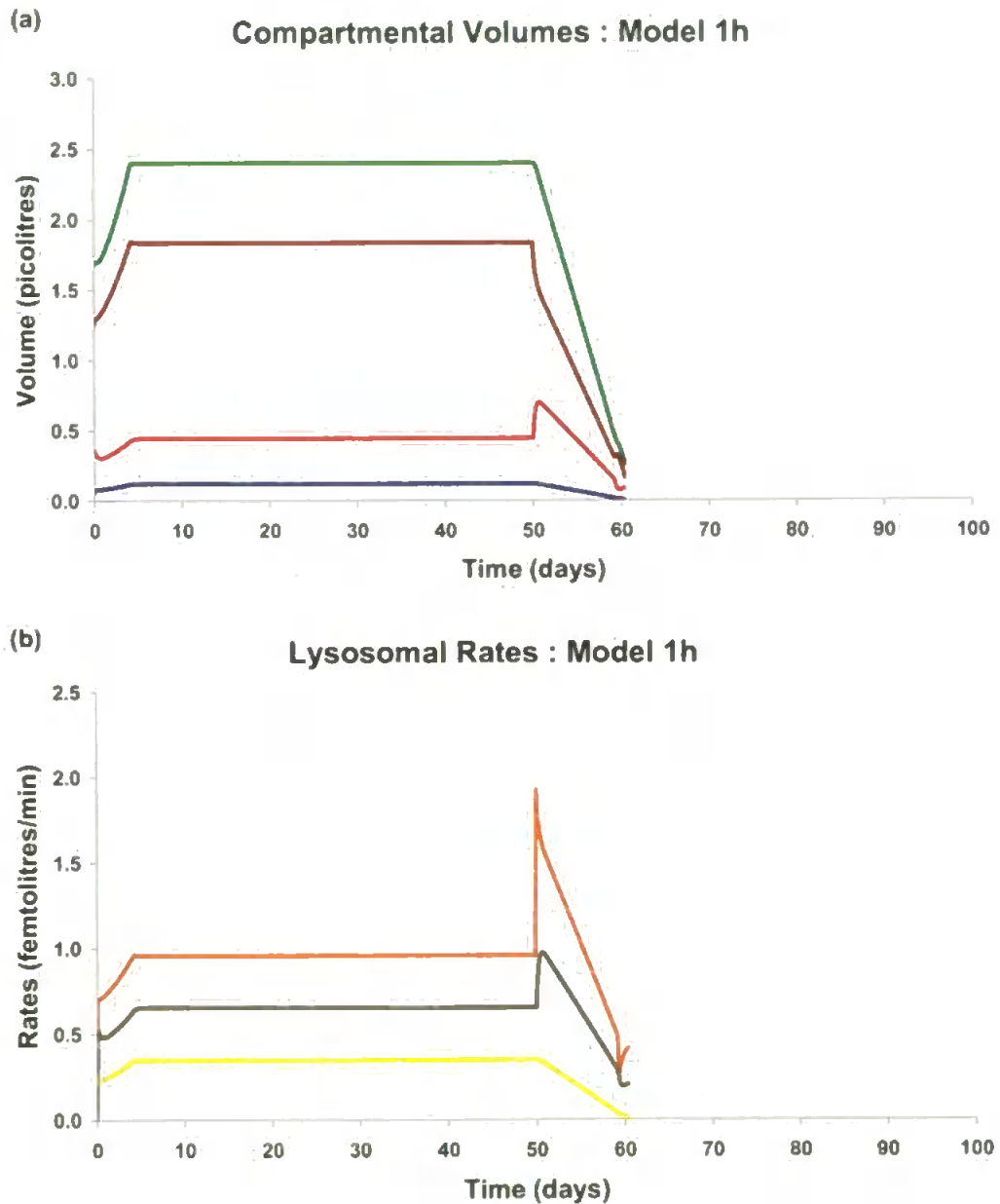


Fig 2.10 100 day simulation, with autophagy increased twofold from day 50 onwards, ICs as detailed for Fig 2.3 and  $S_c = 6.0$ . (a) Compartmental volumes  $E_v$  —,  $L_v$  —,  $C_v$  —,  $Cell_v$  — (b) lysosomal rates  $k_{lys}$  —,  $k_{aut}$  —,  $k_{deg}$  —,  $k_{exo}$  —.

It could be that while the effect of the increased autophagy will have a bearing upon cellular function, in order to compensate for this incurred cost, other processes (unspecified in this model) should have been temporarily halted and the primary task of supplying resources to the cell via endocytotic uptake retained. However, as noted in the previous section, the lysosomal efficiency was a variable quantity and this was used in the next simulation to attempt to preserve the cell during the stressed period.

As was previously noted, during stress the mussel appears to become more dependent on recycling material through autophagy. If digestive efficiency was set at  $f_d = 0.5$  during non-stress and at  $f_d = 0.625$  during a stress period for 28 days, then survival, and subsequently recovery, was exhibited (Fig 2.11a). The effect of this increase was apparent in the division between exocytosis and degradation, which both ran at the same rate when unstressed and split into the set ratio for the period of stress (Fig 2.11b).

Furthermore, the lysosomal relative volume increased from ~18.5% to 30.9% during the stress period (Fig 2.11c), which is a consistently observed cytological occurrence (Cajaraville *et al.*, 1997; Lowe, 1988; Lowe *et al.*, 1981, Marigómez *et al.*, 2005; Moore, 1988; Moore *et al.*, 2007). However, the rate of recovery of the cell (~2 days) was a possible cause for concern.

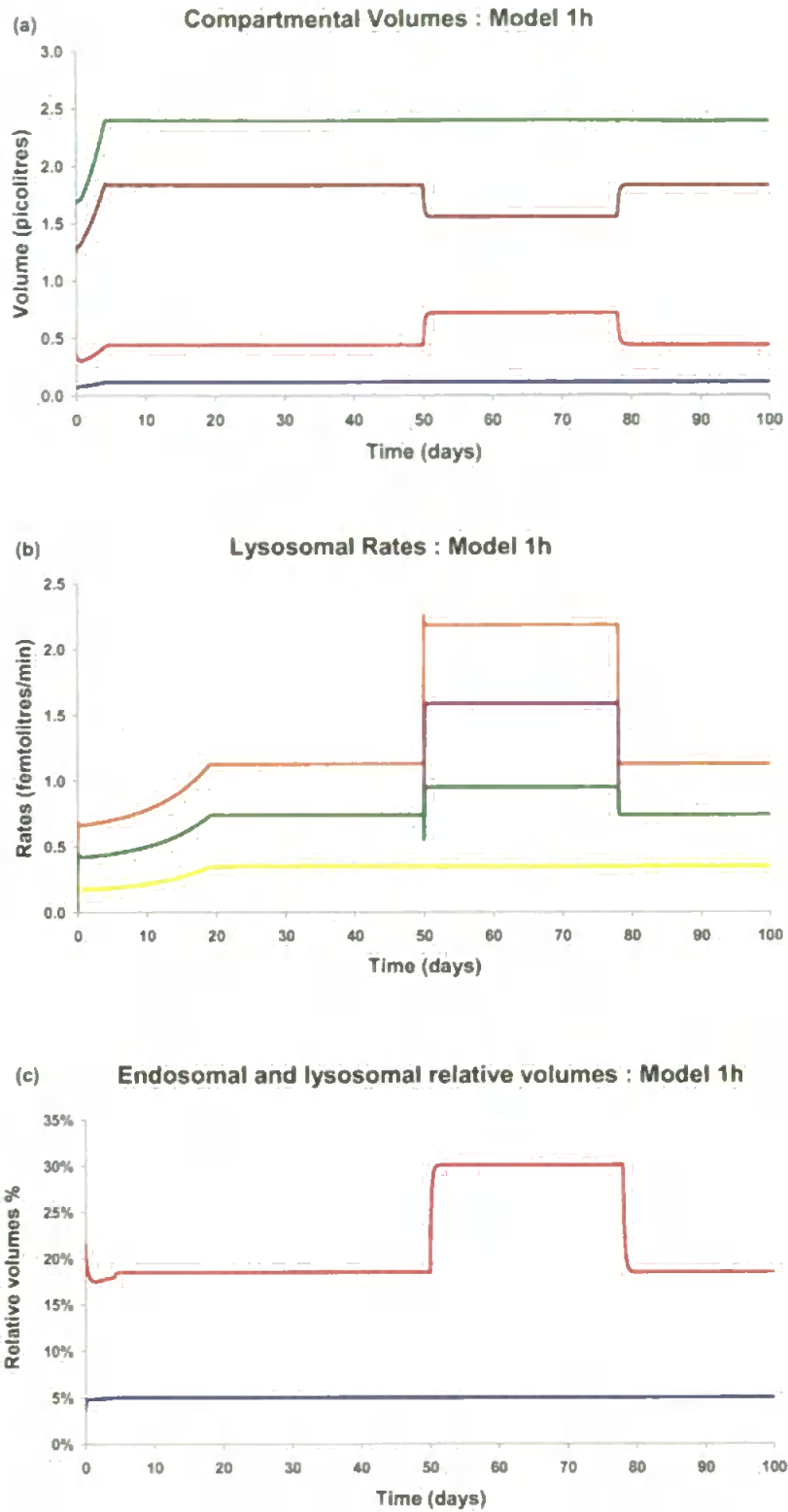


Fig 2.11 100 day simulation, with autophagy doubled and  $f_d = 0.625$  for days 50-78,  $f_{ev} = 3\%$ ,  $f_{lv} = 15.5\%$ ,  $E_c = 11.927$ ,  $L_c = 14.869$  and  $S_c = 6.0$ . (a) Compartmental volumes  $E_v$  —,  $L_v$  —,  $C_v$  —,  $Cell_v$  — (b) lysosomal rates  $k_{lys}$  —,  $k_{aut}$  —,  $k_{deg}$  —,  $k_{exo}$  — (c) relative endosomal (—) and lysosomal (—) volumes.



To compare the model results with biological measurement there is recourse to an observed empirical relationship. There is a strong correlation between lysosomal relative volume and a measurement of lysosomal stability (see introduction for definition; Moore *et al.*, 2006a). Initially a quadratic to describe the relationship between the two correlates was employed (Moore *et al.*, 2006a; Fig 2.12a). This allowed the lysosomal stability of the model cell to be calculated at any timestep.

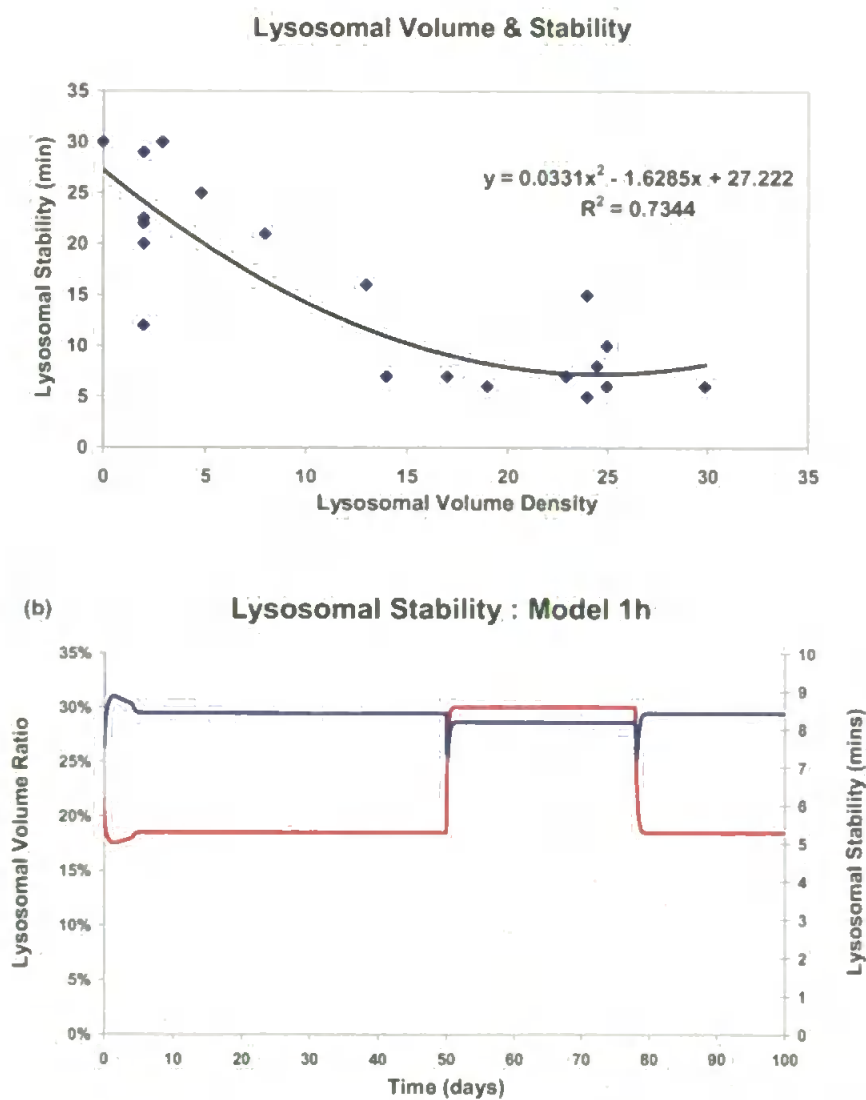


Fig 2.12 Lysosomal stability (a) Empirical relationship between relative lysosomal volume and lysosomal stability (b) previous simulation lysosomal stability — derived from relative lysosomal volume —.



Two anomalies were immediately apparent. First, the quadratic relationship might not have been adequate to express the lysosomal stability to lysosomal volume ratio relationship (Fig. 2.12a). Second, that the initial conditions could not have been correct as the lysosomal stability is never within what might be deemed the healthy range, usually taken to be ~25mins (Fig 2.12b). So alongside the quadratic, a fitted exponential relationship for lysosomal stability:  $LysStab = 24.173e^{-0.0523f_v}$  was derived from the same data and used for comparison. Additionally, the initial lysosomal volume was recalculated by setting the lysosomal relative volume maximum to be 5% to ensure that the lysosomal stability was initially within the “healthy” range. Then a model simulation which exhibited the requisite increase in lysosomal volume when stressed was sought.

With a fivefold boost to the autophagic rate and a rise to 78.7% digestive efficiency for the stressed twenty-eight day period, there was a much larger decrease in lysosomal stability as the lysosome swelled to a relative volume more often seen in stressed animals (Fig 2.13a,b). There was little difference between the quadratic and exponential relations. Furthermore, the volume of the cell started to decline which has been often seen in stressed animals (Fig 2.13a; Bayne *et al.*, 1978; Lowe, 1988; Lowe *et al.*, 1981). The recovery period from this stronger stress extended beyond the two days seen in the previous simulation.

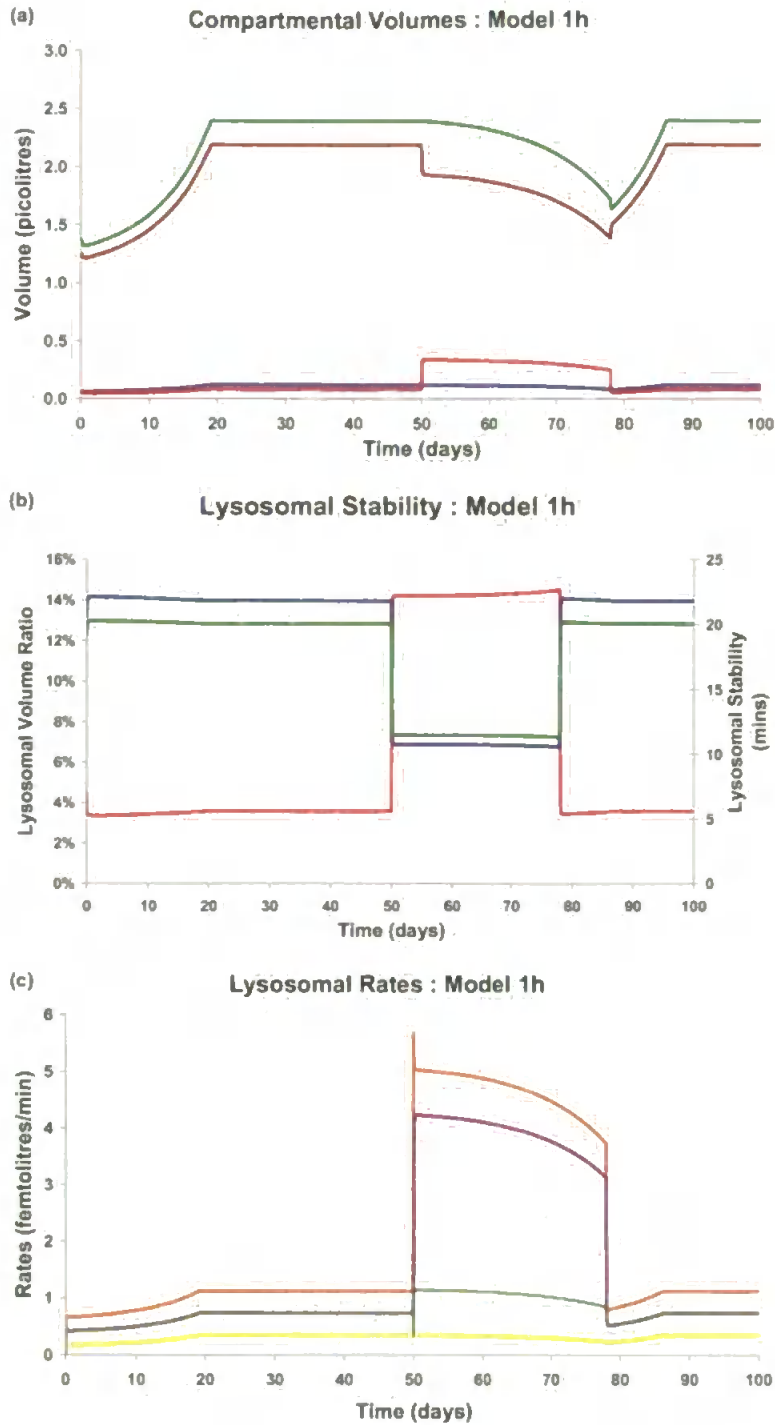


Fig 2.13 100 day simulation of model 1h, with fivefold increase in autophagic boost and  $f_d=0.787$  for days 50-78,  $S_c = 6.0$  throughout and ICs:  $f_{ev}=4.45\%$ ,  $f_{lv} = 4.45\%$ ,  $E_c=11.927$ ,  $L_c = 14.869$ ,  $Cell_v = 1.3764$  picolitres. (a) Compartmental volumes  $E_v$  —,  $L_v$  —,  $C_v$  —,  $Cell_v$  — (b) quadratic derived lysosomal stability —, exponential derived lysosomal stability —,  $f_{lv}$  — (c) lysosomal rates  $k_{lys}$  —,  $k_{aut}$  —,  $k_{deg}$  —,  $k_{exo}$  —.

There was an increase in degradation and exocytosis above the specified parameter limits (Fig 2.13c), due to the reduced maximum relative lysosome volume and their dependence on this parameter. Hence, it was considered that capping these rates at their prescribed maximum, so as to provide a constraint on the amount of digestive processing that the lysosome was capable of, might give a better simulacrum of the actual functioning of the cell.

With the cap on the lysosomal volume dependent rates (Fig 2.14c), a twofold increase in autophagic boost and a small increase in digestive efficiency over a 28 day period, the model showed an initial decline in cellular volume during the stress period (Fig 2.14a) as the cytosolic volume decreased faster than the lysosomal volume increased. Then, there was a recovery as the autophagy, which was cytosolic volume dependent, decreased to a level whereby the carbon content was more than matched by the capped degradation content, and eventually the cell even started exporting during the stressed period, albeit at a slightly lower rate than when in an unstressed condition. The quadratic lysosomal stability is shown to be incapable of dealing with high lysosomal relative volume values, while the exponential works as expected (Fig 2.14b). Once the stressed period was over, there was rapid recovery as the lysosomal volume decreased and the cell returned to the previous equilibrium state.

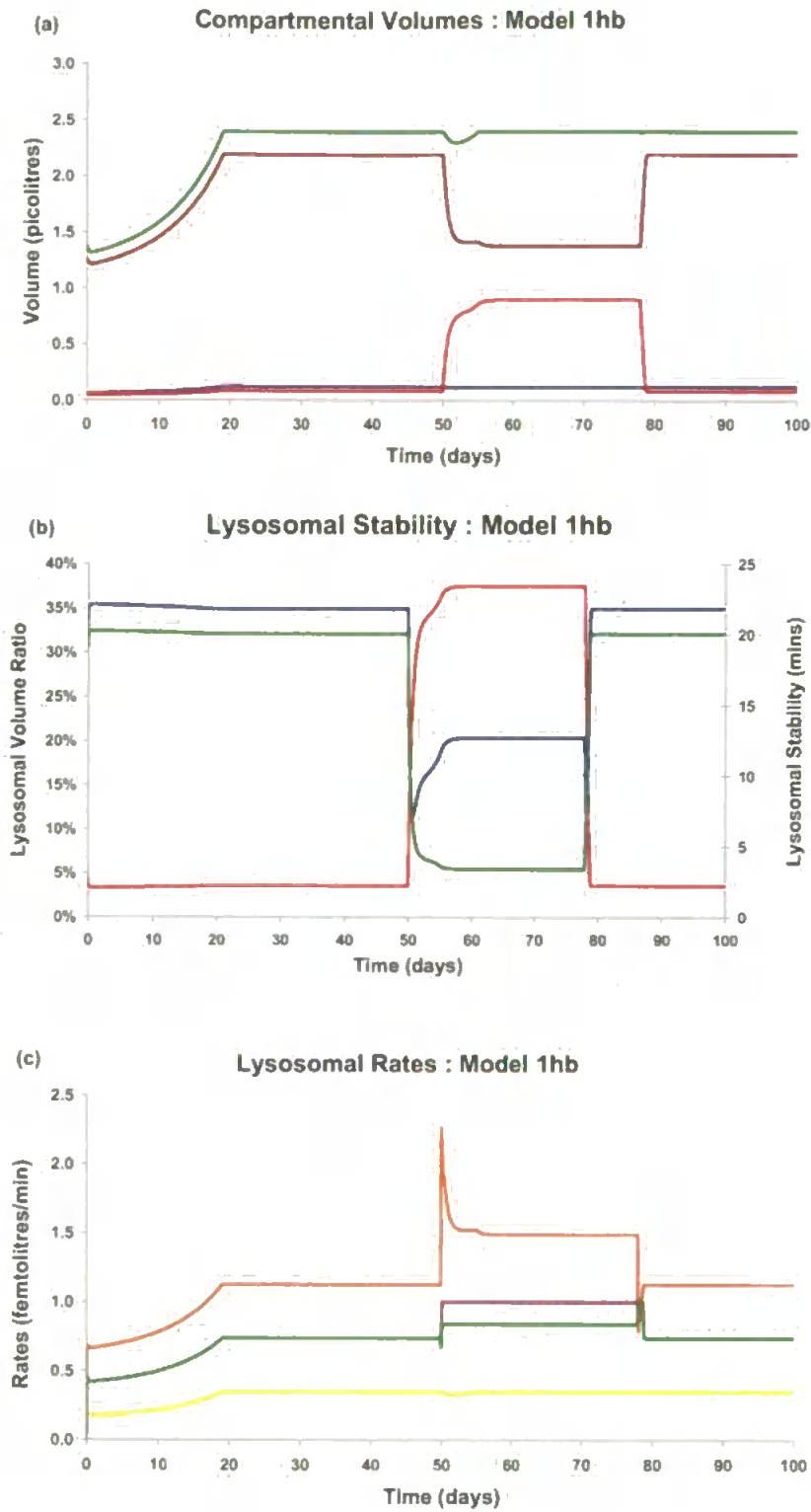
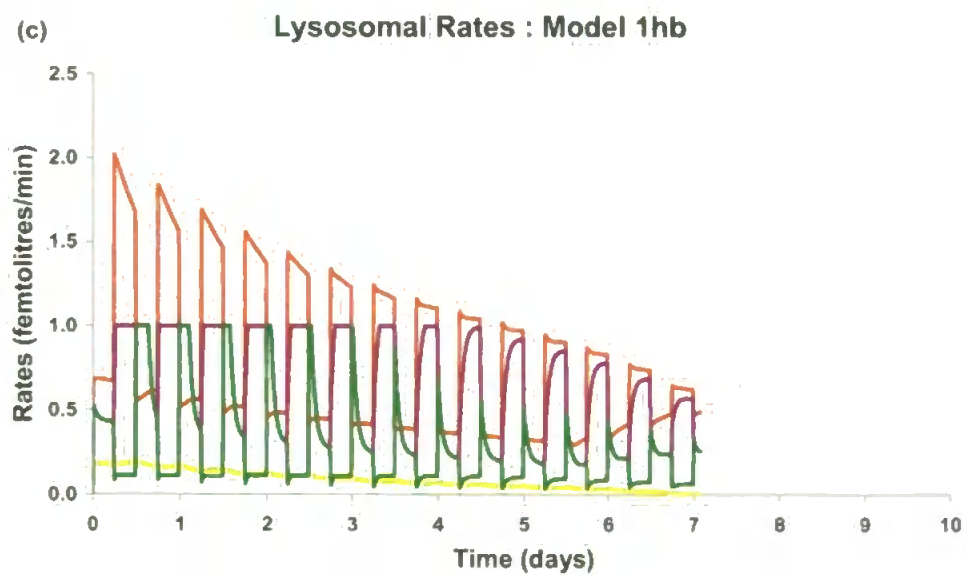
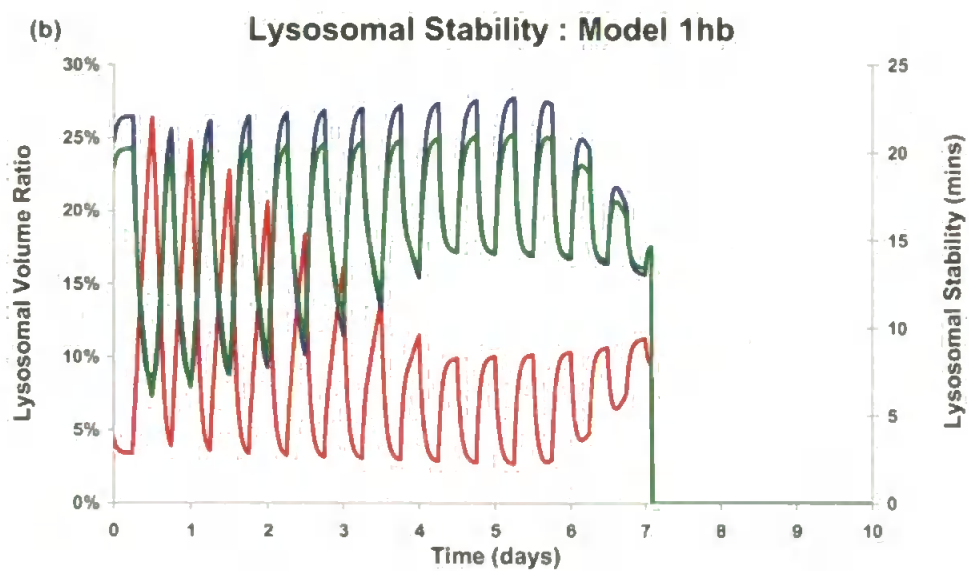
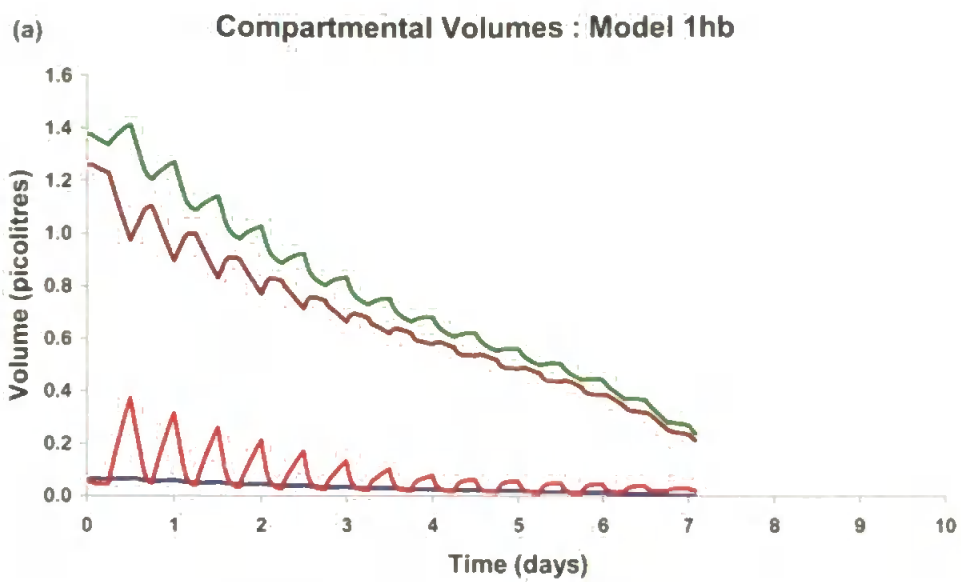


Fig 2.14 100 day capped rate Model 1hb simulation with, twofold increase in autophagy and  $f_d = 0.544$  for days 50-78,  $S_c = 6.0$  throughout and ICs as detailed for Fig 2.13. (a) Compartmental volumes  $E_v$  —,  $L_v$  —,  $C_v$  —,  $Cell_v$  — (b) quadratic derived lysosomal stability —, exponential derived lysosomal stability —,  $f_{lv}$  — (c) lysosomal rates  $k_{lys}$  —,  $k_{aut}$  —,  $k_{deg}$  —,  $k_{exo}$  —.

The observance of the limits imposed on the degradation and exocytosis rates was welcomed. Additionally, the export of material during a stressed period might be feasible as the rest of the animal would still require nutrients during this stage. The exponential formula for the correlation between lysosomal stability and relative volume made more sense than the quadratic function and was adopted hereafter.

With this system, an attempt was made to simulate a hepatopancreatic digestive cell from an animal that was in the inter-tidal range and thus subject to a changing pattern of food availability. Due to their relatively immobile lifestyle, mussels, which are in the littoral zone, do not have food continuously available to them. Instead, they will be subjected to a rhythmic pattern of food availability, dependent on the tidal cycle and their position within the inter-tidal region. To simulate this oscillation the previous model system was next driven by a food concentration modelled as a square wave function, with a 12 hour period and spending half the time submerged and having a high digestive efficiency  $f_d = 0.9$  during periods of exposure.



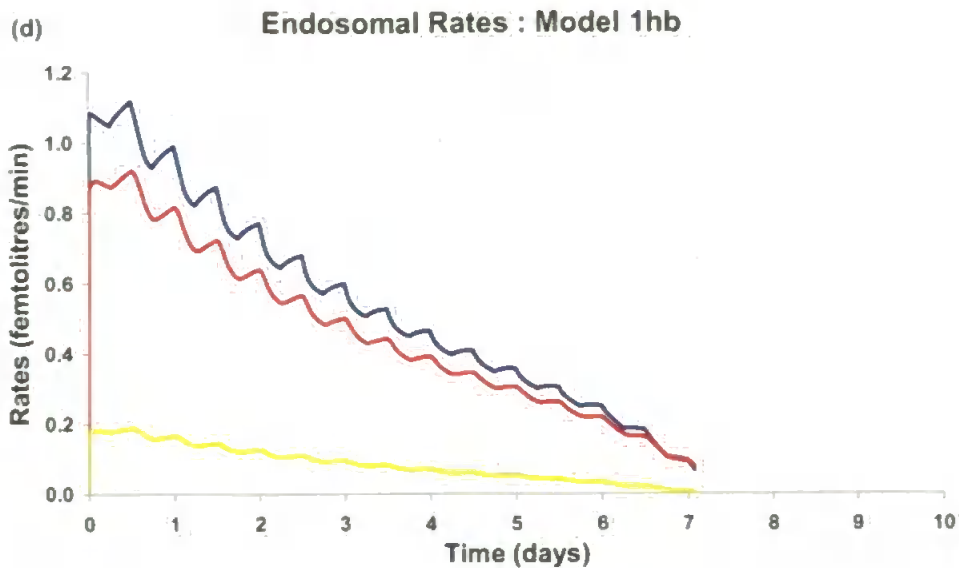


Fig 2.15 10 day capped rate Model 1hb tidal simulation. 6 hours food available, when  $S_c = 6.0$  &  $f_d = 0.5$ , followed by 6 hours no food available when  $S_c = 0.0$  &  $f_d = 0.9$ , and ICs as detailed for Fig 2.13. (a) Compartmental volumes  $E_v$  —,  $L_v$  —,  $C_v$  —,  $Cell_v$  — (b) quadratic — and exponential lysosomal stability —,  $f_{lv}$  — (c) lysosomal rates  $k_{lys}$  —,  $k_{aut}$  —,  $k_{deg}$  —,  $k_{exo}$  — (d) endosomal rates  $k_{end}$  —,  $k_{rec}$  —,  $k_{lys}$  —.

The square wave pattern feeding led to expiry in 7 days; despite feeding at the highest possible food concentration for half the wave period and the increase to the highest possible lysosomal processing efficiency in the other half of the wave period (Fig 2.15a). The lysosomal stability (Fig 2.15b) remained relatively healthy as the autophagy was boosted threefold only during the submerged period (Fig 2.15c). The reason for the decline was the continuation of the endocytotic rate during the exposed period, which added volume at zero food concentration. This was obviously an inadequate simulation of the real situation. Hence, the next system made endocytosis dependent on surface carbon concentration (above threshold) and not cell volume. Under this system the cell fed at the maximum rate

whenever the food was above the maintenance concentration, and decrease in a linear fashion when below this level. When tidally exposed the concentration will be zero and so too, will be the endocytotic rate. This new rate was formulated as:

$$k_{end}(t) = \begin{cases} k_{end\ max} & \text{if } S_c \geq S_{cmain}/k_{end\ max} \\ k_{end\ min} + (k_{end\ max} - k_{end\ min}) \frac{S_c(t)}{S_{cmain}} & \text{if } S_c < S_{cmain}/k_{end\ max} \end{cases} \quad [2.3]$$

With this constraint on endocytosis (Fig 2.16c), the cell became viable once more but never increased in volume nor carbon content (Figs 2.16a & b), as the period of feeding was too short, and eventually settled into an equilibrium pattern around day 44. As the endocytosis decreased, the endosome quickly reduced and in doing so reduced the recycling and lysosomal traffic rates. The lysosomal pattern (Fig 2.16d) started to become dominated by the square wave because of the increase in autophagic input and the loss of material arriving from the endosome.



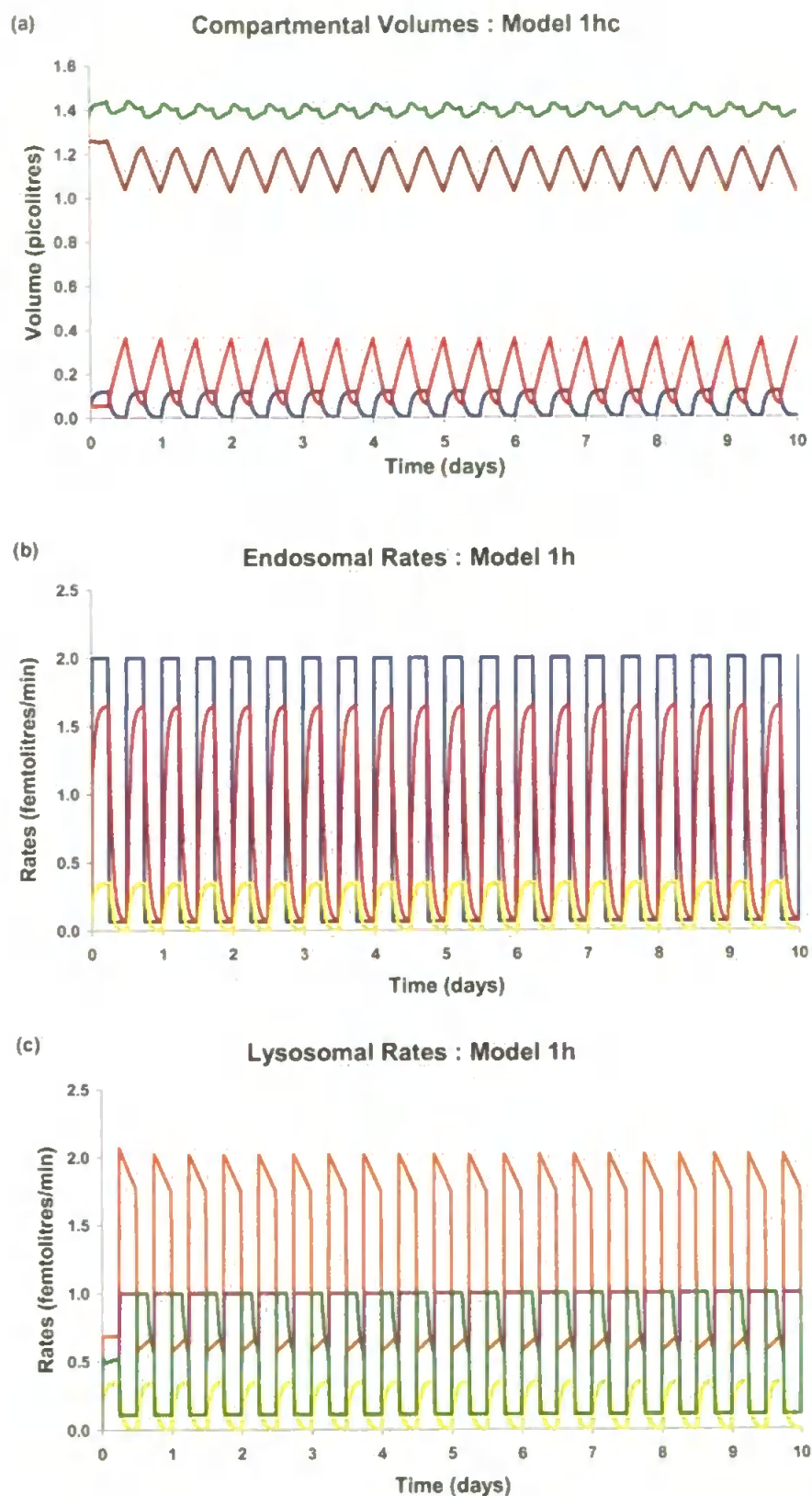


Fig 2.16 10 day simulation of capped rate/endocytosis switching Model 1hc with same feeding regime & ICs as Fig 2.15, (a) Compartmental volumes  $E_v$  —,  $L_v$  —,  $C_v$  —,  $Cell_v$  — (b) endosomal rates  $k_{end}$  —,  $k_{rec}$  —,  $k_{lys}$  — (c) lysosomal rates  $k_{lys}$  —,  $k_{aut}$  —,  $k_{deg}$  —,  $k_{exo}$  —.

## *2.11 Discussion*

The evolution of the model system started with the realisation of the inadequacy of using constant values for the various rates between compartments. Once constant median values for the rates were discounted the simplest functions were chosen to replace them. Under this auspice the assumption was that they are all linearly dependent upon the respective source compartment volume. The notable exceptions to this rule were export and endocytosis.

Endocytosis was clearly one of the primary drivers of cellular behaviour in these cells. As a physical process the rate will be dependent upon the apical surface area and the frequency and distribution of the food available. If the apical cell surface remained proportional to cell volume then making the endocytotic rate dependent upon this variable imposed a spatial and resource restraint. However, constricting endocytosis in this manner restricted the growth of the cell and the ability of the food to be passed to the rest of the animal. If one of the cell's functions was to act as a storage site for energy for the rest of the animal, then the maximum uptake and degradative capacity of the cell would have occurred earlier than upon reaching maximal volume. Furthermore, the shape of the cell and the surface area as cell volume increased did not appear to be linearly correlated. Ingested food particles appeared to be subject to selection according to size and/or nutritional content, but whether or not the uptake of material by these cells, once it has been subjected to an initial crude

degradation in transit through the stomach, was selective is unclear (Owen, 1970).

Continual export was seen to be slowing cell growth when feeding and increasing the likelihood of death when no food was made available. Whilst the cell was obliged to pass on food to the rest of the animal, no data was available which indicated how, under nutritional deprivation, the animal atrophies. It was unclear whether or not all organs shrink at a similar rate simultaneously, or whether particular parts of the animal were partially cosseted under these conditions (Bayne *et al.*, 1978; Lowe, 1988). One possible strategy for the animal would have been to allow the digestive cell to grow to its maximum volume, if this corresponds to its maximum food processing capability, before allowing any export of material. The problem with this model was that if it were a representative cell then the entire organ would be presented with the same food, be in the same state and the entire organ would no longer be performing its primary function. Possibly there is some schedule, whereby some of the constituent cells of any organ are "sacrificed" (programmed cell death – PCD) to provide energy and precursor molecules to guarantee the survival of the remaining cells (Lockshin & Zakeri, 2004; Pipe & Moore, 1985). However, until data to the contrary is provided, or else, until the model is extended to include the dynamics of arrays of cells, tissues and/or organs then the export rate was calculated as only occurring once maximum cell volume was attained.

Similarly, at this early stage of model development the simple cell-volume-dependent endocytotic rate formulation was retained (but see Chapter 6).

The control condition, retaining a constant carbon concentration in the cytosolic compartment in a system (where all flows out of the compartment took material at the average compartmental concentration and the flow in was at the varying lysosomal concentration), enforced the addition of a hypothetical flow of non-carbon solvent. The conceived system was a simplification of an actual cell that regulates a number of physiological and chemical variables (e.g. osmotic pressure and ionic balance) in the fluctuating environment in which they are resident.

Conceivably, the regulation of these other variables might involve diffusion into and out of the cell, which could alter this rate if a compromise had to be found between more than one control condition. However, the osmotic balance is maintained by regulating the size of the free amino acid pool within the cytoplasm (Bayne *et al.*, 1978; Moore *et al.*, 1980). Similarly ion exchange is partially maintained through specific controlled channels, which do not incur bulk fluid transfer. Hence, this introduced rate is to be only partially associated with any real regulatory diffusion rate.

The models presented have been parameterised for one set of constant environmental conditions. This approach necessarily diminished the applicability of the model to “real-life” situations. It was obviously desirable to understand how the digestive cell worked under all environmental conditions. In particular, changes in salinity are shown to

affect cell volume and constitution as well as physiological rates such as diffusion and respiration. Epithelial cells such as those under consideration are directly exposed to the aqueous environment, thus changes in external salinity create an osmotic pressure that must be countered (Pierce, 1971). As an osmocomformer, the mussel increases the amount of free amino acids in response to increased salinity (Bishop, 1976).

However, to be able to construct such a model would require the necessary conceptual framework (detailing how the relevant rates and limits change with the varying environmental conditions) and the necessary data to parameterise such a model. The constraint of available data hinted at the redundancy of this approach; moreover, it was deemed inappropriate to increase the complexity of the model in this respect when the primary focus of the study, modelling the lysosome in response to food and toxic exposure, had not been successfully achieved for a non-varying environment. Nevertheless, the model was constructed in a manner to allow the future incorporation of differing environmental conditions by reparameterisation of the rate limits as functions of salinity or temperature. It is hoped that further work and data acquisition would lead to a model which would have as input, varying food, contaminant exposure and environmental conditions.

Central to the model was the observed response to certain contaminant exposures of an increase in the autophagic rate, possibly as a consequence of increased damage to cellular constituents (Cuervo, 2004;

Moore *et al.*, 2007). Additionally, there was evidence to suggest that the autophagic rate was increased when the available nutritional resource fell below some maintenance threshold. Originally, the model used a threshold food concentration to determine whether or not the autophagy needed augmenting. This had been determined under the assumption that the endocytotic rate was constant. With the varying endocytotic rate this had to be revised to derive a value of carbon entering the cell which could sustain the cell. The model did not, however, provide an inherent reason for the nutritionally induced autophagic enhancement; as it only served to accelerate the demise of the cell when starved.

A further conceptual problem to overcome for the inclusion of this imposition was when food was not made continually available to the cell. Presumably this was the case for an intertidal mussel, unless food continues to pass from the stomach to the digestive gland cells during the period of exposure. Alternatively it could be that once the animal was subject to a lack of food, it could enter a more efficient but slower extraction of available food from the last endocytotically ingested material. Under such circumstances, it could be that the cell required a time averaged threshold condition, whereby the food taken up when the animal was submerged was compared to the cost of survival over an entire tidal cycle. If this was calculated to be deficient then the augmented autophagic sequestration would be invoked.

The simulated recovery from temporary nutritional deprivation also warranted scrutiny. The rate of the recovery of cell volume was in the order of days, dependent upon length of stress. In contrast, the rate of recovery of lysosomal stability was in the order of minutes. This was due to the instantaneous calculation of rates dependent upon compartmental volumes. When the stress condition was revoked the autophagy immediately dropped, whilst the exocytosis and degradation rates continued at maximum level until the lysosomal volume fell below a threshold level.. Thus, the lysosomal volume rapidly declined whilst cellular volume increase was dependent upon endocytosis. As it stood, there was no persistent penalty for previous stress.

Three types of behaviour were distinguishable dependent upon the food concentration and food efficiency: death, with the cell volume declining to below the minimum level allowable; export, with the cell attaining its maximum volume and with enough incoming material to send to the rest of the animal; and equilibrium, the cell reaching a volume level below maximum where incoming and exiting material are in balance. The proportion of the parameter space which was taken up by the equilibrium state was exceptionally small. If the model was taken at face value as an approximation to a single cell then this was not too unsurprising, as the cell should be exporting otherwise it would be redundant and should be deleted by PCD (Lockshin & Zakeri, 2004; Pipe & Moore, 1985). However, if the cell were taken as a proxy for the entire digestive gland then this presented

a serious problem, as there would be times of the year when the rest of the animal would have to survive on reserves built up during the summer months. During these periods the digestive organ would have to utilise its own reserves and slowly cannibalise redundant components (Thompson *et al.*, 1974).

Protein turnover has been shown to be more efficient during times of nutritional stress (Hawkins & Day, 1996). During times of complete starvation the lysosome was only presented with endogenous material. The lysosome has degradative enzymes specifically tailored for the breakdown of proteins (Klionsky & Emr, 2000). Possibly this will lead to less waste than with exogenously sourced material (heterophagy), which will not all be effectively degraded.

Finally, analytical solutions for the variable rate models were not found; hence, numerical methods were used. Initially an Eulerian method was used, then a predictor-corrector method and finally a Runge-Kutta method. However, tests upon the differences in solution showed minimal difference between the higher order methods and the Eulerian method for small timesteps. Hence, the Eulerian method was employed throughout this study.



## Chapter 3 Storage Models

### 3.1 Introduction

The work in this chapter looked at the effect of including storage facilities for cellular carbon on the survivability of the model cell under nutritional stress. To this effect two hypotheses were proposed.

*Hypothesis 2.1:* The introduction of a glycogen store would provide a stockpile which could be utilised under nutritional stress to increase the survival time of the cell

*Hypothesis 2.2:* The division of carbon forms into lipid and non lipid species would provide another means of storage as well as enhancing the verisimilitude of the model cell to a real cell, due to the decreased efficiency of lysosomal catabolism of lipids.

To test hypothesis 2.1 a cellular glycogen store, which provided the cell with a stockpile for potential cellular energy, was first appended to the previous model. The challenge was to design and implement a decision support system which would allow the storage and release of material dependent upon the current cellular condition. The quantification of the effect of the introduction of this store upon cell survival time was conducted to test hypothesis 2.1.

The second variation to the previous model was the splitting of the carbon pathways into two, one purely for the movement of lipid in the cell, and another to account for the remainder. New methodologies for

movement of material, degradative processes and possible transfer between non-lipid and lipid carbon compartments were necessarily introduced. The control condition for the model of a single carbon concentration in the cytosol was also reviewed. The effect on the model behaviour of splitting the carbon was assessed by trying to replicate the seasonal distribution of lipid in the mussel digestive gland. A study of the effect of lysosomal lipid digestive efficiency and food lipid quantity on the relative rates of exocytosis and export was conducted to provide an assessment of the stability of this submodel.

Both were originally introduced as separate amendments to the previous model, in order to assess their individual impacts. They were then combined to produce the complete carbon model and analysed to see if there were either any antagonistic or beneficial effects. Table 3.1 gives a summary of the numerical experiments performed.

ID	Model	Food carbon concentration	Lipid % of food carbon	Lysosomal lipid efficiency	Brief description of experimental goals
1	2a	6.0 Days 0-10,15-20 0.0 Days 10-15	N/A	N/A	Show glycogen store filling and thereafter being utilised
2	2a	As experiment 1	N/A	N/A	Autophagy boost switched off when glycogen present
3	2a	As experiment 1	N/A	N/A	Glycogen concentration increased tenfold
4	2a	6.0 - 17.1875 day period 0.0 - 17.1875 day period	13%	0.1	Square wave food availability to determine when glycogen store is useful for cell survival
5	2b	6.0 Days 0-10	13%	0.1	Show lipid content and volumes inevitable decline
6	2b	6.0 Days 0-100	13%	0.1	Lipid volume and carbon loss breakdown by pathway
7	2b2	6.0 Days 0-243 0.0 Days 243-365	13%	0.1	Seasonal effect on relative cellular lipid content
8	2b2	As experiment 7	0 - 25%	0.1	Effect of lipid food on total carbon export
9	2b2	As experiment 7	0 - 25%	0 - 1	Effect of lipid food & lysosomal efficiency on C export
10	2b2	6.0 Days 0-365	12.5%	0.1	Lipid & total carbon loss by different pathway breakdown
11	2b3	As experiment 10	13%	0.1	As experiment 10 but with new recycling rate distribution
12	2b3	As experiment 10	0 - 25%	0 - 1	Effect of food lipid and lysosomal efficiency on total carbon loss through exocytosis and export
13	2b3	6.0 Days 0-35 3.0 Days 35-50	13%	0.1	Effect of nutrient decline on longevity of lipid model; cell
14	2c	6.0 Days 0-50 3.0 Days 50-100	13%	0.1	Effect of nutrient decline on longevity of combined glycogen and lipid cell model
15	2c2	As experiment 14	13%	0.1	New lipid-glycogen control model effect on longevity and breakdown of carbon 'fate'
16	2c2	6.0 for 6 hour period 0.0 for 6 hour period	13%	0.1	Effect of tidal simulation on lipid-glycogen control model

*Table 3.1 numerical experiments and relevant parameters presented for lipid and glycogen models.*

### 3.2 Glycogen store: Model 2a

The cell utilises the compact form of glycogen to store carbohydrates as a form of potential cellular energy. In the model it was assumed that the formation and release of glycogen was reasonably inexpensive in energetic terms and no regard was given to this cost. This store could then be utilised at times of low food availability or during otherwise energetically demanding periods. For the purpose of the model, these storage molecules have been aggregated together to form a single sub-compartment within the cytosol. In addition, as there was only one type of macromolecule within this notional compartment it was assumed that there is a constant compartmental carbon concentration. The revised schematic is presented below (Fig 3.1).

## COMPUTATIONAL SIMULATION MODEL FOR POLLUTANT UPTAKE AND PATHOLOGY

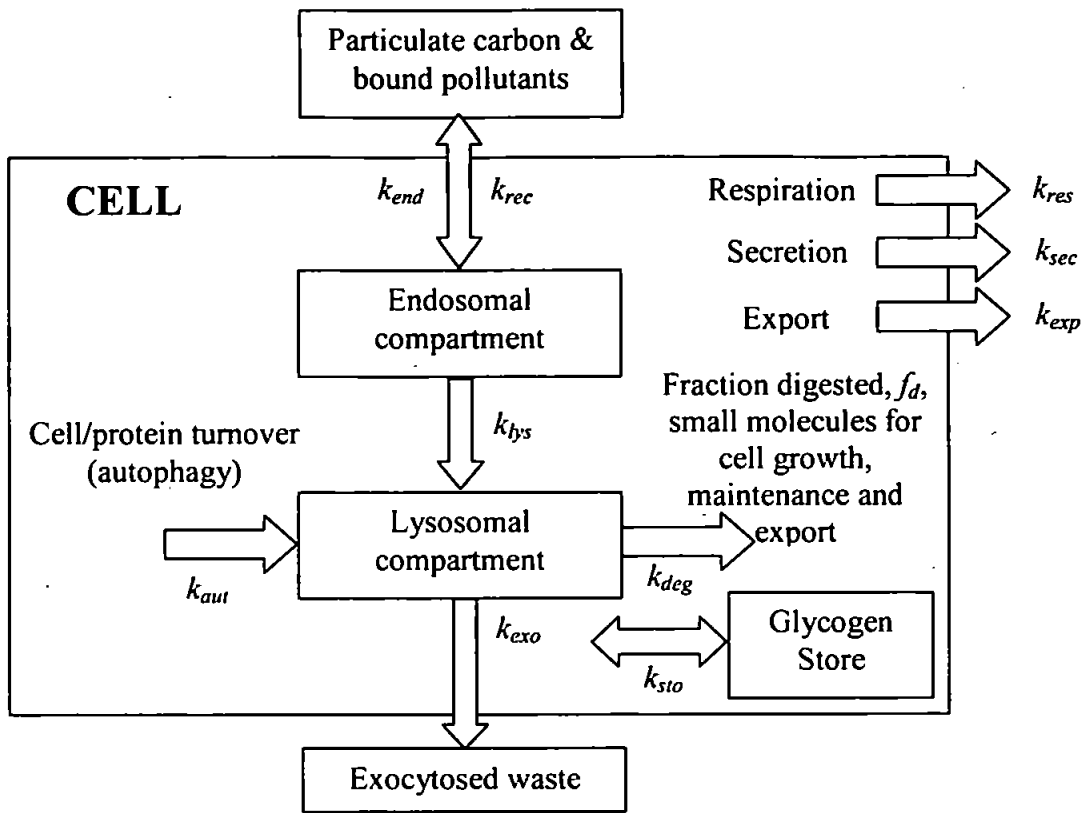


*Fig 3.1 Schematic for model 2a with introduction of glycogen store*

A new two-way pathway was introduced,  $k_{sto}$ , that accounted for either storage when the cell had excess carbon (positive rate) or else for release from the store when the cell so required (negative rate). It was therefore necessary to introduce thresholds when this storage/release was to take place. The following conditions were used in the preliminary model:

- i) When the cell reaches its maximum volume excess carbon was stored in the glycogen store up to a maximum of 20% of the cellular carbon. Once this threshold had been reached excess carbon was exported.
- ii) If the cell volume should fall below maximum level and there was carbon in the glycogen store, then enough of the carbon content was to be released in order to realise this limit. In the case when there was not enough

carbon within the store to realise the cellular maximum volume limit, then all available carbon was to be released.

The reason why this release and storage affected the cellular volume was that it was assumed that there was a higher carbon concentration in this sub-compartment than in the remainder of the cytosol. The effect was then accomplished by the diffusion rate constant either in the case of storage losing cytosolic volume or else in the case of release enhancing cytosol volume. For the store to have an effect the non-glycogen part of the cytosol must have a constant carbon concentration as the control condition for the model. Setting the relevant revised equation to zero allows the diffusion rate to be calculated as shown in Eqn. 3.1.

$$k_{dif} = k_{deg} \left( \frac{L_c}{C_c} - 1 \right) + k_{sto} \left( 1 - \frac{G_c}{C_c} \right) \quad [3.1]$$

It was assumed that the storage capacity of glycogen was up to 20% of cellular carbon. From this premise the storage and release algorithms were formulated as detailed below. The storage algorithm was invoked after a time-step calculation when the newly calculated cell volume exceeded the maximum (Eqn. 3.2 for  $\delta V > 0$ ).

$$Cell_v(t_1) = Cell_{vmax} + \delta V \quad [3.2]$$

For notation a superscripted asterisk is used to indicate the values of variables to be calculated and the extra amount to be added to previously used rates. Then the goal for the storage algorithm was given by Eqn. 3.3.

$$Cell_v(t_1)^* = Cell_{vmax} \quad [3.3]$$

Once the check condition had been flagged the two step storage algorithm was:

Step (1) Calculate rate of glycogen storage and extra diffusion to restore cell volume to maximum

Step (2) Check if glycogen content was greater than 20% of cellular carbon, if so then export excess

Step (1) from [3.1, 3.2 & 3.3] the revised diffusion and storage rates were

$$k_{dif}^* = -\frac{\delta V}{(t_1 - t_0)} \quad \text{and} \quad k_{sto}^* = \frac{C_c}{C_c - G_c} k_{dif}^* = \frac{C_c \delta V}{(G_c - C_c)(t_1 - t_0)} \quad [3.4]$$

Step (2) once the carbon contents are revised then the value of  $\delta X$  in [3.5] is determined

$$5G_{xc}^* = Cell_{xc}^* + \delta X \quad [3.5]$$

When  $\delta X > 0$  then the storage and export rates were revised, as detailed below, so that storage was slightly reduced and export was invoked to take material away.

$$k_{sto}^{**} = \frac{C_c \delta X}{C_c - 4G_c} \quad \text{and} \quad k_{exp}^{**} = \frac{\delta X (C_c - G_c)}{C_c - 4G_c} = k_{dif}^{**} \quad [3.6]$$

Obviously for the storage facility to be of any utility to the cell it needed to be able to release the stored material when required. The release algorithm was invoked when the cell volume became less than the maximum parameter value at the end of a timestep and there was any glycogen stored. Hence, the two flags for this algorithm were:

$$Cell_v(t_1) = Cell_{v_{max}} - \delta V \quad \text{and} \quad G_v > 0 \quad [3.7]$$

Then the following required minimum rate of glycogen release to ensure that the cell volume returned to the maximum if possible would be calculated.

$$k_{sio}^* = \begin{cases} -\frac{G_v(t_1)}{(t_1 - t_0)} & \text{if } G_v < \frac{\delta V C_c}{G_c - C_c} \\ \frac{\delta V C_c}{(t_1 - t_0)(C_c - G_c)} & \text{otherwise} \end{cases} \quad [3.8]$$

And the coincident revised rate of diffusion became.

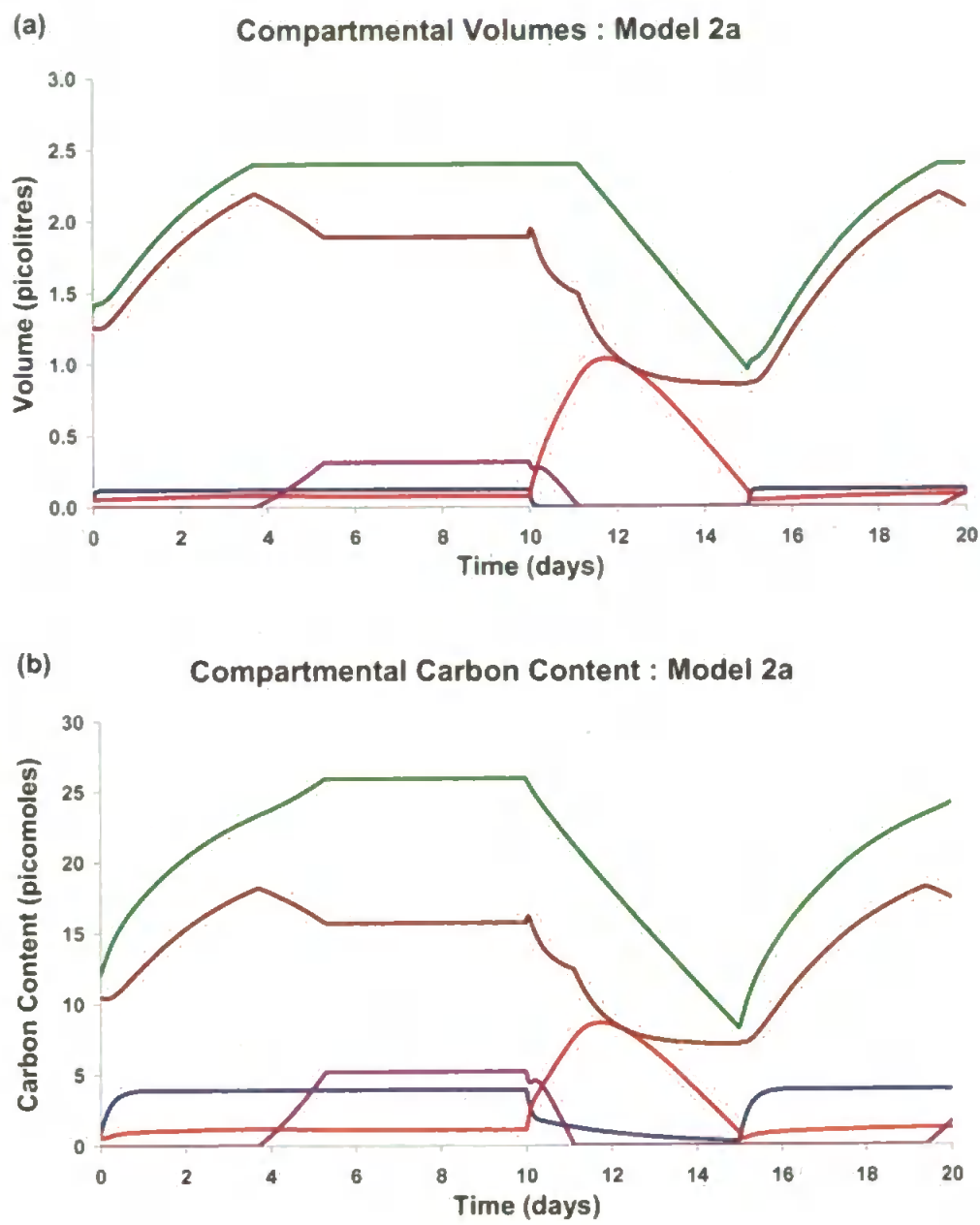
$$k_{dif}^* = \begin{cases} -\frac{G_v(t_1)(C_c - G_c)}{(t_1 - t_0)C_c} & \text{if } G_v < \frac{\delta V C_c}{G_c - C_c} \\ \frac{\delta V}{(t_1 - t_0)} & \text{otherwise} \end{cases} \quad [3.9]$$

In order to see these effects a simulation was run whereby for 10 days a cell was fed at maximum in order to produce a healthy, glycogen-filled cell. It was subsequently deprived of food for 5 days and, finally, feeding was allowed to recommence for 5 days to check recovery.

This system showed exactly the same behaviour as the previous model up until the cell reached maximum volume for the first time (Fig 3.2a). Thereafter the glycogen store started to fill up, taking volume away from the non-glycogen portion of the cytosol. The composite cytosol exhibited an overall behavioural pattern similar to the previous model (see Chapter 2), with the only difference in the non-glycogen compartment volume being a decline, once the steady state had been achieved, to a lower level as cytosolic volume was shifted to the glycogen store. But with the expected increase in overall cellular carbon content (Fig 3.2b). The cell



attained maximum volume around day 3.5 and the glycogen storage algorithm was invoked for the first time (Fig 3.2a). After 5.25 days the storage effectively stopped (Fig 3.2c) as the glycogen content was now 20% of the cellular content and excess material was thereafter exported out of the cell.



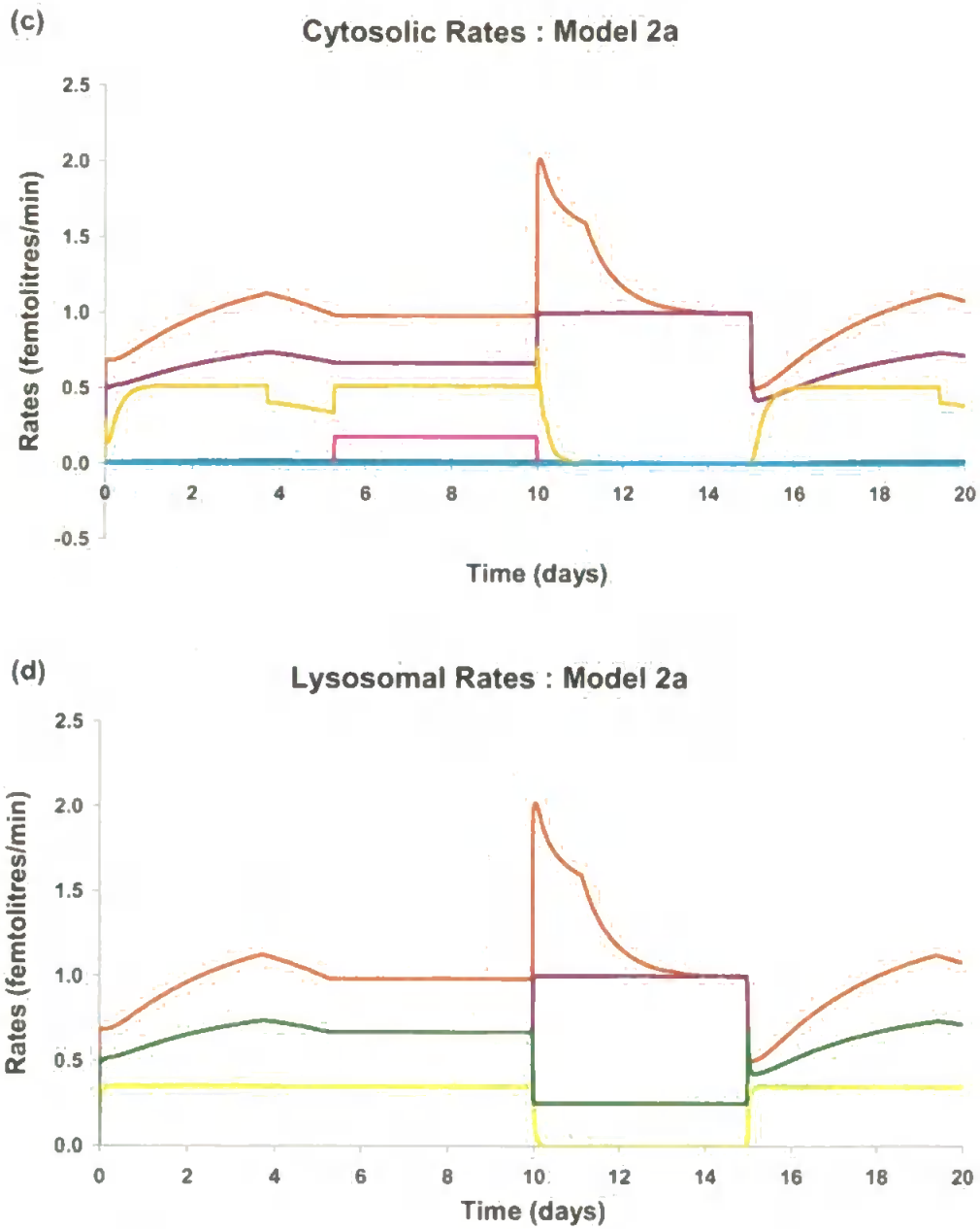


Fig 3.2 20 day simulation of Model 2a. Feeding regime: Days 1-10 & 15-

20,  $S_c = 6.0$ ; Days 10-15,  $S_c = 0.0$ ;  $f_d \equiv 0.5$ . ICs:  $f_{ev} = 4.45\%$ ,  $f_{lv} = 4.45\%$ ,

$E_c = 11.927$ ,  $L_c = 14.869$ ,  $Cell_v = 1.3764$  picolitres,  $G_c = 2 \times C_c = 16.6$  (a)

compartmental volumes  $E_v$  —,  $L_v$  —,  $C_v$  —,  $G_v$  —,  $Cell_v$  — (b)

compartmental carbon contents  $E_{xc}$  —,  $L_{xc}$  —,  $C_{xc}$  —,  $G_{xc}$  —,  $Cell_{xc}$  — (c)

cytosolic rates  $k_{aut}$  —,  $k_{deg}$  —,  $k_{res}$  —,  $k_{sec}$  —,  $k_{exp}$  —,  $k_{dif}$  —,  $k_{sto}$  — (d) lysosomal

rates  $k_{lys}$  —,  $k_{aut}$  —,  $k_{deg}$  —,  $k_{exo}$  —.

Glycogen release commenced after day 10 (see negative storage rate in Figure 3.2c) and continued for approximately 1.12 days leaving the cell at its maximum volume for this extra period (Fig 3.2a). During this period there was transfer of material from cytosol to lysosome (Fig 3.2b) as autophagy was boosted due to lack of food (Fig 3.3d). Since the cell was utilising available reserves, then there was no need within this model for autophagy to be boosted which was previously conditional on food concentration but does not account for cellular reserves. Hence, the model was revised so that the trigger for autophagic boost was changed so as to only be tested when glycogen had been completely utilised.

For this scenario, there was very little change in the overall picture, despite autophagy boost being delayed for 1.12 days. Cytosolic volume was increased during the release period in comparison with the immediate decrease evidenced in the previous simulation (Figs 3.2a & 3.3a). But once the store had been exhausted the increased cytosolic volume led to a greater boosted autophagy rate (Figs 3.2c & 3.3b) which accelerated the relative decline in cell volume to such an extent that by the end of the starvation period both simulations were almost identical.

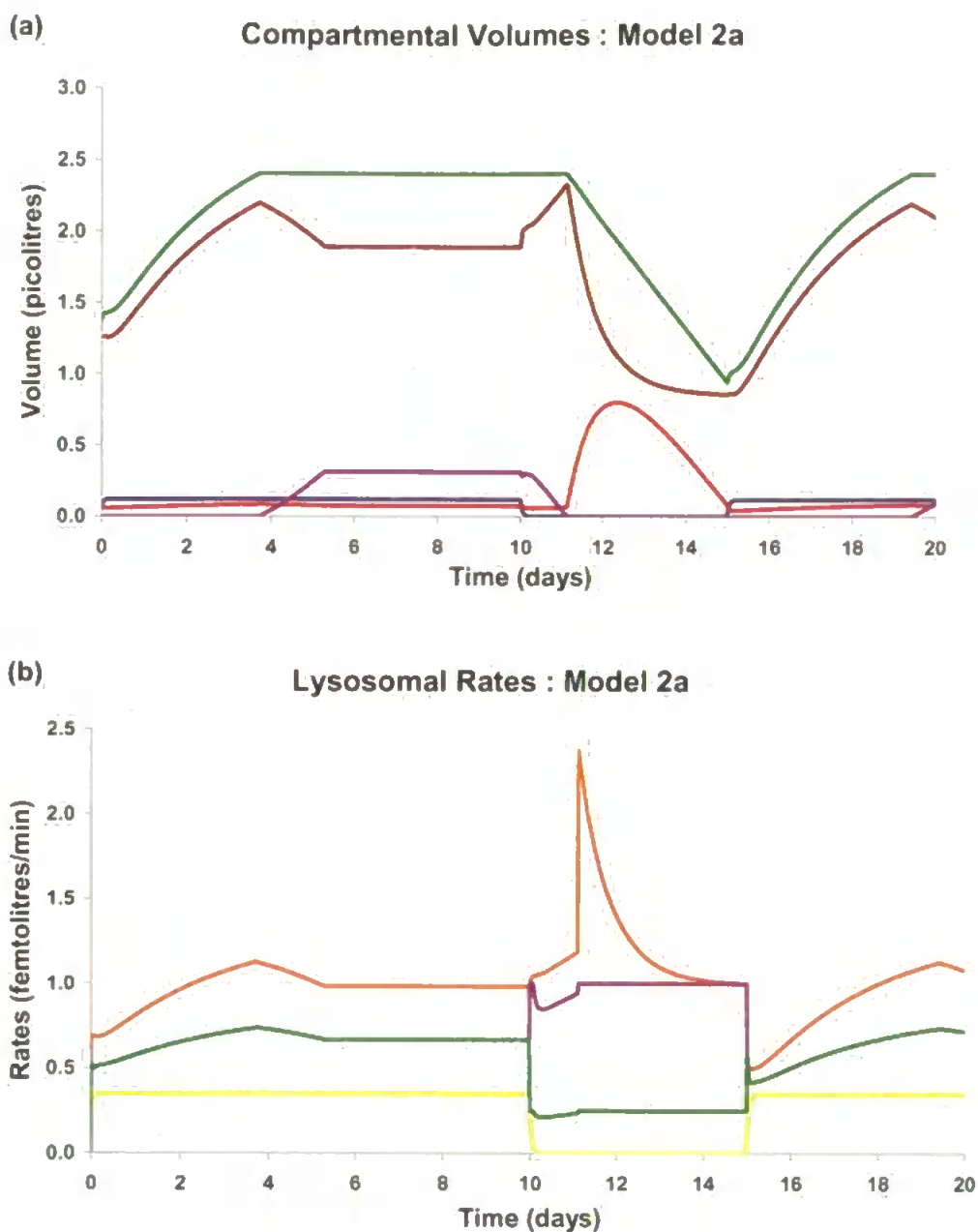


Fig 3.3 Model 2a as detailed for Fig 3.2 but with autophagy boost turned off when glycogen available (a) compartmental volumes  $E_v$  —,  $L_v$  —,  $C_v$  —,  $G_v$  —,  $Cell_v$  — (b) lysosomal rates  $k_{lys}$  —,  $k_{aut}$  —,  $k_{deg}$  —,  $k_{exo}$  —.

To this point the glycogen concentration had been set at twice that of the cytosolic carbon concentration. It was deemed necessary to determine if there was any significant effect of increasing this factor.

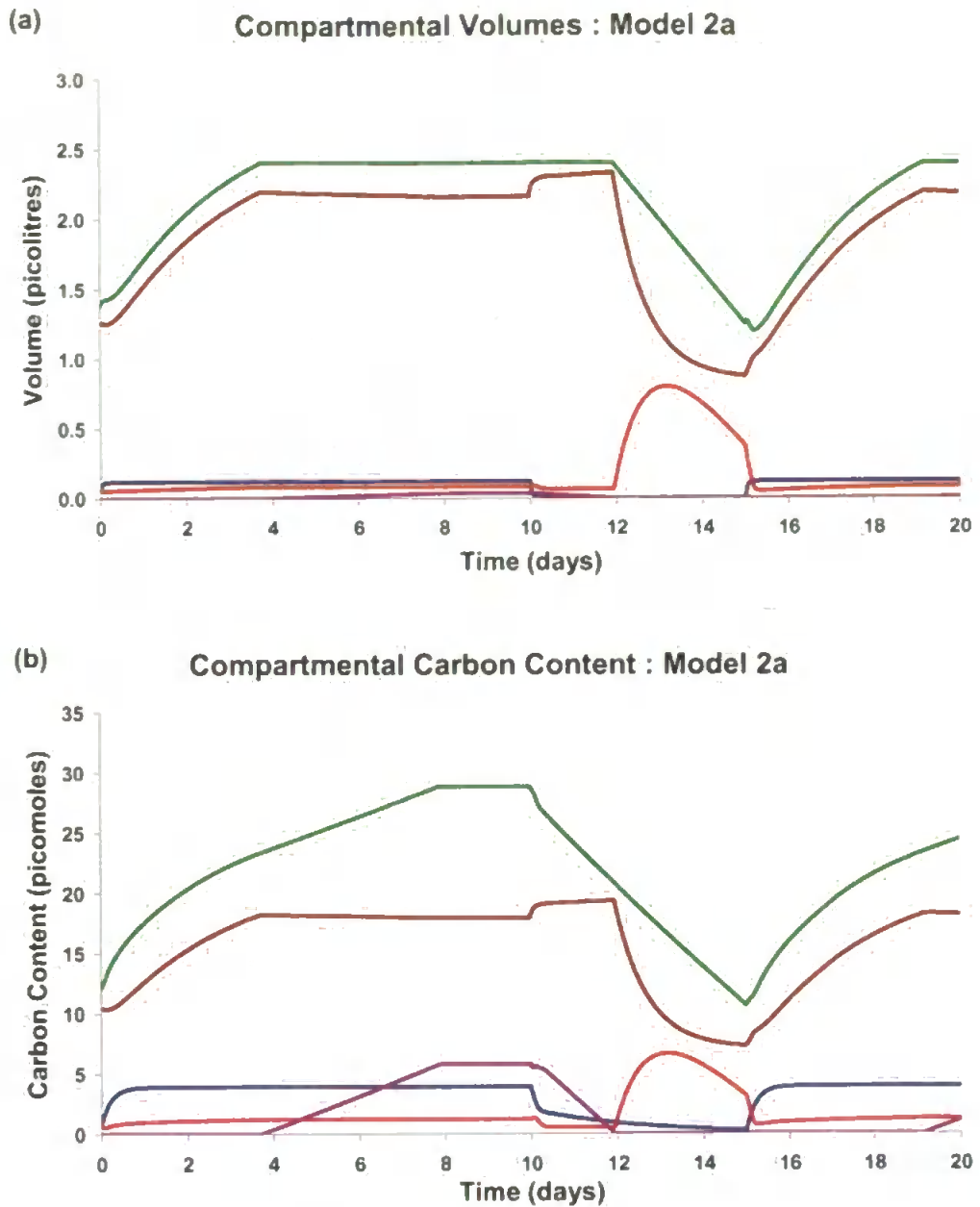
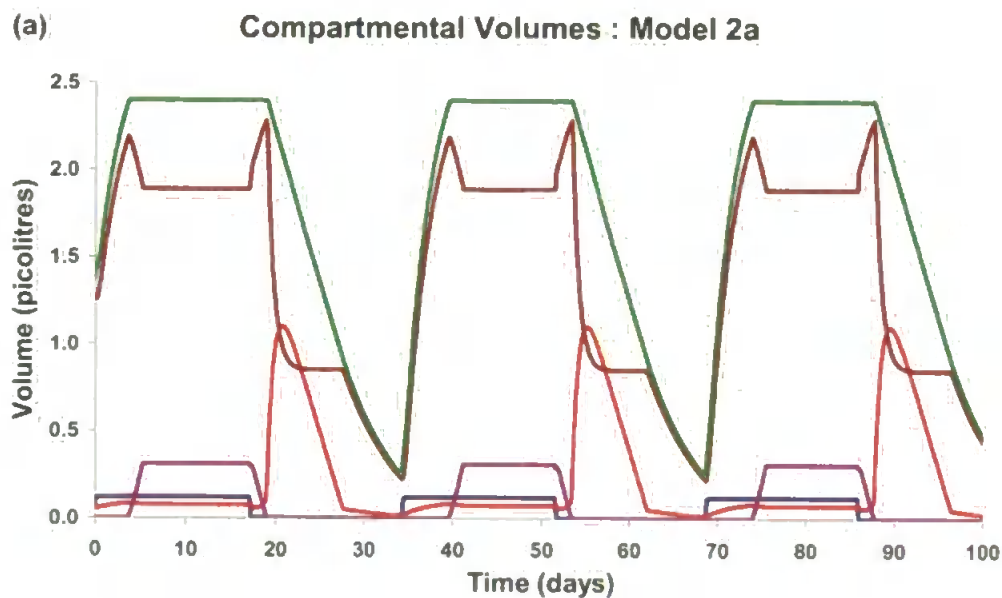


Fig 3.4 Model 2a as detailed for Fig 3.2 but with glycogen concentration increased tenfold,  $G_c = 20 \times C_c = 166 \text{ moles/litre}$ . (a) Compartmental volumes  $E_v$  —,  $L_v$  —,  $C_v$  —,  $G_v$  —,  $Cell_v$  — (b) compartmental carbon contents  $E_{xc}$  —,  $L_{xc}$  —,  $C_{xc}$  —,  $G_{xc}$  —,  $Cell_{xc}$  —.

If the glycogen concentration was increased tenfold then the amount of carbon which can be stored would be slightly increased, as the cytosol volume could be slightly greater and, hence the maximum glycogen carbon

set at 20% of cellular carbon was greater (Figs 3.2b & 3.4b). Compared to the original simulation, cell volume at day 15 is  $1.25 \times 10^{-12}$  to  $9.62 \times 10^{-13}$  litres (Figs 3.2a & 3.4a) from which it was deduced that higher glycogen concentrations would extend cell lifespan, but only to a limited extent.

As already shown mussels exposed to a tidal environment required special consideration. It was considered that the introduction of the glycogen store would have greater impact on their behaviour; as it could provide physiological flexibility for hepatopancreatic digestive cells of tidal animals by seeing them through the periods of no food availability.



*Fig 3.5 100 day simulation of models 2a with periodic food availability.*

*Feeding Regime: Square wave food concentration with 17.1875 day period of food at  $S_c = 6.0$  followed by 17.1875 day period at  $S_c = 0.0$ . ICs: as detailed for Fig 3.2 Compartmental volumes  $E_v$  —,  $L_v$  —,  $C_v$  —,  $G_v$  —,  $Cell_v$  —.*

In order to establish the difference the introduction of a glycogen store had made, the largest cycling food availability/non availability period at which the new cell survived was determined. This proved to be a 34.375 day cycle half at  $S_c = 6.0$ , half at  $S_c = 0.0$  (Figs 3.5). Since this is much greater than any tidal cycle it was concluded that the glycogen store did not provide the model cell with a sensible enhanced survivability for tidal situations.

### 3.3 Lipid subsystem: Model 2b

Model 1 was augmented with a subsystem which modelled the flow of lipid through the cell. The motivation for this was that lipid, as opposed to other nutritional macromolecular types such as carbohydrate and protein, is apparently poorly degraded by the mussel digestive cell lysosome (Fowler & De Duve, 1969; Moore, 1988; Moore *et al.*, 2007). For clarification, the classification of lipid used here does not include the continual recycling of lipid membrane that is part of vesicular traffic. Instead, only lipid that is to be used as an energy source was modelled. In order to model the flow of lipid separately, each of the three cellular compartments was split into two, one containing lipid and everything else in the other. Furthermore, it was assumed that the carbon concentrations of these lipid compartments remain constant and equal. The revised glossary (Table 3.2) and schematic (Fig 3.6) are presented below:

*Table 3.2 Nomenclature used for model 2b.*

Compartment	Variable	Lipid variable name	Non-lipid variable name
Endosome	Volume	$EL_v$	$EN_v$
Endosome	Carbon content	$EL_{xc}$	$EN_{xc}$
Endosome	Carbon	$EL_c$	$EN_c$
Lysosome	Volume	$LL_v$	$LN_v$
Lysosome	Carbon content	$LL_{xc}$	$LN_{xc}$
Lysosome	Carbon	$LL_c$	$LN_c$
Cytosol	Volume	$CL_v$	$CN_v$
Cytosol	Carbon content	$CL_{xc}$	$CN_{xc}$
Cytosol	Carbon	$CL_c$	$CN_c$



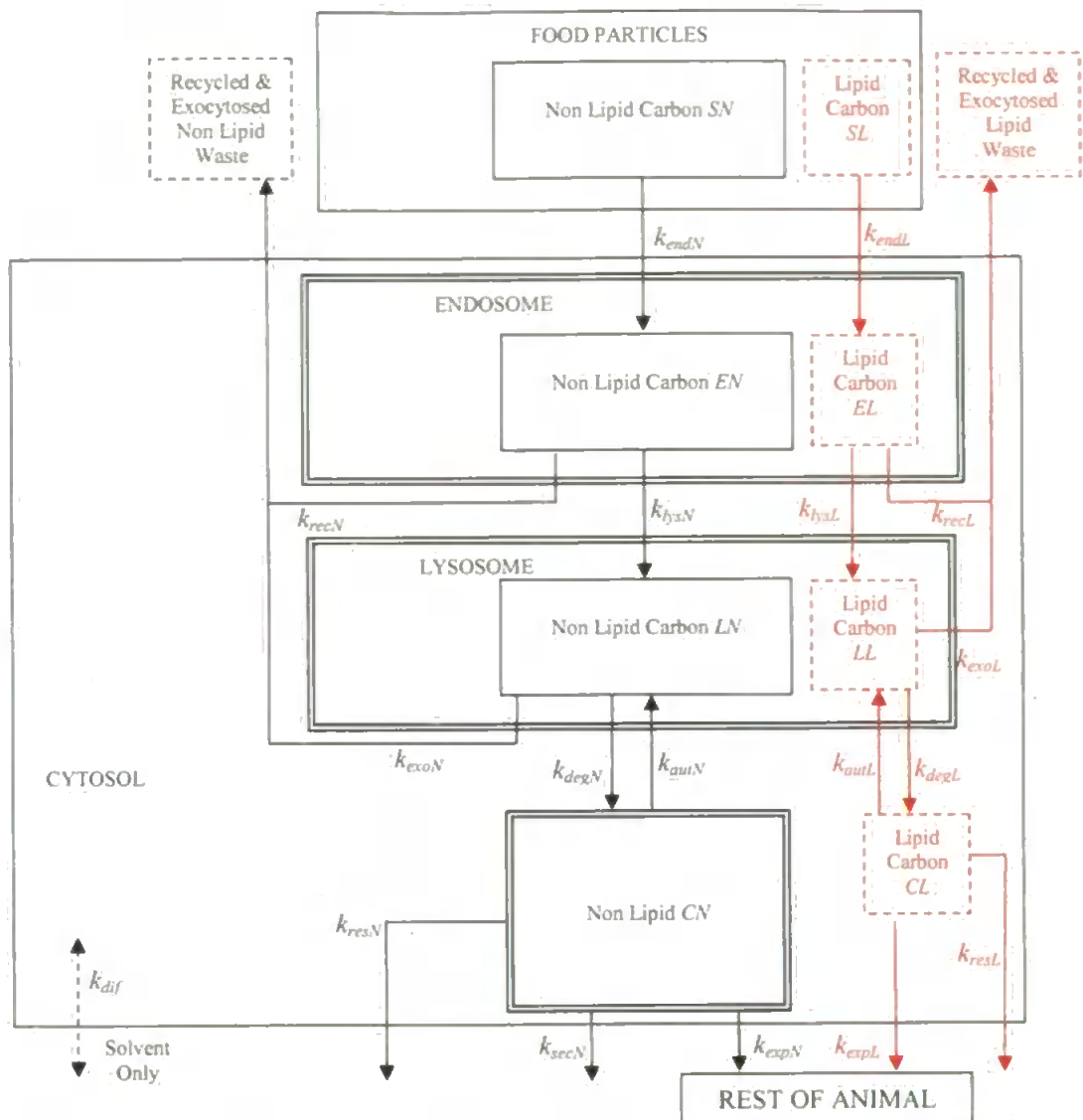


Fig 3.6 Schematic for lipid subsystem model 2b

Some method of calculating the rates of flow between each sub compartment was required. Initially the total rates were calculated as in the last model (1h); and then apportioned according to the relative volumes of lipid and non-lipid volumes of the source compartment e.g. (where  $L$  at the end of subscript denotes the lipid portion and  $N$  the non-lipid portion of total rate, no suffix indicating the total rate.)

$$k_{exoL} = k_{exo} \frac{LL_v}{L_v} \quad \text{and} \quad k_{exoL} = k_{exo} \frac{LN_v}{L_v} \quad [3.10]$$

The digestive cell lysosome appears to be ill-equipped to degrade lipid, hence, the successfully degraded fraction was decreased (Krishnakumar *et al.*, 1994; Moore, 1988, Moore *et al.*, 2007). So the following,  $f_{dn} = 0.5$  and  $f_{dl} = 0.1$ , were taken as basal values for the non lipid and lipid digestive efficiencies respectively, each subject to increase with increased turnover.

Seasonal data for non-mantle tissue (Thompson *et al.*, 1974) was used to set up the initial conditions and concentrations. Lipid dry weight as a percentage of total dry weight was shown to be between 10-13% for most of the year except during May-September where it can reach as much as 30%; presumably as storage occurs, although it remains open to question whether this is in these cells or else in some other part of the non-mantle. In order to employ this data it was necessary to be able to convert a dry weight % into either volume or carbon content (as the concentration was assumed to be static). Consequently, the following technique was formulated.

An average lipid was assumed, e.g. phosphoglyceride, then this was broken down into its chemical constituents and the atomic mass of the various elements was used to find the percentage of its mass contribution that was provided by carbon (Table 3.3).

Table 3.3 atomic breakdown of phosphoglyceride.

		N	H	C	P	O	AM
Fatty acyl chain	Stearic acid	0	36	18	0	0	252
	Glycerol	0	5	5	0	4	97
	Phosphate	0	0	0	1	4	47
Alcohol	Choline	1	13	5	0	0	80
	Phosphoglyceride	1	90	46	1	8	728
	%	0.7%	61.6%	31.5%	0.7%	5.5%	
	Weight	7	90	552	15	64	728
	% By weight	0.96%	12.36%	75.82%	2.06%	8.79%	

Hence the percentage of lipid mass which was provided by carbon was 75.82%. Then the amount of cellular carbon content which was lipid-derived was given by:

Lipid carbon = %Lipid mass carbon  $\times$  % Lipid dry weight  $\times$  Total dry weight

So for the mussel an annual mean (excluding stored summer season) percentage lipid dry weight of 14.35% was used. Total cellular dry weight was taken to be a seventh of the total wet weight and a conversion factor of 1.03 grams per ml was used (Lodish *et al.*, 1993). Then with any initial cell volume the lipid content could be derived and the remainder taken to provide all the necessary initial conditions.

As an initial attempt to see how this system worked, a 10 day simulation was run with  $EL_c = LL_c = CL_c = 33.2$  (four times cytosol concentration) and food at maximum carbon concentration with 13% of the carbon associated being lipid. The overall pattern was similar to model 1h except for an increase in overall cellular carbon. However, the lipid levels quickly fell from the initial 13.7% cellular carbon to almost zero (Figs 3.7a,

b). This drop in lipid was a consequence of the autophagy of lipid and the relatively impaired efficiency of the lysosome to degrade it and return fatty acids and glycerol to the cytosol (Fowler & de Duve, 1969; Moore, 1988).

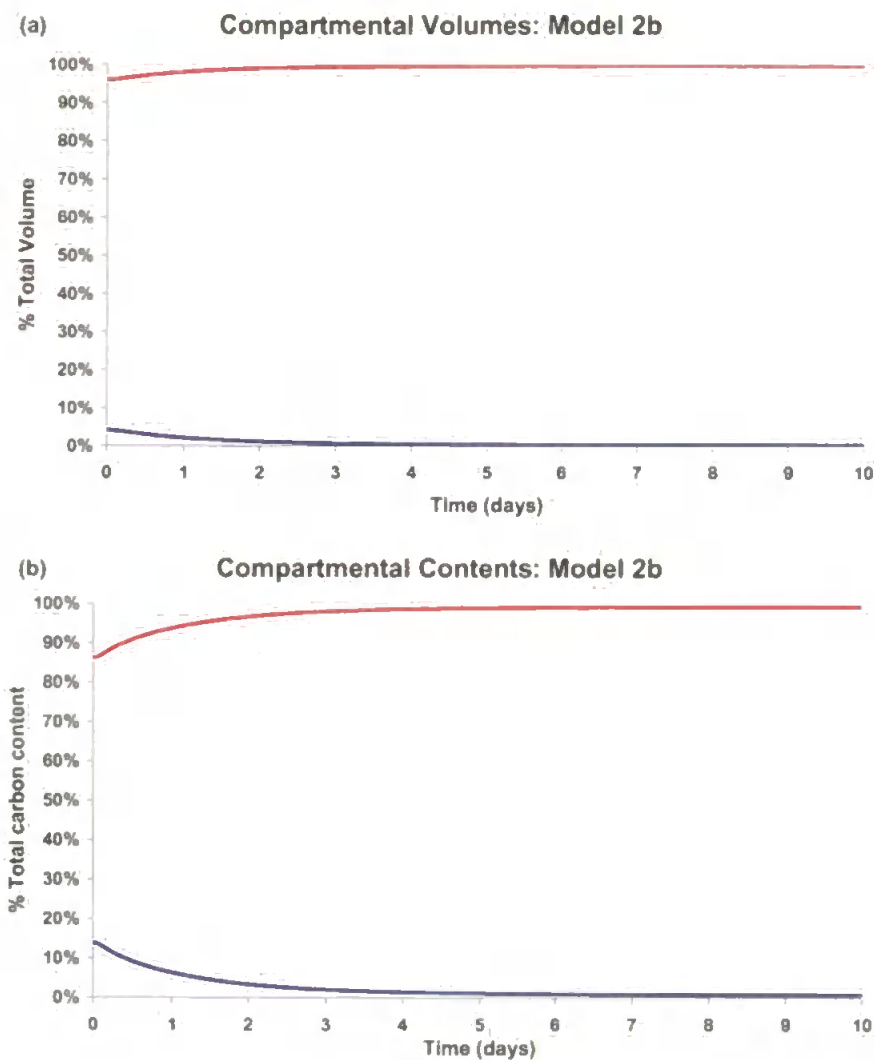


Fig 3.7 10 day simulation for Model 2b. Feeding regime:  $Sc \equiv 6.0$ ;  $f_{dn} \equiv 0.5$ ;  $f_{dl} \equiv 0.1$  &  $L\% = 13\%$ . ICs:  $f_{ev} = 4.45\%$ ;  $f_{lv} = 4.45\%$ ;  $Cell_v = 1.3764$  picolitres;  $E_c = 11.927$ ;  $L_c = 14.869$ ;  $CL_c = 4 \times C_c = 33.2$  and  $CN_c \equiv 8.3$ .

(a/b) Total cell lipid volume — & remainder — expressed as percentages of overall cell volume/carbon content

Consequently, a simulation with limited lipid autophagy was run; under the assumption that as lipid “clogs up” the lysosome, it was less

likely to be taken up in routine cellular maintenance, but more likely when enhanced sequestration was taking place. In fact, as lipid metabolism occurs mainly in peroxisomes and cytosol, the only lipid which should be taken into lysosome is that attached to proteins or associated with damaged organelles (Cuervo, 2004, Moore *et al.*, 2007). In view of this, the following amendments to the rate calculations were made.

$$k_{autN} = MAX\left(k_{aut} \times \frac{CN_v}{C_v}, k_{aut} \times nonlipidsplit\right) \quad [3.11]$$

and

$$k_{expN} = MAX\left(k_{exp} \times \frac{CN_v}{C_v}, k_{exp} \times nonlipidsplit\right) \quad [3.12]$$

For varying values of “non-lipid split”, the overall effect on a 100 day simulation as showed that even with 99.9% of autophagy sourced from non-lipid content, the overall cellular lipid content was bound to decrease (Fig 3.8b). Only with a split of autophagy at 99.99% did the lipid reverse this trend and started to increase.

It seems unlikely that the cell possesses such stringent control to prevent this extremely high proportion of lipid material from entering the lysosome due to the nature of autophagy. However, if this were an adequate representation of the cellular dynamics, then the model would have to include some function to convert lipid to non-lipid material in order to keep the overall lipid concentration within observed limits. Hence, a new model, model 2b2, was proposed with a lipid catabolism rate which

converted lipid above a certain percentage carbon content into non-lipid carbon (see Fig 3.9).

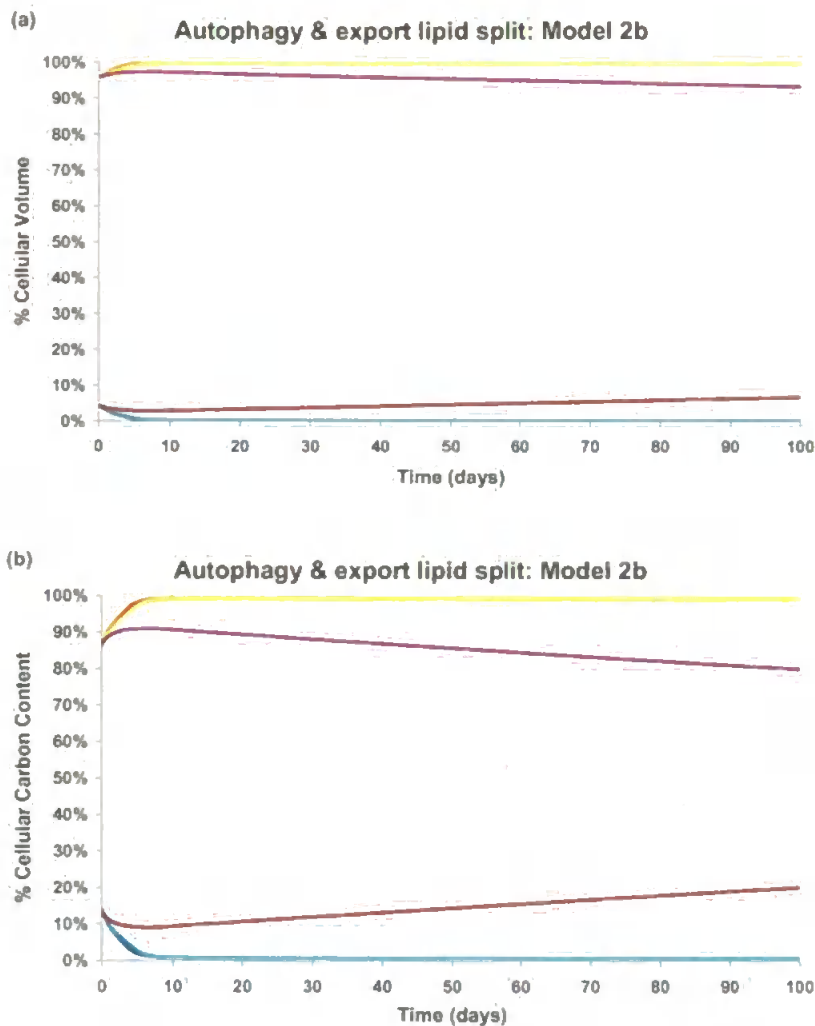


Fig 3.8 100 day simulation of model 2b lipid model with export and autophagy split. ICs and feeding regime as detailed for Fig 3.7. (a) Final lipid and remainder volume expressed as percentage of cell volume (b) final carbon content expressed as percentage of cell volume. Key: nonlipidsplit = 99% non lipid — & lipid —; nonlipidsplit = 99.2% non lipid — & lipid —; nonlipidsplit = 99.99% non lipid — & lipid —.

### 3.4 Lipid catabolism: Model 2b2

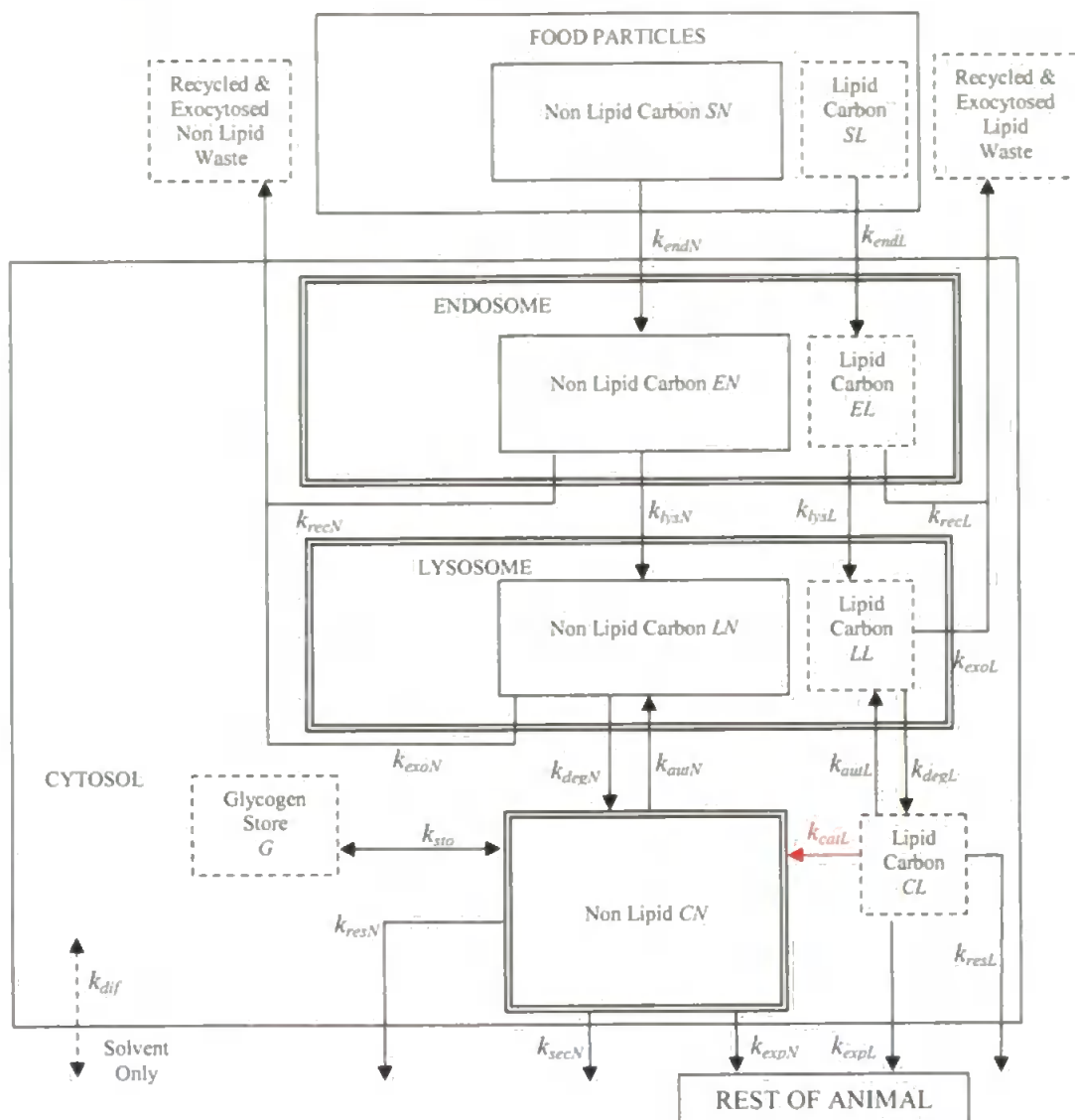


Fig 3.9 Schematic of Lipid submodel including the pathway for catabolism

This lipid conversion rate required a variable cell volume-dependent lipid ratio to enable storage and release, in order for lipid levels to be built up from a small initial intracellular volume. A linear relationship was assumed:

$$\text{Lipid}\% = \text{Lipid}\%_{\text{Min}} + (\text{Lipid}\%_{\text{Max}} - \text{Lipid}\%_{\text{Min}}) \frac{\text{Cell}_v - \text{Cell}_{v\text{min}}}{\text{Cell}_{v\text{max}} - \text{Cell}_{v\text{min}}} \quad [3.13]$$

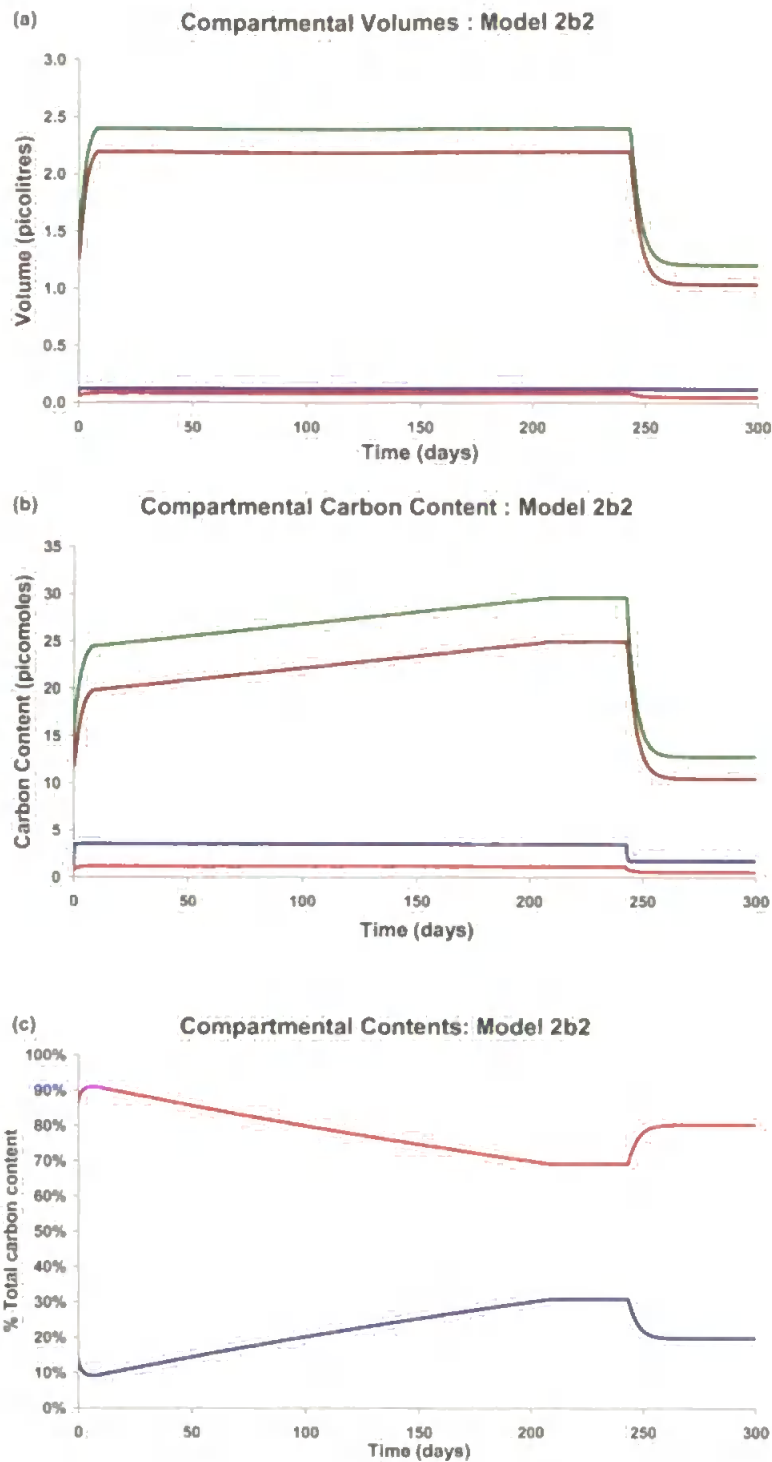


Fig 3.10 300 day simulation for Model 2b2 introducing lipid catabolism. Feeding regime: Days 0-243,  $S_c = 6.0$ , Days 243-300  $S_c = 3.0$ ;  $L\% = 13\%$ ;  $f_{dL} = 0.1$ ;  $f_{dN} = 0.5$ . ICs: as detailed for Fig 3.7. (a) Compartmental volumes  $E_v$  —,  $L_v$  —,  $C_v$  —,  $G_v$  —,  $Cell_v$  — (b) Compartmental carbon contents  $E_{xc}$  —,  $L_{xc}$  —,  $C_{xc}$  —,  $G_{xc}$  —,  $Cell_{xc}$  — (c) Cell carbon conten: lipid — & remainder — expressed as percentages of overall cell carbon content



With this system in place, it was shown that it takes approximately 209 days to achieve an equilibrium state where the lipid levels reach those exhibited in the summer months (Fig 3.10c; Thompson *et al.*, 1974). Obviously, some approach to speeding up this accumulation had to be found to match the observations, but first it was requisite to analyse the rest of the behaviour.

During the period of accumulation, the greater lipid concentration aids the cell in storing more carbon (Fig 3.10b). Once the overall food carbon concentration level was halved, there followed a period of decline in volume and content (Figs 3.10a & b) until a satisfactory equilibrium level was found that could be supported by this reduced nutrient level. During the accumulation of lipid, export of non-lipid material carried on; indicating that one of the primary functions of the cell was still being performed, and as the rest of the animal cells could also convert sugars and protein to lipid, their lipid levels would be under their own regulatory control.

Having included the catabolism rate it was predicted that increasing the lipid content of the food would increase the rate of export. Curiously, when the percentage of food carbon which was lipid was increased from 13% to 16% there was a radical change in the model's behaviour. There was an expected increase in the rate towards cellular lipid saturation, now occurring at day 162, but there was no export of material of any sort from the cell. Indeed the only export that occurs was once the food concentration

dropped and the system had to reduce its lipid content at a faster rate than it could convert it into non-lipid material.

Figure 3.11 shows the effect of lipid food % on the cumulative export from the animal and the final carbon content of the cell, when fed at the maximum food concentration for 1 year. What was evident was that increased lipid in the food reduced the export of carbon from the cell (Fig 3.11). Furthermore, there was an initial increase in the final carbon content due to the higher lipid concentration. But after a threshold limit was passed this too started to decrease.

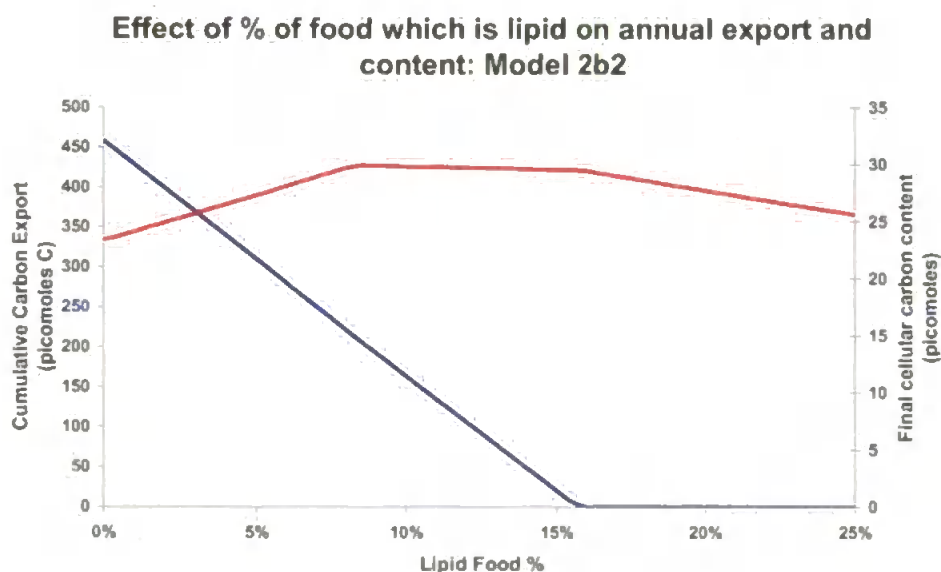


*Fig 3.11 Lipid Food % effect on cumulative carbon export — and final carbon content —:*

Since the lipid food must pass through the lysosome on its way to the cytosol the effect of the lysosomal efficiency was crucial in determining how much was rejected. The effect of lipid degradation efficiency and lipid food% combined was explored. Figure 3.14b shows that increased

degradative efficiency led to a relatively insignificant increase in the amount exported.

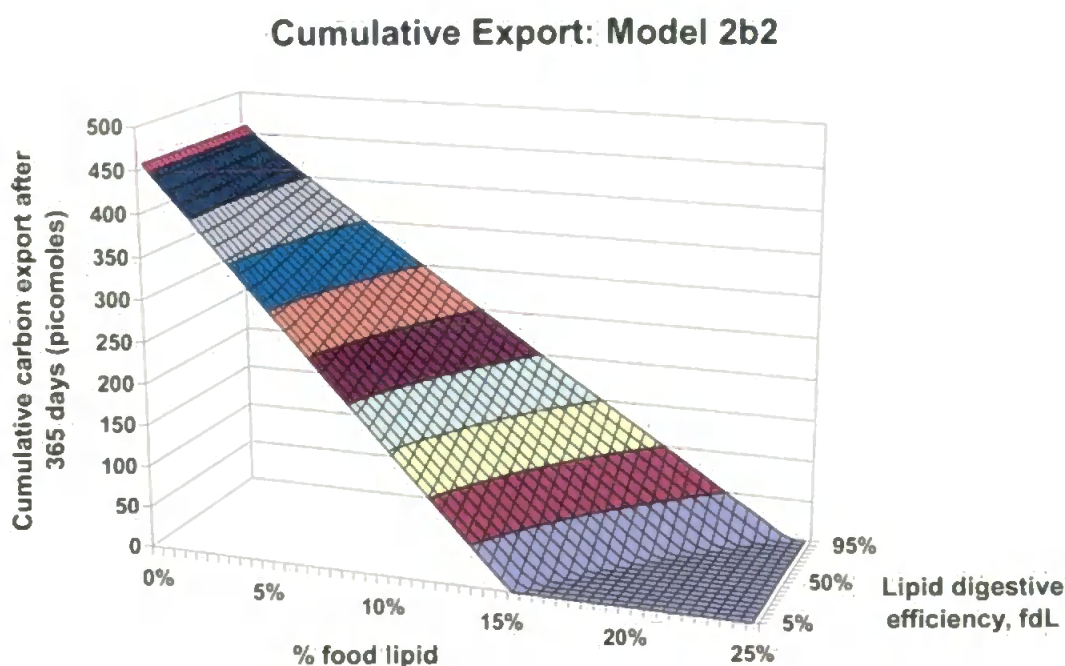


*Fig 3.12 365 day simulation  $S_c = 6.0$  and varying food lipid % and lipid digestive efficiency showing cumulative amount of carbon exported from cell*

An analysis of the percentage breakdown of the pathways by which the cell was losing carbon (cumulative export, respiration, secretion, exocytosis, recycled and in the case of lipid catabolised) was performed. It was evident that the main loss for overall carbon was through exocytosis, accounting for 80% of the loss (Fig 3.13a). However, for the lipid this was replaced by recycling as the major contributor to cellular loss (Fig 3.13b). The lack of significant export, the indicator for a healthy cell, was noted in most cases despite the cell being fed at maximum for over 200 days.

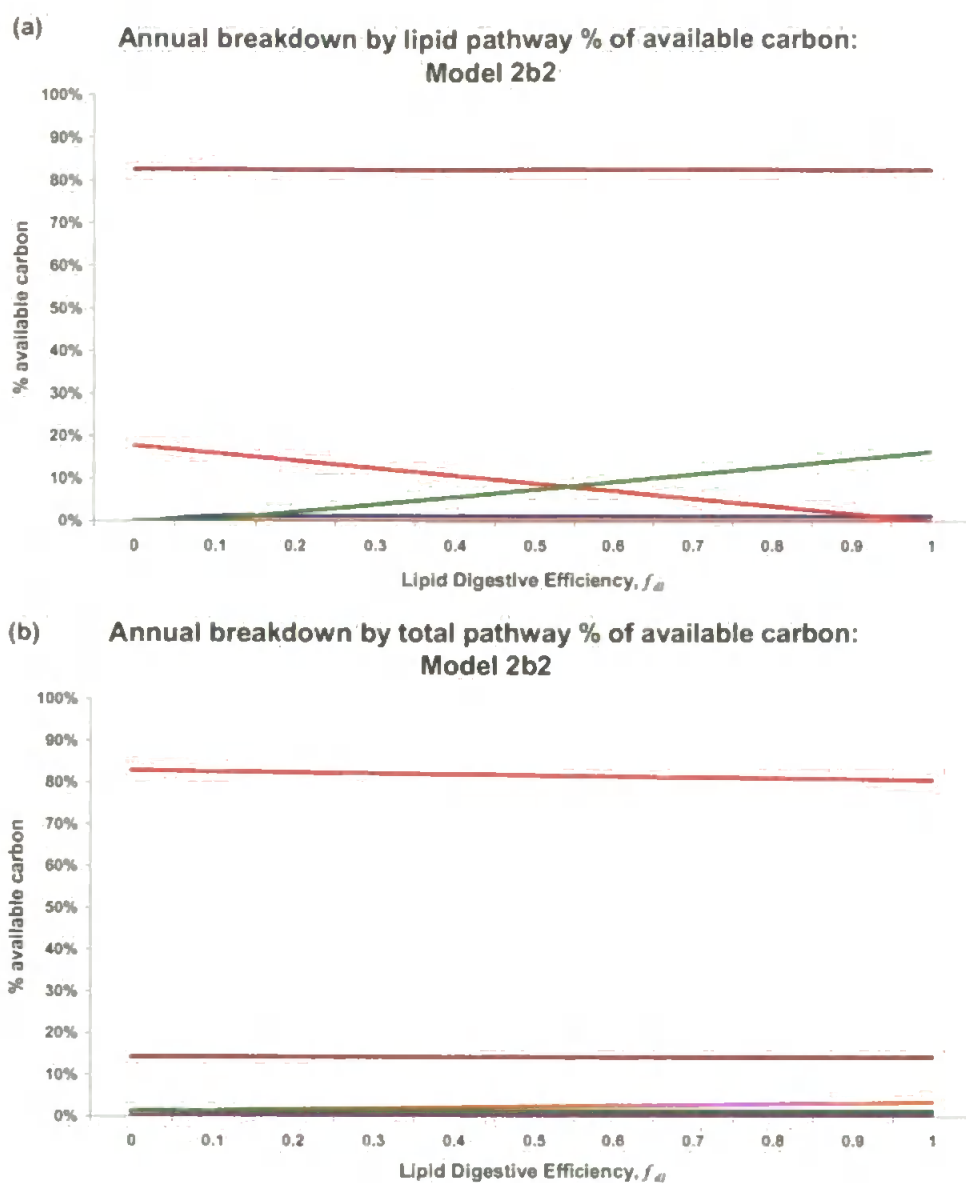


Fig 3.13 Annual simulation for model 2b2. Feeding regime:  $S_c = 6.0$ ;  $L\% = 12.5\%$ ;  $f_{dL} = 0.1$ ;  $f_{dN} = 0.5$ . ICs: as detailed for Fig 3.8. Percentage breakdown of pathways by which carbon is lost from the cell (a) for lipid only (b) total cell as a function of increased lysosomal efficiency in lipid degradation. Key: — Stored; — Exported; — Recycled; — Exocytosed; — Respired; — Secreted.

Perversely it seems, as the food was increased, less was exported due to not only lysosomal loss but also to excessive recycling from the

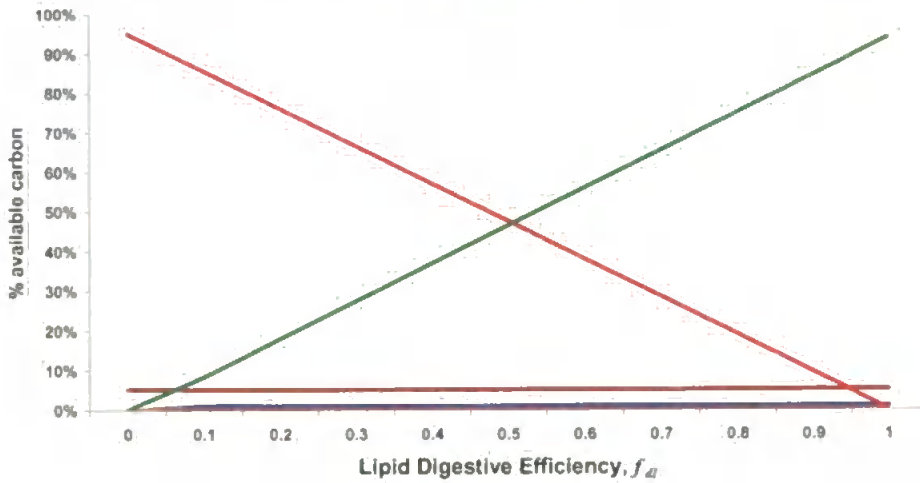
endosome. Recycling in lipid was far more excessive than in non-lipid, due to endocytotic volume being used to apportion the total recycling rate and recycling rate of non-lipid had been given the recycling reducing factor  $f_{rN} = 0.01$ , whereas for lipid  $f_{rL} = 1.0$ , due to the constant lipid carbon concentration. To overcome this problem, the next submodel apportioned the recycling rate into lipid and non-lipid rates as a function of the ratio of their relative endosomal carbon content.

$$\frac{f_{rL}k_{recL}EL_c}{f_{rL}k_{recL}EL_c + f_{rN}k_{recN}EN_c} = \frac{EL_{xc}}{E_{xc}} \quad [3.14]$$

hence

$$k_{recN} = \frac{\left(1 - \frac{EL_{xc}}{E_{xc}}\right) f_{rL} EL_c}{\left(1 - \frac{EL_{xc}}{E_{xc}}\right) f_{rL} EL_c + \frac{EL_{xc}}{E_{xc}} f_{rN} EN_c} \quad [3.15]$$

(a) Annual breakdown by lipid pathway % of available lipid carbon: Model 2b3



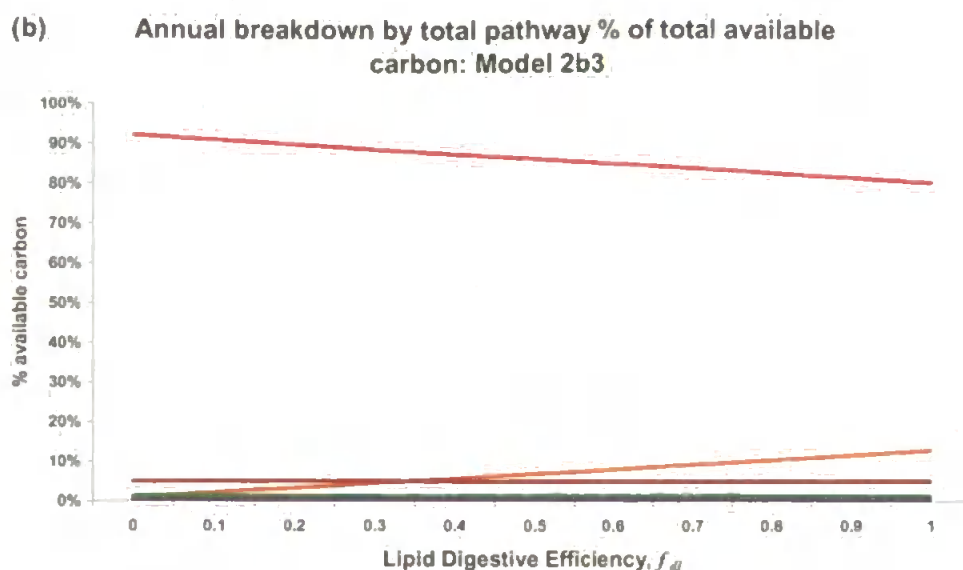
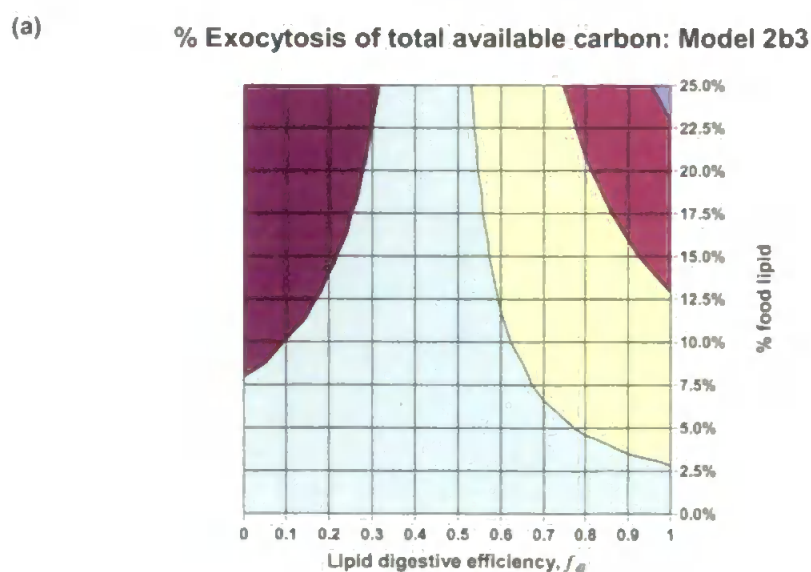


Fig 3.14 Annual simulation for model 2b3. All details the same as for Fig 3.13 except new recycling rate distribution.

Comparing this new sub model, 2b3, to the previous showed the disappearance of the lipid recycling as a significant factor and replaced by exocytosis at low efficiency, which in turn was supplanted by catabolism as the efficiency increase (Fig 3.14a). Also, total cellular loss was affected by this change resulting in improved export at the higher levels (Fig 3.14b).



(b)

## % Export of total available carbon: Model 2b3

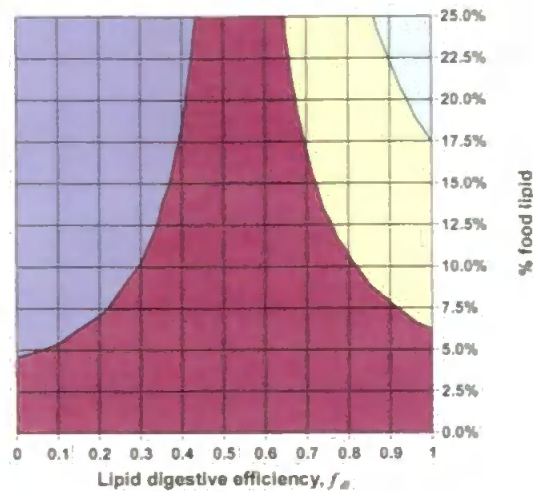
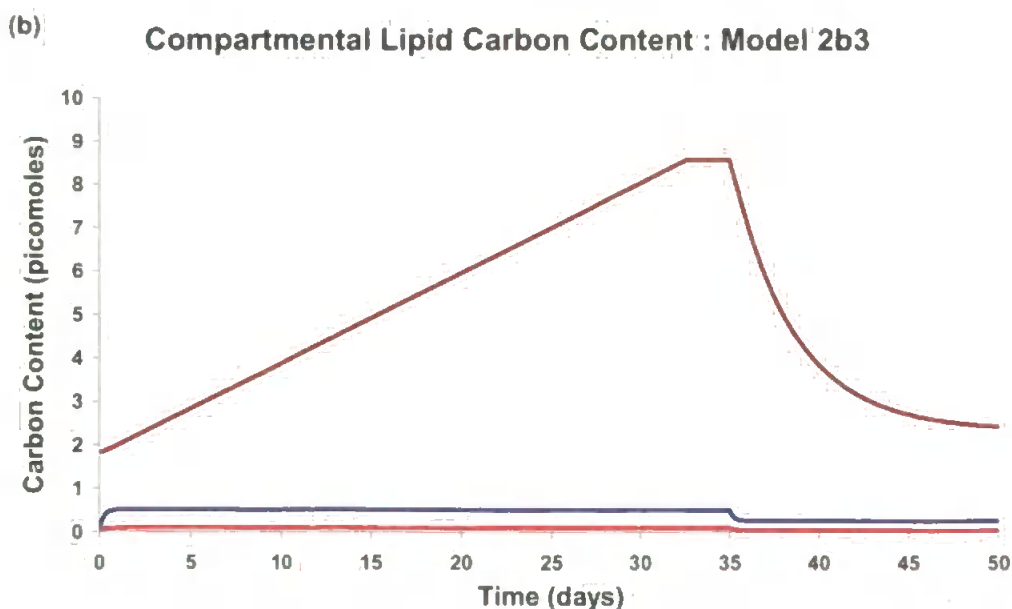
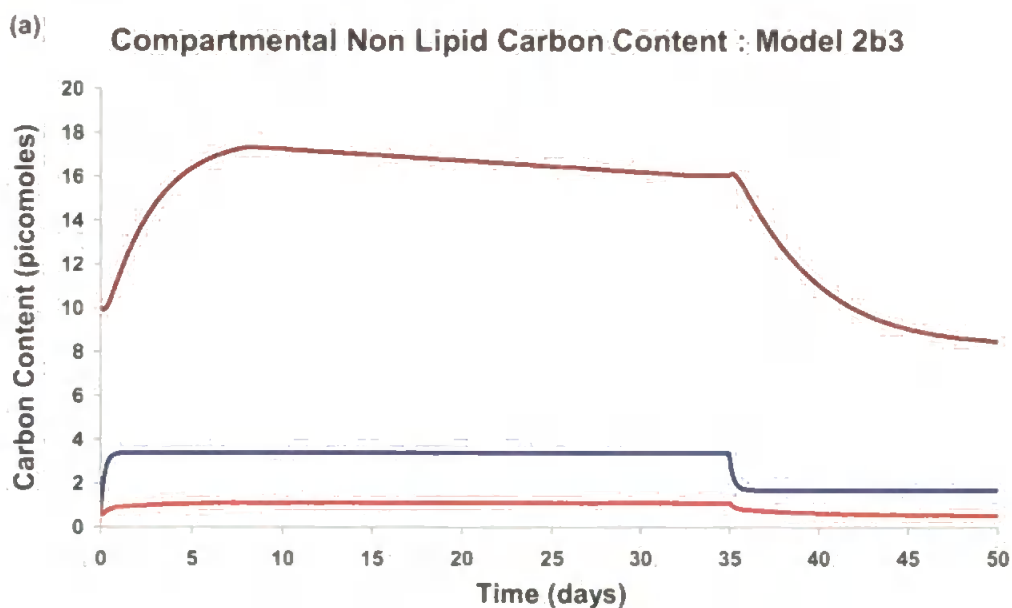


Fig 3.15 Annual simulations of model 2b3 sensitivity analysis. ICs same as detailed for Fig 3.8. Food regime:  $Sc = 6.0$  and  $f_{dN} \equiv 0.5$ . Effect of percentage of food carbon which is lipid ( $L\%$ ) and lysosomal lipid digestive efficiency ( $f_d$ ) on carbon loss through (a) exocytosis: ■ 70-75%; ■ 75-80%; ■ 80-85%; ■ 85-90%; ■ 90-95% and (b) export: ■ 0-5%; ■ 5-10%; ■ 10-15%; ■ 15-20%.

Next, the overall effect of the food lipid content and lysosomal lipid degradative efficiency on total carbon loss was analysed as shown below (Figs 3.15a & b). A general observation was that of increased efficiency increasing the amount of lipid exported at the expense of loss through exocytosis. With a low lysosomal lipid digestive efficiency and high lipid % of food, export was impaired whilst with high efficiency export was increased, which intuitively appears to be a better representation of the actual cellular dynamic.



To see if this had an appreciable effect on the cells ability to survive a nutrient reduction, a 50 day simulation was performed, with food at maximum carbon concentration for the first 35 days (to allow lipid to gain its maximum level; Fig 3.16d) and halved thereafter. Once maximum lipid level was attained the catabolism rate was provoked ensuring export and maximum carbon content (Fig 3.16a).





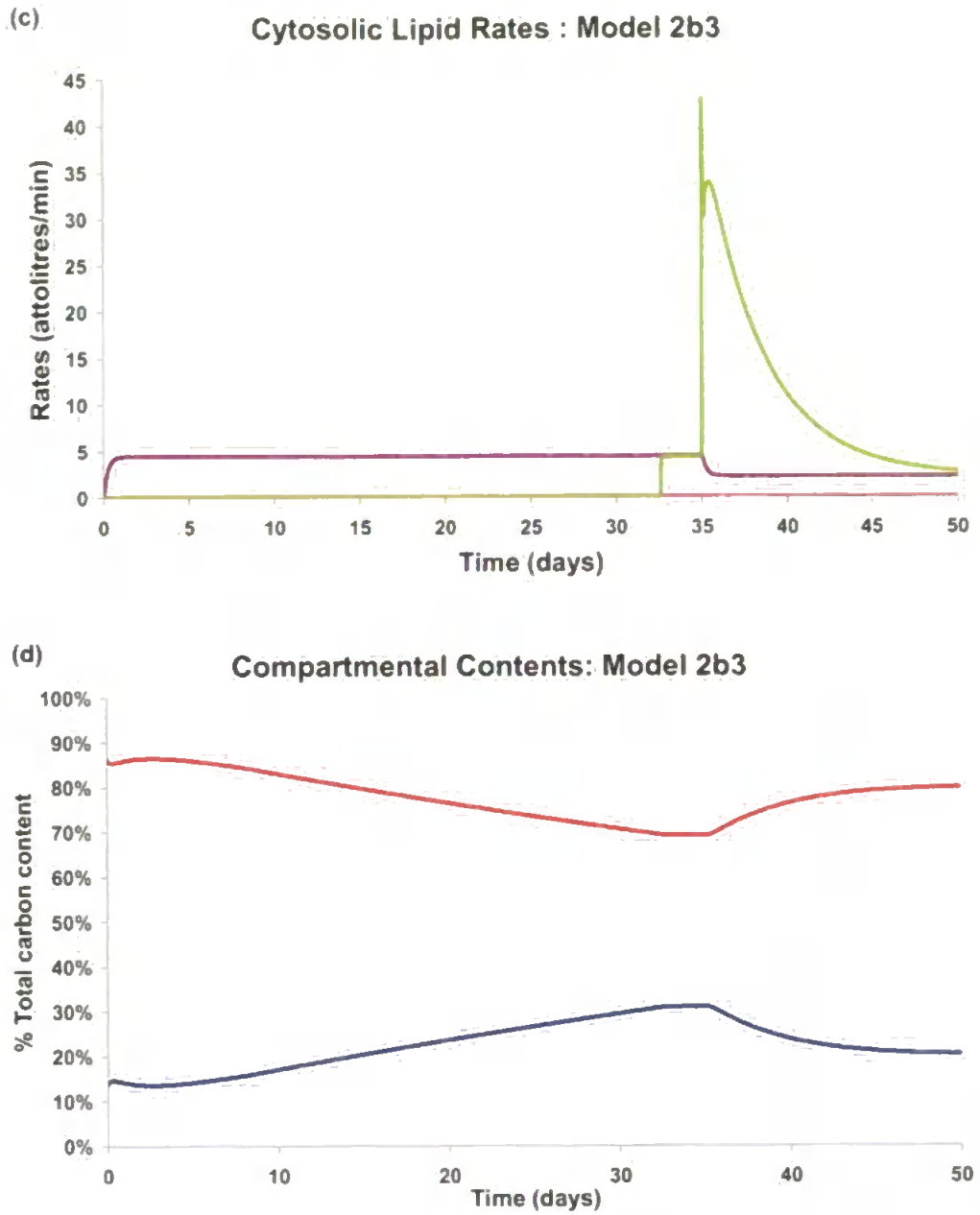


Fig 3.16 50 day simulation of Model 2b3. Feeding regime: Days 0-35  $S_c = 6.0$ , Days 35-50  $S_c = 3.0$ ;  $L\% = 13\%$ ; ICs as detailed for Fig 3.8. (a) compartmental non lipid carbon contents  $E_{xcN}$  —,  $L_{xcN}$  —,  $C_{xcN}$  — (b) Compartmental lipid carbon content  $E_{xcL}$  —,  $L_{xcL}$  —,  $C_{xcL}$  — (c) Cytosolic lipid rates:  $k_{autL}$  —,  $k_{degL}$  —,  $k_{resL}$  —,  $k_{expL}$  —,  $k_{catL}$  —; (d) % of total carbon content split into — lipid and — non-lipid;

Lipid catabolism (Fig 3.16c) provided a small amount of capacity for cellular volume to remain at maximum at the beginning of the stressed period but was quickly utilised. The familiar pattern of the cell's carbon content (Figs 3.16a&b) being gradually built up with lipid, was seen but at a much faster rate than in the first lipid catabolism model (Fig 3.10). Hence the summer values could be effectively established within a month of the onset of higher food availability.

### 3.5 Combined glycogen and lipid system: Model 2c

Having amended each of the glycogen and lipid sub-models so that their behaviour corresponded better and having demonstrated their partial success in making the cell more robust the following model looked at their combined effect (Fig 3.17). The revised system of ODEs for this model are presented in Appendix A.

**MODEL 2C: Combined Glycogen & Lipid Submodel**

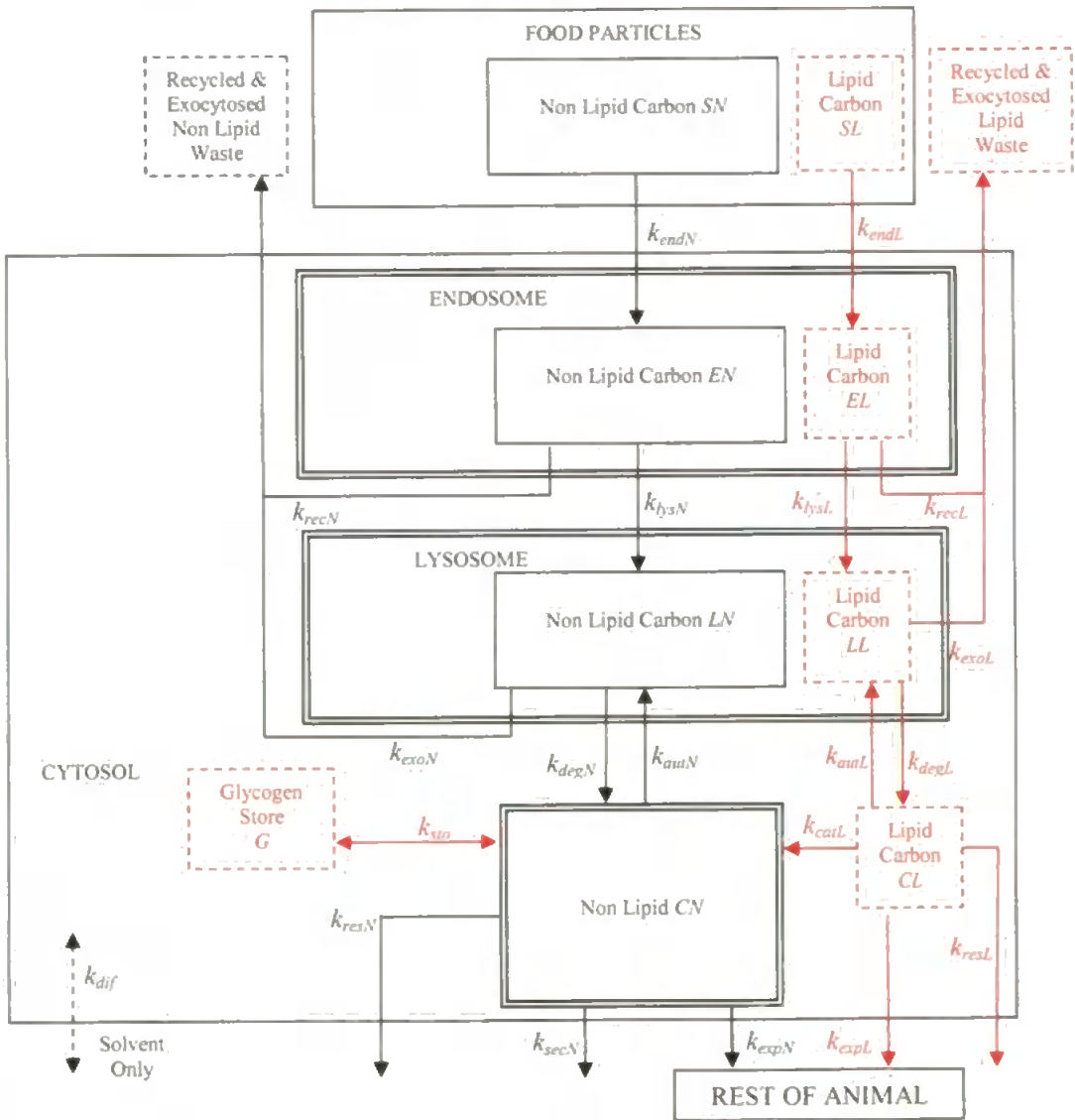


Fig 3.17 Schematic for carbon model with glycogen and lipid included

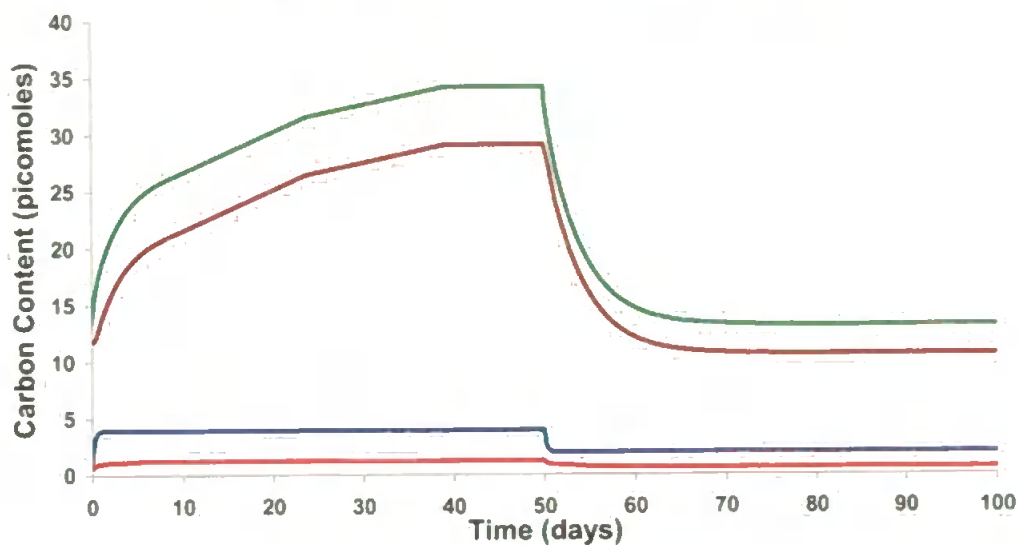
As the cell has recourse to both lipid and glycogen as a means by which it may store cellular reserves, the model needed to incorporate both (Bayne *et al.*, 1978; Thompson *et al.*, 1974). Obviously the means by which the ratio of these two reserves was formed and utilised needed to be developed.

*Algorithm for glycogen and lipid release and storage and overall export*

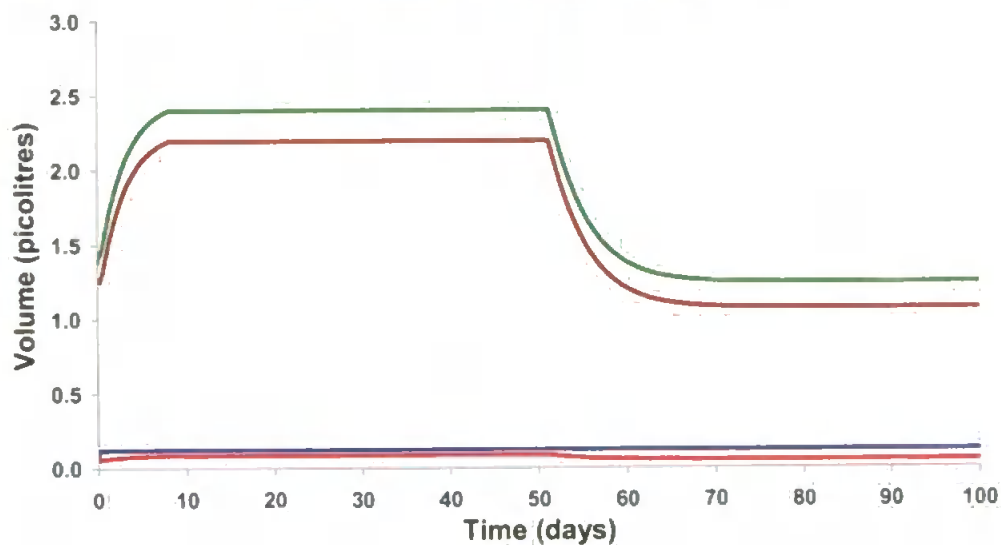
At the end of each calculated timestep the following flags were checked.

- 1) If the cell volume was greater than maximum limit, then enough glycogen was stored so that revised cell volume was equal to this limit.
- 2) Else if the cell volume was less than this maximum limit and there was carbon in the glycogen store, then reserves were released until either cell volume was equal to the maximum limit or there was no more glycogen left.
- 3) If the cellular lipid content was greater than the cell volume-dependent lipid function level, then lipid was catabolised to achieve this level.
- 4) If the glycogen carbon content was greater than 20% of cellular carbon content, then glycogen was released and carbon exported until this level was achieved.
- 5) If the cell volume was as a consequence of the above adjustments greater than its' maximum prescribed limit, then material was exported to achieve this level.

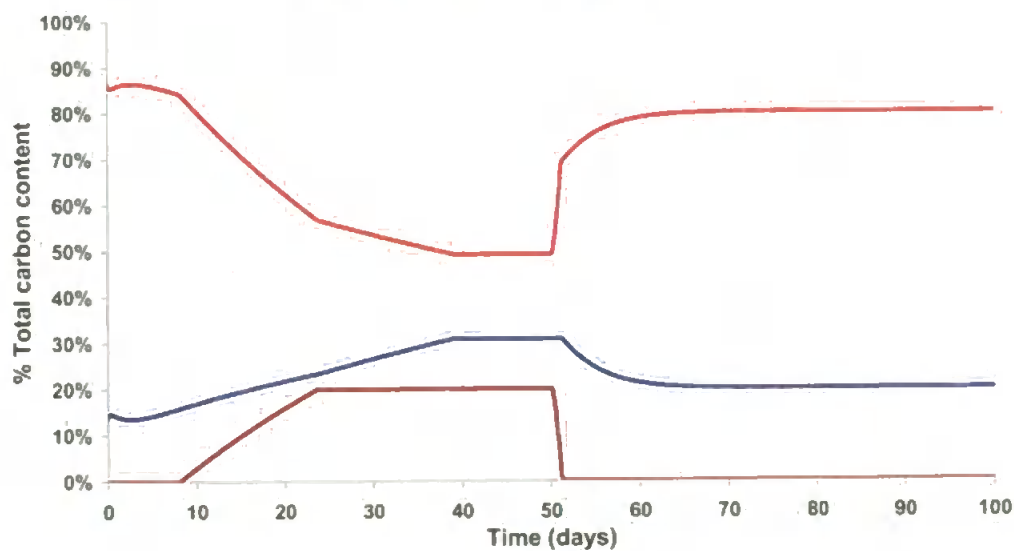
(a) Compartmental Carbon Content : Model 2c



(b) Compartmental Volumes : Model 2c



(c) Compartmental Contents: Model 2c



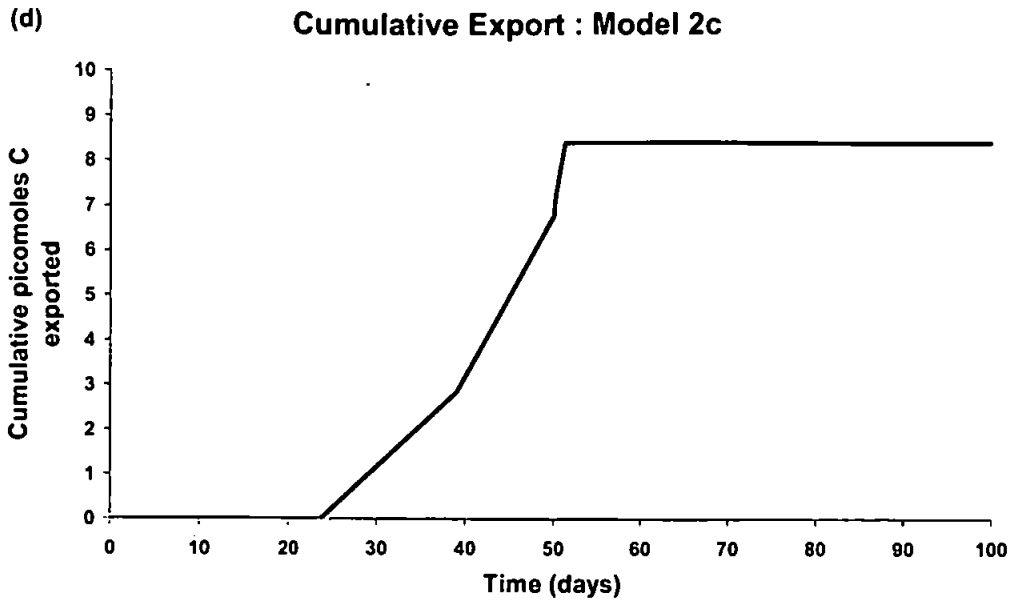


*Fig 3.18 100 day simulation of model 2c combining glycogen and lipid models. Feeding regime: Days 1-50  $S_c = 6.0$ , Days 50-100  $S_c = 3.0$ ;  $L\% \equiv 13\%$ ;  $f_{dN} \equiv 0.5$ ;  $f_{dL} \equiv 0.1$ . ICs:  $Cell_v = 1.38$  picolitres;  $f_{ev} = f_{lv} = 4.45\%$ ;  $E_c = 11.93$ ;  $L_c = 14.869$ ;  $G_c = 16.6$ ;  $CL_c = 33.2$ ;  $CN_c \equiv 8.3$ ; (a) Compartmental carbon contents  $E_{xc}$  —,  $L_{xc}$  —,  $C_{xc}$  —,  $G_{xc}$  —,  $Cell_{xc}$  — (b) compartmental volumes  $E_v$  —,  $L_v$  —,  $C_v$  —,  $G_v$  —,  $Cell_v$  — (c) percentage breakdown of total cellular carbon content into lipid —, glycogen — and remainder — (d) cumulative export*

With this algorithm a simulation was run for 50 days with maximum food, and a further 50 days at half level in order to examine the behaviour generated when storing and releasing both reserve substances in tandem. Cell volume reached its maximum within 10 days and remained constant until food deprivation commenced; thereafter there was a period of roughly 30 days where it advanced towards a new equilibrium level (Fig 3.18b). While the overall volume remained constant after the initial period, the

carbon content still increased until approximately day 40 (Fig 3.18a). Lipid, after an initial decline, started to increase roughly linearly until it reached the maximum allowable level (Fig 3.18c). Glycogen whilst attaining its percentile maximum of cellular carbon around day 20 continued to increase its actual content as the lipid increase allowed the total cellular carbon to rise. Export of carbon started once the glycogen reserve first attained its percentile target but the rate increased once the lipid percentage was achieved (Fig 3.18d).

Once the nutritional stress was initiated, the glycogen reserves were the first to be utilised, taking a paltry 1.8 days to exhaust. Thereafter, the lipid served to slow the rate of cellular volume loss until a new equilibrium was met at around day 80. Of small concern was an anomalous final burst of export, which was initiated upon the onset of nutrient deprivation, possibly as a consequence of the order of the control algorithm. In order to alleviate this perceived problem, the target glycogen level was next modelled as a linear function of cell volume.

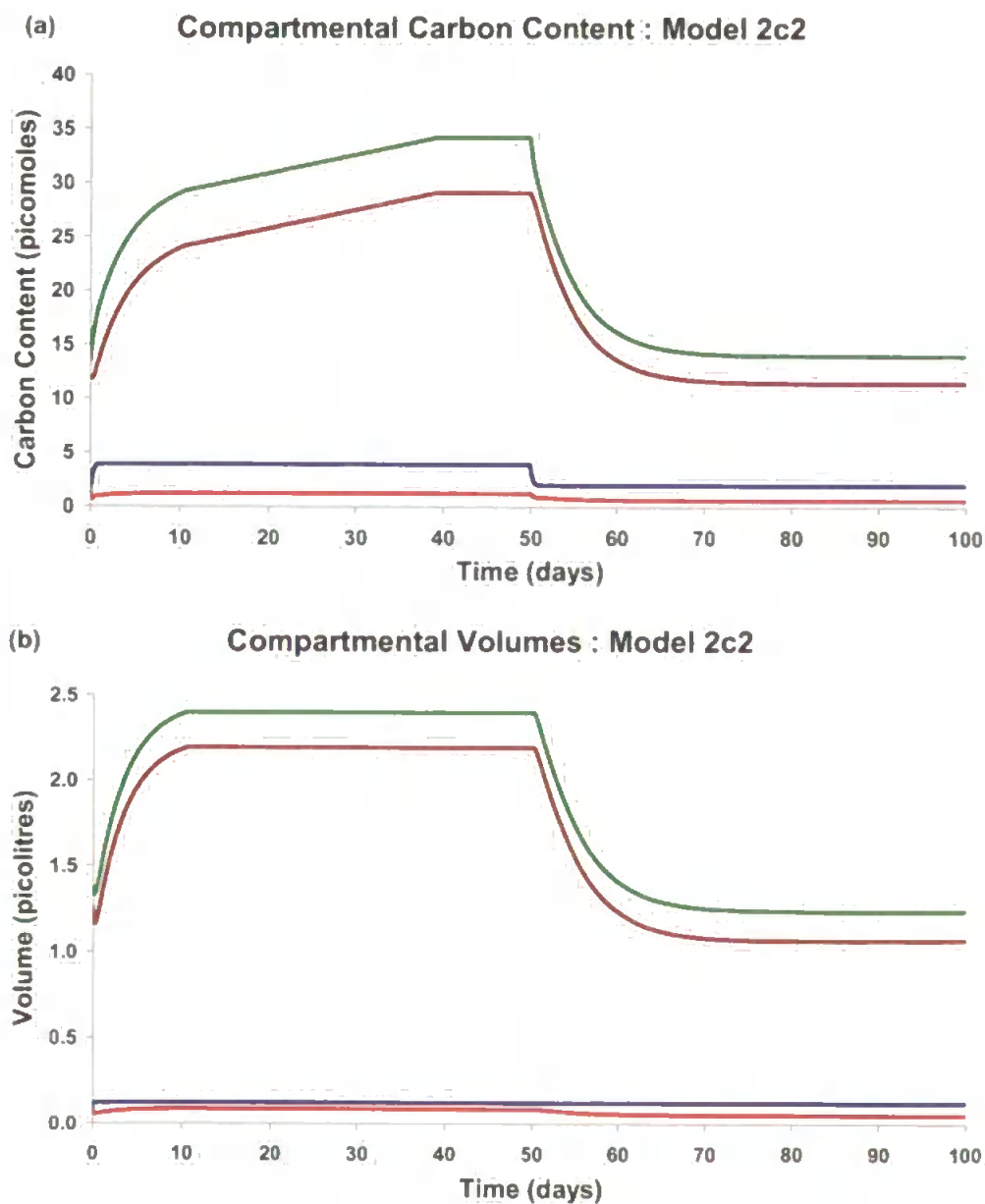
$$G\%(t) = G\%_{\min} + (G\%_{\max} - G\%_{\min}) \left( \frac{Cell_v(t) - Cell_{v\min}}{Cell_{v\max} - Cell_{v\min}} \right) \quad [3.16]$$

Then the following new control algorithm was implemented after the initial calculation for each timestep:

- 1) If the cellular lipid content was greater than the cell volume dependent lipid function level, then catabolise lipid to achieve this level.

- 2) If the cellular glycogen level was not equal to the glycogen percentage split as defined above, then store or release as necessary
- 3) If the cell volume was greater than maximum limit, then store enough glycogen so that a revised cell volume is equal to this limit.

The results of a simulation, with the same initial conditions and feeding regime as the previous one, are shown in Fig 3.19 with the new algorithm implemented.





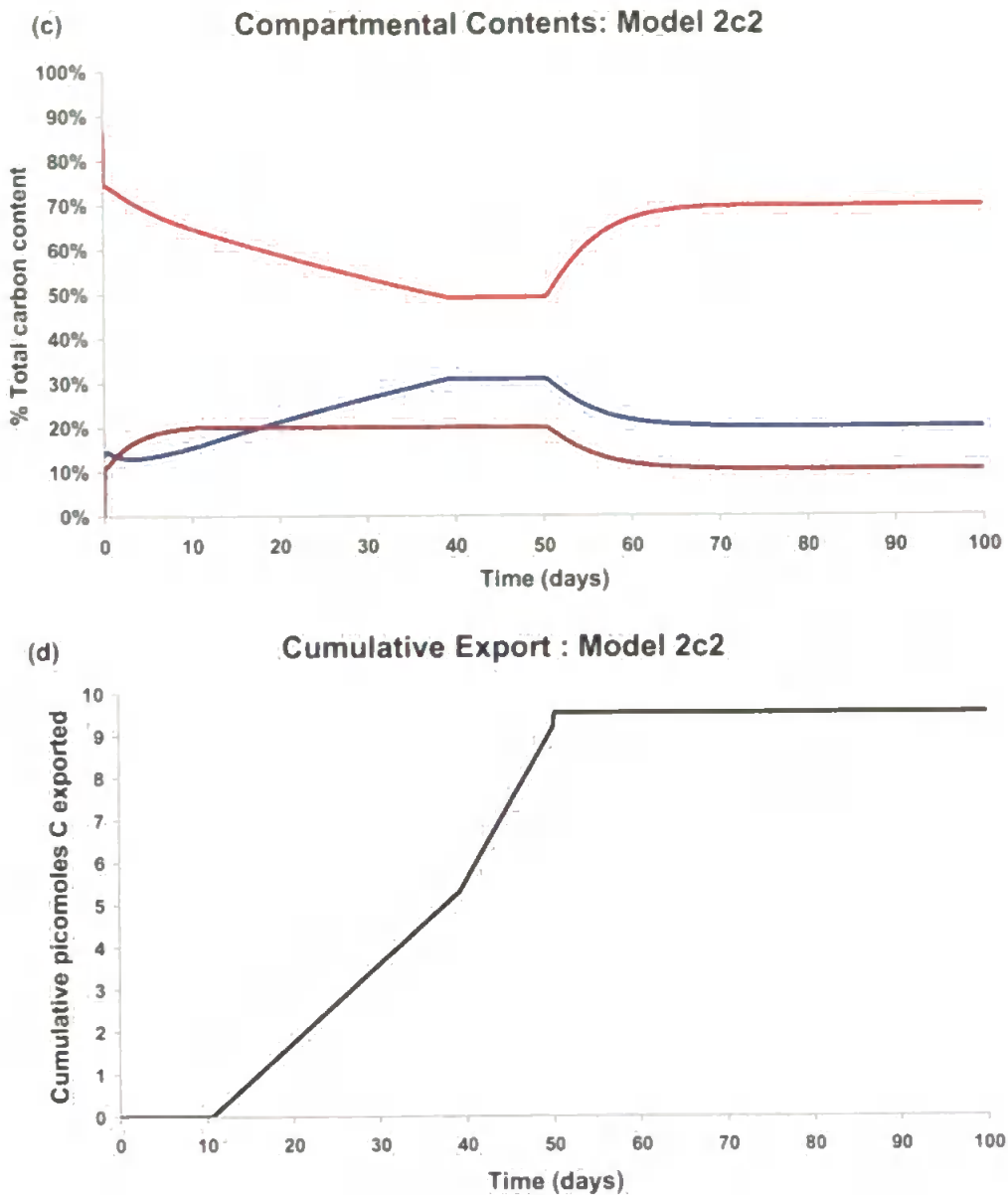


Fig 3.19 100 day simulation of Model 2c2 with new lipid and glycogen control algorithms. ICs and food regime as given for Fig 3.18. (a) Compartmental carbon contents  $E_{xc}$  —,  $L_{xc}$  —,  $C_{xc}$  —,  $G_{xc}$  —,  $Cell_{xc}$  — (b) compartmental volumes  $E_v$  —,  $L_v$  —,  $C_v$  —,  $G_v$  —,  $Cell_v$  — (c) percentage breakdown of total cellular carbon content into lipid —, glycogen — and remainder — (d) cumulative export

In comparison to model 2c this new model had glycogen present at all times to varying degrees (Fig 3.19c) which was considered a better

representation of reality. The algorithm also allowed the cell to attain its maximum volume slightly after 10 days (Fig 3.19b) as the glycogen store was filled, with cell growth requiring more carbon in the initial period to achieve this level. However, from this point the cell was liable to export material and not wait for the glycogen store to fill up as in the previous submodel. Due to this scenario, the cumulative export was increased by approximately an extra 11% (Fig 3.19d). The less well-nourished period settled into an equilibrium state as before, but with slightly larger carbon content than before, as a consequence of this linear glycogen function (Fig 3.19 a).

In order to evaluate how well the model was operating, a calculation was made as to the destination of available carbon. Available carbon was taken to be the sum of the initial carbon and the amount endocytosed. The lost figure was defined as the carbon that was recycled, exocytosed, respired or secreted.

### Pathway breakdown of available carbon : Model 2c2

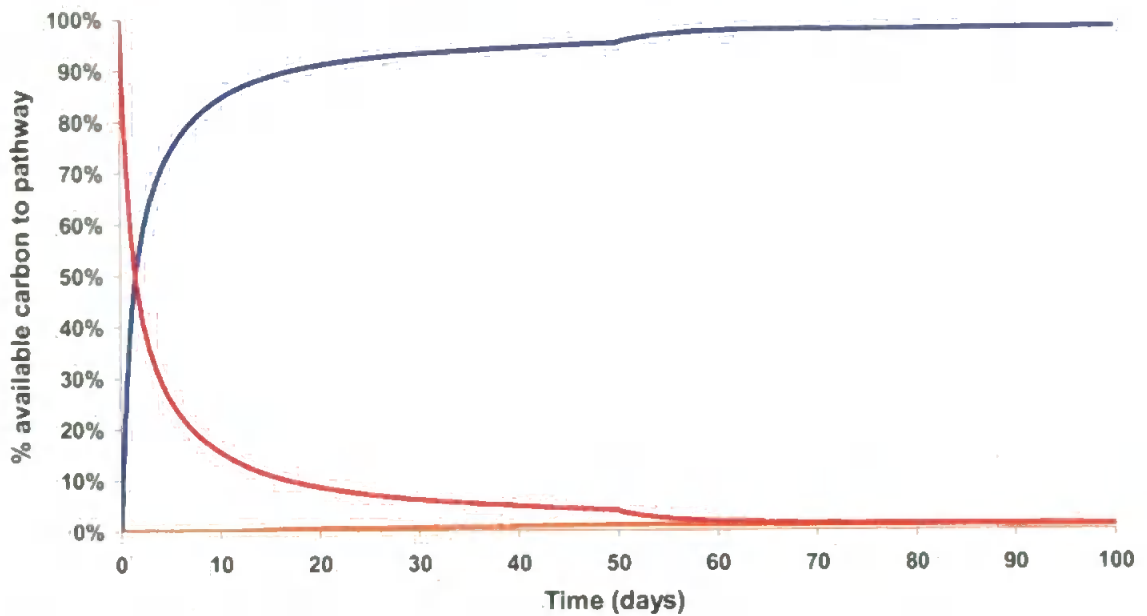


*Fig 3.20 Breakdown of available carbon utilisation into — stored, — lost and — exported in Model 2c2 with glycogen level function.*

Initially the stored % dominated but this inevitably reduced, the longer the simulation is allowed to run, since material was either lost or exported (Figs 3.20 a & b). The initial observation to made was how much carbon was eventually lost. The endocytosed material, as it passed through the endosomal-lysosomal system, lost first 1% through recycling and then 50% of the remainder through the initial lysosomal digestive process. If the simulation were allowed to run for long enough to render immaterial the initial carbon in the cell, then approximately 40% of the cellular carbon loss was derived from cell maintenance (i.e. autophagic turnover and subsequent exocytotic loss).

In order to better compare between the first and the second combined lipid-glycogen models Table 3.4 details the outputs at day 50 prior to nutrient reduction and at the end of the simulation.

By storing carbon as glycogen from the start according to the linear function, model 2c2 reduced the amount of carbon available to loss through autophagy and, hence, by exocytosis or apocrine removal of the apical cytoplasm (Langton, 1975). This accounted for the increased export during the well-fed period and the enhanced storage evinced when the cellular volume dropped to the same level after the under-nourishment.

*Table 3.4 Comparison of percentage breakdown of carbon loss from cell at days 50 and 100 days for models 2c and 2c2 showing effect of new glycogen level control function*

Model	Lost (%)	Export (%)	Store (%)	Cell <sub>v</sub> (end) (litres)	Cell <sub>xc</sub> (end) (moles C)	Lipid (%)	G% (%)
<i>50 days</i>							
2c	91.24	0.77	7.99	$2.4 \times 10^{-12}$	$3.42 \times 10^{-11}$	30.8	20.0
2c2	90.18	1.04	8.78	$2.4 \times 10^{-12}$	$3.42 \times 10^{-11}$	30.8	20.0
<i>100 days</i>							
2c	94.24	0.64	5.11	$1.24 \times 10^{-12}$	$1.31 \times 10^{-11}$	19.9	0.0
2c2	93.45	0.73	5.82	$1.24 \times 10^{-12}$	$1.40 \times 10^{-11}$	19.9	10.32

As a final example of the effects provided by these changes the tidal feeding pattern simulation first introduced for model 1h (Fig 2.16) was replicated.

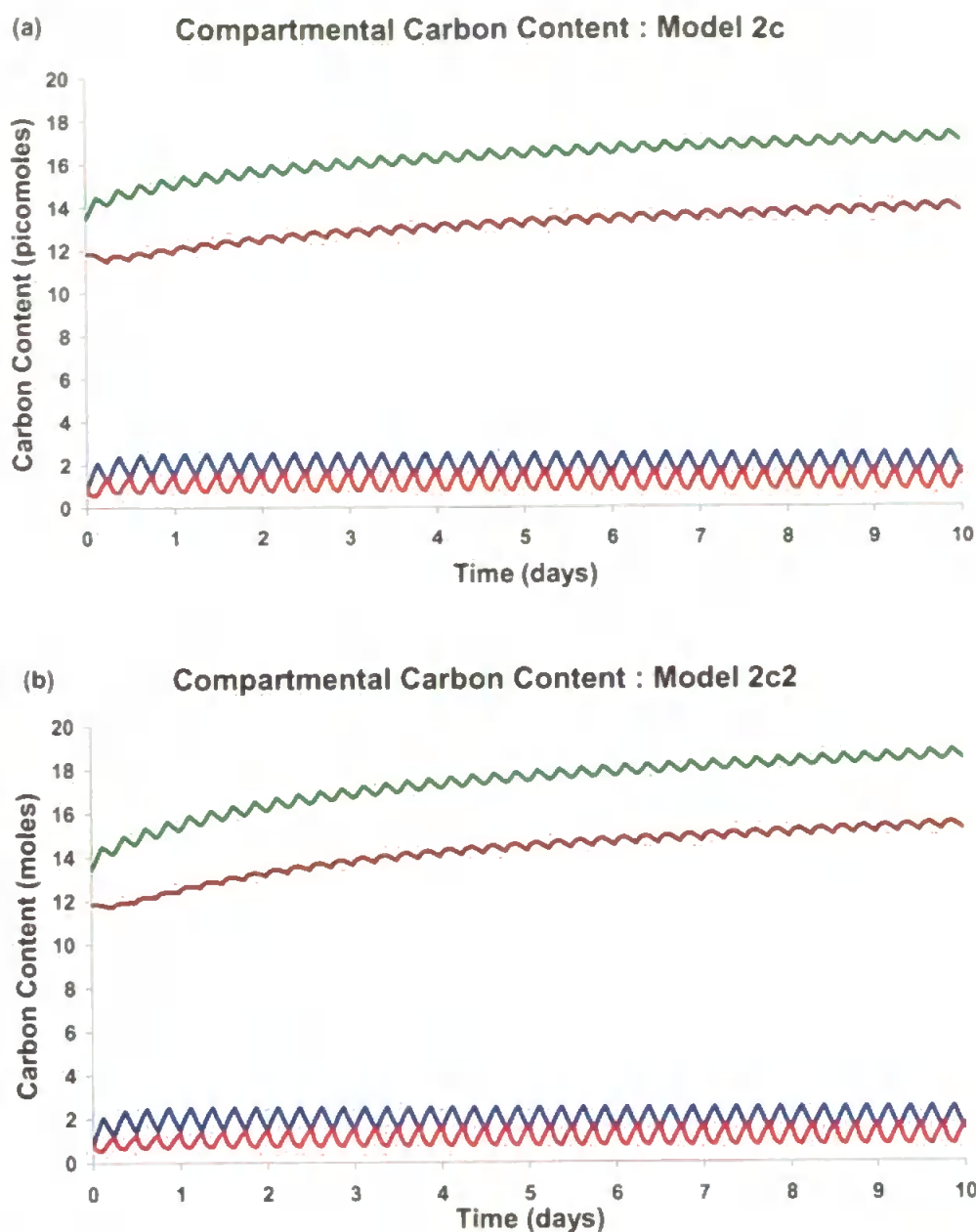


Fig 3.21 Comparison of 10 day simulation of models 2c and 2c2. Feeding regime: 6 hours  $S_c = 6.0$ ,  $f_{dN} = 0.5$  &  $f_{dL} = 0.1$ ; followed by 6 hours of  $S_c = 0$ ,  $f_{dN} = 0.9$  &  $f_{dL} = 0.2$ ;  $L\% = 13\%$ ; ICs same as detailed for Fig 318. Compartmental carbon contents  $E_{xc}$  —,  $L_{xc}$  —,  $C_{xc}$  —,  $G_{xc}$  —,  $Cell_{xc}$  — (a) initial lipid-glycogen model 2c and (b) final volume dependent glycogen model 2c2.

In neither the first or last lipid-glycogen models did the cell ever reach maximum volume (Fig 3.21a) within the model time period and, hence, no export occurred. However, there was an increased carbon content

(Fig 3.21b) and volume compared to model 1h (Fig 2.16). Model 2c2 reached a periodic state if extended to over 20 days, where at the end of feeding the volume is  $1.66 \times 10^{-12}$  litres and the carbon content is  $2.01 \times 10^{-11}$  moles, an increase of 15% volume and 42% carbon on model 1h, which should ensure extended survival under stress. However, the lack of export was a signature of the model not operating correctly and requiring further enhancement.

### 3.6 Discussion

The introduction of storage facilities into the model immediately presented two problems to be solved: 1) how to determine the conditions under which storage takes place; and 2) equally important, how and when these reserves should be utilised. Furthermore, the nature of their incorporation into the previous model needed to be considered in order to allow their effects to be realised.

The twinned introduction of the two storage forms of cellular carbon, glycogen and lipid, also required a model relationship to be formulated between them, in order to be able to explain any observable shared dynamics. Initially, this relationship was disregarded as the two sources were separately introduced to the previous carbon model. However, the later models were constructed in an attempt to utilise the ability of both to enable prolonged survival of the cell. The source of each storage form obviously dictated the construction of each individual sub-model. Thus glycogen, being an internally sourced material and considered in this model to be entirely absent from the food source, was linked only to the cytosolic compartment; whereas lipid, considered as having primarily a dietary source, will by necessity need to be present throughout the three compartment system (Bayne *et.al.*, 1978).

The introduction of glycogen as an entirely separate compartment within the existing model cytosolic compartment bore no resemblance to

the even distribution throughout the cytoplasm commonly observed when it is present (Bayne *et al.*, 1978; Thompson *et al.*, 1974). This form of incorporation was, however, consistent with the premise of compartmentalisation upon which the original model was conceived. Additionally, the idea of imbuing this fictitious compartment with a constant carbon concentration followed in the same vein as the original model. However, the inclusion of this separate compartment within the cytosolic compartment irrevocably altered one of the precepts of the original model; namely, the control condition of a constant cytosolic carbon concentration. If carbon were thought of as a fair indicator of energetic content, then according to the previous model, cell volume was intimately linked to energy levels. By allowing a compact storage form, a smaller cell volume should be able to accommodate a larger energy level than was previously attainable, which from a maintenance perspective appeared to be a more desirable solution. Thus, in order to do so, the model's control condition was chosen to remain exclusive of the glycogen content of the cytosolic compartment.

The initial implementation of the storage mechanism was designed to be the simplest conceivable. If cell volume were below maximum, then it was considered that the cell should utilise all possible incoming resources towards attaining the maximum volume level. Thereafter, the storage of energy in the glycogen form would be initiated until the uppermost level was attained. This storage of energy was linked to the export of material to



the rest of the animal, which was suspended until after the glycogen had reached its maximum limit. Whilst it is recognised that the rest of the animal will continually be requiring and requesting resources from the digestive cells, a simple control algorithm was required to initially incorporate glycogen within the model. What had not been recognised was that by making glycogen levels (and hence storage rates) dependent upon cellular volume the overall cellular metabolic cost would be reduced during growth as the volume of the cytosolic compartment would be fractionally reduced. Furthermore, these methodologies were in better agreement with the observed continual glycogen presence within these cells throughout a seasonal cycle; and, thus, through times of nutritional deprivation and, hence, lower cell volumes.

The release of glycogen to the remainder of the cytosolic compartment was initially reserved for maintaining the cell at maximum volume when appropriate. While this was demonstrated to prolong the survival of a starved cell for a short period as required, the brevity of this extension was disappointing. Indeed, whilst biological similarity was superficially desirable, the inclusion in the model of the glycogen store was essentially a complication, which according to the modelling paradigm should be avoided unless it appreciably allows the simulation results to be validated or converge closer to observation. Hence, the first hypothesis presented in this chapter is refuted, as the function for which this addition was postulated was not shown to yield appreciable heightened survivability

of the cell with this simplistic implementation. However, further enhancements to the model in subsequent chapters reveals that the glycogen store can play a significant role in the cellular dynamics (see Chapter 8).

The separation of lipid from other carbon forms was primarily sought, due to the observed accumulation of this macromolecular form in the lysosome when the cell is subject to toxic stress (reference). This accumulation can be conjectured to impair the lysosomal function as it imbalances the relative concentrations of degradative proteins to target material. Additionally the presence of lipid is a precursor to lipofuscin formation, which can sequester proteins and toxicants within the lysosome, and appears to be trenchantly opposed to removal.

The division of the cellular carbon content into lipid and non-lipid forms required the splitting of all rate processes and the determination of a separate lipid carbon concentration. Since lipid is more often degraded within peroxisomes situated in the cytosol the lysosome is likely to be less efficient at degrading it. Hence, under unstressed conditions it can be speculated that autophagic uptake of lipid would be unpronounced. There are two major problems with this view: firstly, whilst the autophagic process might be targeted against damaged organelles and proteins, due to the act of enveloping this material there would also be an indiscriminant sequestration of ambient material; secondly all material taken up by endocytosis was thought to pass through the endo-lysosomal system and

hence all externally supplied lipid will pass through the lysosome and be subject to the poor degradative rate.

Speculatively these problems might be alleviated if the lysosome were to be possessed of some screening capacity for lipid. Then it could reject this macromolecular form to the cytosol if encountered in small quantities. Then the loss due to degradative inefficiency would be diminished, whilst at greater rates of uptake during stress this screening capacity would be overrun.

Consideration possibly should have been given to adding the peroxisome to the cytosolic compartment. Since this is the site of the majority of lipid breakdown its function under unstressed conditions would have been a further complication. However, under toxic stress the model will be responding to the concentrations of the toxicant in each separate compartment. Possibly the difference in lysosomal and cytosolic toxicant concentrations would have had an important effect on the lipid metabolism, which would not be accounted for under the current scheme.

The lack of an ability, in the model, to synthesise lipid from non-lipid dictated that this storage form was entirely reliant upon external sources for accumulation. This severely restricted the ability to portray this macromolecular form as a storage form in the model. Hence, the second hypothesis of this chapter was undermined from the outset. Equally the poor lysosomal degradative ability led to an evolution which increasingly marginalized the lipid from the main system (e.g. passing only a relatively

small amount to the lysosome). This indicated that the lipid subsystem could not be incorporated into the main model as it stood and be expected to enhance it significantly. Thus this chapter's second hypothesis is also rejected.

Attempts to integrate the lipid and glycogen subsystems highlighted the importance of an overall control algorithm for the model. Given a certain calculated state at the end of a model timestep there was an attempt to backtrack and adjust some relevant rates to meet certain control conditions. This approach was questionable, as these were retrospective adjustments and possibly it would have been better practice to use the state of the cell at the end of the timestep to derive the rates for the next timestep. However, with the given small timesteps the effects are probably trivial.

## Chapter 4 Carbon and Nitrogen Model

### 4.1 Introduction

As part of the original objectives of the project it was considered progressive to augment the carbon-based model by the introduction of a second atomic variable, specifically nitrogen, in order to better incorporate protein turnover and nutritional quality (Hawkins and Bayne, 1991; Hawkins & Day, 1996). The underlying assumption being that the majority of cellular nitrogen was principally either amino acid or protein bound, thus an ability to model the flow of nitrogen in the cell (Fig 4.1) would enhance control and provide a further validation component. In order to achieve this goal, cellular compartments and food were each given a nitrogen content.

The flow of nitrogen in this simple cell model broadly followed that of the carbon. Nitrogen was excluded from the respiration rate which was modelled as being solely a burden on the carbon content; but was connected to a newly added rate of excretion. However, as these are amongst the smallest rates in the model this mutual exclusion provided no significant alteration to the model behaviour. If the inclusion of nitrogen as a second variable was to hold any merit it must significantly contribute to the model performance and its ability to replicate observation. Thus it was postulated that the control of the cytosolic carbon to nitrogen ratio would generate the necessary dynamic variability witnessed in seasonal data (e.g. Thompson *et al.*, 1974) to justify this modification to the model.

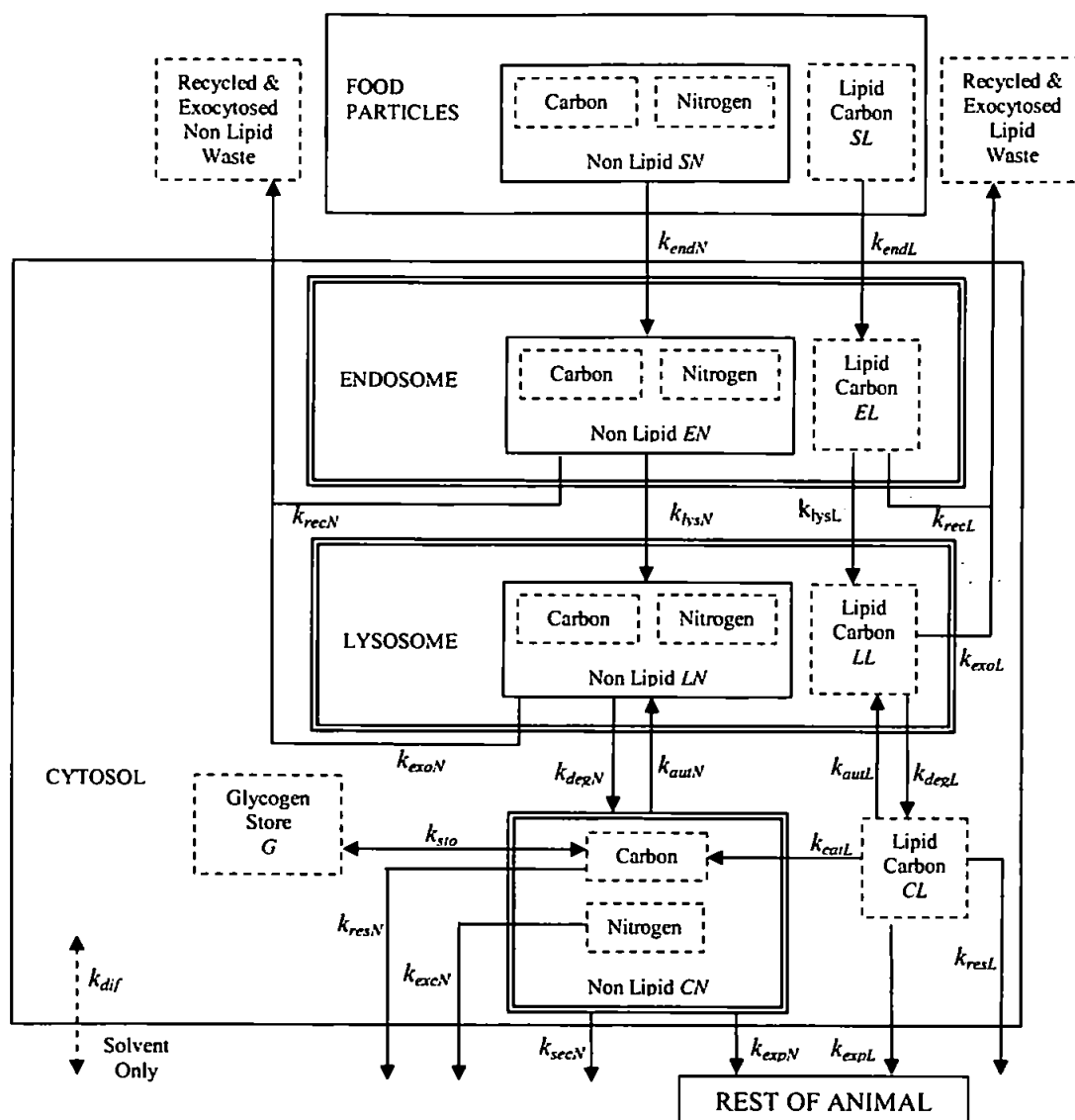


Fig 4.1 Nitrogen and carbon model 3 schematic

The nomenclature for Figure 4.1 and the subsequent ODEs is the same as given in Tables 2.2 & 3.2 appended by Table 4.1.

Table 4.1 Extra variable names for model3 (also see Tables 2.2 & 3.2)

Content variable name	Concentration variable name	Relevant compartment
$EN_{xn}$	$EN_n$	Endosomal non-lipid
$LN_{xn}$	$LN_n$	Lysosomal non-lipid
$CN_{xn}$	$CN_n$	Cytosolic non-lipid
Rate Name	Description	Parameter Values
$k_{excN}$	Rate of excretion	$1.25 \times 10^{-18} - 4.0 \times 10^{-18}$ litres/sec

The system of ODEs under the same assumptions as the initial model is shown below.

### Compartmental Volume Equations

$$\frac{dEN_v}{dt} = k_{endN} - k_{recN} - k_{lysN} \quad [4.1]$$

$$\frac{dEL_v}{dt} = k_{endL} - k_{recL} - k_{lysL} \quad [4.2]$$

$$\frac{dLN_v}{dt} = k_{lysN} + k_{autN} - k_{degN} - k_{exoN} \quad [4.3]$$

$$\frac{dLL_v}{dt} = k_{lysL} + k_{autL} - k_{degL} - k_{exoL} \quad [4.4]$$

$$\frac{dCN_v}{dt} = k_{degN} - k_{autN} - k_{expN} - k_{secN} - k_{resN} - k_{excN} - k_{stoN} + k_{catL} + k_{difN} \quad [4.5]$$

$$\frac{dCL_v}{dt} = k_{degL} - k_{autL} - k_{expL} - k_{catL} \quad [4.6]$$

$$\frac{dG_v}{dt} = k_{stoN} \quad [4.7]$$

### Compartmental Content Equations

$$\frac{dEN_{xc}}{dt} = k_{endN}SN_c - (f_{rN}k_{recN} + k_{lysN})EN_c \quad [4.8]$$

$$\frac{dEN_{xn}}{dt} = k_{endN}SN_n - (f_{rN}k_{recN} + k_{lysN})EN_n \quad [4.9]$$

$$\frac{dEL_{xc}}{dt} = k_{endL}SL_c - (k_{recL} + k_{lysL})EL_c \quad [4.10]$$

$$\frac{dLN_{xc}}{dt} = k_{lysN}EN_c + k_{autN}CN_c - (k_{degN} + k_{exoN})LN_c \quad [4.11]$$

$$\frac{dLN_{xn}}{dt} = k_{lysN}EN_n + k_{autN}CN_n - (k_{degN} + k_{exoN})LN_n \quad [4.12]$$

$$\frac{dLL_{xc}}{dt} = k_{lysL}EL_c + k_{autL}CL_c - (k_{degL} + k_{exoL})LL_c \quad [4.13]$$

$$\begin{aligned} \frac{dCN_{xc}}{dt} = & k_{degN}LN_c - (k_{autN} + k_{expN} + k_{secN} + k_{resN})CN_c \\ & - k_{stoN}G_c + k_{catL}CL_c \end{aligned} \quad [4.14]$$

$$\frac{dCN_{xn}}{dt} = k_{degN}LN_n - (k_{autN} + k_{expN} + k_{secN} + k_{excN})CN_n \quad [4.15]$$

$$\frac{dCL_{xc}}{dt} = k_{degL}LL_c - (k_{autL} + k_{expL} + k_{catL})CL_c \quad [4.16]$$

$$\frac{dG_{xc}}{dt} = k_{sto}G_c \quad [4.17]$$

The total compartmental ODEs are excluded but are merely the addition of the relevant non lipid and lipid ODEs i.e.

$$\frac{dE_v}{dt} = k_{endN} - k_{recN} - k_{lysN} + k_{endL} - k_{recL} - k_{lysL} = k_{end} - k_{rec} - k_{lys} \quad [4.18]$$

The full set of concentration ODEs were derived from the volume and content ODEs but are superfluous to the computational requirements and are not presented; except later in the text where they are necessary for the determination of the rates which control the C:N ratio in the cytosol.



#### 4.2 Control conditions: Model 3

When this model was originally posited the proposition was to have two control conditions: namely, that both the nitrogen and carbon concentration of the cytosol be kept constant. Since the introduction of the lipid and glycogen components in the carbon models, a decision had to be made as to whether or not this would mean the entire cytosol or a select part. Since the glycogen and lipid compartments of the model were bereft of nitrogen content, their increase and decrease would create an imbalance in the carbon to nitrogen ratio of the entire cytosol, so this alternative has been rejected. Instead, it was initially decided to try and achieve the non-lipid and glycogen remainder portion of the cytosol as having constant nitrogen and carbon concentrations, i.e.,

$$\frac{dCN_c}{dt} \equiv 0 \quad \text{and} \quad \frac{dCN_n}{dt} \equiv 0 \quad [4.19]$$

The first of these implied that

$$\frac{dCN_{xc}}{dt} = CN_c \frac{dCN_v}{dt} \quad [4.20]$$

This gave a diffusion rate of

$$k_{diffN} = k_{excN} + k_{degN} \left( \frac{LN_c}{CN_c} - 1 \right) + k_{stoN} \left( 1 - \frac{G_c}{CN_c} \right) + k_{catL} \left( \frac{CL_c}{CN_c} - 1 \right) \quad [4.21]$$

The nitrogen condition required that

$$\frac{dCN_{xn}}{dt} = CN_n \frac{dCN_v}{dt} \quad [4.22]$$

Which led to

$$k_{difN} = k_{degN} \left( \frac{LN_n}{CN_n} - 1 \right) + k_{resN} + k_{stoN} - k_{catL} \quad [4.23]$$

Which if the storage and catabolism was to be determined as before gave a means for calculating the newly introduced excretion rate:

$$k_{excN} = k_{resN} + k_{degN} \left( \frac{LN_n}{CN_n} - \frac{LN_c}{CN_c} \right) + k_{stoN} \frac{G_c}{CN_c} - k_{catL} \frac{CL_c}{CN_c} \quad [4.24]$$

Using the maximum and minimum rates of glycogen storage and lipid catabolism,  $k_{stoN}$  and  $k_{catL}$  from model 2c2 and using other theoretical limits gave the following bounds on possible values for the excretion rate:

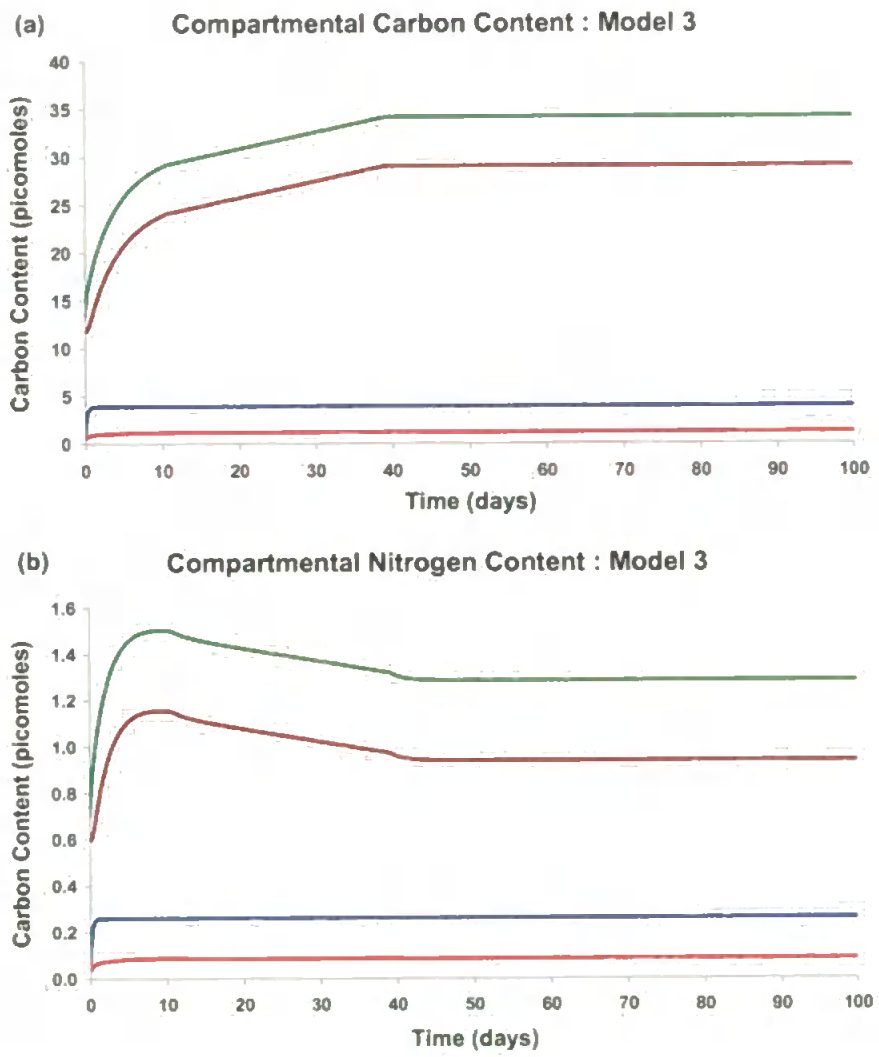
$$-3.92 \times 10^{-15} \leq k_{excN} \leq 1.7 \times 10^{-16} \quad [4.25]$$

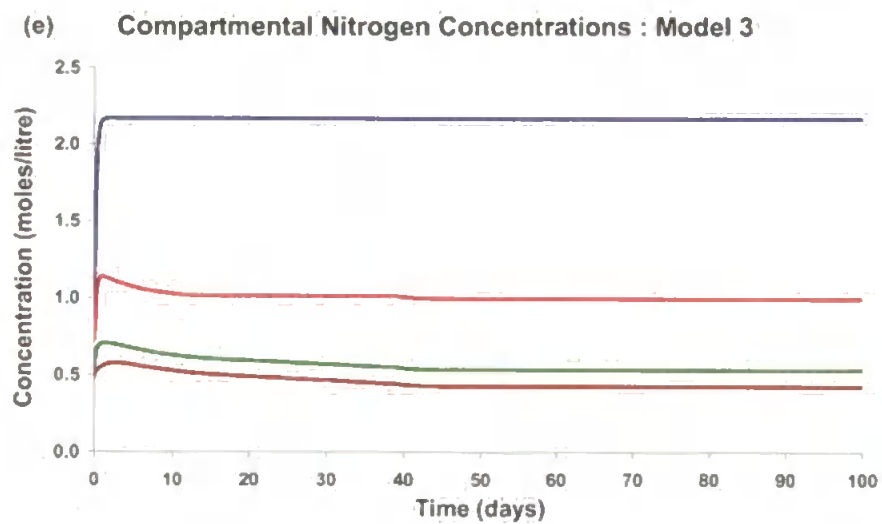
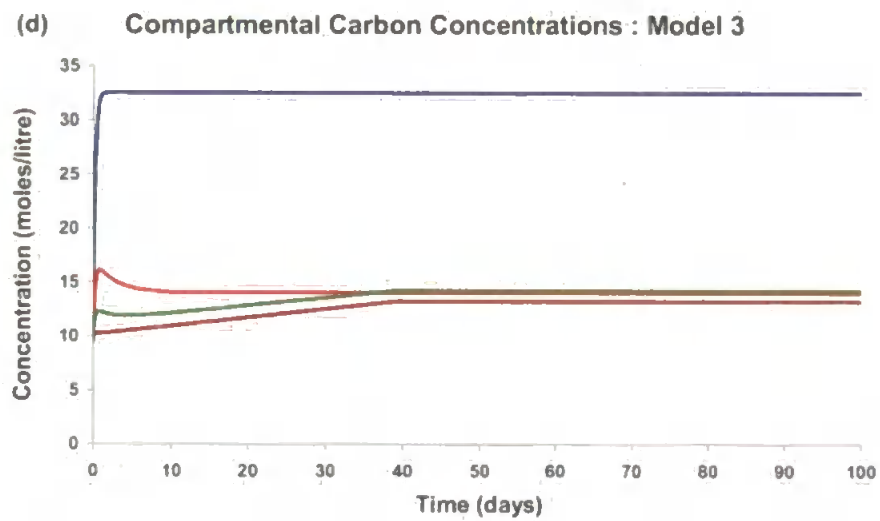
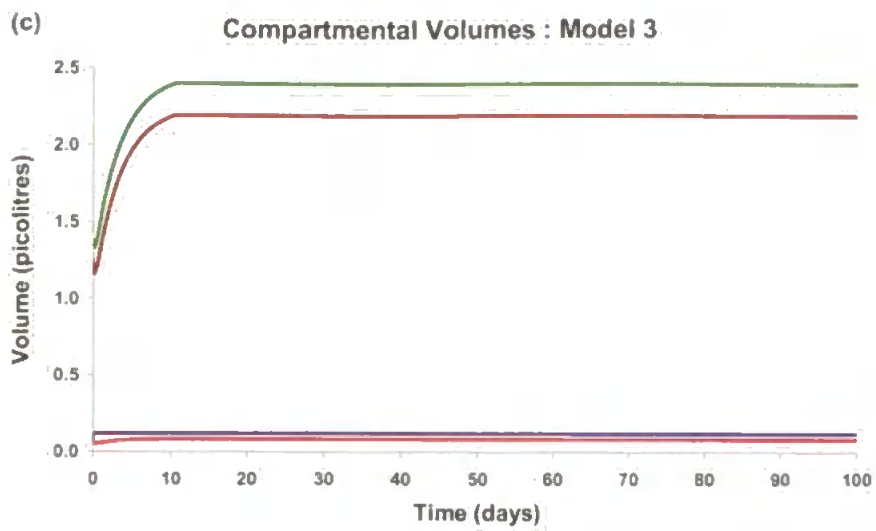
The average value would give a clearly unacceptable negative effluent rate; whilst the maximum rate was far greater than those observed.

The incongruity of these three control conditions was due to two factors. The first was the distinct possibility of material entering the cytosol from the lysosome with a different C:N ratio to a given cytosolic C:N control ratio. The second was the carbon only storage forms which affected only the carbon content. Finally the transfer of either material exclusively by the respiration and excretion rates would upset the C:N balance. Whilst respiration should be considered a function of cellular activity; excretion could be deemed an appropriate control function but did not possess the parameter range to enable the likely necessary flexibility.

In order to see the effects of the nitrogen inclusion, a decision was made to temporarily exclude the nitrogen control condition and proceed

with just the one carbon control condition. With a 100 day simulation and food provided at maximum concentrations for both carbon and nitrogen, recognisable behaviour, similar to model 2c2 was generated for carbon content, concentrations and overall volumes.





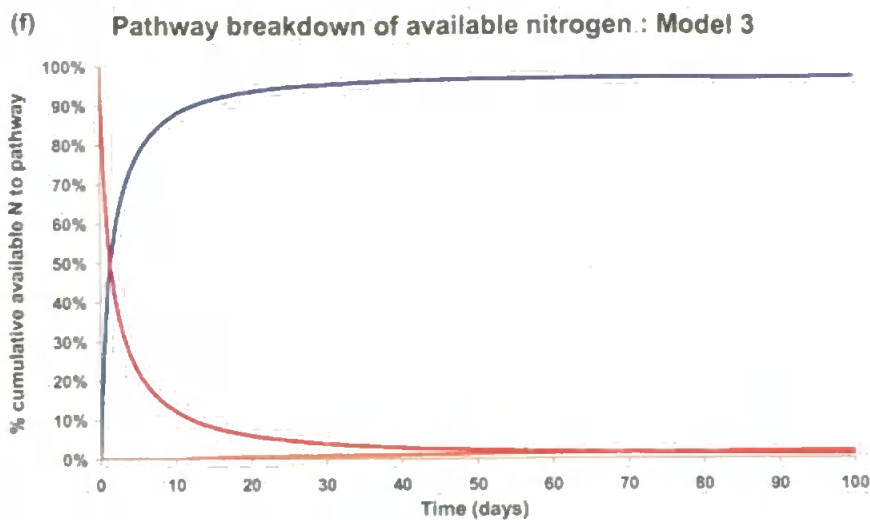
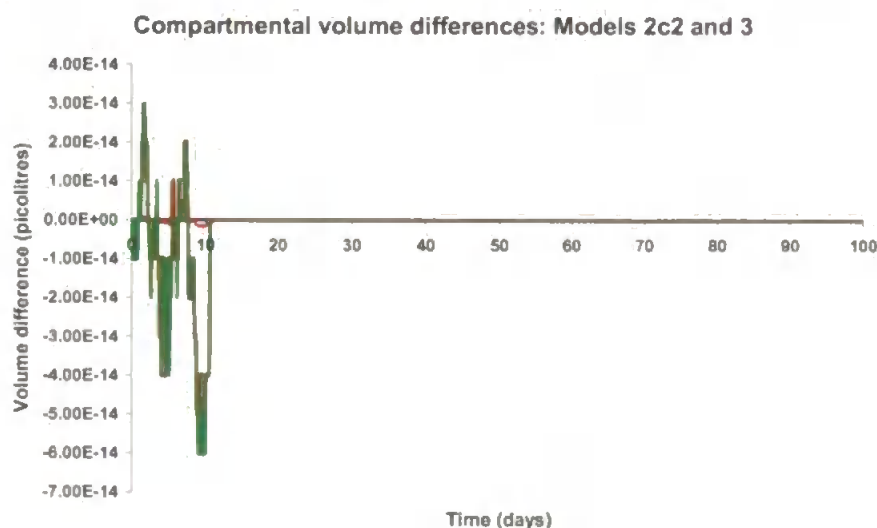


Fig 4.2 100 day simulation of model 3 carbon and nitrogen model. Feeding regime:  $S_c = 6.0$ ;  $S_n = 0.4$ ;  $L\% = 13\%$ ;  $f_{dN} = 0.9$ ;  $f_{dL} = 0.1$ . ICs:  $Cell_v = 1.3764$  picolitres;  $f_{ev} = f_{lv} = 4.45\%$ ;  $E_c = 11.927$ ;  $E_n = 0.794$ ;  $L_c = 14.869$ ;  $L_n = 0.892$ ;  $CL_c = 33.2$ ;  $G_c = 16.6$ ;  $CN_c \cong 8.3$ ;  $CN_n = 0.5$ ; (a) Compartmental carbon contents —  $E_{xc}$ , —  $L_{xc}$ , —  $C_{xc}$ , —  $Cell_{xc}$  (b) compartmental nitrogen contents —  $E_{xn}$ , —  $L_{xn}$ , —  $C_{xn}$ , —  $Cell_{xn}$  (c) compartmental volumes —  $E_v$ , —  $L_v$ , —  $C_v$ , —  $Cell_v$  (d) compartmental carbon concentrations —  $E_c$ , —  $L_c$ , —  $C_c$ , —  $Cell_c$  (e) compartmental nitrogen concentrations —  $E_n$ , —  $L_n$ , —  $C_n$ , —  $Cell_n$  and (f) % breakdown of nitrogen pathway — Lost, — Stored, — Exported.

The nitrogen content had a more rapid initial increase than the carbon content (Figs 4.2 a & b). This was due to the maximum carbon food concentration being relatively less than the carbon control concentration than the equivalent nitrogen ratio. Additionally, there was the necessity to fill the extra storage compartments associated with the total carbon pool i.e. the less well lysosomally degraded lipid and the glycogen store. However, once maximum cell volume was attained (Fig 4.2c) there was a decline in nitrogen content (Fig 4.2b) as the lipid increased, until it too was at its

highest level; thereafter, an equilibrium state was achieved for all variables. Under these feeding conditions, despite having no explicit control mechanism, the cytosolic nitrogen concentration, whilst variable at first, achieved equilibrium close to the real observed value (Fig 4.2e). The comparison of the fate of each element revealed: exported carbon = 1.56%; exported nitrogen = 1.8%; stored carbon = 1.96%; stored nitrogen = 1.11%; lost carbon = 96.48%; and lost nitrogen = 97.09%. Hence, while more nitrogen was lost from the cell and nitrogen reserves in this cell were lower than those for carbon, there had, nonetheless, been more exported to the rest of the animal's tissues for utilisation there.



*Fig 4.3 Comparison of 100 day simulations of models 2c2 & 3. ICs : model 2c2 as described for Fig 2.54; model 3 as described for Fig 4.2; Feeding regime:  $S_c = 6.0$ ;  $S_n = 0.4$  (model 3 only);  $L\% = 13\%$ ;  $f_{dN} = 0.9$ ;  $f_{dL} = 0.1$ . Differences between compartmental volumes. Key: —  $E_v$ , —  $L_v$ , —  $C_v$ , —  $Cell_v$ .*

The relative innocuousness of the introduction of nitrogen into the model was revealed by comparing the differences in volume between the

same simulation on model 2c2 and model 3, which despite the introduction of excretion showed minimal differences after the initial period of accumulation (Fig 4.3).

Further evidence of the insignificance of this particular method of introducing the nitrogen component was revealed when the model was given food at maximum carbon concentration but zero nitrogen. The lack of influence of nitrogen content (Fig 4.4b) on carbon content (Fig 4.4a) was readily apparent and signified that the model, in this state, was not sufficiently well formulated to make the inclusion of nitrogen worthwhile. It was noteworthy that the lack of nitrogen in the food had not reduced the endocytotic rate, since this had remained unchanged and was only a function of the food carbon concentration. This anomaly was addressed in the next section.

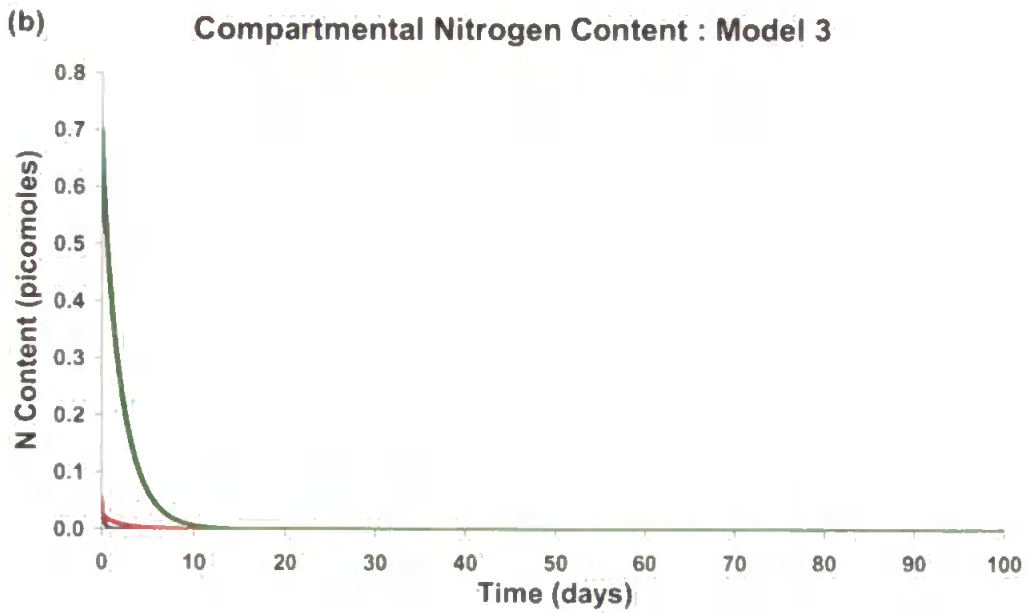
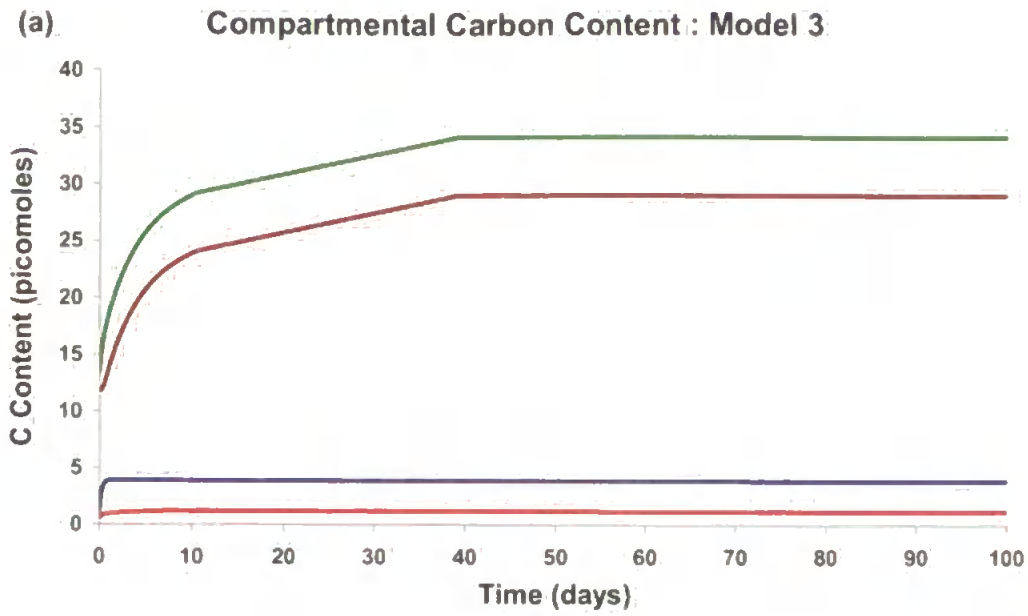


Fig 4.4 100 day simulation of Model 3. Feeding regime:  $S_c = 6.0$ ;  $S_n = 0.0$ ;

$L\% = 13\%$ ;  $f_{dN} = 0.9$ ;  $f_{dL} = 0.1$ . ICs as described for Fig 4.2. and lipid% =

13%. (a) carbon content —  $E_{xc}$ , —  $L_{xc}$ , —  $C_{xc}$ , —  $Cell_{xc}$  (b) nitrogen content —

$E_{xn}$ , —  $L_{xn}$ , —  $C_{xn}$ , —  $Cell_{xn}$ .



### 4.3 Nitrogen control: Model 3a

Thus the next submodel used the second control condition in favour of the first, i.e. non lipid-glycogen cytosolic nitrogen concentration was kept constant. This allowed the possibility that the levels of glycogen and lipid may admit a means for control of the overall cytosolic carbon concentration in circumstance when this measure was less than required.

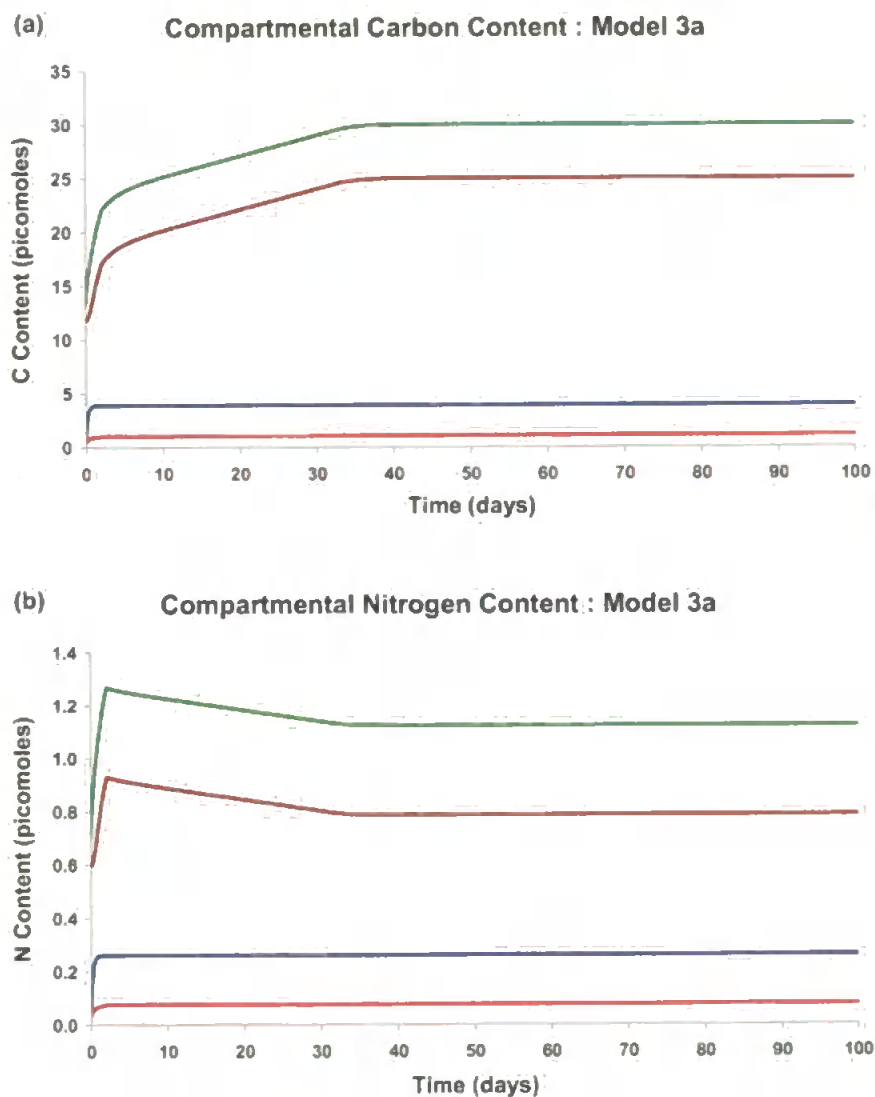


Fig 4.5 100 day simulation of model 3a, nitrogen constraint. Feeding regime:  $S_c = 6.0$ ;  $S_n = 0.4$ ;  $L\% = 13\%$ ;  $f_{dN} = 0.9$ ;  $f_{dL} = 0.1$ . ICs as described for Fig 4.2. (a) carbon content —  $E_{xc}$ , —  $L_{xc}$ , —  $C_{xc}$ , —  $Cell_{xc}$  (b) nitrogen content —  $E_{xn}$ , —  $L_{xn}$ , —  $C_{xn}$ , —  $Cell_{xn}$ .

Under this scheme there was less content of both elements in the cell both at the times of maximum carbon and nitrogen content and in the equilibrium state (Figs 4.5a, b). Furthermore, there was a far sharper change in the nitrogen behaviour once the cell volume limit was reached, which at least recommended itself as the nitrogen having some effect on cellular behaviour.

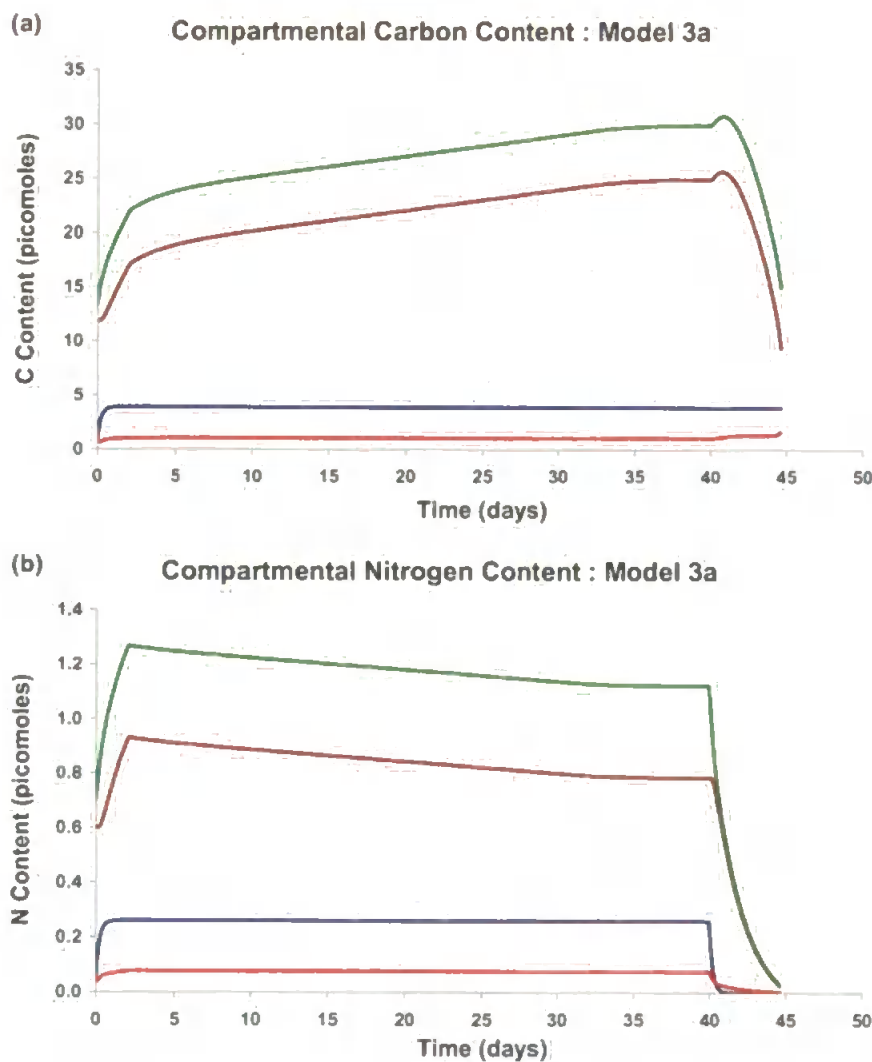


Fig 4.6 50 day simulation of model 3a. Feeding regime: Days 0-40,  $S_c = 6.0$  &  $S_n = 0.4$ , Days 40-50,  $S_c = 6.0$  &  $S_n = 0.0$ ;  $L\% = 13\%$ ;  $f_{dN} = 0.9$ ;  $f_{dL} = 0.1$ . ICs as described for Fig 4.2. (a) carbon content —  $E_{xc}$ , —  $L_{xc}$ , —  $C_{xc}$ , —  $Cell_{xc}$  (b) nitrogen content —  $E_{xn}$ , —  $L_{xn}$ , —  $C_{xn}$ , —  $Cell_{xn}$ .

A simulation designed to show the effect of taking away protein from the diet was conducted (Fig 4.6). The simulation was run for 40 days at maximum food concentrations thereafter the food nitrogen concentration was dropped to zero whilst the carbon remains at maximum. With the current system the model ceased to operate within the prescribed bounds within 5 days. This rapid response to the dietary perturbation was primarily due to the autophagocytosed loss of nitrogen, and was exacerbated by the lack of control exerted by nitrogen deficiency on endocytosis. Similarly, the lysosomal degradative efficiency was still only linked to incoming carbon.

In order to simulate a scenario when there was only proteinaceous material available an “average amino acid” had been constructed; for which a C:N ratio based on the relative frequency of amino acids in proteins have been determined ( Table 4.2; Lodish *et al.*, 1999).

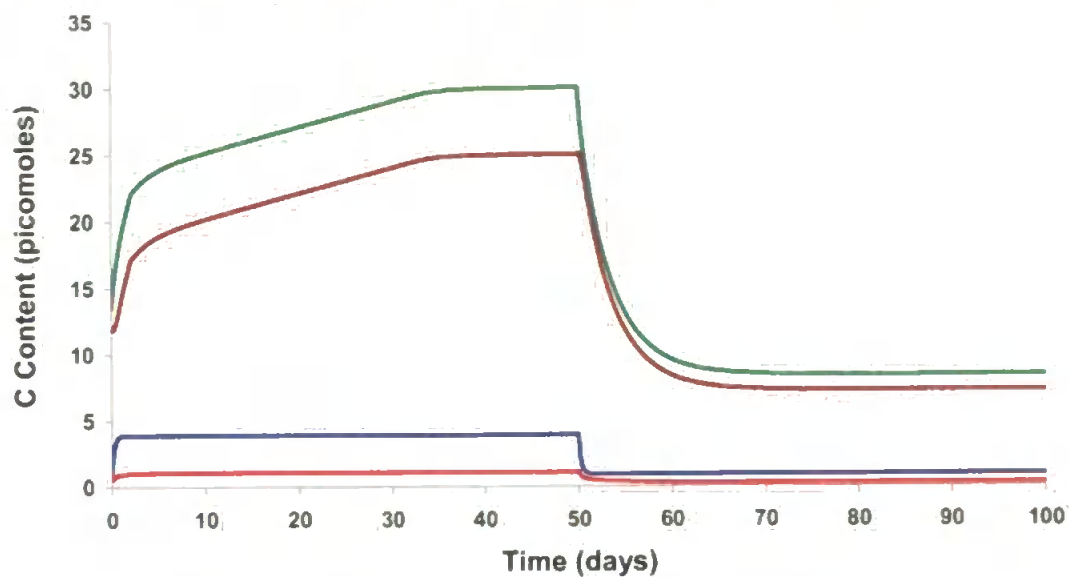
From Table 4.2 it was ascertained that the molar carbon content of proteinaceous material was approximately three and half times that of nitrogen (8.1% to 28.55). One consequence of this was that the carbon concentration of the food must be at least this factor greater than that of the nitrogen; any C:N ratio higher than this would indicate the presence of lipid and/or carbohydrate material.

*Table 4.2 Element composition of relative frequency amino acids*

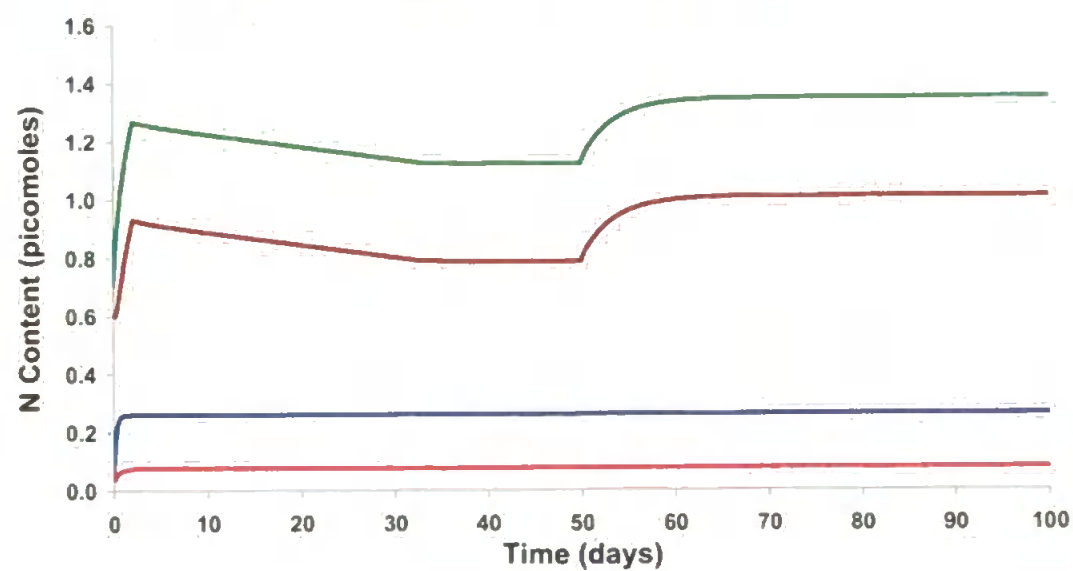
	N	H	C	S	O	AM
Proline	0.048462	0.387692	0.242308	0	0.096923	4.41
Glycine	0.048462	0.242308	0.096923	0	0.048462	2.132308
Cysteine	0.016667	0.116667	0.05	0.016667	0.016667	1.233333
Tryptophan	0.033333	0.216667	0.183333	0	0.016667	2.783333
Tyrosine	0.048462	0.581538	0.436154	0	0.096923	6.93
Phenylalanine	0.048462	0.533077	0.436154	0	0.048462	6.493846
Methionine	0.016667	0.183333	0.083333	0.016667	0.016667	1.7
Leucine	0.08	1.04	0.48	0	0.08	8
Isoleucine	0.048462	0.63	0.242308	0	0.048462	4.264615
Valine	0.048462	0.533077	0.242308	0	0.048462	4.167692
Alanine	0.048462	0.339231	0.145385	0	0.048462	2.810769
Glutamine	0.096923	0.484615	0.242308	0	0.096923	4.846154
Asparagine	0.096923	0.387692	0.193846	0	0.096923	4.167692
Threonine	0.048462	0.436154	0.193846	0	0.096923	3.876923
Serine	0.08	0.56	0.24	0	0.16	5.28
Glutamic	0.08	0.64	0.4	0	0.24	7.92
Aspartic	0.048462	0.290769	0.193846	0	0.145385	4.119231
Lysine	0.24	0.8	0.48	0	0.08	8.88
Arginine	0.193846	0.726923	0.290769	0	0.048462	5.960769
Histidine	0.096923	0.726923	0.290769	0	0.048462	5.282308
Total	1.467436	9.856667	5.16359	0.033333	1.579231	95.25897
%	8.1%	54.5%	28.5%	0.2%	8.7%	
Weight	10.3	9.9	62.0	0.5	12.6	95.25897
% By weight	10.8%	10.3%	65.0%	0.6%	13.3%	

Given a well-fed cell subject to a diet rich in both nitrogen and carbon, which had reached an equilibrium after 50 days, the effects of switching the diet to purely protein was to decrease the overall carbon and increase nitrogen content (Figs 4.7a,b). Lipid content obviously decreased with the switch to the high protein diet, with glycogen following suit, as it was a function of total carbon content (Fig 4.7c). Despite this disruption, the cell was still able to retain maximum volume and continue exporting material to the rest of the animal (Fig 4.7d), albeit at a reduced rate for carbon, but apparently unaffected for nitrogen.

(a) Compartmental Carbon Content : Model 3a



(b) Compartmental Nitrogen Content : Model 3a



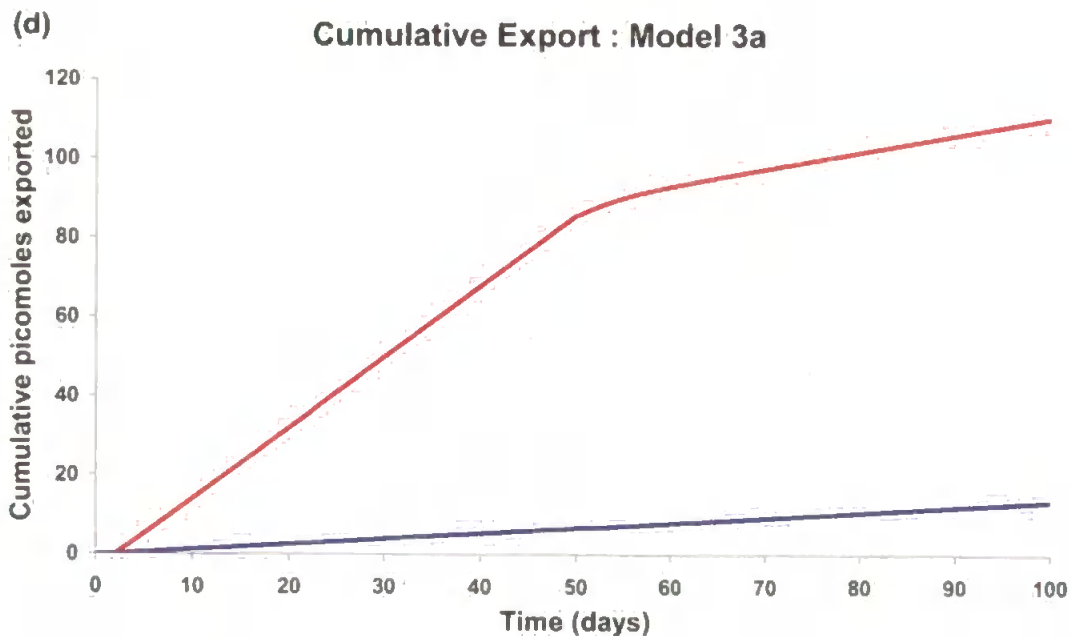
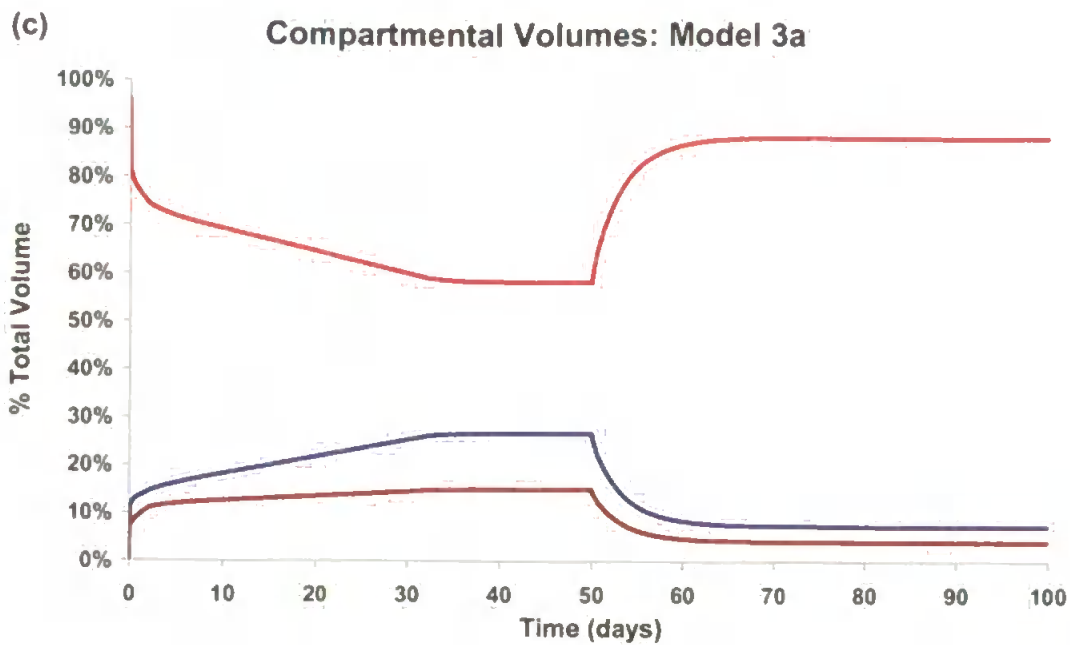


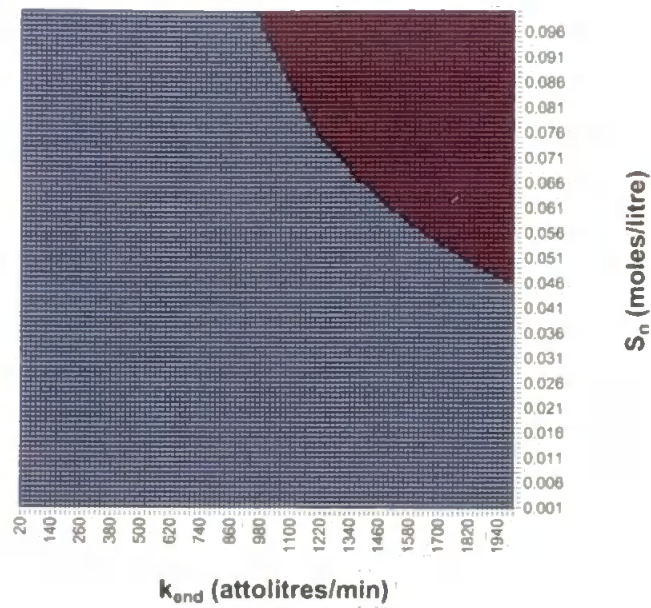
Fig 4.7 100 day simulation of model 3a. Feeding regime: Days 1-50,  $S_c = 6.0$ ,  $S_n = 0.4$  &  $L\% = 13\%$ ; Days 50-100,  $S_c = 1.4$ ,  $S_n = 0.4$  &  $L\% = 0$ ;  $f_{dN} = 0.9$ ;  $f_{dL} = 0.1$ . ICs as described for Fig 4.2. (a) Carbon content —  $E_{xc}$ , —  $L_{xc}$ , —  $C_{xc}$ , —  $Cell_{xc}$  (b) nitrogen content —  $E_{xn}$ , —  $L_{xn}$ , —  $C_{xn}$ , —  $Cell_{xn}$  (c) — lipid; — glycogen and — remainder volumes expressed as percentage of total cell volume (d) cumulative export — Nitrogen & — Carbon.

Since a surfeit of nitrogen appeared to provoke no problems for the system, while deprivation led to swift expiry, a nitrogen maintenance level akin to that found for carbon in the earlier models needed to be evaluated; in order to know when to instigate protective or reactive measures. In terms of the evolving model, these could have included an increase in autophagy and a concomitant increase in degradative recycling efficiency of cytosolic-sourced material, or else, a modification to endocytotic behaviour.

By varying the levels of food nitrogen concentration and the endocytotic rate (Fig 4.8a) the smallest nitrogen molar flux, which keeps the simulation running for over 100 days, could be calculated, with initial conditions based around the cell volume being maximum to start with, and food carbon concentration always at maximum. From this data, the values along the boundary between survival and death gave the series shown in Figure 4.8b, from which a maintenance nitrogen level was derived as the minimum value of this series as  $S_{nmain} = 9.1 \times 10^{-17}$  moles N per minute.

(a)

**Nitrogen Maintenance Model 3a**



(b)

**Maintenance nitrogen: Model 3a**

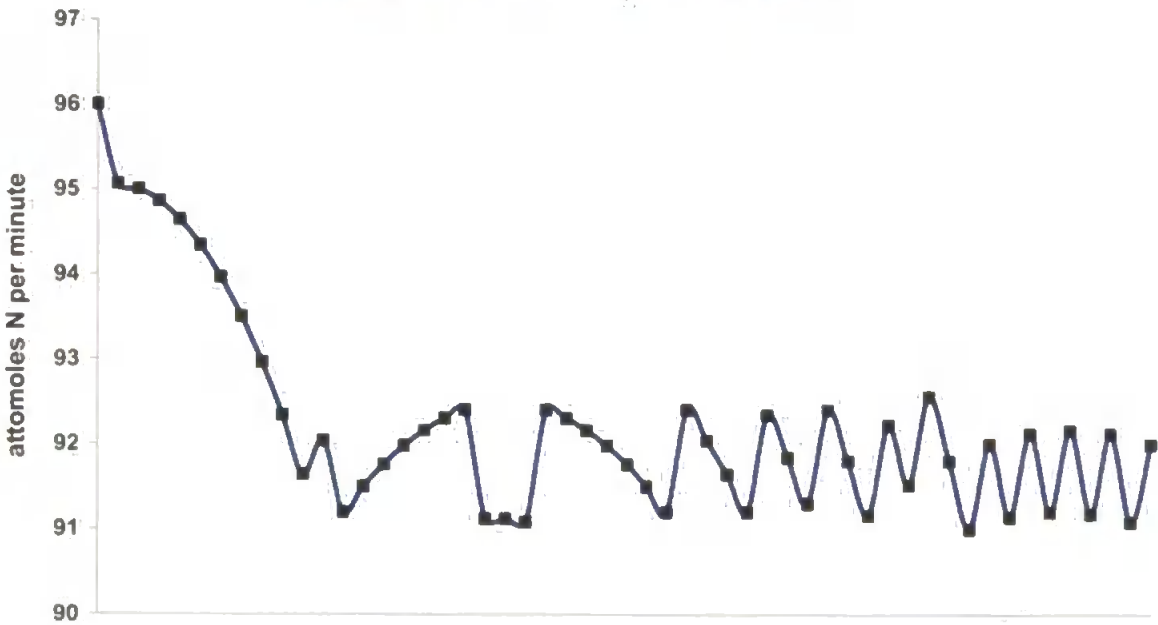


*Fig 4.8 100 day simulations of Model 3a health function. ICs as for Fig 4.2 and varying rates of endocytosis and food nitrogen concentrations (a) Health function showing death before 100 days (■) or survival (■) on small part of parameter space (b) Nitrogen maintenance series*



#### 4.4 Nitrogen controlled autophagy & digestive efficiency: Model3b

Model 3b attempted to utilise this maintenance level of nitrogen by augmenting the previous system with an increase in autophagy and degradative efficiency derived linearly from this value. If there was insufficient nitrogen entering the cell, i.e.  $k_{end} \times S_n < S_{nmain}$  then the revised autophagy (denoted with asterisk) and digestive efficiency were calculated as:

$$k_{aut}^* = k_{aut} \times (1 + 2.0 \times (1 - (k_{end} \times S_n) / S_{nmain})) \quad [4.26]$$

$$f_{dN} = 0.5 + 0.4 \times (1 - (k_{end} \times S_n) / S_{nmain})) \quad [4.27]$$

With a simulation run for 50 days to provide the healthy cell and thereafter with no nitrogen in food the augmented autophagy and degradative efficiency of the lysosome failed to help the cell last for much longer than 10 days (Fig 4.9b). Especially poor, was the proportion of cellular nitrogen which was, upon onset of augmented autophagy, resident in the lysosome, approaching almost entire cellular content (96.55%) at its peak (Fig 4.9a).

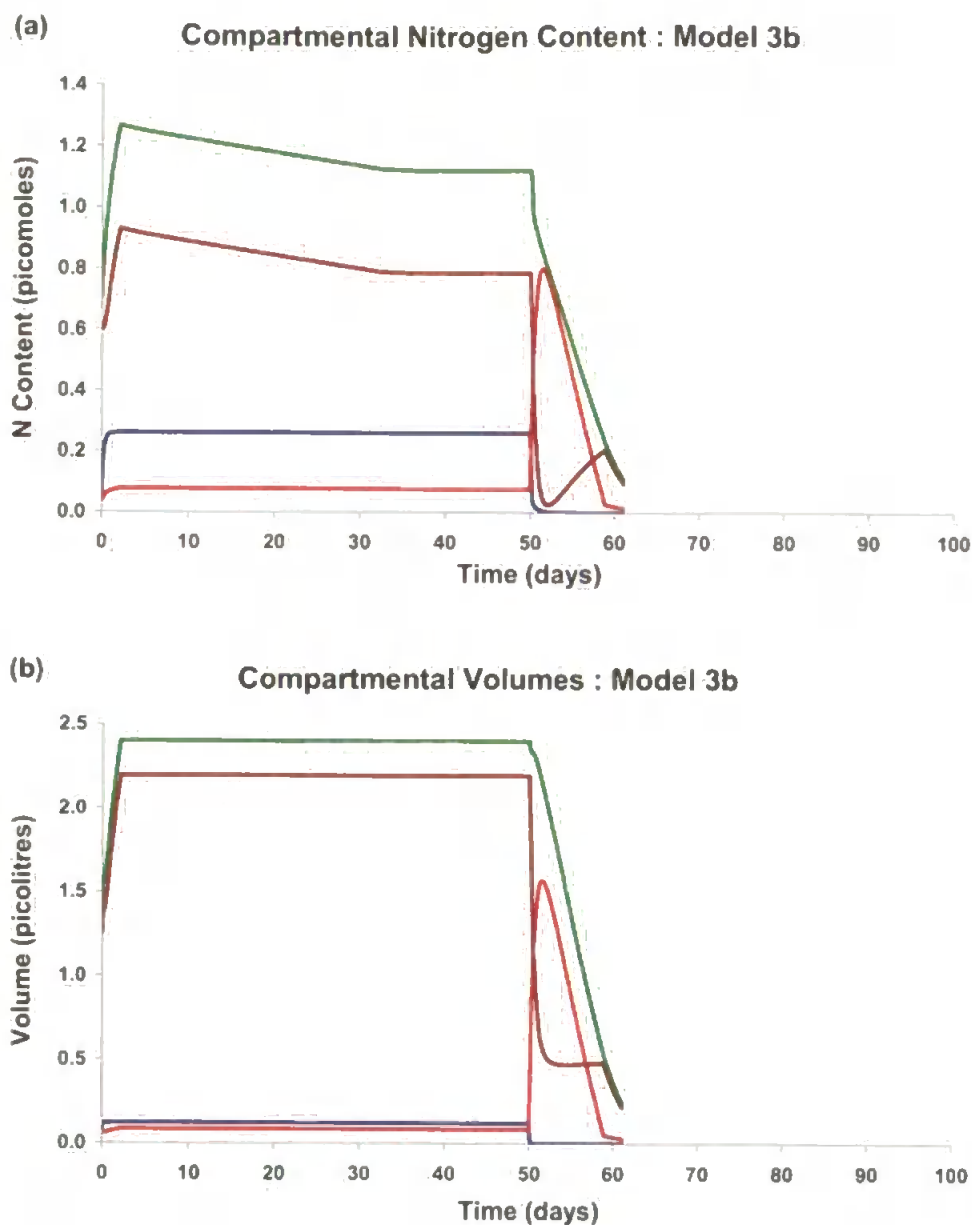
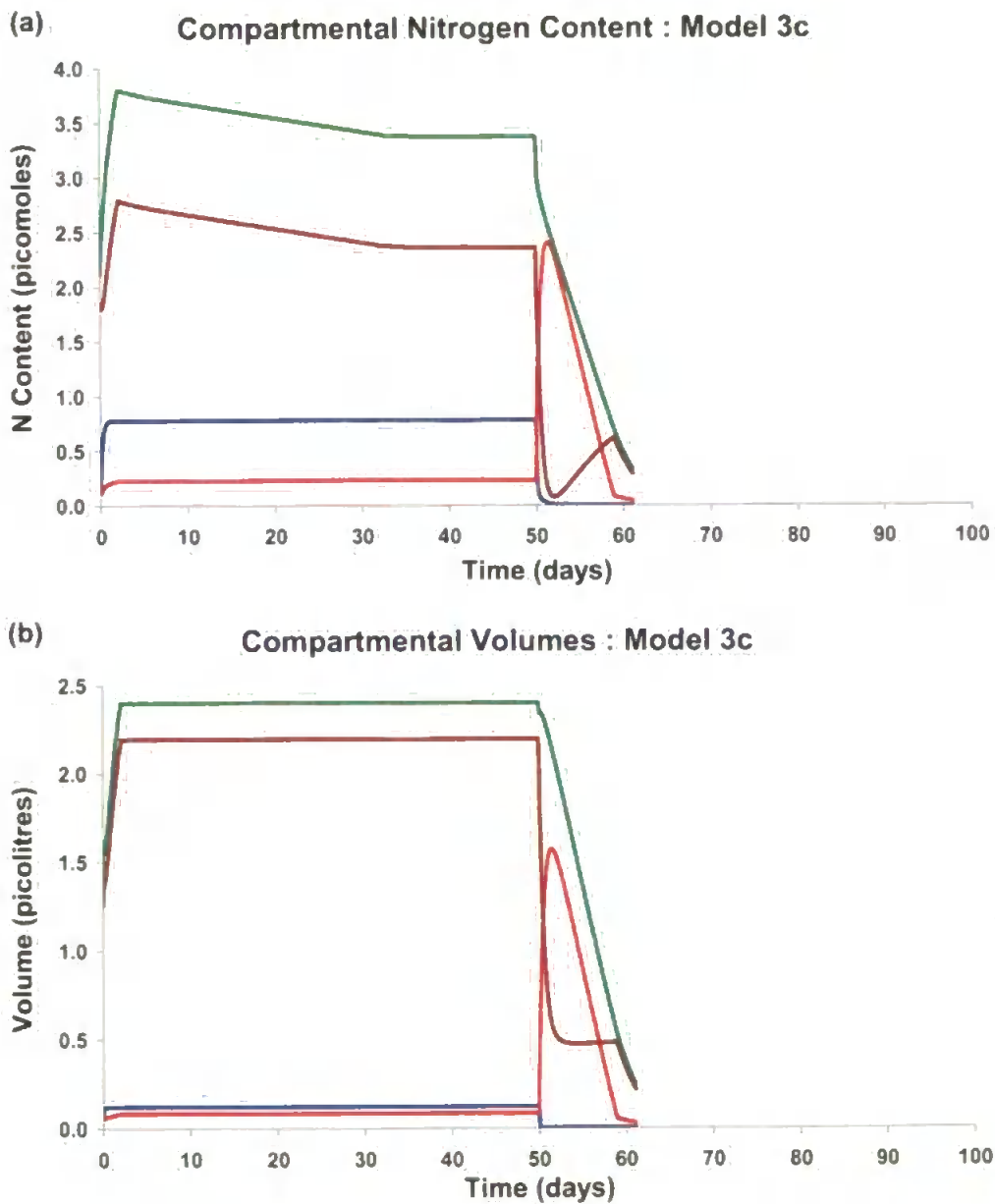


Fig 4.9 Simulation designed to observe survival of model3b, augmented autophagy and digestive efficiency, due to nitrogen deprivation. Feeding regime: Days 0-50  $S_c = 6.0$  &  $S_n = 0.4$ ; Days 50-  $S_c = 6.0$  &  $S_n = 0.0$ ;  $L\% = 13\%$ ; Days 50-100,  $S_c = 1.4$ ,  $S_n = 0.4$  &  $L\% = 0$ ;  $f_{dN} = 0.9$ ;  $f_{dL} = 0.1$ . ICs as described for Fig 4.2. (a) Nitrogen contents —  $E_{xn}$ , —  $L_{xn}$ , —  $C_{xn}$ , —  $Cell_{xn}$  (b) compartmental volumes —  $E_v$ , —  $L_v$ , —  $C_v$ , —  $Cell_v$ .

Reflection on nitrogen dynamics led to a review of seasonal data (see Chapter 6 for details) which provoked a change in parameters. From this

analysis it was established that the C:N control ratio for the model, up to this point, had been far too small - by approximately a factor of three. Hence, it was decided that, henceforth, the parameters for nitrogen should be trebled, e.g.,  $C_n = 1.5$ ,  $S_{nmax} = 1.2$ . In order to see whether this would have an effect on the present system, the same simulation was run again with these values as Model3c.



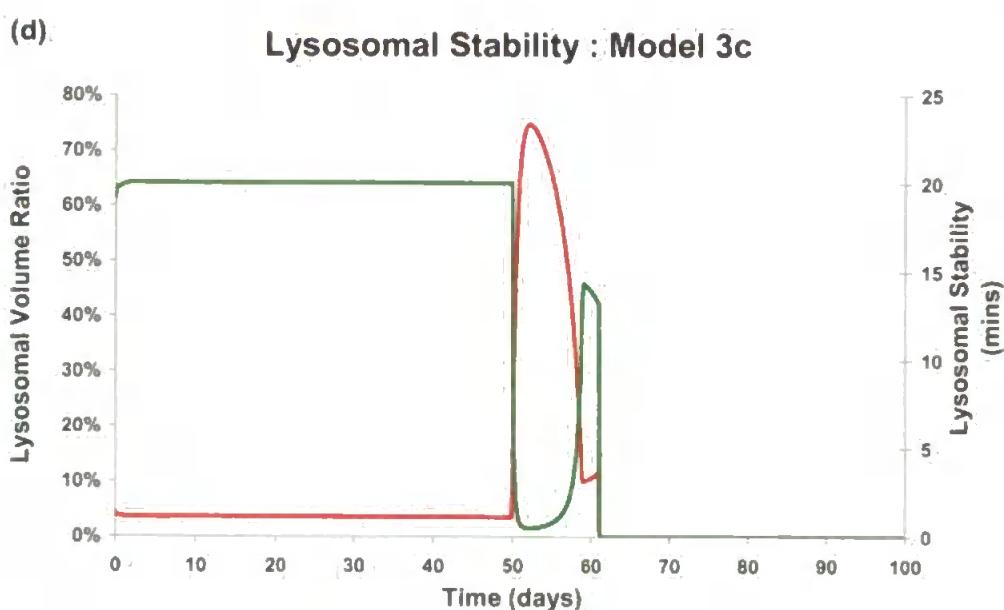
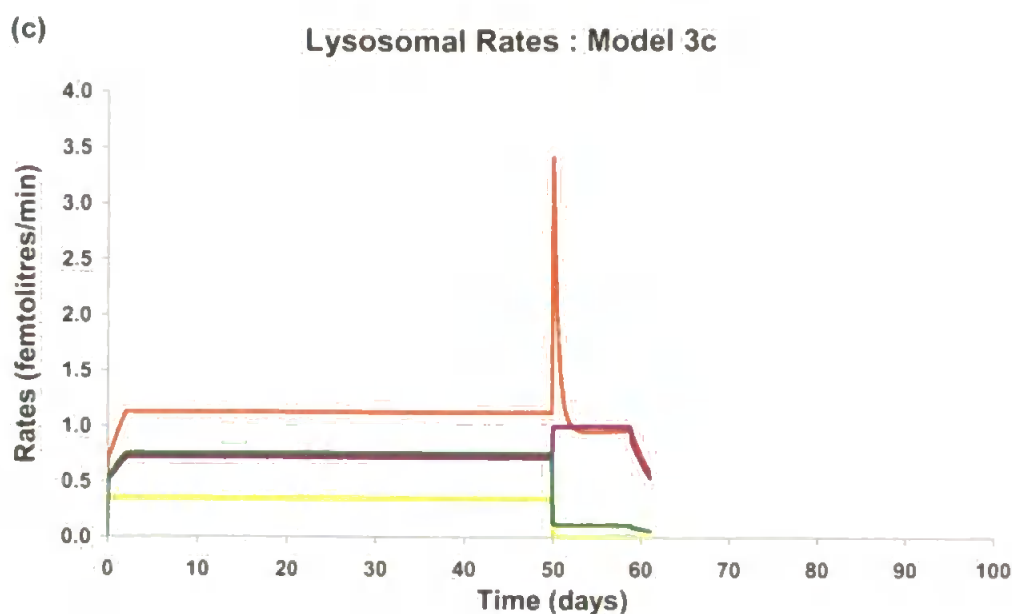


Fig 4.10 Simulation designed to observe survival of model3c, new nitrogen concentrations, with nitrogen deprivation. Feeding Regime: Days 0-50,  $S_c = 6.0$  &  $S_n = 0.4$ ; Days 50-100  $S_c = 6.0$  &  $S_n = 0.0$ ;  $L\% = 13\%$ . ICs:  $Cell_v = 1.3764$  picolitres;  $f_{ev} = f_{lv} = 4.45\%$ ;  $E_c = 11.927$ ;  $E_n = 2.382$ ;  $L_c = 14.869$ ;  $L_n = 2.676$ ;  $CL_c = 33.2$ ;  $G_c = 16.6$ ;  $CN_c = 8.3$ ;  $CN_n \equiv 1.5$  (a) Nitrogen contents —  $E_{xn}$  —  $L_{xn}$  —  $C_{xn}$  —  $Cell_{xn}$  (b) compartmental volumes —  $E_v$  —  $L_v$  —  $C_v$  —  $Cell_v$  (c) lysosomal rates  $k_{lvs}$  —  $k_{aut}$  —  $k_{deg}$  —  $k_{exo}$  — (d) exponential derived lysosomal stability — &  $f_{lv}$  —.

Despite the increased cellular nitrogen content at the onset of deprivation (Figs 4.9a & 4.10a) the dynamics of the cell were similar, with cell death occurring at the same time (Fig 4.9b & 4.10b). The change in nitrogen concentration increased content; but the initial assumption of the model, that has removal of material (carbon or nitrogen) at average concentrations, meant that all material may leave just as quickly as it entered, hence it was the determination of the rates of exit which was crucial. Despite the increased efficiency of the lysosome under stress, the amount of material (carbon and nitrogen) which was being passed to this organelle was too great, and even a 10% loss at this rate was too much for the system to sustain (Fig 4.10c). The increase in autophagy was also called into question as the lysosomal stability (Fig 4.10d) plummeted during this period, due to the swelling of the lysosome relative to cell volume.

It was then concluded that because of its centrality in the stress response, the lysosome required further attention (Moore *et al.*, 2006a, 2007). Hence, with regard to this fact, it was decided to view the lysosome as a blind processing unit. Explicitly, material entering the lysosome would be processed and ejected after a certain delay. This delay and the amount of waste product would be made dependent on the source of the incoming material and the amount of material queuing for attention. However, this necessitated establishing some value for the capacity of the lysosome to do work, i.e. some form of notional throughput based on internal characteristics.

There further remained to be resolved, what to do for imbalanced input from endocytosis? Also, an adaptive mechanism for cellular response to deficiency in one or both of the elemental variables would need to be established if this model were to be developed further.

#### *4.5 Discussion*

The reason for introducing a second chemical variable into the model was to increase biological verisimilitude. Nitrogen was chosen for its crucial association with proteins and amino acids. In order to incorporate the new variable, most existing compartments were imbued with a nitrogen concentration and content. Whilst lipid membranes contain various proteins they were assumed to either remain as a constant proportion and, hence, could be disregarded; or else, taken to contain negligible nitrogen in comparison to other compartments. Similarly, glycogen contains no nitrogen and, hence, this compartment was left in its previous state.

By controlling the cytosolic nitrogen and carbon concentrations, it was originally envisaged that both energy and protein metabolism, and their regulation could be assimilated into the model. However, the only newly introduced rate was cellular excretion; the evacuation of nitrogenous waste material from the deamination of amino acids. This was assumed to take material out of the cell at the average cytosolic nitrogen concentration, but exclusive of carbon. In addition, all other rates were assumed to take material from the relevant source compartment at average nitrogen and carbon concentrations, except for respiration, which took only carbon dioxide and, hence, no nitrogen. However, it became evident that even with a revised diffusion rate, and these exclusive nitrogen or carbon pathways, there was no way the model could manage to keep both control conditions

simultaneously. Partly, this is due to the parameter limits set upon the respiration and excretion rates, as well as the assumed average concentrations they take.

If these control conditions were to be applied simultaneously, then some of the above conditions would have had to have been changed. The maximum limits of these particular rates were a couple of orders of magnitude less than the other rates, making their effect on the cellular behaviour slight. Respiration could be taken to be a measure of cellular exercise and excretion a measure of deamination, taken to be a cellular mechanism to allow amino acid pool size to be regulated (Bayne & Scullard, 1977a; Thompson & Bayne, 1972). However, the role and effect of each was not replicated within the model at this stage.

It was shown that merely incorporating the nitrogen as an attachment to the previous carbon models and disregarding the nitrogen control condition was a relatively pointless exercise. Exclusively using the nitrogen control condition had a slightly more significant effect on cellular behaviour. This condition can be seen as a measure of the importance of proteins in cellular behaviour and structure, but disregarded the energetic state of the model.

This problem was seemingly intractable given the state of the model. However, the applicability of these synchronised control conditions were questionable, given that the digestive gland had been shown to have a seasonal pattern for metabolism and storage of protein, lipid and



carbohydrates (Thompson *et al.*, 1974). Suppose each of these macromolecular forms were imbued with a constant carbon and nitrogen concentration based on a hypothetical 'average' chemical structure. Then applying these to the seasonal dry weight measurements gave neither constant carbon and nitrogen concentrations nor even a constant C:N ratio. Hence, it was proposed that it would be beneficial to reject the current control conditions and instead model the protein, lipid and carbohydrate flow through the cell, and introduce different regulatory conditions to match the seasonal observations.

Prior to the introduction of this new model, closer examinations of both the operation of the lysosome and the endocytotic rate were performed, as described in the following Chapter 5.



## Chapter 5 Endosomal and Lysosomal Models

### . 5.1 Introduction

Hitherto, the autophagic increase at the onset of nutritional deprivation had generally led to rapid cellular disintegration. The existence of empirical evidence to suggest that the relative lysosomal volume does increase significantly under stress also implies that such cells are abundant enough to be detected, and hence are operational and/or persistent; which intimated that the model was seriously flawed under these conditions. Given the central role it has in the model it was thus considered crucial to investigate the dynamics of the endo-lysosomal system in greater detail. Two new models were proposed and tested in order to increase the robustness of the digestive cell model and increase the similarity to the complexity of the endo-lysosomal degradative system.

Both models started from the simple dictum that what goes in must come out. The two degradative organelles were then initially assumed to be intermediate locations along the pathway for the flow of bulk material (Owen, 1970). Vacuolar material remained resident therein for a prescribed period before onward passage along one of two possible pathways.

*Delay Model Hypothesis 5.1:* by making the material exiting the degradative organelle dependent upon the material entering at some prescribed earlier time then the rapid decrease in cellular volume seen with the introduction of an autophagic boost will be mediated.

*Throughput Model Hypothesis 5.2:* by imbuing the degradative organelle with a degradative capacity the rapid decrease in cellular volume seen with the introduction of an autophagic boost will be mediated; whilst the decrease in lysosomal stability observed will also be simulated.

## 5.2 Delay model: Model 4b

After some development the following model was designed to account for the delay from initial entry into the degradative organelle compartment to removal. This required that the volume, carbon and nitrogen into each compartment over a single timestep be matched by exactly the same quantities being removed after a suitable delay. It was found that this formulation of the model requires that the concentrations at which material is moved between compartments would have to be variable.

Essentially, the system sought to determine the rates and concentrations at which material left both compartments dependent upon the volume and content of material entering a set time in the past. Table 5.1 shows the relevant rates at which volume, carbon and nitrogen were entering each compartment. These were equated to the rates at which they leave the compartment to give a system of equations to solve.

For the lipid given that all carbon concentrations were equal this gives a system of 2 equations with 4 unknowns (i.e.  $k_{recL}(t)$ ,  $k_{lysL}(t)$ ,  $k_{degL}(t)$  and  $k_{exoL}(t)$ ). Thus, two parameters  $f_{rL}$  and  $f_{dL}$  were introduced that determined the amount of lipid which was recycled and successfully degraded respectively. For the non-lipid there were 6 equations with 12 unknowns (i.e. the rates  $k_{recN}(t)$ ,  $k_{lysN}(t)$ ,  $k_{degN}(t)$  and  $k_{exoN}(t)$ ; and the concentrations  $EX_{cn}(t)$ ,  $EY_{xc}(t)$ ,  $LX_{cn}(t)$  and  $LY_{cn}(t)$ ). Once again two parameters,  $f_{rN}$  and  $f_{dN}$ , were introduced:  $f_{rN}$  as the fraction of carbon and

nitrogen entering the endosome which left via the recycling pathway; and  $f_{dN}$  parameter as the fraction of material entering the lysosome which was successfully degraded and passed to the cytosol.

Compartment	Volume		Carbon		Nitrogen	
	In	Out	In	Out	In	Out
Endosome Lipid	$k_{endL}(t-\tau)$	$k_{recl}(t) + k_{lysl}(t)$	$k_{endL}(t-\tau)SL_c$	$\left(k_{recl}(t) + k_{lysl}(t)\right)EL_c$	N/A	N/A
Endosomal Non-lipid	$k_{endN}(t-\tau)$	$k_{recN}(t) + k_{lysN}(t)$	$k_{endN}(t-\tau)SN_c(t-\tau)$	$k_{recN}(t)EX_c(t) + k_{lysN}(t)EY_c(t)$	$k_{endN}(t-\tau)SN_n(t-\tau)$	$k_{recN}(t)EX_n(t) + k_{lysN}(t)EY_n(t)$
Lysosome Lipid	$k_{lysl}(t-\delta) + k_{autL}(t-\delta)$	$k_{degL}(t) + k_{exol}(t)$	$k_{lysl}(t-\delta)EL_c + k_{autL}(t-\delta)CL_c$	$\left(k_{degL}(t) + k_{exol}(t)\right)LL_c$	N/A	N/A
Lysosomal Non Lipid	$k_{lysN}(t-\delta) + k_{autN}(t-\delta)$	$k_{degN}(t) + k_{exoN}(t)$	$k_{lysN}(t-\delta)EX_c(t-\delta) + k_{autN}(t-\delta)CN_c(t-\delta)$	$k_{degN}(t)LX_c(t) + k_{exoN}(t)LY_c(t)$	$k_{lysN}(t-\delta)EX_n(t-\delta) + k_{autN}(t-\delta)CN_n(t-\delta)$	$k_{degN}(t)LX_n(t) + k_{exoN}(t)LY_n(t)$

Table 5.1 Instantaneous rates of entry and exit from the endo/lysosomal system for volumes and carbon/nitrogen content.

Where

$EX_{c/n}$  was the concentration of carbon/nitrogen flowing from the endosome back to the surface via recycling.

$EY_{c/n}$  was the concentration of carbon/nitrogen flowing from the endosome to the lysosome.

$LX_{c/n}$  was the concentration of carbon/nitrogen flowing from the lysosome to the cytosol once successfully degraded.

$LY_{c/n}$  was the concentration of carbon/nitrogen flowing from the lysosome to the surface via exocytosis.

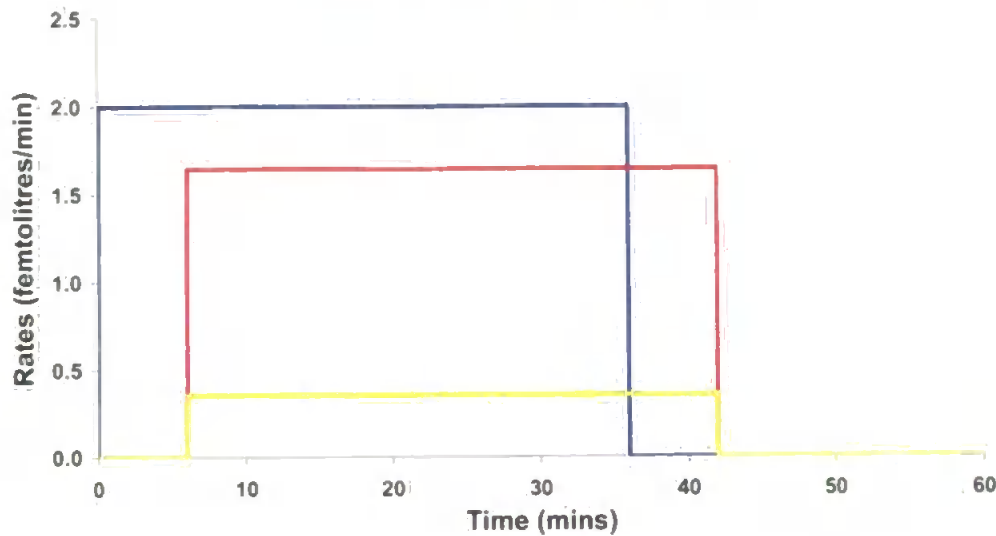
However, the system was such that the number of unknowns could be reduced by observing that the ratio between exiting carbon and nitrogen concentrations must be the same for both pathways from each compartment (e.g for the endosome  $\frac{EY_c}{EY_n} = \frac{EX_c}{EX_n} = \frac{SN_c}{SN_n}$ ). Then two new parameters  $\alpha$  and  $\beta$  were introduced, which related the endosome-to-lysosome to the endocytotic carbon concentration (i.e.  $EY_c(t) = \alpha SN_c(t - \tau)$ ) and the exocytosed carbon concentration to the vesicular traffic from the endosome (i.e.  $LY_c(t) = \beta EY_c(t - \delta)$ ). The biological interpretation of the  $\alpha$  parameter was that the transport vesicles carrying material between the endosomal and the lysosomal compartments must contain greater carbon concentration than the endocytotic vesicles; which appeared sensible as the endosome then acted to reduce the incoming solution to a higher concentrate, which mimicked its sorting role. The  $\beta$  formulation was made as it could be used to calculate the carbon concentration of exocytotic vesicles which should be measurable. It was found that if  $\alpha$  is bound by the constraint,  $1 \leq \alpha \leq 5.66$ , then  $k_{lys}$  would always remain within its parameter limits. Some analytical solutions to this system for the endosome are given in Appendix B

Lauffenburger & Linderman (1993) suggest the rejection of unwanted endocytotic material in mammalian cells takes in total 20 minutes and recycling of either pinocytotic or endocytotic surface vesicles

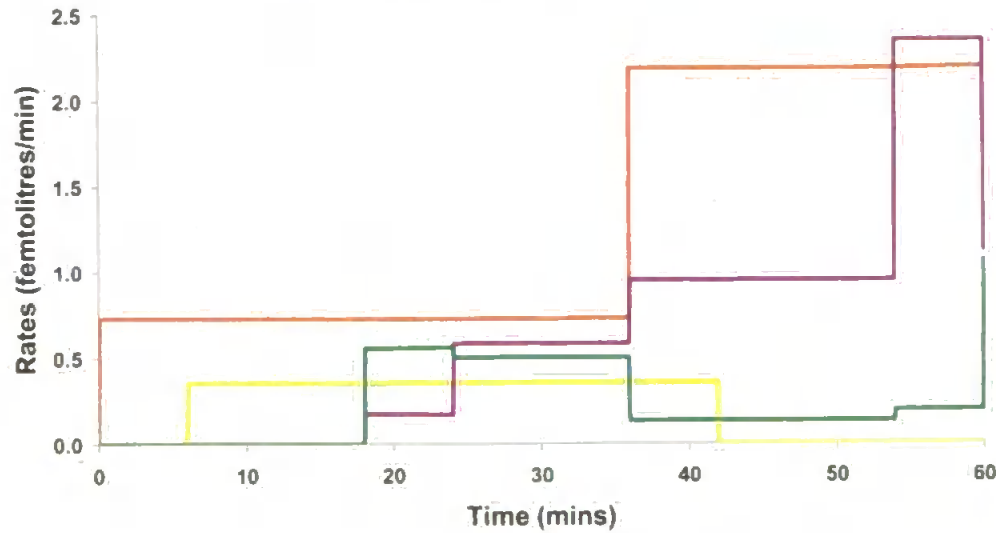


takes approximately 5 minutes. Hence the system was parameterised with  $\tau$  = 5 minutes and  $\delta$  = 15 minutes.

(a) Endosomal Rates : Model 4b



(b) Lysosomal Rates : Model 4b



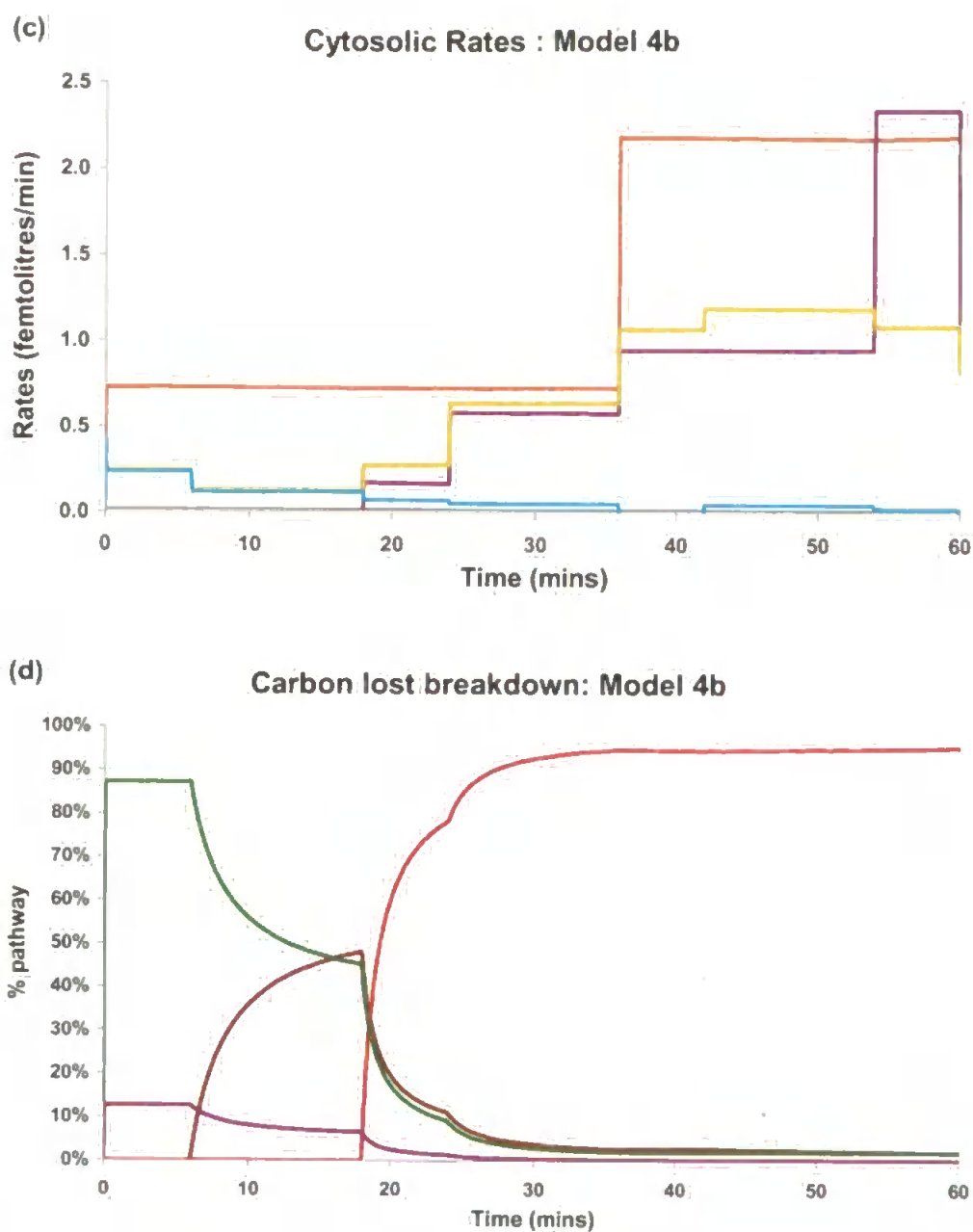


Fig 5.1 1 hour simulation of first delay model 4a. Feeding regime: First 30 minutes,  $S_c = 6.0$ ,  $S_n = 1.2$  &  $L\% = 13\%$ ; last 30 minutes,  $S_c = S_n = 0.0$ , ICs:  $E_c = 11.93$ ;  $E_n = 2.38$ ;  $L_c = 14.87$ ;  $L_n = 2.68$ ;  $f_{ev} = f_{lv} = 4.45\%$ ;  $Cell_v = 1.38$  picolitres. (a) Endosomal rates —  $k_{end}$ , —  $k_{rec}$  and —  $k_{lys}$  (b) lysosomal rates —  $k_{lys}$ , —  $k_{aut}$ , —  $k_{deg}$  and —  $k_{exo}$  (c) cytosol rates —  $k_{aut}$ , —  $k_{deg}$ , —  $k_{res}$ , —  $k_{sec}$ , —  $k_{sto}$ , —  $k_{exp}$ , —  $k_{dif}$  and —  $k_{exc}$  (d) breakdown of pathways by which carbon is lost from cell: — Exocytosed; — Recycled; — Respired; — Secreted.

Figure 5.1a shows the 5 minute delay between the start and finish of endocytosis and the commencement of material leaving the endosome. The split between the two exiting pathways was now approximately half each, as the amount of material leaving at the endosomal concentration to the lysosome required that the endosome-to-lysosomal pathway be increased. This raised the value of the rate constant over the parameter maximum. The lysosomal rates show the introduction of material from the cytosol via autophagy from the onset and then the introduction of material from the endosome after 5 minutes, once it has been processed (Fig 5.1b). Then at 15 minutes the exiting of the cytosol sourced material began followed at 20 minutes by an increase as the cytosol and endosome sourced material combined started to be allowed to leave. Once again, the split between the two exiting pathways was determined by both the condition that one pathway be taken to flow at average concentration and the degradative efficiency parameter. After 30 minutes feeding stopped and the autophagic rate was boosted accordingly. Then at 35 minutes the material from endocytosis no longer entered. Increase in the exiting rates was shown at 45 minutes, the delay period after the inception of the autophagy boost, and was subsequently reduced somewhat at 50 minutes, as the last of the endocytosed food was successfully processed through the system. The cytosolic rates (Fig 5.1c) were dominated by autophagy and degradation as seen previously: the only other significant rates were the diffusion rate, which increased as material sourced from the lysosome entered at a higher

concentration, thus needing solvent to retain the constant control condition, and the storage rate for glycogen. The breakdown of carbon loss through the appropriate pathways (Fig 5.1d) revealed that for 5 minutes, loss is only via secretion and respiration; thereafter, recycling started to increase in importance until after 20 minutes the exocytosis commenced, and quickly becoming the dominant factor in cellular carbon loss.

Furthermore, it was now possible to determine those initial conditions (Fig 5.2) which would allow this delay model endosomal compartment to remain within its bounds over the first delay period, which, as its concentration inevitably decreased thereafter, ensures these bounds are no longer exceeded as in previous models. The maximum values occurred for relatively small nitrogen concentration and were utilised hereafter for the initial conditions.

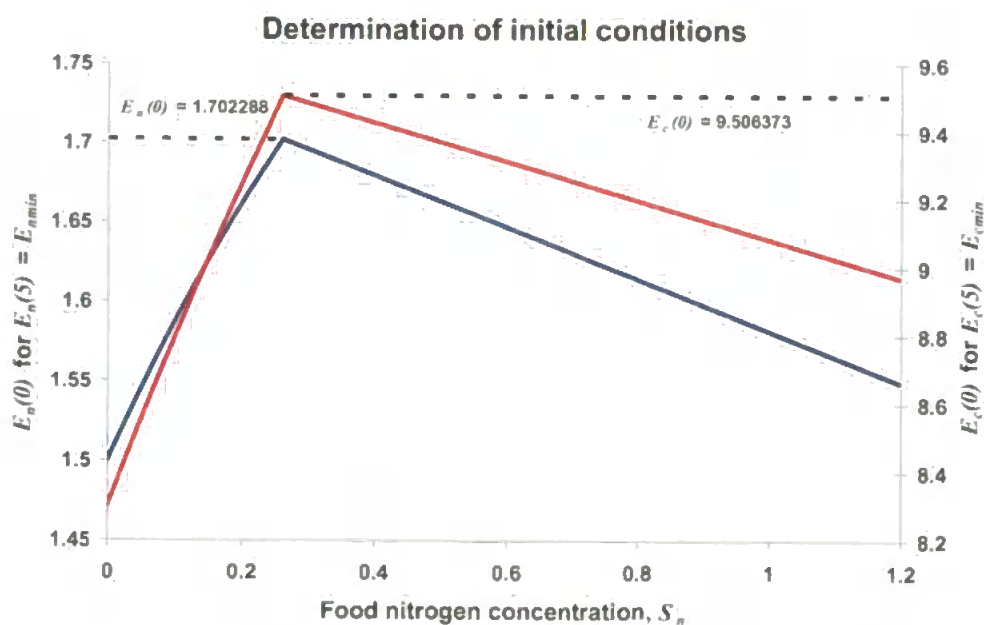
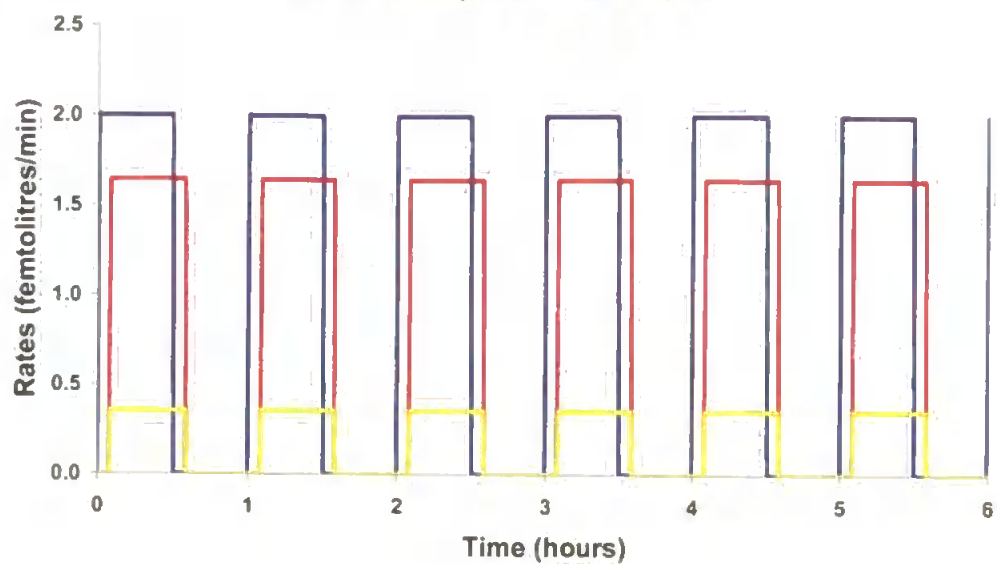


Fig 5.2 Determination of initial endosomal concentrations which allow for endosomal concentration to remain within bounds

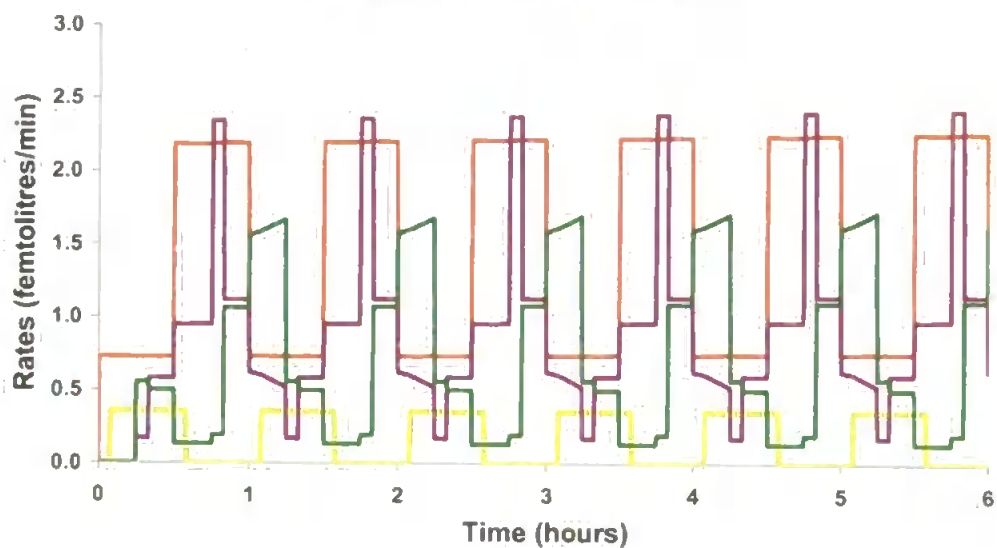
To be able to observe this new system a short square wave food pattern was used, so that the feeding signal was switched off periodically. The endosomal rates followed a highly regular pattern (Fig 5.3a), and with the delay in response excepted, they all switched on and then off over an hourly cycle. The lysosomal responses, although seemingly more complicated (Fig 5.3b), also followed a regular pattern, which was principally driven by the different forcing factors during each of the phases of the cycle. These forcing factors were either the material transported from the endosome during feeding, or else, the increased autophagy during the rest phase. Any long-term cellular volume trend away from equilibrium would change the scale of the autophagic response.

The cytosolic response (Fig 5.3c) to this feeding pattern was principally driven by the feedback between the autophagy and digestion rates. Nitrogen (Fig 5.3d) and carbon concentrations once removed from the initial period, were also affected by the square wave pattern but with linear increases and decreases in peaks as food entered and left the lysosomal and endosomal compartments.

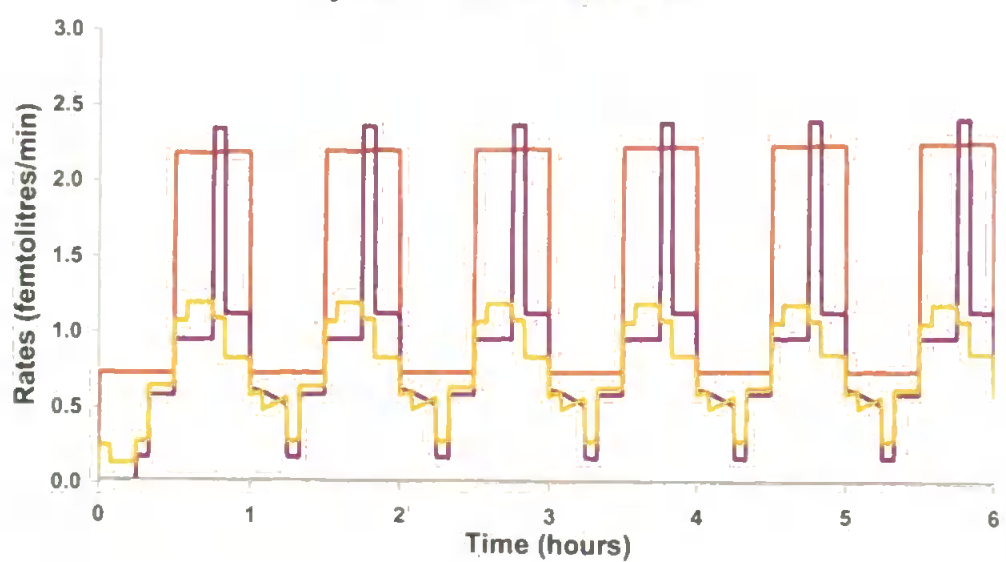
(a) Endosomal Rates : Model 4b



(b) Lysosomal Rates : Model 4b



(c) Cytosolic Rates : Model 4b



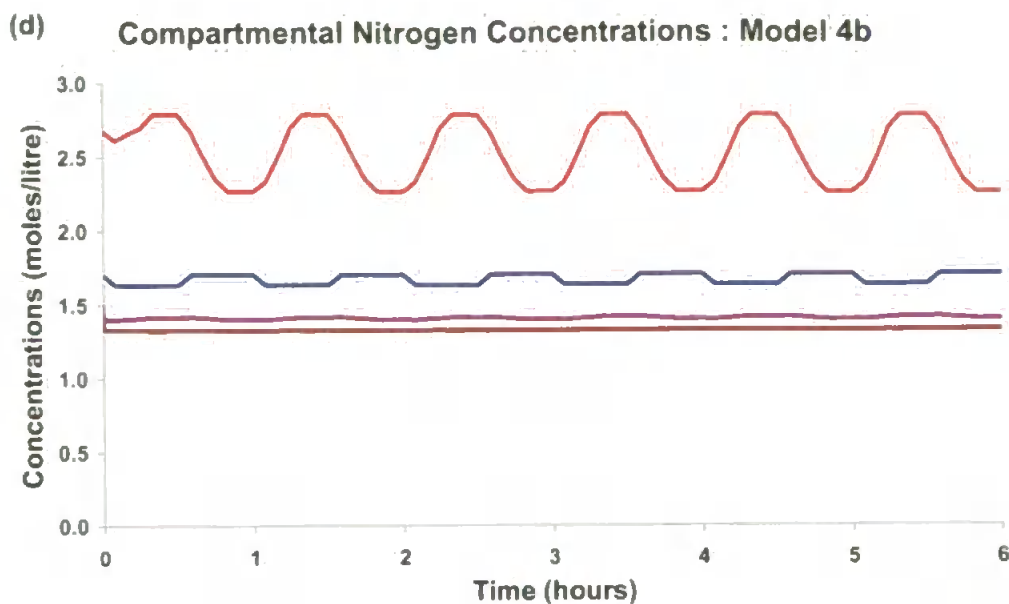


Fig 5.3 6 hour simulation of second delay model 4b with hourly food pattern. Feeding regime: 30 minutes,  $S_c = 6.0$  &  $S_n = 1.2$ ; 30 minutes at  $S_c = 0.0$ ,  $S_n = 0.0$ ;  $L\% = 13\%$ . ICs as described for Fig 5.6. (a) Endosomal rates —  $k_{end}$ , —  $k_{rec}$  and —  $k_{lys}$  (b) lysosomal rates —  $k_{lys}$ , —  $k_{aut}$ , —  $k_{deg}$  and —  $k_{exo}$  (c) cytosol rates —  $k_{aut}$ , —  $k_{deg}$ , —  $k_{res}$ , —  $k_{sec}$ , —  $k_{sto}$ , —  $k_{exp}$ , —  $k_{dif}$  and —  $k_{exc}$  (d) nitrogen concentrations —  $E_n$ , —  $L_n$ , —  $C_n$ , —  $Cell_n$

### 5.3 Throughput model: Model 4c

Whilst these delay models appeared acceptable for a normal unstressed animal, the burden of stress was now only met by an increase in the augmented autophagic rate and the subsequent sequestration of extra material from the cytosol to lysosome. Under conditions of nutritional stress this represented material from the cytosol replacing that from outside the cell, which would rarely constitute enough to provoke the reaction seen in experimental studies. Moreover, the lysosome and endosome operate at maximum optimality regardless of the size and condition of the cell. Furthermore the dysfunction of the lysosome, so often seen in real cells was not captured in the simulation (Moore *et al.*, 2006a, 2007). Hence a new approach was subsequently adopted whereby the organelles were imbued with a notional throughput to reflect the constraints on their 'productivity'.

In order to better formulate the functioning of the endosomal and lysosomal compartments it was necessary to look at their internal composition and potential for processing macromolecules when they were first synthesised. In this initial state each of the degradative organelles was only a sac of digestive hydrolytic enzymes awaiting material to process. Once a portion of material ready for degradation had entered it would be dependent upon its proximity to the appropriate enzymes before it is subdivided into the constituent monomeric parts, which the rest of the cell



required as building blocks for new macromolecules. This digestive process generally occurred more than once for each macromolecule. For example, proteins are broken into polypeptides, denuded of side chains, and eventually into individual amino acids, which implies that a chain of events, possibly ordered or not occurred on each piece of 'target' material (Doherty & Mayer, 1992). Thus if a package of similar material entered the system at a point in time, then the rate of total passage through the lysosome was principally dependent upon the various enzyme concentrations within the lysosome (under the assumption that the lysosome had perfect environmental conditions and the target and internal enzymes formed a reasonably well mixed solution). However, the hydrolytic enzymes might be spatially organised into functional arrays which extend their overall degradative capacity (Doherty & Mayer, 1992).

In order to simulate this action consider the material entering the lysosome going through a number of stages along the way to full degradation. Suppose there are  $n$  sequential stages of degradation, with a particular enzyme,  $m_i$  say, responsible for each cleavage (Fig 5.4). Then the overall rate of degradation would be dependent on the enzyme concentration distribution.

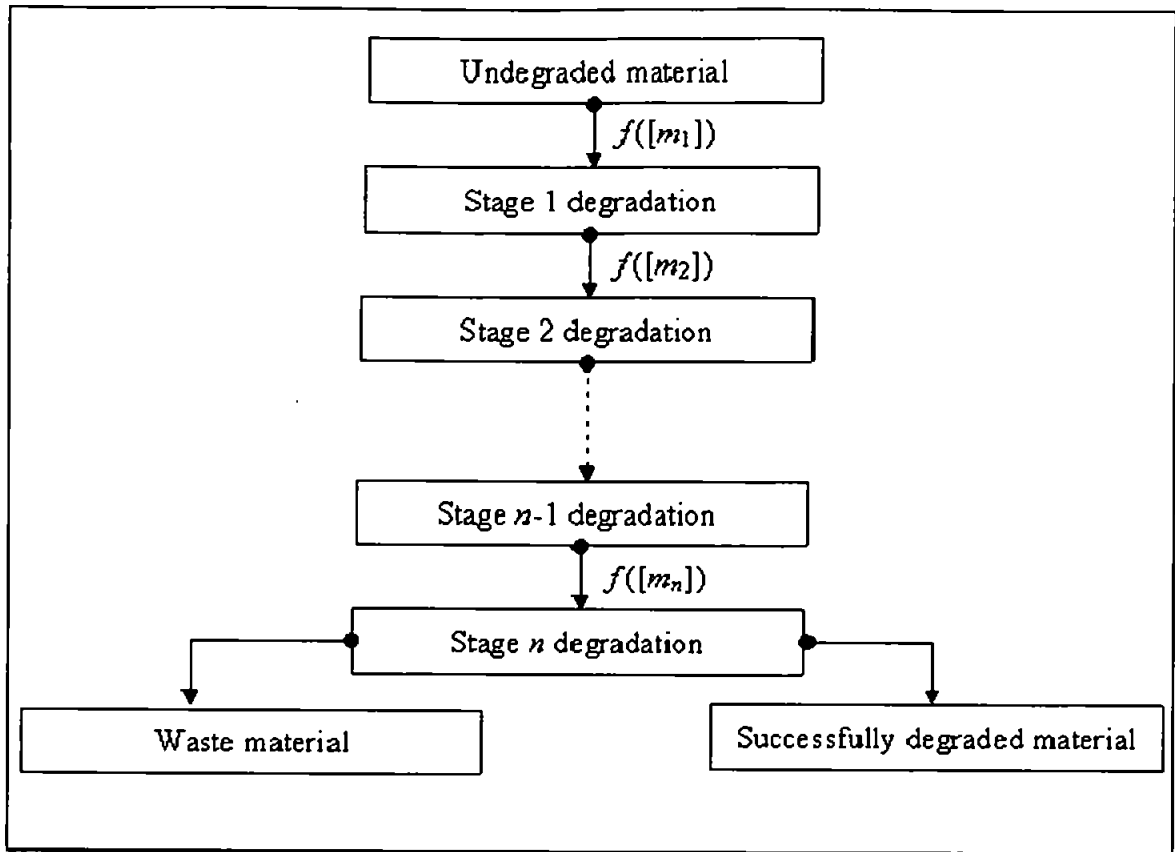


*Fig 5.4 Model 4c degradative organelle scheme*

Two possible implementations of this idea were originally considered. First to simplify the implementation of this scheme the capacity for degradation between each step is assumed to be homogenous. Then suppose that under normal conditions the endosome/lysosome could deal with a certain amount of material in 5/15 minutes and that it progressed along a number of predestined steps towards final degradation into constituent parts.

Example: suppose the timestep was 1 minute then the endosome would have 5 steps along which 10 pieces of material per minute may pass.

Initial Endosome Volume 5  
Throughput 10 per step

TimeStep	0	1	2	3	4	5	6	7	8	9	10	11	12	13	14	15	16	17	18	Total
Incoming material	10	10	20	30	40	5	0	0	0	0	0	0	0	0	0	0	0	0	0	115

step compartments	1	0	10	10	20	40	70	65	55	45	35	25	15	5	0	0	0	0	0	0
	2	0	0	10	10	10	10	10	10	10	10	10	10	10	5	0	0	0	0	0
	3	0	0	0	10	10	10	10	10	10	10	10	10	10	10	5	0	0	0	0
	4	0	0	0	0	10	10	10	10	10	10	10	10	10	10	10	5	0	0	0
	5	0	0	0	0	0	10	10	10	10	10	10	10	10	10	10	10	5	0	0

Exiting material	0	0	0	0	0	0	10	10	10	10	10	10	10	10	10	10	10	5	0	115
------------------	---	---	---	---	---	---	----	----	----	----	----	----	----	----	----	----	----	---	---	-----

Endosome volume	5	15	25	45	75	115	110	100	90	80	70	60	50	40	30	20	10	5	5	
-----------------	---	----	----	----	----	-----	-----	-----	----	----	----	----	----	----	----	----	----	---	---	--

Alternatively if the endosome was assumed to have the capacity to make 50 steps independent of order per timestep then the best strategy to minimise endosomal volume would be to move 10 pieces of material through the endosome and out every timestep when available.

Initial Endosome Volume 5  
Throughput 50

TimeStep	0	1	2	3	4	5	6	7	8	9	10	11	12	13	14	15	16	17	18	Total
Incoming material	10	10	20	30	40	5	0	0	0	0	0	0	0	0	0	0	0	0	0	115

step compartments	1	0	0	0	10	30	60	55	45	35	25	15	5	0	0	0	0	0	0	0
	2	0	0	0	0	0	0	0	0	0	0	0	0	0	0	0	0	0	0	0
	3	0	0	0	0	0	0	0	0	0	0	0	0	0	0	0	0	0	0	0
	4	0	0	0	0	0	0	0	0	0	0	0	0	0	0	0	0	0	0	0
	5	0	0	0	0	0	0	0	0	0	0	0	0	0	0	0	0	0	0	0

Exiting material	0	10	10	10	10	10	10	10	10	10	10	10	5	0	0	0	0	0	0	115
------------------	---	----	----	----	----	----	----	----	----	----	----	----	---	---	---	---	---	---	---	-----

Endosome volume	5	5	5	15	35	65	60	50	40	30	20	10	5	5	5	5	5	5	5	5
-----------------	---	---	---	----	----	----	----	----	----	----	----	----	---	---	---	---	---	---	---	---

In a comparison of these two approaches (Fig 5.5) it was shown that the second method reduced endosome volume throughout the simulation. Moreover, it processed the material more rapidly than the first method.

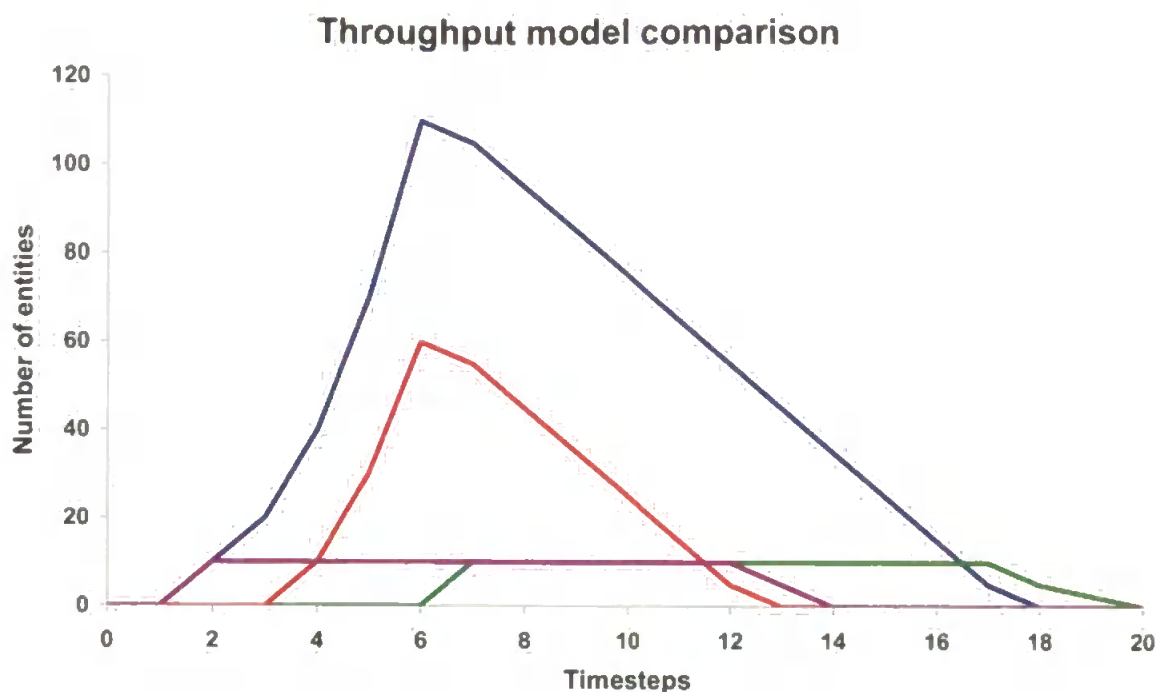


Fig 5.5. Throughput model comparison. — Endosomal volume method 1 — Endosomal volume method 2 — Target material exiting endosome method 1 — Target material exiting endosome method 2.

Since the endosome and lysosome were known to swell from a minimum of 1% cell volume to 5% when unstressed and presumably this occurred when feeding, the first method appeared more suitable (Lowe, 1988; Lowe *et al.*, 1981; Moore *et al.*, 2007). Moreover, the sequential approach fits better with the idea of different enzymes being used in sequence to process material targeted for degradation. Whilst the degradative capacity of each step was implemented as being homogenous, this could be changed in future if data were available for specific enzyme concentrations (Doherty & Mayer, 1992). Hence, for the endosome the model had  $n = \tau \div (t_1 - t_0)$ , so for the normal setup  $n = 500$  (5 minutes  $\div$  0.01 minute)

Then all enzymes involved were assumed to be equally well distributed; then the maximum amount of material passing between each timestep must be equal to the maximum amount coming in. Thus, between each degradative stage there would be a maximum unstressed throughput for each of the three degraded class of materials, denoted  $T_{EC}$ ,  $T_{EN}$  &  $T_{EL}$ , per timestep per stage equal to the maximum non lipid carbon, nitrogen and lipid entering per timestep.

$$T_{EC} = (t_I - t_0) SN_{cmax} k_{endNmax} \quad [5.1]$$

$$T_{EN} = (t_I - t_0) SN_{nmax} k_{endNmax} \quad [5.2]$$

$$T_{EL} = (t_I - t_0) SL_c k_{endLmax} \quad [5.3]$$

Which can be calculated given that:

$$k_{endLmax} = \frac{k_{endmax} S_{cmax} L\%_{max}}{SL_c} \quad \& \quad k_{endNmax} = k_{endmax} \left( 1 - \frac{S_{cmax} L\%_{min}}{SL_c} \right) \quad [5.4]$$

$$SN_{cmax} = S_{cmax} \frac{(1 - L\%_{min})}{\left( 1 - L\%_{min} \frac{S_{cmax}}{SL_c} \right)} \quad \text{And} \quad SN_{nmax} = \frac{S_{nmax}}{\left( 1 - L\%_{max} \frac{S_{cmax}}{SL_c} \right)} \quad [5.5]$$

A similar set up for the lysosome gave  $n = 1500$  and the throughput per degradative stage per timestep was given by the maximum unstressed carbon and nitrogen arriving per timestep

$$T_{LC} = (t_I - t_0) ( EY_{cmax} k_{lysNmax} + CN_{cmax} k_{autNmax} ) \quad [5.6]$$

$$T_{LN} = (t_I - t_0) ( EY_{nmax} k_{lysNmax} + CN_n k_{autNmax} ) \quad [5.7]$$

$$T_{LL} = (t_I - t_0) ( EL_c k_{lysLmax} + CL_c k_{autLmax} ) \quad [5.8]$$

Unstressed this model produced results as seen in the previous model; but with sufficient perturbation provided by stress there was movement away from this behaviour.

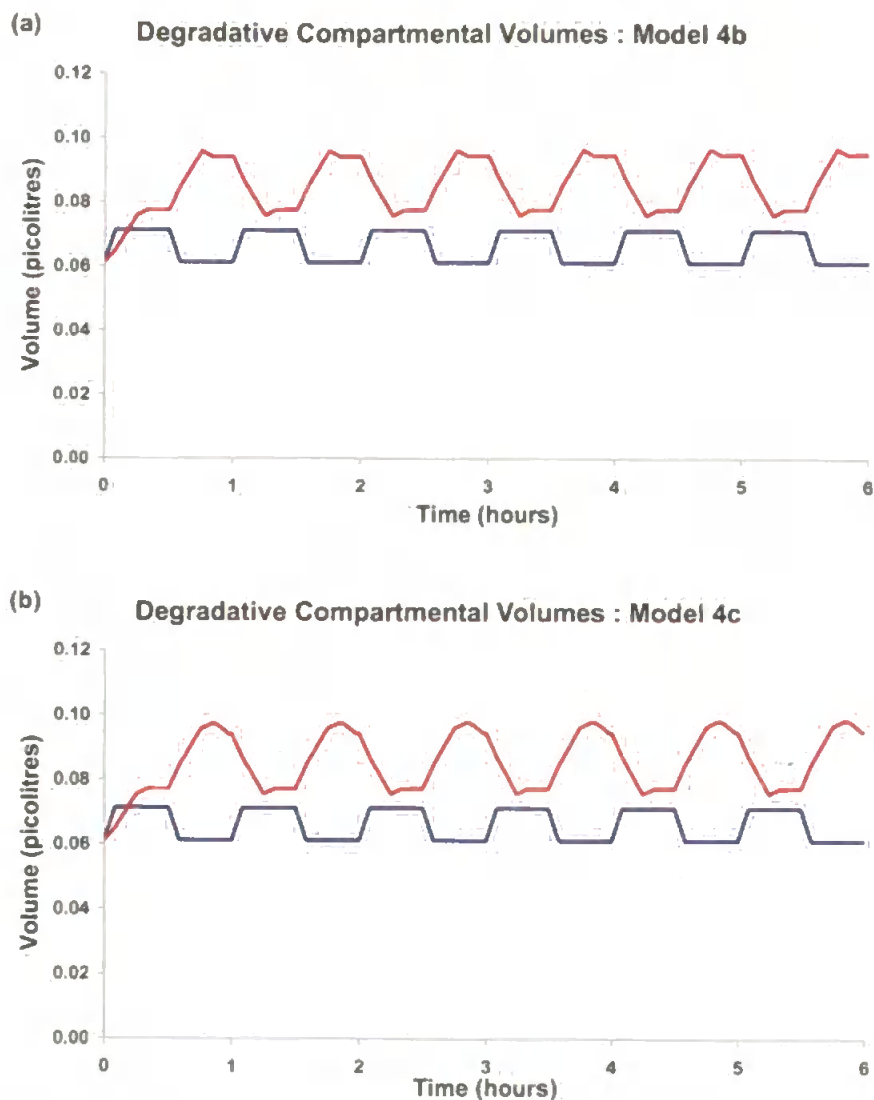
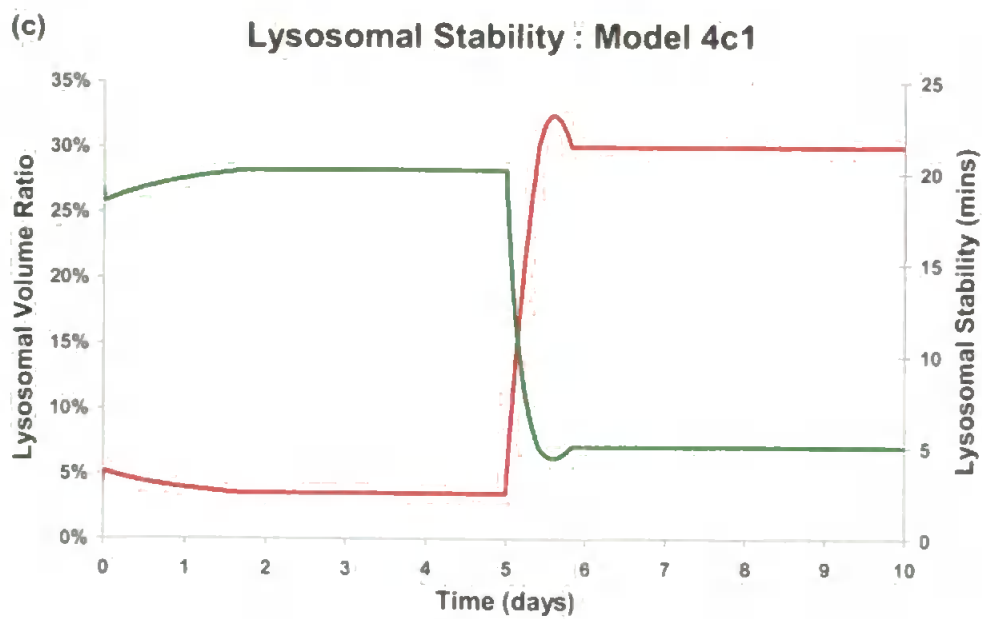
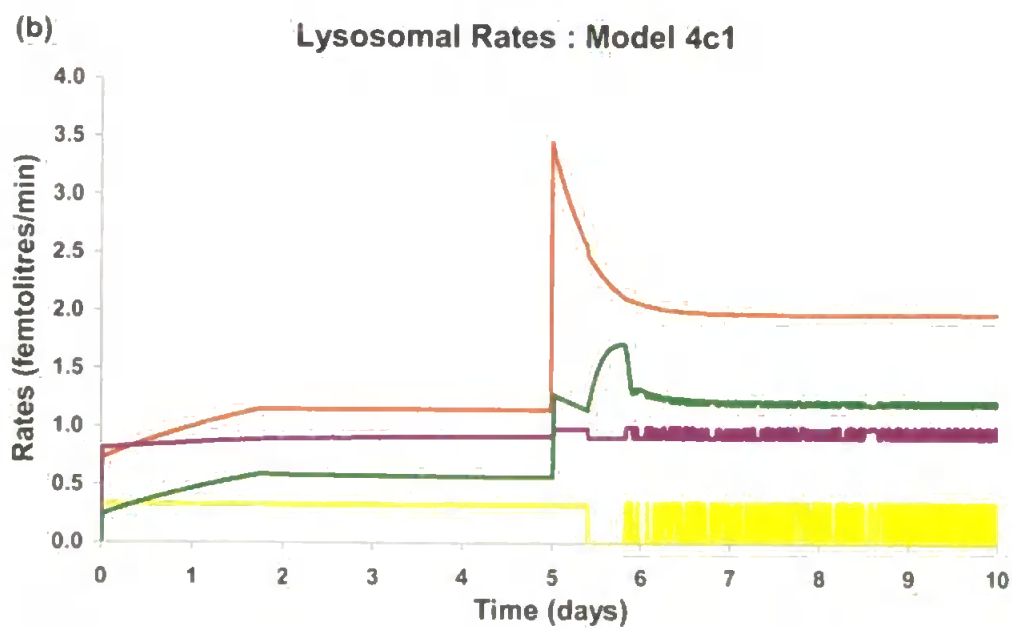
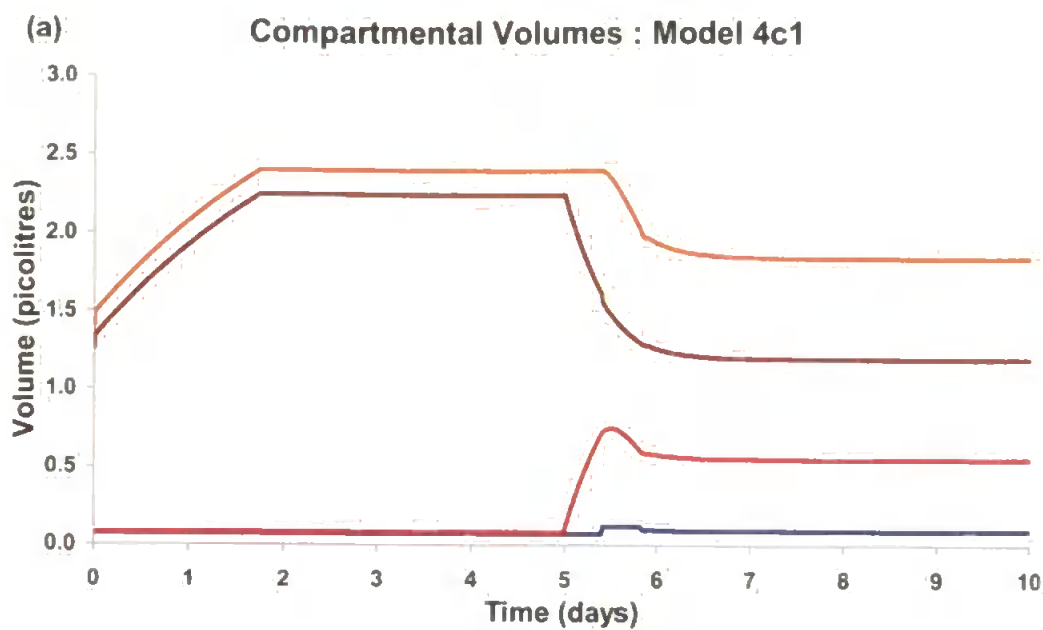


*Fig 5.6 Degradative organelle volumes with periodic feeding, — endosome — lysosome (a) Delay Model (b) Throughput Model*

The delay model revealed that no matter what the amount of material was passed to the lysosome, there was only the delay period during which swelling occurs and then material inside was in equilibrium with material coming out. Hence, the peaks for volume are flat (Fig 5.6a). Swelling in the

throughput model (Fig 5.6b) was exacerbated by the lysosomes' inability to deal with the material above this level, when autophagy was augmented following the end of feeding and the processed material being passed from the endosomes to the lysosomes. Hence, there was a rounded peak as this material was gradually removed by the extra capacity over the received autophagocytosed material when not feeding.

In order to provoke a greater response, a simulation whereby an additional "pollutant" stress was added to the model, by increasing the autophagic rate threefold after a certain time period, was presented. One final enhancement had been made to this model in order to keep the endosomal and lysosomal relative volumes within their parameter limits. If  $f_{ev} \geq f_{ev\max}$  then  $k_{end}$  was temporarily suspended until this was no longer true. Similarly, if  $f_{lv} \geq f_{lv\max}$  then  $k_{lys}$  was suspended, but not autophagy as this was taken to be a 'reflex' response (pathological reaction) to the pollutant stress and, therefore, not controllable.





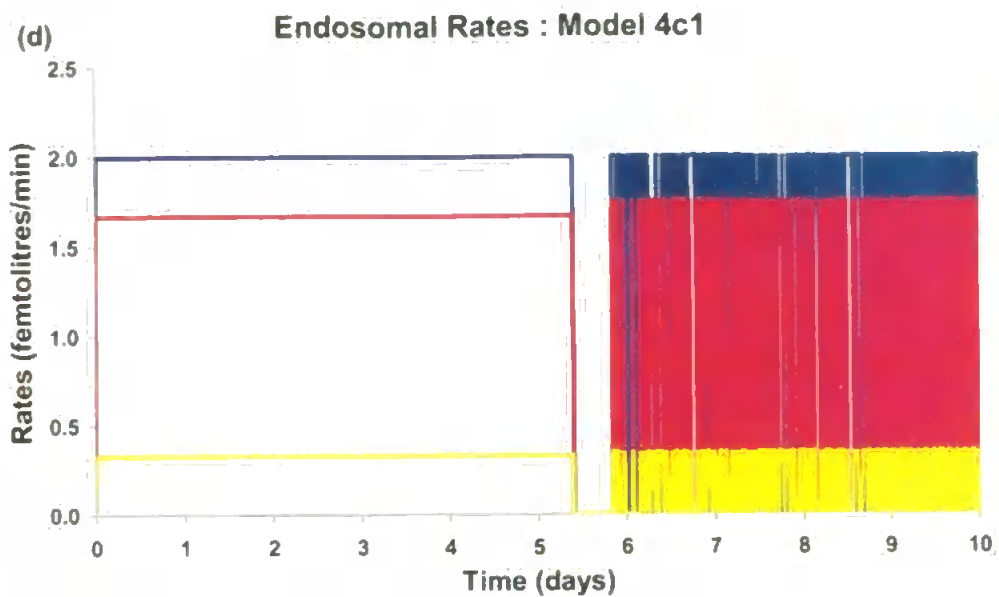


Fig 5.7 Model 4c1: endosomal and lysosomal relative volume dependent endocytosis and lysosomal traffic suspension. Threefold autophagy after 5 days.  $S_c = 6.0$  &  $S_n = 1.2$ . ICs as described for Fig 5.6. (a) Volumes —  $E_v$ , —  $L_v$ , —  $C_v$ , —  $Cell_v$  (b) lysosomal rates —  $k_{lys}$ , —  $k_{aut}$ , —  $k_{deg}$  and —  $k_{exo}$  (c) — lysosomal relative volume, — lysosomal stability (d) Endosomal rates —  $k_{endo}$ , —  $k_{rec}$  and —  $k_{lys}$

Once the autophagic boost was introduced (Fig 5.7b) there was an automatic loss in cell volume and an increase in lysosomal relative volume, due to the increased material for degradation (Figs 5.7a & c). However, in previous models lysosomal rates were determined only by volume and the incoming material was dealt with immediately. Then, whilst the majority of this material was returned to the cytosol, there was a much greater feedback loop established which quickly diminished both cytosolic and lysosomal volume to such an extent that the cell was no longer viable (e.g. Fig 4.10d). In this model the increased autophagy was dealt with more effectively

allowing longer survival combined with the observed decrease in lysosomal stability. However, the increased lysosomal volume inhibited endocytosis during the lattermost part of the first day of increased autophagy and intermittently thereafter (Fig 5.12d).

#### *5.4 Discussion*

In order to increase the functionality of the cell, whereby certain rates are a consequence of preceding actions performed in the cell, the delay models for the endosome and lysosome were developed. The amended lipid flow through the cell required only an appreciation of the percentage of material to be recycled and degraded and the residence time within the respective compartments, because of the consistent concentrations in all three compartments. The non-lipid flow required that the concentrations at which material leaves the cell had to be adjusted, in order to keep the compartmental concentrations within the set parameter limits. This provoked the perception of the endosome as a body whose primary role is to concentrate the incoming extracellular fluid from the lumen of the digestive tubule and mainly eject the excess water entering the cell through bulk endocytosis.

The delay was, of course, not exhibited with continual feeding; however the effect was apparent on the dependent outgoing rates. However, the idea of the endosome taking 5 minutes to return material to the cell surface led to a consideration of the rate of endocytosis. Was the site of endocytosis a fixed locus on the cell surface, and if not were there a relatively constant number of sites? Did the apical cell surface area change for varying cell volume, and was there a maximum or minimum? When the surface invaginated to form an endocytotic vesicle did the site remain

active or was it rendered inactive due to the loss of the membrane proteins? Did whatever attraction the site have on external material continue during any inactive periods, thus allowing the site to continually be replenished and ready to invaginate as soon as the endocytotic delay period was over? Such considerations were the impetus behind Chapter 6, which is a more detailed examination of the rate of endocytosis (Doherty & Mayer, 1992; Lauffenburger & Linderman, 1993).

Whilst the delay model increased the functionality of the model it did not provide an altogether adequate framework for describing the changes to lysosomal performance under stress. In order to allow for the characteristic lysosomal swelling the throughput model was developed. Of the two separate systems proposed the sequential model was chosen to model the system. It was supposed that protein degradation was the primary lysosomal function and each lysosomal enzyme targetted the link between two separate amino acids. Thus, if the concentration of enzymes within the lysosome was in the same ratio to the distribution of amino acid links, the sequential approach would not be the best representation of lysosomal performance.

The throughput for both the lysosome and endosome remained constant despite any loss in volume, thus enabling the smallest cell to deal with the same amount of endocytosed or autophagocytosed material as the largest cell: this was unacceptable. The throughput was governed by the

enzyme concentration and the amount of material to be degraded; hence, it should be introduced as a function of the integral compartmental volume.

Nevertheless, this all disregarded the initial endosomal volume and content prior to degradation. Presumably the rate of synthesis of primary endosomes and lysosomes grows relative to the volume of the cell, so that the degradative capability of the cell increases with increased cellular volume providing a stimulus for cell growth and division (Marigómez *et al.*, 1999; Szego, 1975). But in order to incorporate this facet of cellular behaviour there was a requirement for the depletion and refreshment of the integral endosomal and lysosomal components, which was beyond the capability of this present model but shall be addressed in model 6 (see chapter 7).



## Chapter 6 Endocytosis

### 6.1 Cellular Feeding – Objectives and Hypotheses

The objective for this chapter was to develop a better simulation of the rate of endocytosis. The primary external signal in the mussel digestive cell model was that of the process of endocytosis. Given the influence of the rate of endocytosis on the cellular behaviour, attempts were made to secure a more functional footing for its calculation.

The tubules, composed of the digestive cells, exhibited a phasic cycle that could be reduced to three phases: a feeding phase whose length was dependent upon the amount of food left in the tubule lumen; a disintegrating phase where the superfluous by-products of feeding were discharged back into the tubule lumen; and a resting phase when either feeding was unwarranted or else to produce the necessary metabolites for the feeding phase.

*Objective 6.1:* Develop a tubule phase model which would provide the model cell with a discontinuous feeding pattern and provide the capability to cease feeding when food availability make this energetically inefficient.

Subsequently, a model for the uptake of the food during the feeding phase and expulsion of waste during the disintegrating phase needed to be established. Movement of material from tubule lumen into the brush border appeared to be accomplished by passive diffusion.

*Objective 6.2:* Develop conceptual, spatial models of the digestive tubules and cells, in order to be able to assess relative volumes.

*Hypothesis 6.1:* Movement of new material from the tubule lumen to the sites of endocytosis can be simulated with a stochastic model based on the relative volumes of the lumen, brush border and endocytotic sites.



## 6.2 Mussel and cellular feeding

The animal takes in food particles (algal cells and detritus coated with bacteria) suspended in the external environment through an inhalant siphon (Owen, 1970). This solution is passed through the gills, where oxygen is extracted for respiration, and food particles are roughly disassociated from the main body of fluid (Owen, 1970). The particles are subject to initial degradation by extracellular digestion in the stomach, where they become associated with a string of mucus which is passed on into the digestive diverticula and ultimately delivered to a digestive tubule (Langton, 1975; Owen, 1970). The tubule is composed of the modelled digestive cell and also some pyramidal secretory basophile cells (Langton, 1975; Marigómez *et al.*, 1999; Owen, 1970). Enzymes released into the tubule breakdown the mucus attachments and the particles into a size suitable for endocytotic uptake by the digestive cells ( $< 100\text{nm}$  diameter). During this process, waste material builds up in residual bodies in the cytoplasm. Presumably after the cell has reached a saturation point, or else the concentration of food particles no longer makes uptake cost effective, endocytosis stops and the waste portion of the ingested food ration is passed back into the tubule lumen for eventual passage out as faeces (e.g. Mathers, 1972). The digestive tubule epithelium is then reconstituted ready for the next endocytotic/digestive phase (Langton, 1975).

### 6.3 Tubule phase model

The pattern of animal feeding and its influence on cellular uptake will be driven by such gross environmental factors like spatial position in the intertidal zone in relation to the tidal cycle and food concentration in the water column. Whilst the original food concentration can feasibly be calculated by measurement of the tubule lumen this will change with the digestive cell uptake and volumetric variation.

It has been proposed on the basis of the morphology of digestive tubule sections of bivalve molluscs that the tubule possesses four possible phases or states. These have been characterized by Langton (1975) as:

Holding/Normal; Absorptive; Disintegrating and Reconstituting.

Cajaraville *et al.* (1992) describe a fifth phase, necrotic, for tubules which are being eliminated to allow the organ to remain functional. The observed relative frequency of each phase for intertidal mussels across two tidal cycles in October is shown in Figure 6.1. The feeding and resting phases dominate throughout regardless of exposure or immersion.

The feeding phase remains high even while exposed; under the assumption that there is no internal store of gut fluid; this may be indicative of an extra long and less energetic feeding period as the mussel attempts to extract the most nutritional content out of the final recharged lumen from the immersed period. The reconstituting phase is observed so infrequently and poorly defined that a three phase cycle is proposed to simulate the uptake of food.

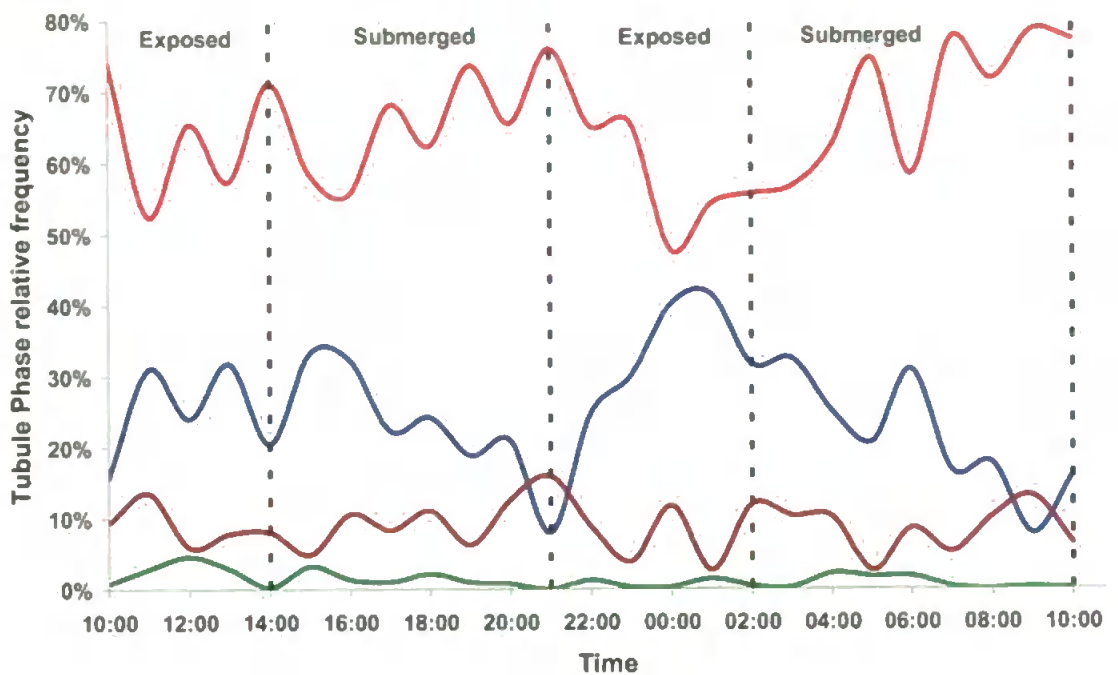


*Fig 6.1 Relative frequency of tubule phase over two tidal cycles — absorptive phase, — disintegrating phase, — holding phase & — reconstituting phase*

Suppose that food entered the tubule in the form of a mucus string: this would be the start of an absorptive phase, over the course of which the string would be attacked by various secreted digestive enzymes which released the food particles attached. The digestive cell absorbed the material in the lumen through endocytosis in this absorptive phase. Assume also that the cell pushed into the tubule central core rather than outwards as a consequence of the extra volume taken up during endocytosis (given that density of the cell remains constant); this would serve to reduce the available volume for the food particles in the tubule solution, making them

more susceptible to a bulk fluid phase endocytotic sequestration (Langton, 1975; Owen, 1970). This scenario should reflect the morphological information whereby the digestive cells extend into the lumen during the absorptive phase while the basophile cells remain in their original position, thus forming the commonly observed crypts (Owen, 1970).

At some point, due to either low food concentration in the tubule lumen making uptake inefficient, or else from some other internal signal the cell would stop absorbing food. Then the cell would need to rid itself of the tertiary lysosomes (residual bodies) and excess fluid which it had taken up, hence next entering a short disintegrating phase (Langton, 1975). In the model this was based upon the period taken for the most recently ingested food to be processed by the lysosome (i.e. the sum of the normal endosomal and lysosomal sortation periods). The tubule lumen would fill up with exocytosed residual bodies and apical cytoplasm (i.e., apocrine secretion) and the cell would shrink in volume to reflect the observed pattern (Langton, 1975). Once the last of the material was discharged the tubule core can be 'flushed' out to the stomach and removed as faeces (Langton, 1975, Owen, 1970).

Thereafter, the observed cell type frequency suggested that the cell entered the holding phase for some unknown reason, possibly to build up the necessary secretory enzymes or to enter a rest period for cellular housekeeping. The relative length of this phase could then be calculated

from Langton's data and compared to the feeding phase length (Langton, 1975). Then the cycle could start again in response to more available food.

The proposed three step tubule phase model to satisfy objective 1 of this chapter was, in summary, then:

***Holding Phase:*** Disregarding normal cellular metabolic rates (respiration, excretion, secretion) only autophagy was to occur, waste material accumulated in residual bodies. Replenishment of endosomal and lysosomal components to be incorporated, cell height and tubule epithelium adjusted to compensate for previous nutritional uptake. This state remained until replacement of the tubule lumen with fresh food before entering next phase.

***Absorptive Phase:*** Endocytosis will be initiated until the process becomes energetically unfavourable and then the next phase will be entered. The tubule radius would remain constant and the digestive cell height increase radially towards the centre of the tubule.

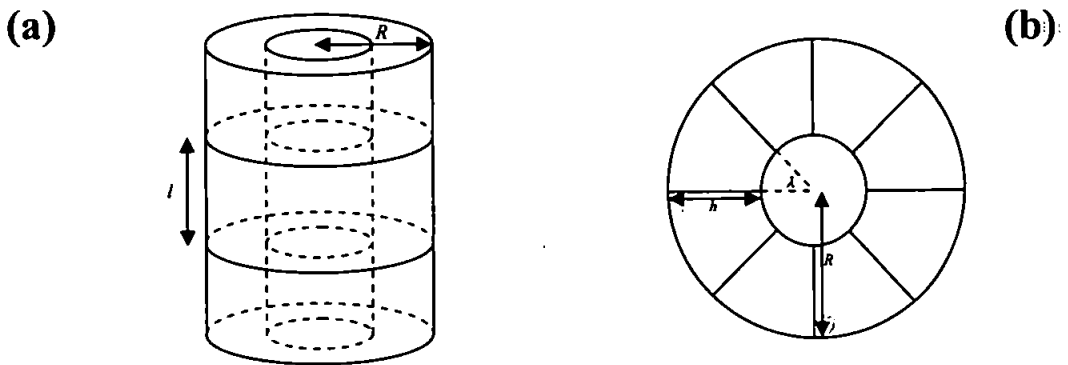
***Disintegrating Phase:*** The waste products from the lysosome, including autophagic debris from holding phase and food waste, which have accumulated in the residual bodies, would be expelled into the tubule lumen. Cell height will be decreased. Once the majority of waste material has been expelled the cell will return to the initial holding phase.

Since feeding only occurs when the exterior particle count is above a certain threshold to make the expenditure viable the length of the holding phase will vary throughout the year (Langton, 1975, 1977; Langton &

Gabbott, 1974). Similarly the feeding phase length will be determined by the amount and possibly quality of the food available throughout the year.

#### 6.4 Spatial tubule and cell model

In order to arrive at a stochastic model for endocytosis based on spatial distribution of food particles in the tubule lumen, digestive cell epithelial brush border and endocytotic site catchment areas a speculative spatial model was proposed for the digestive tubule. Initially, it assumed that the cells form layers of an outer circular core of a circular toroidal layers of even height,  $l$ , which were stacked upon one another to form the tubule (Fig 6.2a), ignoring the blind end. A perpendicular cross section (Fig 6.2b) through any of these levels gave the tubule radius,  $R$ . One measure often made of the cell is “height”,  $h$ , shown in the cross-section to be the distance from the radial distance that the cell extends into the lumen. Suppose there are  $N$  cells (basiphil and digestive) in each cross-section and each cell covers the same area. Then each digestive cell subtended an angle  $\lambda = \frac{2\pi}{N}$  from the centre. If an apical brush border extending distance,  $m$  into lumen, were added then a model of the spatial aspect of a cell which looks like a slice of cake with a central bite taken from it (Fig 6.2c).



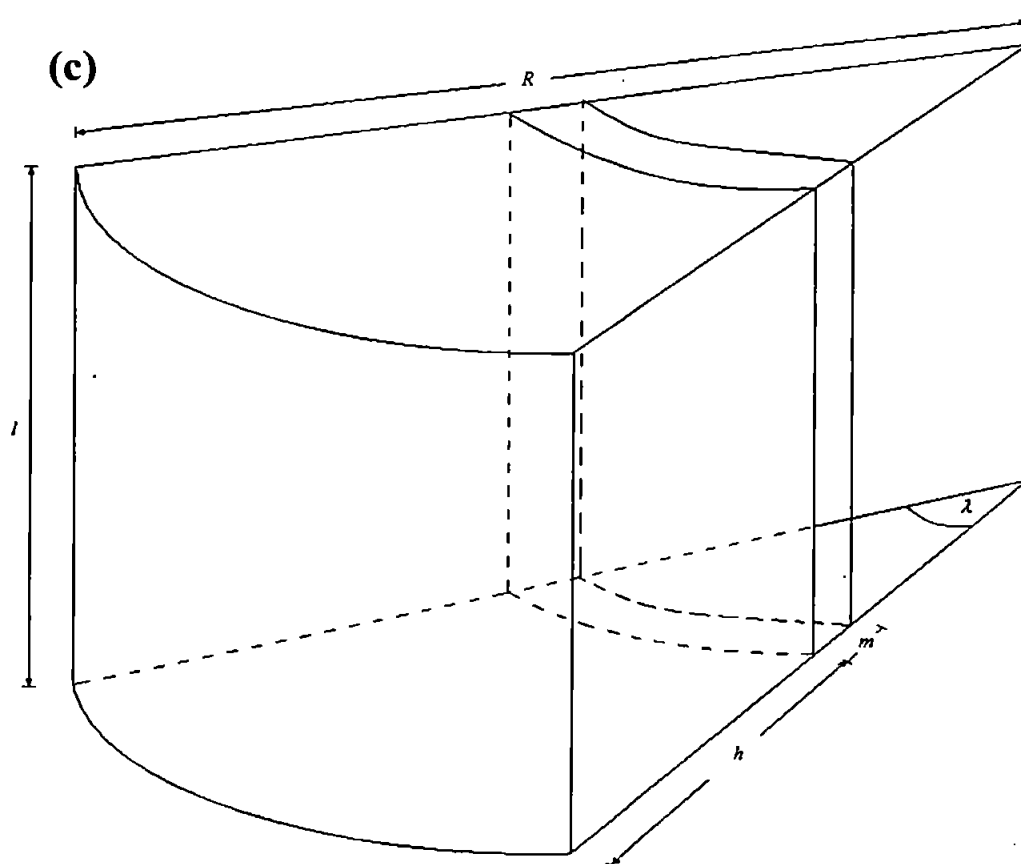


*Fig 6.2 Spatial models of (a) digestive tubule (b) cross-section of tubule layer and (c) cell spatial model*

To find some average values for  $R$ ,  $\lambda$ ,  $h$ ,  $N$  and  $l$  cross-sections, commonly used in histopathology, were utilised. If the conceptual spatial model was correct then when looking at cross-sections the more oblique the cut away from the perpendicular the more elliptical the cross-section will seem, as often observed. In such cases then the smallest diameter through the centre was taken. Using the morphological data of Langton (1975), the following measurements were taken for each particular phase and compared to observed data (Table 6.1).



Table 6.1 Average values for radial heights during different tubule stages.

All values in  $\mu\text{m}$ .

Phase	$R$	$h$	$R/h$	$R - h$
Feeding	33.66	18.66	0.55	15.0
Disintegrating	34.66	13.33	0.38	21.33
Resting*	29.0	15.33	0.53	13.66
Weighted Average	32.58	17.36	0.53	15.22
Cajaraville (1992)	33.34	15.06	0.45	18.28
Widdows <i>et al</i> (1982) day 1	-	21.6	-	-
Widdows <i>et al</i> (1982) day 100	-	23.0	-	-
Moore (1985)	-	~15	-	-

Notably, the tubule radius from Langton (1975) weighted by the distribution of the type of phase showed good agreement with Cajaraville (1992). Similarly the epithelial heights were close for all figures except Widdows (1982). The number of cells in the tubule lumen varied but was taken to be equal to 20 for this parameterisation. No data was found to show epithelial cell layer height,  $l$ , but this was also assumed to vary according to cellular volume. In order to create a hypothetical system of cell growth and deterioration an algorithm for calculating  $R$ ,  $h$  &  $l$  according to cell volume was devised. Excluding volume occupied by the brush border then:

$$Cell_v = \frac{l\lambda}{2} \left( R^2 - (R - h)^2 \right) \quad [6.1]$$

and specifically

$$l = \frac{2Cell_v}{\lambda \left( R^2 - (R - h)^2 \right)} \quad [6.2]$$

The following assumptions were adopted: (a) the weighted averages above apply to maximum cell volume; (b) that tubule radius decays more slowly than the cell height; (c) cell height and layer height decay in the same manner. Then a relative cell volume was defined as shown in Eqn 6.3.

$$Cell\% = \frac{Cell_v - Cell_{vmin}}{Cell_{vmax} - Cell_{vmin}} \quad [6.3]$$

Then the tubule radius was calculated as shown in Eqn 6.4.

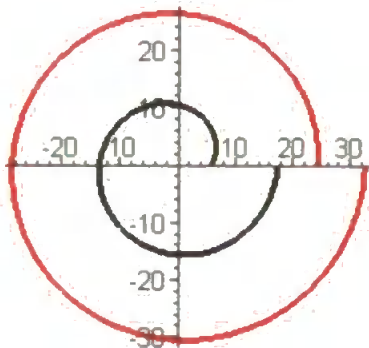
$$R = R_{max} (0.75 + 0.25 Cell\%), \quad h = h_{max} p(Cell_v) \text{ and } l = l_{max} p(Cell_v) \quad [6.4]$$

Where  $R_{max}$  and  $h_{max}$  were taken as the weighted averages from Table 6.1 and used to calculate  $l_{max}$ .  $p(Cell_v)$  was a polynomial, which gave the best fit to the desired cell volumes, specified below for  $Cell_v$  in  $\mu m^3$ .

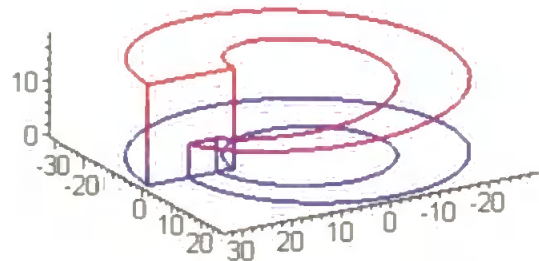
$$p(x) = 0.156 + 8.354 \times 10^{-4} x - 4.333 \times 10^{-7} x^2 + 1.456 \times 10^{-10} x^3 - 2.046 \times 10^{-14} x^4$$

With this scheme the three spatial parameters were derived from the cell volume (Figs 6.3a & b). Specific regard for the different morphological feeding extension into the tubule lumen were considered in section 6.8.

(a)



(b)



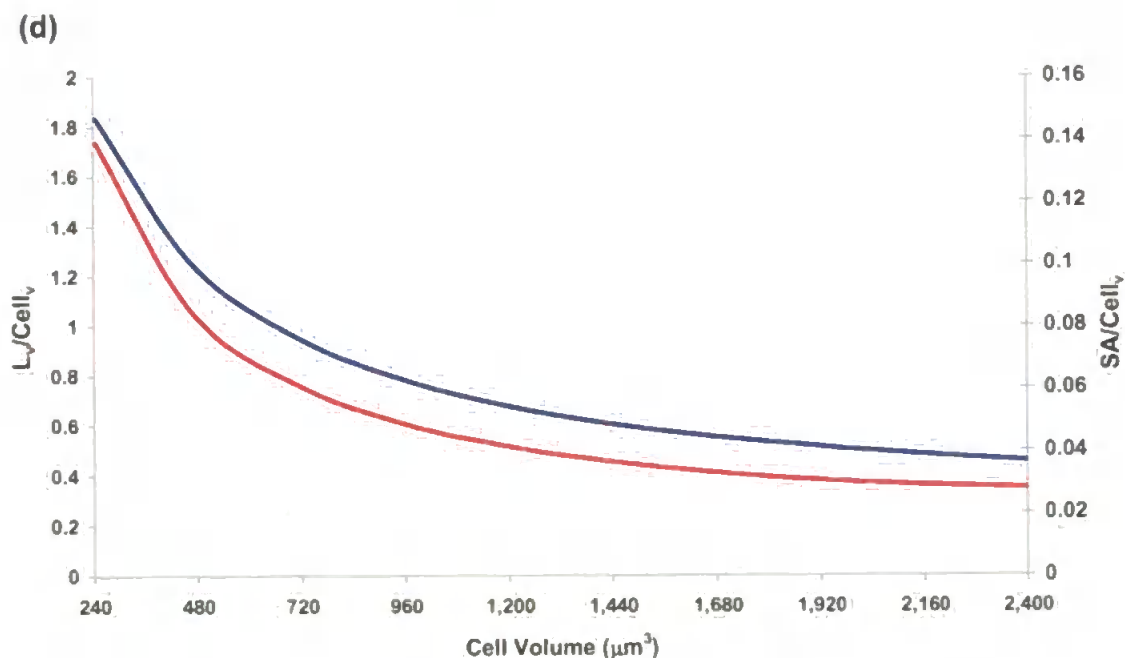
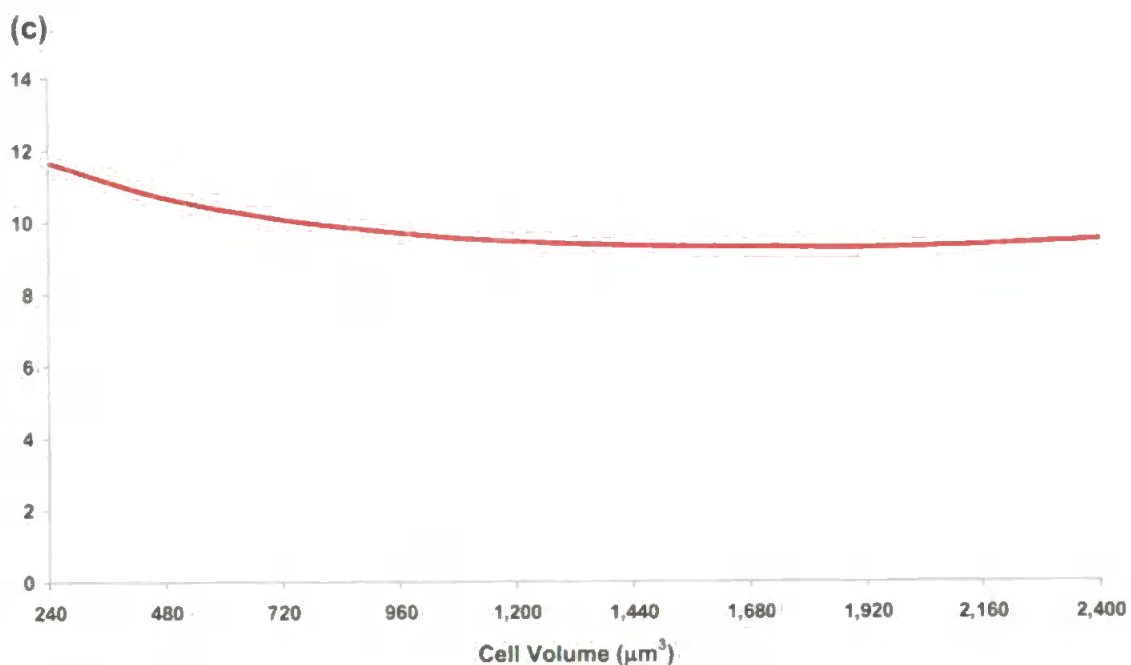


Fig 6.3 Spatial dimension variations with cell volume. (a) From minimum to maximum cell volume anticlockwise from 0 to  $2\pi$  showing — Tubule Radius,  $R$ , and — Cell height,  $h$ . (b) Complete tubule and digestive cell spatial components (c) Lumen Volume / Cell Surface Area (d) — Lumen Volume / Cell Volume and — Cell Surface Area / Cell Volume

The cell model was predicated on the assumption that the cell volume was a measure of how much food it could process; additionally the tubule lumen volume could be seen as a measure of the amount of food that could be supplied to the cell, and the cell surface as a measure of how much food could be taken up whether through endocytosis or diffusion. Thus, the ratio between the lumen to cell volume nominally shows the relationship between processing ability and availability. Under the proposed scheme, the lumen to cell volume ratio drops to a fifth of its highest value (Fig 6.3d) as cell volume increases by a factor of 10. However, this discounted the speed at which the cell was capable of processing nutrients, and this apparent shortfall was accommodated by refreshing the tubule more often. Similarly, the cell surface area to volume ratio drops to a quarter of its highest value when cell volume increased to a maximum, reflecting a relative fall in endocytotic capacity. However, the net rate of uptake would have been 2.5 times greater than the original and, given the higher capacity of the cell, the frequency of refreshment of the tubule could be increased concomitantly to increase the amount of nutrients processed. There was a much smaller variation in the lumen volume to cell surface area ratio (Fig 6.3c) indicating that the amount of food made available to the uptake capacity of the cell was not seriously impaired by this cellular spatial algorithm. This conceptual, spatial model satisfied objective 2 of this chapter and was next used in the determination of probabilities for a stochastic feeding mechanism.

### 6.5 Stochastic model: Model 5a

All of the probability driven models that follow started with food particles entering the core of the tubule lumen signifying the end of the holding phase. Thereafter, for each timestep of the simulation a probability, constant or variable, was used to model the flow of food particles into the brush border,  $P(toBB)$ . Food in the epithelial microvillous (brush) border then had a probability of either becoming associated with an endocytotic site  $P(toES)$ , returning to the tubule lumen  $P(toL)$  or remaining in the brush border. The desired rate of endocytosis was then be determined by the number, capacity and turnover of the endocytotic sites and the number of particles therein. A pictorial representation is shown in Fig 6.4.

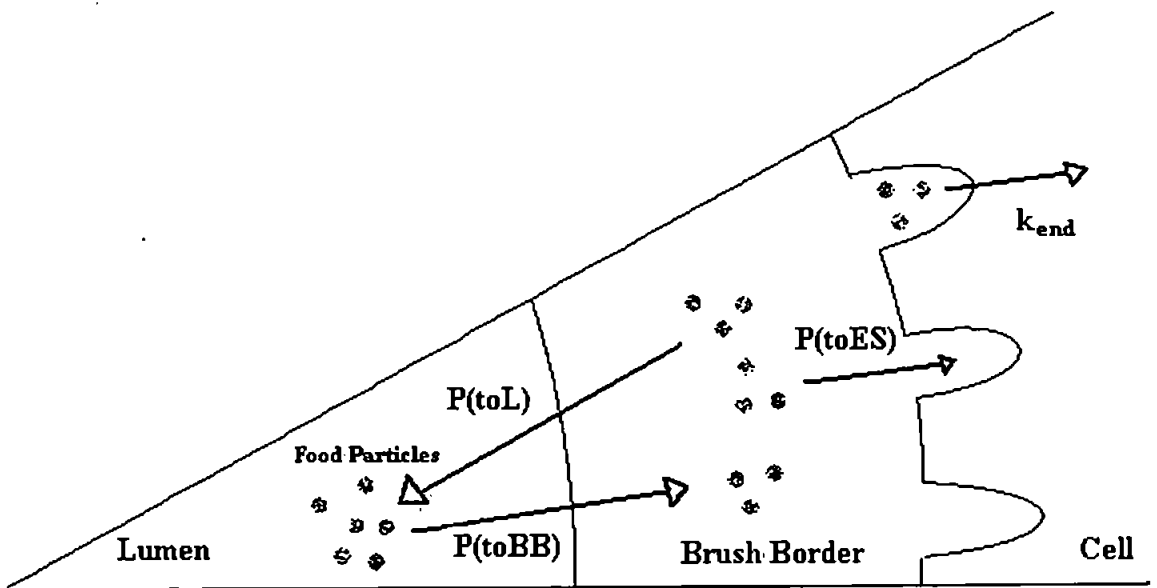


Fig 6.4 Stochastic feeding model

The first model, model5a, initially neglected the calculation rate of endocytosis and concentrated on the dynamics of the particles into the endocytotic sites. The following rules and simplifications were made:

1. The ratio of the volume occupied by the brush border,  $BB_v$ , of the digestive epithelium to the total tubule lumen volume,  $T_v$ , was considered constant throughout a single feeding phase and equal to the probability of particles in the lumen entering the brush border. i.e.

$$P(\text{toBB}) = \frac{BB_v}{T_v} \quad [6.5]$$

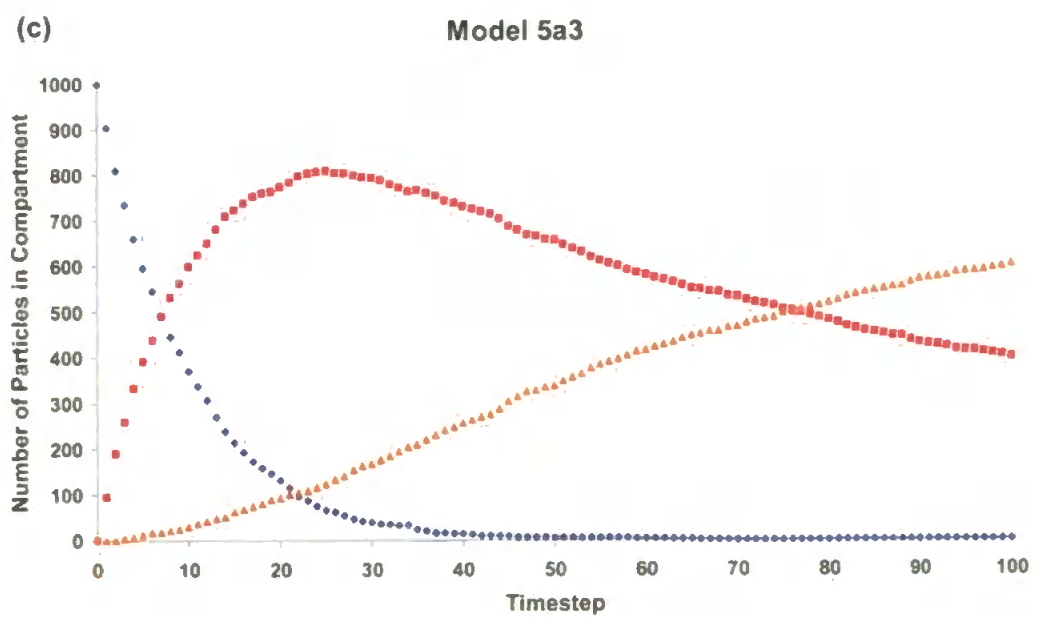
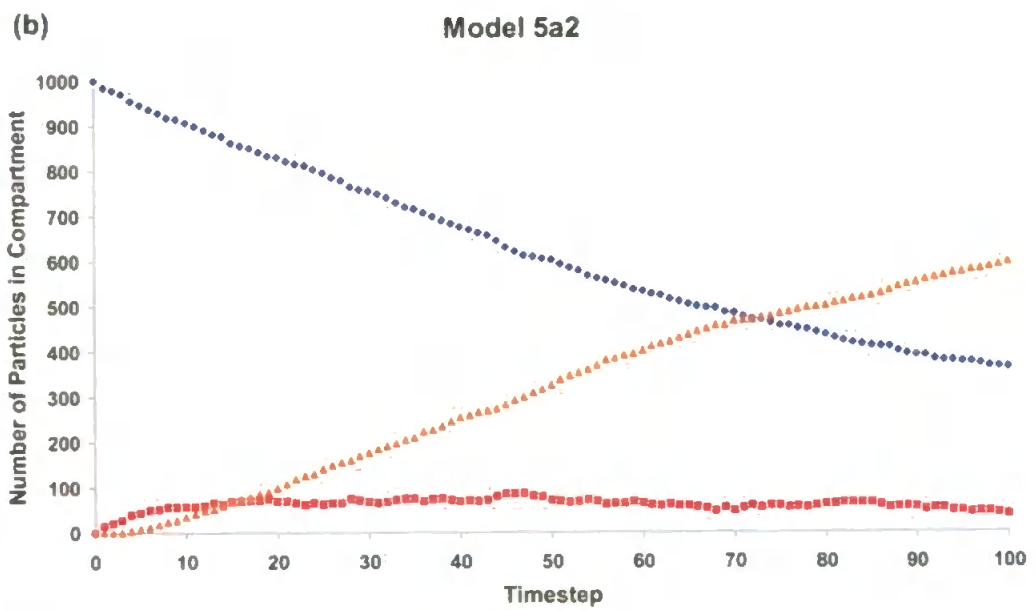
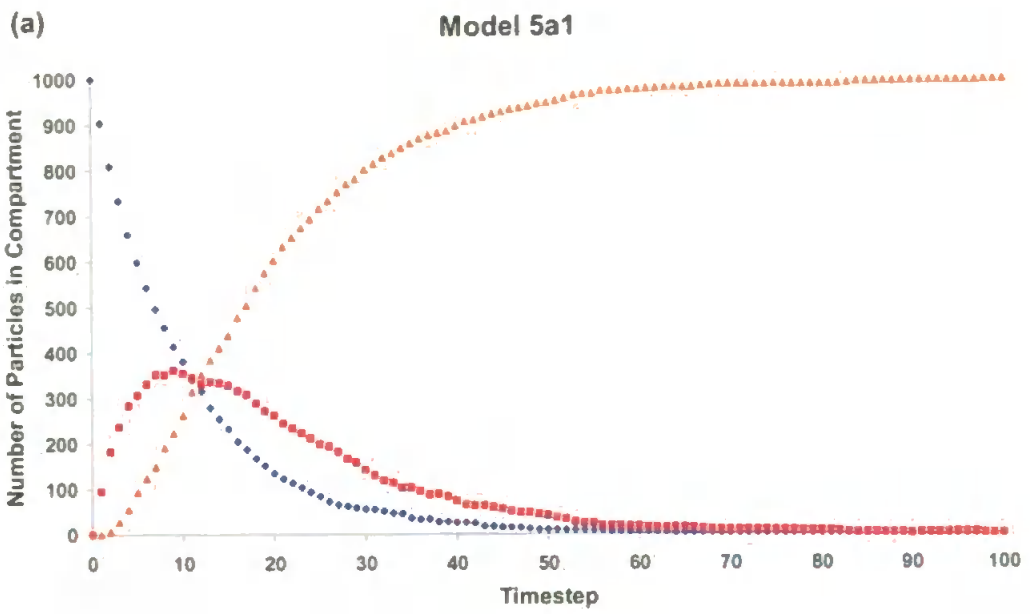
2. Material entering brush border did not return to lumen. i.e.

$$P(\text{toL}) = 0 \quad [6.6]$$

3. The number of endocytotic sites,  $NES$ , remained constant and each site was considered to exert an attractive influence over a constant neighbourhood,  $ES_v$ . Then the probability of brush border particles entering the endocytotic sites was calculated from the ratio of total endocytotic site attractive neighbourhood volume to brush border volume. i.e.

$$P(\text{ToES}) = NES \times \frac{ES_v}{BB_v} \quad [6.7]$$

In order to highlight the issues this model did not address adequately, consider as a base case, a tubule for which the brush border comprises 10% of the tubule lumen. Suppose there are 100 endocytotic sites, each with a catchment zone of 0.0001 units<sup>3</sup>. Then suppose the tubule feeding phase period is 100 time units. Finally, let there be 1000 particles in the newly charged tubule layer. The solutions to this model are shown in Figure 6.4.



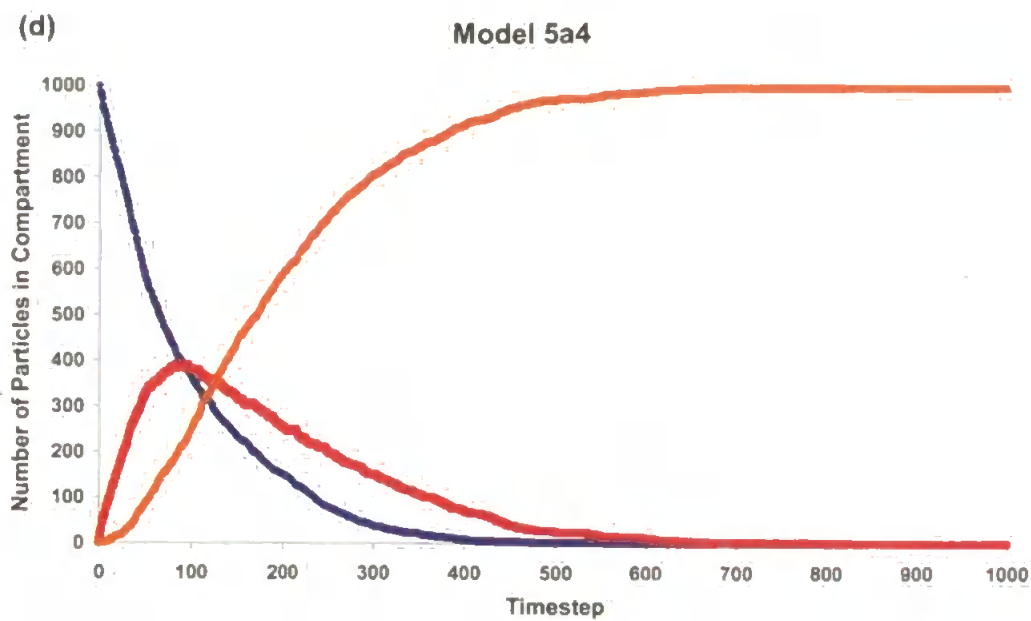


Fig 6.5 Model5a showing flow of particles from tubule core at beginning of feeding cycle to endocytotic sites of digestive cell. ♦ Particles in tubule lumen, ■ particles in brush border & ▲ particles attached to endocytotic sites. (a) Base case  $P(toBB) = 0.1$ ,  $P(toES) = 0.1$  (b)  $P(toBB) = 0.01$ ,  $P(toES) = 0.1$  (c)  $P(toBB) = 0.01$ ,  $P(toES) = 0.1$  (d)  $P(toBB) = 0.01$ ,  $P(toES) = 0.01$  (Note change in time axis).

The expected exponential decrease in the number of particles in the tubule lumen was evident from Figure 6.5. With ‘perfect’ brush border capture of the food particles,  $P(toL) = 0$ , the number of food particles in the tubule lumen at timestep  $n$  was given by:

$$T(n) = T(0)(1 - P(toBB))^n \quad [6.8]$$

The smaller the value of  $P(toES)$  the closer the increase in number of brush border food particles, which reflected the decrease in the tubule lumen. The number in the brush border at timestep  $n$  was given by Eqn 6.9.



$$BB(n) = T(0)P(toBB) \left( P(toES)^n + P(toES)^{n-1} P(toBB) + P(toES)^{n-2} P(toBB)^2 + \dots + P(toES)^{n-i} P(toBB)^i + \dots + P(toBB)^n \right) \quad [6.9]$$

Reducing the flow from the lumen to the brush border, by one order of magnitude, stretched out and flattened the brush border particle curve as the lumen particles obviously decreased at a far slower rate (Fig 6.5b).

Reducing the brush border to endocytotic site probability by the same scale served to increase the number of particles retained in the brush border (Fig 6.5c). Reducing both probabilities led to the same curves as seen in Figure 6.5a but stretched out by a factor of 10 (Fig 6.5d).

## 6.6 Endocytotic model: Model 5b

As a first attempt at using the probability model to provide the endocytotic rate for the cell model the following used a random number generator to assign probabilities to each particle. Furthermore, it used the generator and the following algorithm to decide whether or not an endocytotic site initiated or 'fired'; thereby releasing a vesicle and the associated particles into the cell interior. The particular site was then classified as inactive until the endosome sortation period had expired.

A maximum number of particles,  $M$ , were allowed at any endocytotic site which defined a probability function for a site firing at each timestep by:

$$P(\text{fire } ES_i) = \frac{NEP_i}{M} \quad [6.10]$$

Where  $NEP_i$  was the number of particles at endocytotic site  $i$ . There may be a lower limit of particles to make the energetic cost of the operation economically viable but this was not included.

If it were supposed that each vesicle formed was of uniform size then the endocytotic rate was readily calculated. For the following simulation  $P(\text{toBB}) = 0.1$ ,  $P(\text{toL}) = 0$ ,  $P(\text{toES}) = 0.1$ , endosomal sortation period  $\tau = 5$ ,  $M = 10$  and vesicle diameter = 0.15 microns. In all cases the random number generator is a Fibonacci Lagged Generator. The simulation has been run 1000 times with differing seeds and the average values at each timestep have been taken. The site attached number fell as various sites

'fired' and sent particles by vesicle to the endosome. Then the site became inactive for 5 time units, during which particles were free to associate with the site. Once associated with a site particles did not disengage under this model.

The brush border and lumen particle behaviour remained unaffected by the changes to the system (Fig 6.6a). However, the number at endocytotic sites started to decrease as the invagination of endocytotic vesicles commenced almost immediately. A peak of activity was seen around timesteps 15-20. Presumably, if there were an energetic cost involved in endocytosis, an optimal strategy would be sought. At present the average number of particles per vesicle was only 1.72, during the peak period (Fig 6.6b). Furthermore the rate of endocytosis never reached anywhere close to the maximum limit and was often below the prescribed minimum limit. Increasing vesicle diameter would increase the rate of endocytosis, but the content and concentration would still be determined by the number of particles associated with each vesicle.

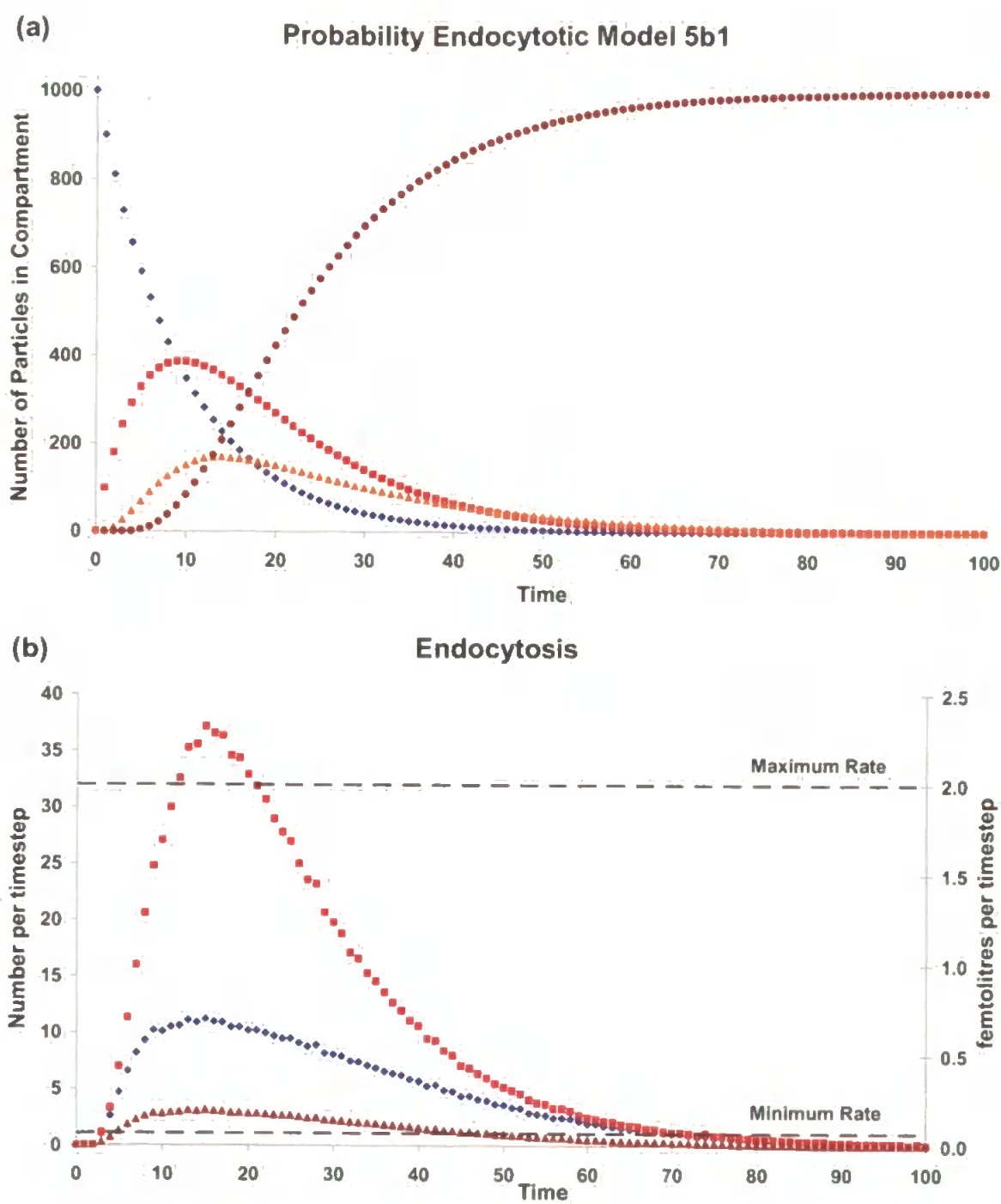


Fig 6.6 Probability model5b1 to determine endocytotic rate (a) ◆ Particles in tubule lumen, ■ particles in brush border, ▲ particles attached to endocytotic sites & ● particles ingested by cell (b) Number of vesicles (◆) and particles(■) taken in by cell at every timestep and rate of endocytosis (▲).

The algorithm was modified so that the number of particles associated with each endocytotic site was allowed to surpass the maximum for triggering endocytosis. This variation provoked an oscillatory pattern to emerge with a period equal to the endosomal sortation period (Fig 6.7b). This was due to the model allowing the number of particles at a site to increase whilst it was inactive after firing. This allowed the average number of particles at each site to tend towards the preset maximum; and forced the site to fire immediately once active. This pattern was repeated until the number of particles in the brush border was depleted to an extent where there was no longer enough to fill all of the endocytotic sites.

The relative number of particles within the brush border had a higher maximum than the previous model (Figs 6.6a & 6.7a). The maximum proportion of particles attached to an endocytotic site awaiting endocytosis was, perhaps surprisingly, diminished.

By increasing the vesicle diameter from 15 to 23 $\mu$ m the rate of endocytosis intermittently achieves its maximum limit, but the average rate over the entire simulation was 0.793 femtolitres/minute which was not far away from the minimum.

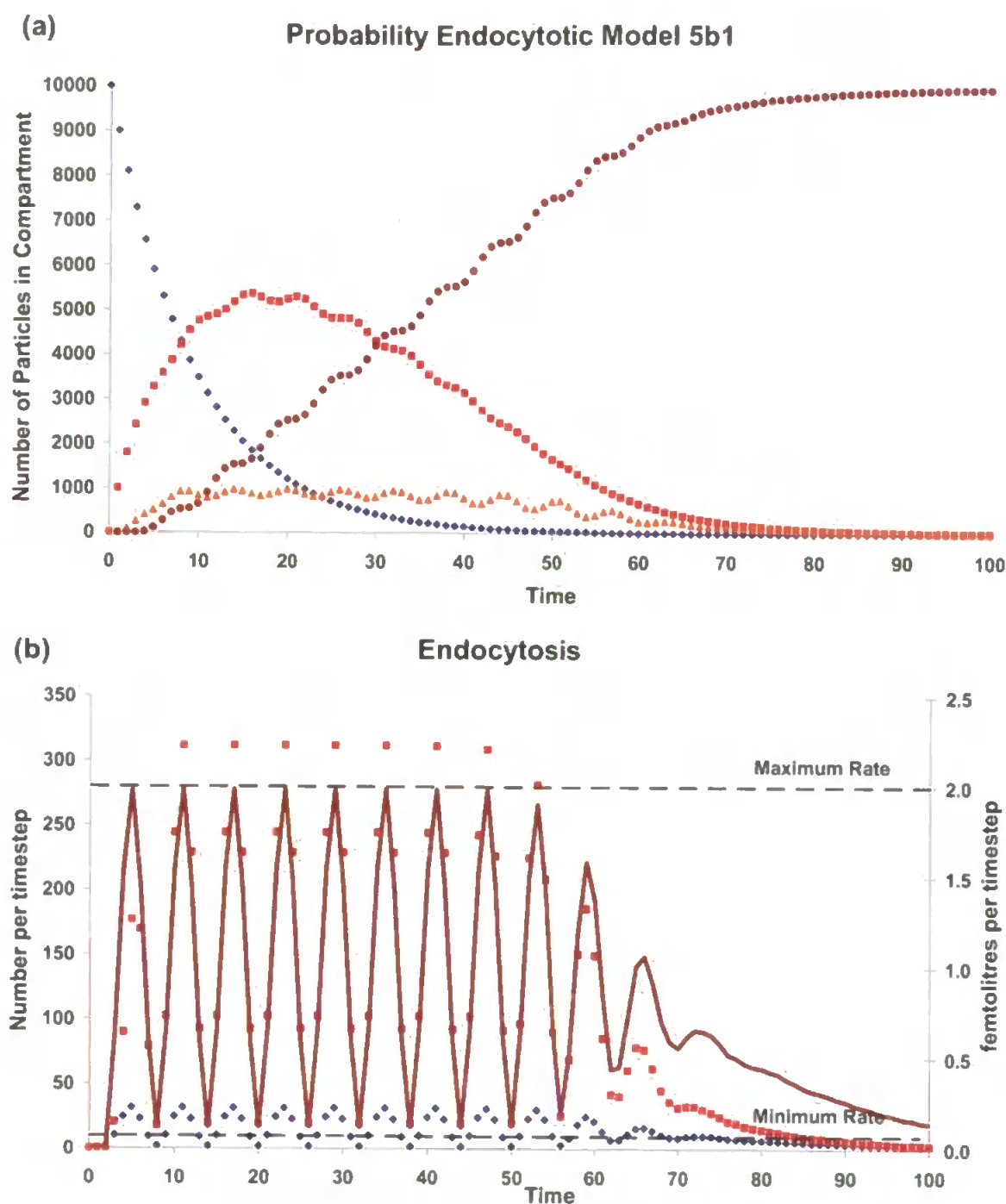


Fig 6.7 Model5b1 10,000 initial particles, vesicle diameter =  $23\mu\text{m}$   
 otherwise as described for Fig 6.5 (a) ♦ Particles in tubule lumen, ■  
 particles in brush border, ▲ particles attached to endocytotic sites & ●  
 particles ingested by cell (b) Number of vesicles (♦) and particles(■) taken  
 in by cell at every timestep and rate of endocytosis (▲).

### 6.7 Partial derivative equation model: Model 5c

A degree of mechanical/functional interpretation had gone into the construction of the brush border and endocytotic pits and the dynamics involved therein. In contrast, the probability for food particles to brush border based on relative volume sizes was relatively arbitrary. The flow of particles from the mucus string, i.e. luminal core towards the brush border could be described by a partial differential equation with the following assumptions.

- a) the mucus string to which the particles are initially attached can be described as a circular tube which was situated in the middle of the tubule
- b) any vertical difference was negligible across a cell layer
- c) the concentration was independent of angular variation

Then the concentration of particles will be given by the solutions to the following boundary value problem. Let  $u(r, t)$  be the concentration of particles at radial distance  $r$  at time  $t$ . Then using the parabolic heat equation in cylindrical polar coordinates this led to:

$$\frac{\partial u}{\partial t} = k \left( \frac{\partial^2 u}{\partial r^2} + \frac{1}{r} \frac{\partial u}{\partial r} \right) \text{ for } 0 < r < L \text{ and } t > 0 \quad [6.11]$$

Where  $L$  is the distance from the tubule centre to the brush border and  $k > 0$  is some coefficient of diffusion. Given that, initially, there was a core of equally spread particles in the middle of the tubule over a distance  $L$ , then the initial condition were formulated (Eqn 6.12).

$$u(r,0) = f(r) = \begin{cases} A & 0 \leq r \leq L_1 \\ 0 & L_1 < r < L \end{cases} \quad [6.12]$$

For the boundary condition it was required that  $u$  should remain finite at the tubule centre. Furthermore, it appeared plausible that at the border of the membrane that the flow of particles to the brush border was proportional to the particle concentration at the border; thus the Neumann boundary condition in Eqn 6.13 was adopted.

$$u(L,t) = B \frac{\partial u}{\partial r}(L,t) \quad [6.13]$$

This is then a Sturm Liouville boundary value problem which by separation of variables i.e. suppose  $u(r,t) = R(r)T(t)$  has solutions:

$$R(r) = C_1 J_0(\mu r) \quad \text{and} \quad T(t) = D e^{-\mu_n^2 k t} \quad [6.14]$$

with eigenvalues  $\lambda_n = \mu_n^2$  given by  $J_0(\mu_n L) - B \mu_n J_1(\mu_n L) = 0$

By the principle of superposition this gives the solution

$$u(r,t) = \sum_{n=1}^{\infty} c_n J_0(\mu_n r) e^{-\mu_n^2 k t} \quad [6.15]$$

where  $c_n$  are the Fourier Bessel coefficients given by

$$c_n = \frac{\int_0^L r f(r) J_0(\mu_n r) dr}{\int_0^L r J_0^2(\mu_n r) dr} = \frac{A \int_0^{L_1} r J_0(\mu_n r) dr}{\int_0^L r J_0^2(\mu_n r) dr} = \frac{2 A L_1 J_1(\mu_n L_1)}{\mu_n L^2 (J_0^2(\mu_n L) + J_1^2(\mu_n L))} \quad [6.16]$$

In order to test the effects of the various parameters, approximations to the necessary Bessel functions were needed (see Appendix C). Once established, the effect of the number of eigenvalues on the precision of the approximation to the concentration function was investigated (Fig 6.8).



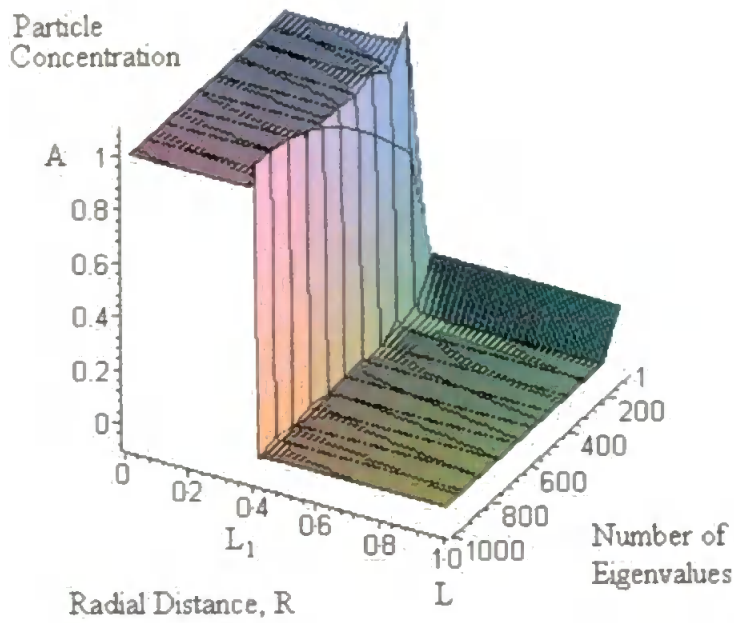


Fig 6.8 Initial condition dependence on number of eigenvalues used in approximation with  $L = 1$ ,  $L_1 = 0.4$  &  $A=1.0$

Once past 100 eigenvalues the only real problem occurred at the discontinuity and to a lesser degree around 0. For the following analysis the number of eigenvalues was curtailed to 100 for computational ease.

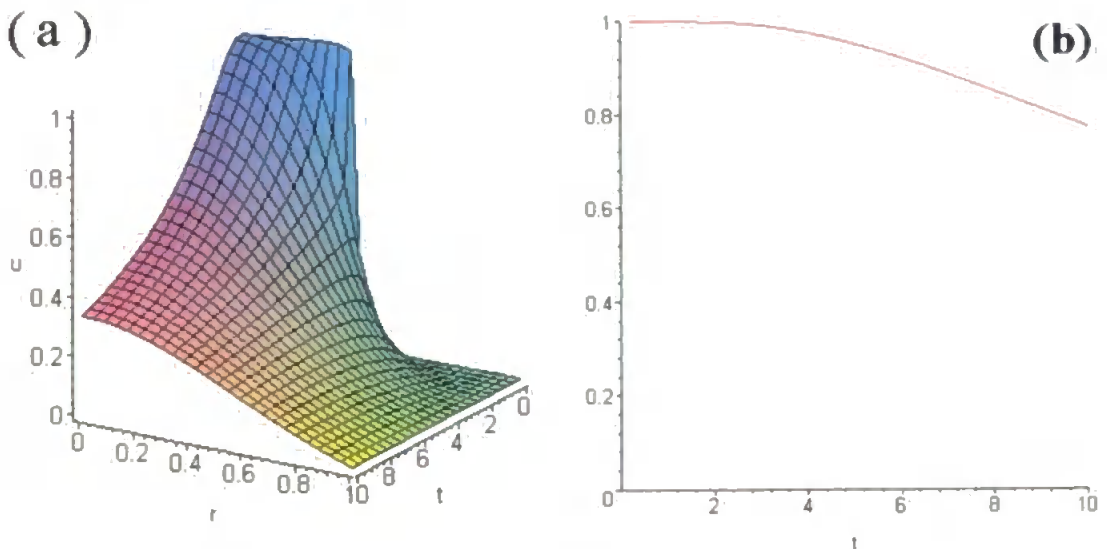


Fig 6.9 Particle migration.  $k = 0.01$ ,  $B = 0.001$ ,  $L = 1$ ,  $L_1 = 0.4$ ,  $A = 1.0$  &  $N_E = 100$  (a) particle concentration over radial profile progressing in time (b) fraction of initial particles remaining in tubule lumen.

The solution for a particular set of parameters is shown in Fig 6.9a.

What was required for the model was the number of particles left in the tubule lumen at any time. As a fraction of the initial number this can be found by calculating the formula in Eqn 6.17.

$$\frac{\int_0^L ru(r,t)dr}{AL_1^2} \quad [6.17]$$

It was deemed beneficial to determine how the parameters involved affected the solutions.  $A$  &  $L_1$  were based on the initial conditions and it is hoped that they should be derivable from study of the mucus string, possibly prior to delivery to the tubule.  $L$  could be derived from the spatial model discussed above.

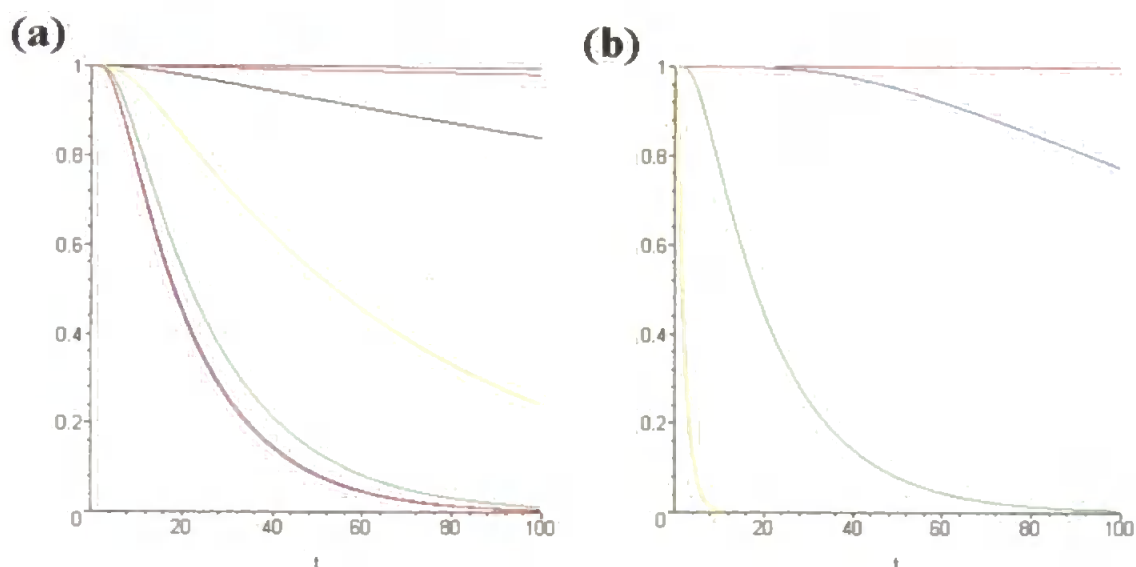


Fig 6.10 Time course development of tubule lumen particle concentration expressed as a fraction of initial condition:  $A = 1.0$ ,  $L = 1.0$ ,  $L_1 = 0.4$ ,  $N_E = 100$  (a) effect of boundary condition coefficient  $k = 0.01$ ,  $B = -1000$  —  $100 - 10$  —  $1 - 0.1 - 0.01 - 0.001$  (b) effect of diffusion coefficient with  $B = 0.001$ ,  $k =$  —  $1.0 - 0.1 - 0.01 - 0.001 - 0.0001$

The dynamic effects were controlled by  $B$  and  $k$ . The diffusion coefficient,  $k$ , would only affect the profile in the time direction, whilst  $B$  affected the solution in the radial direction. The Neumann boundary condition revealed that if  $B$  was greater than 1 the diffusion out of the tubule would be sluggish (Fig 6.10a). If  $B \geq 0$  then the diffusion will follow an exponential nature. The same pattern was generated for all  $k$  values but stretched across the time axis (Fig 6.10b).

However, due to the lack of data and the length of computational time for this model, it was appropriate to seek a numerical approximation to this function. This approximation could then be used in lieu of the full solution.

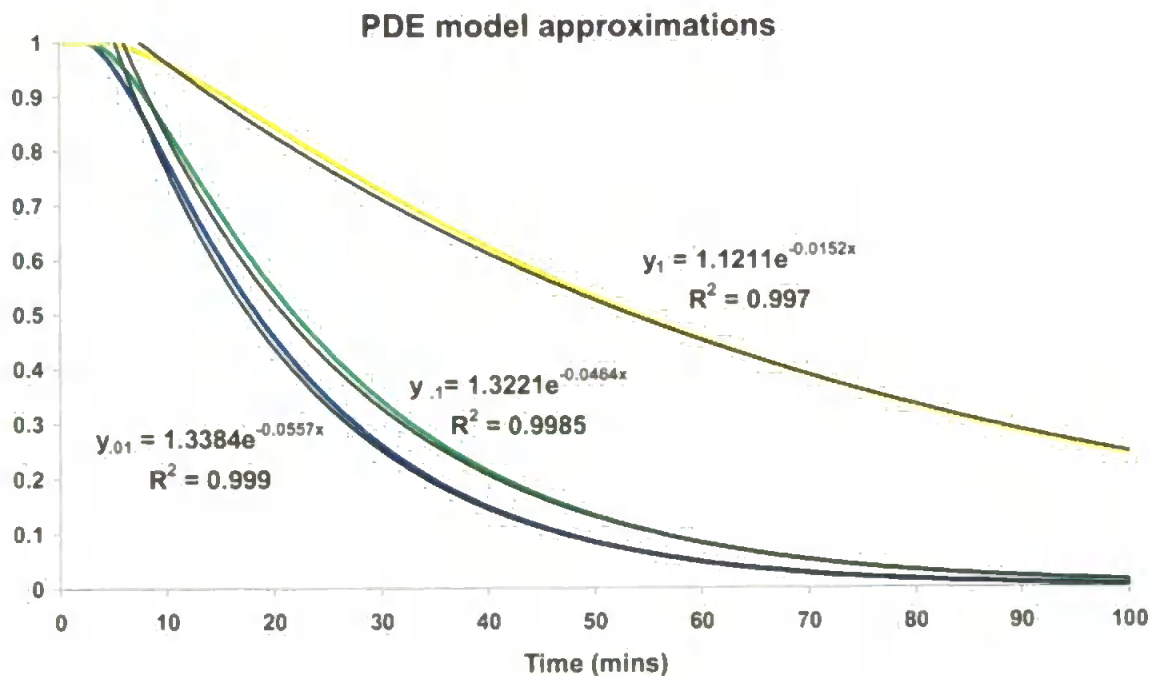


Fig 6.11 Exponential approximations to tubule lumen particle counts for  $B=1-0.1-0.01$ .

Exponential functions approximated the particles in the tubule lumen with fair degrees of accuracy (Fig 6.11). Hence the approximation function was considered to be of the form  $ae^{-bt}$ . Then to be able to approximate for all interceding values of  $B$  the values for  $a$  &  $b$  were made dependent upon this parameter.

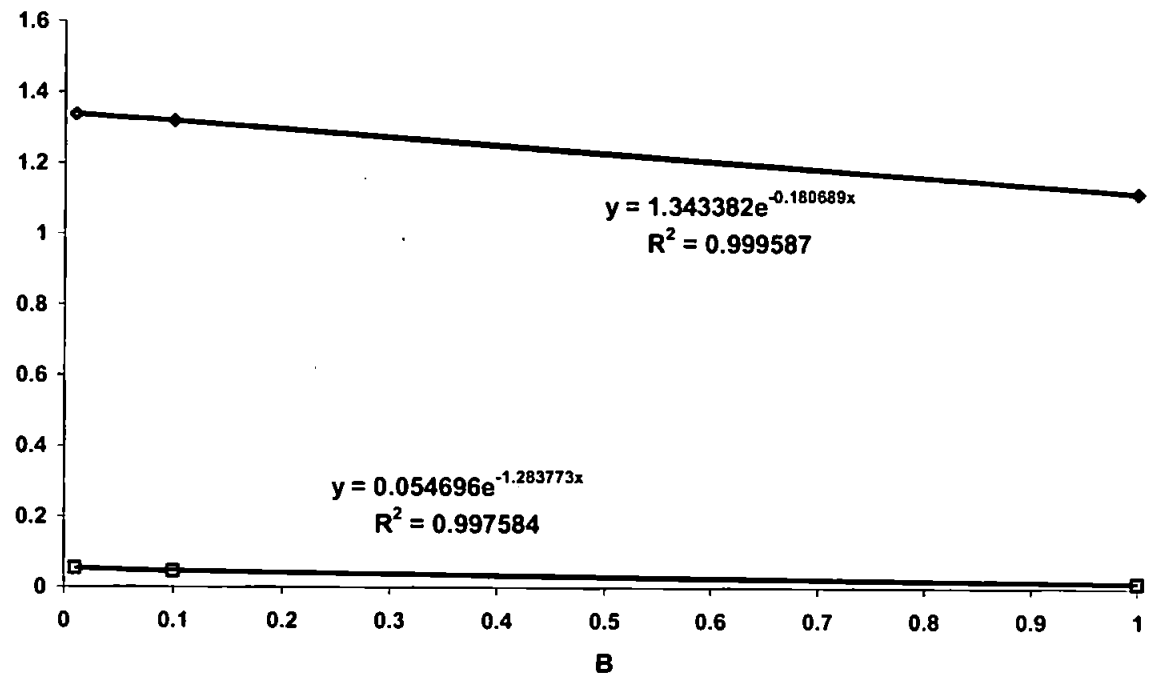


Fig 6.12 Parameter determination for exponential approximation —  $a$  —  $b$

Exponential approximations were once again taken to determine these parameters to retain the smoothness. Hence the approximation used was:

$$y(B,t) = 1.35e^{-0.18-0.00547te^{-1.28B}} \tag{6.18}$$

The resulting interpolation between the values of  $0.01 \leq B \leq 1.0$  is shown in Fig 6.12. Only at the start of the simulation was there a problem as the exponential function would only start at  $t = 0$  if there was no constant

coefficient multiplying it other than 1. Hence at the initial step the approximation was divided by the starting value to alleviate this.

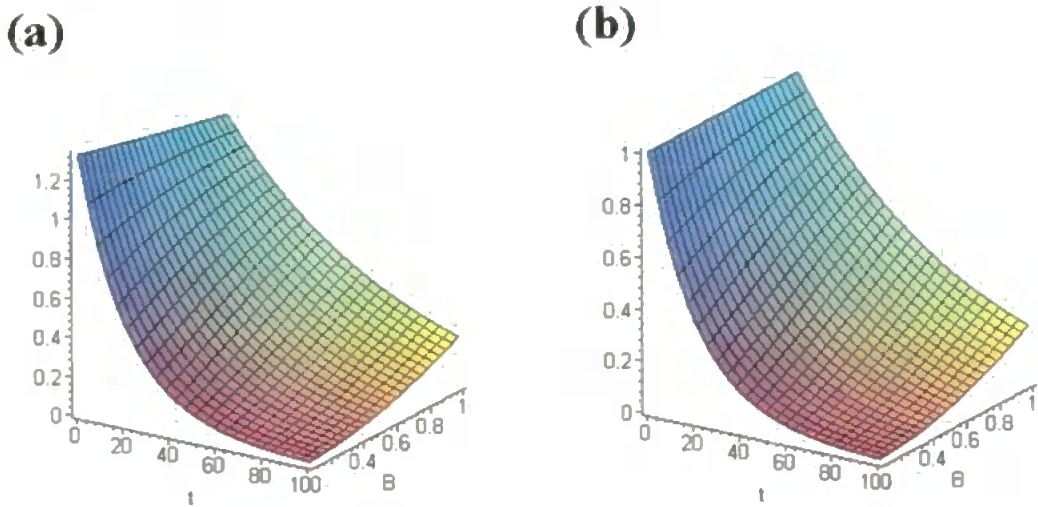


*Fig 6.13 approximation to the time series of particles in the tubule lumen across the  $B$  parameter space (a) initial model (b) adjusted model*

However, the overall dynamics exhibited by this more complicated model are remarkably similar to the original stochastic variant proposed in section 6.5 (Compare Figs 6.13a & 6.13b). This, coupled with the lack of available data to parameterise this algorithm, compelled the abandonment of this more complex alternative for the original.

Both proposed variants for the movement of material from the lumen to the brush border were only appropriate, if the shape of the brush border/lumen interface and their relative volumes remained constant. However, examination of the cross-sections of tubules during the feeding phase provided evidence that the cell extended into the lumen during this phase. It was considered necessary to investigate whether this motion would have a significant effect on the proposed model.

### 6.8 Variable lumen volume: Model 5d

Consideration was given to the extension of the cell into the tubule lumen, whilst feeding, to ascertain whether this could significantly alter the flow and capture of particles from the tubule lumen to the brush border, and hence the overall endocytotic rate. To this end  $R$  and  $l$  were supposed to remain static during the absorbing phase and were subsequently adjusted in the holding phase to reflect the growth once the cell had determined how much new material it had ingested. Then, during feeding, the only adjustment was of the cell height towards the lumen centre (Fig 6.14). The simplest extension model is to adjust  $h$  according to the amount of new volume acquired.

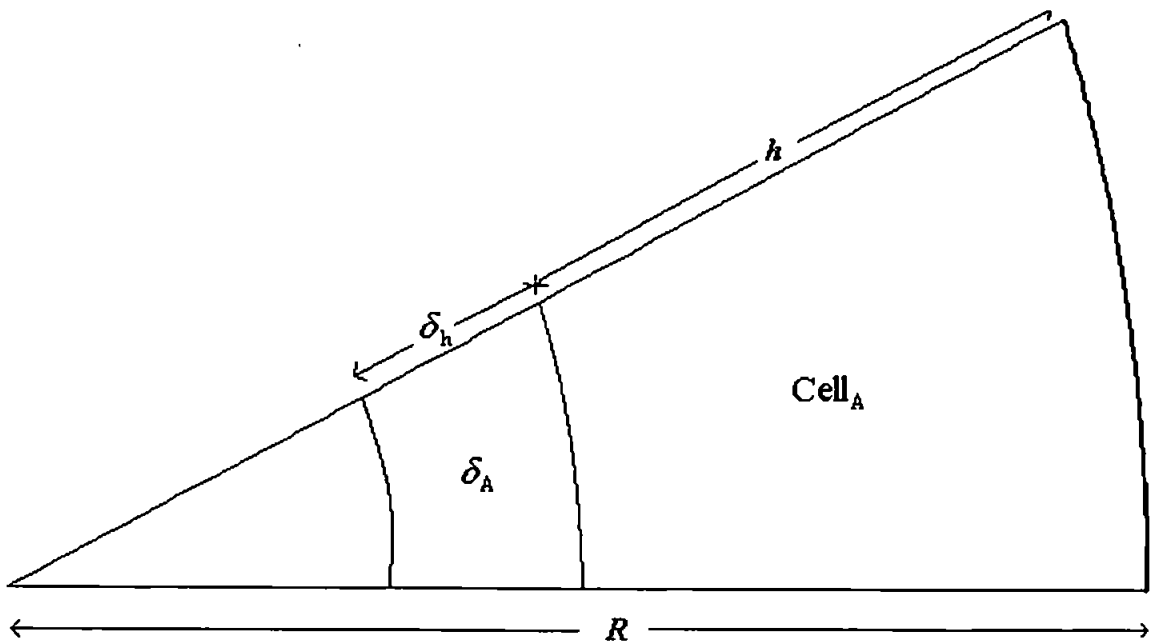


Fig 6.14 Schematic for simplest tubule lumen extension model.

Extending the cell height into the lumen by a distance  $\delta h$  gave a change in surface area  $\delta S = -\delta h \lambda$ , a change in 2D area  $\delta A = \lambda \delta h (2(R - h) - \delta h)$  and a change in cell volume  $\delta V = l \delta A = l \lambda \delta h (2(R - h) - \delta h)$ .

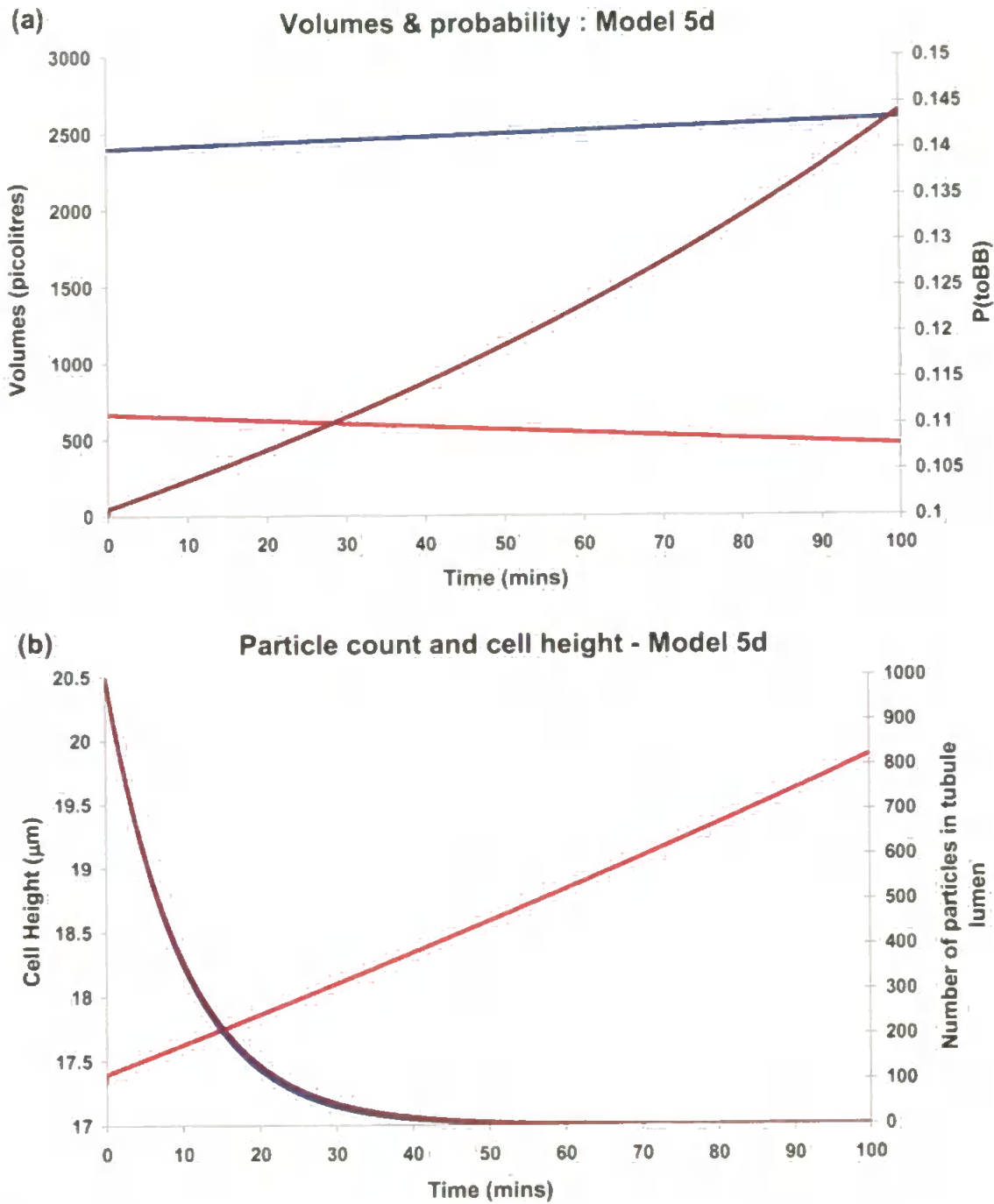


Fig 6.15 Model 6c 100 mins simulation (a) — Cell volume — Tubule Volume — P(toBB) (b) — Number of particles in tubule — Cell height — Number of particles in tubule with  $P(\text{toBB}) \equiv 0.1$ .

It was assumed that the brush border remained constant and that over 100 minutes the cell volume was growing at the maximum endocytotic rate, with nothing leaving the cell. The initial condition was set to be that the cell was at maximum volume and that the brush border volume was a tenth of the tubule volume, hence  $P(toBB) = 0.1$  per minute.

The cell volume grew linearly from 2400 to 2600  $\mu\text{m}^3$  after 100 minutes which meant the tubule volume fell from 671 to 471  $\mu\text{m}^3$  (Fig 6.15a). From which it was apparent that the  $P(toBB)$  rose from  $\frac{67.1}{671} = 0.1$  to  $\frac{67.1}{471} = 0.1425$  (4dp). Whilst this was a reasonable increase in the probability, the increase was too slow to significantly alter the particle dynamics as the majority have left the tubule before the probability was radically enhanced (Fig 6.15b).

Such a model would, however, reduce the apical surface area which, dependent upon how sparsely the endocytotic sites were originally distributed, could adversely affect the capacity for endocytotic activity. Consideration was given as to how the surface might deform into the lumen whilst keeping the surface area constant. Several different deformation models were tested to varying degrees of success, due to the small changes in volume at each timestep. However, there was no benefit to the probability model of modelling this extension exactly, as the only assumption used is that the proportion of tubule volume to brush border volume determined the probability of particle diffusion between the two.



## *6.9 Discussion*

The phasic behaviour described by Langton (1975, 1977) motivated the use of a discontinuous feeding signal. However several problems beset the development of this model. The most obvious being no concrete definition of what was occurring during the reconstituting phase and how it differed from the resting phase, which was the closest observationally. This and its relative infrequency led to its exclusion from the conceptual feeding-disintegrating-resting sequential phase cycle proposed.

Secondly, there was a problem with what occurred when an intertidal animal was exposed to the air. The proportion of feeding tubules decreased over the exposed period but still remained above 50%. If the tubule was still being supplied with nutrient rich water then the mussel must have some store higher up in the alimentary system. Otherwise, the last refresh of the tubule lumen with nutrient rich gut fluid/mucus was subject to an extended feeding phase, presumably allowing the cell to extract a greater proportion of the available nutrient. It would have been beneficial to know how much food was extracted from the tubule lumen, both during immersion and exposure, to see if some efficiency strategy was employed when food was readily available or not. Until this problem was resolved, the model has been considered only for mussels which were continually submerged.

The phasic behaviour observed also threw doubt on the prescribed parameter limits for endocytosis. For example the minimum value of the rate of endocytosis was greater than zero hence stipulating continual feeding even when food was not available: but if the tubule spent a substantial proportion of time 'resting' then there would be no need for endocytosis. Similarly, if the maximum rate limit was derived from an average ingested value, then if the model were to use a phasic model with a proportion of downtime then the upper limit needed to be raised. Thus, where originally endocytosis had been modelled as a continuous rate based on cellular volume, it was subsequently replaced by a discontinuous rate which was unrestricted by cellular constraints.

In order to incorporate this phasic pattern, a spatial model had to be constructed of the digestive gland. If the cylindrical layer height of the digestive tubule could be derived under similar conditions to the cell height a more complete model could be constructed of cell volume adjustments in accordance with feeding activity. Similar consideration should be given to determining the dynamics of the number of cells in a tubule layer through varying conditions. Equally, the probability models introduced work under a number of assumptions which require checking, such as the constant number of endocytotic sites.

Various attempts had been made to consider the effect of the type of deformation which the apical cell surface undergoes with increased volume due to food uptake and retention. It was considered that by reducing the

volume of the lumen the cell would concentrate the number of leftover particles enabling a greater efficiency in uptake. However, upon reflection these have been dropped, due to the reliance of uptake only upon the surface area and tubule volume.

Finally, the signal of food received in the tubule core needs to be related to the environmental signal. Then the model may be able to take on real input data for the food. However, this may well have to be a much simplified function to start with due to the various factors which have been shown to influence the rate and efficiency of food selection by the mussel (Bayne, 1973a, b; Bayne & Scullard, 1977b; Widdows *et al.*, 1992).



## Chapter 7 Macromolecular Model

### 7.1 Objectives

The objective of this chapter was to introduce a model based on the flow of macromolecules and their constituent forms rather than carbon and nitrogen alone. This was prompted by observation that the problematical constant carbon and nitrogen concentrations stipulated to control the previous models were unrealistic. Equally the response of the cell to energetic requirements varied across an annual cycle due to the availability of different forms of storage.

*Hypothesis 7.1:* moving to a model based upon macromolecules will allow the simulation of the observed variable seasonal C:N ratio.

Initially, the new model formulation was introduced, and then the various functions governing the flow of material were explicated. The initial conditions were then derived. Subsequently, a sensitivity analysis was performed to ascertain the effects of energy storage, nitrogen as a limiting factor and the various concentrations on the annual signal. The possible consequences of cell division on this signal were then explored. Finally the effect of a varying annual demand from the rest of the animal was considered.

## 7.2 Introduction

The models in this chapter were based on modelling the dynamics of the three major organic macromolecules (proteins, carbohydrates and lipid) and their constituents/storage forms (amino acids, glycogen, and triglyceride) throughout the compartmentalised cell (Figure 7.1). This allowed for

- 1) Enhanced flexibility in the cellular response to feeding, dependent on composition as well as quality of food and state of the cellular macromolecular balance., i.e. whether to store or release energy forms, deaminate amino acids when the only available energy was stored within amino acids or export suitable forms when in excess
- 2) The capability to model the lysosome less arbitrarily

In these final models the endosome and lysosome were considered to be composed of two types of material, the intrinsic digestive enzymes and lipoprotein membrane, and the target material delivered for degradation. The flow through each degradative organelle remained as described in model 5, except the throughput was now formulated as a function of the intrinsic protein content. Hence, functional perturbation or damage to these enzymes reduces throughput capability and subsequently provoked some of the customary swelling of the lysosome (Lowe *et al.*, 1981). Damage to the intrinsic lipid and or proteins in the membranes reduces the membrane

stability and either undigested materials or the lysosomal enzymes were allowed to diffuse through the membrane into the cytosol, where it then joined a pool of cytosolic material which had been damaged and awaited sequestration by autophagy (Cuervo, 2004; Moore *et al.*, 2006b, 2007). This then provided a feedback loop of undigested material re-entering at the start of the digestive process.

Cytosolic material was damaged as a consequence of the reactive oxygen/nitrogen species present in the cell (Cuervo, 2004; Regoli, 2000). Autophagy was then modelled as a reflex action carrying a steady fraction of damaged cytosolic material to the lysosome. Damage to intact material was modelled as a percentage of this material per timestep, i.e. as a first order dynamic relationship.

In order to incorporate these refinements a number of rates and constraints needed to be addressed. The initial model presented in this chapter lacked the ROS, lipofuscin and triglyceride storage form and concentrated on the following in order to be able to get a feel for the dynamics of the new system and to be able to try and obtain a seasonal response for validation against a data set (Gabbott & Bayne, 1973).

*Table 7.1 Description of various compartments and nomenclature for*

*Figure 7.1*

Compartment		Carbohydrates	Proteins	Lipid
Surface		<i>SS</i>	<i>SP</i>	<i>SL</i>
Endosome	internal	<i>N/A</i>	<i>EP</i> <i>degradative</i> <i>enzymes</i>	<i>EL</i> <i>lipid membrane</i>
	target material	<i>ETS</i>	<i>ETP</i>	<i>ETL</i>
Lysosome	internal	<i>N/A</i>	<i>LP</i> <i>degradative</i> <i>enzymes</i>	<i>LL</i> <i>lipid membrane</i>
	target material exogenously sourced	<i>LTES</i>	<i>LTEP</i>	<i>LTCL</i>
	target material endogenously sourced	<i>LTCS</i>	<i>LTCP</i>	<i>LTCL</i>
Cytosol	internal	<i>CS</i> <i>free sugar</i> <i>pool</i>	<i>CP</i> <i>functional</i> <i>proteins</i>	<i>CL</i> <i>free fatty acid</i> <i>pool &amp;</i> <i>membranes</i>
	Storage /Constituent Forms	<i>G</i> <i>glycogen</i>	<i>AA amino</i> <i>acid pool</i>	<i>T</i> <i>triacylglyceride</i>
	Damaged Pools	<i>CDS</i>	<i>CDP</i>	<i>CDL</i>
	Residual Bodies	<i>RB</i>		



## Model 6: Macromolecules

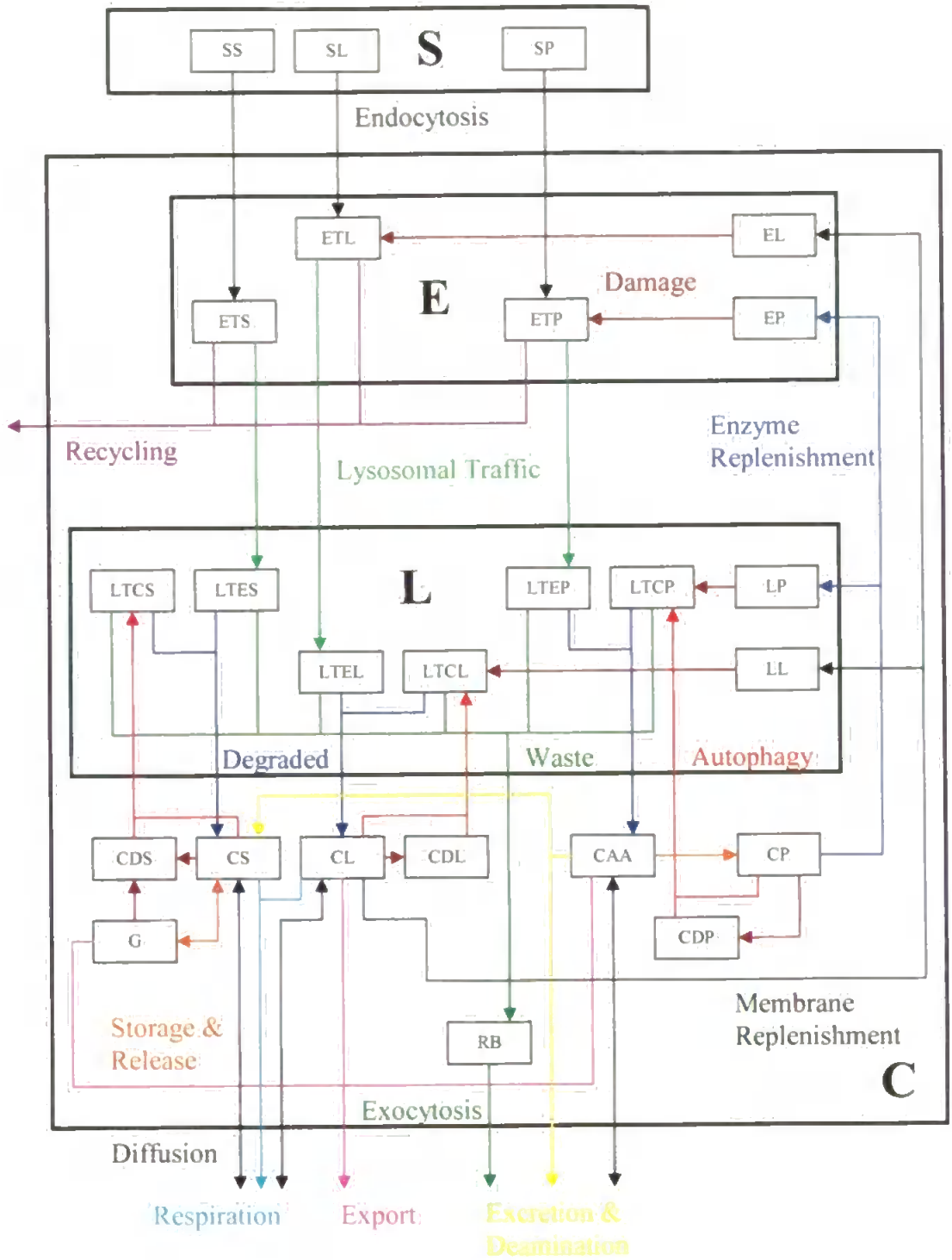


*Fig 7.1 Model 6 Schematic*

7.3 Macromolecular model initial set up

Compartmental Concentrations and Initial Conditions

This model focused on the ratio of the different macromolecules within the cell. Utilising the previous values for carbon and nitrogen contributions to the differing macromolecular composition and seasonal data from Thompson *et al.* (1974) for non-mantle tissue, a seasonal plot of overall carbon and nitrogen ratio was produced (Figure 7.2).

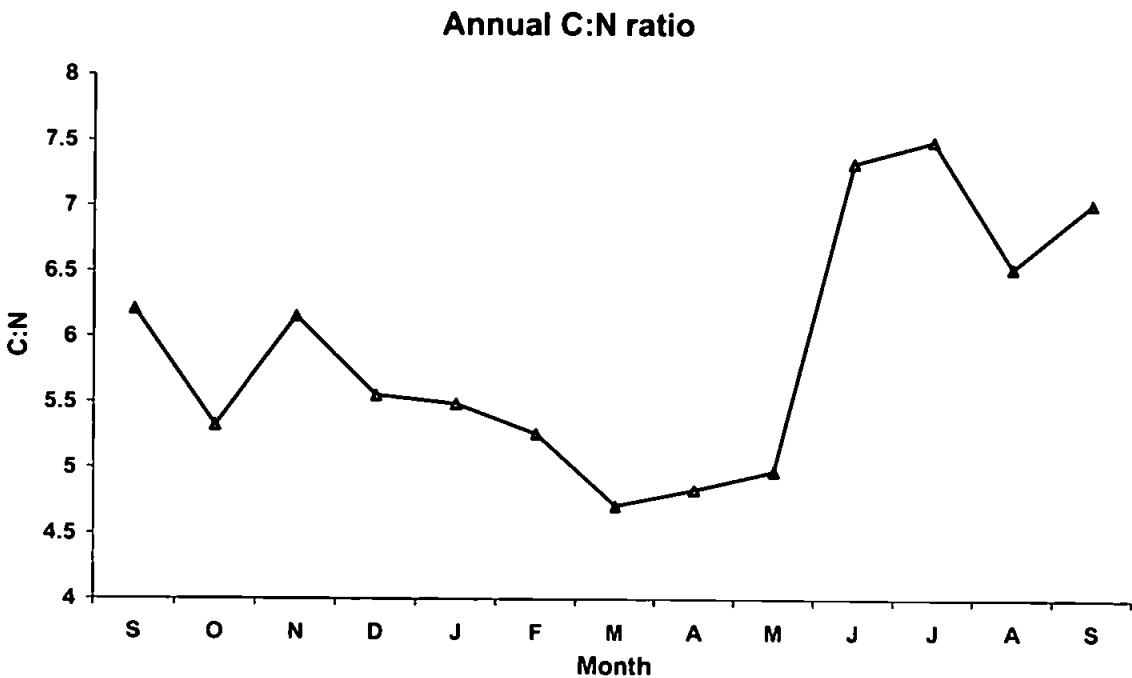


Fig 7.2 Annual C:N ratio

The minimum C:N ratio was during the spring when carbohydrate and lipid reserves were at their lowest. Once food availability increased over the summer these stores were filled in anticipation of food depletion over the autumn and winter, whereupon they were utilised. The summer increase in C:N ratio was opposite to that observed by Gardner &

Thompson (2001). However, their measurements were made on all soft tissue and not just the digestive gland.

Consequently, the assumption of constant carbon and nitrogen concentration controls assumed in previous models was seen to be inadequate. However, the hypothesis behind this new approach was that by imposing constant concentrations on each of the sub-compartments the observed values could be achieved by varying the proportional volume of each of the compartments to one another. By utilising a conventional wet to dry weight conversion factor of 7 (Lodish *et al.*, 1999) and accounting for the ash content of the cell, the following seasonal concentration trends were also elicited (Fig 7.3).

Two points were made at this juncture:

- (1) The data was extrapolated from total somatic weight and a digestive gland index. This gave data for the entire digestive gland, thus any other cell type within the gland, such as basophile cells, will if they are composed differently skew any comparison. Hence, it was assumed that their distribution in the digestive gland was small enough for the one model cell to be representative of the entire gland
- (2) The model cell had to simulate the entire gland, whereas in the real gland reserves can be utilised to create new digestive cells, thus enhancing feeding capacity of the animal when food was plentiful up to some optimal degree. Assuming that their upkeep in less nutritionally-viable times would be wasteful, then these excess cells

would undergo programmed cell death, providing an additional source of nutrient to the extant cells

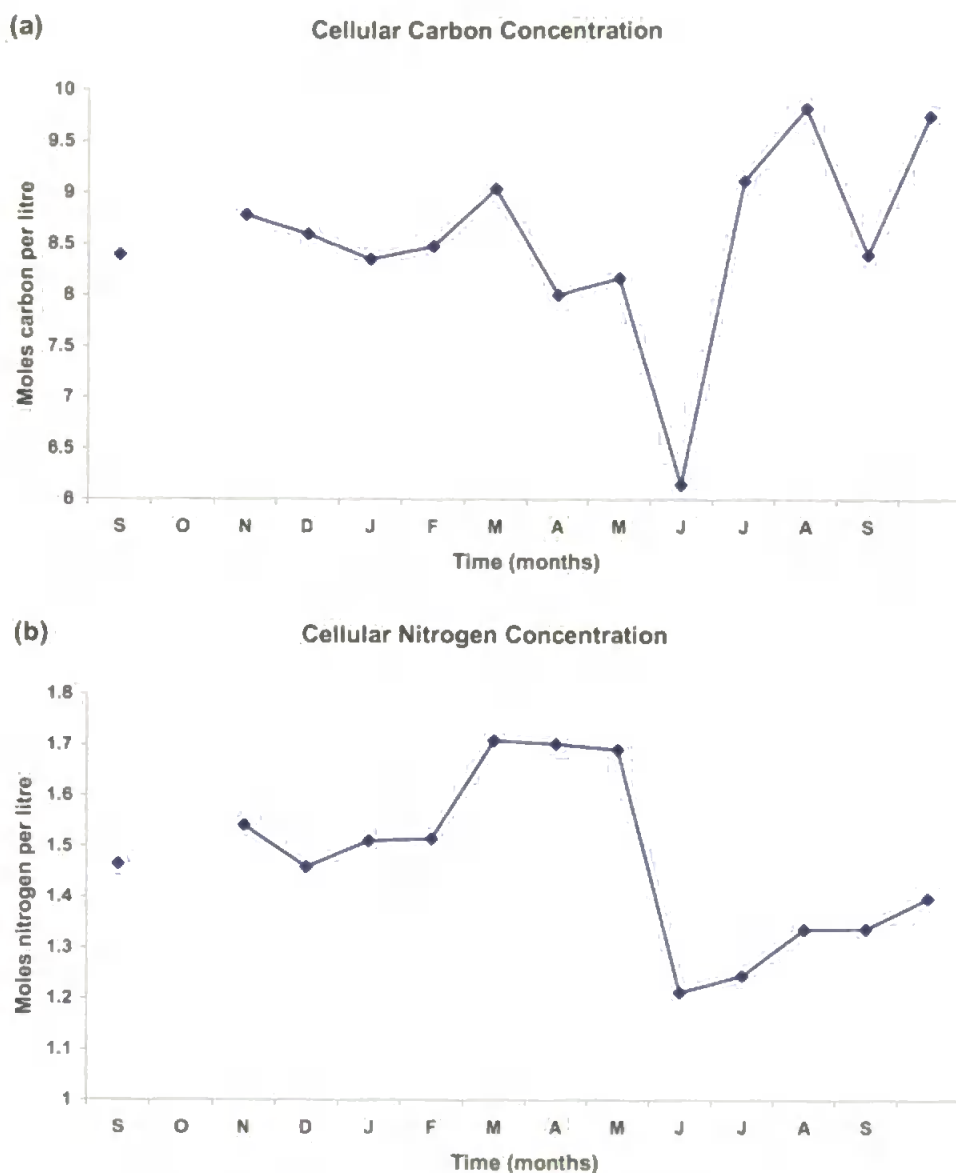


Fig 7.3 Annual (a) carbon & (b) nitrogen cellular concentrations.

A generalisation was made of the seasonal trend of a mussel; from a lowest ebb/spent state in the late spring/early summer post spawning; followed by rapid recovery coincident with the presence of abundant food during the summer, then an allocation of nutrient consumed to both growth and a build up of reserves for survival and reproductive purposes over the barren winter/ early spring, during which there is a gradual decline in body

mass. Additionally, there was also the possibility of a second spawning at the end of the summer if the animal had enough reserves and conditions are favourable. Thus, the model was initialised at the lowest point, which originally was deemed equivalent to the lowest cell volume, however upon reflection this was reset to 3 times the lowest volume as this coincided with the 30% of maximum seasonal dry weight observed. The remaining initial conditions were derived as follows:

As incoming material would add to the volume of the endosome it would be the case that it was at its smallest possible volume prior to feeding hence:

$$f_{ev}(0) = \frac{E_v(0)}{Cell_v(0)} = f_{evmin} = \frac{1}{100} \quad [7.1]$$

Thus, it was assumed that

$$E_v(0) = L_v(0) = 0.01 \times Cell_v(0) \quad [7.2]$$

The newly formed endosome was considered to be a sphere of radius  $r$ , with a lipid membrane of thickness,  $d$  (Fig 7.4).

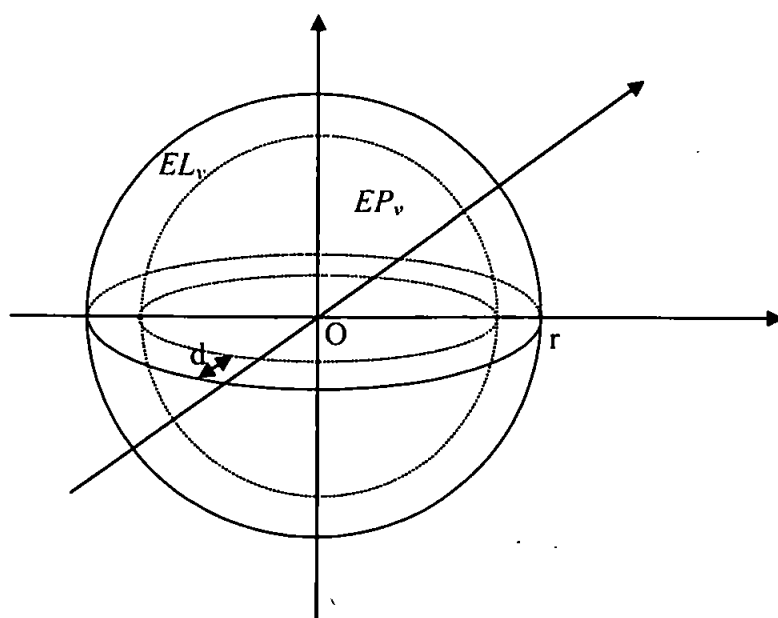


*Fig 7.4 Conceptual model of newly synthesised or 'clean' endosome.*

Then the volumes of the enzyme and membrane sub compartments were given by:

$$E_v(0) = \frac{4\pi}{3} r^3 \quad [7.3]$$

$$EP_v(0) = \frac{4\pi}{3} (r-d)^3 \quad [7.4]$$

$$EL_v(0) = \frac{4\pi}{3} (r^3 - (r-d)^3) \quad [7.5]$$

$$\frac{EP_v(0)}{E_v(0)} = \left(1 - \frac{d}{r}\right)^3 \quad [7.6]$$

Hence, the internal lumen and membrane volumes were calculated (Eqn 7.7).

$$EP_v(0) = E_v(0) \left(1 - \frac{d}{r}\right)^3 \quad \text{and} \quad EL_v(0) = E_v(0) \left(1 - \left(1 - \frac{d}{r}\right)^3\right) \quad [7.7]$$

Taking average measurements from Owen (1970) and Pal (1972) measurements of microvesicles, which were identifiable as early endosomes and primary lysosomes, the following values were taken (See Appendix D):  $EP_v(0) = 0.81E_v(0)$  and  $EL_v(0) = 0.19E_v(0)$  with the same ratios used for the lysosome.

The model also required the constant protein, lipid and carbohydrate concentrations, and factors for glycogen storage compared to free sugar and free amino acids to protein concentrations. Using the seasonal data and rounding up the following were obtained:

When	$Cell_v = Cell_{vmax}$	When	$Cell_v = Cell_{vmin}$
	$Cell_c = 12.0$		$Cell_c = 8.0$
	$Cell_n = 1.2$		$Cell_n = 1.7$

Additionally, the glycogen level was assumed to follow a linear relationship with cell volume ranging from 30-75% of total carbohydrate carbon content.

$$\frac{G_{xc}}{G_{xc} + CS_{xc}} = 0.3 + 0.45 \left( \frac{Cell_v - Cell_{vmin}}{Cell_{vmax} - Cell_{vmin}} \right) \quad [7.8]$$

Then the following relationship was introduced to the free amino acid pool size relative to bound protein.

$$AA_{xn} = 0.05(AA_{xn} + CP_{xn}) \quad [7.9]$$

This was designed so that changes to this factor might incorporate responses to changes in salinity, when amino acid pool size is either up or down-regulated.

From all of which the following were derived:

$$CP_n = EP_n = LP_n = 2.4$$

$$CP_c = EP_c = LP_c = 3.5 \times CP_n = 8.4$$

$$AA_c = 0.5 \times CP_c = 4.2$$

$$CS_c = 5.0$$

$$G_c = 2.5 \times CS_c = 12.5$$

$$CL_c = 10.0$$

From which the initial conditions for all initial cell volumes were taken.

*Endosome, lysosome, cytosol damage and autophagy*

In the model, damage to the lysosomal and endosomal integral components occurred as a function of degradative activity. To date, this had been set at 0.5% of the endosomal and 1.0% of the lysosomal integral components volume per minute when active. As will be seen later, the degradative capacity of these two organelles was derived in the model from the concentration of integral proteins, hence a long feeding phase became more inefficient the longer it was extended, providing a rationale for the splitting of the model phase cycle.

The cytosolic damage was considered to be primarily affect the proteinaceous matter, hence the following rates were utilised initially.

$$k_{CdamP} = 0.001 \times CP_v \text{ per minute} \quad k_{CdamL} = 0.0001 \times CL_v \text{ per minute}$$

$$k_{CdamS} = 0.0001 \times CS_v \text{ per minute.}$$



Damaged cytosolic material was then accumulated in conceptual damaged compartments; the rate of autophagy was then a function of the amount of damaged material present in the cytosol.

$$k_{autP} = 0.1 \times CDP_v \text{ per minute} \quad k_{autL} = 0.1 \times CDL_v \text{ per minute}$$

$$k_{autS} = 0.1 \times CDS_v \text{ per minute}$$

### *Endosome and lysosome replenishment*

Replenishment had two meanings in this context, first with increased cell volume after feeding the endosome would necessarily need an increase in integral content to remain within the parameter limit of minimum cell volume ratio. Additionally, as the integral components were damaged when the endosome was active, they will need replacing to retain its efficiency and capacity. As the cell did not feed during the resting period and, hence, the endosome was inactive, it was obviously a suitable time for replenishment to take place. Furthermore, the model endosome was flushed clean of excess transient material at the end of the disintegrating phase. Thus, the model sought to replace endosomal content and volume to the prescribed ratios according to the cell volume at a capped rate; failure to replenish the endosome to the required level provoked an extended resting period once again creating a limit on the amount of feeding that could be done in one phase cycle. Lysosomal replenishment was treated slightly different, as this organelle was always active, but it has been set up to mirror endosomal replenishment within the resting period. Replenishment

was subject to the applicable material being available within the cytosol, which established a further control on cell growth.

#### *Control rates and conditions*

The cell volume was constrained by the amount of proteinaceous material: not enough protein for structure and function and the cell would shrink; excess proteinaceous material and the cell was able to grow, the exception being when there was not enough energy available, then the energy stored in amino acids could be utilised by deamination and excretion. Additionally, these cells also served as a repository of stored energy forms, principally glycogen and lipid. To an extent, the constraint on cell volume should not have been affected by these stores, since they required only the structural proteins to accommodate the extra volume required, but their densely packed storage forms, glycogen bundles and mycelins, should minimise this effect and hence this factor was ignored in the model. The decision tree implemented in the model is shown in Figure 7.5.

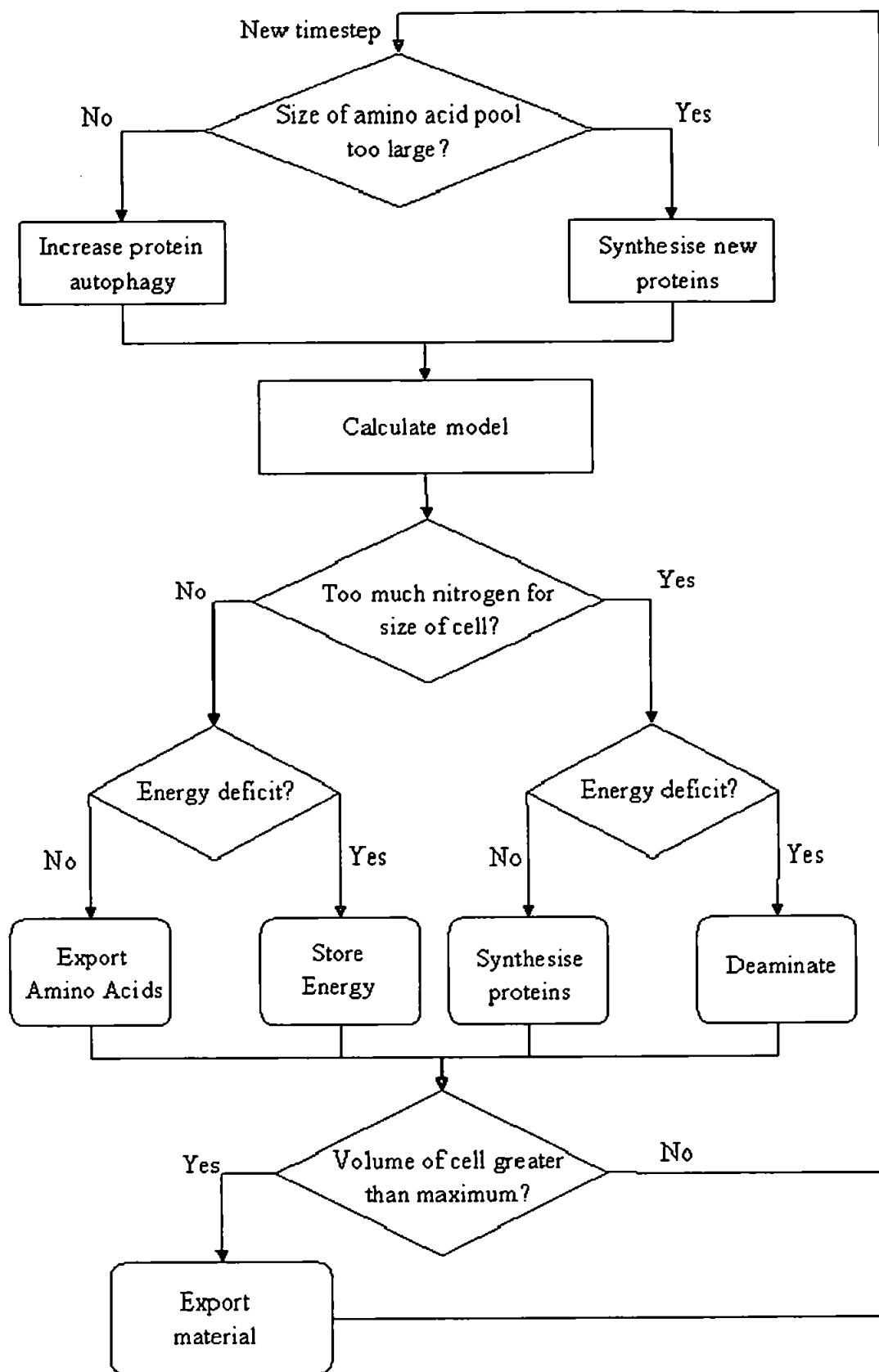


*Fig 7.5 Decision tree for control of cell behaviour due to content at beginning and end of timestep.*

### *Metabolic Rates*

Cellular respiration was now modelled as a function of the activity of the cell. Once again a linear function was produced between maximum and minimum observed values, with cellular activity as the independent variable. Activity in this toxin free model was split into basal (as a function of cell volume, but excluding basal protein turnover and lysosomal degradation), lysosomal function ( to model synthesis of degradative proteins, lipid membrane and the electron pumps required to keep the lysosome at the correct pH) and endosomal function. Observation (Widdows & Hawkins, 1989) showed that the increase in respiration during feeding was dependent on the ingestion rate and accounted for between 15-20% of total energy expenditure, but as these were whole animal measurements they do not account for the primacy of these hepatopancreatic cells in the digestive process. Thus, the model was initially set to:

60% basal excluding nominal lysosomal cost

30% lysosomal

10% endocytotic

Thereafter, the choice of which energy substrate to be utilised by the model was made according to whether or not there was an excessive amount of lipid. In order to do so a simple control mechanism was employed as follows:

$$S_{Split} = \begin{cases} 1 & \text{if } \frac{CL_{xc}}{CL_{xc} + CS_{xc}} < 0.5 \\ \text{MIN}\left(1, \frac{CS_{xc} + G_{xc}}{CL_{xc} + CS_{xc}} \times \frac{f_{cdS}}{f_{cdS} + f_{cdL}}\right) & \text{otherwise} \end{cases} \quad [7.10]$$

This factor was then applied to the total respiration rate calculated to find the carbohydrate fuelled respiration and the remainder was taken to be lipid fuelled.

Additionally, secretion was now forced to coincide with the feeding phase of the cycle to simulate the release of digestive enzymes into the tubule lumen to perform a final pre-ingestive breakdown of material; and, presumably, to release the material from the mucus string which it had adhered to in order to pass through the digestive tract.

#### *Lysosomal material split*

Material entering the lysosome was modelled according to its source in accordance with the increased digestive efficiency seen during starvation. It was assumed that exogenous material contained unrecognisable or un-utilisable components which the mussel had to eject, whereas endogenous material would be mainly composed of recognisable and recyclable components. Thus, the digestive efficiency was set at 50% for material from the endosome, and 90% for cytosolic sourced material. Movement through the digestive organelles was as before, but weighted according to content from either source.

### *Residual bodies*

In order to encapsulate the swelling of the cell into the tubule lumen, during the feeding phase, residual bodies were included in the cell. Waste material from the lysosome was stored in these until the disintegrating phase. As far as this model was concerned all cellular volume dependent functions exclude this portion of the total volume, but in the results this meant the total cellular volume sometimes exceeded the maximum limit as these bodies start to build up in volume between disintegrating periods.

### *Annual simulation*

The tubule phases provided a means of determining the input signal to the cell (Langton, 1975, 1977). By varying the lengths of both the resting and feeding phases an annual signal was established; whereby feeding activity was elevated in the summer when food sources were plentiful; and depressed thereafter as food became scarcer with a concomitant increase in the resting phase.

Increasing the actual feeding phase period, during the summer months to a capped highest limit, was supposed to simulate the growth of the entire digestive gland, thus increasing digestive capacity at this time of year (Fig 7.6a). It was capped as the digestive gland was restricted by the size of the mussel. The disintegrating phase was kept constant throughout the year to reflect the cell ridding itself of the majority of the waste material that had accumulated within. The resting phase was at its minimum during the summer as the animal fed as much as possible, but

increased concomitantly with increasing scarcity of available food. The reconstituting phase was ignored due to its relative infrequent observation and obscure function. The observed mean average for each of the resting, feeding and disintegrating phase excluding the reconstituting phase was 25.22%, 65.96% & 8.82%, which were reflected in the well fed period in the annual simulation adopted (Figure 7.6b).

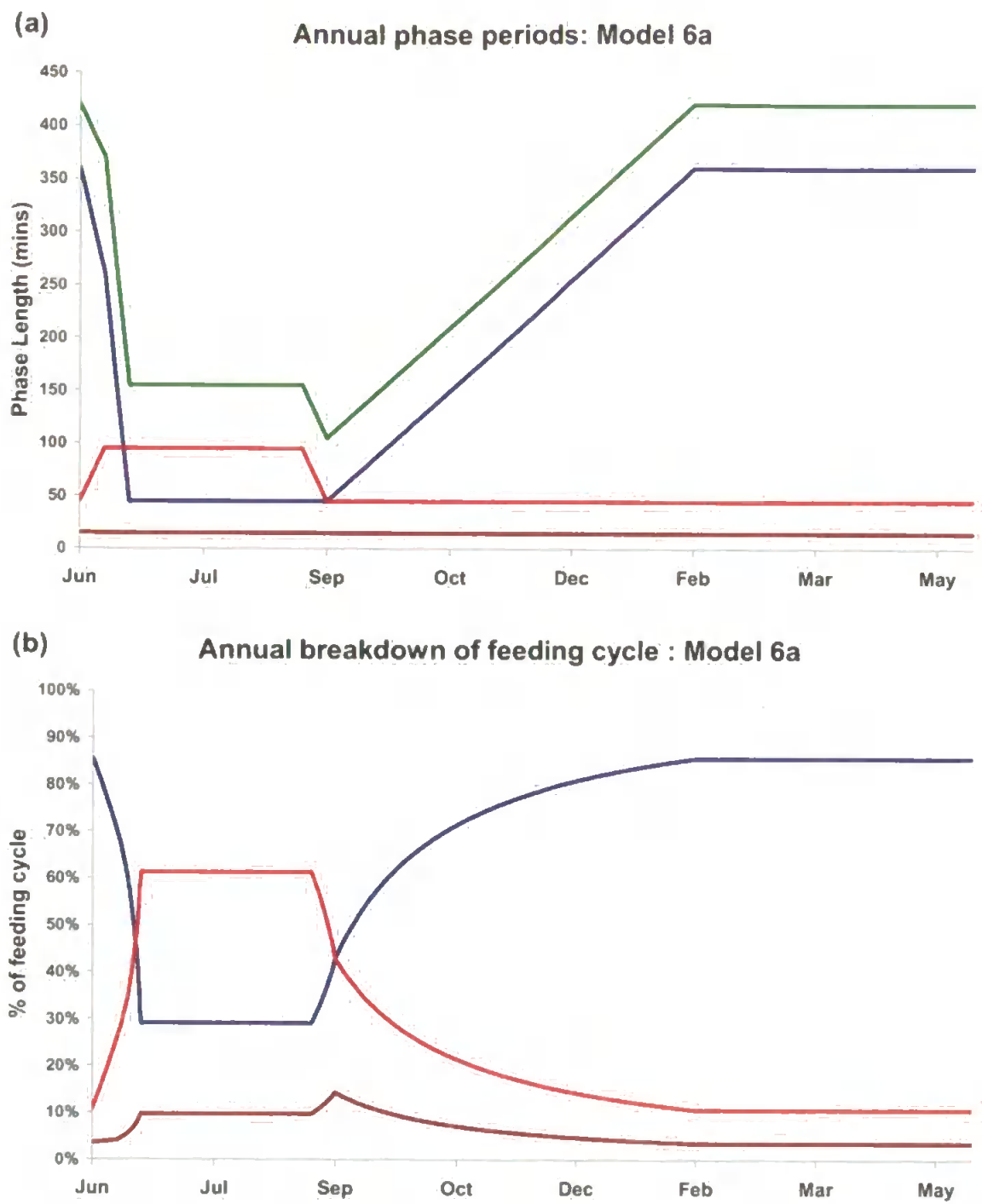
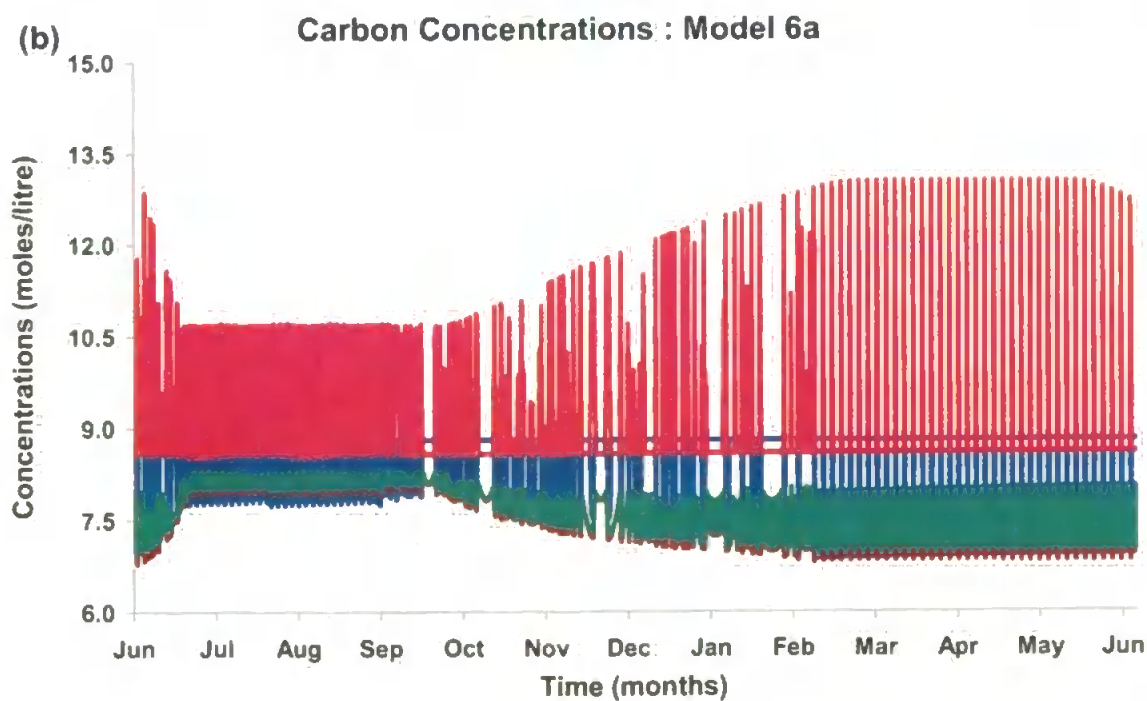
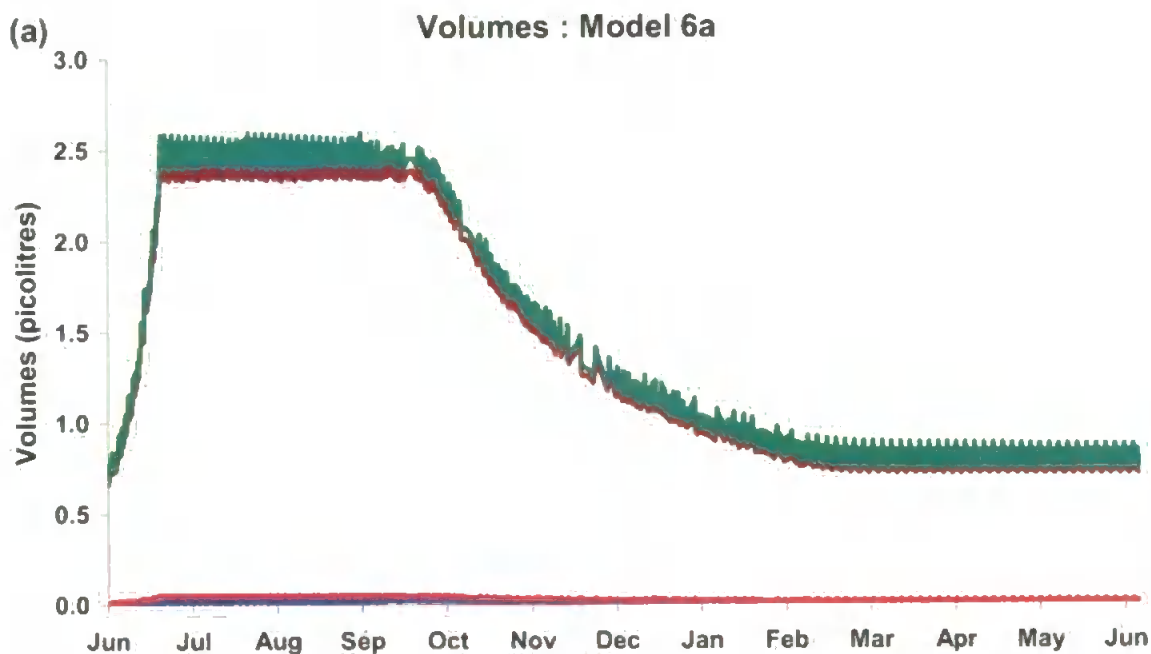


Fig 7.6 Annual tubule phase feeding regime setup for model 6a. (a) Number of minutes for — feeding phase, — disintegrating phase, — resting phase & — total cycle (b) % of each tubule cycle taken up by — feeding phase, — disintegrating phase & — resting phase respectively.



#### 7.4 Initial macromolecular model: Model 6a

An initial, annual simulation was run to investigate the new models behaviour. Model 6a was run with the food concentrations set throughout the year at  $S_c = 6.0$ ,  $S_n = 1.2$  & the proportion of non-proteinaceous material which is lipid,  $L_{Split} = 0.25$ .



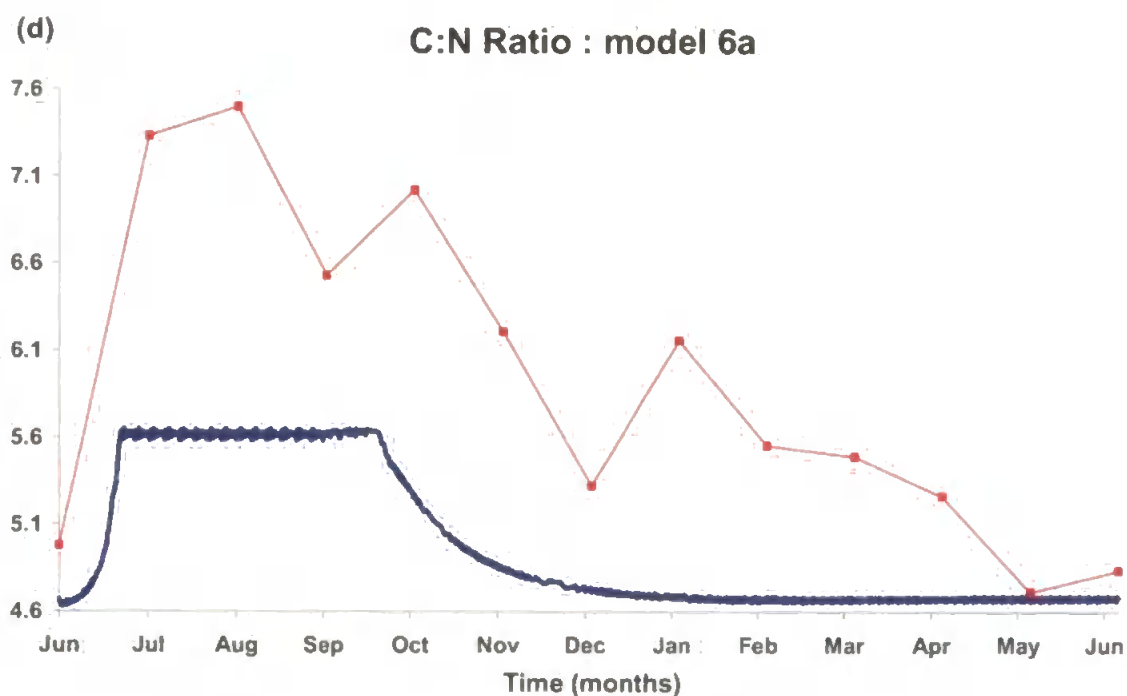
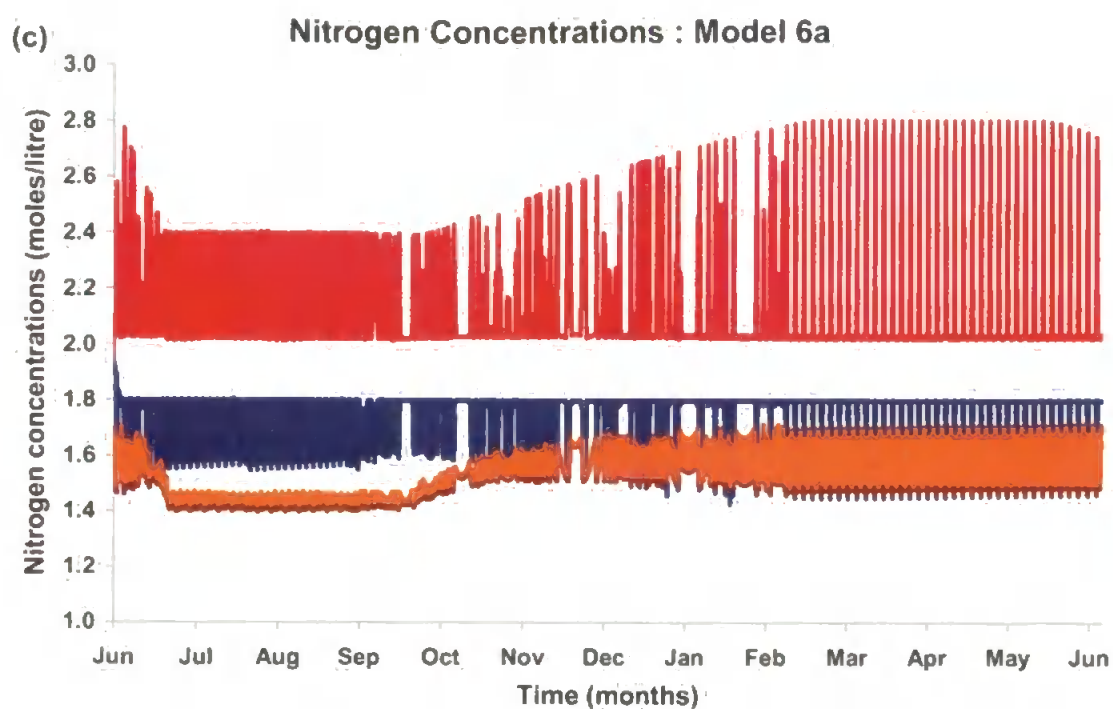


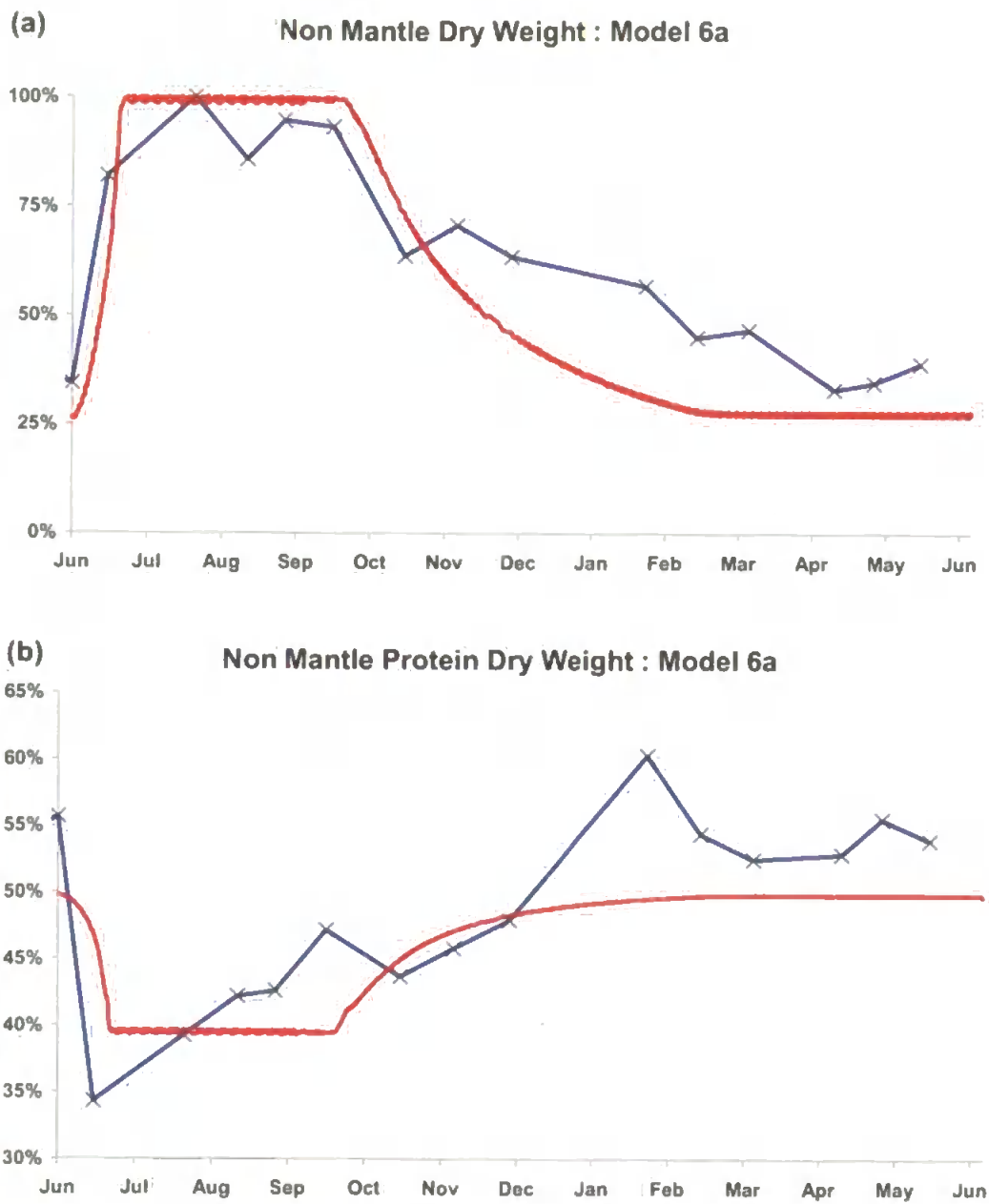
Fig 7.7 Annual simulation of Model 6a — Endosome, — Lysosome, — Cytosol, — Cell (a) volumes (b) carbon concentrations (c) nitrogen concentration (d) C:N ratio — Model — Observed

The annual simulation provoked a rapid increase from the lowest level of cell volume to the maximum capped limit within 18 days of commencement (Fig 7.7a). This was followed by a plateau until day 111, which meant that the effect of food reduction was innocuous for 11 days.

There followed a period of steady decline until day 260, where a lower bottom limit was reached, albeit slightly higher than the initial cell volume. Cellular and cytosolic carbon concentrations rose and fell in a similar fashion, due to the increased higher carbon concentration lipid and carbohydrate forms present when food was high (Fig 7.7a). The major variability was seen in the lysosome and endosome but, due to their relative insignificance in total volume, did not significantly affect the cellular pattern.

The endosomal concentration fell following feeding as more diffuse material entered the enzymatic mixture, while lysosomal concentration rose as the condensed material from the endosome was passed on. Despite the food concentrations remaining constant throughout the year, a seasonal pattern emerged for the lysosome as the cytosolic composition was changed and transferred in through autophagy. Endosomal and lysosomal nitrogen concentrations followed the same pattern as the carbon (Fig 7.7c). The cytosolic and cellular nitrogen concentrations were suppressed through the summer, due to the increased presence of glycogen and lipid in the cell, but recovered once the cell started to decrease in size. The C:N ratio followed the same annual pattern as the cell volume (Fig 7.7d). While the pattern vaguely reflected the observed seasonal data, either the degree of carbon increase or nitrogen decrease during the summer was inadequate, or else, the prescribed concentrations to the various components of the model were deficient.

A comparison between the simulation and observed annual dry weight data by macromolecular type was then made.



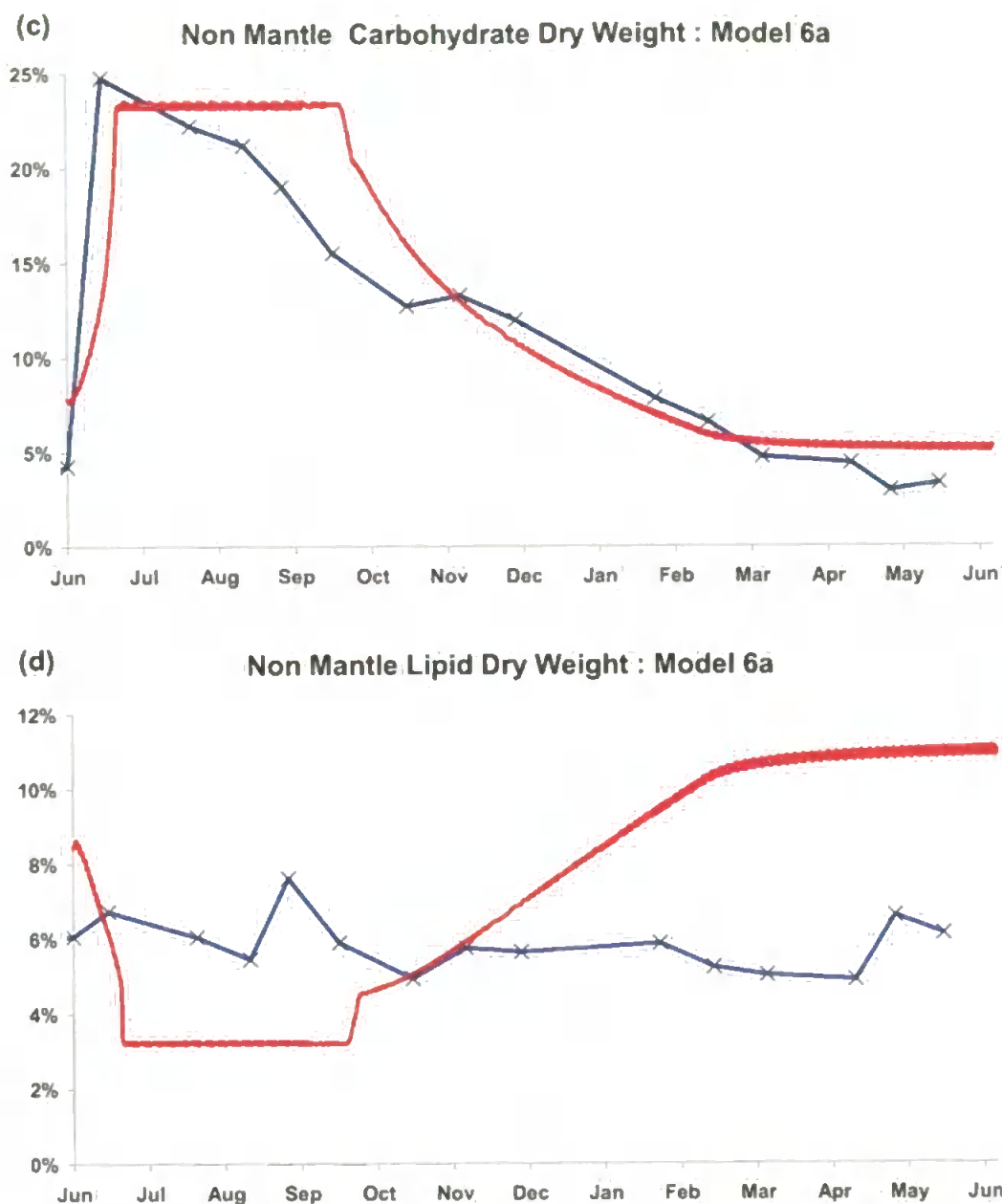


*Fig 7.8 Dry weight comparison for Model 6a — Observed — Model. (a) Total cellular dry weight as a percentage of maximum attained throughout annual cycle. (b) Protein, (c) Carbohydrate and (d) Lipid dry weight expressed as a percentage of cellular dry weight*

Total dry weight followed the observed trend in a reasonable fashion (Fig 7.8a), although the observed decline after the summer followed a smoother descent than the model. The observed immediate drop in protein

and increase in carbohydrate were both evident (Figs 7.8b & c), but the degree of each was smaller in the simulation. The subsequent simulated constant proportions until October were not observed; rather the protein should have increased in a linear fashion to mid September followed by a fairly constant period to December and then an increase to February followed by another constant period; and the carbohydrate should decrease linearly throughout the rest of the year. The lipid dynamics (Fig 7.8d) are more difficult to judge as the percentage of total dry weight was small, but in general keeping a constant percentage seemed a better way to proceed, to which end some form of lipid storage, such as triacylglyceride, was required and was addressed in Model 7 in chapter 8.

The nitrogen and glycogen control functions were the major, internal factors responsible for the response to the external signal. The average export rates per timestep were the gross major response mechanisms (Fig 7.9). The cell exported material throughout the year as a consequence of the control mechanism, whereas in previous models this only occurred during periods of plentiful food supply. However, only carbohydrate was exported during the non-summer months, which would have required the rest of the animal to survive on its own amino acid stores throughout the rest of the year. In comparison, the digestive gland was having its amino acid pool restocked throughout the year. Both the lipid and the amino acid export were only evident during the summer, when food was high, and were invoked as a response to the cell attaining maximum volume and

excess volume,  $\delta V$ , being exported by the following proportions: if glycogen and lipid were low then export was only amino acids; if lipid alone was low then export was 75% amino acid and 25% glycogen by volume; if just glycogen was low then export was 75% amino acid and 25% lipid; if neither glycogen nor lipid was low then export was 50%

amino acid,  $k_{exp,S} = \frac{\delta V}{(t_1 - t_0) \left( 1 + \frac{G_c CL_{xc}}{CL_c CS_{xc}} \right)}$  and the remainder was lipid.

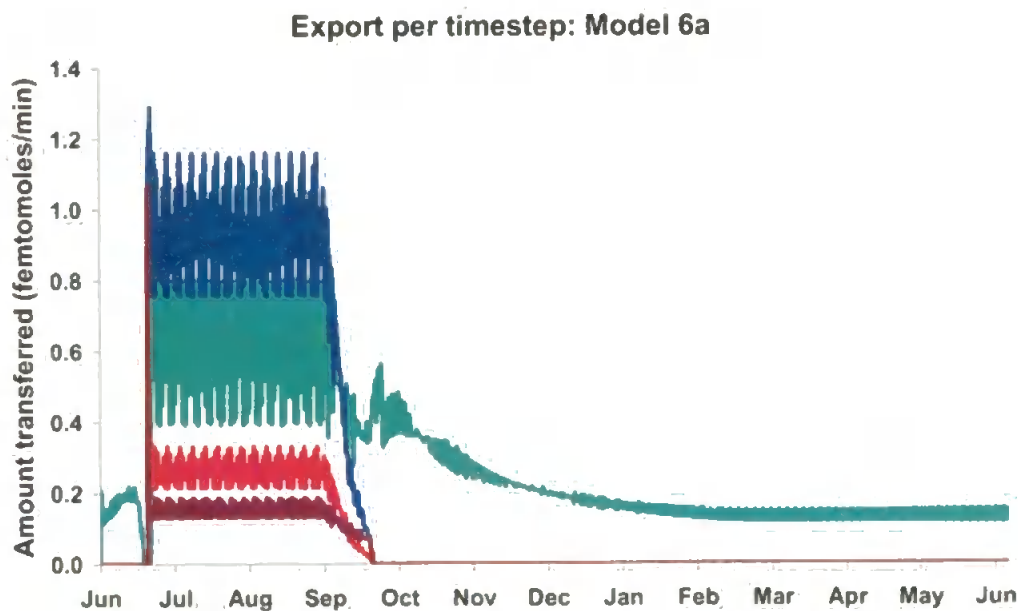


Fig 7.9 Model 6a average export per timestep through annual simulation.

— Protein carbon, — Protein Nitrogen, — Lipid Carbon & — Carbohydrate Carbon.

There then followed a sensitivity analysis of this model and annual simulation with model 6a taken as a control for comparison. To this end three new models were subject to the same simulation with the following differences: Model 6b looked at differing glycogen control functions;

Model 6c tested the effect of changing the nitrogen content control ratio; whilst Model 6d explored the effect of the prescribed concentrations and the differing factors between storage forms and their precursors.



### 7.5 Glycogen functions: Model 6b

The amount of glycogen contributed to the control rates, the control model used a linear function of cell volume to determine the split of carbon content between the free sugars and this storage form, being at its greatest when the cell was at maximum volume and capable of storing the greatest amount of energy. As notation let this ratio be called,  $G\%$ .

$$G\% = \frac{G_{xc}}{G_{xc} + CS_{xc}} \quad [7.11]$$

and for each submodel 6bn, let this be denoted  $G\%_n$

As the carbohydrate level did not peak as high as the observations in the Model 6b1 increased the capacity of the glycogen store at maximum from 75 to 90%.

$$G\%_1 = 0.3 + 0.6 \left( \frac{Cell_v - Cell_{vmin}}{Cell_{vmax} - Cell_{vmin}} \right) \quad [7.12]$$

Since the carbohydrate dynamics for Model 6a were incorrect Model 6b2 kept the same limits as the control, i.e.  $0.3 \leq G\%_2 \leq 0.75$ , but modelled it as exponentially dependent on cell volume.

$$G\%_2 = 0.3e^{\left( \frac{0.91629073}{Cell_{vmax} - Cell_{vmin}} (Cell_v - Cell_{vmin}) \right)} \quad [7.13]$$

Model 6b3 was also exponential but had the increased limits of Model 6b1 as well (i.e.  $0.3 \leq G\%_3 \leq 0.9$ ).

$$G\%_3 = 0.3e^{\left( \frac{1.0986123}{Cell_{vmax} - Cell_{vmin}} (Cell_v - Cell_{vmin}) \right)} \quad [7.14]$$

Model 6b4 made the glycogen split as a power law, with exponent 3 and the limits were  $0.3 \leq G\%_4 \leq 0.75$ .

$$G\%_4 = 0.3 + 0.45 \left( \frac{Cell_v - Cell_{v\min}}{Cell_{v\max} - Cell_{v\min}} \right)^3 \tag{7.15}$$

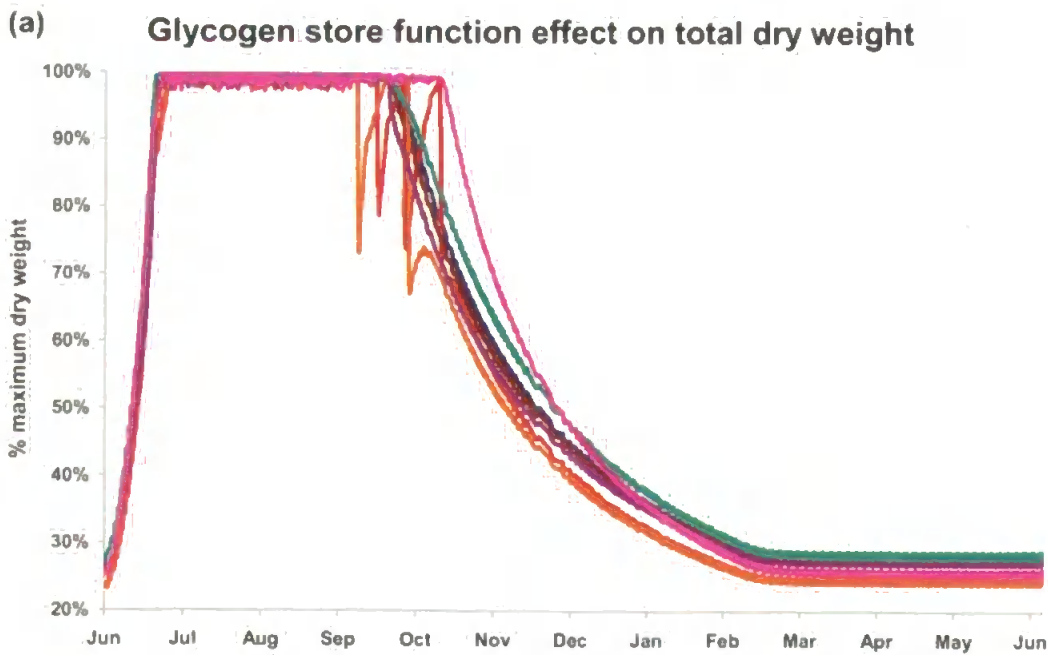
Model 6b5 looked at the glycogen split as a fractional power law, with exponent 1/3 and the limits were  $0.3 \leq G\%_5 \leq 0.75$ .

$$G\%_5 = 0.3 + 0.45 \sqrt[3]{\frac{Cell_v - Cell_{v\min}}{Cell_{v\max} - Cell_{v\min}}} \tag{7.16}$$

Model 6b6 looked at the glycogen split as a fractional power law, with exponent 1/3 and the limits were  $0.3 \leq G\%_6 \leq 0.9$ .

$$G\%_6 = 0.3 + 0.6 \sqrt[3]{\frac{Cell_v - Cell_{v\min}}{Cell_{v\max} - Cell_{v\min}}} \tag{7.17}$$

Before comparing all the sub models together it was noted that sub-models 6b1 and 6b3 showed some unstable behaviour.



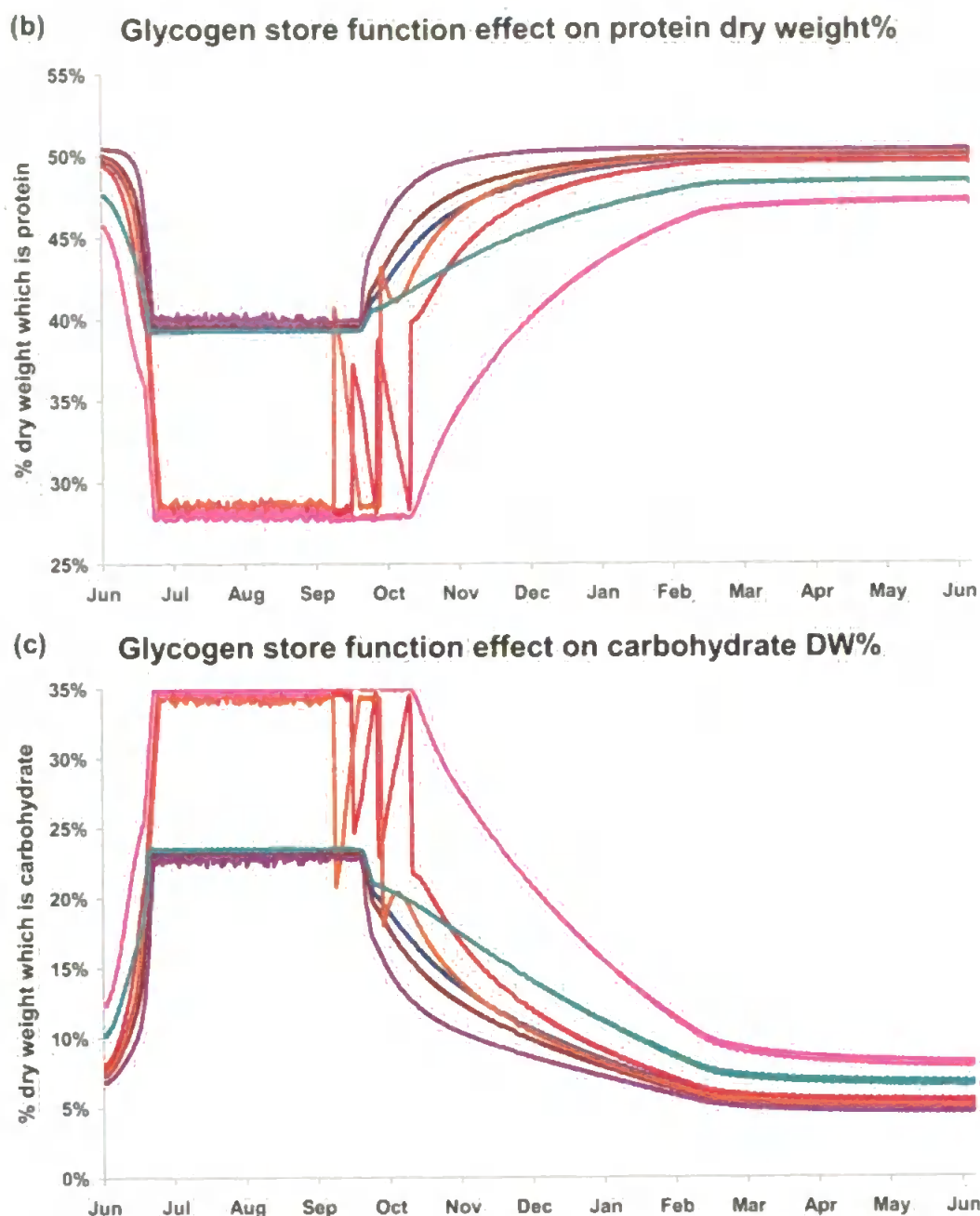


Fig 7.10 Comparison of models 6b, glycogen store functions, and 6a for annual simulation. 6a —, 6b1 —, 6b2 —, 6b3 —, 6b4 —, 6b5 — & 6b6 — (a) Total cellular dry weight as a percentage of maximum attained throughout annual cycle. (b) Protein and (c) Carbohydrate dry weight expressed as a percentage of cellular dry weight

The effect on the cell volume of the differing models was negligible, apart from the instabilities of models 6b1 and 6b3 with the higher limits

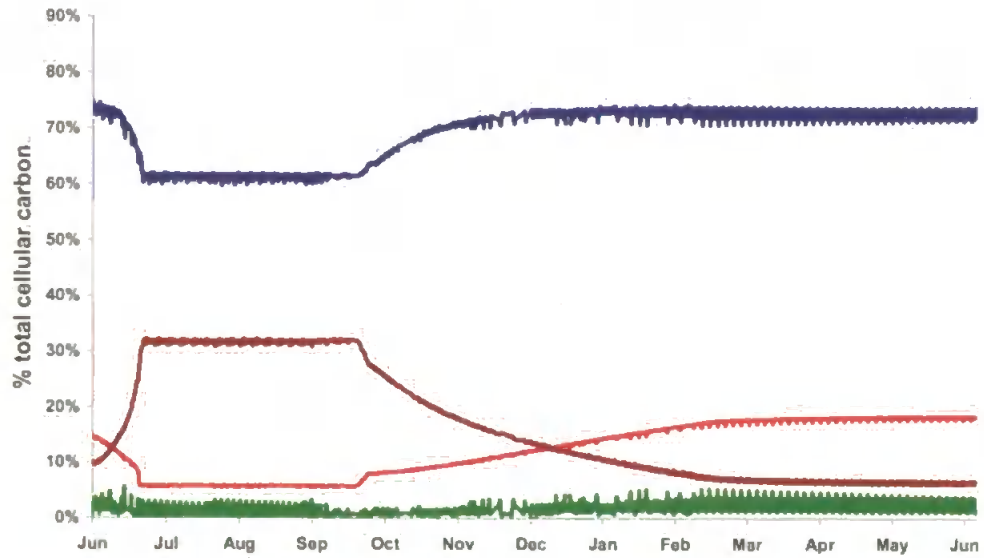
(Fig 7.10a). While this indicated that the amount of allowable stored material must have a higher limit, model 6b6 shared this upper limit but did not have this problem. This was because the function climbed rapidly at the beginning of its domain, and then only slightly in the uppermost part of its domain. This meant that as it decreased from the maximum, the cell only had to export a small fraction of material to achieve the glycogen control level; and this fraction was too small to invoke the cycle of decrease evidenced in the other two sub-models with the higher limit. Naturally, the higher limit models had an overall increase in carbohydrate dry weight due to glycogen's compact macromolecular form (Fig 7.10c). The decreases in the models from their respective upper summer carbohydrate limits to the winter/spring constant period differed in their rates of decrease. In Models 6b5 & 6b6, the cube root functions reduced the glycogen level least rapidly as expected, while the power function Model 6b4 reduced it most quickly. The final constant level that they all settle on is coincident with their rate of decrease, with the quickest to descend reaching the lowest levels and vice versa. The proportional amount of protein and lipid reflected the proportion of carbohydrate in the cells for all of the models, one rising as the other falls (Figs 7.10b & c). However, none of these differing functions, regardless of limits, had exchanged the period of summer constancy for an initial rise followed by steady decline of the carbohydrate as seen in the observed data in Figure 7.7c.

### *7.6 Nitrogen control factor: Model 6c*

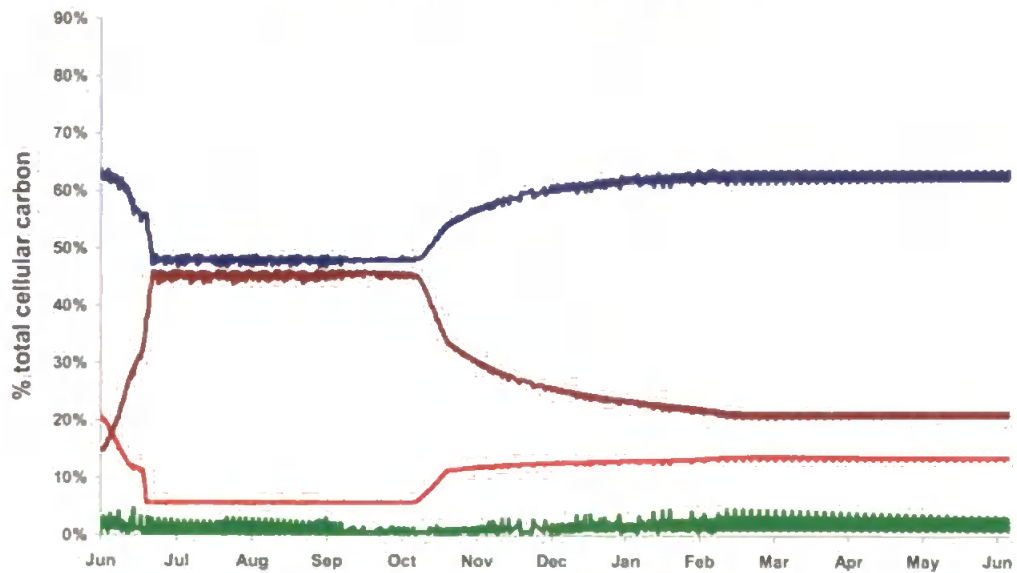
For model 6a, the nitrogen control factor was set at  $N_v = 1.74$  and was determined from the seasonal data of Gardner & Thompson (2001). Due to its central role in the models configuration this was adjusted to test its influence. The values used were: Model 6c1:  $N_v = 1.5$ ; Model 6c2:  $N_v = 2.0$  & Model 6c3:  $N_v = 1.25$

Models 6a, 6c1 & 6c3 shared similar features (Figs 7.11a, b & d): the summer decrease in protein and lipid with a concomitant increase in carbohydrate, followed by a slow increase in both lipid and protein and a slow decrease in carbohydrates. The reduced nitrogen control factor for model 6c1 decreased the amount of protein carbon initially; and the proportion also reduced to almost the same levels as the carbohydrates in the summer, whereas for model 6c3 the carbohydrate exceeded the protein during this period. Both models 6c1 and 6c3 showed a sharper increase in lipid after the summer period than model 6a. Both models 6a and 6c3 showed greater deamination as a result of this factor than model 6c1, but both were dwarfed by that produced by model 6c2.

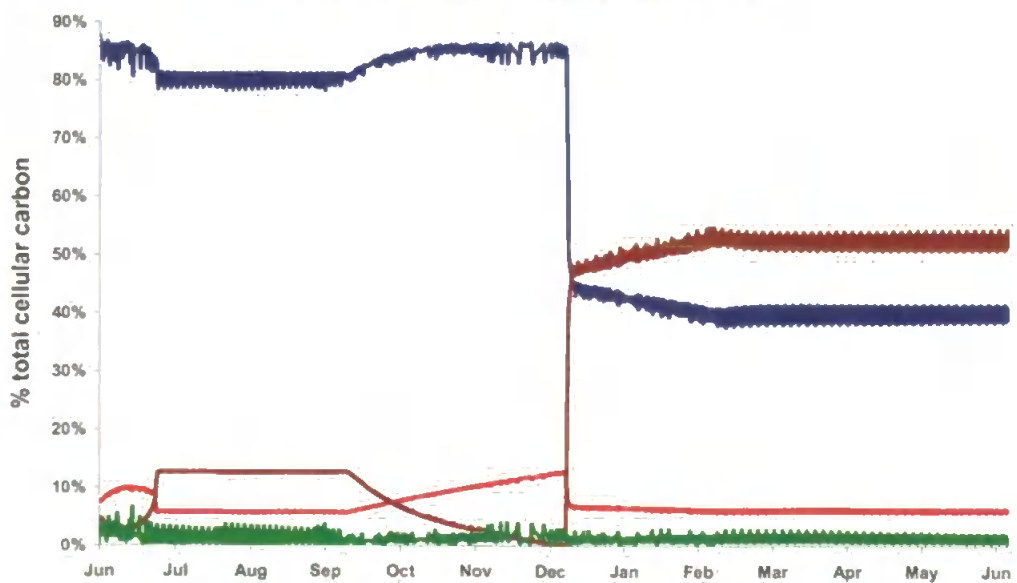
(a) Carbon Content Distribution : Model 6a



(b) Carbon Content Distribution : Model 6c1



(c) Carbon Content Distribution : Model 6c2



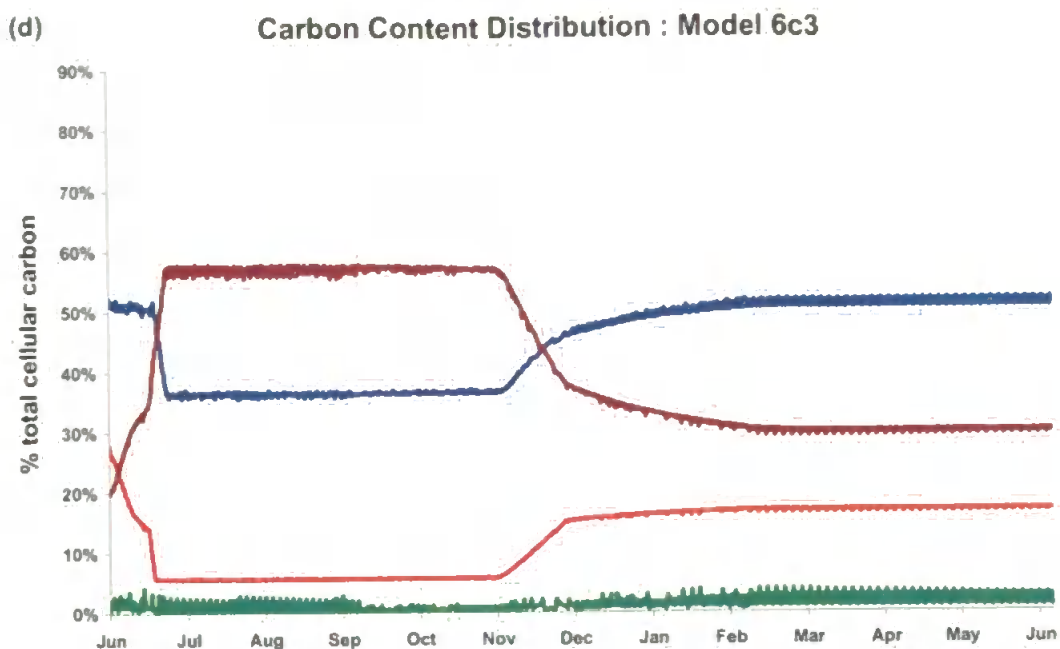


Fig 7.11 Total cellular carbon content split into — Protein, — Lipid, — Carbohydrate & — Waste for (a) Model 6a  $N_v = 1.74$  (b) Model 6c1,  $N_v = 1.5$  (c) Model 6c2,  $N_v = 2$  (d) Model 6c3,  $N_v = 1.25$ .

With the higher factor (Fig 7.11c) the summer seasonal increase in carbohydrates was depressed in comparison to model 6a (Fig 7.11a). In the control simulation the majority of the carbohydrate increase in its proportional share had come from the protein, whereas in model 6c2 it was shared equally with the lipid loss. Then after the summer there was a move towards protein and lipid increase which was interrupted by a critical event in December. Thereafter, the results cannot be considered reliable due to this irregularity.

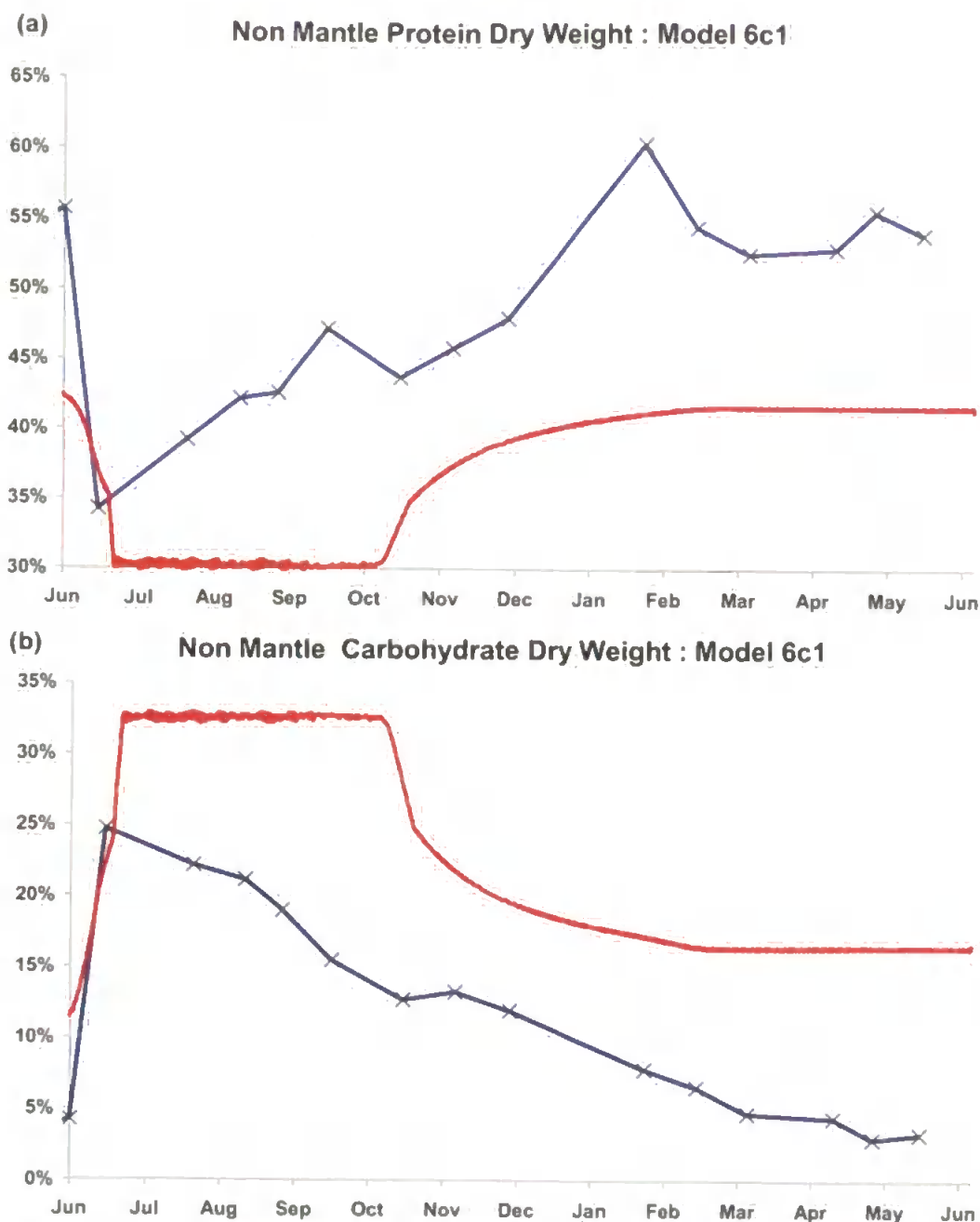


Fig 7.12 Model 6c1 comparison — Observed — Model. (a) Protein and (b) Carbohydrate dry weights as percentage of total cellular dry weight

Model 6c1 was then checked against the seasonal observational data.

While the total cellular dry weight appeared much as for model 6a, there is a much greater discrepancy between the protein and carbohydrate dry weights across the simulation (Figs 7.12a & b). Hence, there was some vindication for the control figure used in model 6a for this nitrogen control factor.



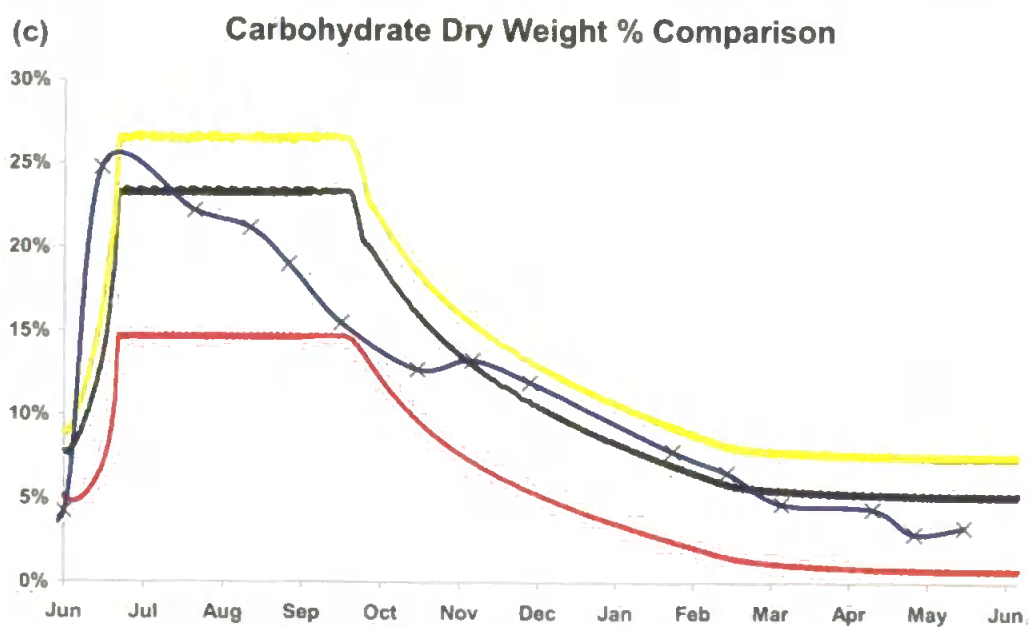
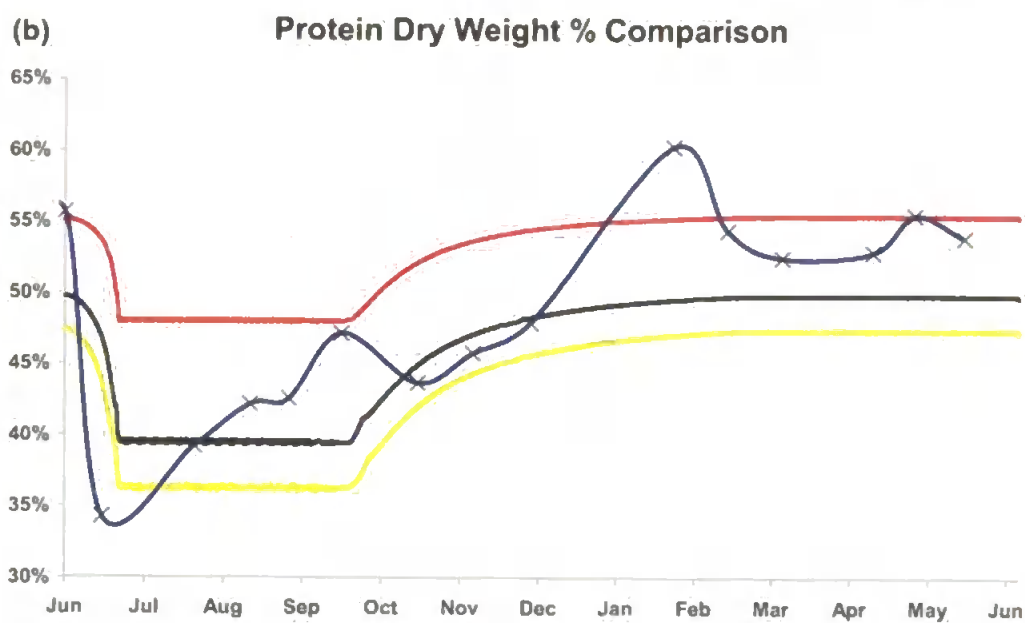
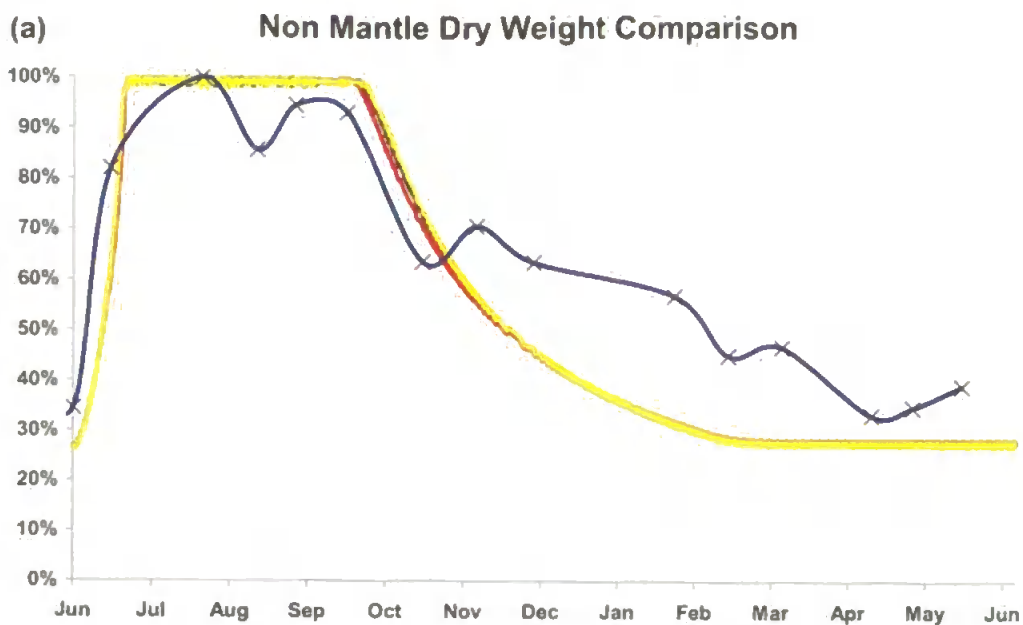
### 7.7 Concentrations sensitivity analysis: Model 6d

Model 6d was constructed to show the effect of varying pertinent relative concentrations upon the annual simulation. As was shown, by the previous comparison of models 6b, the amino acid and protein nitrogen portion is part of the cellular control algorithm; hence, the amino acid and protein concentrations were seen to be of particular importance. To this end let *aminofactor* be defined as the carbon and nitrogen concentrations of the amino acid pool relative to the bound protein compartment i.e.

$$\text{aminofactor} = \frac{AA_c}{CP_c} = \frac{AA_n}{CP_n}.$$

For the control model 6a this had been set at *aminofactor* = 0.4. The importance of this factor was tested by using submodel 6d1 *aminofactor* = 0.2 and submodel 6d2 *aminofactor* = 0.8.

The effect on total dry weight was negligible (Fig 7.13a) as the behaviour for each of the components was relatively unaffected except for the scale (Figs 7.13b-d), and was expressed as a percentage of the maximum achieved for each model. The protein proportion was raised for the higher *aminofactor*, which depressed the carbohydrate proportion, whilst the reverse was true for the lesser *aminofactor*. Only the recovery of the lipid percentage after the summer differed significantly for the lesser *aminofactor*. The higher *aminofactor* pushed the initial increase and decrease of carbohydrate and protein, respectively, towards the observed peaks and troughs, but its performance deteriorated thereafter.



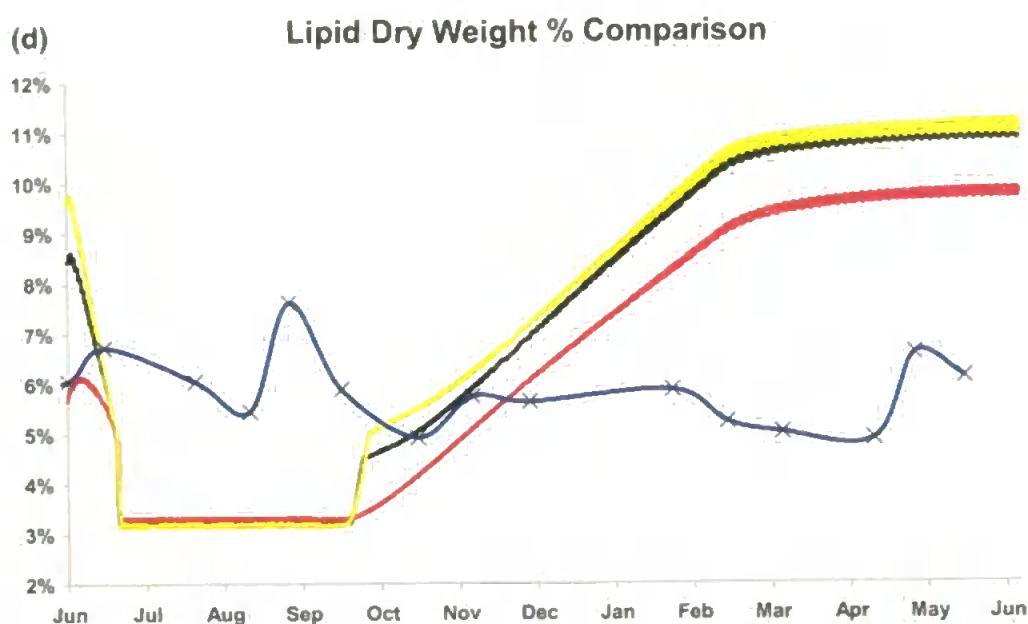
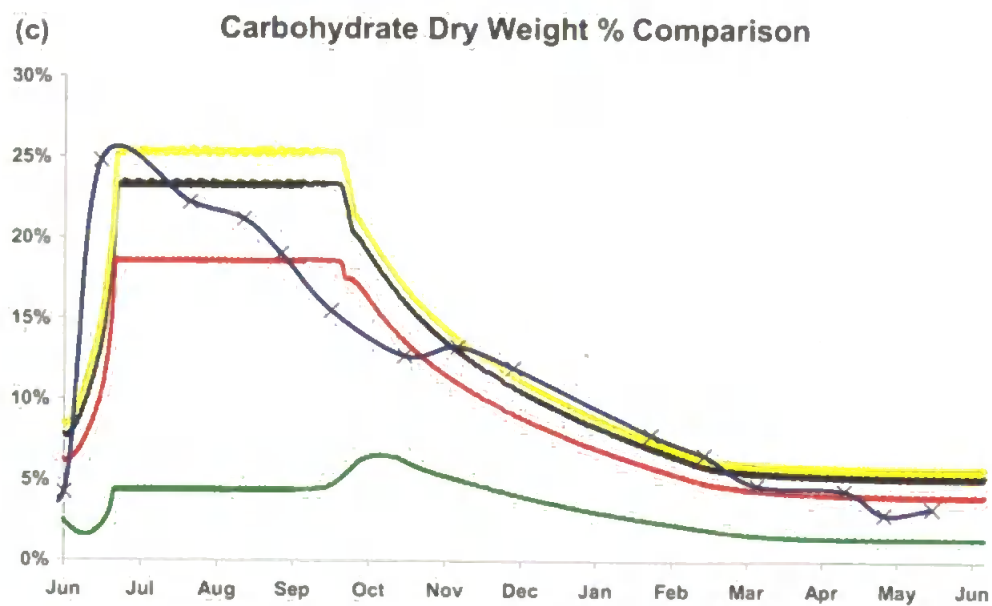
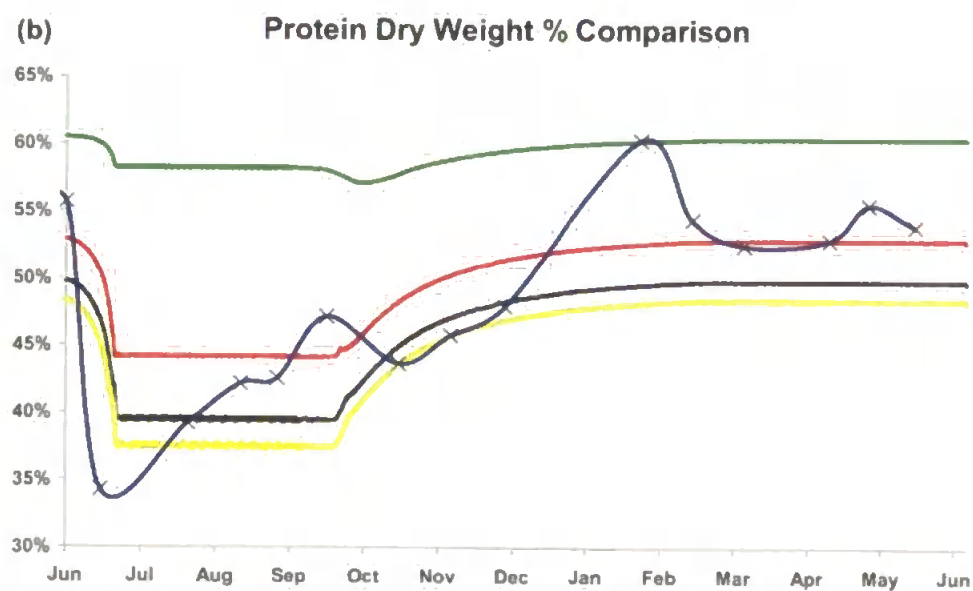
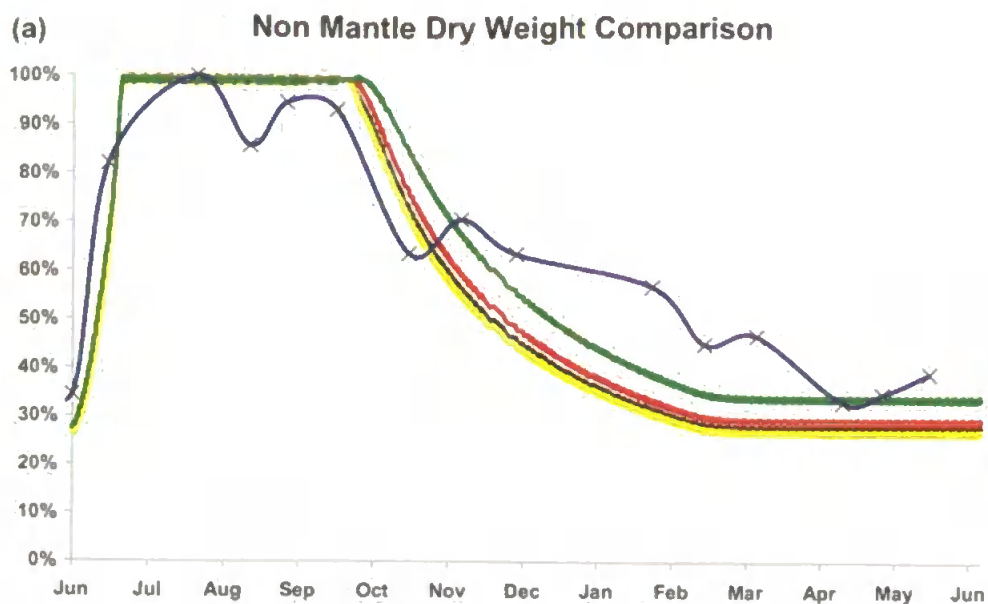
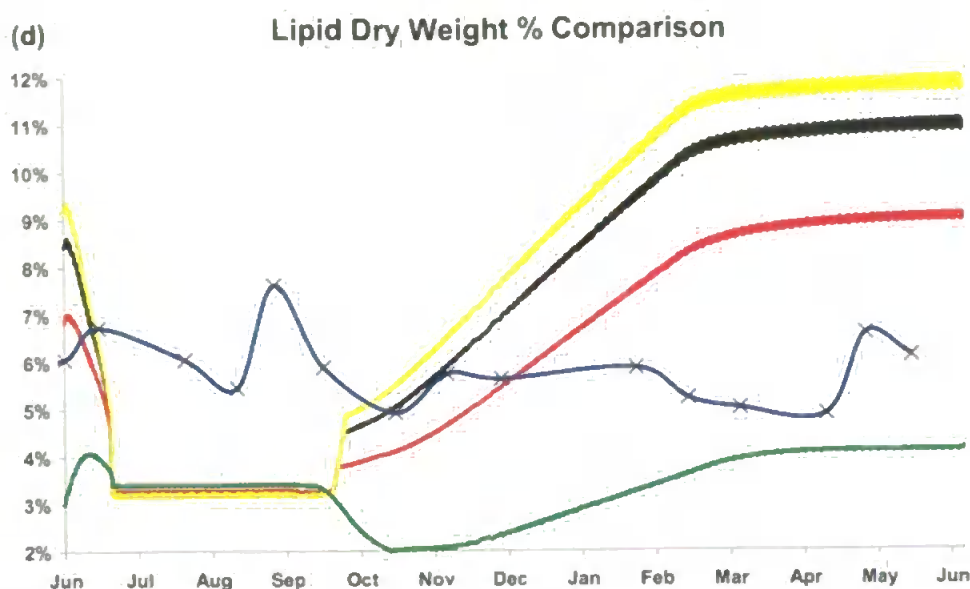


Fig 7.13 Comparison of the effect of amino acid concentration relative to that of bound protein on annual dry weight proportions. — Observed, — Model 6a, — Model 6d1 & — Model 6d2. (a) Total dry weight (b) protein dry weight relative to total (c) carbohydrate dry weight relative to total (d) lipid dry weight relative to total.

As well as the concentrations between the amino acid and protein compartments being set at a constant factor, there was also a mechanism for ensuring that the nitrogen content was also conserved by a set factor. This had previously defined as,  $aa\%$ , and its effect was also tested. For the control model this factor had been set as  $aa\% = 0.05$  (Eqn 7.9); for model 6d3  $aa\% = 0.1$ ; for model 6d4  $aa\% = 0.025$  & for model 6d5  $aa\% = 0.2$ .





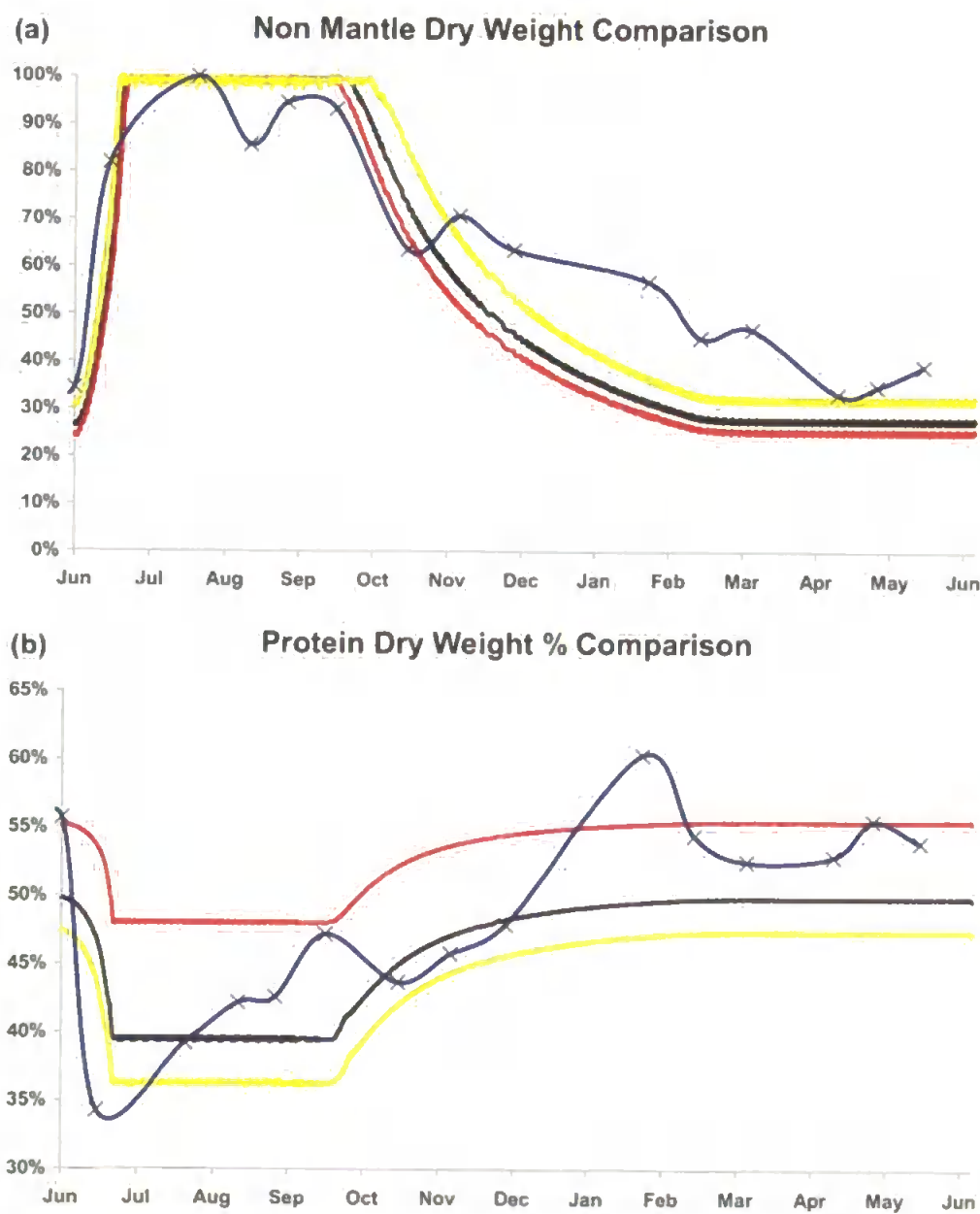
*Fig 7.14 Amino acid split comparison on annual dry weight effect. — Observed, — Model 6a, — Model6d3, — Model6d4 & — Model6d5. (a) Total dry weight (b) protein dry weight relative to total (c) carbohydrate dry weight relative to total (d) lipid dry weight relative to total.*

Clearly, the highest of these amino acid pool ratios was unacceptable (Fig 7.14b), even given that the dry weight total was, marginally, the closest to the observed trend in the lattermost parts of the annual cycle (Fig 7.14a). There was a dampening of most of the seasonal signal for protein dry weight and as a consequence, there was a drop in carbohydrate at the very beginning of the year that had not been seen in any previous model. Later on, this was followed by a rise when food becomes less plentiful at which time there was also a reduction in lipid (Figs 7.14b-d). The closer factors to the control (models 6d3&4) show a similar pattern to the control with only variations in scale.

Another factor that had been introduced, which required exploration, was the storage factor for glycogen. For a storage facility to provide value to the cell model the storage form had to be more compact than its precursor, hence the model had a factor defined in Eqn 7.18.

$$glycogenfactor = \frac{G_c}{CS_c} \tag{7.18}$$

For model 6d6 this was set to be double the original and for model 6d7 half.



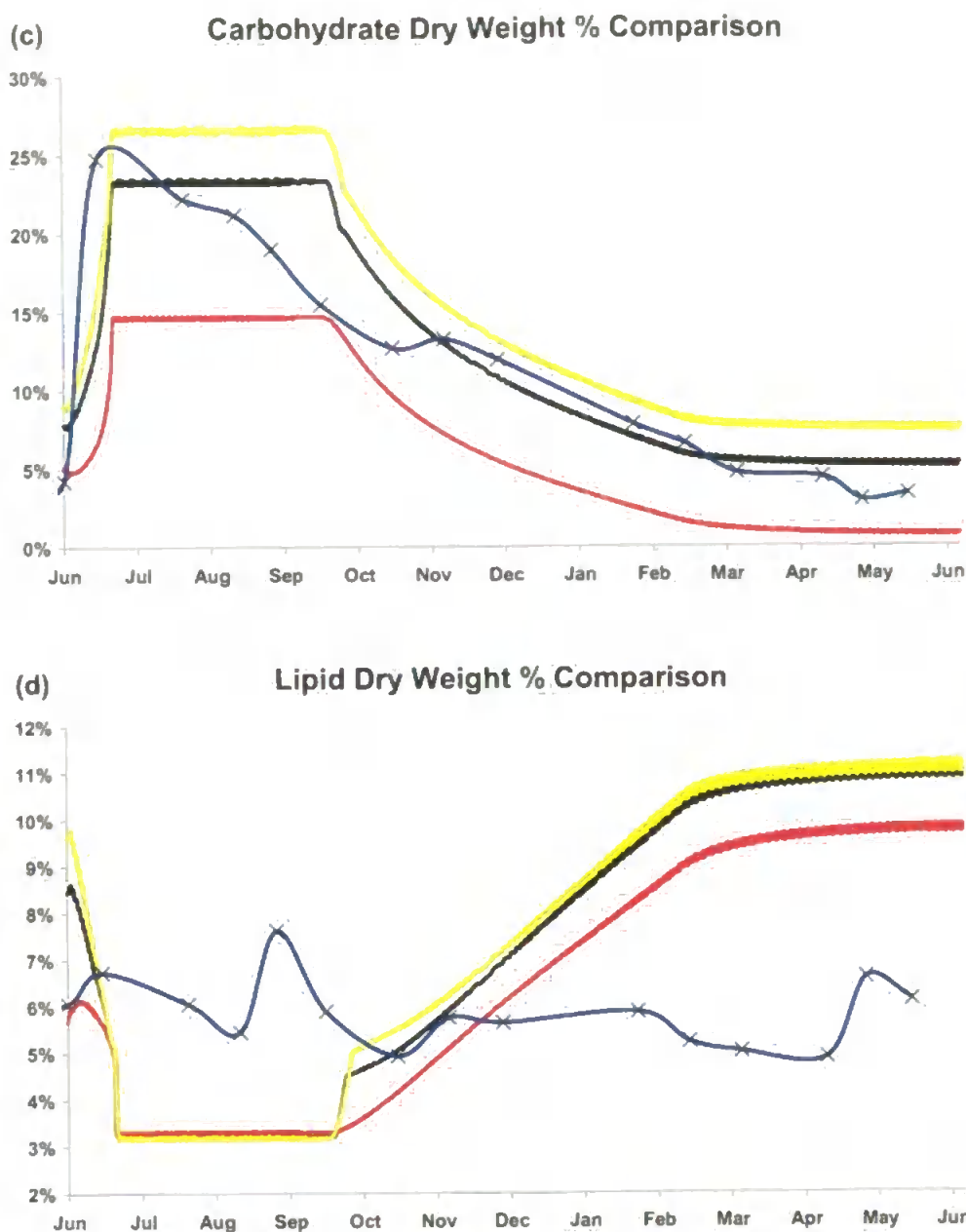


Fig 7.15 Annual simulation comparison of effect of glycogen concentration relative to free sugar compartment. — Observed, — Model 6a, — Model6d6 & — Model6d7. (a) Total dry weight (b) protein dry weight relative to total (c) carbohydrate dry weight relative to total (d) lipid dry weight relative to total.

The changes to the model response were confined to effects of scale rather than pattern (Figs 7.15a-d). The higher concentration, model 6d6, provoked a drop in overall carbohydrate dry weight with a complementary

increase in protein. The extent of carbohydrate loss was well below the observed figures, but the protein levels during the winter and spring are closer to the observed than the control model. The reverse was true for the lower concentration, model 6d7. These were a consequence of the amount of glycogen that was stored. With the change in glycogen concentration, the maximum carbon contents in the glycogen compartment during the summer varied from 4.1 picomoles with the highest concentration to 5.16 picomoles with the lowest. Cumulatively the lower concentration enabled the cell to export 41% more protein at the expense of 0.3% less carbohydrate.

The problems with matching the model to the observed data have not been addressed by any of these amendments. Specifically, the summertime constancy, whilst acceptable for the total dry weight was clearly not reflected in the protein and carbohydrate observed dynamics. The initial rapid increase in carbohydrate was seen in the simulation, but the increase in protein thereafter, given that the dry weight stays was interpreted to imply that glycogen levels must decrease and protein increase over the summer. Two possible explanations for this phenomenon were explored next.

- 1) The anomaly was a consequence of extrapolating from single cell results to the organ level, thereby ignoring the growth of the digestive gland during this period to enhance feeding capacity.



- 2) The rest of the animal may require protein earlier on relatively more than energy stores to regenerate after the winter and be able to function correctly with the increased summer demand, subsequently the storage of energy reserves within the animal could take place.

### *7.8 Simple cell division model: Model 6e*

Consideration was now given to the first of these possible explanations for the incongruity in the C:N model results. Under the presumption that the cellular model was correct and that this anomaly was a result of the discrepancy with the data being taken at the organ level. The digestive gland increased the number of cells in order to facilitate the degradation of an optimal amount of the abundant food available in the summer months. Each new cell being created as an old cell split in two through mitosis. If this split was equal and relatively inexpensive in terms of energy, then the organ would have two cells of half volume with half the amount of glycogen, which would be above the glycogen function levels. If this occurred during the first couple of weeks and the glycogen level was retained then the consequence, for the model cell, would be heightened carbohydrate initially followed by a steady increase in protein. So Model 6e1 was designed as a simple exercise in cell division to attempt to validate this hypothesis.

For the first 100 days of abundant food availability the cell was allowed to divide every time it reached the maximum cell volume. After this cell division it did not export excess glycogen, thus control in this model came only from storing and releasing glycogen. Also the act of mitosis in the model incurred a cost of 25% of all resources. Then the cell results were multiplied by the number of cells present.

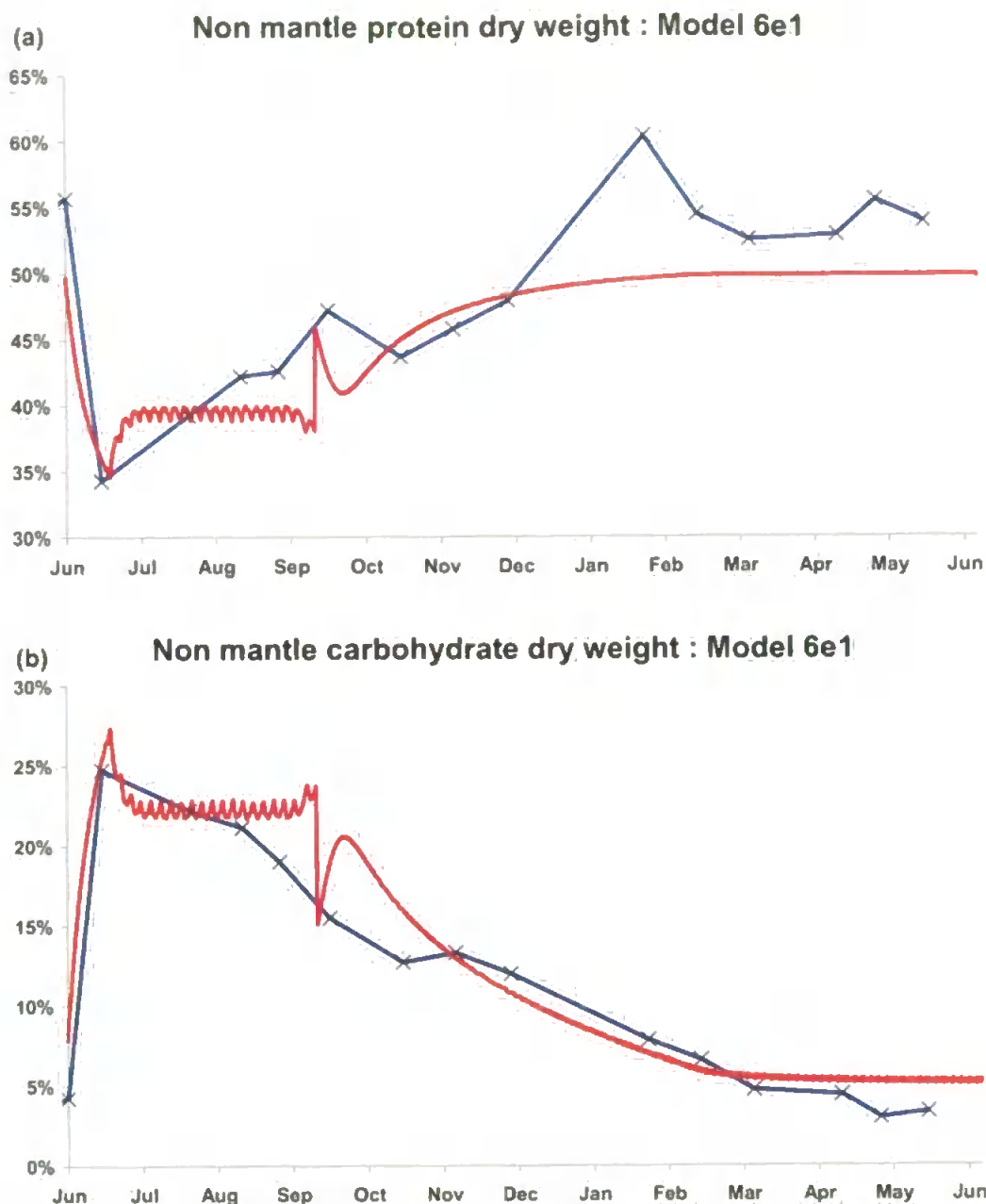
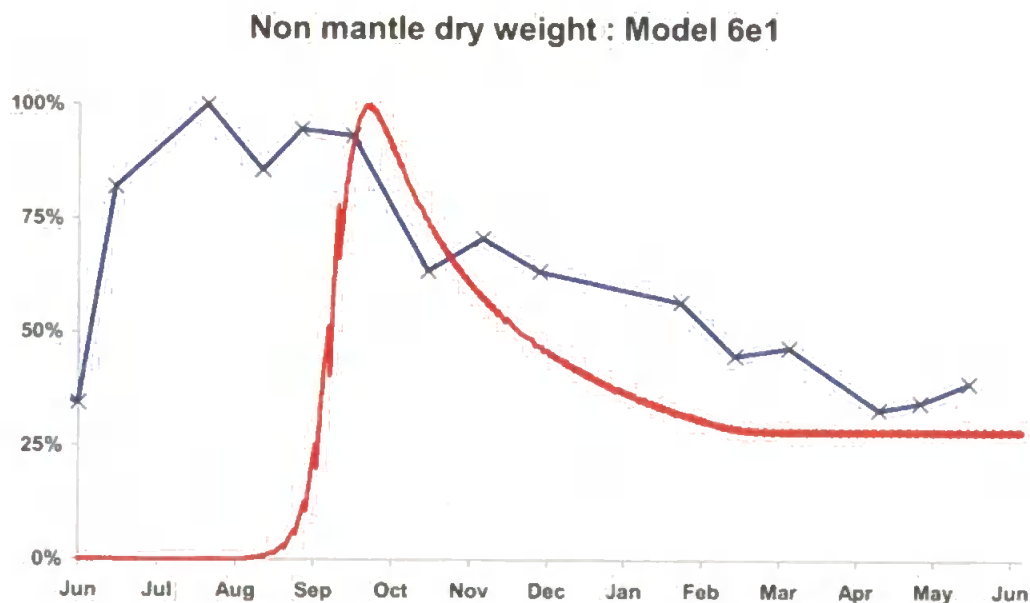


Fig 7.16 Annual simulation with cell division, — Observed & — Model6e1 .  
 (a) Protein dry weight (b) carbohydrate dry weight.

The initial rise in carbohydrate and drop in protein, which peaked at day 17, occurred before the first cell division (Figs 7.16a & b). After the first cell division the carbohydrate started to decrease as the protein started to rise. However, around day 35 after the fifth cell division the carbohydrate and protein started to fall into a period of constancy as they

fluctuate minutely around a mean figure. This continued until day 100, whereupon the algorithm allowed glycogen to be exported again as the food started to decline, hence the sudden drop in carbohydrate. The carbohydrate then started to rise once more as food is still available but eventually dropped along with the ever declining food stock.



*Fig 7.17 Annual simulation of total cellular dry weight with cell division, — Observed & — Model6e1.*

The main problem with this model is that by day 100 there had been 20 cell divisions which resulted in 1,048,576 cells generated from initial cell. Hence, the total dry weight peaks at the last cell division, which occurred at the end of the summer, and did not coincide with the observed data (Fig 7.17). In order to address this problem the model was amended to cap the number of splits to 5, resulting in a maximum of 32 cells.

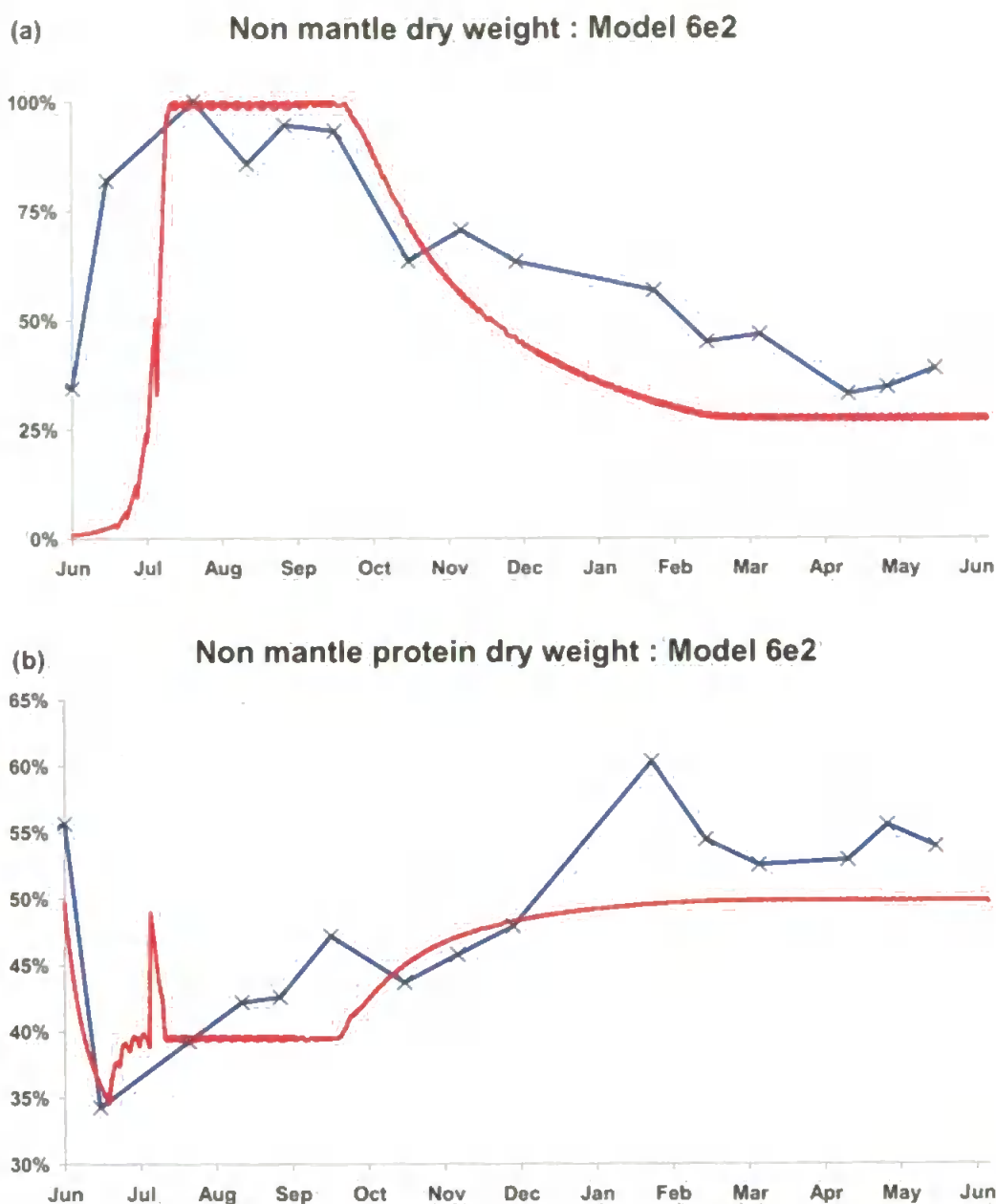


Fig 7.18 Annual simulation of total cellular dry weight with capped cell division, — Observed & — Model6e2.

The carbohydrate and protein relationship was still unresolved with problems occurring after the last cell division (Fig 7.18b) and a summer plateau was still in evidence. But the irresolvable problem with this idea was that with the number of cells involved after the last cell division then the initial value was never going to be 35% of maximum as observed. Also,

over the winter period there would need to be some way of modelling the cannibalisation of the majority of newly generated cells in order to account for return to previous size (excluding animal growth). This would require inclusion of a sub-model for programmed cell deletion as was observed in real tubules (Pipe & Moore, 1985).

### 7.9 Annual variable rest of animal signal model: Model 6f

Since there appeared no way of surmounting these difficulties this idea was abandoned and the second idea for addressing the problem of the summer plateau was investigated. In this idea the cell was receiving a signal from the rest of the animal demanding differing compositions of export at different times of the year. Initially, protein was demanded in order to build functionality and then carbohydrate to store as reserves. In order to implement this idea, model 6f supposed that the glycogen control function was affected by signals coming from the rest of the animal.

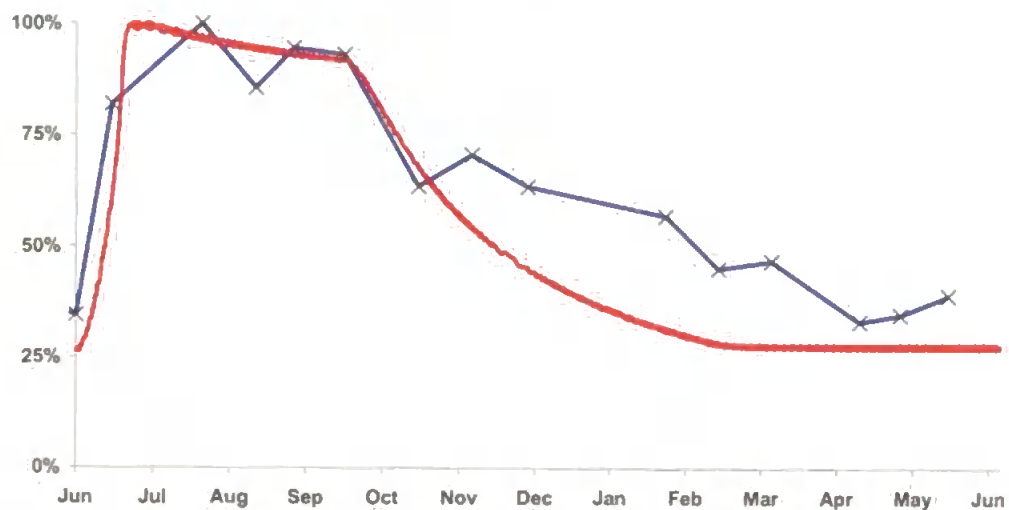
During days 1-30, the glycogen control function stayed as previously reported, with the cell gaining more carbohydrate. Then for the rest of the summer, the upper limit for glycogen was linearly reduced to force the cell to export more carbohydrate for storage elsewhere in the body. For days 30-100 the formula in Eqn 7.19 was applied, reducing the glycogen split to 0.5 by the end of the summer.

$$G\% = 0.3 + \left( 0.45 - \frac{0.25 * (DayNumber - 30)}{70} \right) \times \left( \frac{Cell_v - RB_v - Cell_{vmin}}{Cell_{vmax} - Cell_{vmin}} \right) \quad [7.19]$$

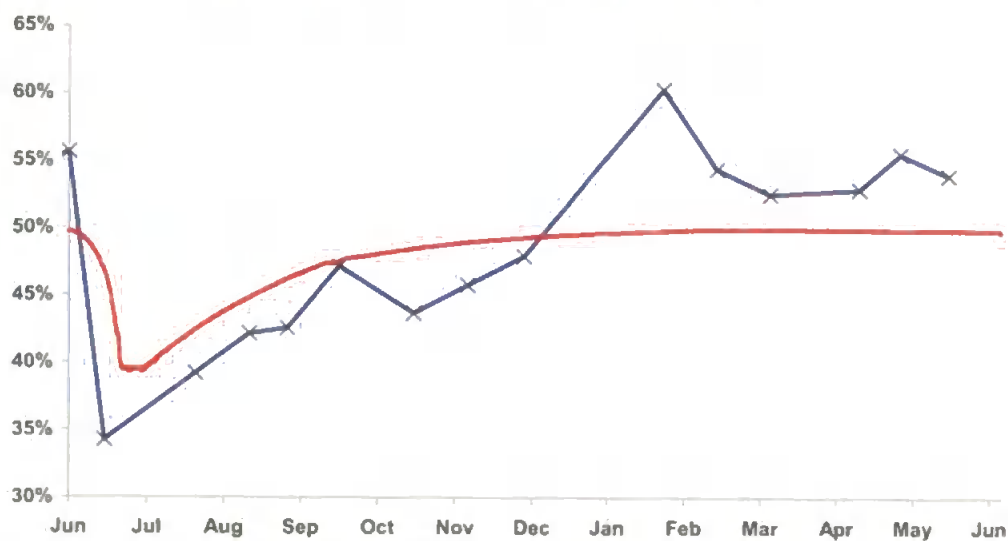
Then for the rest of the year, days 150-365, this glycogen split was increased once again (Eqn 7.20), so that it would return to its original value at the start of the next year.

$$G\% = 0.3 + \left( 0.2 + \frac{0.25 * (DayNumber - 100)}{265} \right) \times \left( \frac{Cell_v - RB_v - Cell_{vmin}}{Cell_{vmax} - Cell_{vmin}} \right) \quad [7.20]$$

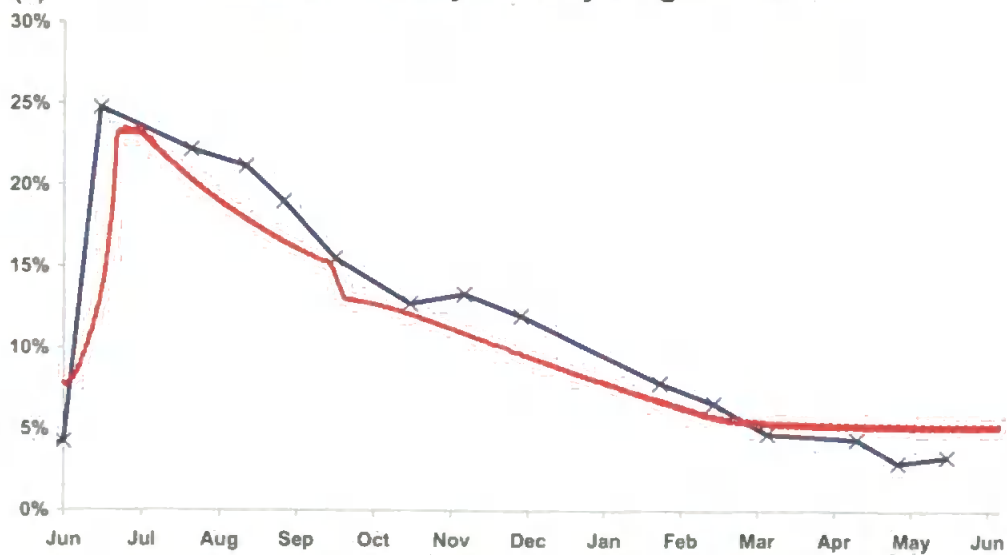
(a) Non mantle dry weight : Model 6f



(b) Non mantle protein dry weight : Model 6f



(c) Non mantle carbohydrate dry weight : Model 6f





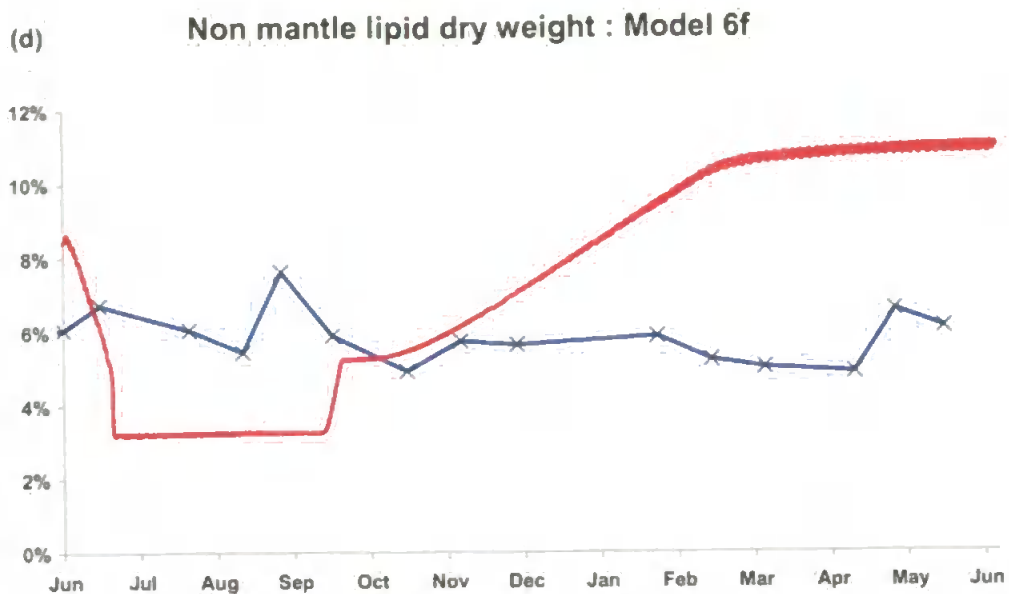


Fig 7.19 Model 6f annual dry weight comparison — Observed — Model6f.

(a) Total cellular dry weight as a percentage of maximum attained throughout annual cycle. (b) Protein, (c) Carbohydrate and (d) Lipid dry weight expressed as a percentage of cellular dry weight

With the change in the glycogen control function there was a slow decrease from the maximum dry weight at the start to the end of summer followed by the greater decrease over the autumn/winter period (Fig 7.19a). The protein dry weight now increased after it had reached its minimum point at the start of the summer in accordance with the data, although the scale of the initial decrease was not quite enough (Fig 7.19b). The carbohydrate dynamic was very close to the observed throughout the annual cycle (Fig 7.19c), with only a small questionable decrease over days 100-110 as the food started to decline. This small decrease was reflected in a small increase in the lipid at the same time, but the overall lipid behaviour showed poor agreement with the data (Fig 7.19d).

### *7.10 Discussion*

The macromolecular model was implemented by considerations of the various ratios of the different molecular components. These provided the necessary control for the model, and allowed for the seasonal variation seen in the C:N ratios which had been problematic previously. By varying the storage forms of energy throughout the year an annual signal was derived. The notion of varying certain parameters on an annual timescale to reflect the physiological demands and requirements of the whole animal (e.g., reproductive and growth imperatives) was achieved through a series of gradually refined functions.

The modelling dictum of simplicity has lead to linear functions being used. Due to the lack of "time dense" data for different regimes over annual cycles these were not improved upon. A lack of data detailing how the organism responded under differing circumstances, in terms of the rates and concentrations, precluded an accurate validation of the system devised.

The main question to ask was whether or not this model is any better than the previous model? On the positive side, it was more adaptive than its predecessor and had been shown to adequately simulate a seasonal pattern for protein, carbohydrates and overall dry weight. But as a consequence, it had to have more processes added and more assumptions had to be made. Whilst the inclusion of these processes was appealing - because they are

readily recognisable as biological activities – the problem was the lack of validation of their rates against the proposed scenarios.

Since the validation data was for an entire annual cycle, the definition of the model became unclear once more. Should it have represented a single cell or stand as a proxy for the entire gland? The loss of dry weight over the winter was presumed to represent degeneration of cells to reduce inefficiency and running costs. A core subset could then be left to regenerate when the food supply was bountiful once more in the spring. The sacrificed cells, presumably, could then form part of the diet of the remaining cells in times of hardship (i.e., by phagocytosis of apoptotic fragments). But with a single eternal cell model, this cannot be simulated. Equally, an ensemble composed of individual cell models could not be implemented without consideration of intracellular effects and how to characterise each cell. Whilst the cell characterisation may have been implemented via a probability distribution linked to the cellular parameters the introduction of more unknown processes was prohibitive. Digestive cells do undergo mitosis (Marigómez *et al.*, 1999), hence, a simple cell division model was investigated to determine whether or not this could account for the seasonal variation in cellular ratios.

Whilst the homogeneity of the cells generated in this model could conceivably be a reason for its inadequacy (in accounting for the summer trend of drop in protein and rise in carbohydrate) the general conclusion was that it was the demands of the rest of the animal which provoked this

response. Hence, some signal was needed, as an input to the model, to incorporate the demands from the rest of the animal if the C:N ratio signal was to be replicated. While a typical annual signal might be postulated in line with the reproductive cycle, there would also have to be regard for demands placed on the animal by various irregular exogenous factors such as change in environmental conditions.

## Chapter 8 Lipid Metabolism & Starvation Models

### 8.1 Introduction

The previous model was developed further to produce a model which could be used in the toxicity experiments detailed in Chapter 9. Initially, development of the previous model was concentrated on producing better results with specific regard to the lipid dry weight result. Consequently, the importance of the control algorithm under varying dietary regimes was highlighted. It was deemed important to develop a model adaptive to both food quality and quantity.

The objectives of this chapter were, thus, twofold.

- 1) To address the poor performance of the annual lipid dry weight results. To this end, a lipid storage form was added to the model and the control algorithm changed to ensure that a constant proportion of the cellular carbon was contained within the lipid compartments.

*Hypothesis 8.1:* Adjusting the model to keep a constant lipid dry weight will allow for better overall annual simulation results.

- 2) To remove the arbitrary seasonal feeding and resting phase lengths of the previous model and make these variables dependent upon the availability and quality of food.

## 8.2 Lipid metabolism model: Model 7a

Under the model's auspices, lipid referred to the major water insoluble molecules, notably phospholipids (as the basis of cellular membranes) and triacylglycerols and their basic component building block, free fatty acids. A simple model of lipid metabolism was proposed to enhance the model.

Whatever the form of dietary fat, it is considered to be degraded by the lysosome into fatty acid. Fatty acids are stored as triacylglycerols, which are converted back to fatty acids when required (Lodish *et al.*, 1999). Fatty acids are either utilised through the fatty acid spiral in energy release or else used in the de novo synthesis of phospholipids or sterols. The other possible source of sterols is the uptake of extracellular material, either from the rest of the animal or else in the diet.

In the simplified model proposed the phospholipids, which equate to cellular membrane in the model, were taken to be a constant proportion of cell content and are ignored. The exception was the retention of the lysosomal and endosomal membrane lipids, to allow for the damage and replenishment to these critical components of the model.

Additionally, excess carbohydrate could be incorporated into the triacylglyceride pool as a means of long term storage. Initially this flow of material was implemented uni-directionally. Subsequently, it was seen to

be necessary to allow for the lipid to transfer to the carbohydrate compartment as well (see Section 8.5).

The revised model lipid metabolism is shown in schematic form in Figure 8.1. From the schematic it was evident that it was necessary to develop a procedure for controlling triacylglyceride release, storage and export in conjunction with the overall cellular metabolism. For simplicity, the level of triacylglyceride carbon content was set equal to that of cytosolic lipid at the end of each timestep by retrospectively setting the rates of storage or release.

From the observed seasonal data it was apparent that the lipid levels do not fluctuate significantly, hence, the control algorithm which was applied at the end of the timestep calculation was amended to include a facility to keep the proportional lipid dry weight at a constant level (Thompson *et al.*, 1974). If there was not enough lipid then material was taken from the glycogen store and converted into fat. If there was too much lipid then triacylglyceride was exported to the rest of the animal.

Finally the degree of compaction which the storage form afforded needed setting. Since this was a long term storage form and the model had material coming from the glycogen compartment, this was taken to be a multiple of the lipid constant carbon concentration. Initially, it was set at twice the normal lipid concentration. An annual simulation was then performed to see the effect of these changes.



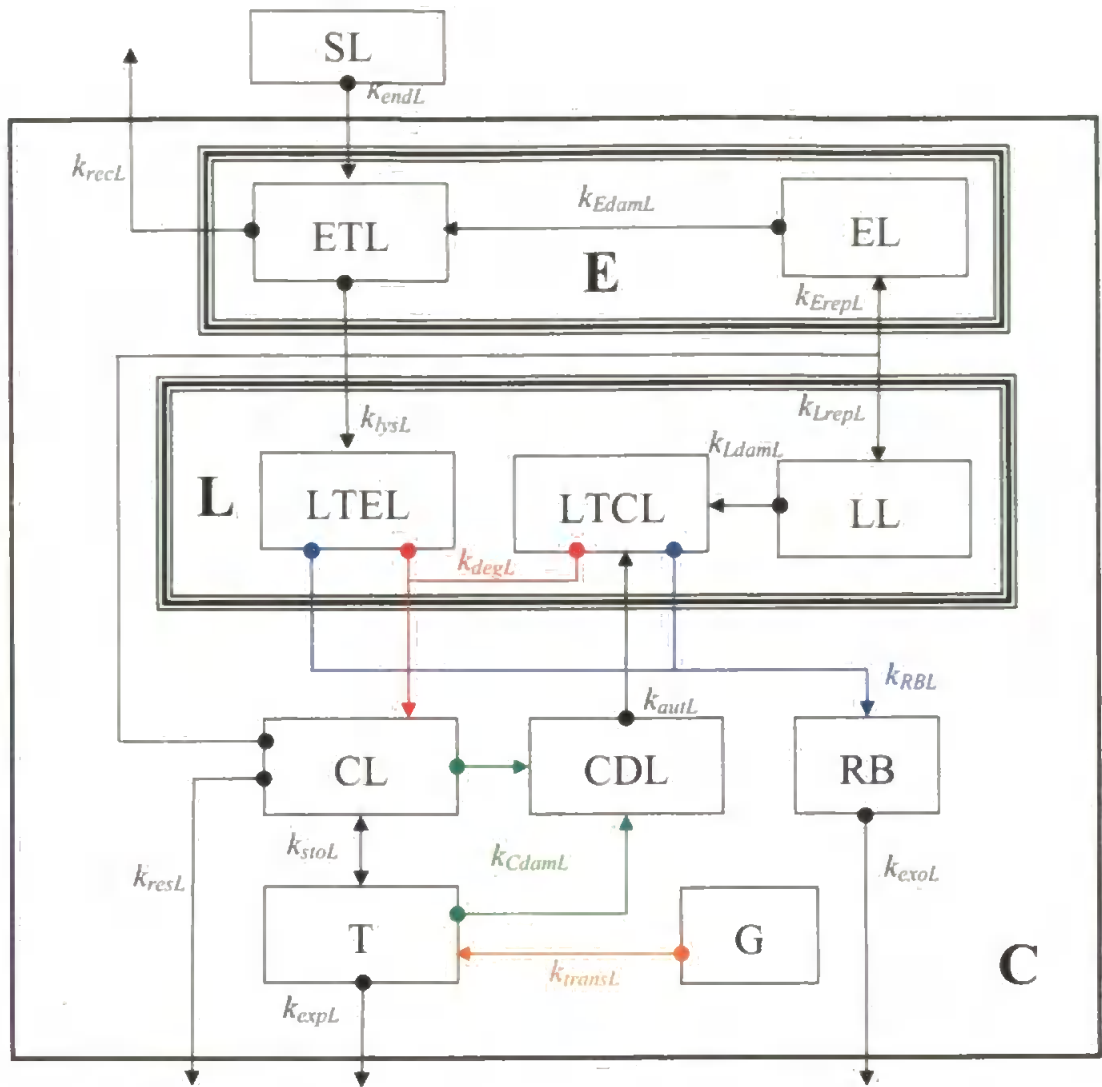
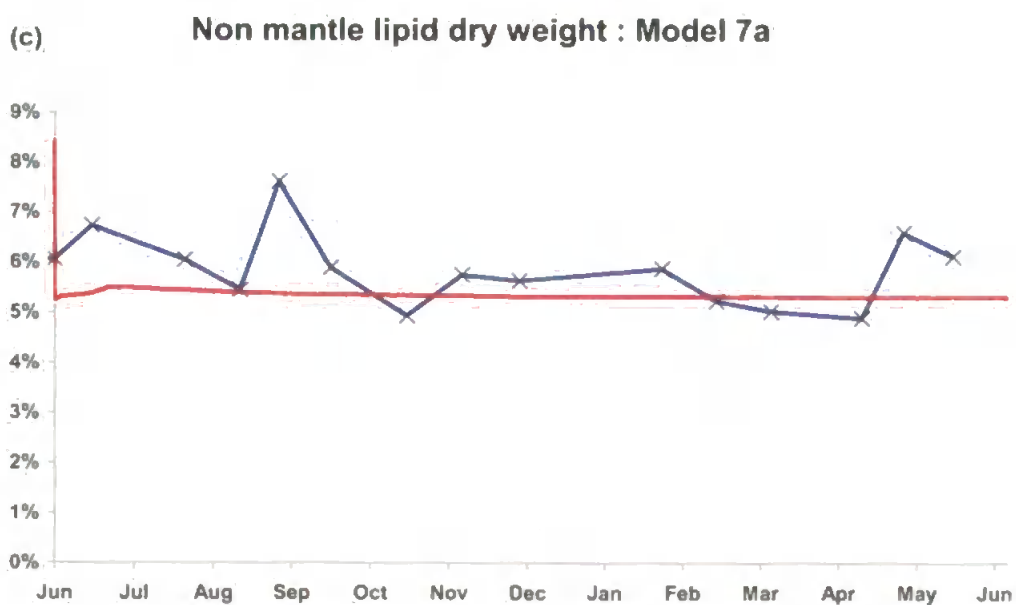
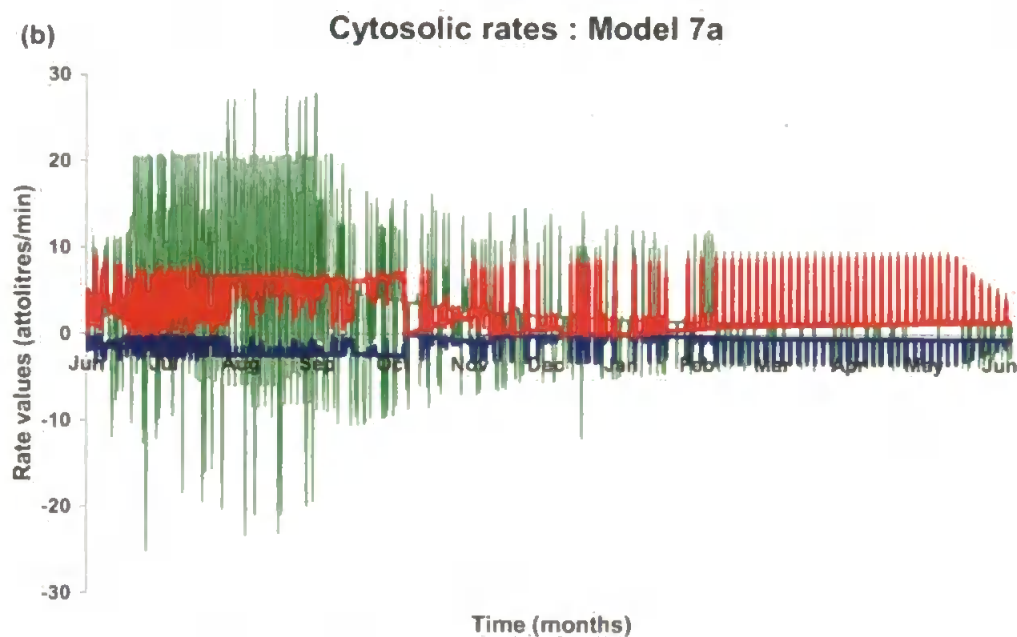
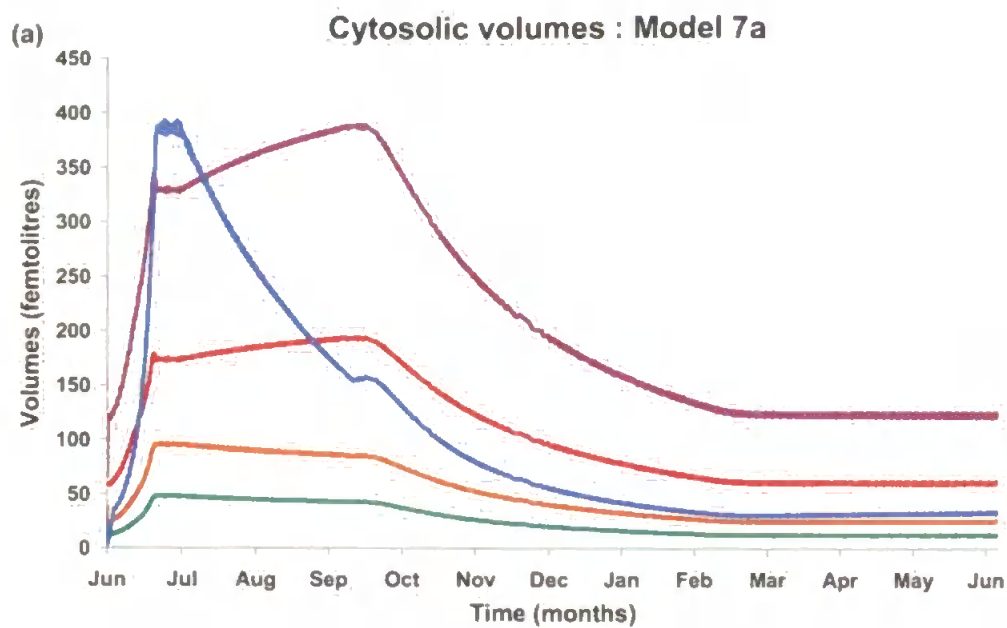


Fig 8.1 Cellular lipid metabolism schematic; SL – surface lipid (food source); ETL – endosomal target lipid; EL – endosomal integral lipid (membrane; LTEL – lysosomal target lipid sourced from endosome; LTCL – lysosomal target lipid sourced from cytosol; LL – lysosomal integral lipid (membrane); CL – cytosolic lipid (includes); CDL – cytosolic damaged lipid; RB – residual bodies; G – glycogen store;  $k_{endL}$  endocytosis of lipid;  $k_{recL}$  recycling of lipid;  $k_{hysL}$  lipid from endosome to lysosome;  $k_{degL}$  lysosomal degradation of lipid;  $k_{RBL}$  removal of waste lipid to residual bodies;  $k_{autL}$  autophagy of lipid;  $k_{exoL}$  exocytosis of lipid;  $k_{resL}$  respiration fuelled by lipid;  $k_{stoL}$  storage/release of lipid;  $k_{expL}$  export of lipid to rest of animal;  $k_{E/L/CdamL}$  damage of lipid in endosome/lysosome/cytosol;  $k_{E/LrepL}$  replenishment of lipid membrane to endosome/lysosome;  $k_{transL}$  transfer of glycogen to lipid.



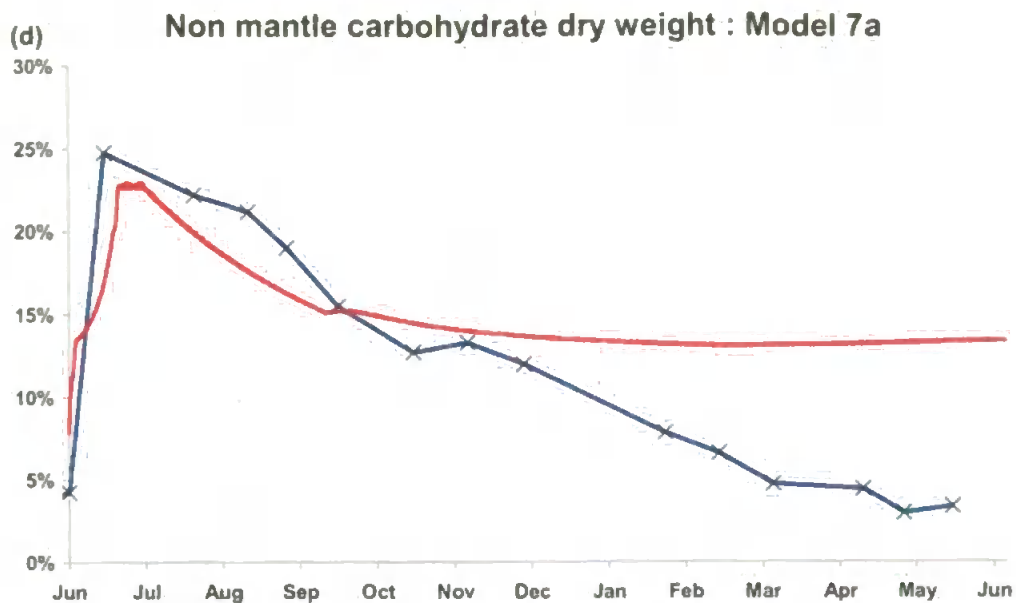


Fig 8.2 Model 7a Annual cycle as in model 6f but with constant lipid condition (a) small compartmental cytosol volumes:  $AA_v$ ,  $CS_v$ ,  $G_v$ ,  $CL_v$ ,  $T_v$  (b) New rates calculated:  $k_{transL}$ ,  $k_{GdiffT}$ ,  $k_{stoL}$  (c) Lipid and (d) Carbohydrate as percentage of total dry weight — Model, — Observed.

The cytosolic lipid and triacylglyceride volumes (Fig 8.2a) differed only by the triacylglyceride being half the scale of the other compartment, due to the presumption of sharing equal content and possessing double the concentration. As the lipid dry weight was constrained to remain close to the 7% of cell dry weight (Fig 8.2c), the annual shape of their curves was coincident with that of the total dry weight. The newly introduced rates showed that there was a fairly consistent amount of glycogen being transformed into lipid throughout the year, while the storage and release of triacylglyceride oscillated throughout as the correct balance was strived for (Fig 8.2b). There was a 4.6% overall increase in lipid & carbohydrate

carbon export over model 6f, but the split between two types differed with more lipid being exported in this simulation.

Unfortunately the effect on the carbohydrate dry weight dynamic was not favourable (Fig 8.2d), this value remained relatively constant from late autumn to the spring and not decreasing as before. It was considered productive at this stage to address the imposed seasonal tubule phase lengths. Since experimentation with these parameters showed significant effects on the model output, it was speculated that this might address the newly arisen problem with the carbohydrate result.

### 8.3 Food availability: Model 7b

Previously the resting phase and feeding phase signal had been used to invoke an annual nutritional signal into the cell. It was decided it would be more beneficial to actually derive a response to the food signal arriving at the cell surface. To this end, model 7b was developed to simulate how the cell copes with nutritional deprivation. Consequently, a new variable *FoodAvailability* was introduced which ranged from 0-1, indicating the abundance of food: with 0 representing no food available and 1 indicating food at or above the feeding capacity of the mussel. Model 7b1 made the feeding phase length linearly dependent on cell volume excluding the accumulating residual bodies. The following [8.1] was calculated daily in the model:

$$FP = FP_{\min} + (FP_{\max} - FP_{\min}) \left( \frac{Cell_v - RB_v - Cell_{v\min}}{Cell_{v\max} - Cell_{v\min}} \right) \quad [8.1]$$

The resting phase was made dependent on the *FoodAvailability* variable and calculated daily:

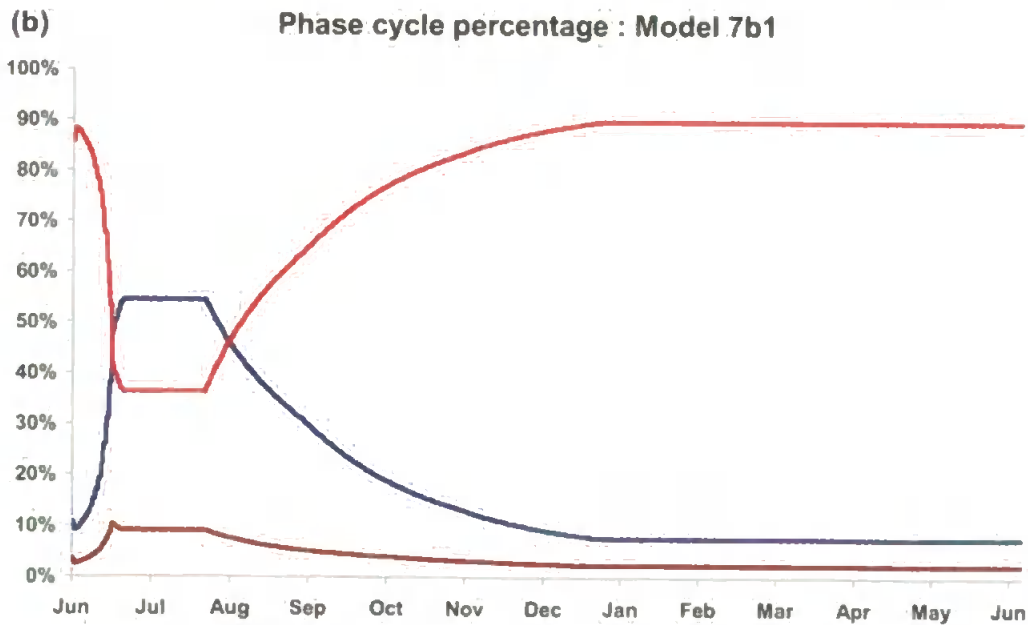
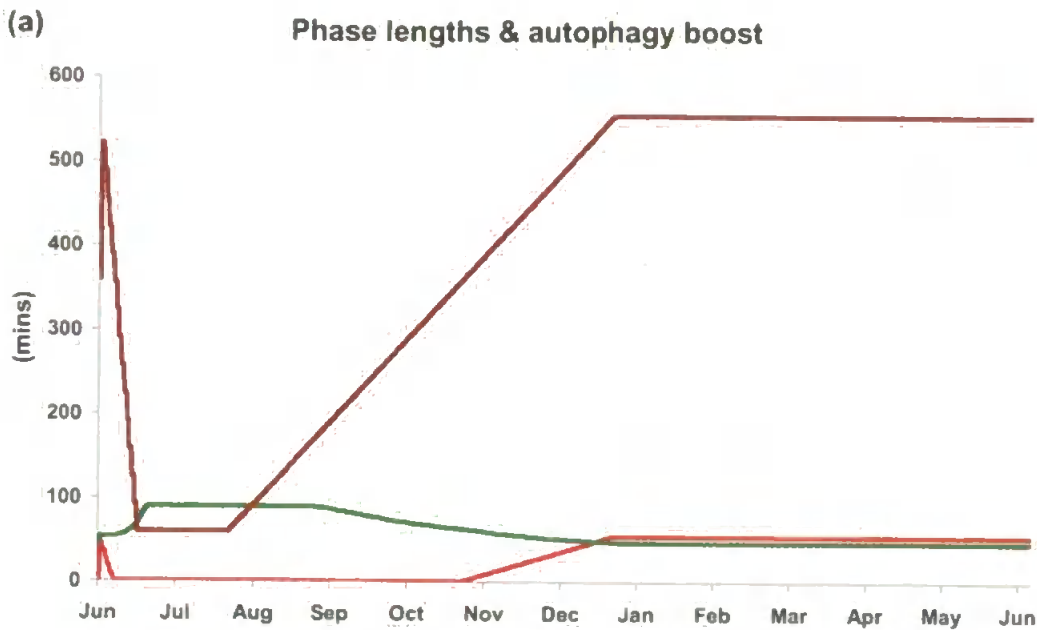
$$RP = RP_{\min} + (RP_{\max} - RP_{\min}) Foodavailability \quad [8.2]$$

Then the *FoodAvailability* signal was modelled as a rapid increase over the first 15 days from 0.25 to 1, then remaining at 1 until day 50 then linearly decrease to 0.25 to day 200, and remaining at 0.25 thereafter (Fig 8.5a). Obviously, this signal needs to be validated for future studies.

Furthermore, the decrease in food was used to boost the basal autophagy of

non-damaged proteins as detailed below [8.3] to allow up to a hundredfold increase.

$$AutophagyBoost = \begin{cases} 1 + 99 \times \left( \frac{RP}{360} - 1 \right) & \text{IF } RP > 360 \\ 1 & \text{Otherwise} \end{cases} \tag{8.3}$$



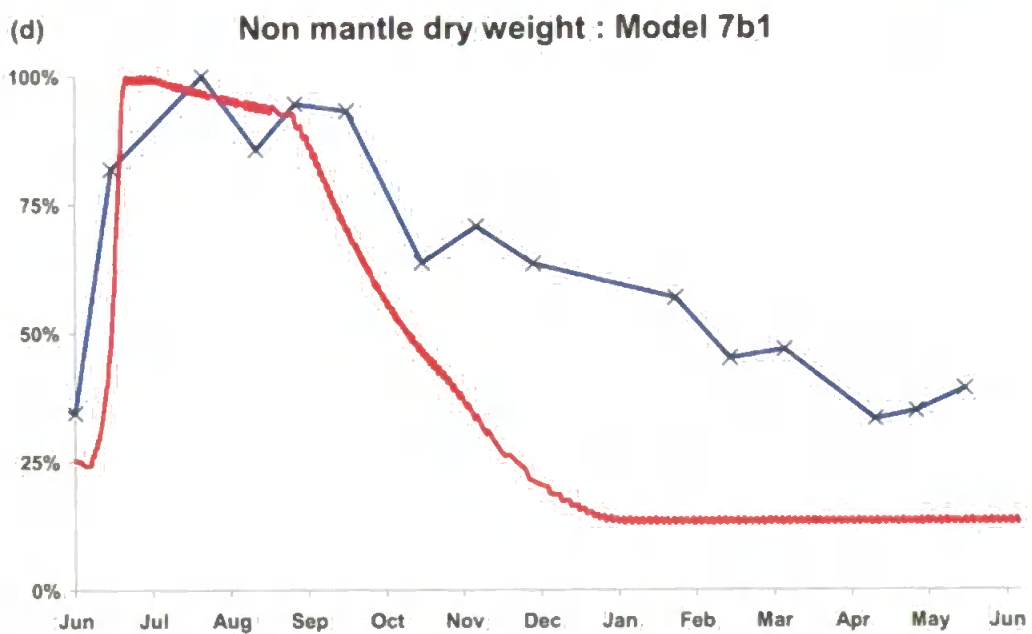
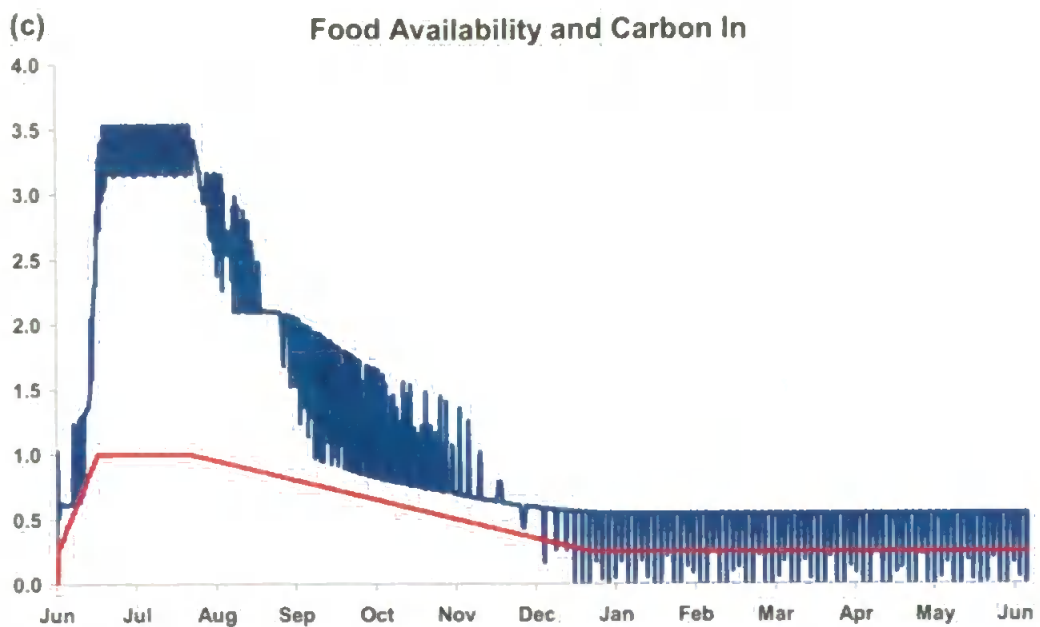
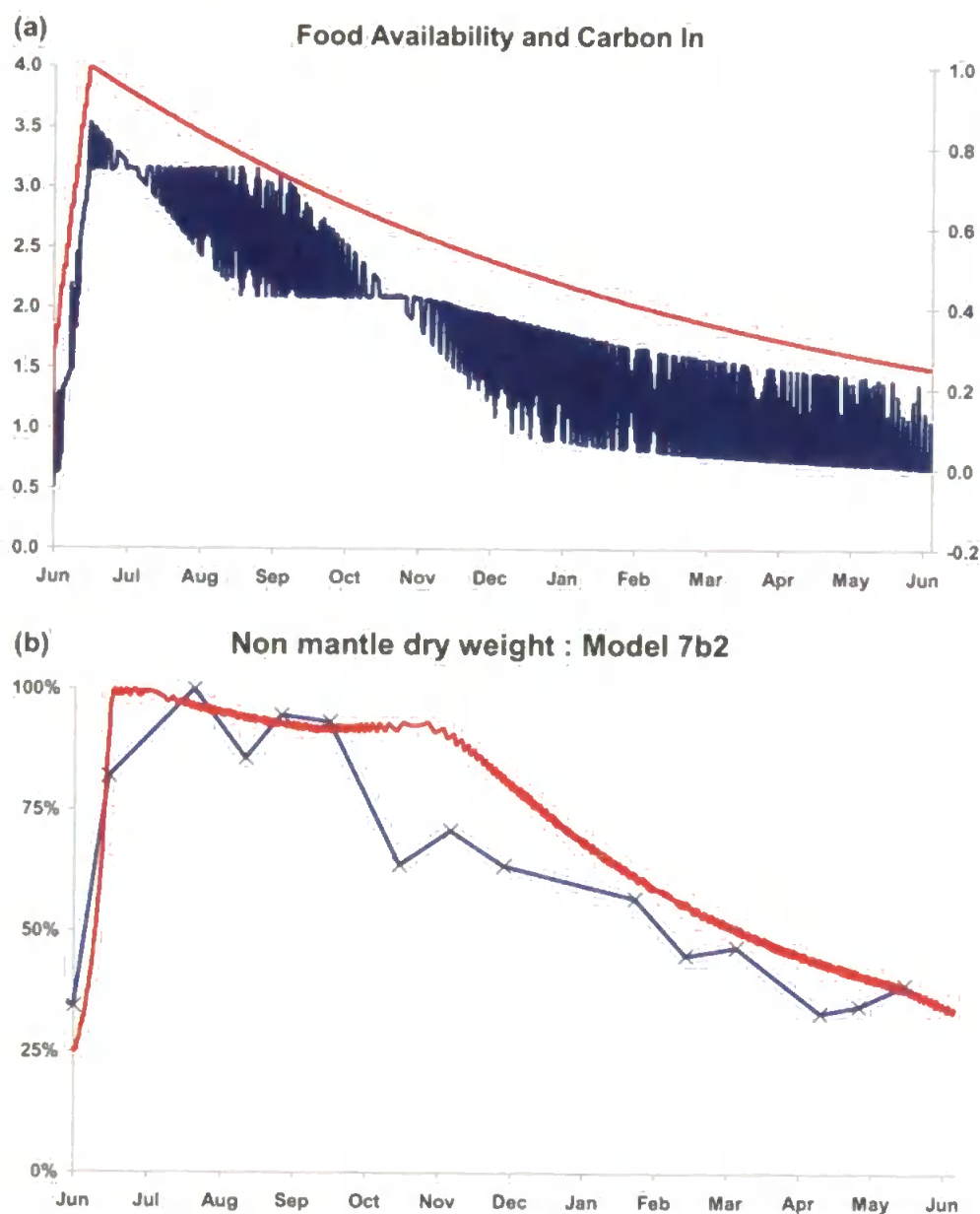


Fig 8.3 Feeding and resting phases, based on food availability with autophagic boost, Model 7b1. (a) – Resting phase length, – feeding phase length, – basal undamaged autophagic boost (b) phase length as percentage of total phase cycle – feeding phase, – resting phase & – disintegrating phase (c) – FoodAvailability signal & – carbon taken up by endocytosis in a timestep (d) – observed & – simulation total dry weight as percentage of maximum.

The *FoodAvailability* signal was reflected in the amount of carbon ingested by the cell as expected, with a seven and a half fold increase in the bountiful summer over the average winter/early spring daily average (Fig 8.3c). The overall dry weight, however, fell to a lesser average value in the winter/spring than before, due to the increased autophagy of stored reserves (Figs 8.3a & d). Comparison of the previous relative phase lengths (Fig 7.6b & 8.3b) showed the decrease of the feeding phase over the last of the summer period; and provoked the smoother decline in dry weight.





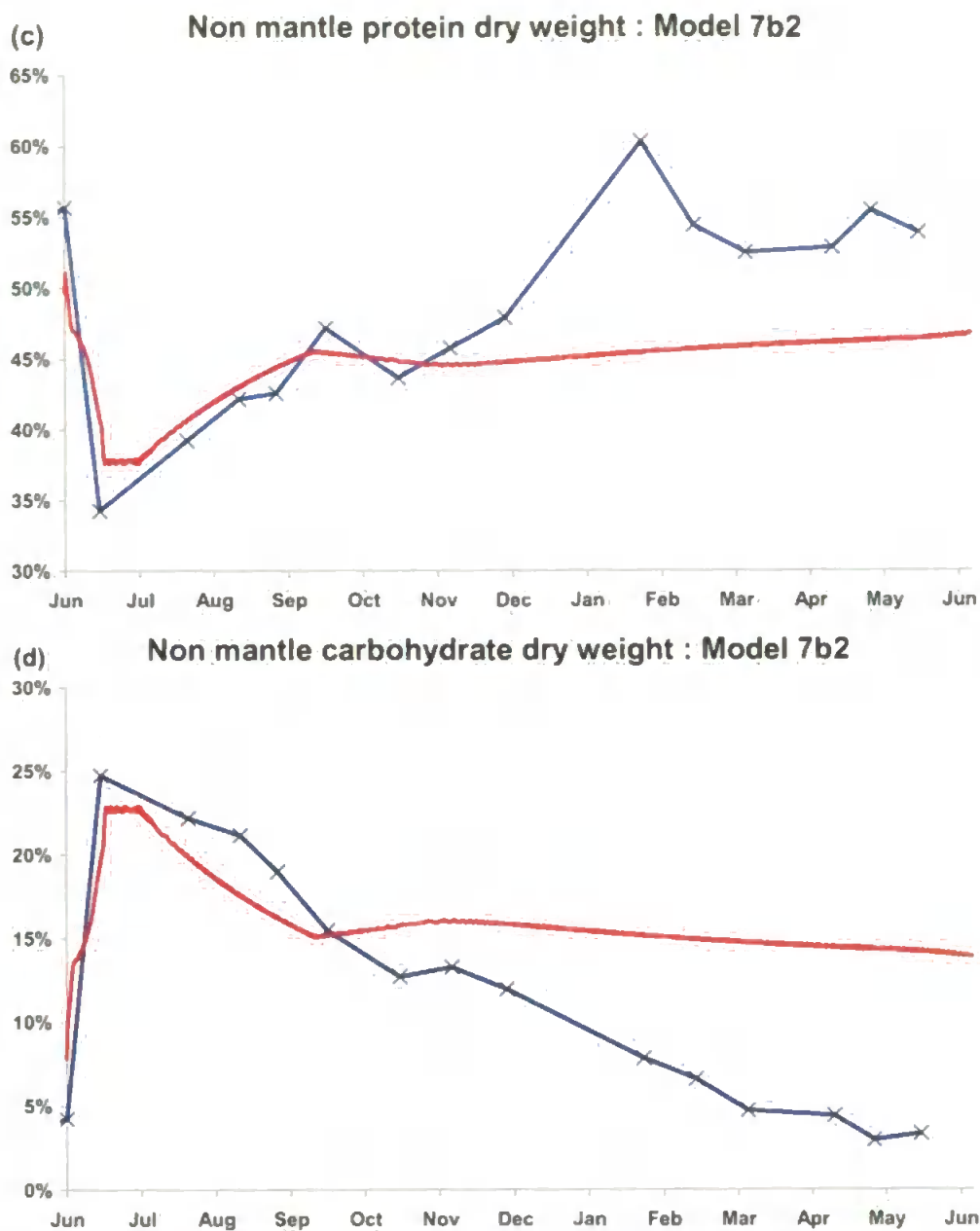


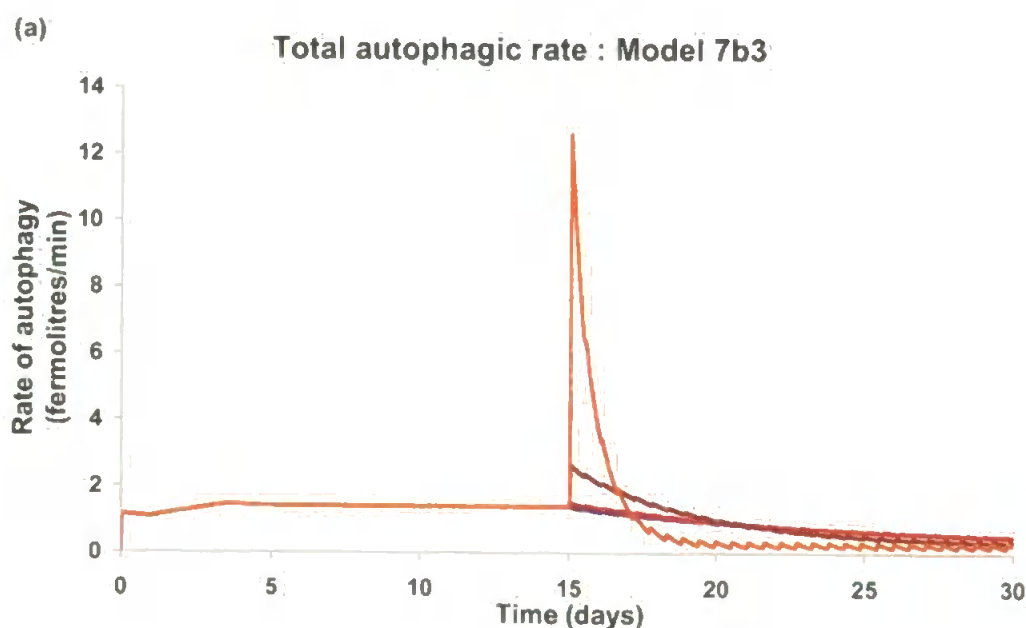
Fig 8.4 Model 7b2 exponential decrease in FoodAvailability from day 50 to low at day 365. (a) — FoodAvailability and — total carbon in (b-d) — observed and — simulation (b) total dry weight (c) protein dry weight (d) carbohydrate dry weight.

Model 7b2 attempted to rectify the excessive dry weight decline by decreasing the FoodAvailability value from day 50 to day 365 exponentially (Fig 8.4a). The total dry weight then decreased to around the

end of year figure, however the initial decrease was quite slow followed by a more rapid increase from day 150 (Fig 8.4b). However, at this time the carbohydrate and protein dry weights started to diverge from the observed trends (Figs 8.4c & d).

It was concluded that during this period either: the control algorithm was converting too much protein to carbohydrate; or too much protein was being degraded; or too little carbohydrate was being used. It was deemed prudent to consider the autophagic boost due to food deprivation as this was heavily weighted to choose protein over the other two macromolecular forms. Actual *AutophagyBoost* increase is only minimal and started on day 338.

To test the effect of increased autophagic boost, Model 7b3 varied the autophagic boost from no boost to a thousand-fold increase of the undamaged portion of autophagy. In this simulation, the cell was well fed for 15 days and not at all for the next 15 days.



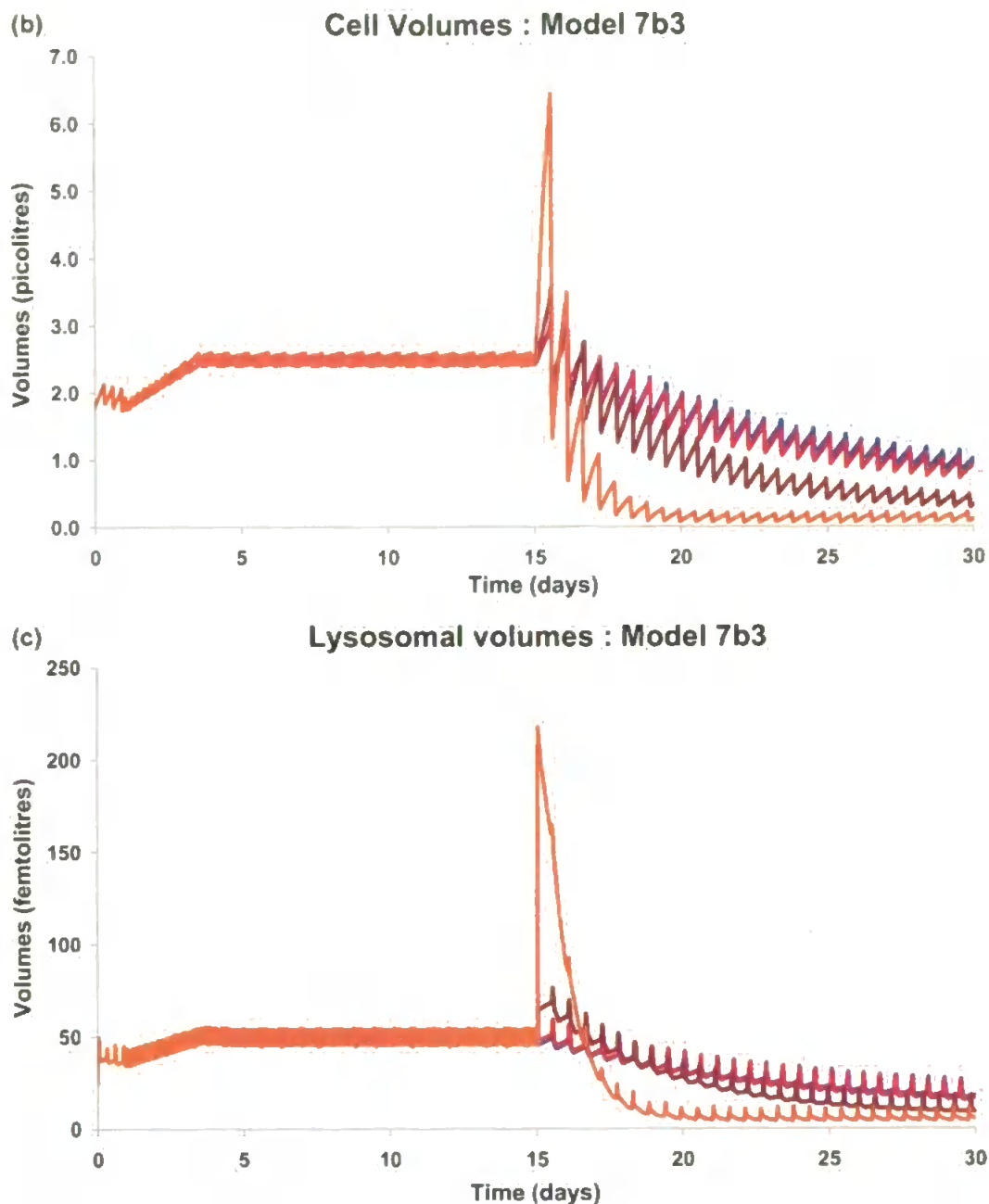


Fig 8.5 Autophagy boost test - Model 7b3. FoodAvailability = 1.0 during days 0-15, FoodAvailability = 0.0 during days 15-30; Autophagy Boost = 1 —, 10 —, 100 —, 1000 —. (a) Total autophagic rate (basal  $\times$  boost + damaged) (b) Total cellular volume (c) Lysosomal Volume.

By increasing the *AutophagyBoost* parameter a thousand-fold, the total autophagic rate was eight and half times the normal rate to begin with but rapidly decreased to the lowest observed value (Fig 8.5a). This

occurred because as the cytosolic volume decreased less material was made available for autophagy than for the other values, which had slower rates of decrease of autophagy from the initial boost. The initial increase in lysosomal volume reflected the increased autophagic rates (Fig 8.5c). The cell volume showed an overall decreasing pattern as a consequence; however, there was a period during which cell volume increased as the residual bodies increase as the lysosome degraded this new material. The relative lysosomal volume did not increase to those values which would represent poor lysosomal stability.

The problem with the residual body volume artificially inflating the cell volume (Fig 8.5b) and hence affecting the lysosomal stability calculation were noted during this simulation. Hereafter, it was decided to exclude the residual body volume from that of the cell volume for these purposes.

A sensitivity analysis based on the AutophagyBoost parameter space revealed a threshold where cell expiry does not occur before day 100 (Fig 8.7a), which was arbitrarily taken to indicate poor model performance. This simulation was run with complete starvation after day 15, but there was still a feeding phase being invoked. This was due to the algorithm being purely based upon food quality. It was determined that the feeding phase should be disregarded completely when *FoodAvailability* = 0. Hence, model 7b4 was run with no feeding phases when there is complete starvation to explore the effect on cell expiry. The lack of material entering the cell

made cell expiry occur for all cells no matter what level of autophagy boost was applied (Fig 8.6b).

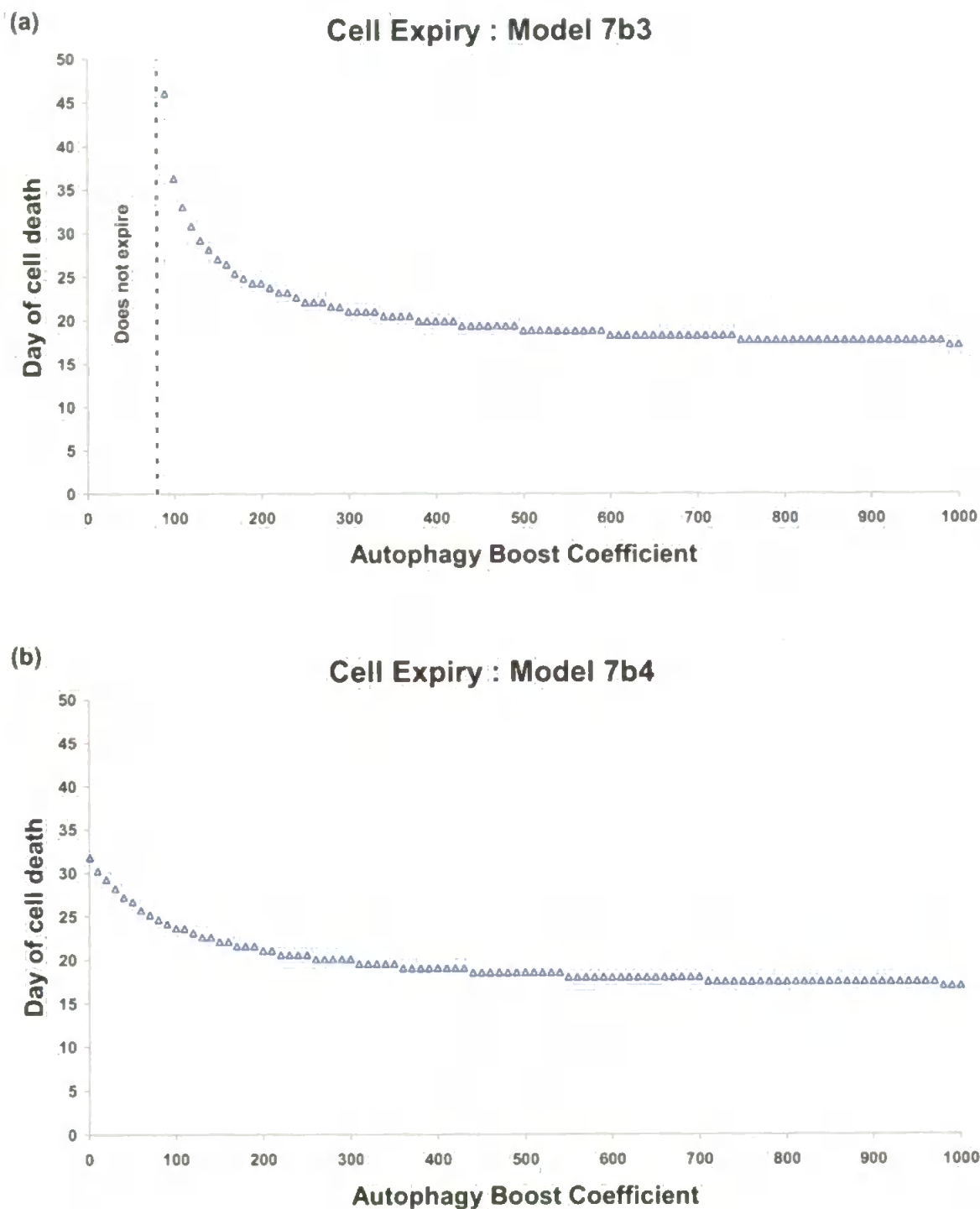
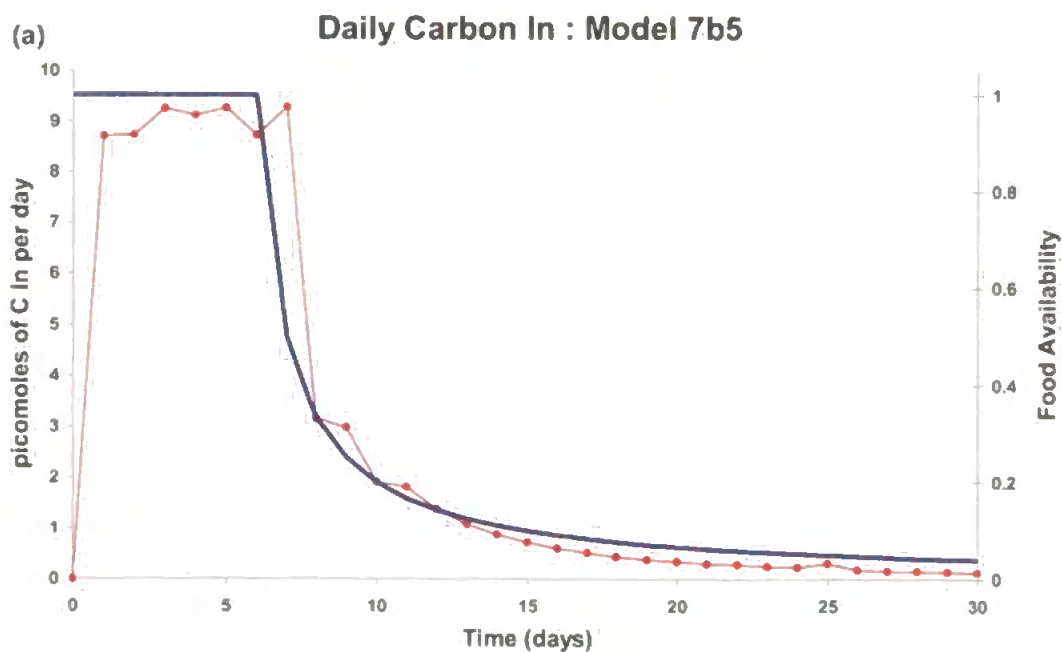


Fig 8.6 No feeding phase on complete starvation - Model 7b4. Otherwise as Fig 8.5. Autophagy Boost = 1 —, 10 —, 100 —, 1000 —. (a) Cell Volume excluding residual bodies (b) lysosomal stability (c)  $\Delta$  cell expiry date

However, this condition was considered too narrow and instead a broader directive to decrease the feeding phase length (FP) in line with decreasing food availability was adopted. Hence, for *FoodAvailability* < 0.25 the following calculation was used in Model 7b5:

$$FP = \left( FP_{\min} + (FP_{\max} - FP_{\min}) \left( \frac{Cell_v - RB_v - Cell_{v\min}}{Cell_{v\max} - Cell_{v\min}} \right) \right) \frac{Foodavailability}{0.25} \quad [8.4]$$

*AutophagyBoostMax* = 10 was chosen because it had exhibited increased survival. The results of model 7b5 showed an approximate doubling of overall autophagic rate and no discernible change in lysosomal stability as a consequence of starvation. Although in an experiment where mussels had been starved there was no observed affect after 10 days but after 20 days the lysosomal stability had declined to approximately 15minutes (Bayne *et al.*, 1978). Hence, it was acknowledged that the since the cell volume fell as expected the lysosomal volume must be depressed and would require further consideration.



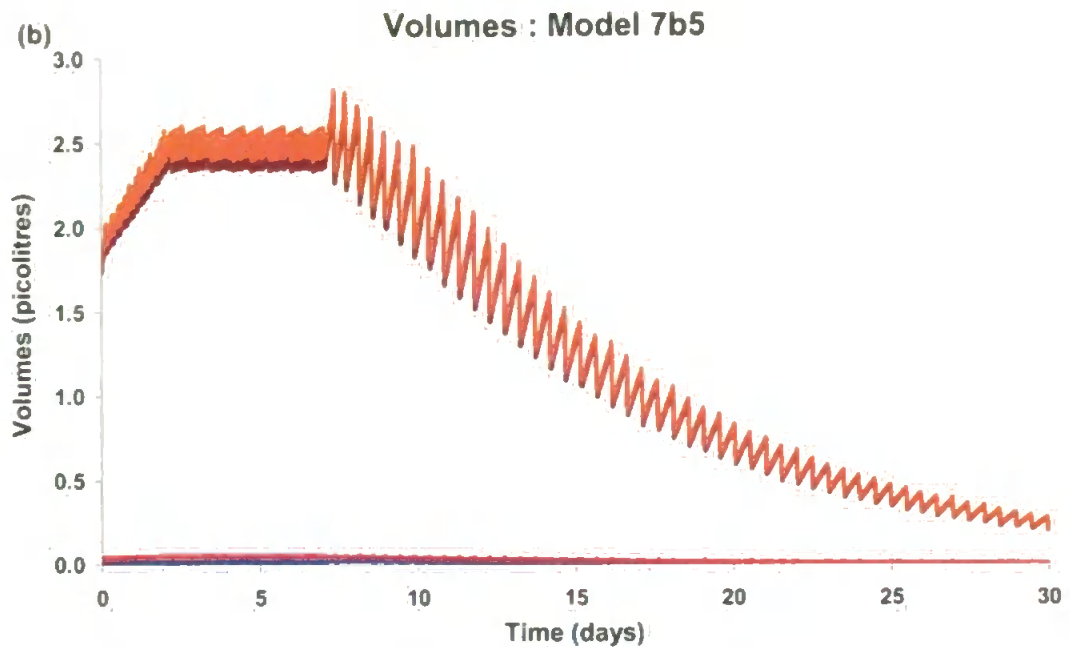


*Fig 8.7 Decreasing food availability Model 7b5. 6 days full food availability, thereafter FoodAvailability was recalculated daily as  $FoodAvailability = 1/(Day - 5)$  (a) — FoodAvailability and — carbon in (b) volumes — Endosome, — Lysosome, — Cytosol & — Cell.*

The link between decreased *FoodAvailability* and the amount of carbon ingested was closely interrelated (Fig 8.7a). The cell volume decreased at a lesser rate than the food availability (Fig 8.7b) and survivability was primarily determined by the protein content of the cell. The rate of cell volume loss was, however, exacerbated by the control algorithm which demanded that the carbohydrate and lipid be exported to achieve the stipulated equilibrium state given the superior loss of protein due to autophagy.

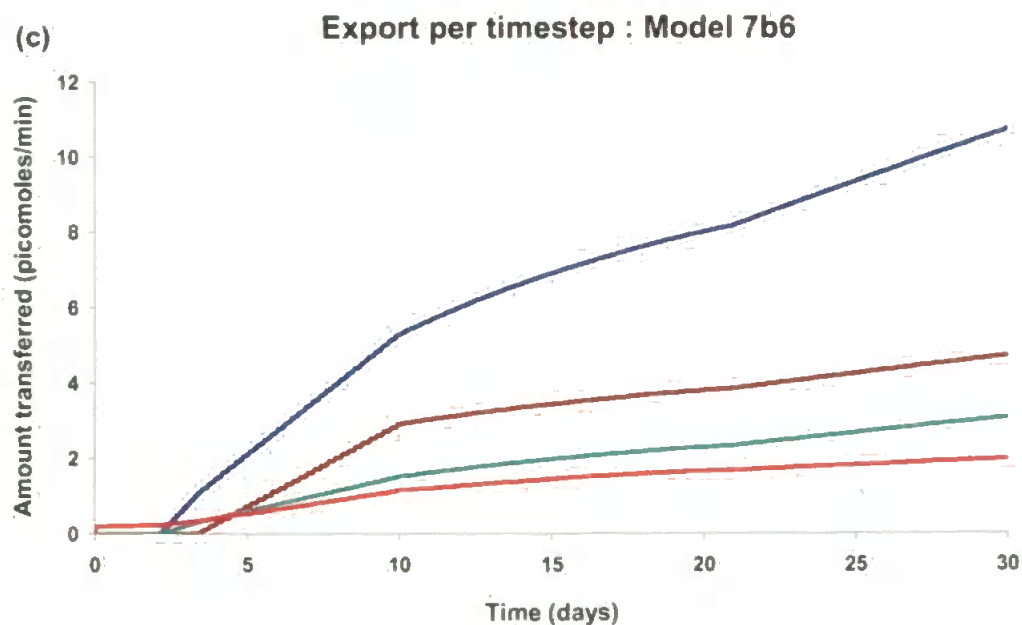
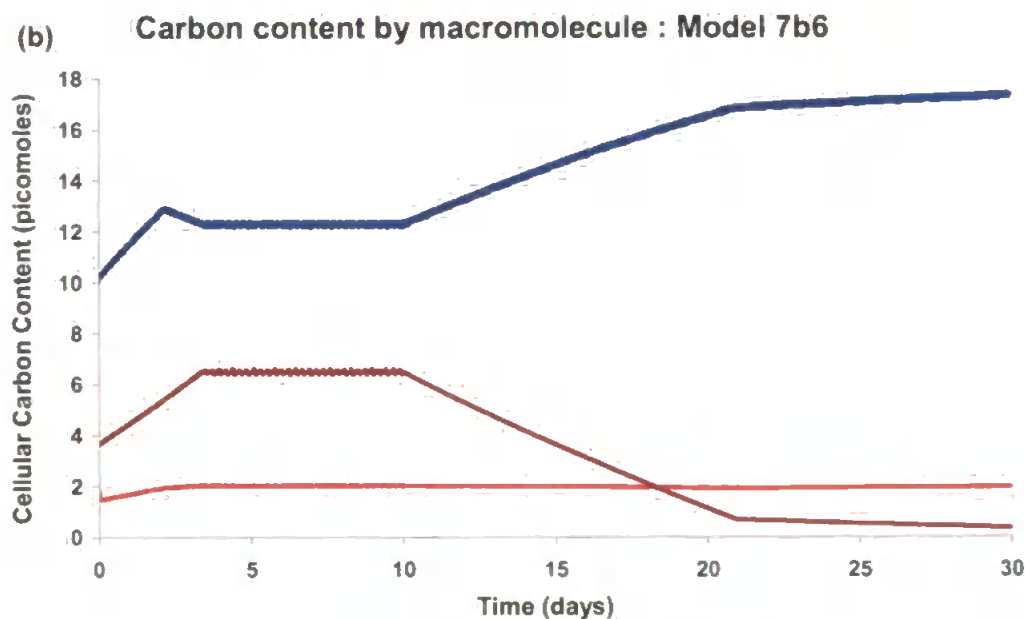
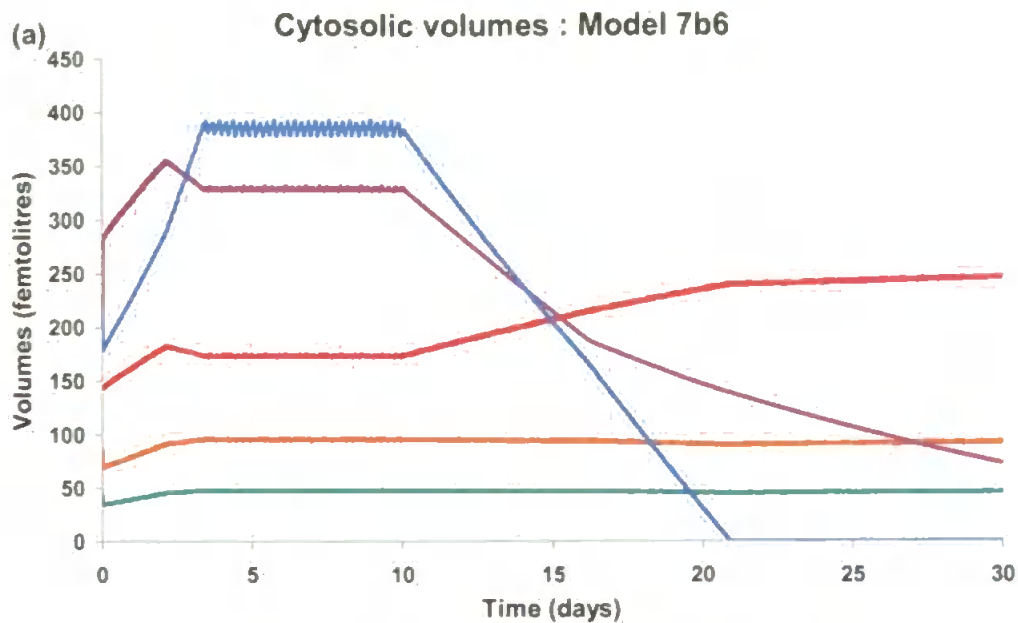
#### 8.4 Dietary quality: Model 7b6

The effects of the dietary quality upon the system were then investigated. With regard to the model, dietary quality concerned the carbon and nitrogen concentrations in the source material. The effect of an all protein diet was explored as this was considered the most taxing case for the control algorithm to manage. Subsequently, a diet with no protein was examined in order to see the rate of expiry.

For 10 days the cell was well fed with a varied diet ( $S_c = 6.0$ ,  $S_n = 1.2$ , *lipid%* = 25%), then for the next 20 days *FoodAvailability* was kept at its highest but the carbon concentration of the food dropped to the extent where all the incoming material was protein ( $S_c = 4.2$ ,  $S_n = 1.2$ ).

The initial period was dominated by the accumulation of glycogen; free sugars and amino acids initially rose and later fell as the energy stores fill more of the cell. By day 3.75 the cell had settled into a relatively constant state with the ratio of protein: carbohydrate: lipid carbon settled at approximately 6:3:1, with small variations as the cell fed (Fig 8.8b). Also the cell volume peaked at this point and remained there even when the food quality changed.





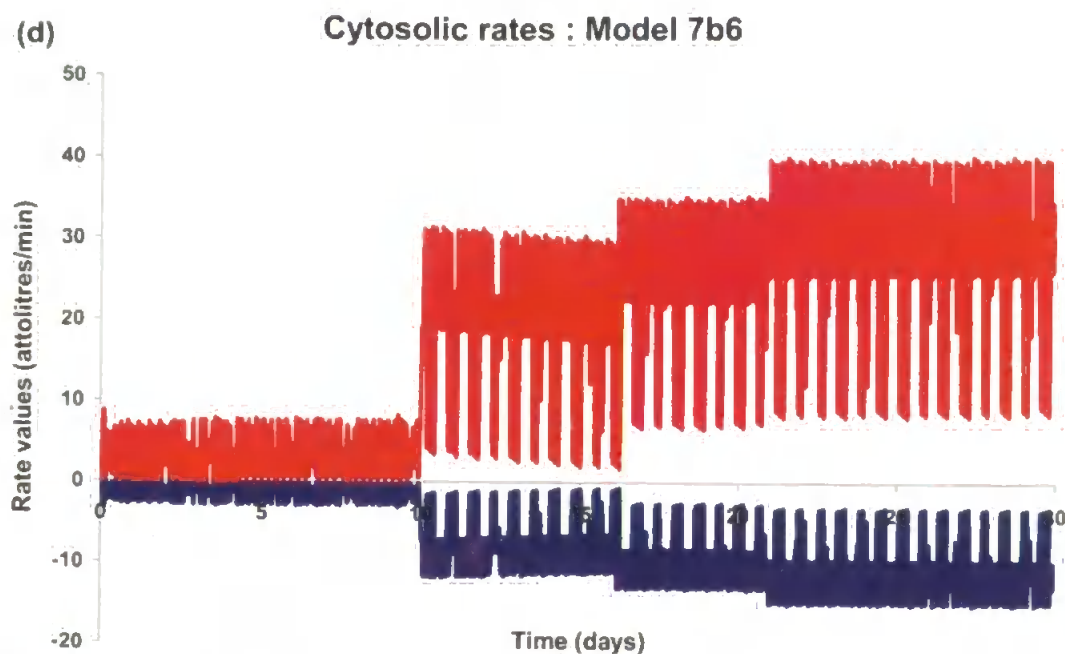


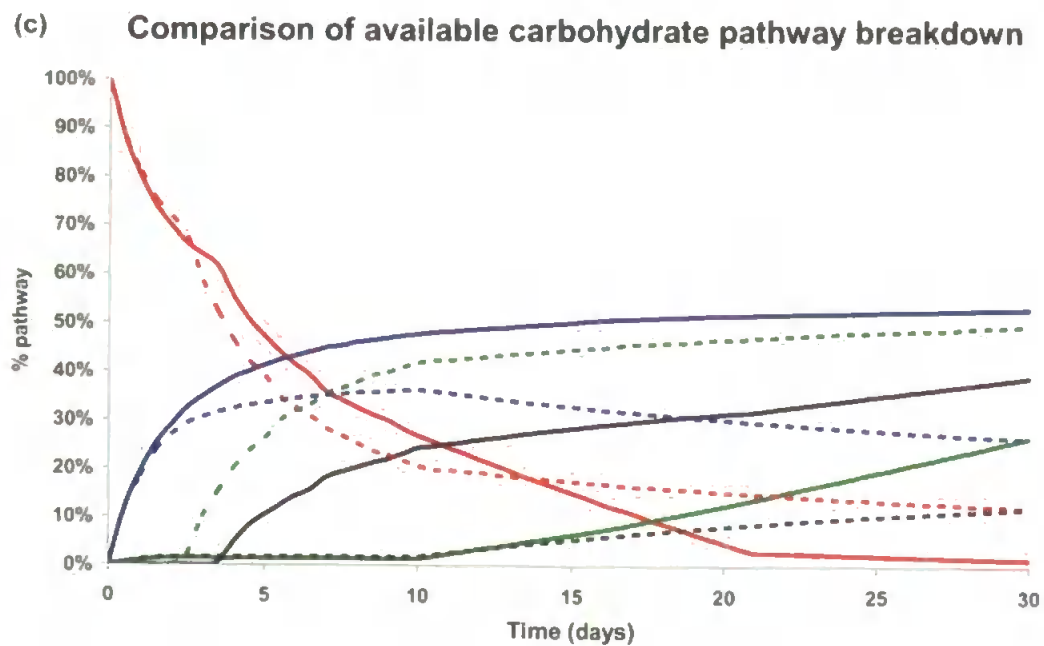
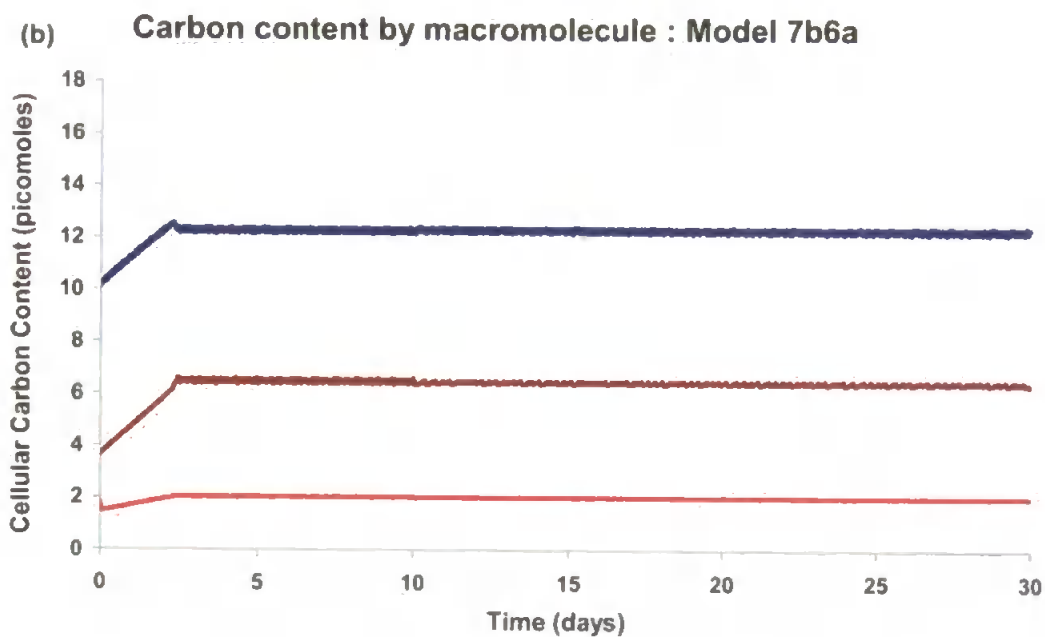
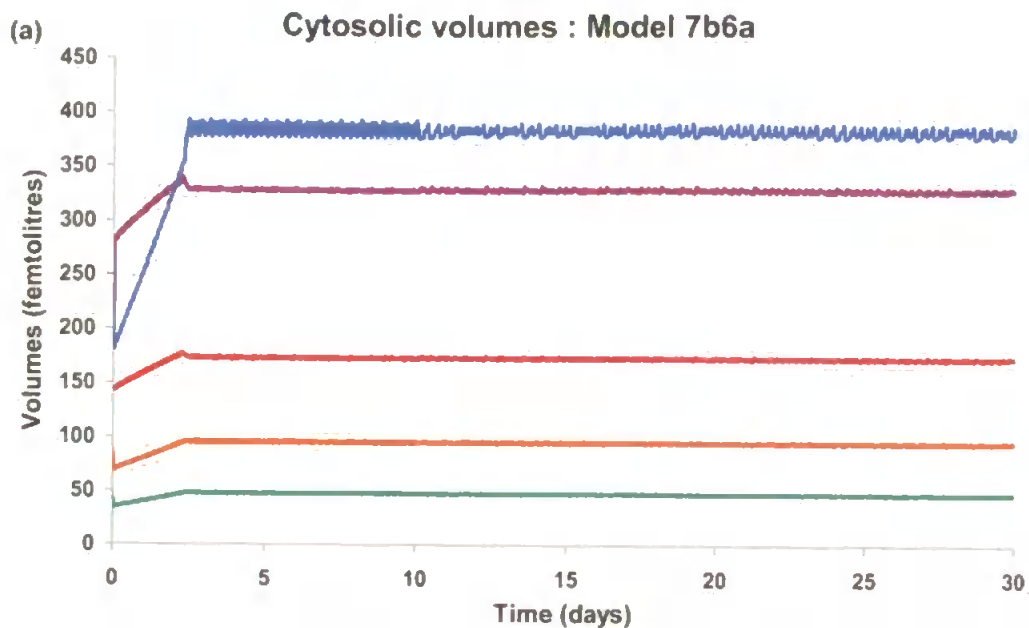
Fig 8.8 Model 7b6, all protein diet after day 10. (a) Cytosolic volumes — glycogen — free sugars — lipid — triacylglyceride — amino acid pool (b) Cellular carbon content breakdown — protein — carbohydrate — lipid (c) Export — protein carbon — protein nitrogen — carbohydrate — lipi (d) — Glycogen to triacylglyceride — Associated diffusion rate.

After day 10 there was a dramatic decrease in glycogen volume, with a slightly less rate of reduction in free sugars, a rise in amino acids and the lipid forms remained fairly consistent (Fig 8.8a). Eventually, the glycogen volume became zero which was not what the control algorithm was designed to provoke. This was determined to have been a consequence of the order that the various tests and reactions in the control algorithm were made in. Of particular concern was the export of glycogen which continued even after the inception of the all protein diet, albeit it at a lower rate than before (Fig 8.8c). This in itself was not considered a problem as long as glycogen stores remain sufficiently high for the cells own utilisation in

times of stress. Also of concern, was the transformation of carbohydrate to lipid which has increased under these dietary conditions (Fig 8.8d). If lipid is considered to be a long term storage form, then this compartment should not have been filled upon the initiation of stress, but rather chosen as the initial form of energy utilised.

As there was a lot of food available, what was expected was the deamination of amino acids to provide free sugar. Clearly this did not occur as expected and hence, Model 7b6a repeated the simulation with an additional final check on the control algorithm at the end of each timestep. It now checked the glycogen level and nitrogen controls, and deaminated if necessary, with associated nitrogen excretion.

This final check solved a lot of the problems with the all protein diet. There was enough nitrogen coming in as protein to sustain the nitrogen requirement and the excess carbon could be used to sustain the energy requirement, evidenced by the maintenance of high glycogen volume (Fig 8.9a). Also evident was the constant protein: carbohydrate: lipid carbon ratio (Fig 8.9b), which indicated that the control algorithm had enabled the desired homeostasis to be achieved under these restricted dietary conditions.



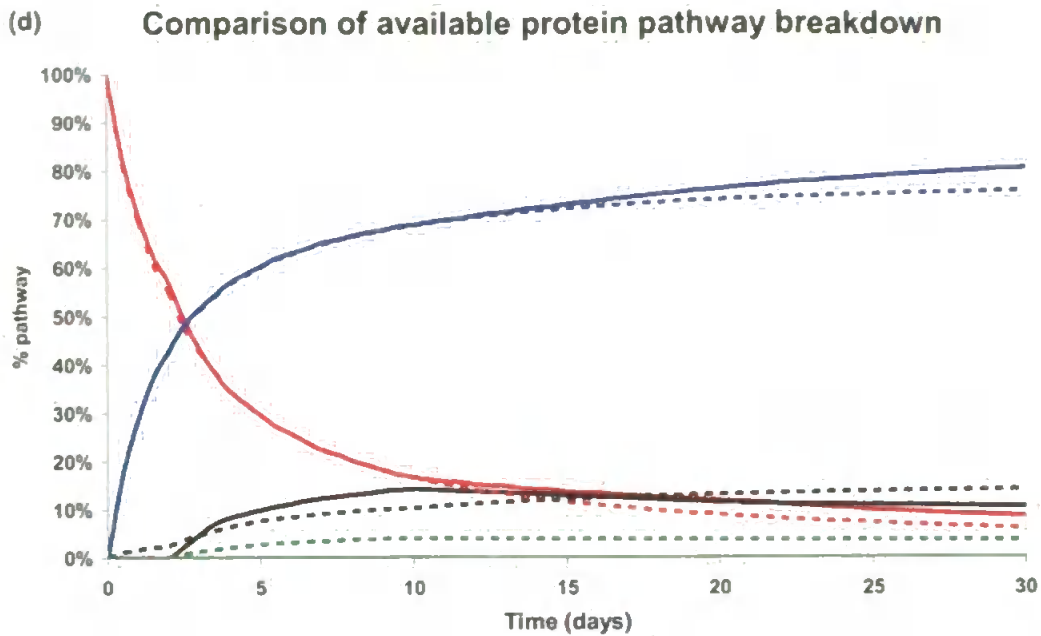


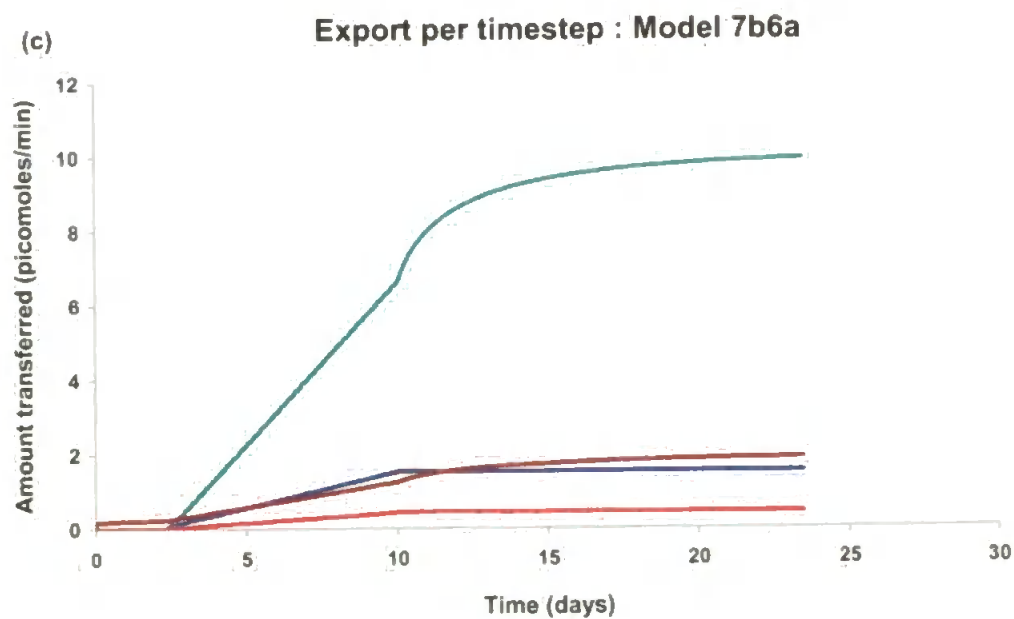
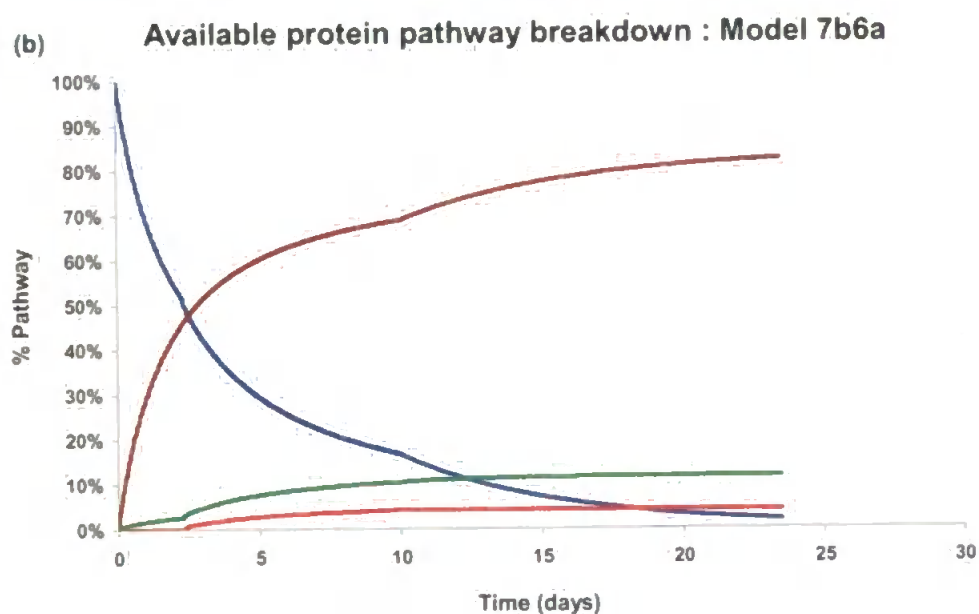
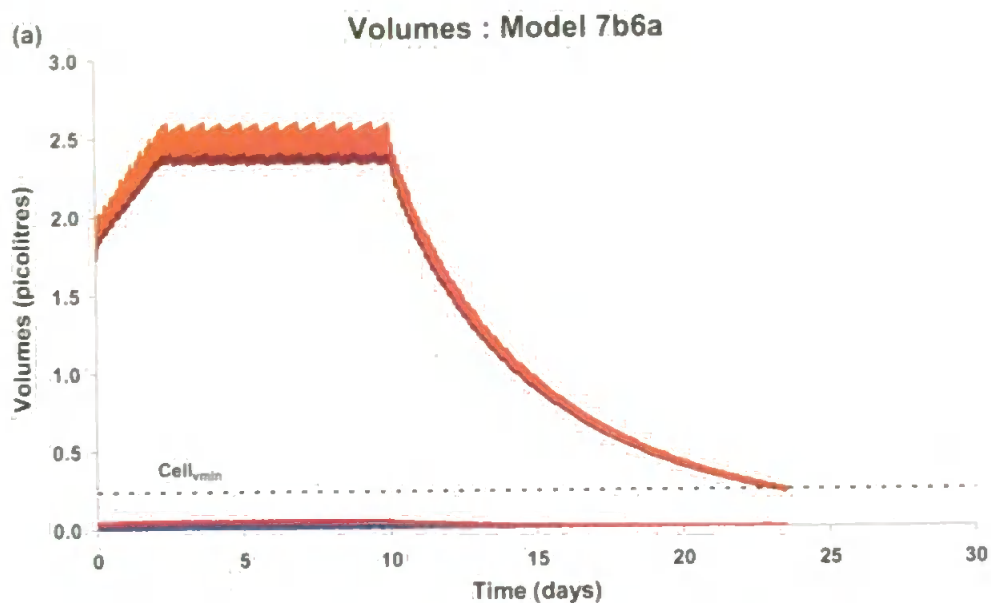
Fig 8.9 All protein diet after day 10, Model 7b6a had a final deamination check (a) cytosolic volumes — glycogen — free sugars — lipid — triacylglyceride — amino acid pool (b) cellular carbon content breakdown — protein — carbohydrate — lipid. Figs(c-d) show comparisons between model 7b6 and 7b6a for cumulative figures of carbohydrate and protein, respectively, into the cell broken down into — stored — exported — lost & — transformed (protein deaminated, carbohydrate stored as lipid). Model 7b6 unbroken line Model 7b6a broken lines.

Only slightly less carbohydrate was transformed into lipid in model 7b6a, but proportionally this was more significant, due to the increased carbohydrate in as a result of the protein deamination (Figs 8.9c & d). Whilst this had the effect of reducing the amount of proteinaceous material exported by two thirds, there was still amino acid export, as well as 2.8 times the amount of carbohydrate export. Therefore, the cell fed on a “protein only” diet can sustain itself, both in terms of energy and protein

synthesis, and still perform its function of providing the rest of the animal with all three forms of storage molecules.

The same model was then tested with a diet which had no nitrogen in it. Fed as normal for the first ten days ( $S_c = 6.0$ ,  $S_n = 1.2$ ,  $lipid\% = 25\%$ ) and thereafter with no nitrogen ( $S_c = 6.0$ ,  $S_n = 0.0$ ,  $lipid\% = 25\%$ ). The lack of nitrogen should lead inevitably to the deterioration of the model, but the rate and manner at which this is achieved will be affected by the rate of autophagy, the efficiency of recycling of proteins and the control algorithm.

With no incoming nitrogen the cell reaches its minimum volume value at day 23.49 (Fig 8.10a). However, there were two issues which warranted further investigation. First, there was deamination occurring after there ceased to be any incoming nitrogen (Fig 8.10b). Second, the endocytotic rate decreased due to the lack of nitrogen (Fig 8.10c), thus allowing neither carbohydrate nor lipid to enter; this partly explained the need to deaminate to provide the energy required.



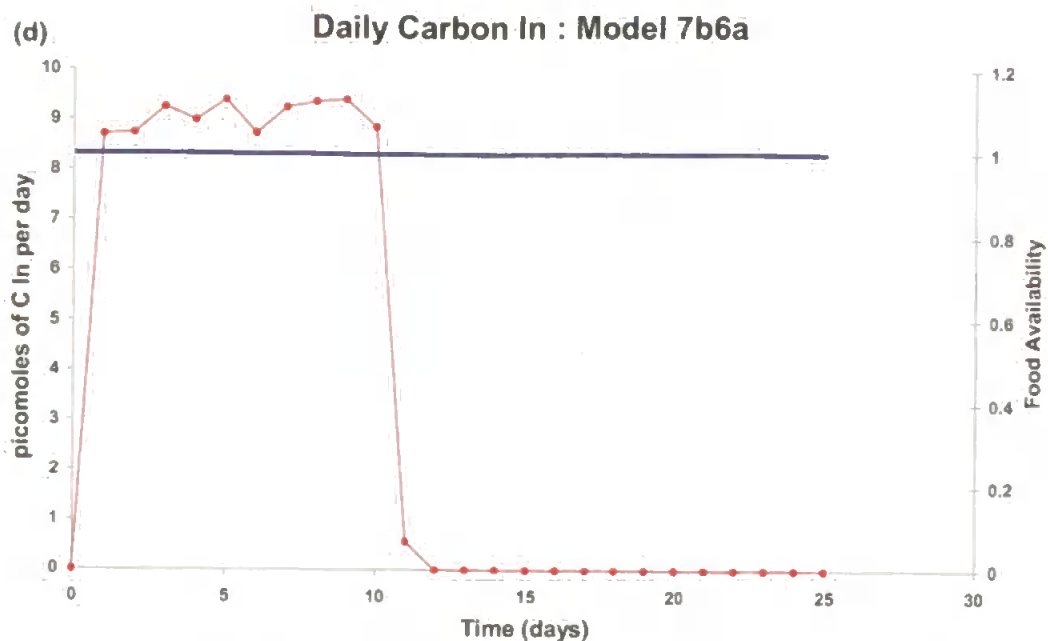


Fig 8.10 Model 7b6a 10 days full food, thereafter no nitrogen in diet. (a) volumes — endosome, — lysosome, — cytosol & — cell (b) protein in fate — stored — exported — lost & — deaminated (c) export — protein carbon — protein nitrogen — carbohydrate — lipid d (d) — FoodAvailability and — carbon in.

Realistically, it would have been more appropriate to still take in energy forms and allow no deamination. Thus the following amendments were made to the previous model to create model 7b6d.

- 1) No deamination if  $S_n < S_{nmain}$
- 2) Endocytosis was only slowed if both of the following conditions are met:

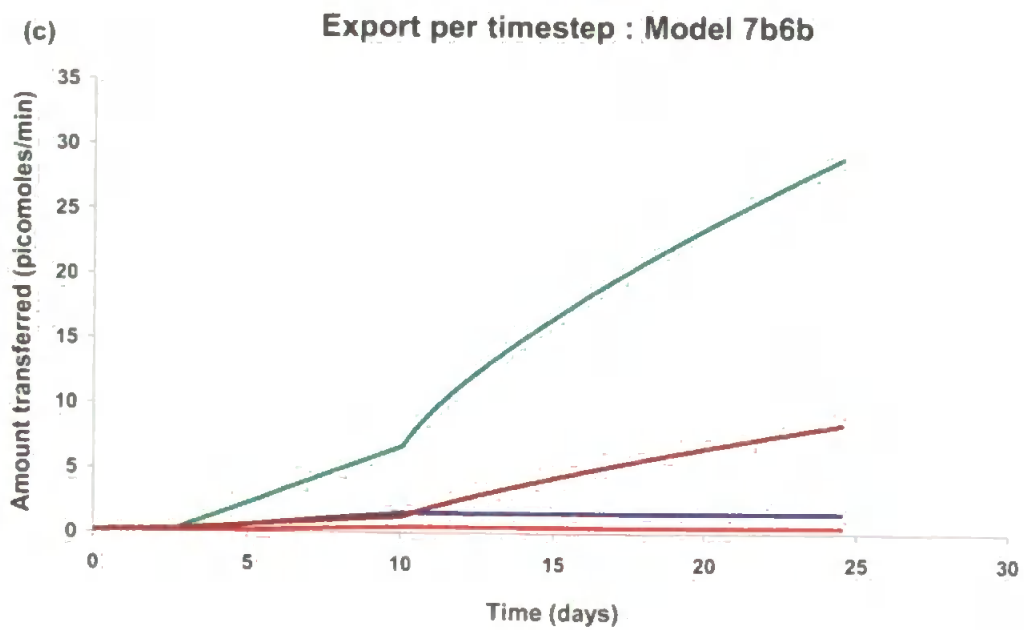
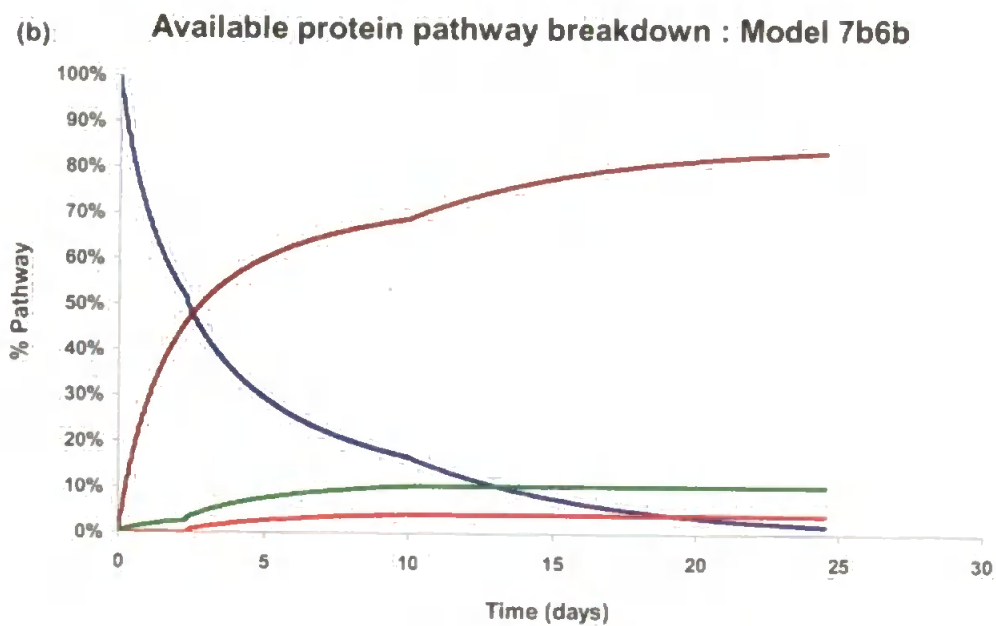
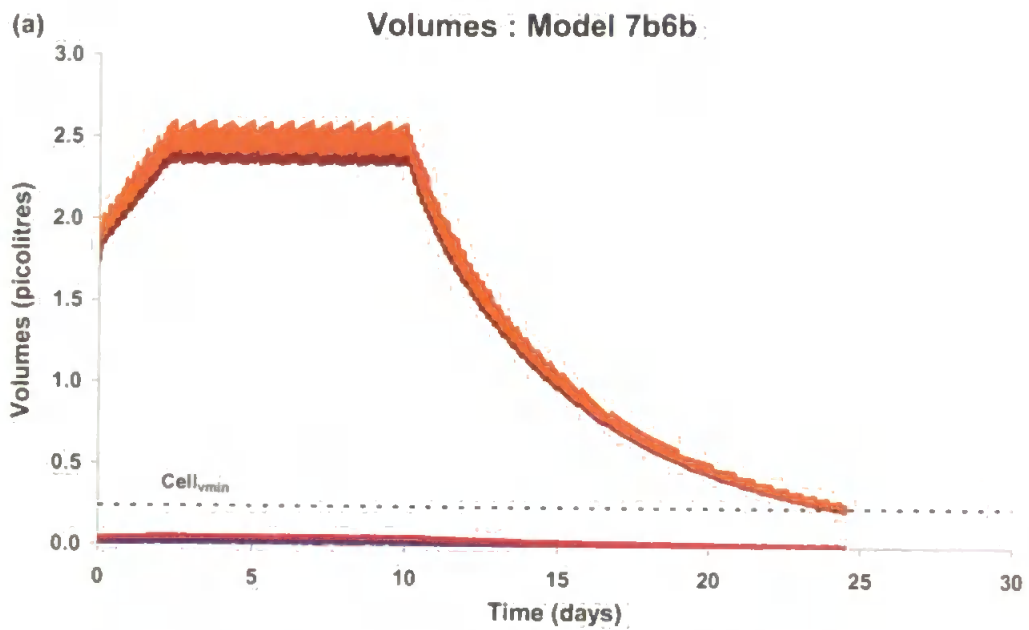
$$S_n < S_{nmain} \text{ \& } S_c < S_{nmain} \times \text{ProteinCN}$$

Model 7b6b increased survival to 14.54 days (Fig 8.11a) an extra day's survival in comparison to model 7b6a. The new endocytotic



condition allowed an increase in the amount of carbon entering the cell (Fig 8.10c & 8.11d).

Although most of this increased uptake simply passes through the cell to the rest of the animal through a threefold overall increase in lipid and carbohydrate export (Fig 8.10c & 8.11c), the time it remains resident in the cell, and specifically the cytosol, increases the cell volume, which in turn increases the rates of autophagy and respiration and thus appears to accelerate the cells decline. The heightened endurance is thus due to the lack of deamination (Fig 8.11b) once the diet lacks nitrogen.



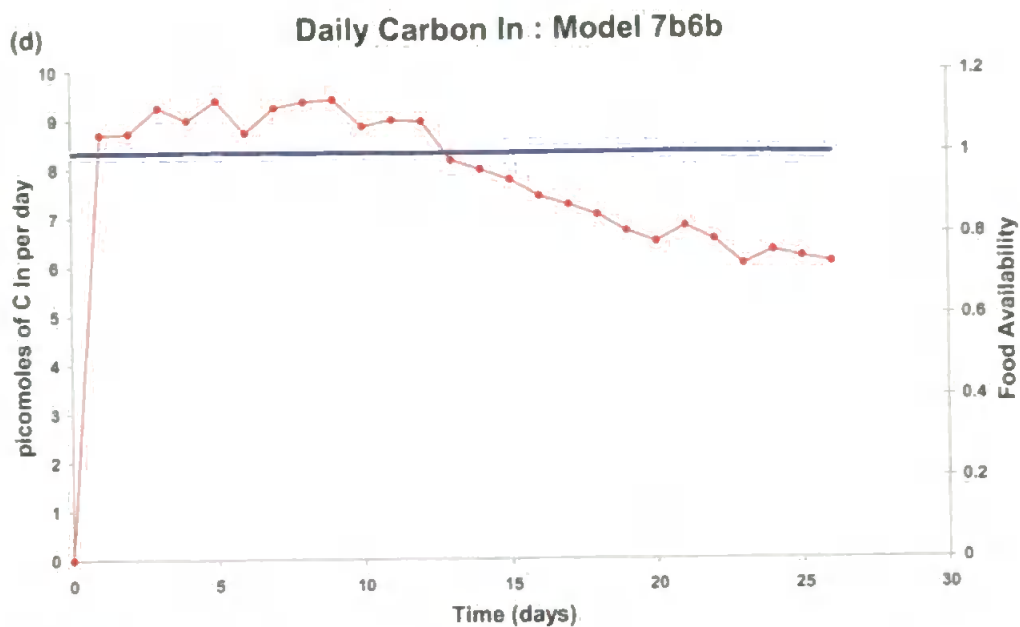
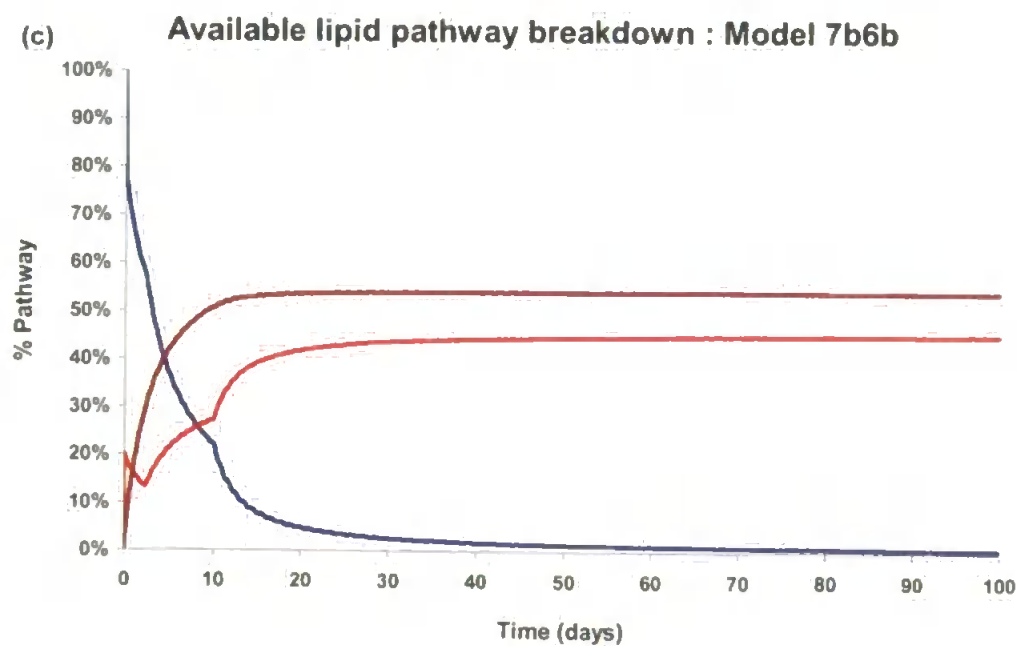
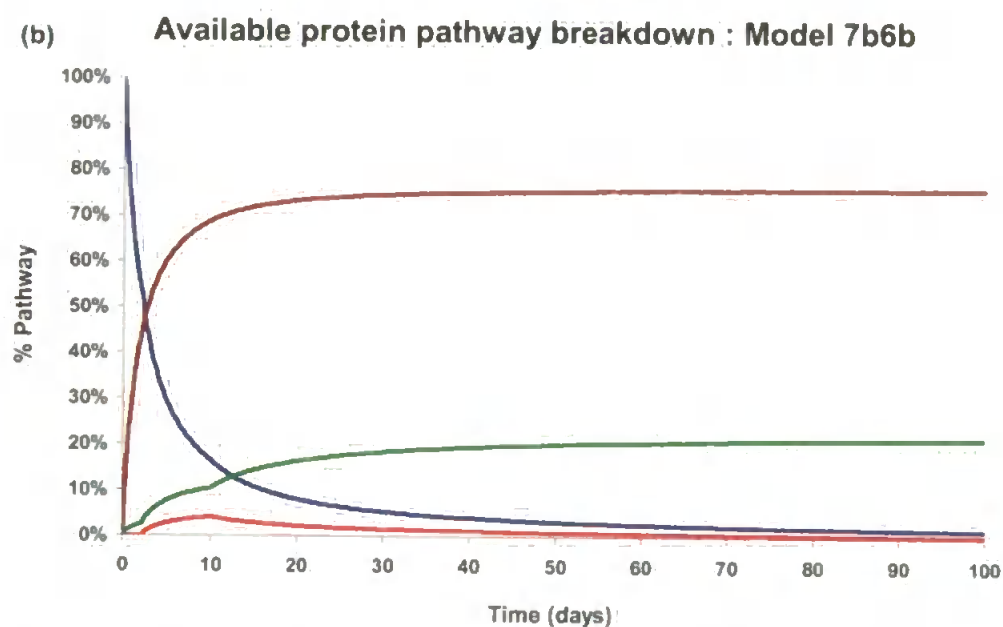
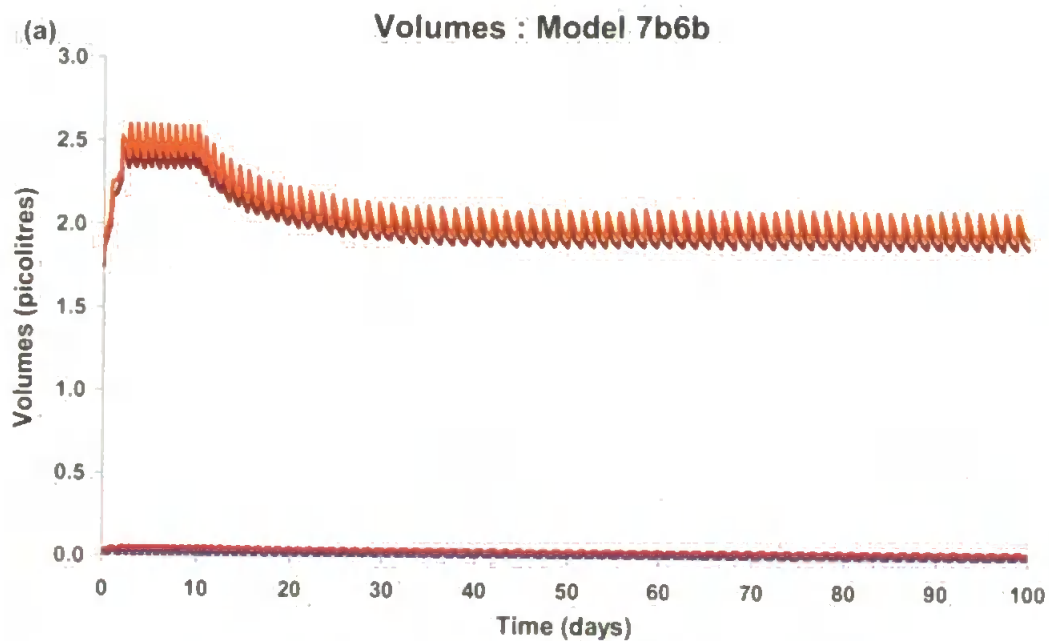


Fig 8.11 Model 7b6b 10 days full food, thereafter no nitrogen in diet. (a) volumes — endosome, — lysosome, — cytosol & — cell (b) protein in fate — stored — exported — lost & — deaminated (c) export — protein carbon — protein nitrogen — carbohydrate — lipid (d) — FoodAvailability and — carbon in.

The next food regime to be tested was for no carbohydrate but adequate lipid within the diet (after day 10:  $S_c = 6.0$ ,  $S_n = 1.2$ ,  $lipid\% = 100\%$ ). This was designed to test whether with sufficient food entering in energy form, the obligation to deaminate would be low and the lipid would carry the majority of the burden of energy requirement.



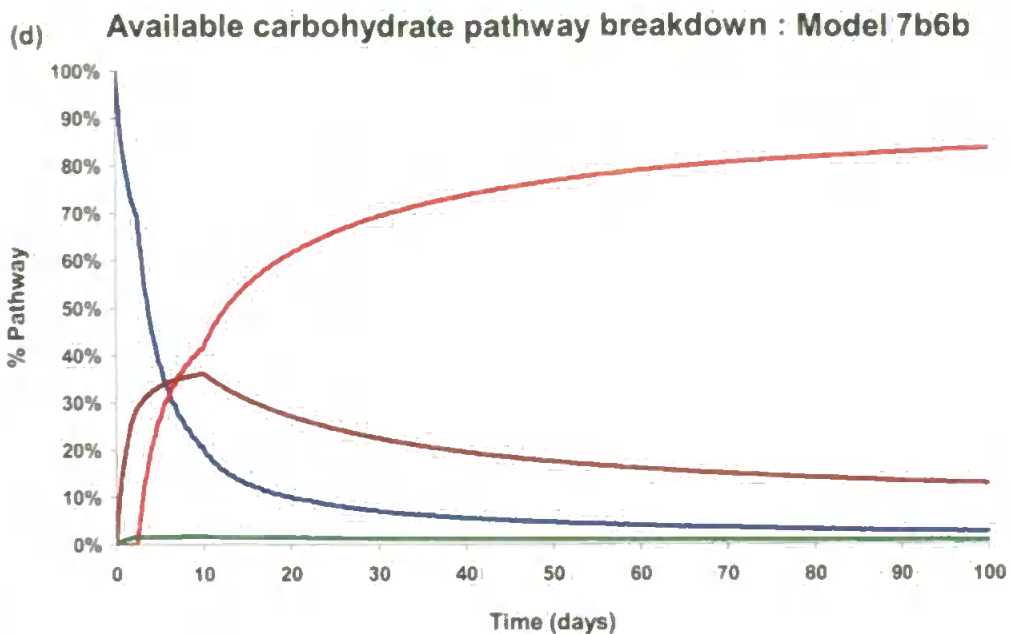


Fig 8.12 100 day simulation of Model 7b6b 10 days full food, thereafter maximum nitrogen and carbon but no carbohydrate in diet. (a) volumes — endosome, — lysosome, — cytosol & — cell (figs c-d) — stored — exported — lost & — transformed (b) protein (c) lipid (d) carbohydrate.

Once the carbohydrate was removed from the diet, the lipid entering increased, as the amount of carbon entering the cell remained constant. The cell volume initially dropped but then reached a fairly high stable level after 20 days (Fig 8.12a). From the start of the diet change, no amino acids were exported as the rate of deamination increased (Fig 8.12b), whilst the lipid and carbohydrate rates of export increased at the same time (Figs 8.12c & d). The control algorithm still provoked storage of carbohydrate as lipid, which seemed incorrect given the imposed dietary constraint. If the rest of the animal could transform long-term lipid storage back to carbohydrate, then it would require only lipid and amino acid export from the digestive cell.

8.5 Lipid to carbohydrate: Model 7c

Hence the next model sought to include the ability for the cell to transfer lipid to carbohydrate. As this was the final version of the model the schematic is presented below in Figure 8.13.

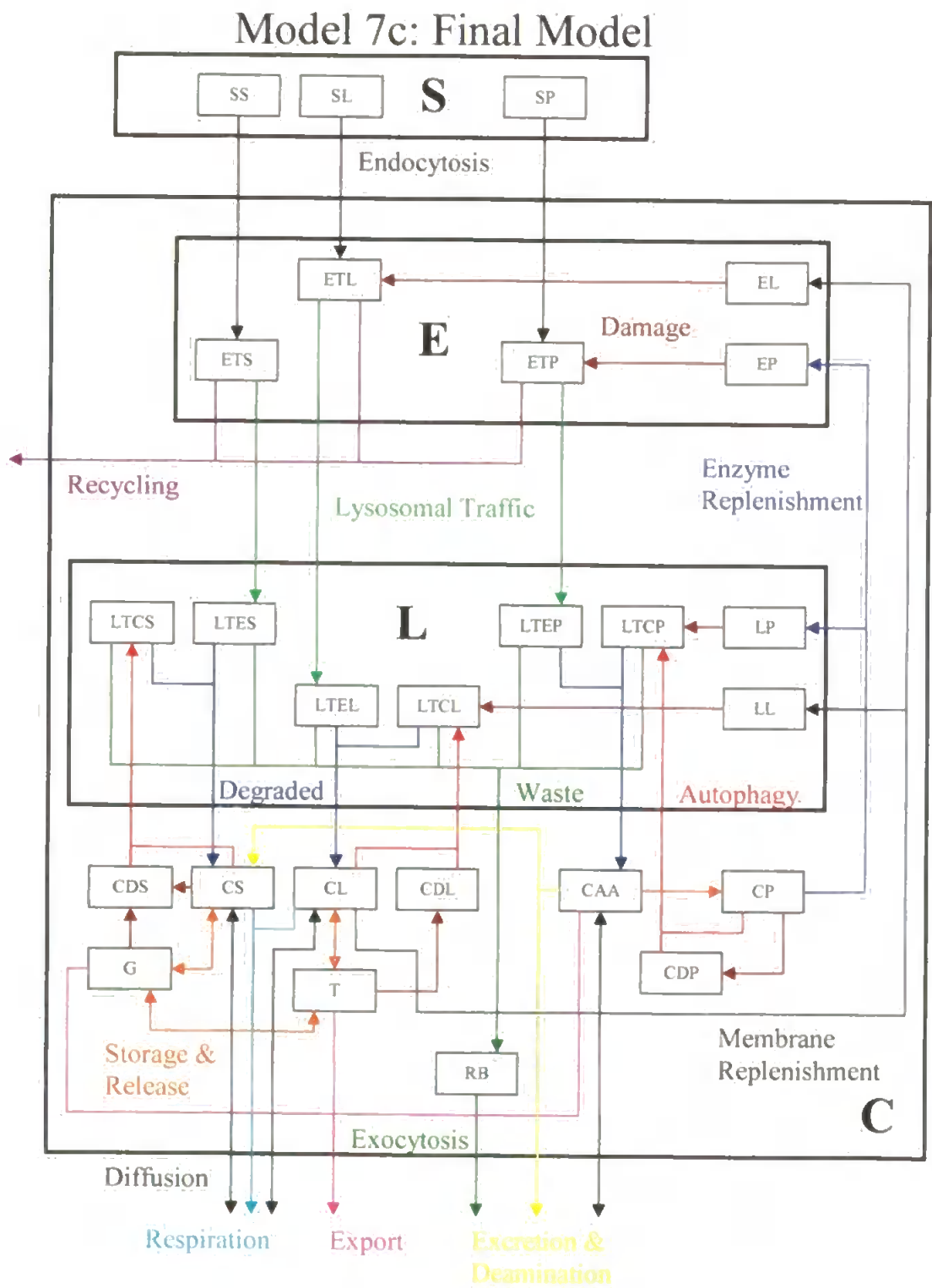
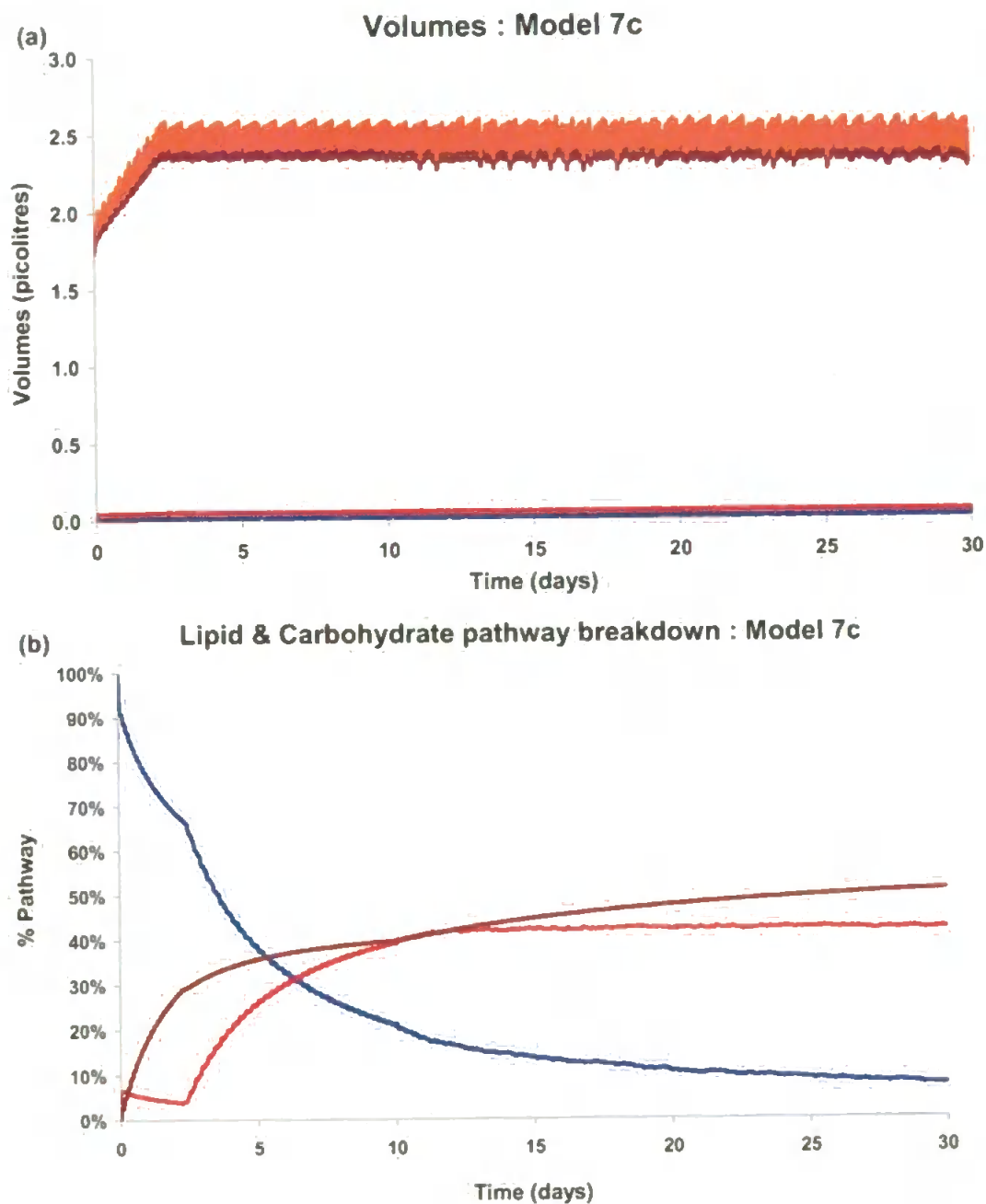


Figure 8.13 Schematic of model 7c

This model allowed the transformation rate from carbohydrate to lipid to be negative to simulate release of lipid stores back to free sugars. The control algorithm was then amended to produce the final Model 7c.



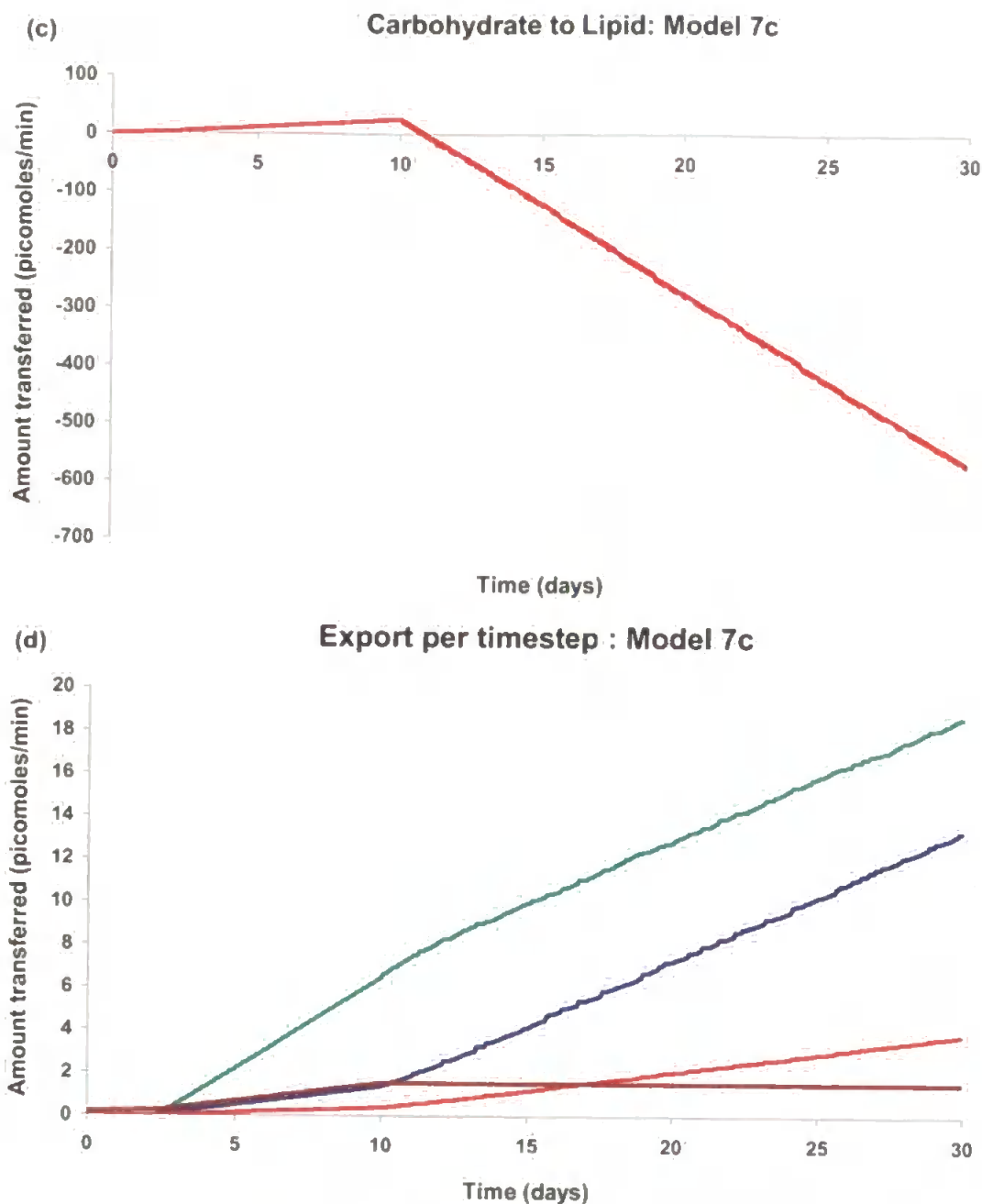
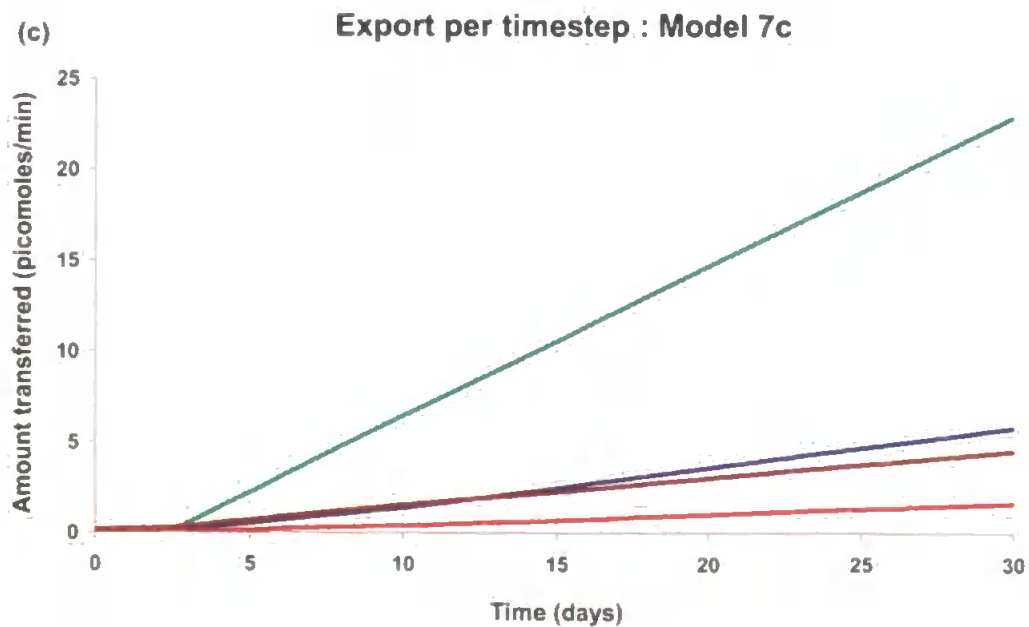
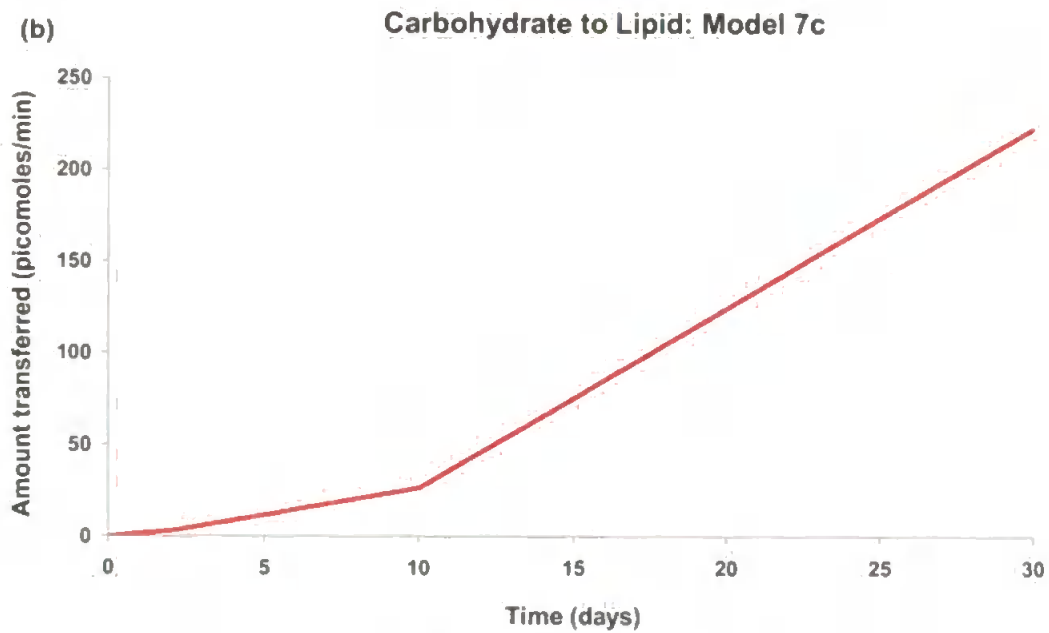
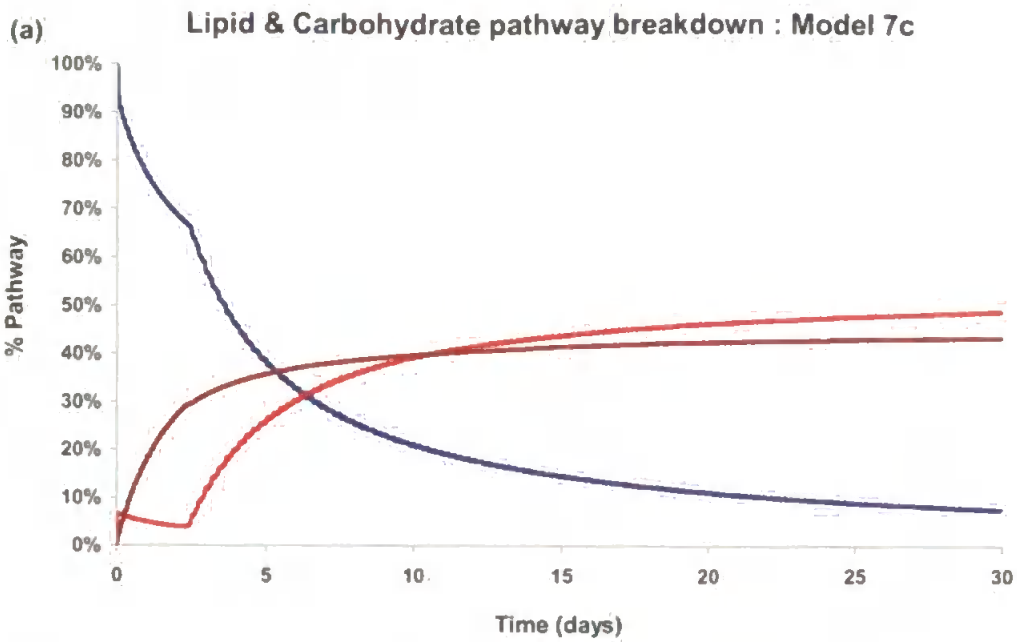


Fig 8.14 30 day simulation of Model 7b6c 10 days full food, thereafter maximum nitrogen and carbon but no carbohydrate in diet. (a) volumes — endosome, — lysosome, — cytosol & — cell (b) combined lipid and carbohydrate — stored — exported — lost & — transformed (c) — carbohydrate to lipid rate (d) export — protein carbon — protein nitrogen — carbohydrate — lipid.



With the conversion of lipid back to sugar introduced to the model cell the system once again survived with a “no carbohydrate” diet (Fig 8.14a) but the relative behaviour of the separate storage forms was quite different. From day 10 onwards, the lack of carbohydrate in the diet forced the cell to convert incoming lipid into sugar (Fig 8.14c) and this precluded any need for the cell to deaminate amino acids to provide the free sugars. This enabled the cell to accelerate the rate of amino acid export, continue carbohydrate export and stop lipid export (Fig 8.14d). The overall breakdown of total carbohydrate and lipid behaviour reveals the export stabilising at around 42% of total carbohydrate and lipid made available to the cell (Fig 8.14b).

Finally, model 7c was tested with no lipid in the food after 10 days (after day 10:  $S_c = 6.0$ ,  $S_n = 1.2$ ,  $lipid\% = 0\%$ ). There was no loss of cell volume after day 10. The carbohydrate to lipid rate was invoked once the lipid was lost from the diet, and attained a level approximately three times as seen in previous models (Fig 8.15b). This created very little change to the rates of export (Fig 8.15c), due to the homeostasis in carbon content distribution (Fig 8.15d) afforded by the control algorithm. There was lipid export, which may seem perverse given the diet, but overall the total carbohydrate and lipid behaviour was tending towards 50% of total available non-protein carbon being exported (Fig 8.15a).



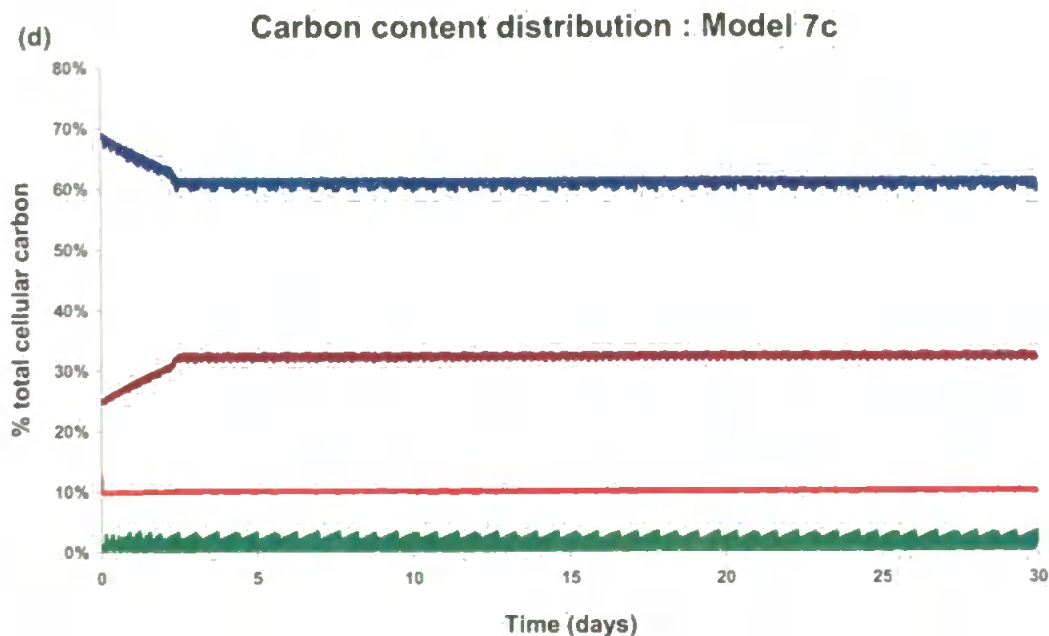


Fig 8.15 30 day simulation of Model 7b6c 10 days full food, thereafter maximum nitrogen and carbon but no lipid in diet. (a) Combined lipid and carbohydrate — stored — exported — lost & — transformed (b) — carbohydrate to lipid rate (c) Export — protein carbon — protein nitrogen — carbohydrate — lipid (d) Carbon content distribution — protein, — lipid, — carbohydrate & — residual body.

Thought was given to re-conducting the annual simulations with the new control algorithm with the final model. However, there was a lack of the relevant seasonal data on the food quality that would be necessary for any impact to be made on the cell results. Therefore, this final model was subject to a sensitivity analysis instead to determine those combination of parameters under which it would survive.

## 8.6 Sensitivity analysis

A test of the previous model cells survivability was conducted, taking into account the combined effects of variable dietary availability and quality. The survival space of the mussel cell was determined: when subject to food availability ranging from complete starvation to maximal amounts; and from food quality which was designed to range from no protein to total protein (the lipid/carbohydrate split of the remainder of food was kept constant throughout).

The results for varying the nitrogen content and food availability are shown in Figure 8.16.

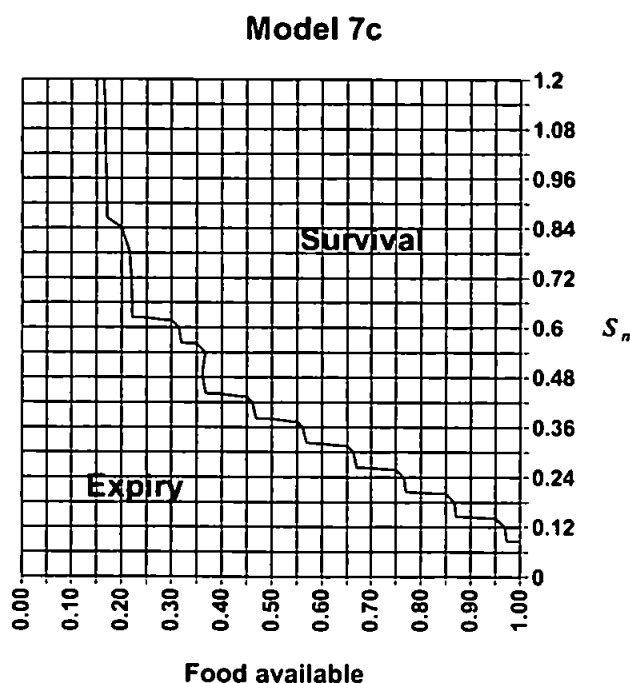


*Fig 8.16 Sensitivity analysis for food availability and protein content of food.  $S_c = 6.0$ , Lipid% = 25%*

As expected with small food amounts available the cell eventually expired. Also, with absolutely no available protein, the cell eventually ran out of the necessary metabolites for healthy function. The cell was seen to survive on a relatively small amount of “protein only” food, converting the amino acids for energy. The simulation suggested that for a large majority of the parameter space the cell falls into a quasi-steady state, approximately returning to the same cell volume after each feeding cycle. A study of the date of expiry from a initially well fed cell was also conducted. It was found that a threshold just above 50 days was reached. If the cell had survived this date then it would survive indefinitely (Fig 8.17).

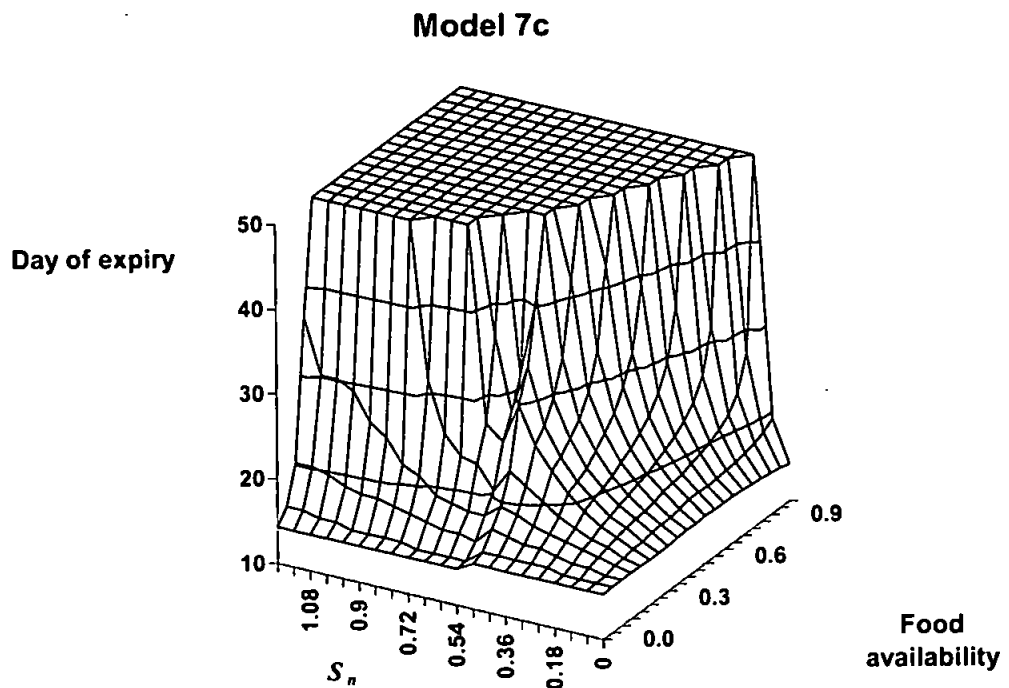
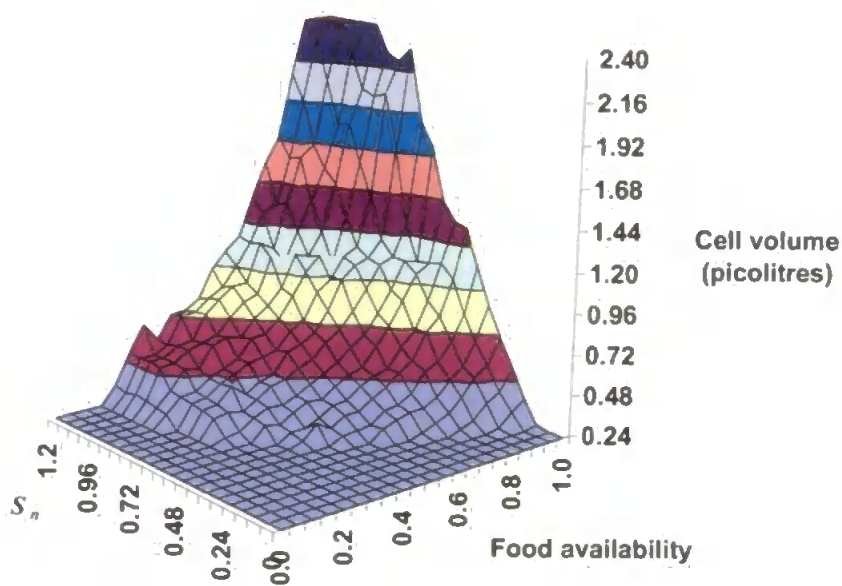


*Fig 8.17 Model 7c showing date of expiry of cell over food availability and nitrogen concentration space, details as for Fig 8.1. Plane at day of expiry = 50 indicates survival.*

The maximum cell volume did not coincide with the maximum rate of carbon export from the cell (Figs 8.18a &b). With low protein content the cell was forced to export a lot of carbohydrate and lipid in order to retain the designated balance of storage molecules. Thus growth was seen to depend upon both the amount of food available and its composition.

(a)

Model 7c



(b)

Cumulative carbon export : Model 7c

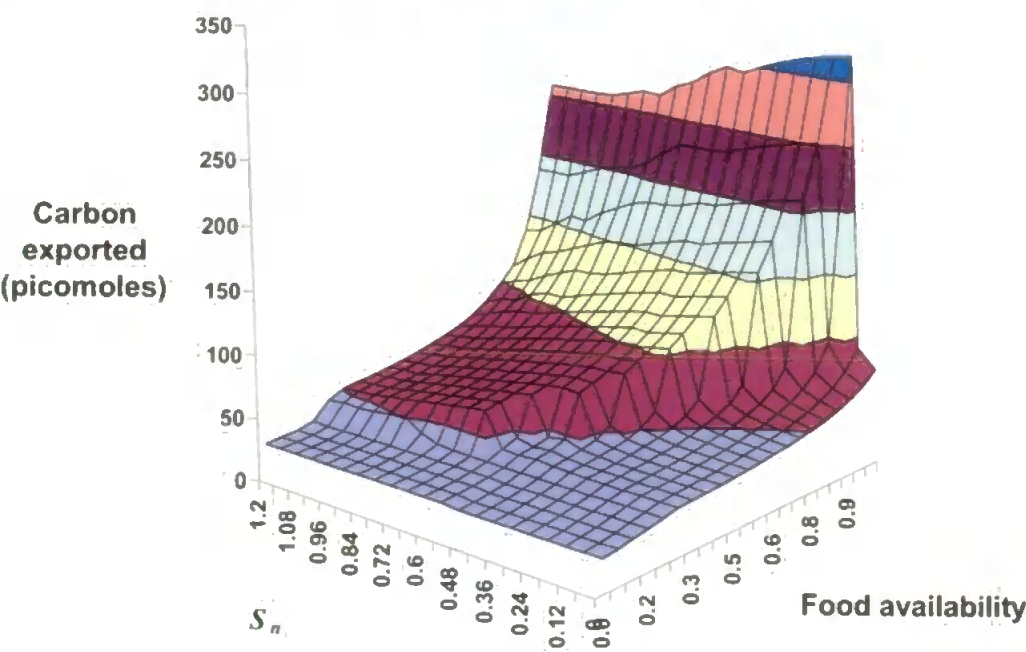


*Fig 8.18 Model 7c sensitivity analysis. Simulation details as for fig 8.16 (a) Cell Volume & (b) Carbon export from cell.*

In conclusion, model 7c was seen to be relatively robust and possessed a suitable adaptability with regard to food received. The overall annual results could not be improved upon, but the significance of the demand from the rest of the animal was indeterminable and considered to be a significant factor.

## 8.7 Discussion

The lipid metabolism of the cell was reviewed, due to the inferior performance of the model in predicting lipid levels over the annual cycle. The observed data of Thompson *et al.* (1974) suggested a constant level of lipid over the year. However, variation in lipid content was seen to occur in other studies (Gabbott & Bayne, 1973). Due to the various roles that lipid can play in cellular metabolism this discrepancy may have been due to the widely varying environmental conditions each mussel colony was subject to at different geographic locations.

The principle assumptions made in this model were that the lipid level was constant and that it was principally a long term energy store. Hence conversion pathways from sugar to lipid and back again were introduced. It was not necessary for the model to understand why there needs to be both a short term and long term storage format (glycogen and lipid) as the relative proportions of each was controlled by a seasonal control signal.

Hypothesis 8.1 was, however, seen to fail. Adjusting the lipid had an effect on the overall dry weight, and, more strikingly on the carbohydrate dry weight. The reasons for this failure are linked to the control algorithm. The model has been designed to allow transfer of material between all three macromolecular forms to generate greater flexibility. The hub of these transfers was the carbohydrate compartments; hence the greater impact on



the results of this form. This failure, however, provoked greater consideration of how to adapt the model to varying available diet.

Adaptation to varying food quality and quantity was implemented in changes to the control algorithm. By the end of its evolution, this algorithm had become quite Byzantine and the ramifications of modifications became quite unpredictable. Of particular concern was that the order of the checks and operations, involved in the control algorithm, were becoming increasingly important in deciding the model behaviour. Consideration was given to implementing a fuzzy logic control system instead, whereby a number of 'probability' rules would be tested simultaneously and the system would head towards an optimal solution over the next timestep. Refinements at each timestep would enable a flexible approach to the changing internal and external environments. However, this attempt was abandoned due to the prohibitive nature of the number of rules that would have to be devised.

As an isolated cell, the model suffered from a lack of context, which required that the control algorithm be solely based on the internal environment. Equally, there was latterly identified a possible source of contention with the internal lysosomal state. If the lysosome were primed with a plentiful supply of material to degrade then should this be considered within the control algorithm as a future source of material? In a relatively inactive cell this would prove less critical as a stable state might be reached; however, in these particular cells, with their intermittent

feeding activity, this state would probably never be attained. Hence a time-averaged state of the lysosome might be considered to further influence the control algorithm. Unfortunately, this lack of 'memory' afflicts the cell model on other levels. A history of the export of material would possibly benefit the control algorithm to identify the optimal strategy to employ for survivability and utility for the rest of the animal.

At this late stage, however, the model was considered relatively robust enough to incorporate the toxicity element of the study for which it had been originally devised.

## Chapter 9 Toxicity Models

### *9.1 Introduction, Objectives & Hypotheses*

The effect of exposure of the model cell to toxicants was finally explored. The rationale behind the models developed was that the previous model could be given dysfunctions to simulate the observed effects of toxic exposure. Equally the recovery from toxic stress was explored in an attempt to match observation. In particular a single experiment was chosen showing the effect of dietary restriction on the recovery of a cell exposed to a toxicant. The unusual protection afforded by one stressor to the response to another was explored (Table 9.1 gives a list of simulations performed).

*Hypothesis 9.1:* Dietary restriction (DR) in the cell prior to exposure to a-toxicant enhances the lysosomal system, such that impact of subsequent exposure is lessened and recovery may occur at a faster rate than in cells only exposed to the toxicant.

In order to test this main hypothesis it was necessary to consider the uptake, movement within the cell, possible transformation, and expulsion of the toxicant. Simultaneously the effect of toxicants within the cellular compartments had to be simulated. Equally, the cellular defence mechanisms to toxic insult were considered.

*Hypothesis 9.2:* Effects of toxic exposure can be adequately simulated by increasing the basal damage rates by a factor determined by internal toxicant concentrations.

Test	Model ID	Fed/Unfed	Brief description of experimental goals
1	8a1	Fed	Decreased lysosomal throughput & enhanced autophagy.
2	8a2	Unfed	Exposure: Double autophagy, lysosomal throughput halved. Recovery: Double autophagy, lysosomal throughput increasing to 0.7 of normal calculated rate.
3	8a2a	Unfed	“Drip feed” from rest of animal to ensure survival.
4	8b1	Fed	Contaminant flow modelled: diffusion based on surface concentration, autophagic uptake of contaminant; restricted flow from lysosome to residual bodies. Boost to cytosolic autophagic rate and lysosomal damage, decrease in lysosomal throughput based on contaminant concentration.
5	8b2	Fed	Lysosomal throughput not decreased (extra damage only) & feeding phase maximum length of 30mins
6	8c1	Fed	Contaminant induced cytosolic damage reduced and capped.
7	8c	Fed	Sensitivity analysis of rate of removal of contaminant from cytosol.
8	8c2	Fed	Sensitivity analysis of contaminant boost to cytosolic damage and rate of removal from cytosol.
9	8d1	Fed	Contaminant diffusion allowed to go greater than surface concentration.
10	8d2/a	Fed/Unfed	Surface concentration dependent upon lumen volume.
12	8d2b/c	Unfed/Fed	As above with “drip feed”.
14	8d2d/e	Fed/Unfed	Contaminant cytosolic damage boost and residency time doubled.
16	8e/1	Fed/Unfed	Lysosomal damage increased.
18	8e2	Fed	Lysosomal residency time increased.
19	8e3	Fed	Sensitivity analysis of lysosomal stability of various lysosomal damage levels and residency times.
20	8f	Fed	Cellular contaminant defence added.
21	8f1/2	Fed	Contaminant defence only when above a certain threshold & with reduced upregulation capability.
23	8g	Fed	Sensitivity analysis of bio-transformation of contaminant.
24	8h1	Fed	Lipofuscin generation and accumulation.

*Table 9.1 Experimental tests run for toxicity model.*

## 9.2 Experimental Paradigm

The effect of exposure to a toxicant can be explored in the model cell. The simulation which shall become the standard for the development of the toxicity model is based upon the following experimental treatments (Moore, 2004). These involved 3 days exposure to a contaminant followed by a 12 day recovery period over the course of which different treatment groups of mussels were either fed or not. (Nutritional deprivation (diet restriction) is, perhaps seemingly perversely, shown to have a salutary effect on recovery of lysosomal stability following exposure to toxic chemicals (Moore, 2004).

Nutritional deprivation or dietary restriction (DR) confers protection against ageing and oxidative stress in many animals and induced lysosomal autophagy is part of this mechanism (Aksenova *et al.*, 1998; Cavallini *et al.*, 2001; Ramaiah *et al.*, 2000). The effects of dietary restriction on the toxicity of copper and the polycyclic aromatic hydrocarbon phenanthrene have previously been investigated in the common marine mussel *Mytilus edulis* (Moore, 2004). DR-induced autophagy facilitates the recovery of the digestive gland (i.e., molluscan liver analogue) from cell injury caused by both copper and phenanthrene (Fig 9.1). The concentrations of copper and phenanthrene in the digestive gland tissues were essentially the same in both treatments after 3 days with and without food. A similar experiment for fed mussels only (Moore *et al.*, 1984), with exposure to copper or

phenanthrene showed that there was no significant decline in either phenanthrene or copper concentration during the recovery period.

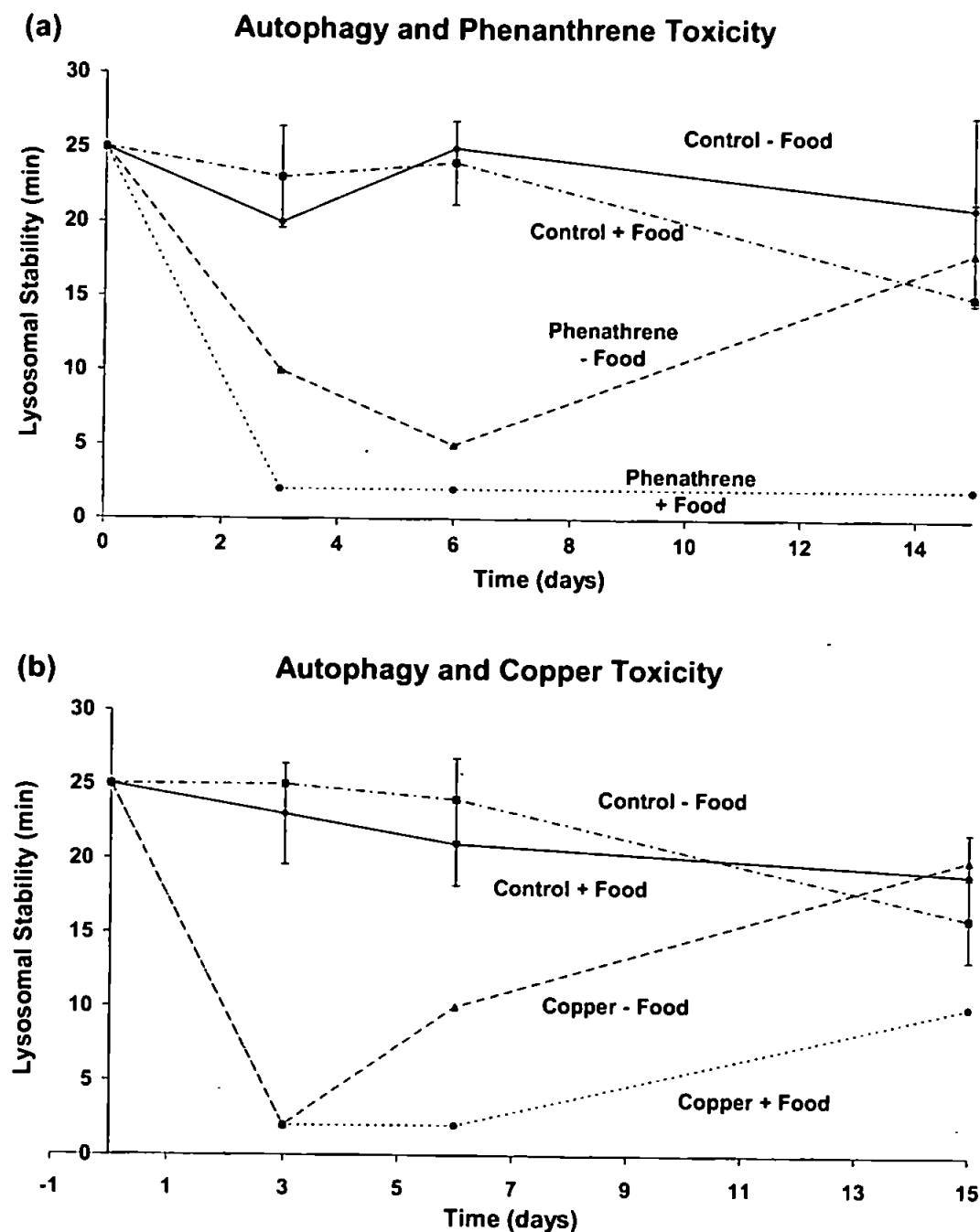


Fig 9.1 Lysosomal stability of the treatments fed/unfed exposed to (a) Phenanthrene & (b) Copper.

It was concluded that DR induced autophagy and lysosomal proteolysis results in improved cellular “housekeeping” through the more efficient removal of oxidatively and pollutant damaged proteins (e.g., protein carbonyls, protein adducts, etc.) and that this probably contributed to stress resistance (Cavallini *et al.*, 2001).

### *9.3 Theoretical model: Model 8a*

The initial assumption for the phenomenon exhibited in the experiment was that the recovery of the cell with diet restriction was a consequence of both initial increased autophagy (provoked by diet restriction) and spare lysosomal capacity within these cells (due to lack of food to process). Model 8a was a simple model based on these two assumptions.

Model 8a1 attempted to simulate response of the fed cell by subjecting it to a sustained constant decrease (0.4 of calculated level) in lysosomal throughput to reflect the accretion of contaminant, thus preventing correct functioning. Additionally, autophagy was enhanced to represent cytosolic damage done by the initial accumulation and then continued contaminant presence within this compartment. This took the form of an initial linear increase of the rate over the three days of exposure and thereafter remaining at double the otherwise calculated level.

Model 8a1 showed that despite the immediate decline in lysosomal throughput, it was still able to cope with both autophagocytosed material and the food entering via the endosome (Fig 9.2a). However, as the autophagic rate increased there was not enough capacity to deal with both sets of material which caused the lysosome to swell in size. A low in lysosomal stability occurred around one and a half days after exposure had ceased (Fig 9.2b). Cell volume dropped from maximum due to the



increased autophagy and reached a minimum at the same point, but was subsequently increased as the overall amount of autophagocytosed material fell due to the smaller size of the cytosol. A relatively stable situation was achieved 17 days after the start of the exposure with a lysosomal stability oscillating minutely around 6.61 mins.

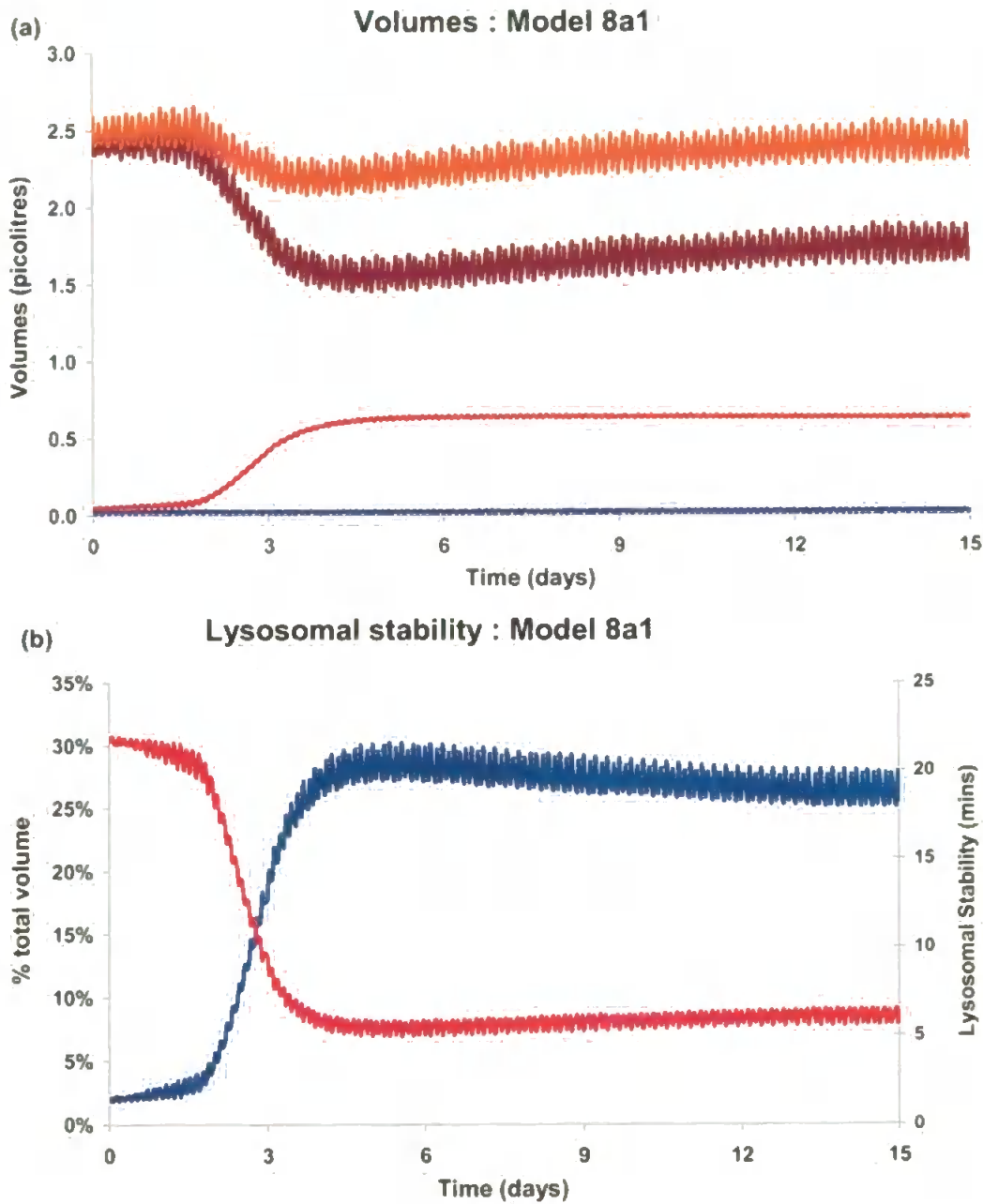


*Fig 9.2 Model 8a1 3 day contaminant exposure simulation. (a) Volumes — endosome, — lysosome, — cytosol & — cell (b) — lysosomal relative volume — lysosomal stability.*

Model 8a2 replicated the unfed exposure by doubling the autophagic rate throughout the time course of the experiment. During the period of exposure the lysosomal throughput was halved; to simulate the recovery, under the presumption of less lysosomal activity and, hence, capacity to deal with the sequestered contaminant, the lysosomal throughput was increased thereafter linearly to 0.7 of its normal value by the end of the simulation.

With no food entering the cell and the increased autophagy due to the contaminant exposure, the cell relentlessly declined to below its minimum value (Fig 9.3a) ten and a half days from the start of the exposure. The lysosomal relative volumes increased more rapidly (Fig 9.3b), due to the immediate autophagic boost and lysosomal throughput decrease, than the previous model (Fig 9.2b) and reached a minimum lysosomal stability value of 4.3 minutes at day 3.075. However, the recovery of lysosomal throughput after day 3 was reflected in the decrease in lysosomal relative volume thereafter, as the lysosome can deal with the extra autophagocytosed material as there was no food to process as well.

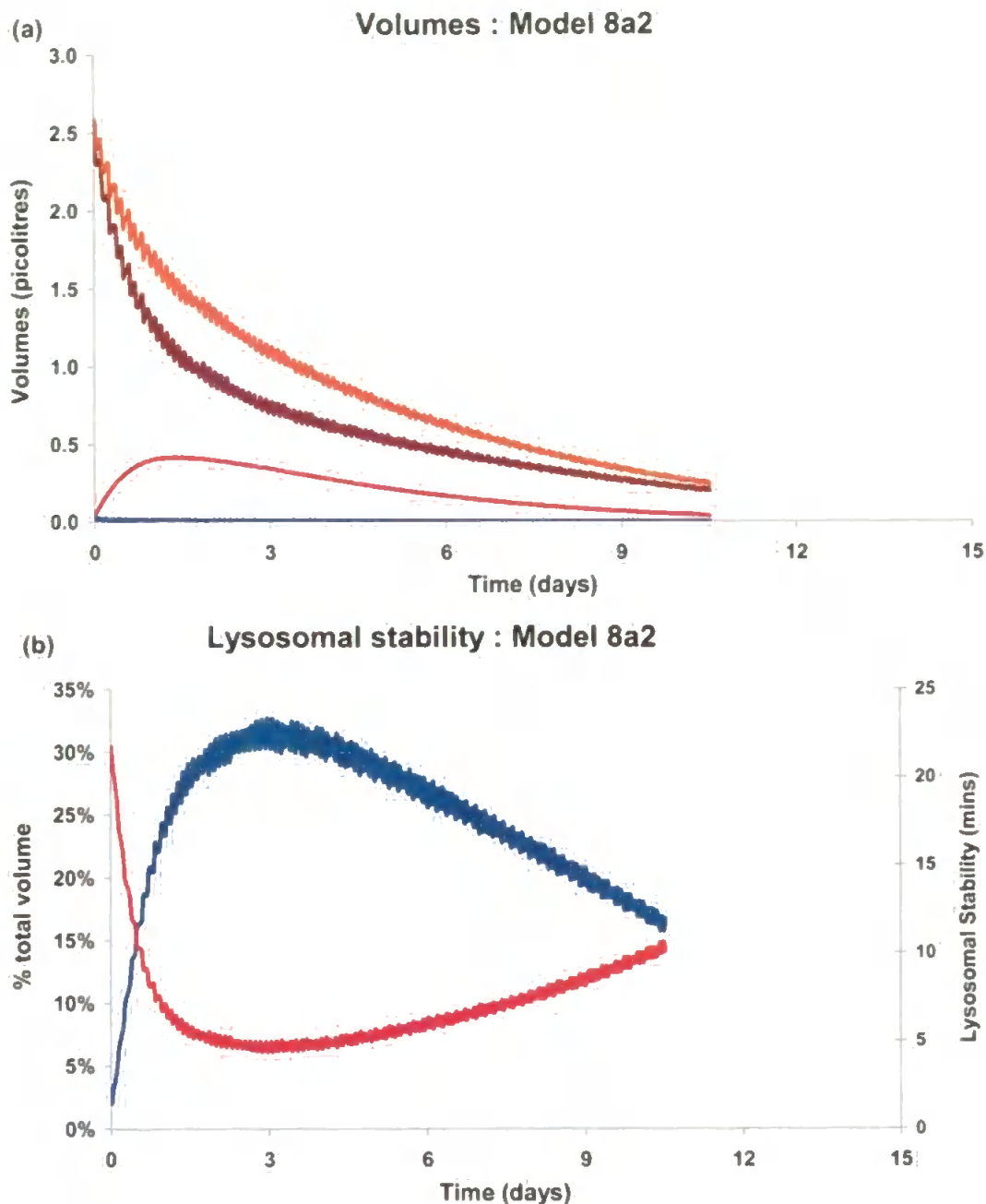


*Fig 9.3 Model 8a2 3 day contaminant exposure 12 day recovery simulation, but unfed throughout. (a) Volumes — endosome, — lysosome, — cytosol & — cell (b) — lysosomal relative volume — lysosomal stability.*

As the unfed cells were still evident at the end of the experiment for measurements to be taken, either the rate of decrease in volume was incorrect or else there was some other source of food entering the cell. The primary factor in cell volume loss was the rate of autophagy, which as a

necessary component of the theoretical toxic model was left alone. Hence, a nominal 'drip feed' from the rest of the animal or other 'sacrificial' digestive gland cells was proposed to ensure the cell survives once the minimum cell volume was attained (Model 8a2a).

With a drip feed of amino acids back into the cytosol of the cell, Model 8a2a was seen to last the experimental distance (Fig 9.4a). Moreover, the recovery of lysosomal stability continued unabated from the previous model and eventually reached a value of ~15 minutes which was not too far from the 18minute experiment values. Aside from this fix needed to keep the cell alive, the main problem with the model results is that the experimentally unfed and exposed cell decreased its lysosomal stability at a lower rate than observed and reached a minimum around day 6 not day 3.

Regardless of these misgivings, with this partial validation of the premises of the theoretical toxic model, the aim thereafter was to make the model behaviour dependent upon exposure and nutritional profiles, which will determine the uptake and internal contaminant dynamics.

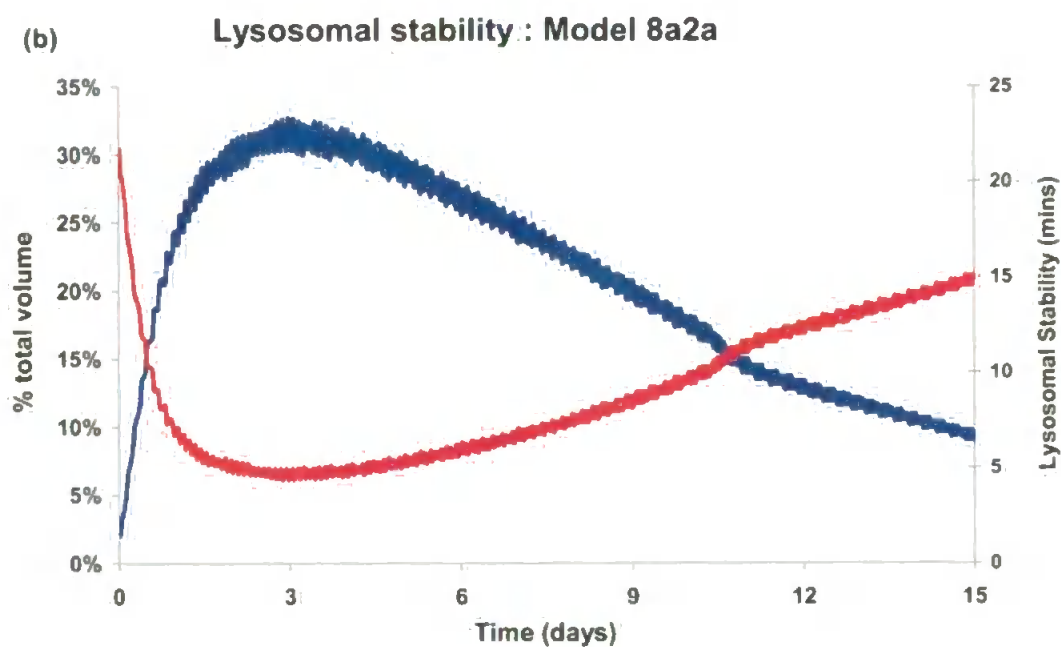
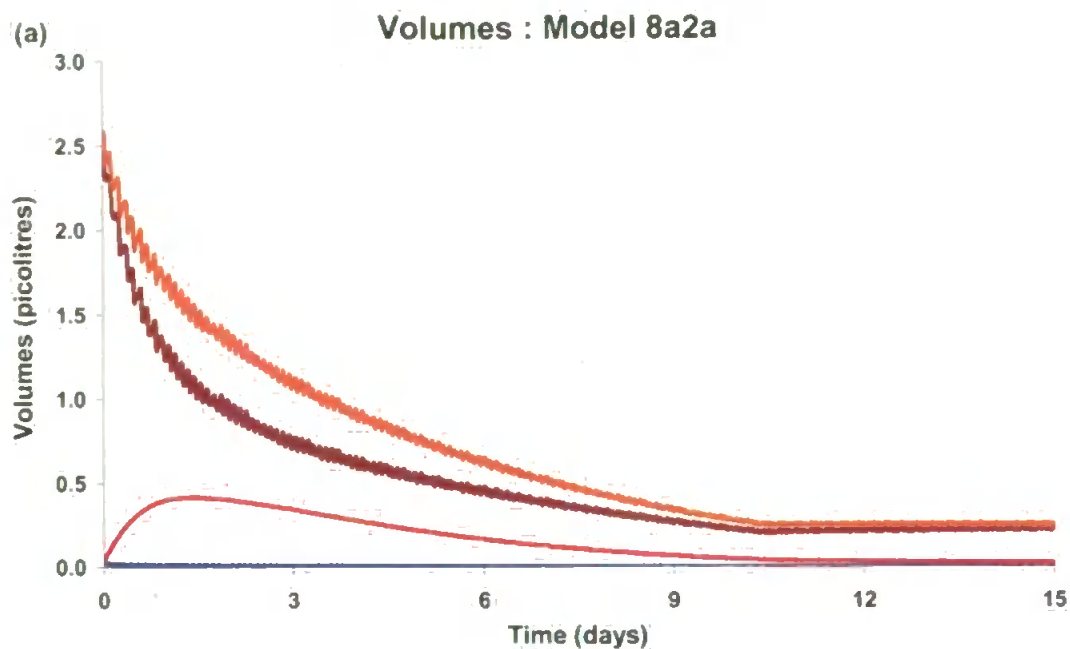
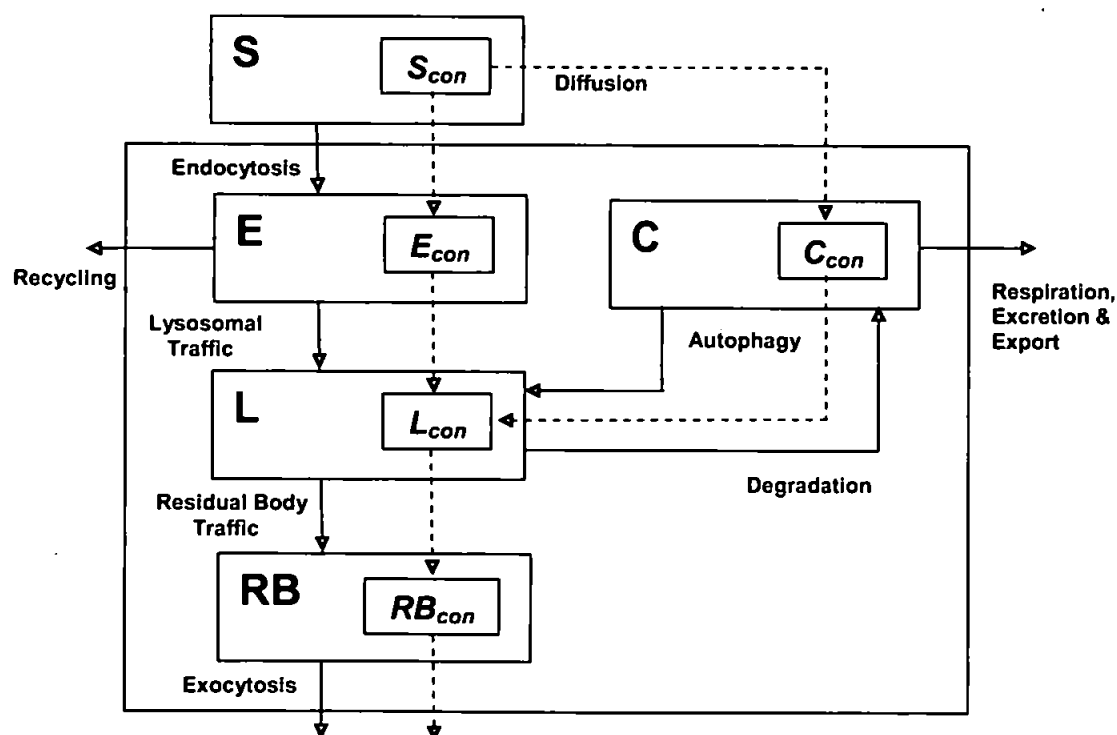


Fig 9.4 Model 8a2a 3 day contaminant exposure 12 day recovery simulation, but unfed throughout with "dripfeed". (a) Volumes — endosome, — lysosome, — cytosol & — cell (b) — lysosomal relative volume — lysosomal stability.

#### 9.4 Contaminant flow: Model 8b

Initially a single, hypothetical generic contaminant was utilised to enable the introduction of the necessary pathways and modifications. In the following schematic (Fig 9.5), two possible routes of entry to the cell were made available to the contaminant, either by endocytosis through attachment to the food or else by diffusion through the cellular membrane. Contaminant presence in the lysosome was designed to invoke two modifications to the normal operating conditions, a decrease in lysosomal throughput and an increase in the rate of damage to internal lysosomal components. Contaminant in the lysosome exited to the residual bodies and thereafter left the cell via exocytosis.



*Fig 9.5 Contaminant model schematic. Unbroken lines show non contaminant pathways and dashed lines the associated contaminant flow.*

From Figure 9.5 the following rate equations for the amounts of contaminant are derived based on the initial assumption of average concentration flow between compartments:

$$\frac{dE_{xcon}}{dt} = k_{endC} S_{con} - k_{lysC} E_{con} \quad [9.1]$$

$$\frac{dL_{xcon}}{dt} = k_{lysC} E_{con} + k_{autC} C_{con} - k_{RBC} L_{con} \quad [9.2]$$

$$\frac{dC_{xcon}}{dt} = k_{difC} S_{con} - k_{autC} C_{con} \quad [9.3]$$

$$\frac{dRB_{xcon}}{dt} = k_{RBC} L_{con} - k_{exoC} RB_{con} \quad [9.4]$$

The notation is as before, with the following additions: a subscripted  $C$  on a rate constant indicating contaminant flow; the subscript  $xcon$  for the compartmental contaminant content and the subscript  $con$  for the respective concentration.

Contaminant entry to the cell was simplified to the two routes of endocytosis and diffusion. The decision as to which route was taken was determined by the lipophilicity of the contaminant. To accommodate this property a variable, *OctCoeff*, was introduced as follows:

$$0 \leq OctCoeff \leq 1: \quad 0 \text{ all endocytosis; } 1 \text{ all diffusion.}$$

Then the endocytotic uptake of food/particle associated contaminant was calculated proportional to the total endocytotic rate as a linear function of its lipophilic coefficient:

$$k_{endC} = (1 - OctCoeff) k_{end} \quad [9.5]$$

Diffusion into the cell of a contaminant was initially defined as the product of two linear functions of both the lipophilic coefficient and the ratio of the difference between the cytosolic and external concentrations as follows:

$$k_{diffC} = \begin{cases} k_{endmax} \times OctCoeff \times \left( \frac{S_{con} - C_{con}}{S_{con}} \right) & \text{if } C_{con} \leq S_{con} \\ 0 & \text{Otherwise} \end{cases} \quad [9.6]$$

As all the cells, including those unfed, accumulated contaminant this variable was initially set to  $OctCoeff = 1$  for the following simulations. An arbitrary, constant, external contaminant concentration of 200 units/litre was initially used.

Since the mussel has been shown to bioaccumulate certain contaminants greatly above environmental concentrations the rate was not allowed to go negative. Of course this could be accumulation in different parts of the visceral mass of the mussel, or else accumulation within the lysosomal system of the hepatopancreatic cells, or less plausibly the presentation to these cells of a greatly contaminantly enriched aqueous phase due to some sortation process between the labial palps (mouth) and the digestive gland. The reality may be that there is a two-way diffusion between the external phase and the cytosol but, as the surface concentration was initially assumed to be constant, this was disregarded.



The rate of contaminant flow from the endosome to the lysosome was assumed to be the same as the total flow between these two compartments as follows:

$$k_{h3c} = \begin{cases} k_{h3} & \text{if } E_{con} > 0 \text{ and } k_{h3} > 0 \\ 0 & \text{Otherwise} \end{cases} \quad [9.7]$$

One of the commonly observed effects of contaminant exposure is the increase in the autophagic rate (Moore *et al.*, 2007). Whilst presumably this is in part due to an increase in the rate of damage to cytosolic constituent structures, the initial implementation of this effect was solely as an increase in the autophagic rate of non-damaged components. This reflected a purely defensive mechanism to remove the contaminant from the cytosol, but at the 'cost' of turnover of non-damaged components therein. The boost to the autophagic rate was calculated as a linearly dependent function of cytosolic contaminant concentration as follows:

$$\text{ContaminantBoost} = \begin{cases} \frac{999 \times C_{con}}{100} + 1 & \text{if } C_{con} > 0 \\ 1 & \text{Otherwise} \end{cases} \quad [9.8]$$

Explicitly, the non-damaged rate of autophagy was now calculated as:

$$k_{autP} = 0.01 \times k_{DautP} \times \text{FoodBoost} \times \text{ContaminantBoost} \quad [9.9]$$

Where *FoodBoost* was the boost due to food below maintenance as previously described. Then the rate of contaminant flow from cytosol to lysosome was taken to be proportional to the total autophagic rate.

$$k_{autC} = \begin{cases} k_{Dau} + k_{au} & \text{if } C_{con} > 0 \\ 0 & \text{Otherwise} \end{cases} \quad [9.10]$$

The increase in relative lysosomal volume which correlates to lysosomal stability could be solely due to a decrease in cellular volume but observational evidence is that the lysosomes swell (Lowe, 1988, Moore, 1988; Moore *et al.*, 2007). Hence, either material is entering at a greater rate, or else material is leaving at a lesser rate. With the delay model for lysosomal degradation, what came in left after a specified time delay. Hence, solely increasing autophagy would increase lysosomal volume for a short initial period; thereafter the increased incoming material will be matched by the same amount of material leaving. However, cell volume would start to decrease if autophagy were above a certain level, at which point the lysosomal relative volume would increase. But under these conditions the vicious circle of increased autophagy and decreasing cell volume would never allow the lysosomal stability to reach a stable minimum value as seen in the paradigm experiment (9.1a Phenanthrene + Food). So instead it was speculated that lysosomal performance was adversely affected by the contaminant, then the throughput values would start to decrease and the residency time of material within the lysosome would start to increase, hence swelling the lysosome at the lower autophagic boosts.

Consequently, a new coefficient, *ConFactor*, was defined, which would linearly (up to a threshold) decrease lysosomal throughput (Eqn

9.11). It was implemented by simply multiplying all the existing lysosomal throughputs by this coefficient.

$$ConFactor = \begin{cases} 1 - MIN(0.5, L_{con} / 100) & \text{IF } L_{con} > 0 \\ 1 & \text{Otherwise} \end{cases} \quad [9.11]$$

Alternatively or additionally the presence of contaminants in the lysosome could have injurious effects upon the degradative enzymes and membrane components (Brunk & Terman, 2002; Moore *et al.*, 2007). Since the throughputs were dependent upon the enzyme concentration, damaging these components should also lead to a reduction in the lysosomal throughput. Hence, another coefficient was defined, *DamFactor*, also linearly dependent on the lysosomal contaminant concentration (Eqn 9.12) and the lysosomal damage rates were multiplied by this factor.

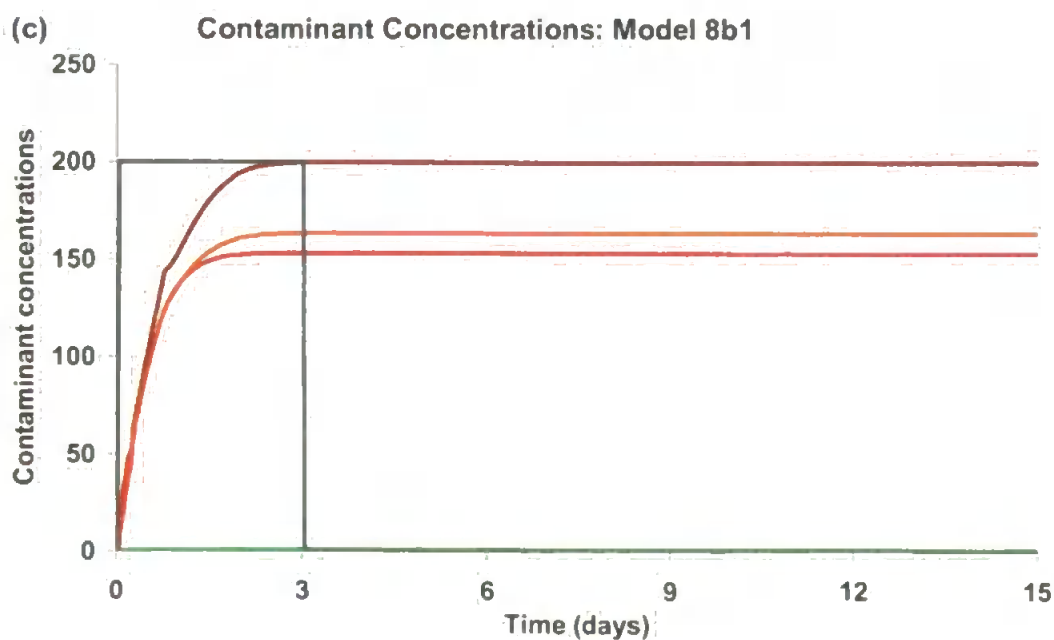
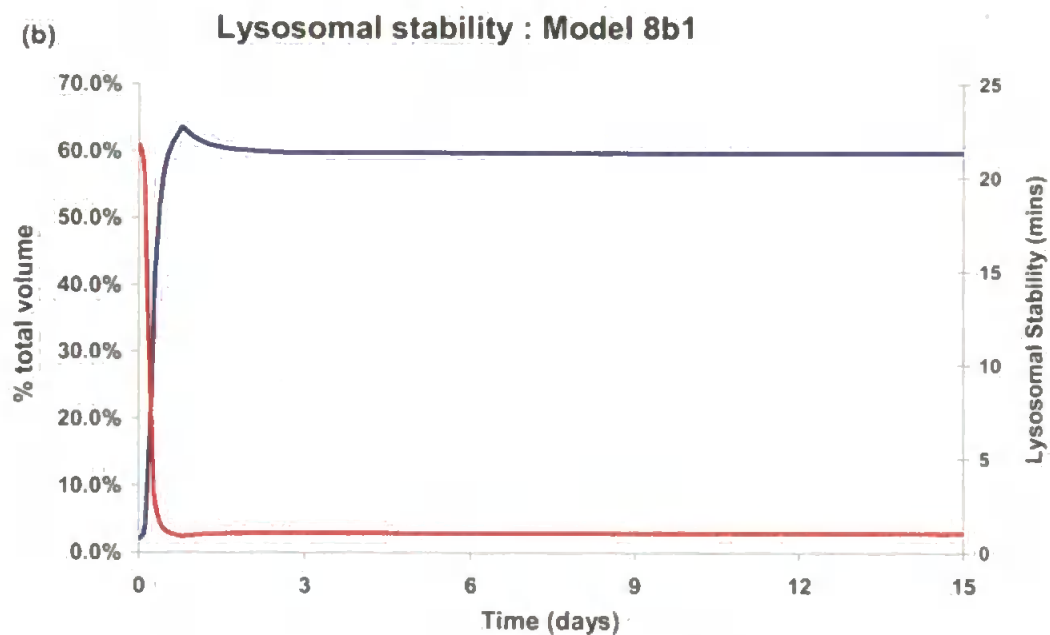
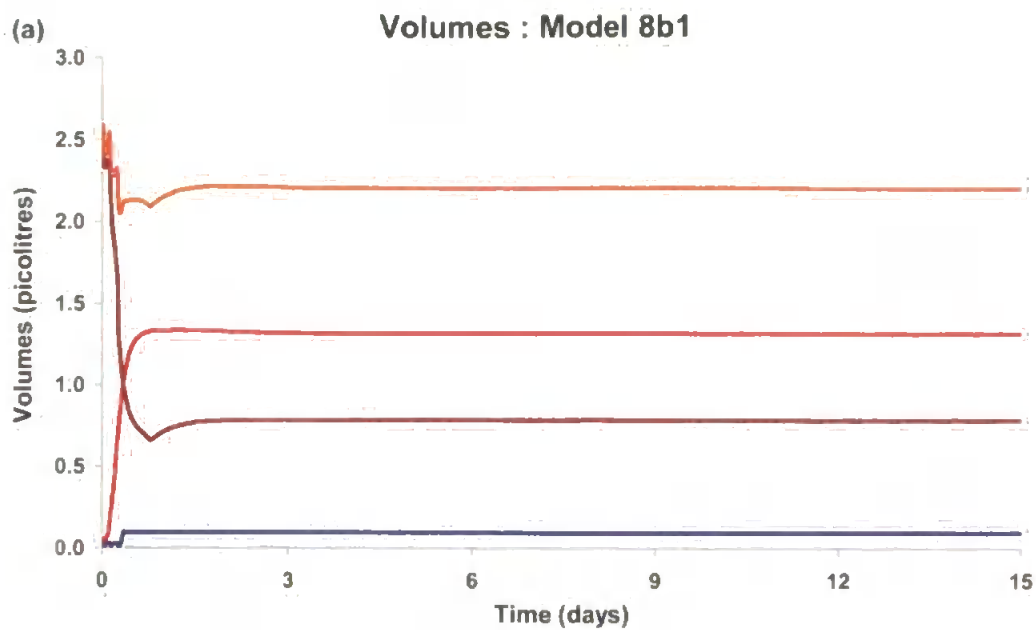
$$DamFactor = \begin{cases} 1 + MIN(1, L_{con} / 100) & \text{IF } L_{con} > 0 \\ 1 & \text{Otherwise} \end{cases} \quad [9.12]$$

To allow the contaminant to exit the cell a rate for transfer from the lysosome to the residual bodies needed to be introduced. Under the assumption that lysosomes were the sites of accumulation for the contaminant, this rate was introduced as a reduced proportion of the flow of normal debris from the lysosome to the residual body compartment.

$$k_{RBC} = \begin{cases} (k_{ERB} + k_{CRB}) / 100 & \text{IF } k_{ERB} + k_{CRB} > 0 \& L_{con} > 0 \\ 0 & \text{Otherwise} \end{cases} \quad [9.13]$$

As the residual body was ejected from the model cell in its entirety, any contaminant therein will leave at the same rate (Eqn 9.14).

$$k_{exoc} = k_{eto} \quad [9.14]$$



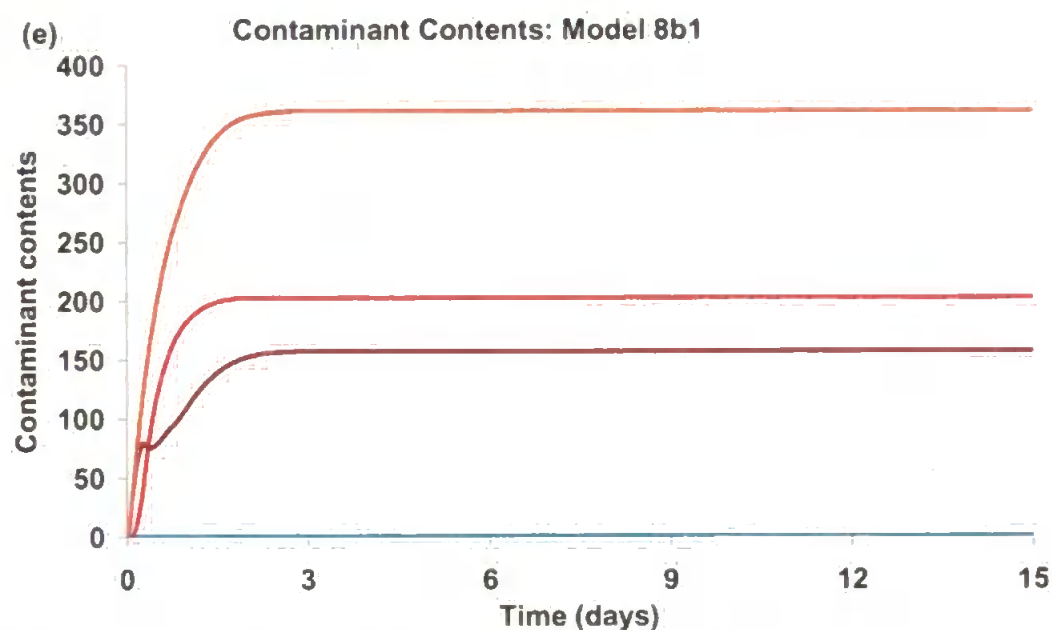
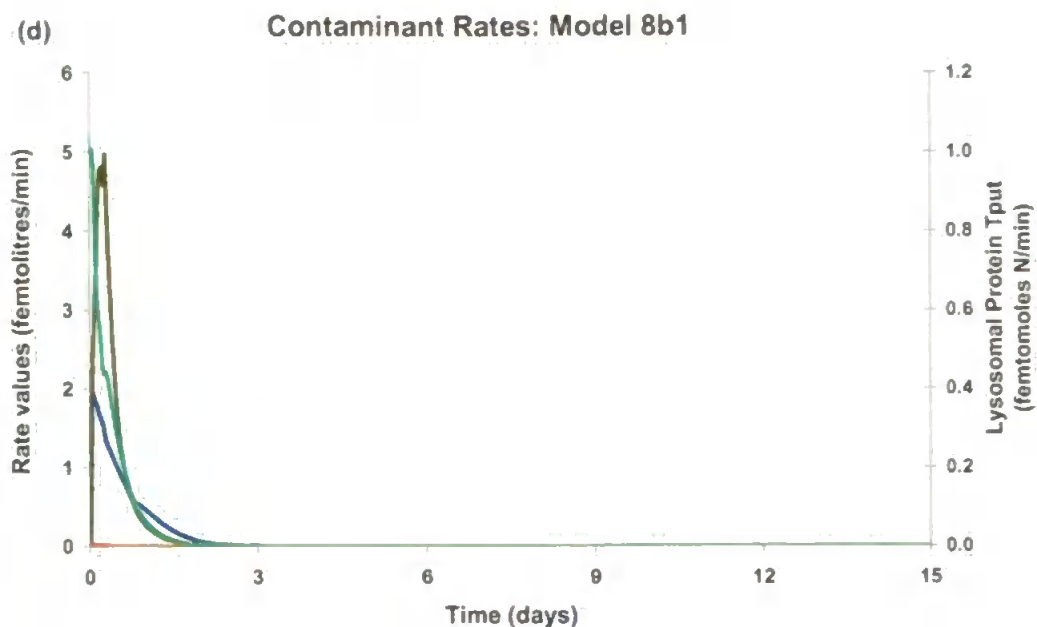


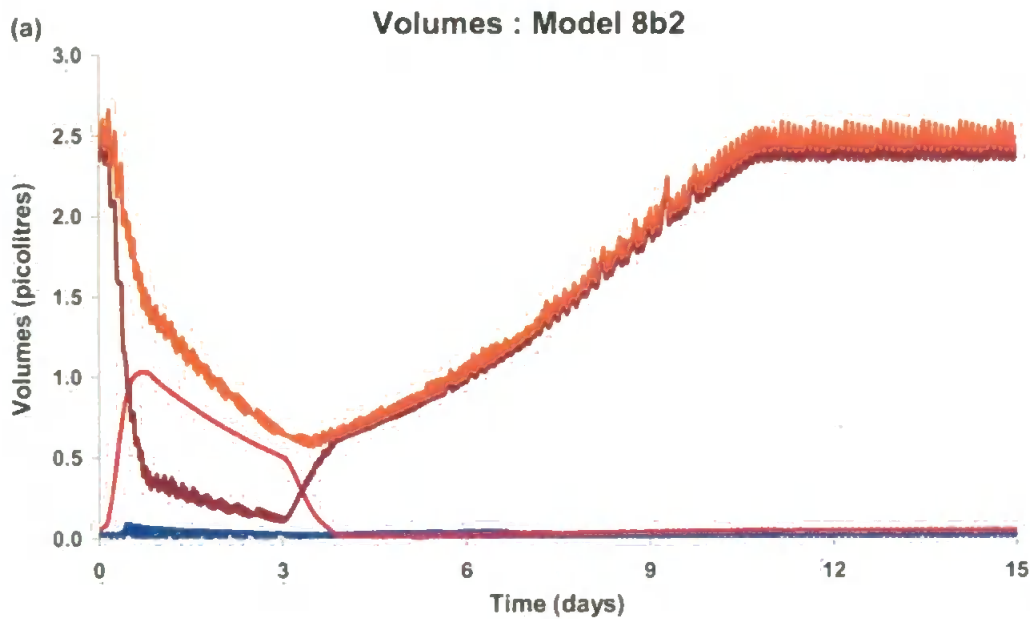
Fig 9.6 15 day simulation of toxicity model 8b1, days 0-3 exposure, days 3-15 recovery period. ICs:  $Cell_v - RB_v = 2.4$  picolitres,  $f_{ev} = 1\%$ ,  $f_{lv} = 2\%$ . (a) Volumes,  $-E_v$ ,  $-L_v$ ,  $-C_v$ ,  $-Cell_v$  (b)  $-$  relative lysosomal volume,  $-$  lysosomal stability (c) Contaminant concentrations, in arbitrary units,  $-S_{con}$ ,  $-L_{con}$ ,  $-C_{con}$ ,  $-RB_{con}$  &  $-Cell_{con}$  (d) contaminant rates  $-k_{diffC}$ ,  $-k_{autC}$ ,  $-k_{RBC}$  &  $-LPxnTput$  (e) contaminant contents  $-L_{xcon}$ ,  $-C_{xcon}$ ,  $-RB_{xcon}$  &  $-Cell_{xcon}$ .

An initial simulation of the fed replicate in the toxicity experiment was performed (Fig 9.6). Contaminant entered the cytosol quite rapidly until it approached the asymptote of the surface concentration, the rate of diffusion decreased as this limit was approached, until the initiation of the recovery period whereupon it ceased altogether (Figs 9.6c, d & e). The lack of significant change after this point indicated that the implementation of the depuration mechanisms was seriously flawed. However, the increased autophagic rate removed ~60% of the cumulative contaminant entering the cell into the lysosome within 1.8 days. The lack of transfer from the lysosome to the residual bodies of the contaminant was the cause of this accumulation. Investigation of the total compartmental volumes (Fig 9.6a) revealed the lysosome swelling to an outsize 62% of cell volume within 0.85 days of the commencement of the exposure (Fig 9.6b). The low return of traffic to the cytosol and to the residual body, coupled with this high proportion of cell volume indicated that the decrease in lysosomal throughput had been too severe.

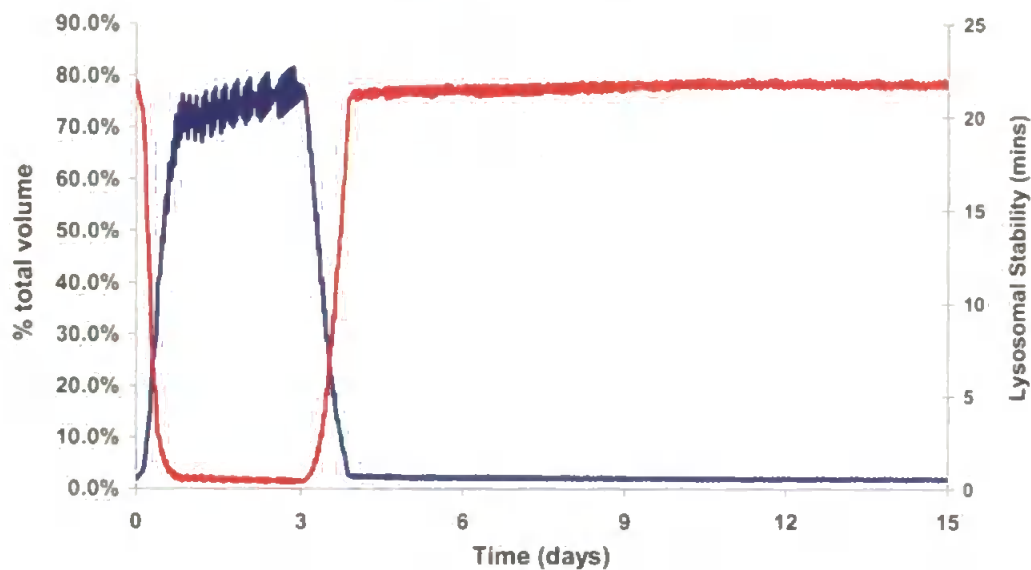
The lysosomal throughput had been decreased to 50% of its normal value, but the major reason for its net reduction was the continued damage to the lysosomal degradative proteins without replenishment. Replenishment of the lysosome had been constrained to the resting phase, however, due to the rapidity of the lysosomal swelling during the initial feeding period the endosome had stopped sending material to the lysosome.

This in turn had suspended the cell phase cycle in the feeding phase awaiting lysosomal reduction.

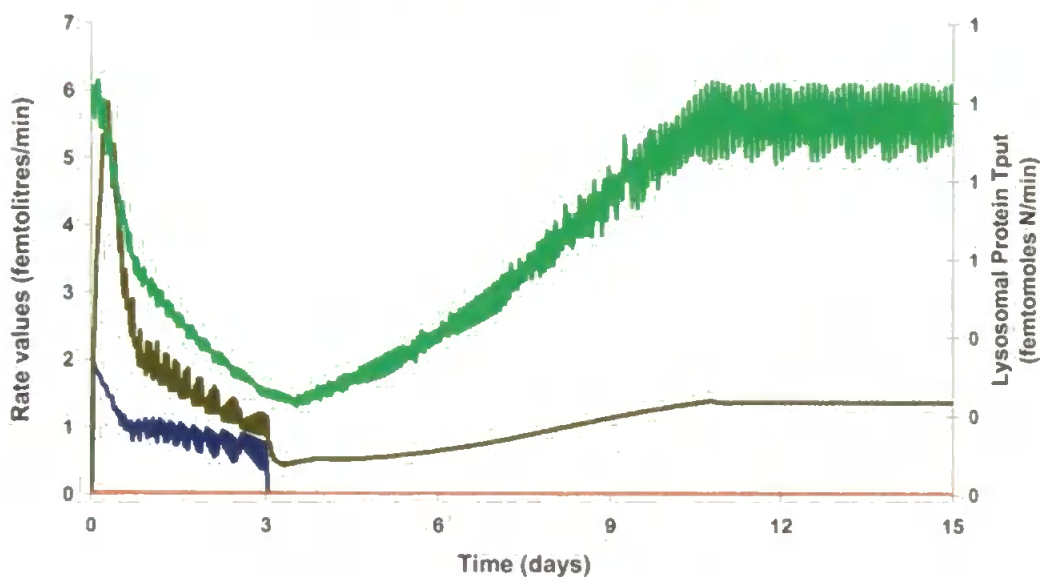
This realisation prompted two changes to the toxicity model. First, the lysosomal throughput was only, hereafter, reduced as a consequence of damage to the lysosomal degradative proteins. Second, the feeding phase was given a maximum period of 30 minutes, to allow the cell to initially await any lysosomal reduction, but to pass on if necessary to the disintegrating phase and then the replenishment phase.



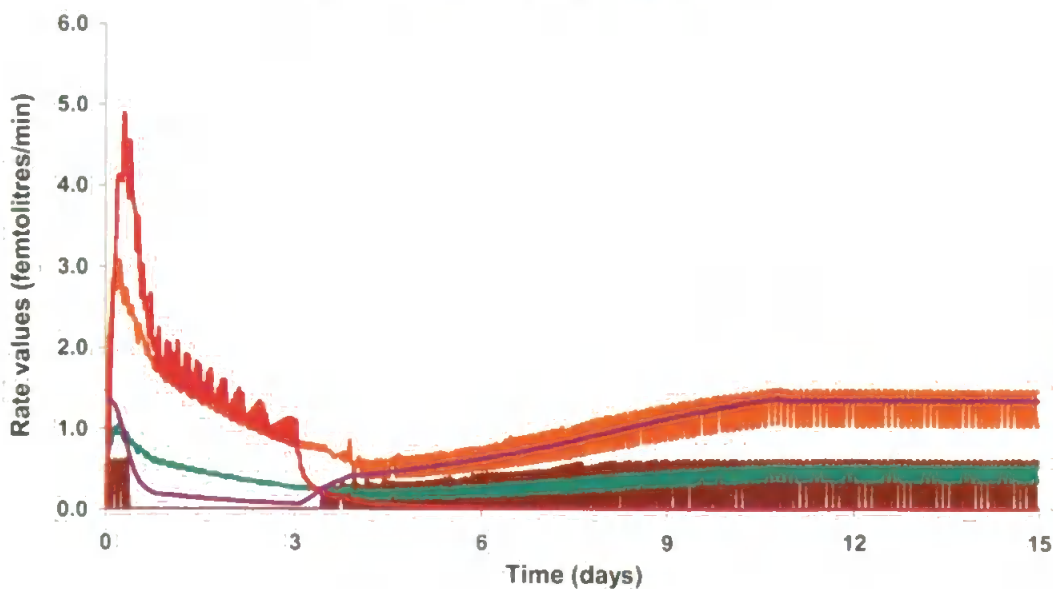
(b) Lysosomal stability : Model 8b2



(c) Contaminant Rates: Model 8b2



(d) Lysosomal rates : Model 8b2





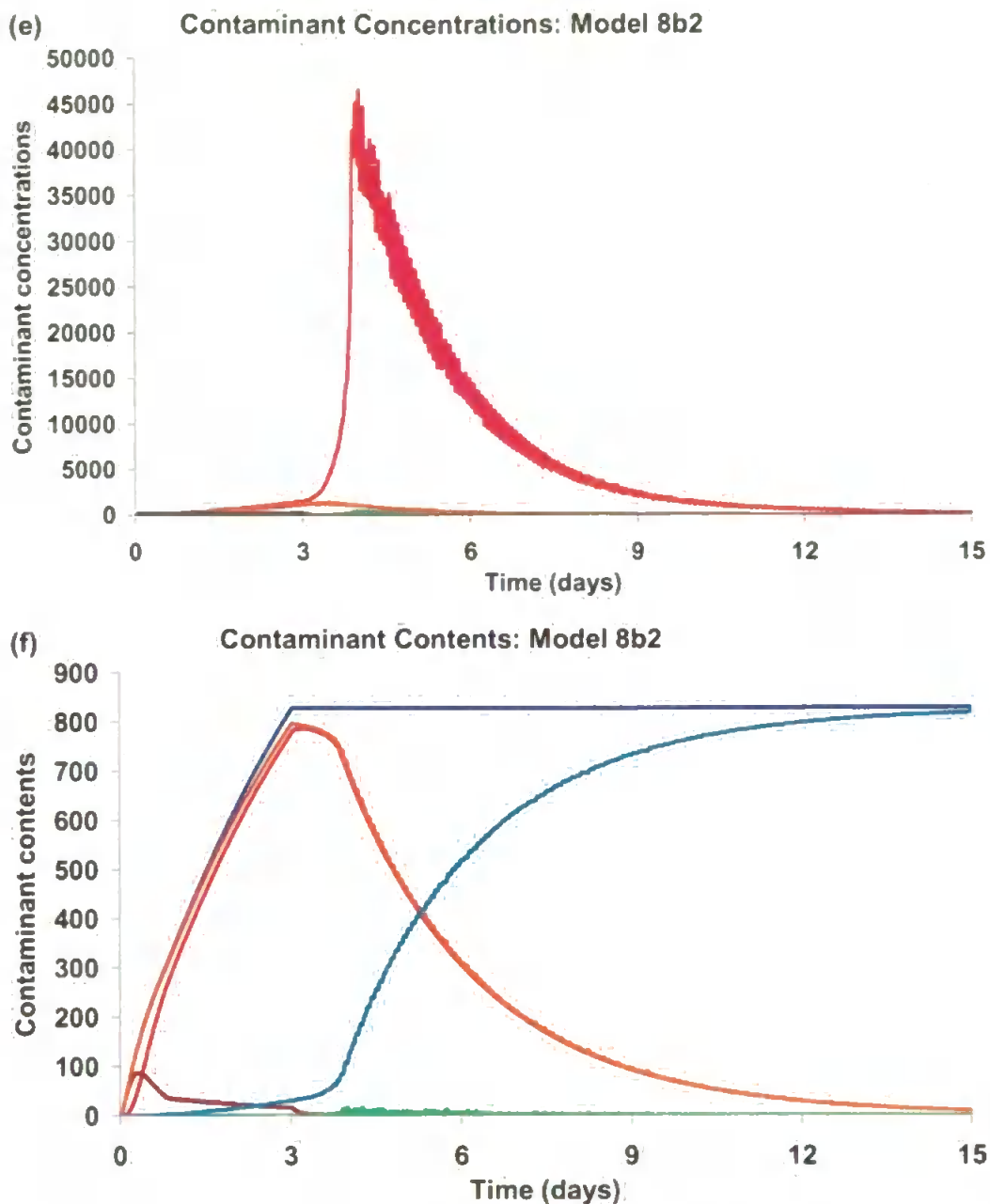


Fig 9.7 Model 8b2 toxicity simulation as described for Fig 9.6. (a)

volumes,  $E_v$ ,  $L_v$ ,  $C_v$ ,  $Cell_v$  (b)  $\text{relative lysosomal volume}$ ,  $\text{lysosomal stability}$  (c) contaminant rates  $k_{difC}$ ,  $k_{autC}$ ,  $k_{RBC}$  &  $LP_{xnTput}$  (d) Lysosomal rates,  $k_{lys}$ ,  $k_{Daut}$ ,  $k_{aut}$ ,  $k_{deg}$ ,  $k_{RB}$  (e)

Contaminant concentrations, in arbitrary units,  $S_{con}$ ,  $L_{con}$ ,  $C_{con}$ ,  $RB_{con}$  &  $Cell_{con}$  (f) contaminant contents  $L_{xcon}$ ,  $C_{xcon}$ ,  $RB_{xcon}$  &  $Cell_{xcon}$ , Cumulative contaminant In: & Out:

First, it was noticeable that the contaminant now exited the cell through the residual bodies and by the end of the recovery period the cell had almost expelled everything it had taken in (Fig 9.7f). Furthermore the system behaviour was such that 2.29 times as much contaminant entered the cell compared to the first model, due to the greater contaminant flux from cytosol via lysosome to the residual body, which kept the cytosolic concentration depressed, thus enabling more contaminant to enter by diffusion (Fig 9.7c & e). Experimental evidence suggested that the overall cellular contaminant concentration at the end of the 12 day recovery period was 5 times higher than the basal concentration (Moore, 2004; Moore *et al.*, 1984). Although this needed further parameterisation to determine an initial value, it was likely that the contaminant in this model was not resident in the cell for long enough.

Also evident, was the decrease in cell volume and lysosomal stability over the exposure period, the almost immediate recovery, after exposure stopped, of the lysosomal stability and the eventual recovery of cell volume (Figs 9.7a & b). However, continued exposure until day 5.44 would result in the cell reaching its minimum volume which could have been unrealistic.

The lysosome became the major site of contaminant accumulation (Fig 9.7f; Moore *et al.*, 2006a; 2007; Viarengo *et al.*, 1985). When the lysosome volume reduced at a greater rate than the contaminant content this increased the concentration drastically. In the initial model, this would have resulted in continued maximal lysosomal throughput reduction, but as

this is now solely based on the damage done to the degradative proteins, and this was capped for high lysosomal contaminant concentrations, the throughput recovered as the damaged enzymes were replaced at a greater rate (Figs 9.7c & e).

The autophagic uptake of contaminant was seen to follow that of the increased undamaged autophagic uptake until the beginning of the recovery period, where the basal damaged autophagic uptake began to dominate once more (Figs 9.7c & d). The augmented rate of undamaged autophagy was some 600 times the normal mean rate but overall the total autophagic rate peaked at 5 times the unaffected mean (Fig 9.7d).

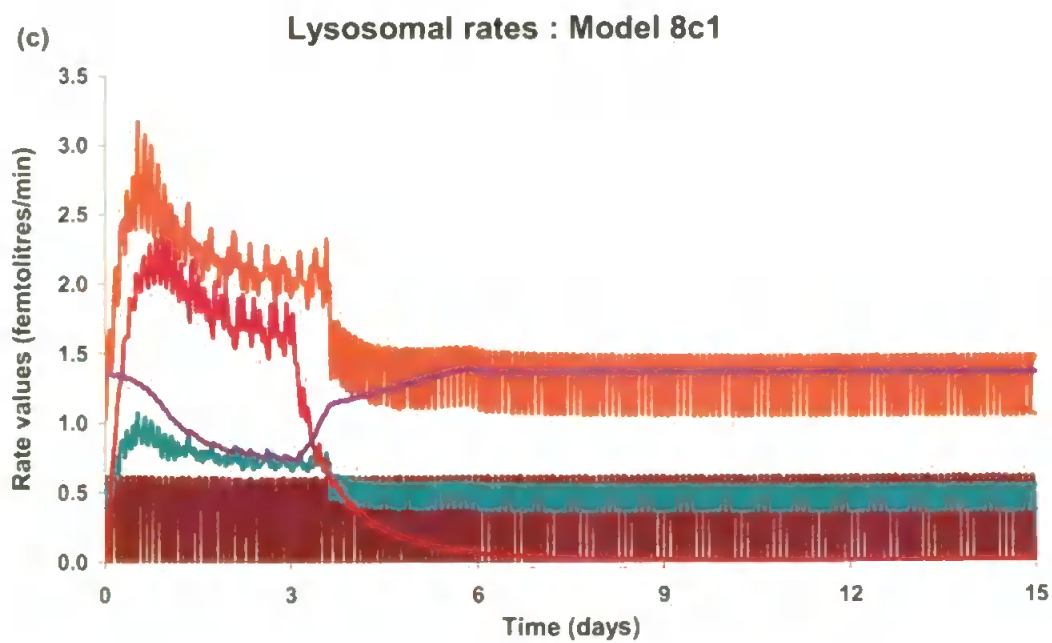
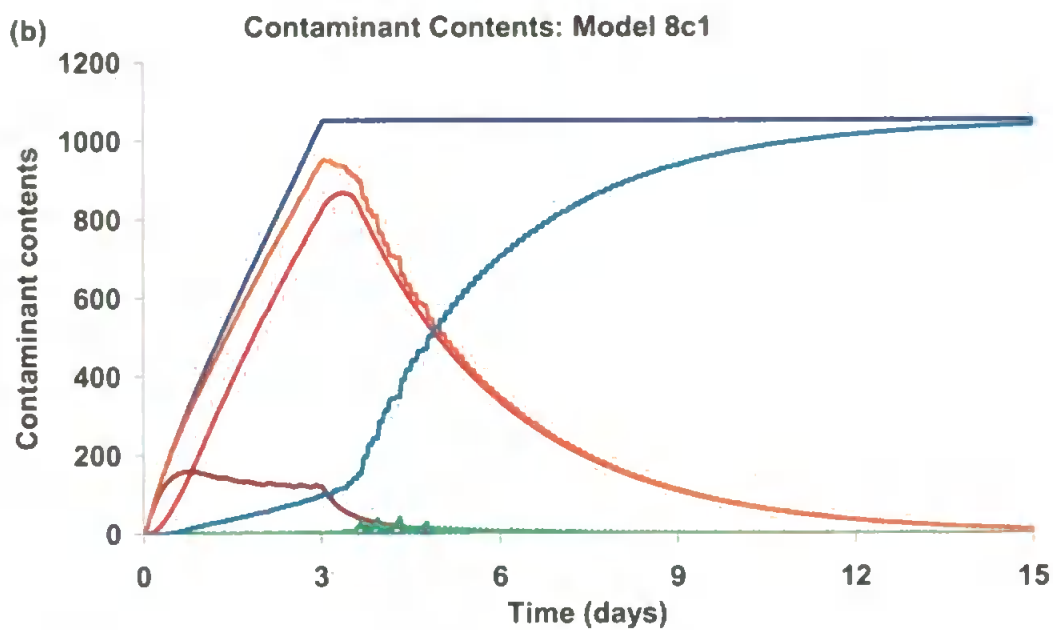
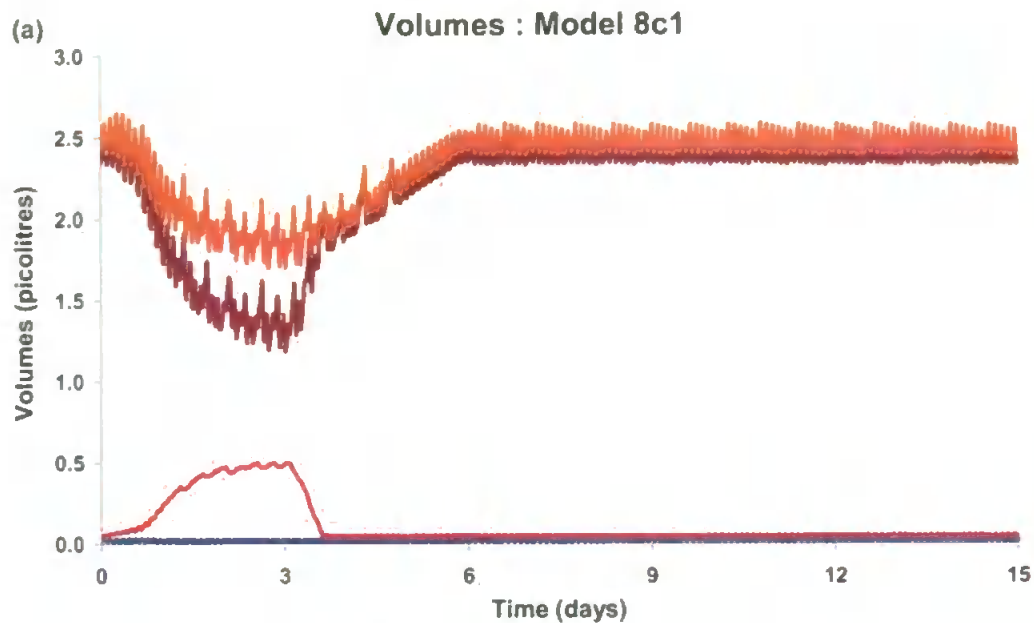
The rate of decrease in cell volume was remarkable and constituted one of the major factors in the system's behaviour. This drop was due almost entirely to the increased autophagy and subsequent exocytosis of 10% of that volume. In total under unexposed conditions, the model sends 82.4% of its daily volume for degradation via autophagy. In both this and the previous model cytoplasmic turnover rose to 235.1% of the nominal rate during the first three days of exposure and then fell to 84.4% over the recovery period. Furthermore, the lysosomal contaminant concentration rose to a maximum of 233 times the source concentration, although the cellular concentration is only 6.91 times at its highest point.

### 9.5 Cytosolic contaminant removal and effects: Model 8c

The residency time of the cytosolic contaminant was the key factor for the increased autophagy. The boost to autophagy as a consequence of cytosolic contaminant concentration may have initially been set too high. The effects of reducing this factor by a quarter and capping the autophagic boost at higher concentrations were considered (Eqn 9.15) in Model 8c.

$$\text{ContaminantBoost} = \begin{cases} \text{MIN}\left(250, \frac{249C_{con}}{100} + 1\right) & \text{if } C_{con} > 0 \\ 1 & \text{Otherwise} \end{cases} \quad [9.15]$$

The decreased autophagic boost sent less material to the lysosome for degradation, which enabled the cell to recover from an initial loss of volume over the exposure period (Fig 9.8a). The lysosomal volume swelled over the exposure period, but not enough to temporarily stop the endosome passing on material, as it did previously (Figs 9.6a); but quickly recovered upon the start of the recovery period (Fig 9.8b). Moreover, the lysosomal stability did not decrease as much as seen in the previous model (Figs 9.7b & 9.8d) and remained within realistic levels. The amount of contaminant that entered the cell also slightly increased in comparison to the last model (Figs 9.7f & 9.8b). The reduced autophagy prolonged the cytosolic residency time but this was counterbalanced by greater cytosolic volume enabling a smaller concentration, which provoked greater diffusion.



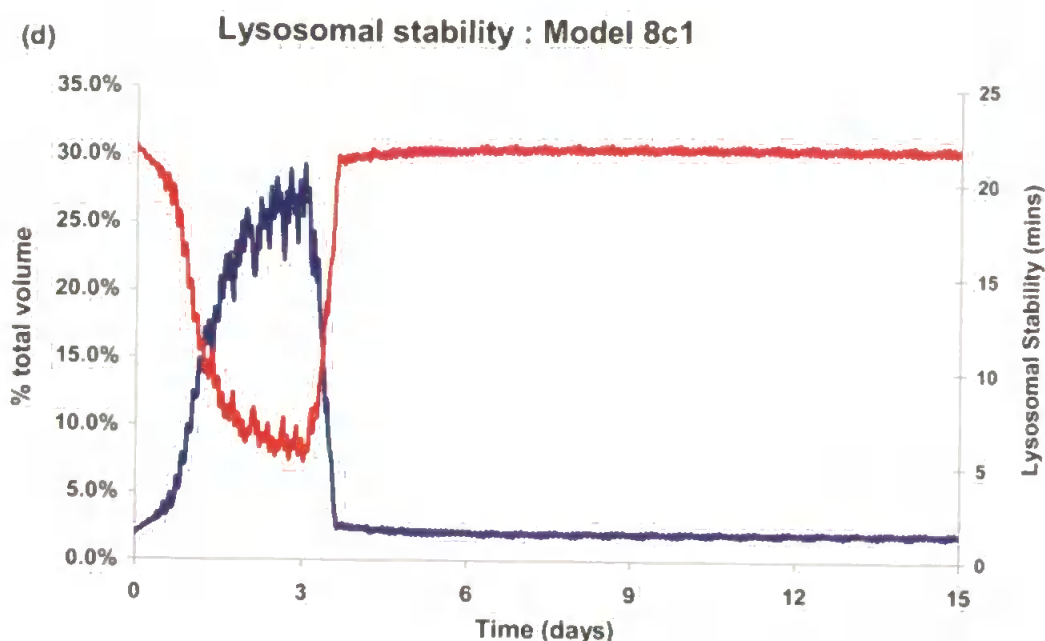
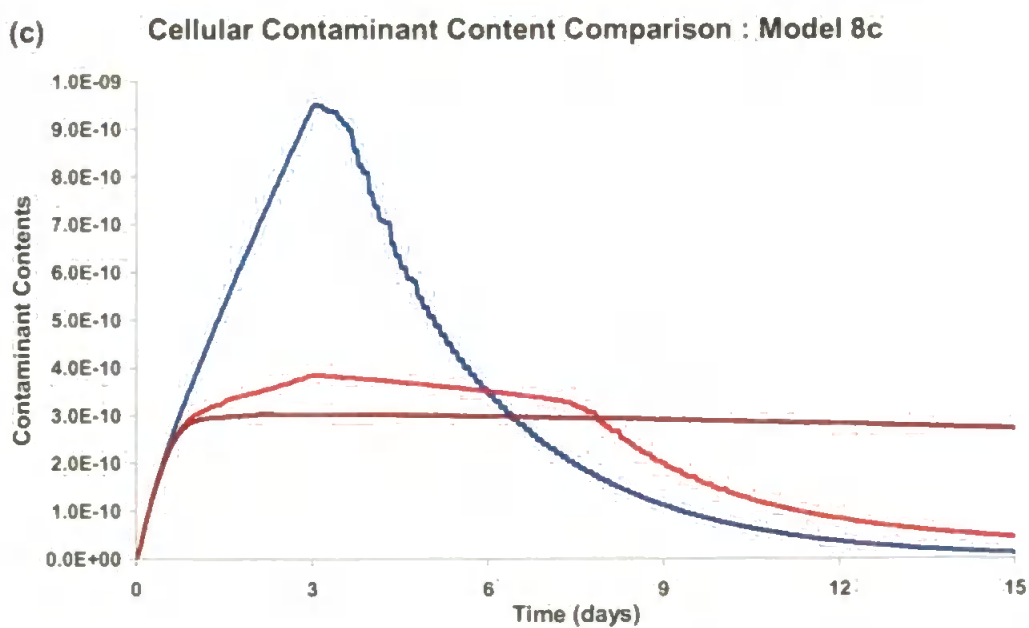
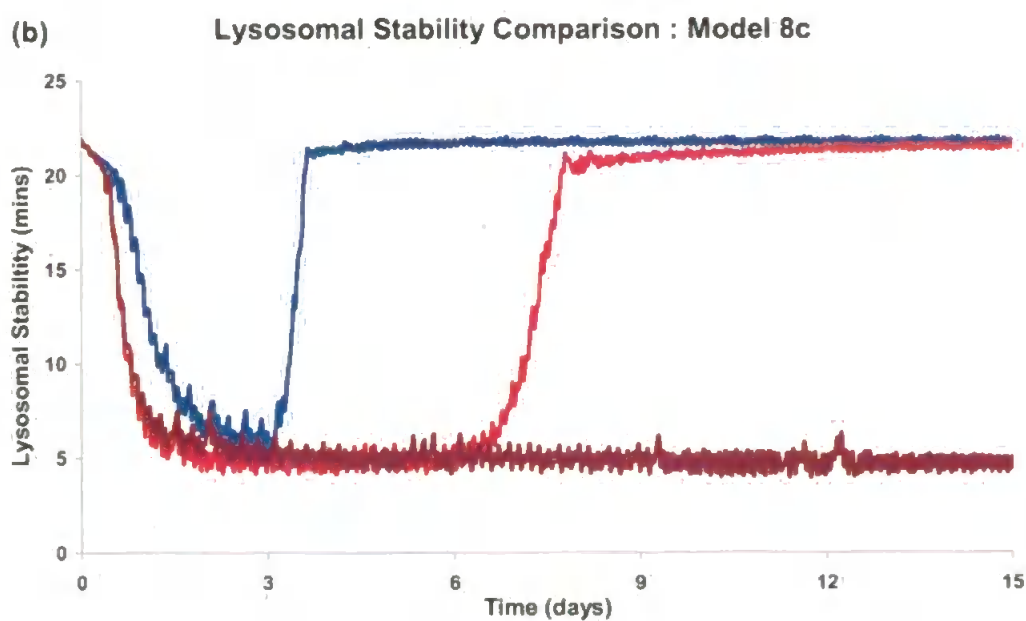
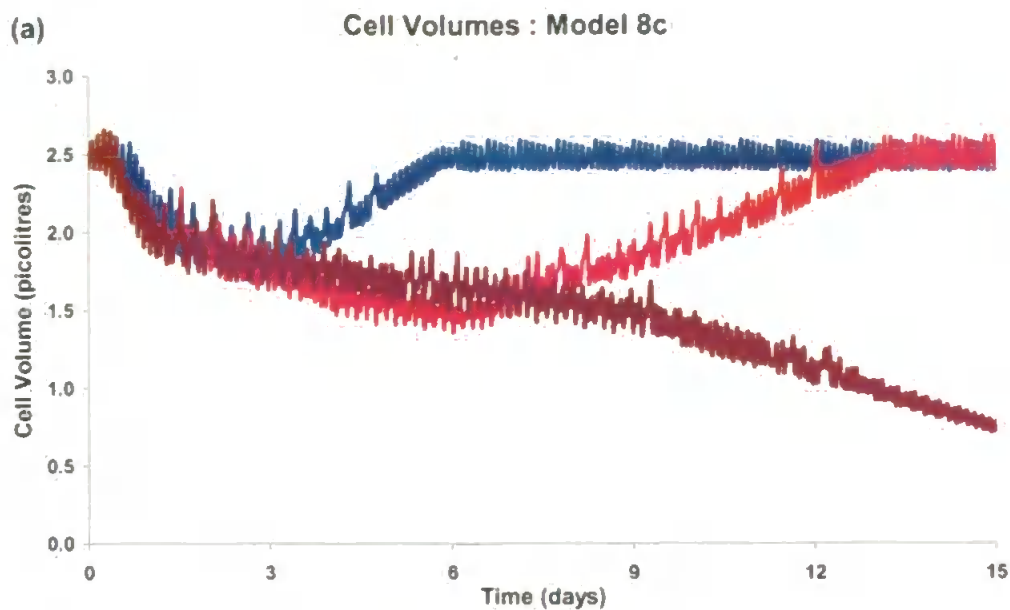


Fig 9.8 Model 8c1 reduced autophagy boost otherwise as previous simulation (a) Volumes, —  $E_v$ , —  $L_v$ , —  $C_v$ , —  $Cell_v$  (b) contaminant contents —  $L_{xcon}$ , —  $C_{xcon}$ , —  $RB_{xcon}$  & —  $Cell_{xcon}$ , Cumulative contaminant In — & Out — (c) Lysosomal rates, —  $k_{lys}$ , —  $k_{Daut}$ , —  $k_{aut}$ , —  $k_{deg}$ , —  $k_{RB}$  (d) — relative lysosomal volume, — lysosomal stability.

With the reduced autophagic boost (Fig 9.8c), the overall daily turnover of cell volume during the exposure period was now 2.4 times the unexposed level. This decreased the maximum volume loss to 35.45% of the maximum limit (Fig 9.8a) compared to 78.62% in the previous model (Fig 9.7a), which was the primary factor for recovery of cell volume. The major concern with this model was the length of time that contaminant was resident in the cellular compartments, which appeared very short in comparison to the observed results. To force the residency time to increase, the flow between cytosol and lysosome of contaminant was reduced by applying a factor,  $ConAut$ , to the average flow between them (Eqn 9.16).

$$k_{autC} = ConAut(k_{Daut} + k_{aut}) \quad [9.16]$$



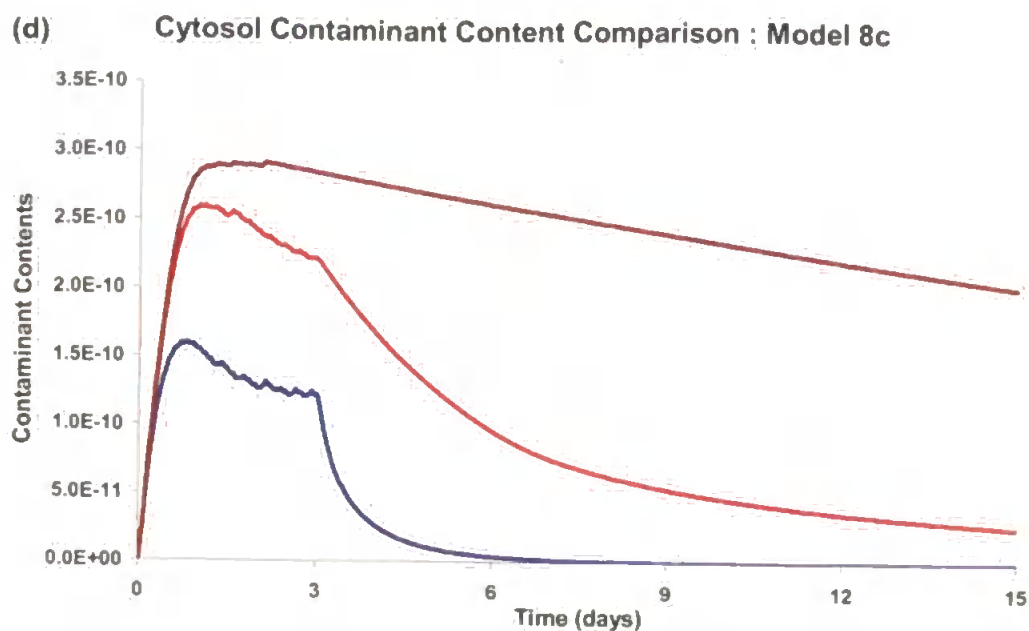


Fig 9.9 Model 8c contaminant autophagic factor comparison:  $ConAut = -$  1,  $-0.1$  &  $-0.01$ . (a) Cell volume (b) lysosomal stability (c) cellular contaminant contents (d) cytosolic contaminant contents. (NB no contaminant autophagic reduction,  $conaut = 1$ , is exactly the previous model 8c1)

With  $ConAut = 0.1$ , the cell volume continued to fall beyond the end of the exposure period, as the protein autophagic boost was still operational due to the increased cytosolic residence time of the contaminant.

Additionally, the cell volume fell to 48.5% of the maximum and the relative lysosomal value oscillated around 30% between days 2-6 of the simulation, which allowed feeding to continue intermittently. The fall in cytosolic volume and the decrease in removal of cytosolic contaminant increased the cytosolic contaminant concentration to above that of the surface, which inhibited diffusion into the cell. Hence, there was a reduction in contaminant entering the cell. Enough contaminant was



leaving the cytosol to allow recovery of cell volume to commence from around day 6 onwards.

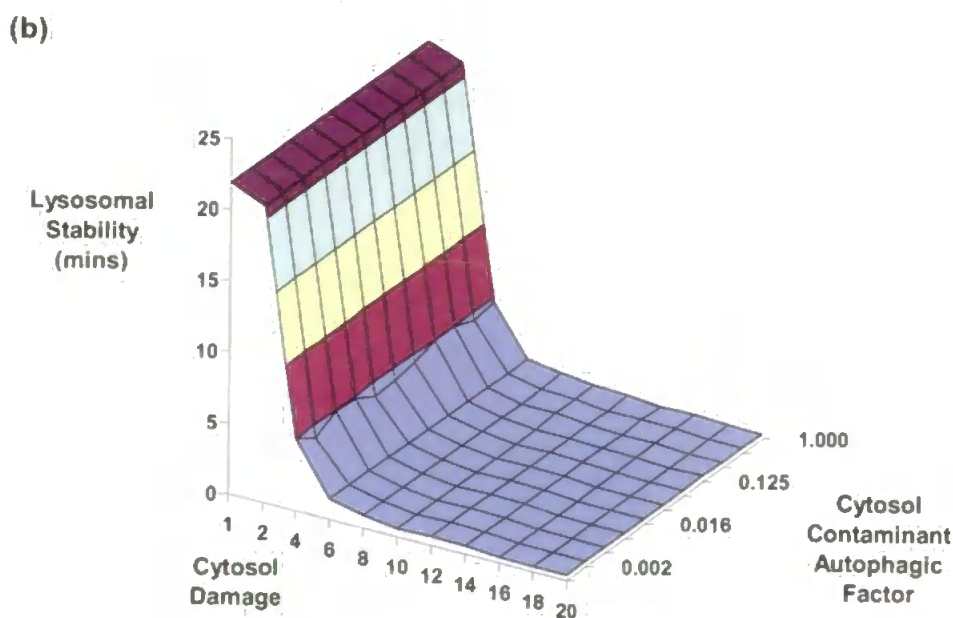
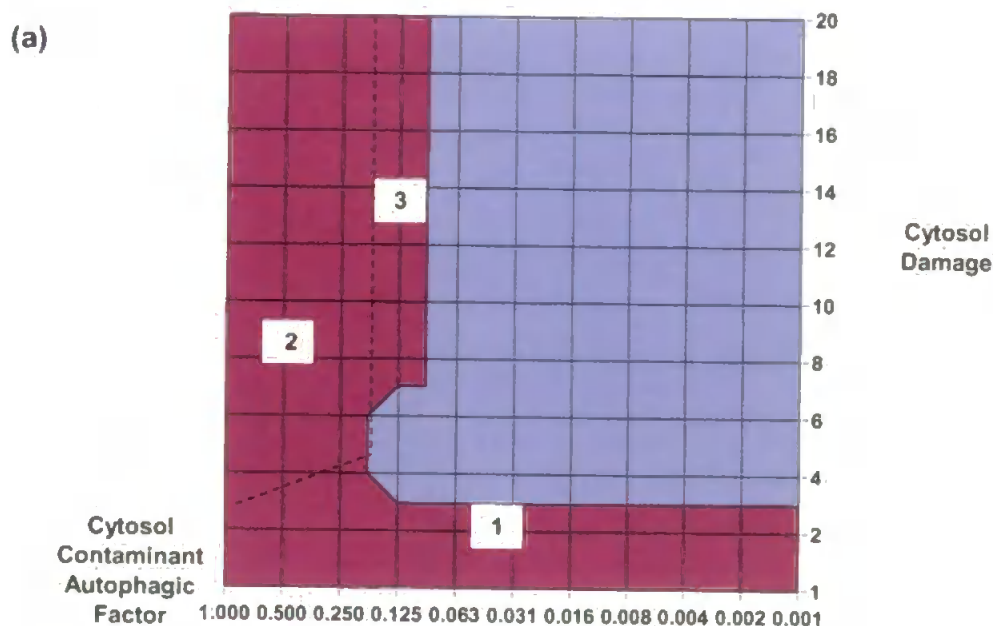
With  $ConAut = 0.01$ , the cell volume continued to decline throughout the simulation and the lysosomal stability rapidly attained, and thereafter remained, at a low value. If the simulation were extended, then the cell volume would reach the minimum prescribed value at day 33.09 due to the continued heightened autophagy of protein. This was a consequence of the cell volume declining at a faster rate than the contaminant content, which meant the contaminant concentrations grew rapidly. Thus, since the deleterious autophagic effects are based upon concentrations the autophagic rate was increased and prolonged.

It would appear evident that the extra autophagy, which occurs as a result of contaminant exposure, is due to extra damage on the constituent parts of the cytosol (Moore *et al.*, 2006b, 2007). Instead then of increasing the autophagic rates by an arbitrary amount, it made more functional sense to increase the amount of damage to the components of the cytosol as a consequence of the contaminant presence. Then the pool of damaged material requiring autophagic uptake would increase, and hence, the damaged autophagic rate would rise accordingly. Model 8c2 was conceived with the following changes to the previous model:

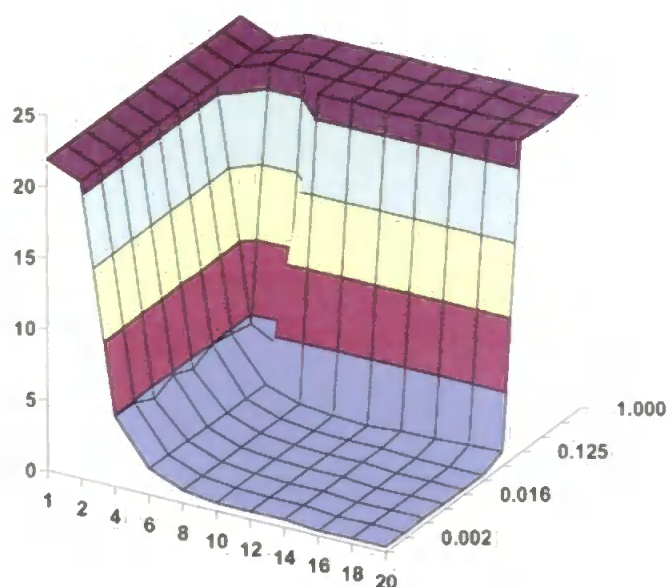
$$ContaminantBoost = \begin{cases} MIN\left(ConDam, \frac{(ConDam - 1)C_{con}}{100} + 1\right) & \text{if } C_{con} > 0 \\ 1 & \text{Otherwise} \end{cases} \quad [9.17]$$

$$k_{CdamP} = 0.001 \times CP_v \times \text{ContaminantBoost} \quad [9.18]$$

Autophagy of compartmental material returned to the previous specification as dependent solely on size of the pool of damaged material. The relationship between two factors, the increased damage and the rate of removal of contaminant by autophagy, determined the overall cellular behaviour. Even when the damage was high, there existed a removal rate high enough so that the cell could recover.



(c)



(d)

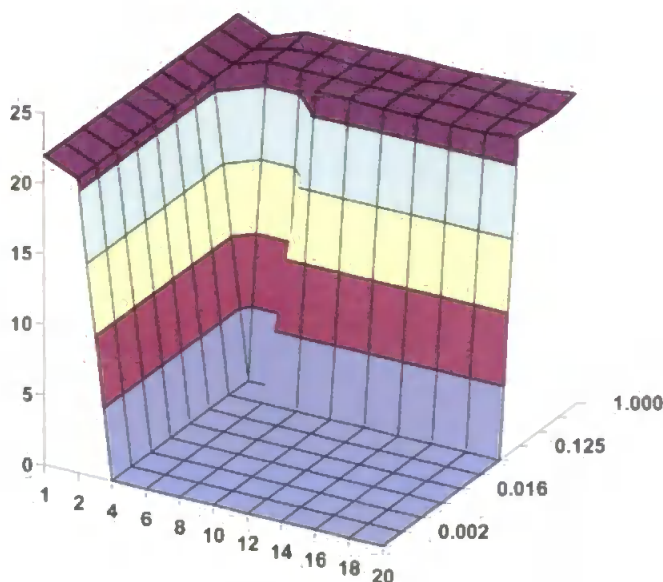


*Fig 9.10 Model 8c2 survival across the contaminant autophagic factor and cytosolic damage factor parameter space (a) Survival ■ Expiry ■ (b-d) Lysosomal Stability (b) after 3 days exposure (c) after 3 days recovery (d) at end of experiment.*

When the contaminant was allowed to move from the cytosol to the lysosome at the same rate as normal material, then even 20 times the normal amount of damage does not stop the cell from recovering, due to

the lack of contaminant residency time restricting the opportunity for damage to accrue. Even at 25% and 50% of the normal flow this remained true (region 2, Fig 9.10a). Similarly, when the rate of normal damage was doubled then the cell can recover regardless of the flow of the contaminant from the cytosol (region 1, Fig 9.10a).

Once the flow was reduced to 12.5% of normal, the cell's recovery capacity was violated when the rate of damage was 4-6 times of normal. For this autophagic uptake of contaminant and above these rates of damage, the cell did recover but with pathological levels of lysosomal swelling (region 3, Fig 9.10a).

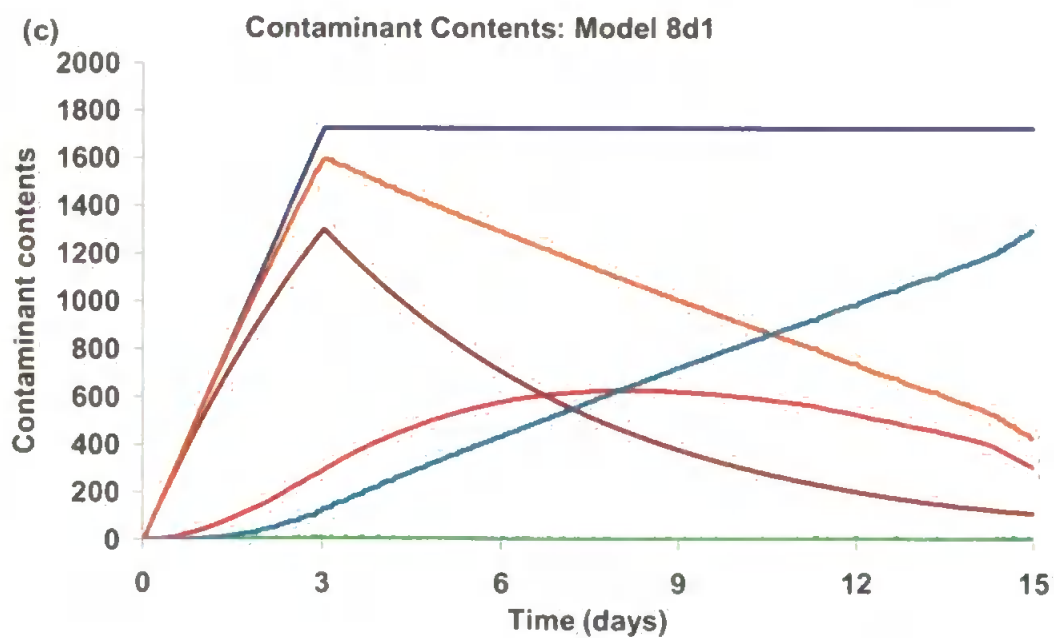
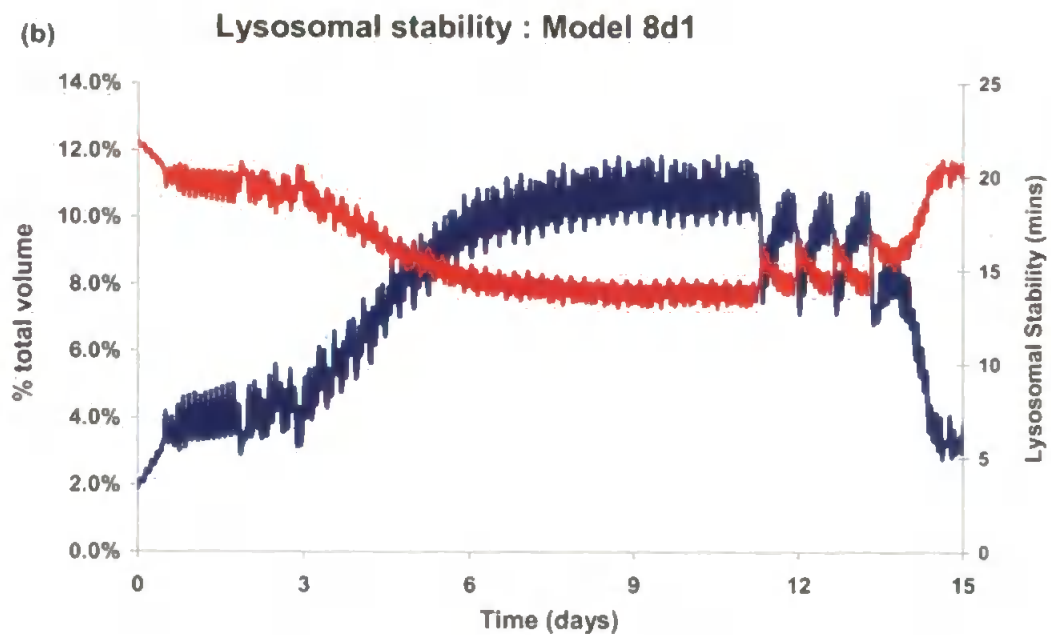
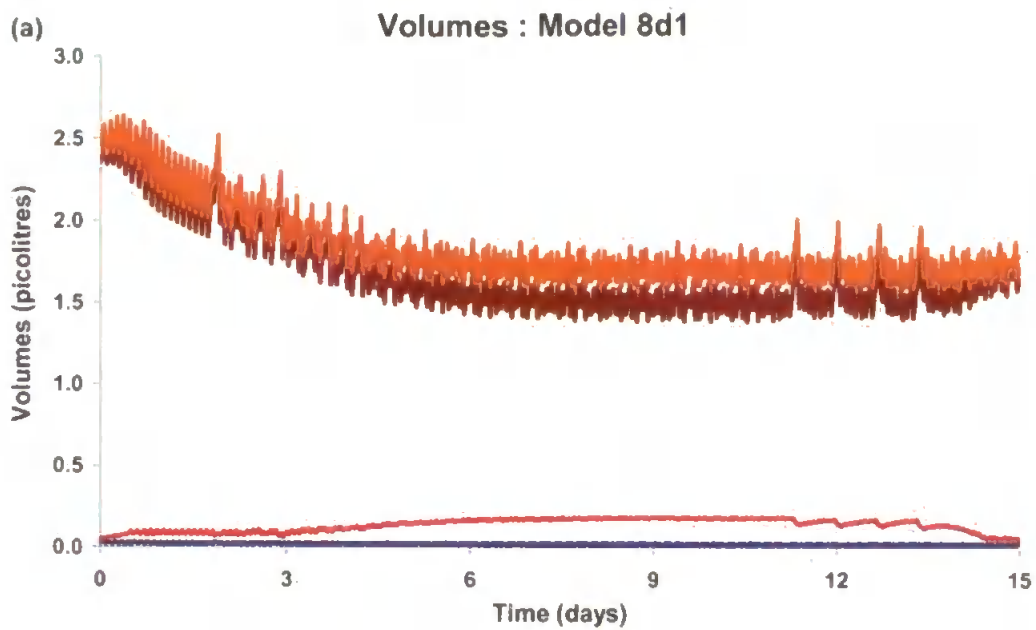
Within the 'survival' section of the parameter space there were two distinct regions. Within the low cytosolic damage factor (region 1, Fig 9.10a), the cell never shows any appreciable lysosomal instability through the course of the simulation (Fig 9.10b & c). However, for damage factors which are above double the normal rate and high rates of contaminant flow (region 2, Fig 9.10a), there was significant lysosomal instability at the end of the exposure period (Fig 9.10b). The recovery of models in this region of the parameter space resulted in total recovery of lysosomal stability to normal levels by the end of 3 days of recovery (Fig 9.10c).

## 9.6 Contaminant diffusion: Model 8d

The amount of uptake of contaminant was controlled by the assumption that the cell membrane was permeable in one direction. This has been crudely simulated by stopping the flow of contaminant once the cytosolic concentration was greater than that at the surface. However, as the mussel has been shown to bioaccumulate contaminants in greater concentrations than in their natural environments then, if there were no significant cell shrinkage, more contaminant must be allowed to enter the cell, disregarding possible sequestration in other membrane compartments. Equally, if the contaminant was transformed into another equally reactive and damaging species this would enable possible further diffusion (Livingstone *et al.*, 2000b; Regoli, 2000).

Model 8d1 lets the diffusion continue at a steady rate during the exposure period regardless of the cytosol concentration (with the following parameters  $conaut = 0.1$   $ConDam = 2.5$ ).

$$k_{diff} = \begin{cases} k_{end\ max} \times OctCoeff & \text{if } S_{con} > 0 \\ 0 & \text{Otherwise} \end{cases} \quad [9.19]$$



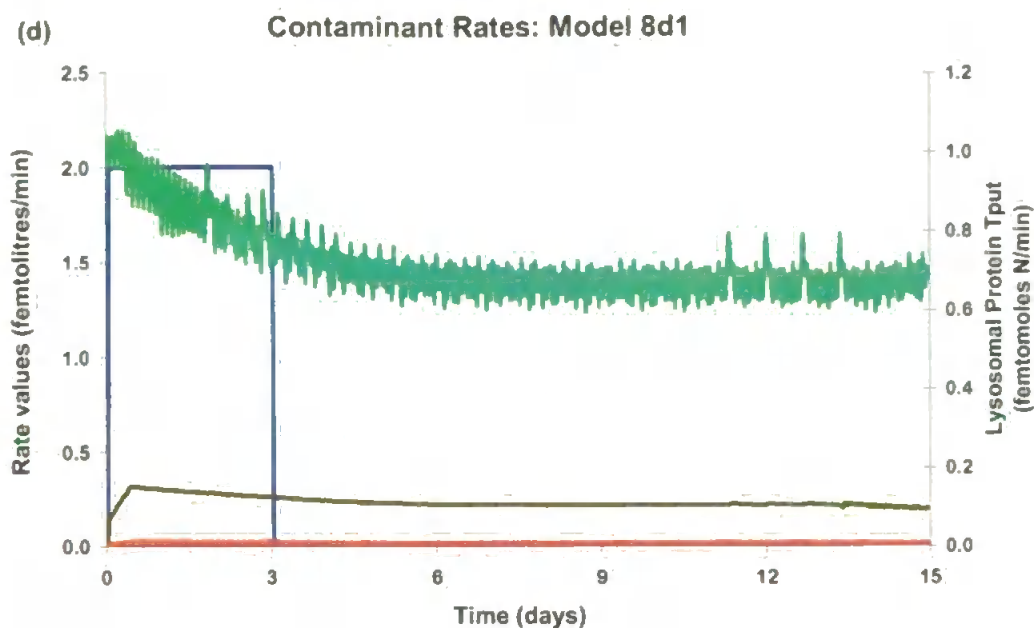


Fig 9.11 Model 8d1 continual exposure diffusion. (a) Volumes,  $-E_v$ ,  $-L_v$ ,  $-C_v$ ,  $-Cell_v$  (b)  $-$  relative lysosomal volume,  $-$  lysosomal stability (c) Contaminant contents  $-L_{xcon}$ ,  $-C_{xcon}$ ,  $-RB_{xcon}$  &  $-Cell_{xcon}$ , Cumulative contaminant In  $-$  & Out  $-$  (d) Contaminant rates  $-k_{diffC}$ ,  $-k_{autC}$ ,  $-k_{RBC}$  &  $-LPxnTput$ .

The cell volume declined until 2 days into the recovery period, due to the continued presence of contaminant in the cytosol and the damage it was causing (Figs 9.11a & c). Lysosomal throughput follows a similar pattern, due to the lysosomal contaminant content damaging the digestive enzymes (Fig 9.11d; Moore *et al.*, 2007). 3.36 times as much contaminant enters the cell when compared with the previous model with the same parameter values (Table 9.1). The retention of the contaminant in the cytosol prevented the lysosomal throughput from falling sufficiently to swell the lysosome to the observed size despite the enhanced autophagy (Fig 9.11b).

In a comparison of this and the previous model, both showed the cell retaining contaminant by the end of the experiment. If the cell were taken to have a density of 1.03g/ml and the water in the cell accounts for 6/7 of the weight: then the latest model cell would have, after three days exposure, added approximately 28 times the exposure concentration, which is significantly higher than the previous models (Table 9.2).

*Table 9.2 Comparison of Model 8c2 and 8d1.*

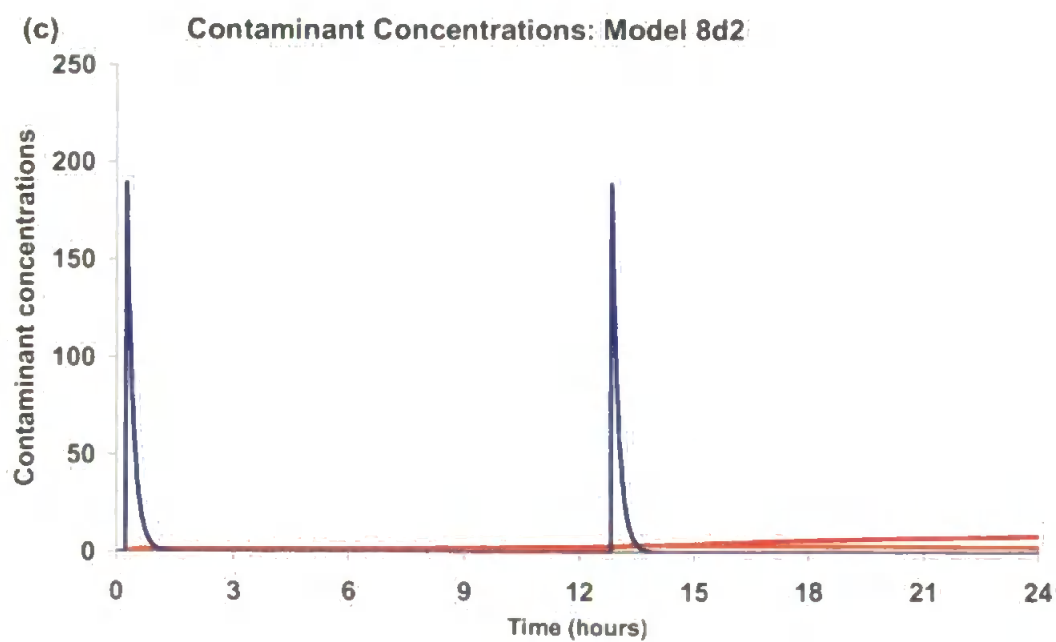
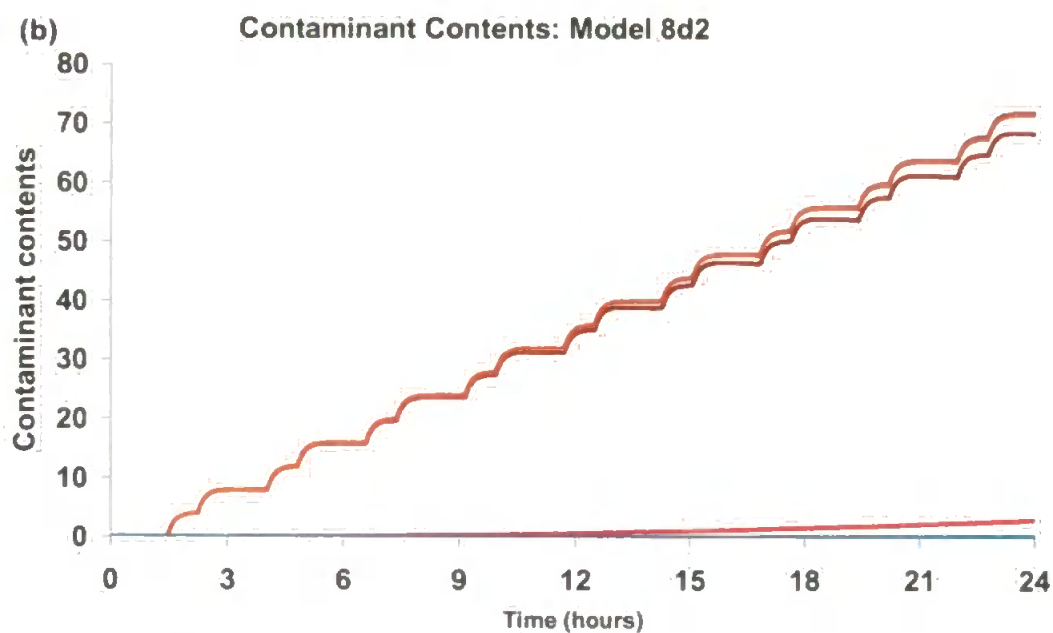
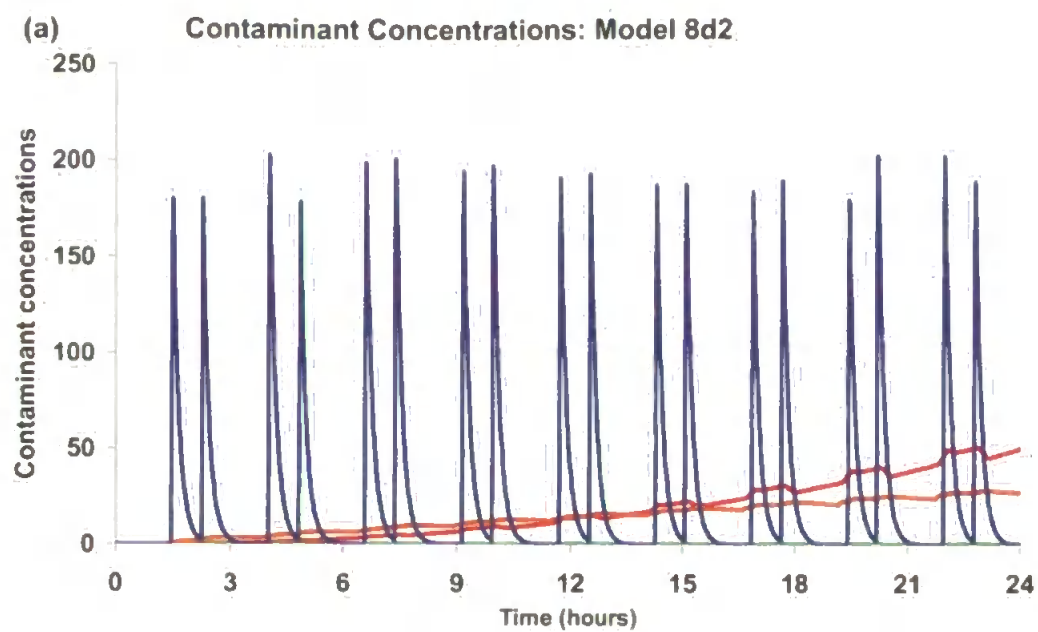
Variable name	Model 8c2	Model8d1
$Cell_{con}(15)/S_{con}$	0.14	1.24
$Cell_{con}(max)/S_{con}$	1.24	4.38
Contaminant In	0.5135	1.7278
Contaminant Out	85.5%	75.8%
$Cell_v(min)/Cell_{vmax}$	60.85%	60.24%

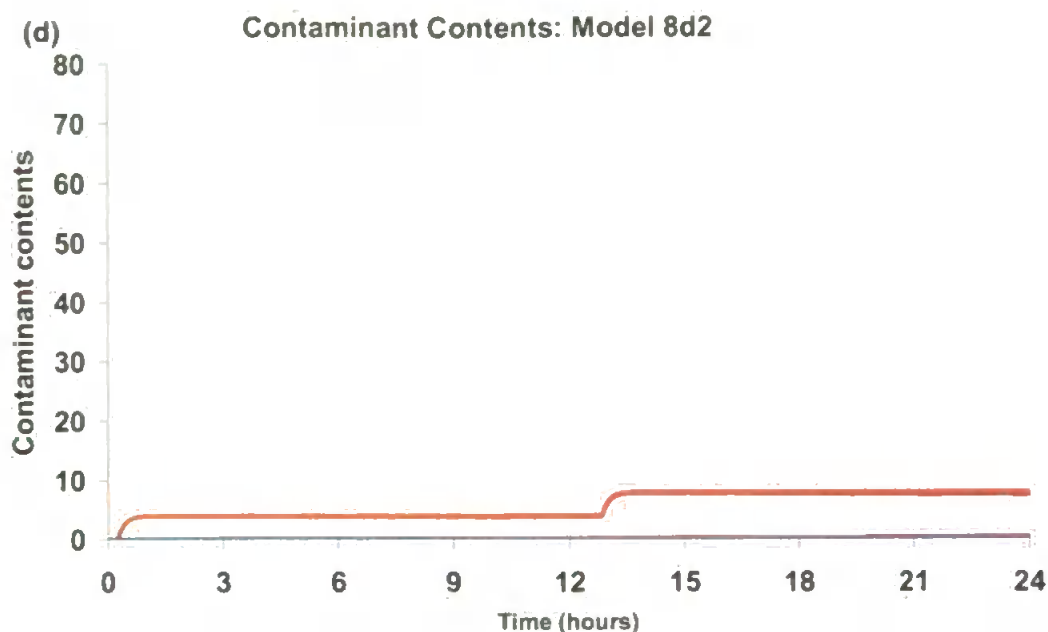
Even with these amendments, the issue of contaminant entry was not yet complete. As has been shown, a starved mussel will decline in volume at a greater rate than a fed mussel, which should boost the concentrations therein, but the phenanthrene minus food treatment results in a slightly lower internal contaminant concentration (Bayne *et al.*, 1978). It has been proposed that recovery of the lysosomal stability is due to the relative rapidity with which an unfed cell can deal with the contaminant; but what could also affect this is the relative amount of contaminant entering the cell.



If, as proposed by the digestive tubule phase cycle, the tubule lumen were replenished at the beginning of the feeding phase with fresh luminal fluid/mucus and then flushed and replenished once more at the end of the disintegrating phase; then the length of the particular phases would partly determine how much of the contaminant in the lumen would diffuse into the cell. As this has been designated a one way flow, then as the period between flushes extended there would be less contaminant in the tubule phase. For the feeding cell this would occur at regular intervals. However, for the unfed cell the resting phase was greatly extended and there was no feeding phase, thus making the relative time between fresh, contaminant-rich, extracellular, luminal fluid/mucus far longer and possibly decreasing the amount presented to the cell.

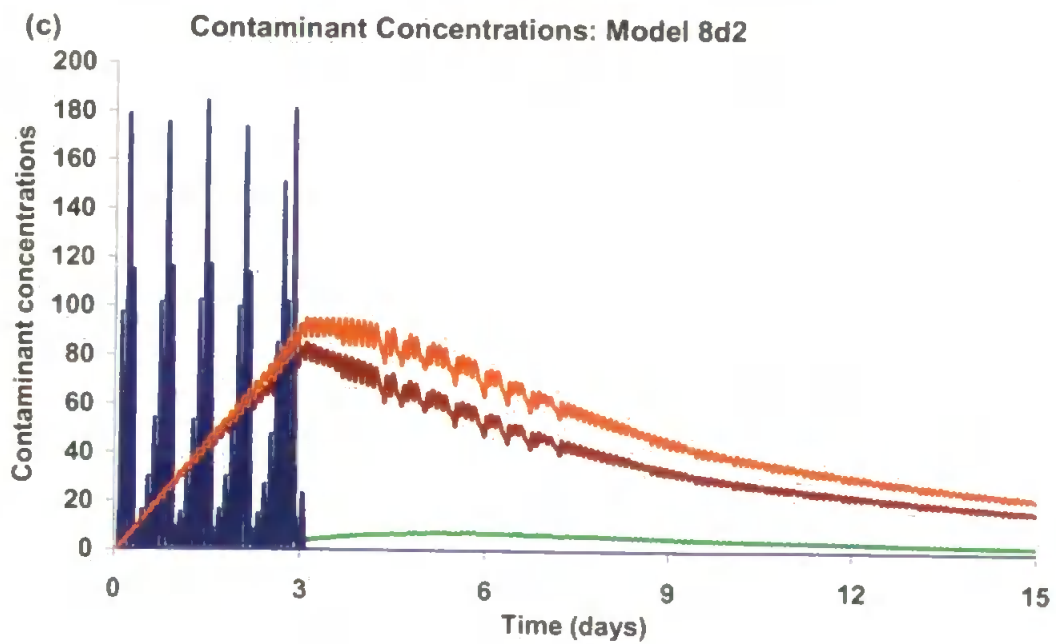
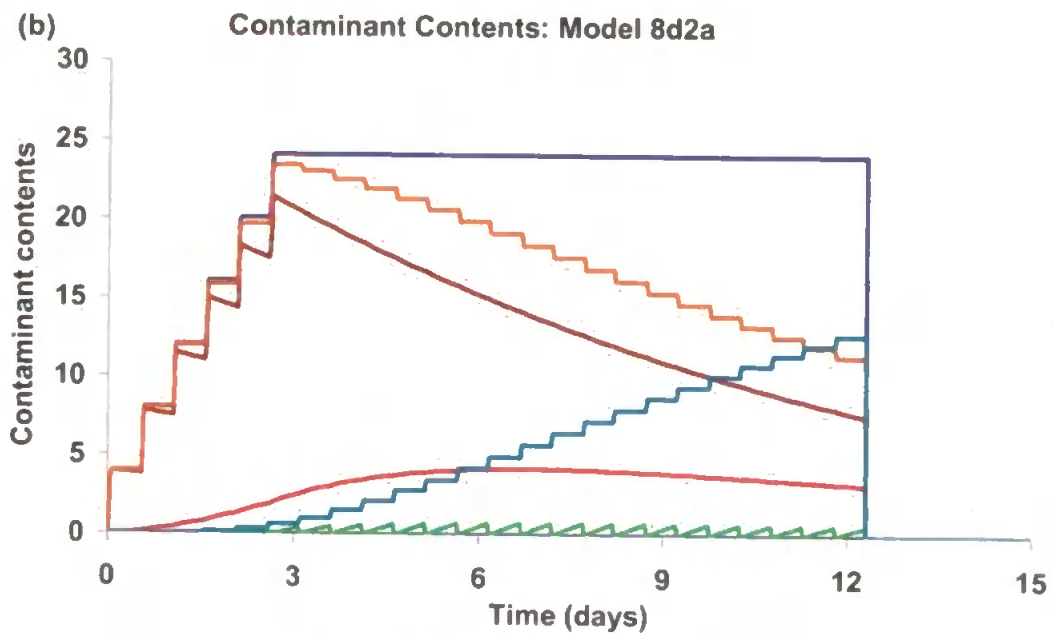
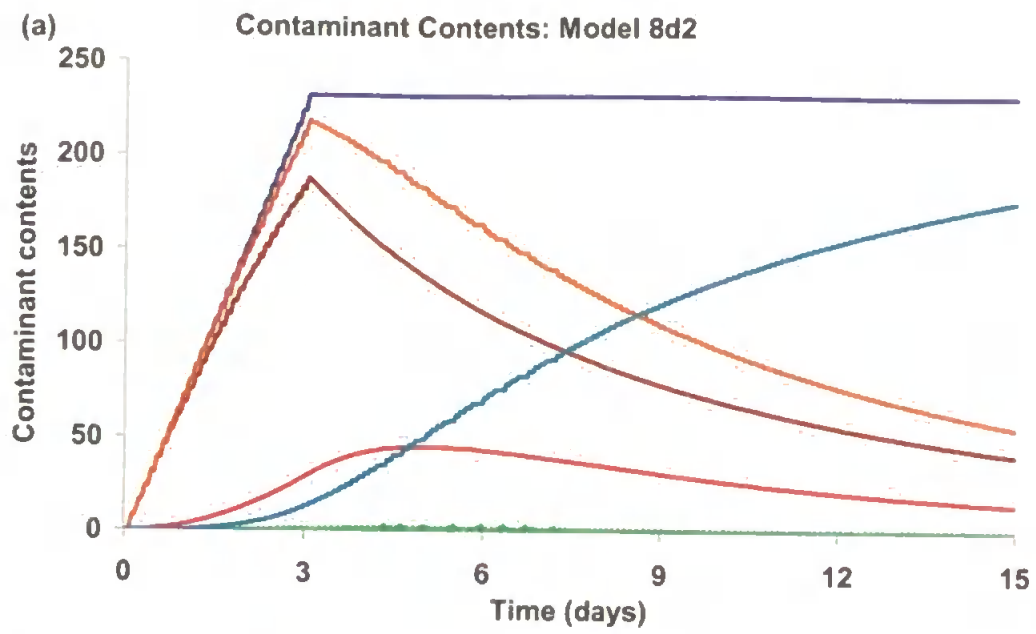
Model 8d2 implemented this idea by calculating the tubule lumen volume and contaminant content at these points in the phase cycle and updating them as they progress to the next recharging point. Model 8d2a was exactly the same, except with the extra stress of starvation imposed.





*Fig 9.12 Recharging tubule lumen model fed 8d2 (a & b) and starved 8d2a (c & d): — surface, — lysosome, — cytosol & — cell (a&c) Contaminant concentrations (b&d) compartmental contaminant contents.*

For the fed animal, the recharging of the tubule occurred 18 times during the first day of exposure compared to just twice for the starved animal (Figs 9.12a & c). This resulted in a much greater amount of contaminant entering the cell for the fed over the starved treatments (Figs 9.12b & d). The refreshment of the tubule was followed rapidly by a decrease in surface contaminant concentration due to the rate of uptake. Whilst feeding, the rate of surface contaminant concentration was slightly less than during the resting period, as the cell pushed into the tubule lumen, but the effect was only marginal. Even whilst feeding the greater length of the resting phase is such, that all of the contaminant was taken into the cell during this part of the phase cycle.



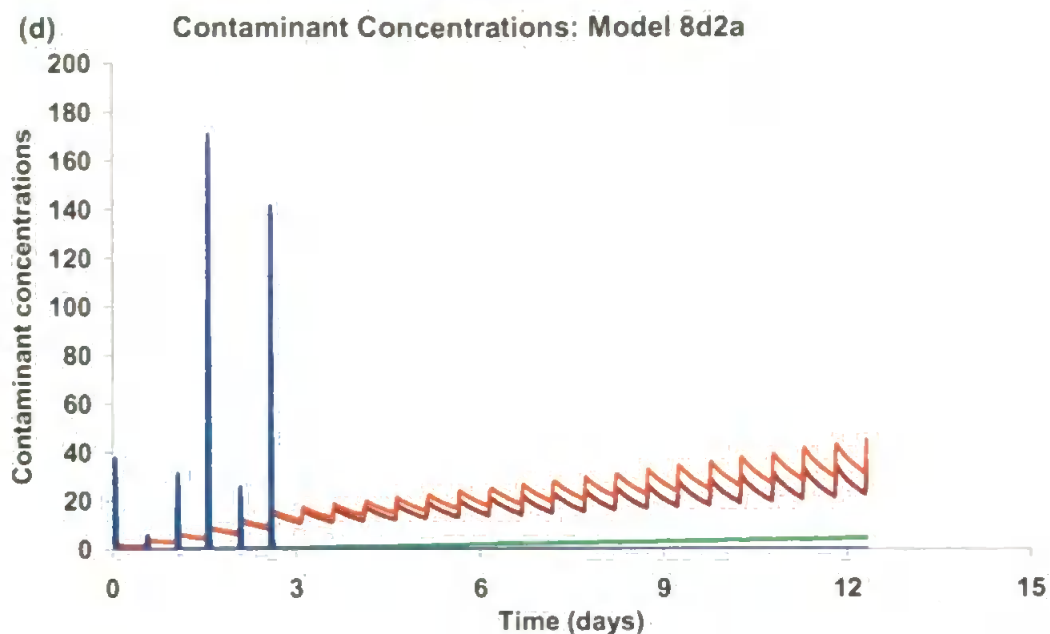


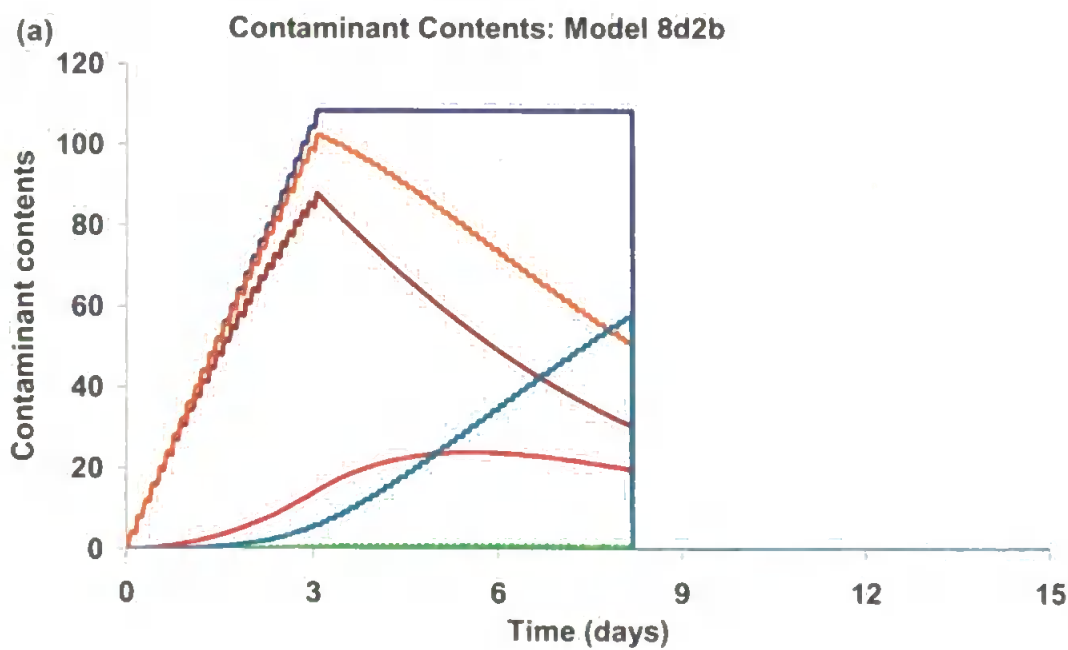
Fig 9.13 Recharged lumen tubule models fed 8d2 (a & c) & starved 8d2a (b & d). (a & b) Contaminant concentrations —  $S_{con}$  —  $L_{con}$  —  $C_{con}$  —  $RB_{con}$  & —  $Cell_{con}$  (c & d) contaminant contents —  $L_{xcon}$  —  $C_{xcon}$  —  $RB_{xcon}$  & —  $Cell_{xcon}$ , Cumulative contaminant In — & Out —.

Inevitably, the starved cell died before the end of the simulation but the major contributory effect was due to the starvation and not contaminant exposure. The fed cell did not significantly lose cellular volume during the simulation, although during days 6-9 the average volume fell to 94.3% of the unexposed average. The lysosomal relative volume peaked at day 3 but only at 3% of cell volume which barely registered as a perturbation to the lysosomal stability. The lysosomal stability of the starved cell slowly decreased until its expiry but even then, it only fell to 20.6 minutes, which was well within the healthy part of the spectrum.

By the end of the exposure period the starved cell had taken on only 10.39% of the contaminant load as compared with that of the fed cell due to

the recharging algorithm (Figs 9.13a & b). The rate of decrease in volume of the starved cell was not sufficient to make its cellular contaminant concentration (12.65) equal to that of the fed cell (92.13) by the end of the exposure (Figs 9.13c & d). In order to allow more contaminant in, the next submodel decreased the resting phase maximum when not feeding to 150 minutes.

With the lower resting phase the starved cell took on 46.8% of the contaminant compared to the fed cell (Figs 9.13a & 9.14a). The starved cellular contaminant concentration at the end of the exposure period was, however, now comparable to that of the fed cell (Figs 9.13c & 9.14b). However, the cell now reached its deletion point (cell death) even earlier than before, due to the increased cytosolic damage. Hence a drip feed as detailed for Model 8a2 was assimilated into the next model to impose survival for both fed and unfed cells.



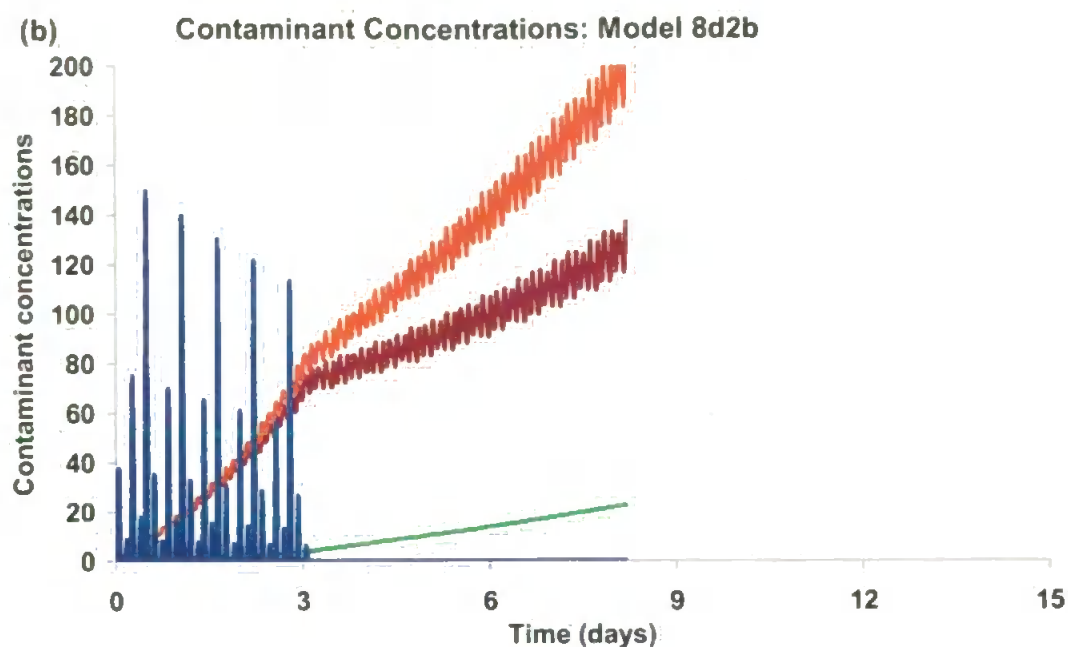


Fig 9.14 Model 8d2b starved mussel with maximum resting phase reduced to 150mins (a) Contaminant concentrations —  $S_{con}$ , —  $L_{con}$ , —  $C_{con}$ , —  $RB_{con}$  & —  $Cell_{con}$  (b) contaminant contents —  $L_{xcon}$ , —  $C_{xcon}$ , —  $RB_{xcon}$  & —  $Cell_{xcon}$ , Cumulative contaminant In — & Out —.

The overall concentration deficit between experiment and simulation was significant, as there had been very little exit from the cell of any contaminant by the end of the exposure period. Disregarding this discrepancy the cytosolic damage, *ConDam*, invoked by contaminant concentration was doubled and the residency time in the cytosol of contaminant was increased by halving *conaut*.



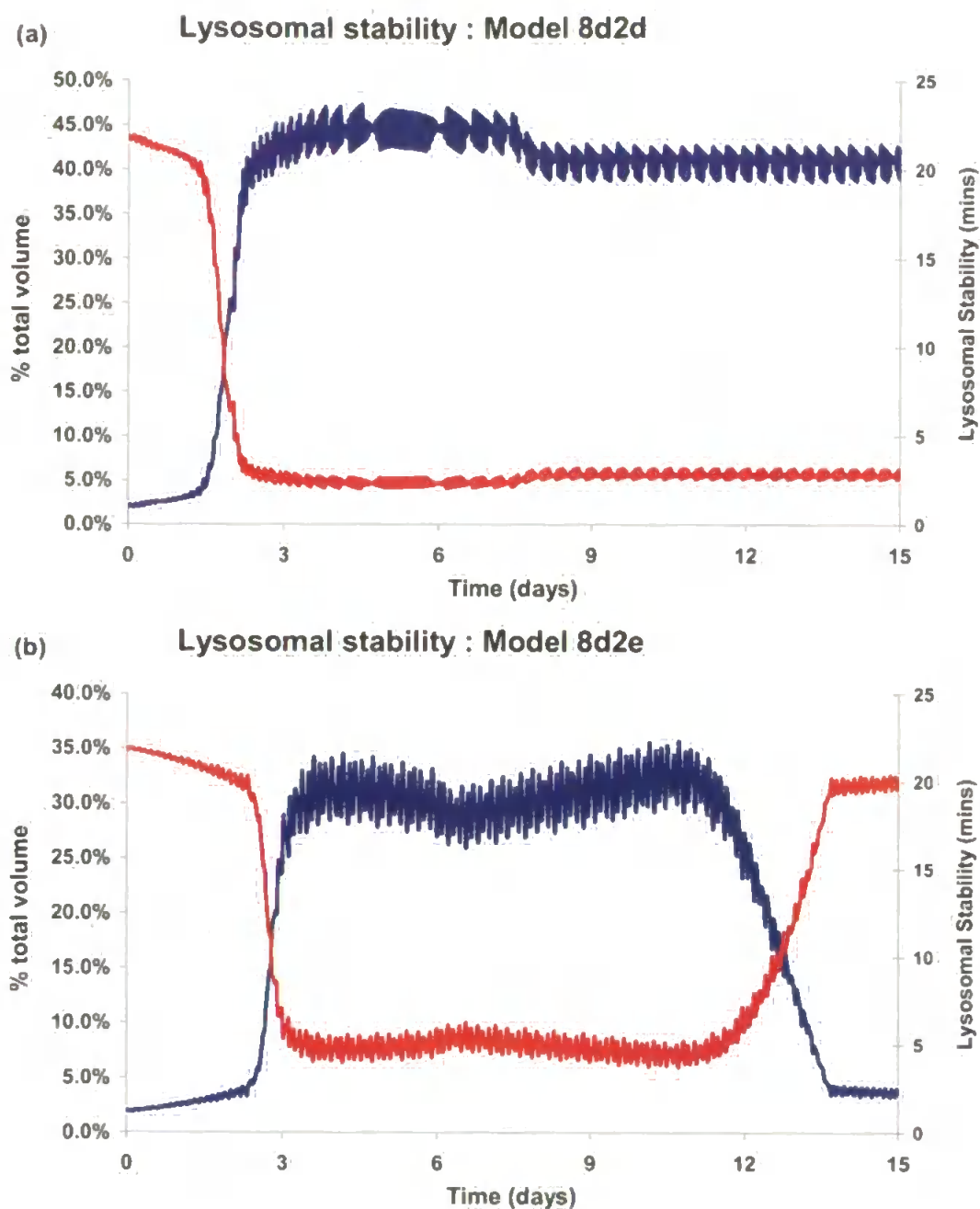


Fig 9.15 Double contaminant cytosol damage and residency. — lysosomal relative volume — lysosomal stability (a) fed Model 8d2d (b) starved Model 8d2e.

With respect to the fed cell, by doubling the amount of damage done by the cytosolic contaminant and increasing its residency in the cytosol, the lysosomal stability rapidly reached a minimum value before the end of the exposure period, from which it only very slowly recovered (Fig 9.15a) and



can be considered a reasonable reflection of the observed experimental results.

The lesser concentration in the unfed cell's cytosol reduced the rate of lysosomal instability decrease, but it too reached a hazardous minimum around the end of the exposure period (Fig 9.15b). However, the reduced concentration allowed the cell to recover lysosomal stability by the end of the simulation as in the real experiment (Moore, 2004).

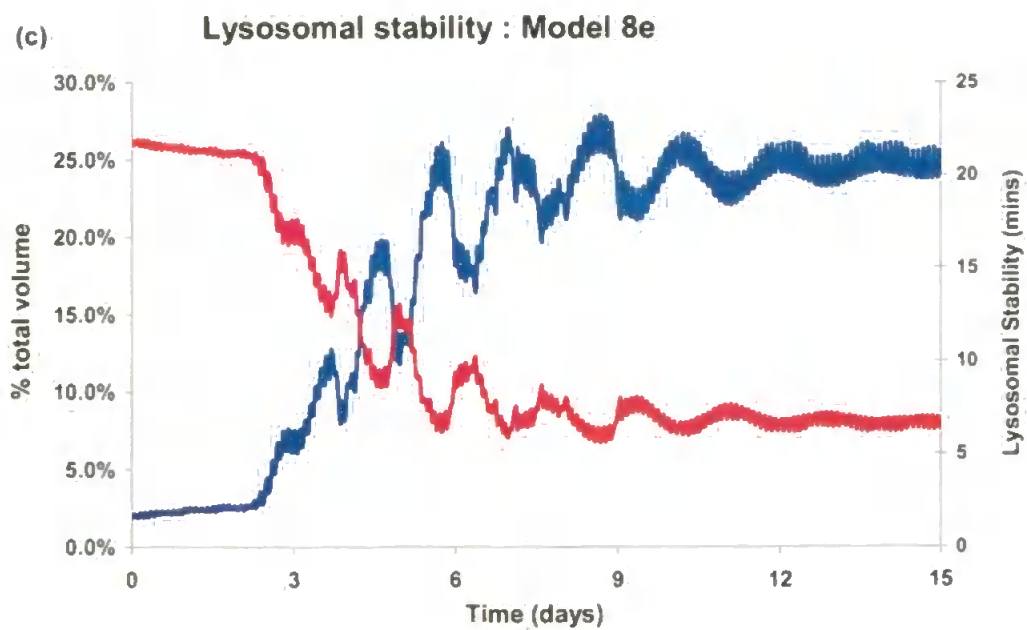
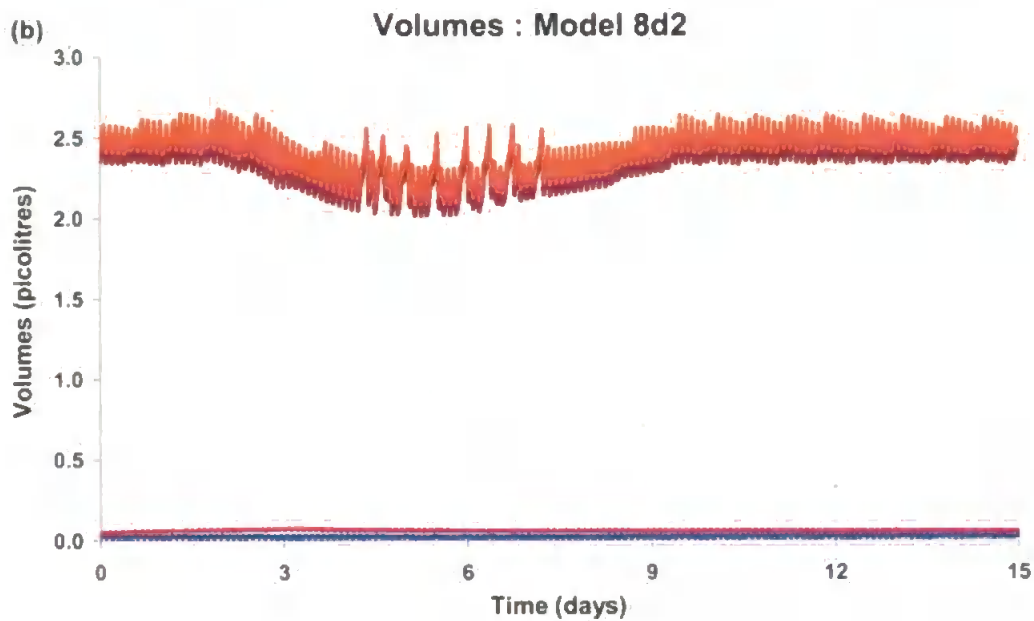
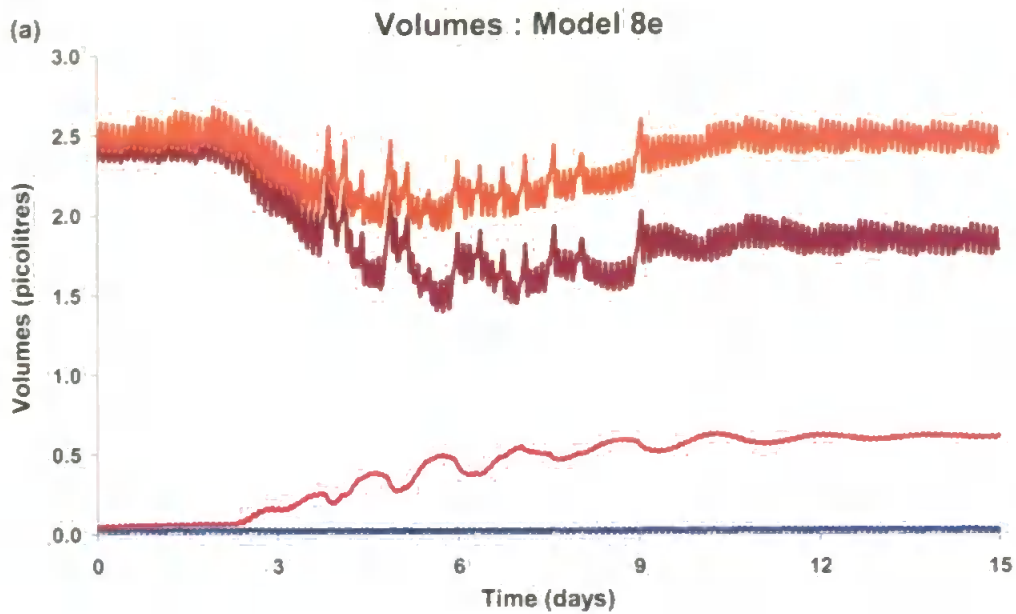
### 9.7 Lysosomal damage & release: Model 8e

As has been noted, the lysosomal throughput was dependent upon the lysosomal enzyme concentration, which was reduced by a basal rate of damage and replenished in the resting phase of the phase cycle. The current contaminant model enhanced the amount of damage done to these enzymes dependent on the lysosomal contaminant concentration. This was updated for Model 8e so that the varying degrees of damage to the lysosomal enzymes could be assessed, by introducing a new parameter, *LysConDam* (Eqn 9.20).

$$DamFactor = \begin{cases} 1 + MIN(LysConDam, L_{con} / 100) & \text{IF } L_{con} > 0 \\ 1 & \text{Otherwise} \end{cases} \quad [9.20]$$

In all models to date this had been set to *LysConDam* = 1. Model 8e made *LysConDam* = 5 and reverted to *ConDam* = 2.5 and *ConAut* = 0.1.

When Model 8d2 was run, with the same cytosolic parameter values as used for Model 8e, it exhibits an insignificant level of cell volume change (Fig 9.16b). Significantly however the lysosomal volume did not increase radically, producing a very weak lysosomal response. With the increased lysosomal damage, there was still no significant loss in cell volume; but there was a much more marked increase in relative lysosomal volume (Fig 9.16a). Hence, the radical change in lysosomal stability behaviour (Fig 9.16c).



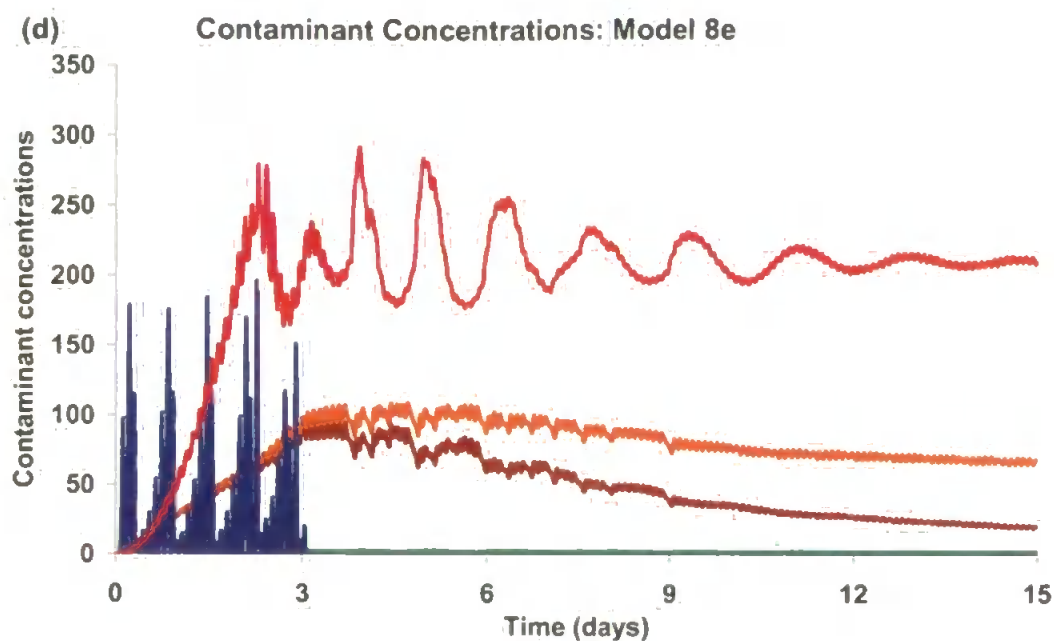


Fig 9.16 Increased Lysosomal damage Model 8e. (a & b) volumes ( (a) Model 8e & (b) Model d2),  $-E_v$ ,  $-L_v$ ,  $-C_v$ ,  $-Cell_v$  (c)  $-$  relative lysosomal volume,  $-$  lysosomal stability (d) Contaminant concentrations, in arbitrary units,  $-S_{con}$ ,  $-L_{con}$ ,  $-C_{con}$ ,  $-RB_{con}$  &  $-Cell_{con}$

The oscillatory nature of the lysosomal volume was due to the periodic replenishment of the lysosome with new digestive enzymes which temporarily increased the lysosomal throughput (Fig 9.16a). The increased damage, however, soon returned this to a lower value over the course of the simulation until a stable situation was attained around day 12. The increased lysosomal damage also reduced the release of material to the residual bodies, which was also the outlet for contaminant from the lysosome. This increased the lysosomal concentration, but as this quickly exceeds the minimum requirement for the damage rate to be capped, the injurious effects were not compounded (Fig 9.16d).

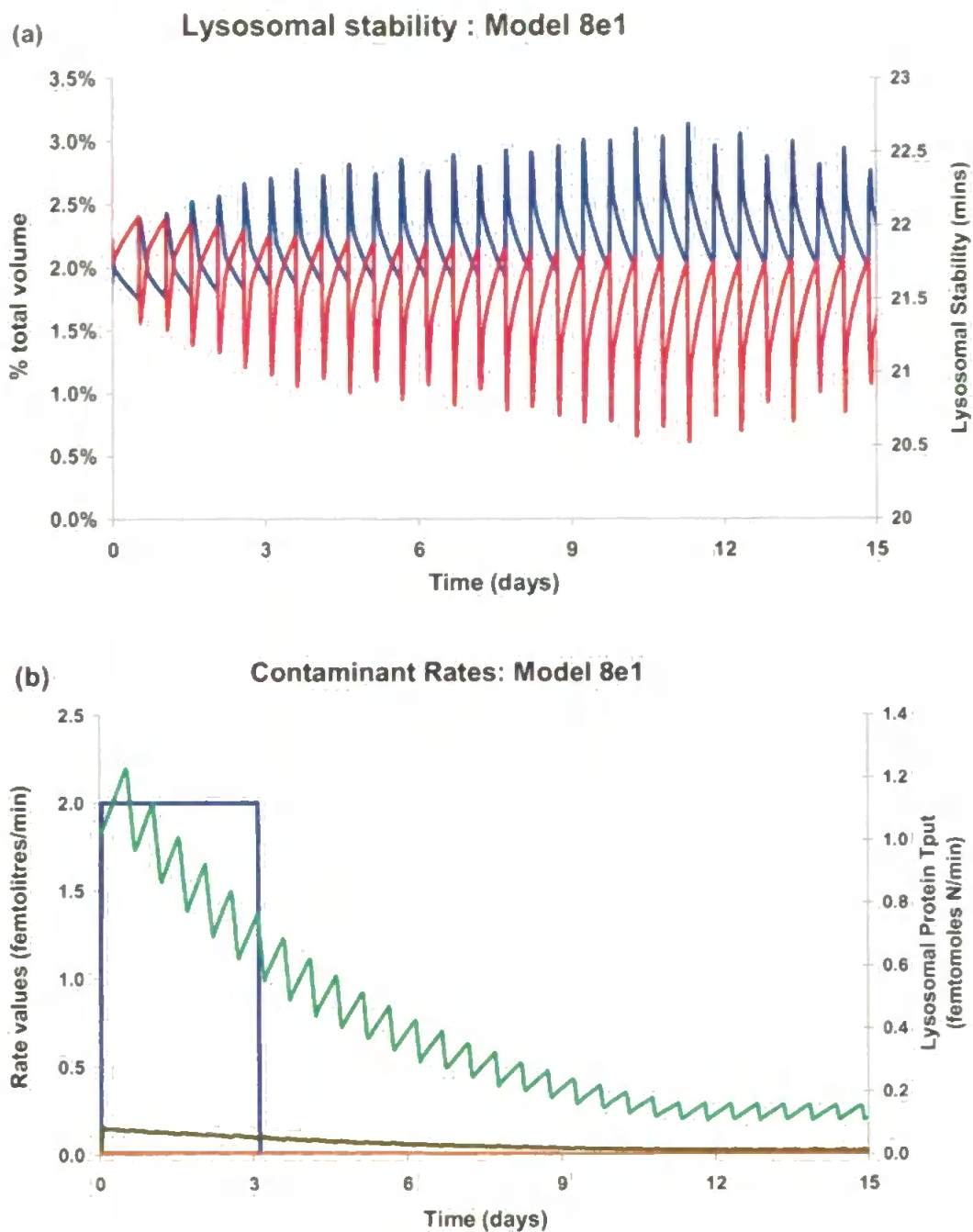


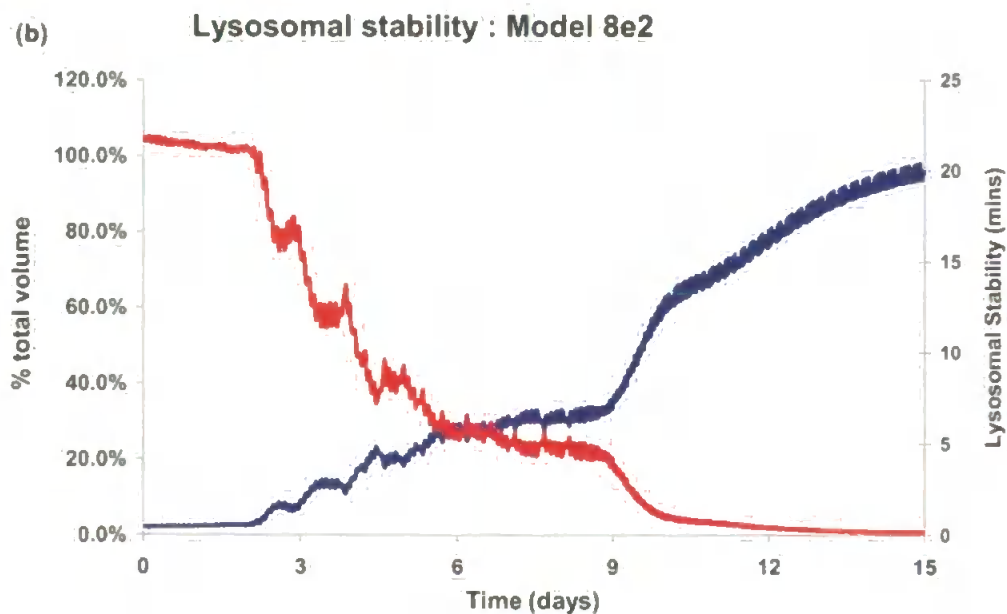
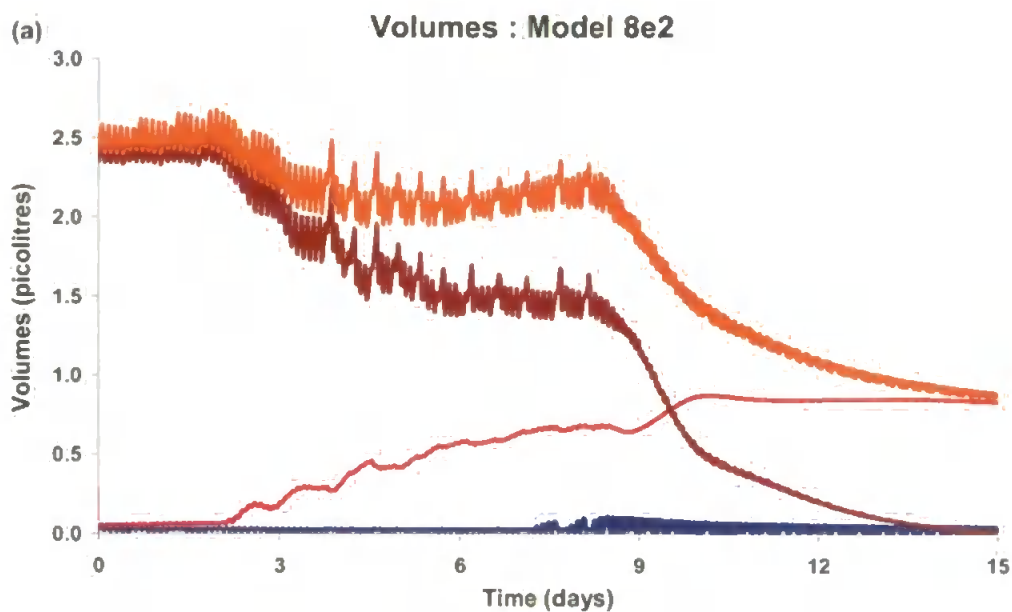
Fig 9.17 Model 8e1 starved simulation with increased lysosomal damage

(a) — relative lysosomal volume, — lysosomal stability (b) contaminant rates —  $k_{difC}$ , —  $k_{autC}$ , —  $k_{RBC}$  & —  $LP_{xnTput}$ .

By comparison, Model 8e1 without food showed that, despite the increased lysosomal damage and concomitant decrease in lysosomal throughput (Fig 9.17b), the cellular behaviour invoked does not adequately

replicate the experimentally observed pattern. Lysosomal stability remained well within the 'healthy' range of possible values (Fig 9.17a)

Once again the residency time of the contaminant in the compartment under scrutiny affected the nature of the disabling effects. In order to adjust the residency time in the lysosome a new parameter, *ConRB*, was defined as the rate of contaminant flow from lysosome to residual body relative to the flow of other material.



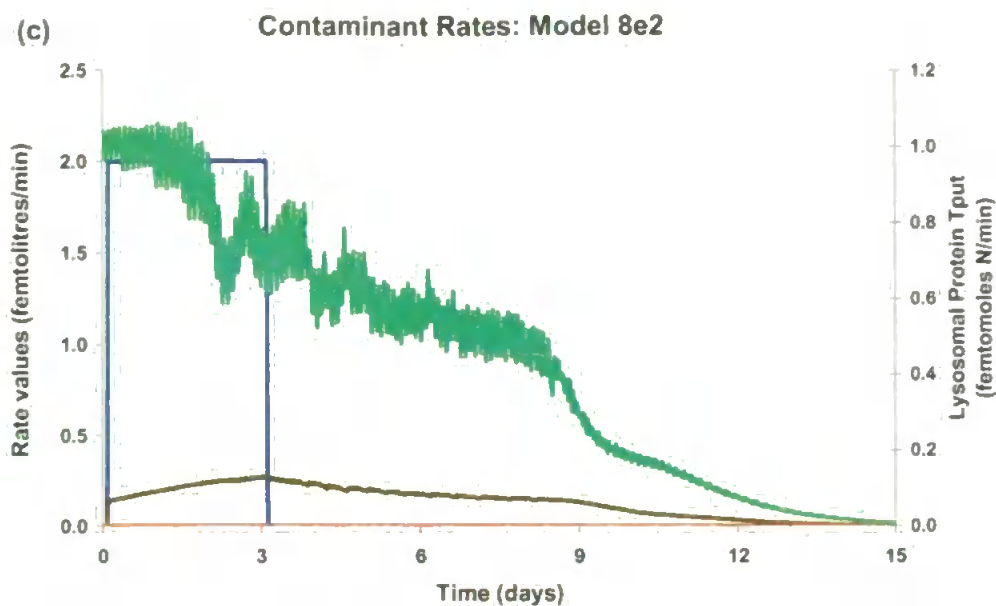


*Fig 9.18 Model 8e2 tenfold reduction in lysosomal to residual body contaminant flow,  $ConRB = 0.001$ . (a) Volumes —  $E_v$ , —  $L_v$ , —  $C_v$  & —  $Cell_v$  (b) — relative lysosomal volume, — lysosomal stability (c) contaminant rates —  $k_{diffC}$ , —  $k_{autC}$ , —  $k_{RBC}$  & —  $LP_{xn}T_{put}$ .*

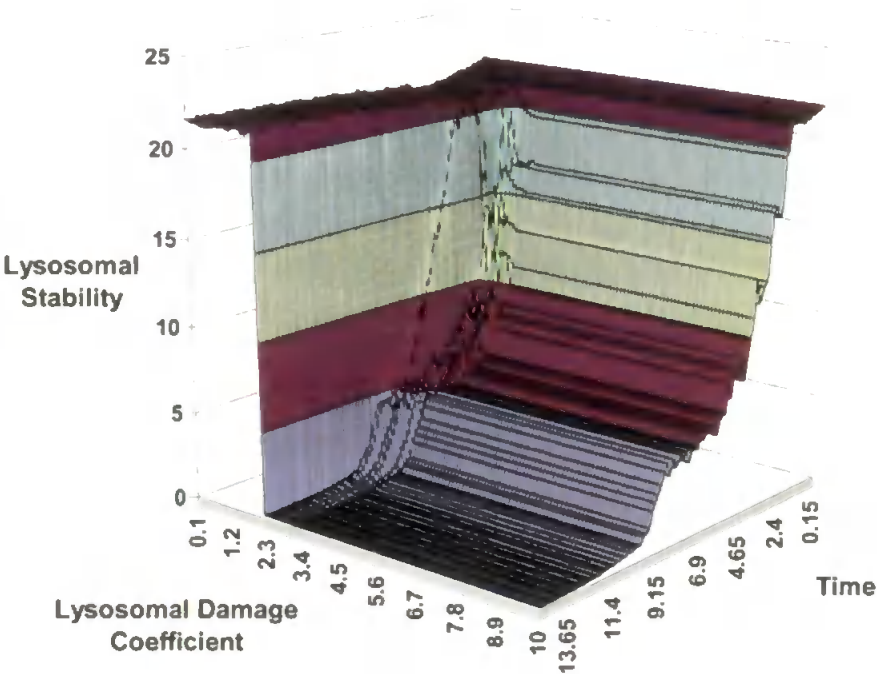
With the lysosomal flow reduced by a factor of ten from the previous model, the cell eventually reached an unsatisfactory state with almost all of its volume being lysosomal (Fig 9.18a). This was due to endocytosis being switched off once the lysosome swelled too much. As soon as this occurred, with the increased lysosomal damage and subsequent throughput decline (Fig 9.18c), the cell entered into a state of inevitable decline. Consequently, the lysosomal stability (Fig 9.18b) also declined to terminal levels.

A sensitivity analysis of the lysosomal stability, over time and a range of lysosomal damage coefficients, was performed (Fig. 9.20) to



determine the effect of two different rates of flow between lysosome and residual bodies.

(a)



(b)

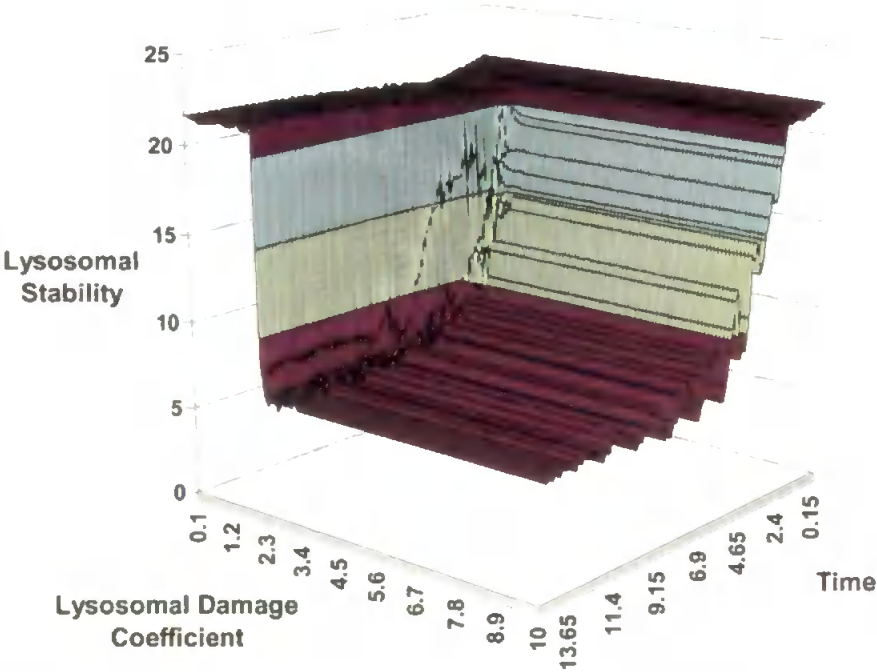


Fig 9.19 Model 8e3 lysosomal stability (minutes) over time (days) and varying lysosomal damage coefficients for (a)  $ConRB = 0.001$  (b)  $ConRB = 0.01$



This sensitivity analysis, predictably, revealed that the rate of contaminant removal from lysosome to the residual bodies was essential to the continued survival of the cell. If the value was too low (Fig 9.19a) then the cell generally declined to the state seen in the previous simulation (Fig 9.18a); if the value was an order of magnitude higher the lysosome did not become dominant (Fig 9.19b). Equally, it was evident that there was a clear cut off point for the factor multiplying the lysosomal damage: on one side of this threshold the lysosomal stability was unaffected; whilst on the other side of this threshold all values led to the decline of the lysosomal stability to some minimum value.

### 9.8 Cellular contaminant defence: Model 8f

To this point, there has been no regard given to any 'defensive' cellular reaction to toxic insult. The only method of elimination introduced has been via exocytosis but there are cellular systems which mitigate the damaging effects of contaminants. Cytochrome P4501A is involved in the biotransformation of organic contaminants (Shaw *et al.*, 2004) and one of the functions of metallothioneins is in the detoxification of non-essential metals (Viarengo, 1985).

An attempt to introduce such systems was made by incorporating a varying base level of contaminant concentration which the cell can comfortably deal with. The level of damage induced, as a response to contaminant exposure, had been capped for high concentrations; but prior to a certain level being attained it had risen linearly. The level at which this cap occurs had, up to this point, been arbitrarily set at 100 for both cytosol and lysosome. Two new base levels were introduced, *LysBase* & *CytBase*, which were originally set equal to 100. Thereafter at the start of every resting phase these figures are re-evaluated by the following method.

$$NewCytBase = \begin{cases} 1.5 \times OldCytBase & \text{IF } Ccon \geq OldCytBase \\ MAX(100, 0.9 \times OldCytBase) & \text{Otherwise} \end{cases} \quad [9.21]$$

$$NewLysBase = \begin{cases} 1.5 \times OldLysBase & \text{IF } Lcon \geq OldLysBase \\ MAX(100, 0.9 \times OldLysBase) & \text{Otherwise} \end{cases} \quad [9.22]$$

These factors were then applied to the damaging variables as follows:

$$DamFactor = \begin{cases} \frac{LysConDam \times L_{con}}{NewLysBase} + 1 & \text{if } L_{con} > 0 \\ 1 & \text{Otherwise} \end{cases} \quad [9.23]$$

$$ContaminantBoost = \begin{cases} \frac{ConDam \times C_{con}}{NewCytBase} + 1 & \text{if } C_{con} > 0 \\ 1 & \text{Otherwise} \end{cases} \quad [9.24]$$

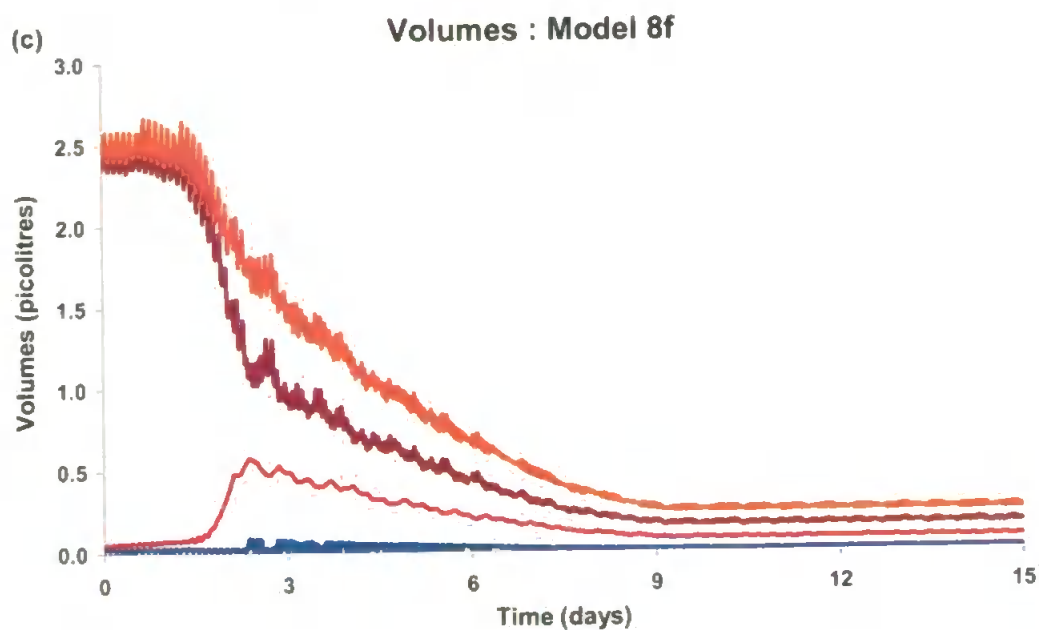
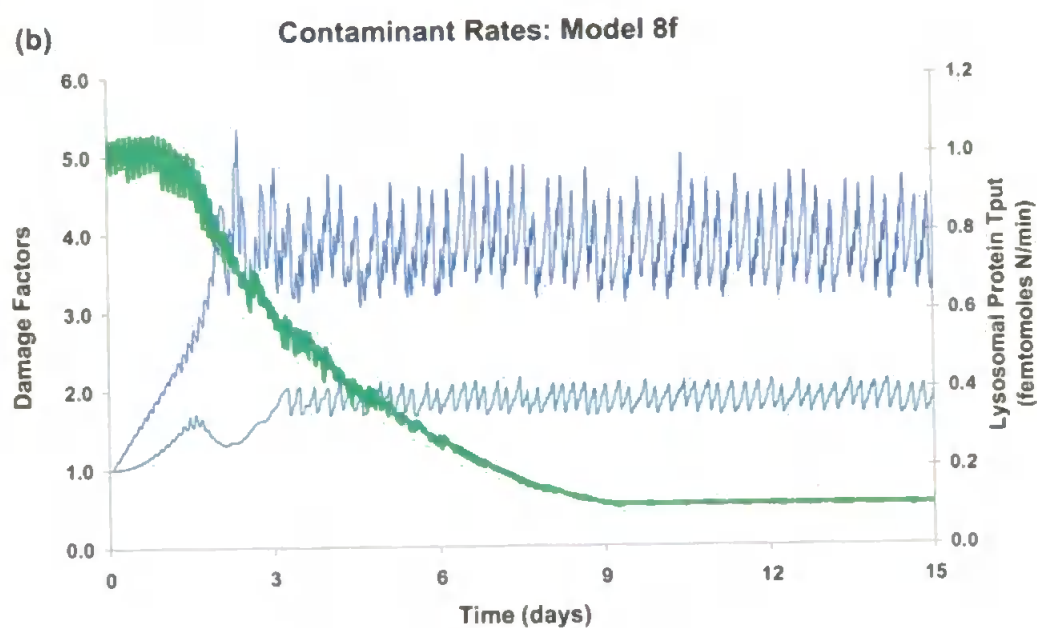
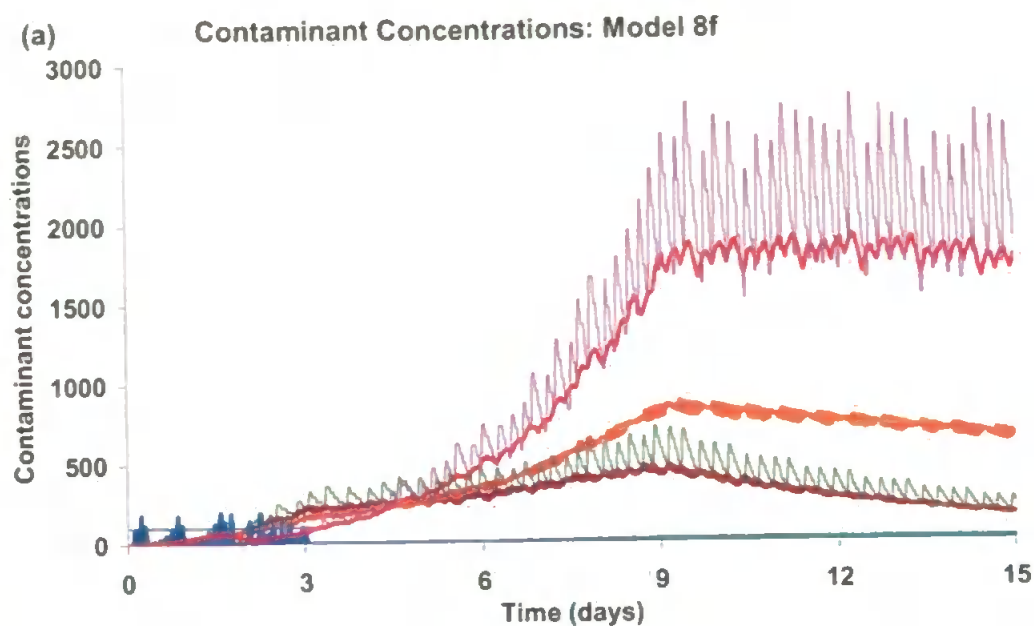
$$k_{CdamP} = 0.1\%CP_v \times ContaminantBoost \quad [9.25]$$

$$k_{LdamP} = 0.1\%LP_v \times DamFactor \quad [9.26]$$

$$k_{LdamL} = 0.1\%LL_v \times DamFactor \quad [9.27]$$

Model 8f was run with this system in place and the following parameter values  $LysConDam = 1$ ,  $ConDam = 3.5$ ,  $ConAut = 0.05$  &  $ConRB = 0.01$ . For almost all the exposure period the contaminant concentrations were below that of the initial base figures (Fig 9.20a), but the amount of damage increased over that period (Fig 9.20b). As the initial base figure was exceeded for the first time, the damage factors exceed those of the previous model. As more material was autophagocytosed there was an inevitable decrease in cell volume (Fig 9.20c) that increased the cytosolic contaminant concentration which caused the damage to increase still further (Fig 9.20a). The decline in actual, but not relative, lysosomal volume as the cell volume decreased augmented the lysosomal concentrations. However, the varying base algorithm enabled the cell to cope with this increase, due to its relatively slow rate of increase compared to that of the lysosomal base. This could be interpreted as the cell utilising

reserves to ensure the continued functioning of the central lysosomal system.



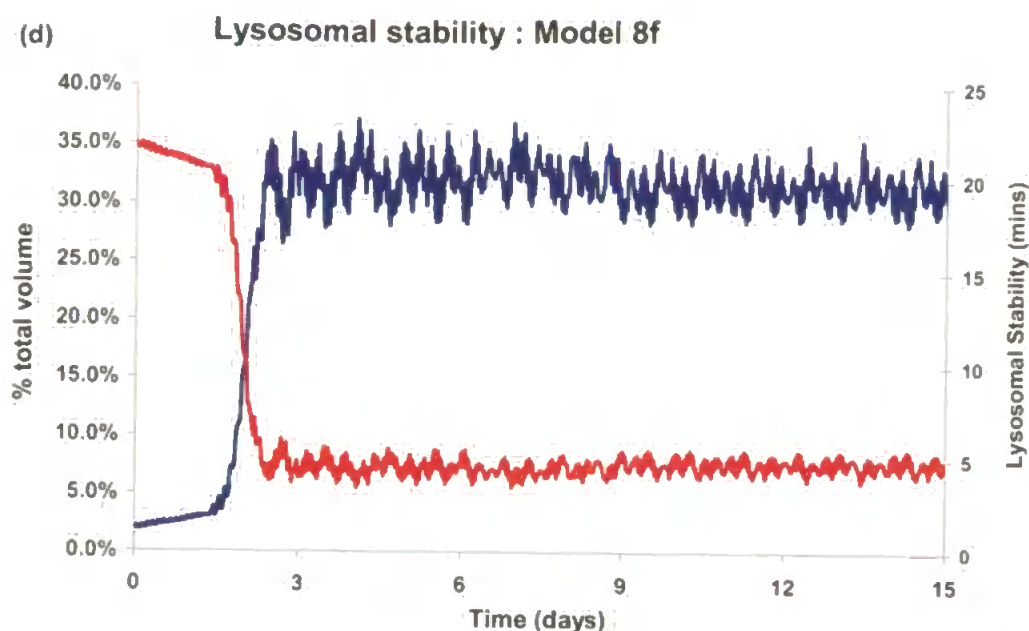


Fig 9.20 Model 8f varying cytosolic and lysosomal contaminant bases (a) Contaminant concentrations —  $S_{con}$ , —  $L_{con}$ , —  $C_{con}$ , —  $RB_{con}$ , —  $Cell_{con}$ , —  $LysBase$  & —  $CytBase$  (b) Contaminant factors — lysosomal damage, — cytosol damage & — lysosomal throughput (c) —  $E_v$ , —  $L_v$ , —  $C_v$  & —  $Cell_v$  (d) — relative lysosomal volume, — lysosomal stability.

The lysosomal stability was close to the observed behaviour (Figs 9.1a & 9.20d). But the survival 'drip-feed' mechanism was invoked around day 9 and endocytosis became intermittent due to lysosomal size. If continued, the model finally started to feed and regain volume 22 days after the start of the exposure, which coincided with the cytosolic contaminant concentration falling beneath the minimum base level. Full recovery of the cell to a 'normal' state was achieved quite rapidly, thereafter, as the lysosomal contaminant concentration declined with the drop in autophagy.

The continued response of the base algorithm to the varying concentration forced the multiplying damage factors to be relatively stable

around the maximum value. It was only this tendency to keep the damage boost around the maximum factor, that this implementation of a defence mechanism actually provided the cell.

So a further attempt, Model8f1, was made to create a defence system in the model cell. This time extra damage was only incurred if the compartmental contaminant concentration was greater than the base defensive value. The ability of the cell to upregulate the defensive value was lessened from the previous model to ensure that there was some response. The lysosomal upregulation of defensive capability was heightened in comparison to the cytosol to reflect the acidic environment of this organelle.

$$NewCytBase = \begin{cases} 1.1 \times OldCytBase & \text{IF } C_{con} \geq OldCytBase \\ MAX(100, 0.9 \times OldCytBase) & \text{Otherwise} \end{cases} \quad [9.28]$$

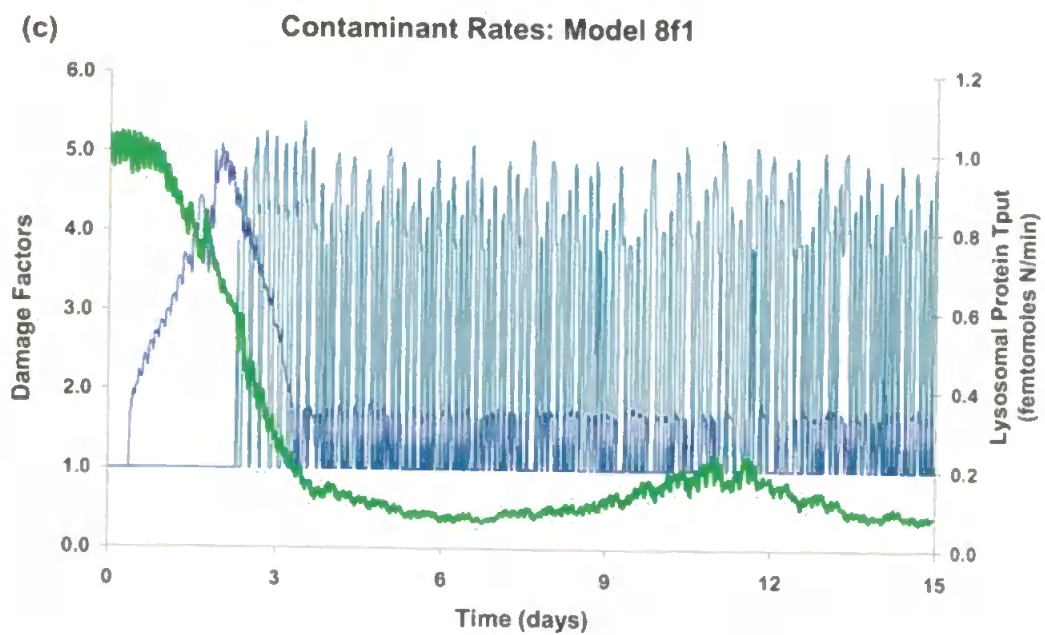
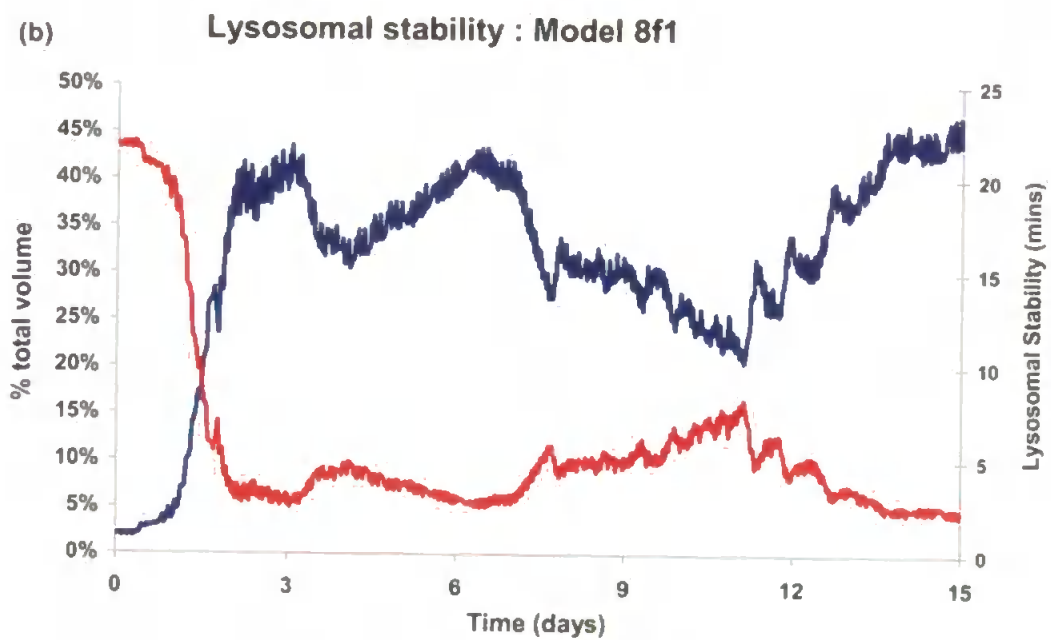
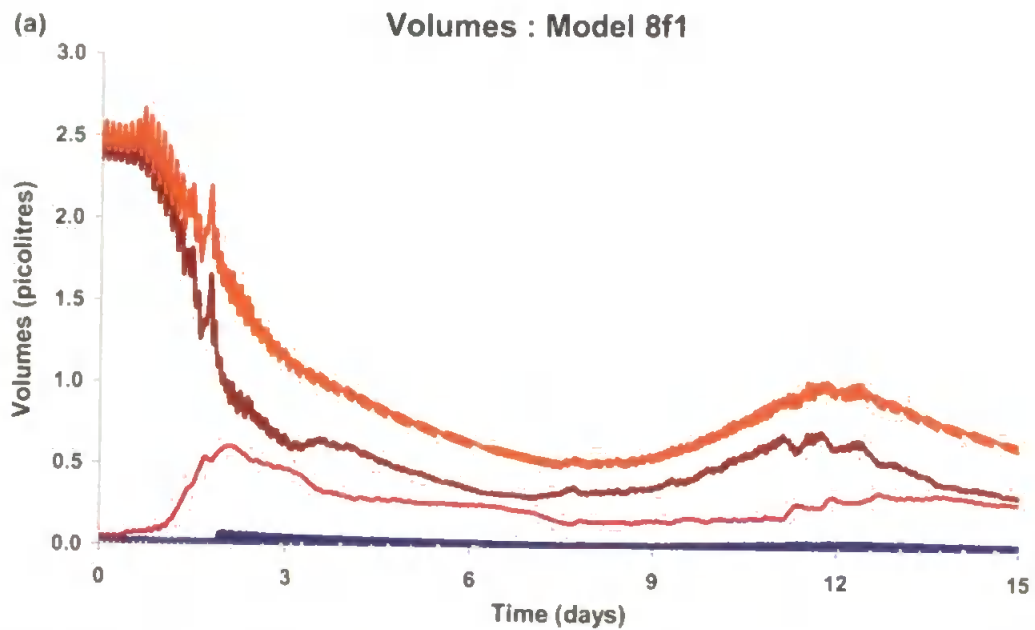
$$NewLysBase = \begin{cases} 1.25 \times OldLysBase & \text{IF } L_{con} \geq OldLysBase \\ MAX(100, 0.75 \times OldLysBase) & \text{Otherwise} \end{cases} \quad [9.29]$$

$$DamFactor = \begin{cases} \frac{LysConDam \times L_{con}}{NewLysBase} & \text{if } L_{con} > NewLysBase \\ 1 & \text{Otherwise} \end{cases} \quad [9.30]$$

$$ContaminantBoost = \begin{cases} \frac{ConDam \times C_{con}}{NewCytBase} & \text{if } C_{con} > NewCytBase \\ 1 & \text{Otherwise} \end{cases} \quad [9.31]$$

The following parameter values were used in the next simulation:

$LysConDam = 3.75$ ,  $ConDam = 1.625$ ,  $ConAut = 0.01$  &  $ConRB = 0.01$ .





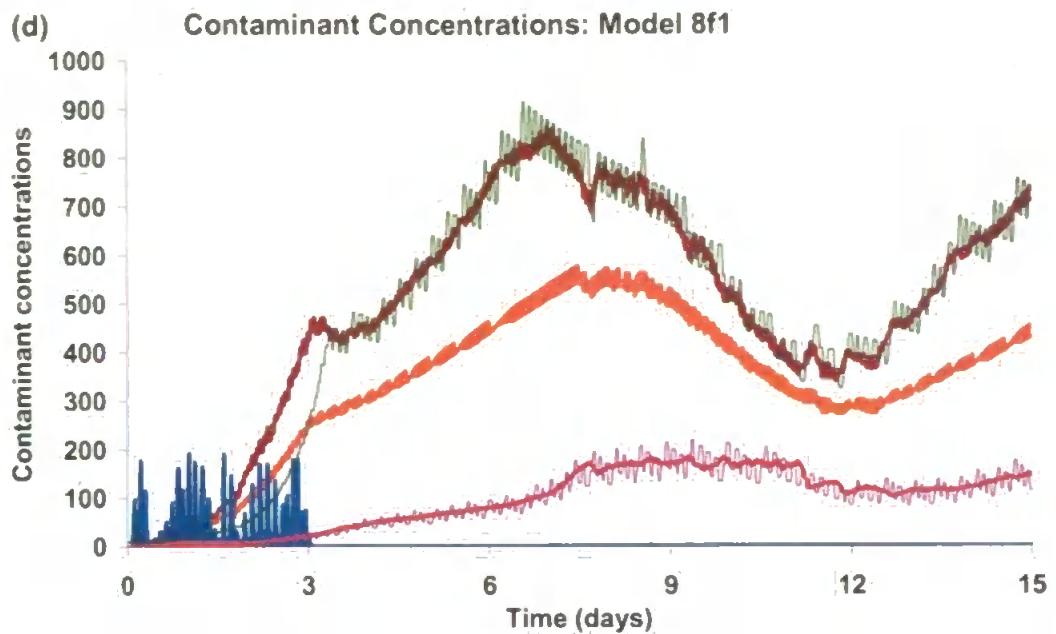


Fig 9.21 Model 8f1 below base defensive value precludes damage boost.

(a) Volumes —  $E_v$ , —  $L_v$ , —  $C_v$  & —  $Cell_v$  (b) — relative lysosomal volume, — lysosomal stability (c) Contaminant factors — lysosomal damage, — cytosol damage & — lysosomal throughput (d) Contaminant concentrations —  $S_{con}$ , —  $L_{con}$ , —  $C_{con}$ , —  $RB_{con}$ , —  $Cell_{con}$ , —  $LysBase$  & —  $CytBase$ .

There was an initial period when the extant basal cellular defence systems were able to cope with the incoming contaminant. The cytosolic system was the first to be overwhelmed, as the contaminant concentration increased rapidly the defence values increasing beneath this rate allowed for an initial burst of severe damage, which was reflected in the decrease in cell volume (Fig 9.21a) and increase in relative lysosomal volume. This provoked a much sharper decrease in lysosomal stability during the exposure period (Figs 9.20d & 9.21b). However, once the exposure period was over cytosolic concentrations diminish (Fig 9.21d) and the cytosolic damage, thereafter, was markedly reduced (Fig 9.21c). The lysosomal

defence was only overrun at day 2.35, but the greater damage factor created more damage, which decreased the lysosomal throughput to such an extent that the lysosomal stability remained low (Fig 9.21c), despite the decrease in autophagic activity.

From days 7-12 there was an increase in cellular volume as normal feeding activity was resumed; this had been affected between days 2-7 by the increased lysosomal volume. However, there was still 85% of the contaminant which came into the cell resident in the cytosol. Thus, the increased cytosolic volume reached a point where the doubled autophagic rate soon exceeded lysosomal capacity; once more creating a further depression in cellular volume from day 12 onwards. If the simulation were continued the cell started to increase cellular volume once more at day 17, and proceeded to the maximum volume despite the continued presence of contaminant.

The simulation was then repeated but with an unfed cell. As with all previous starved simulations, there was the decline of cell volume to the point when the survival 'drip-feed' was necessary to prolong the cell's existence. Only a third of the amount of contaminant entered the cell in comparison to the fed cell. But with the more rapidly diminishing cytosol volume the boost to damage is increased around day 1.25 as before. However, due to the lower contaminant load that entered the cell, the contaminant concentration did not outpace the defensive capability to the same extent as in the previous model (Figs 9.21d & 9.22a) and, hence, the

damage boost was much less. This provoked a much decreased initial decline in lysosomal stability (Figs 9.21b & 9.22b). Lysosomal damage follows a similar pattern to the previous model but the decreased autophagy ensures that even the reduced capacity of the lysosome is not exceeded by demand. This enabled the lysosome to recover its stability fairly quickly and remain in the healthy range (Fig 9.22b).

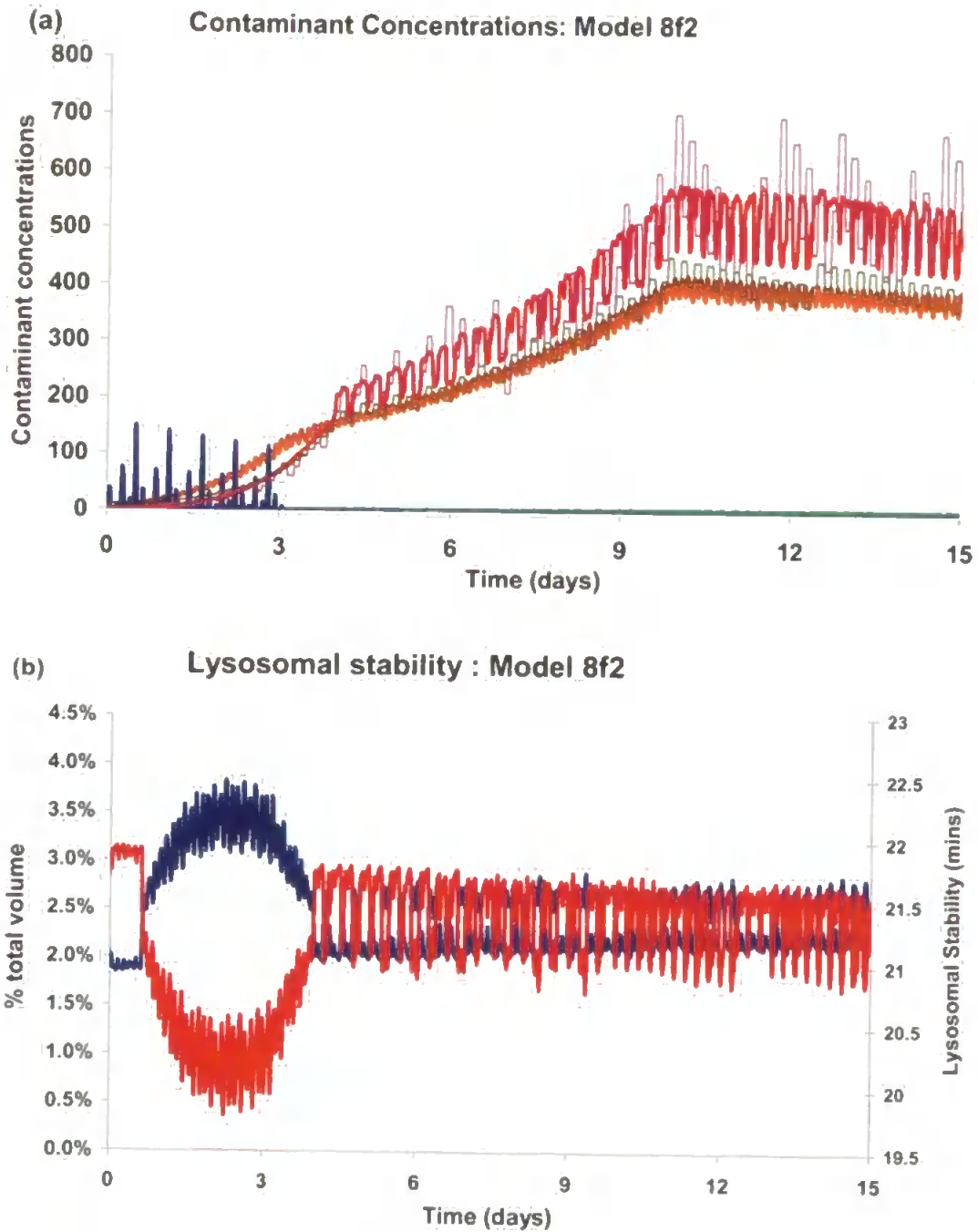


Fig 9.22 Model 8f2 as previous model except starved (a) Contaminant concentrations —  $S_{con}$  —  $L_{con}$  —  $C_{con}$  —  $RB_{con}$  —  $Cell_{con}$  —  $LysBase$  & —  $CytBase$  (b) — relative lysosomal volume, — lysosomal stability.

### 9.9 Contaminant bio-transformation: Model 8g

Model 8g introduced the ability of the cell to transform the contaminants by cellular mechanisms into a different form, which would prove innocuous to the cellular constituents. This was achieved by adding two new rates  $k_{transL}$  and  $k_{transC}$  which would leech contaminant from the lysosome and cytosol pools respectively. Each rate was made dependent upon the contaminant content.

$$k_{Ltrans} = \begin{cases} 0 & \text{If } L_{con} = 0 \\ TransFactorL_{xcon} & \text{Otherwise} \end{cases} \quad [9.32]$$

$$k_{Ctrans} = \begin{cases} 0 & \text{If } C_{con} = 0 \\ TransFactorC_{xcon} & \text{Otherwise} \end{cases} \quad [9.33]$$

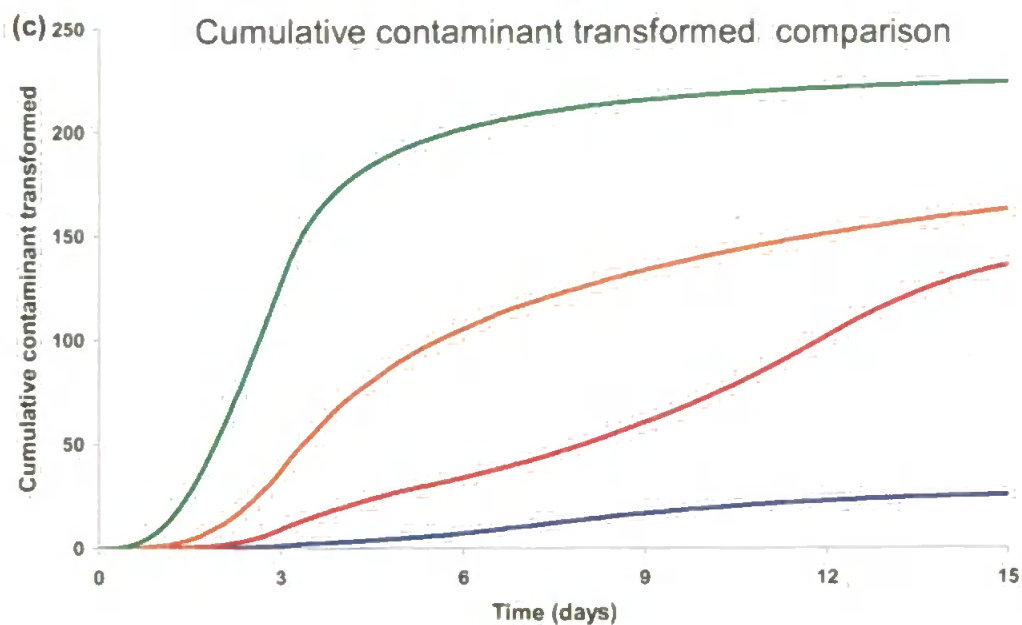
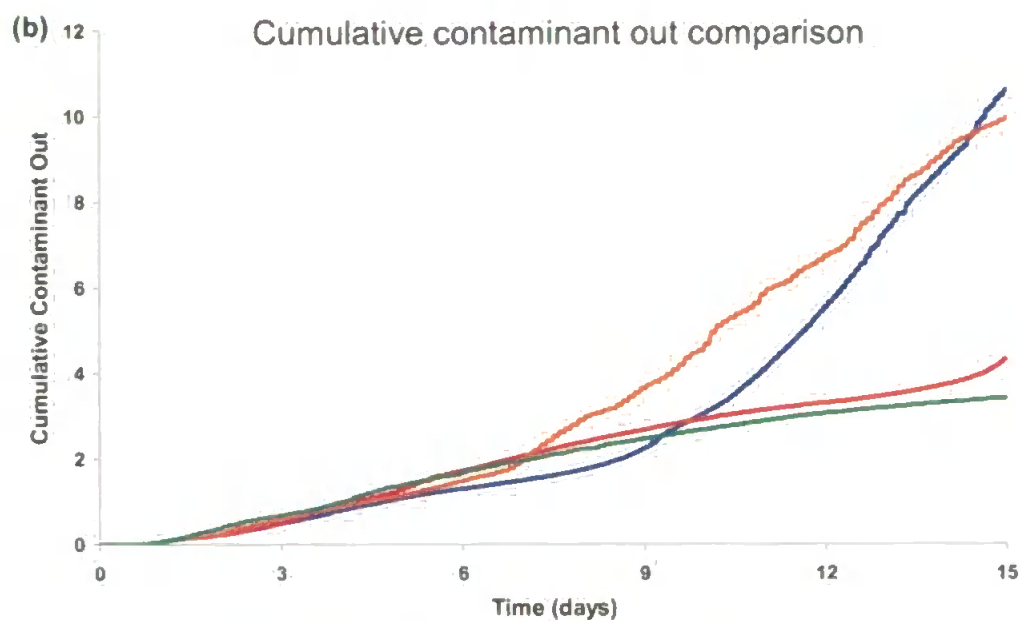
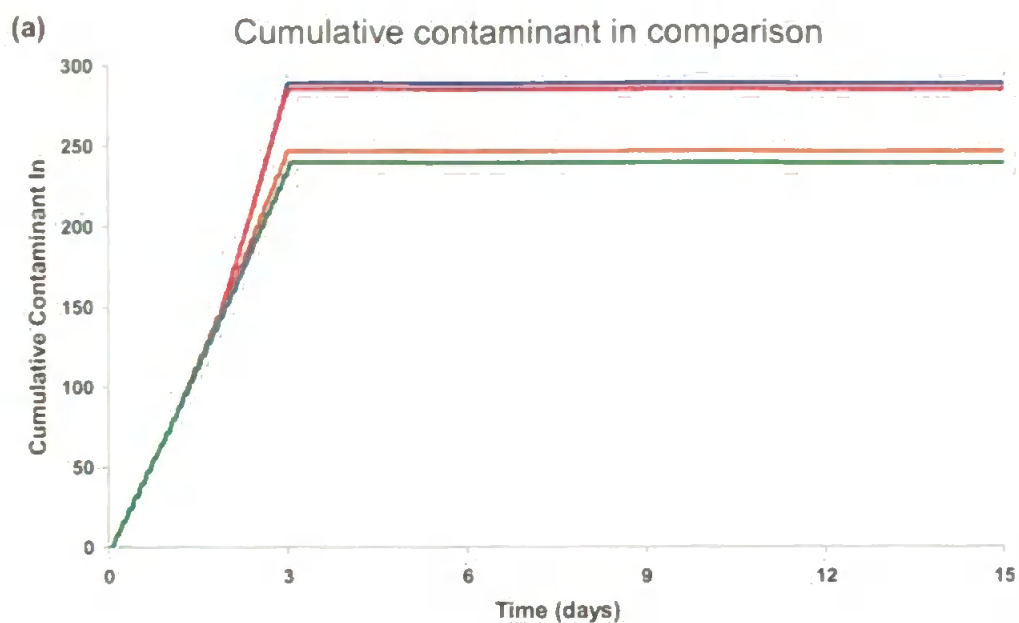
Where *TransFactor* was a measure of how much of the percentage of resident contaminant is processed per timestep. The revised ODEs then become:

$$\frac{dL_{xcon}}{dt} = k_{lysC} E_{con} + k_{autC} C_{con} - (k_{RBC} + k_{transL}) L_{con} \quad [9.34]$$

$$\frac{dC_{xcon}}{dt} = k_{diffC} S - (k_{autC} + k_{transC}) C_{con} \quad [9.35]$$

The higher the rate of transformation of contaminant the less entered the cell (Fig 9.23a). This was due to the lesser damage, which allowed for an uninterrupted phase cycle. The cell volume declined more rapidly than the lysosome for the higher rates of damage, associated with the lower transformation rates, thus provoking the temporary cessation of

endocytosis, which allowed the contaminant in the tubule to enter more frequently.



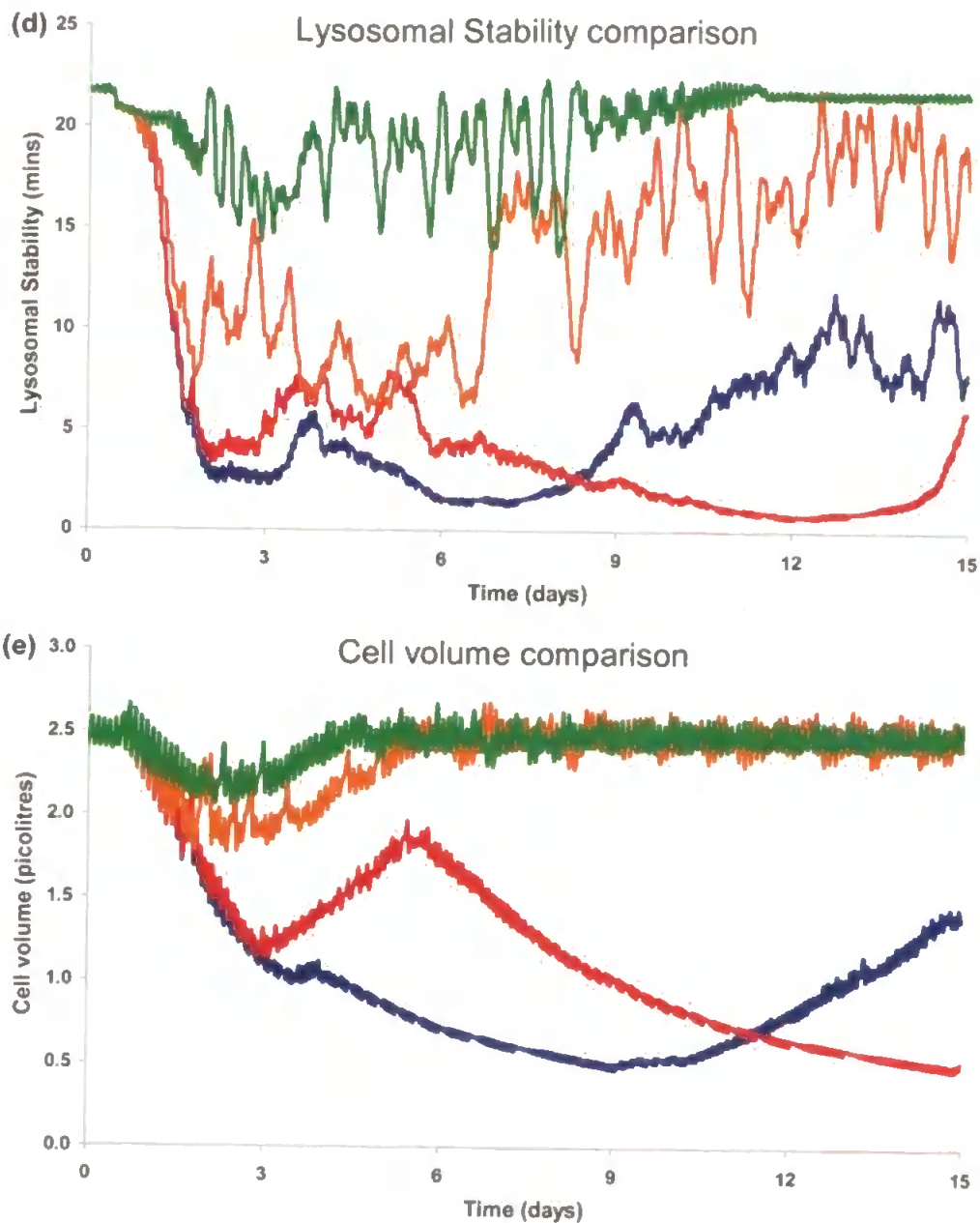


Fig 9.23 Bio-transformation Model 8g. TransFactor —  $10^{-8}$  —  $10^{-7}$  —  $10^{-6}$  —  $10^{-5}$ . Cumulative (a) contaminant in (b) contaminant out (c) contaminant transformed & (d) lysosomal stability (e) cell volume.

The amount of contaminant which left the cell untransformed did not follow the expected trend of decreasing along with the increase in the transformation rate (Fig 9.23b & Table 9.2). This was due to the transformation allowing the cell to recover more quickly, due to the



lessened damage. This in turn led to an increased autophagic rate, allowing contaminant to be removed from the cytosol more rapidly. However, the increased or earlier burden on the lysosome impeded the recovery rate of the cell.

The relatively tardy evacuation of the contaminants did not impinge on the relationship of contaminant content exiting the cell via biotransformation increasing as the rate of transformation increased (Fig 9.23c & Table 9.3).

The effect on lysosomal stability of the introduction of the biotransformation of contaminants was marked, with a far more erratic pattern exhibited for all values of *TransFactor* (Fig 9.23d). The two upper values for *TransFactor* ( $10^{-6}$  &  $10^{-5}$ ) provided enough of a defence for the cell so that little volume change was invoked or sustained (Fig 9.23e). A greater decrease was seen for the lower two values of *TransFactor* ( $10^{-8}$  &  $10^{-7}$ ). The upper value showed a slow, steady decline followed by recovery around day 9. The next higher value reached a low around day 5.8 but gradually increased thereafter. Interestingly the lowest transformation rate value showed more recovery than the rate set one order of magnitude greater (Figs 9.23d & e).

The reason was the interplay between the recovery of the cell volume (marked by an increased basal autophagy), the lysosomal throughput impairment and the contaminant defence base value. The contaminant concentration was far greater for the lowest of the contaminant

transformation rate simulations, and yet as no cost was attached to an increased contaminant base this cell can cope adequately well allowing for the smooth recovery. The biotransformation level above this increased and accelerated the lysosomal impairment, due to the initial cell recovery over and above that which it can cope with. The endosome then became too high a percentage of the cell volume stopping the feeding cycle and the cell fell into a vicious cycle of autophagic uptake which slightly exceeded lysosomal throughput. The accelerated accumulation of lysosomal contaminant served only to further enforce this cycle. Eventually, enough cytosolic contaminant would have been biotransformed or evacuated from the cell for it to enter a recovery period.

*Table 9.3 Table of model 8g results for various transformation factors revealing cumulative contaminant in by end of exposure period and % of material exiting via exocytosis and % of material rendered harmless by biotransformation at tend of the recovery period.*

Variables	Transformation Rate Factor				
	0.0	$10^{-8}$	$10^{-7}$	$10^{-6}$	$10^{-5}$
Contaminant In (dimensionless)	289	289	285	247	239
Contaminant Out %	2.7	3.7	1.5	4.0	1.4
Contaminant Transformed %	0.0	8.8	47.7	66.0	93.7

### *9.10 Lipofuscin: Model 8h*

Another widely observed component of the toxic process in the cell is the generation of lipofuscin, the implementation of which formed the basis for Model 8h. Two factors were considered for inclusion in the model: the production of lipofuscin from other components of the cell which will affect the energy budget of the cell; also lipofuscin can bind contaminants (Brunk & Terman, 2002; Moore & Willows, 1998). The ability of lipofuscin to bind contaminants was considered to have two possible effects: either it sequestered them within its bulk thus rendering them inactive for the purpose of damage to the cellular components, additionally the extensive lifespan of lipofuscin within the cell might provide an explanation for heightened concentrations detected therein long after exposure (Moore & Willows, 1998; Nott & Nicolaidou, 1989); or else the sequestration of the contaminant (possibly on the surface area of the lipofuscin mass) only extended their cellular lifespan and their damaging effects continue unabated throughout this increased time (Brunk & Terman, 2002). Both responses were considered in the models below.

Unfortunately, the contaminant binding role was excluded from the lipofuscin model due to time constraints. Initially, it was then assumed that lipofuscin was only present in two compartments, the lysosome and the residual bodies. Then lipofuscin generation was made dependent on lysosomal contaminant concentration and the material of which it was

comprised was taken from the lysosomal contents. Finally, it was assumed that it was removed from the cell along with other material via exocytosis.

First a lipofuscin generation rate,  $k_{LFgen}$ , was determined based upon the lysosomal contaminant concentration and defence status.

$$k_{LFgen} = 10^{-18} \times \begin{cases} MIN(1, L_{con} / LysBase) & \text{IF } L_{con} > 0 \\ 0 & \text{Otherwise} \end{cases} \quad [9.36]$$

The source of this lipofuscin generation was from each of the lysosomal compartments whether considered transient or integral. Hence, this rate was divided according to volume and subtracted from the various compartments. This would have the effect of reducing the amount of material to be processed and would also diminish the degradative enzyme content and, hence, lysosomal throughput.

To allow for the observed accumulation of lipofuscin in the lysosome, it was sent to the residual body compartment at a much reduced percentage of the normal flow between these compartments.

$$k_{LFRB} = MIN\left(10^{-6} \times k_{RB}, \frac{LF_v}{100(t_1 - t_0)}\right) \text{ IF } k_{RB} > 0 \quad [9.37]$$

The additional and revised ODEs are then:

$$\frac{dLP_v}{dt} = k_{LrepP} - k_{LdamP} - k_{LgenP} - k_{LdifP} \quad [9.38]$$

$$\frac{dLL_v}{dt} = k_{LrepL} - k_{LdamL} - k_{LgenL} - k_{LdifL} \quad [9.39]$$

$$\frac{dLTEP_v}{dt} = k_{lysP} - k_{EgenP} - k_{EdifP} - k_{EdegP} - k_{ERBP} \quad [9.40]$$

$$\frac{dLTEL_v}{dt} = k_{lysL} - k_{EgenL} - k_{EdifL} - k_{EdegL} - k_{ERBL} \quad [9.41]$$

$$\frac{dLTES_v}{dt} = k_{lysS} - k_{EgenS} - k_{EdifS} - k_{EdegS} - k_{ERBS} \quad [9.42]$$

$$\frac{dLTCP_v}{dt} = k_{autP} + k_{DautP} + k_{LdamP} - k_{CgenP} - k_{CdifP} - k_{CdegP} - k_{CRBP} \quad [9.43]$$

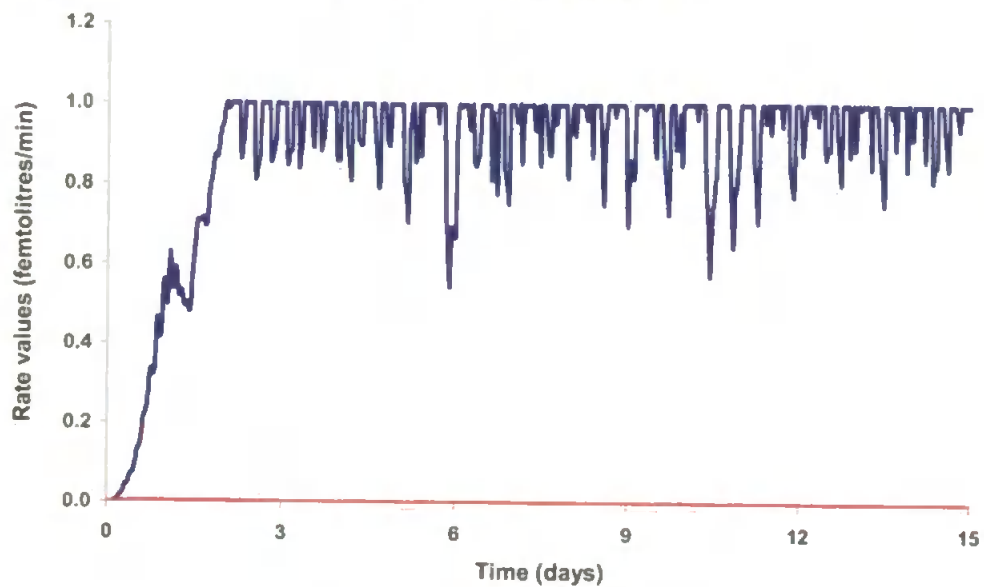
$$\frac{dLTCL_v}{dt} = k_{autL} + k_{DautL} + k_{LdamL} - k_{CgenL} - k_{CdifL} - k_{CdegL} - k_{CRBL} \quad [9.44]$$

$$\frac{dLTCS_v}{dt} = k_{autS} + k_{DautS} - k_{CgenS} - k_{CdifS} - k_{CdegS} - k_{CRBS} \quad [9.45]$$

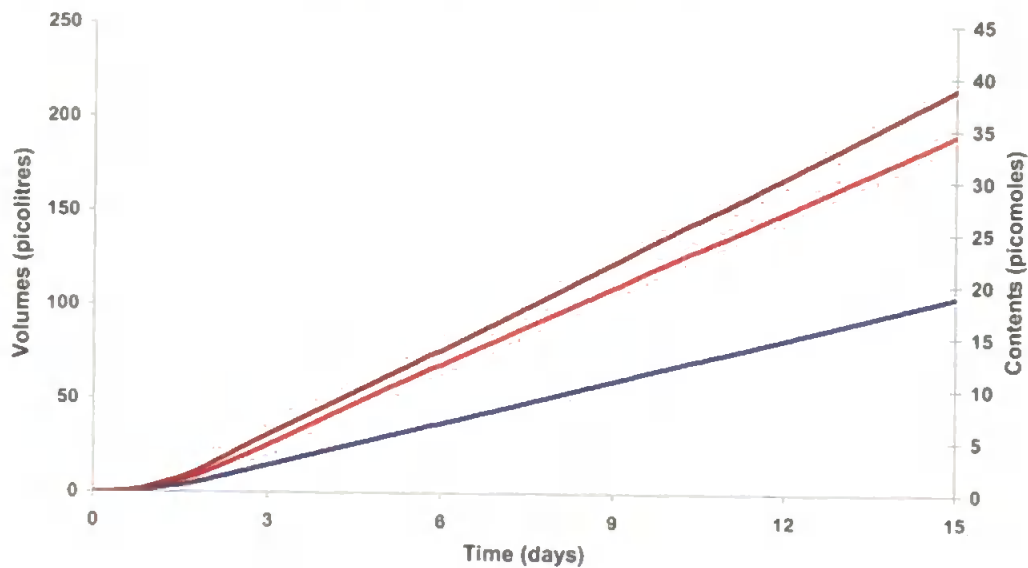
$$\frac{dLF_v}{dt} = k_{gen} - k_{LFRB} \quad \frac{dRB_v}{dt} = k_{RB} + k_{LFRB} - k_{exo} \quad [9.46]$$

It was then assumed that all of these flows take carbon and nitrogen at average source concentration and the content ODEs were revised accordingly.

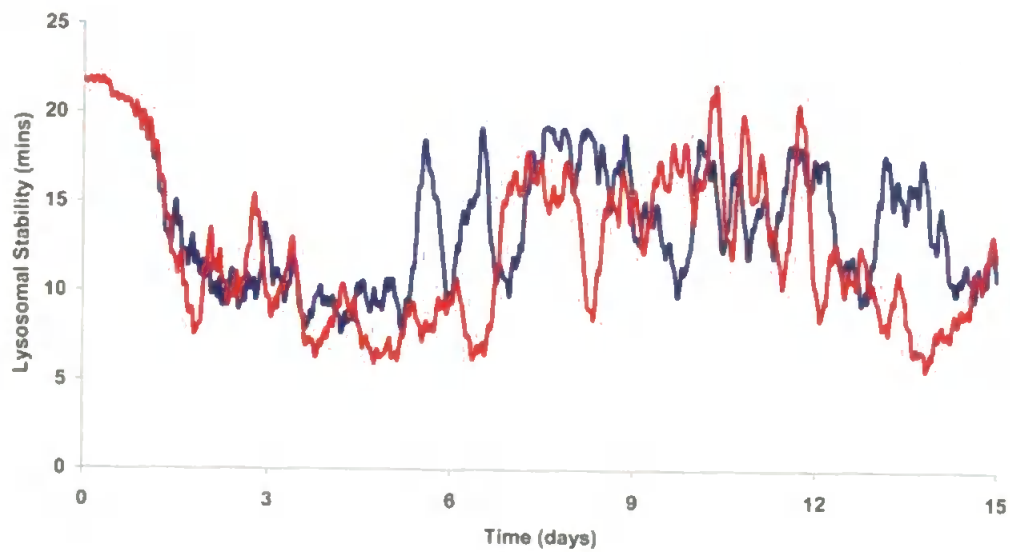
(a) Lipofuscin Rates: Model 8h1



(b) Lysosomal volumes : Model 8h1



(c)



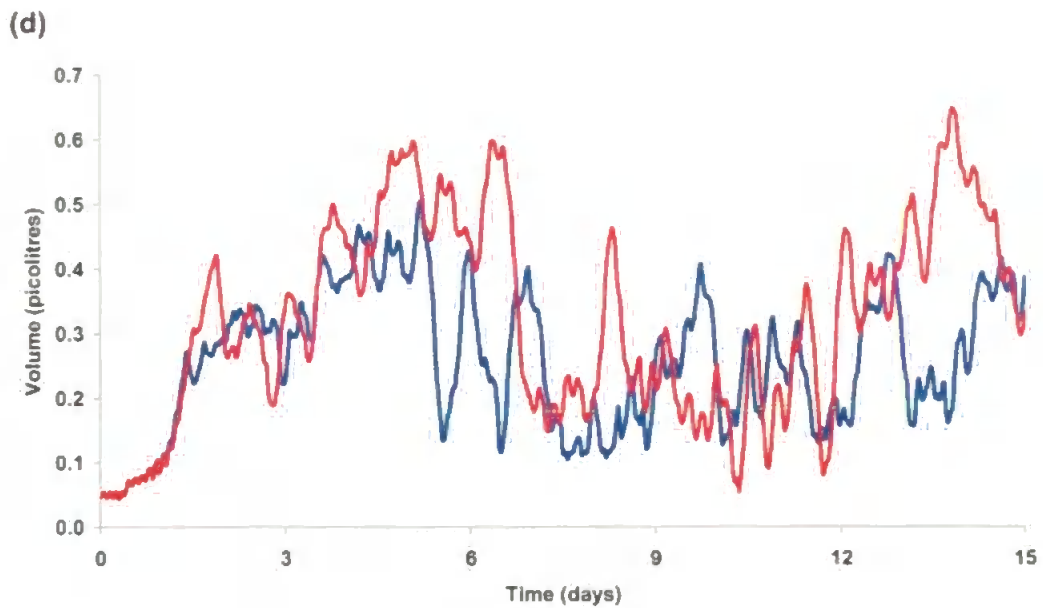


*Fig 9.24 Lipofuscin Model 8h1. (a) Lysosomal lipofuscin rates —  $k_{LFgen}$  —  $k_{LFRB}$  (b) — Lysosomal lipofuscin volume — lipofuscin carbon content — lipofuscin nitrogen content (c) Lysosomal Stability — Model 8h1 — Model 8g (d) Lysosomal Volume — Model 8h1 — Model 8g*

Initially, lipofuscin generation reached the prescribed maximum as the lysosomal contaminant concentration increased towards the contaminant basal defence value. Thereafter, it oscillated in a fashion dictated by the contaminant and variable defence value (Fig 9.24a) which provoked a linear increase in lipofuscin content and volume (Fig 9.24b). The effect on overall cell volume appeared negligible; however, there were changes in lysosomal volume significant enough to alter the pattern of lysosomal stability (Figs 9.24c & d). Extending the simulation a lot further showed that lipofuscin production and expulsion eventually stabilised to cancel each other out (Fig 9.25a) and allow the model cell to live in perpetuity with a low lysosomal stability (Fig 9.25b).

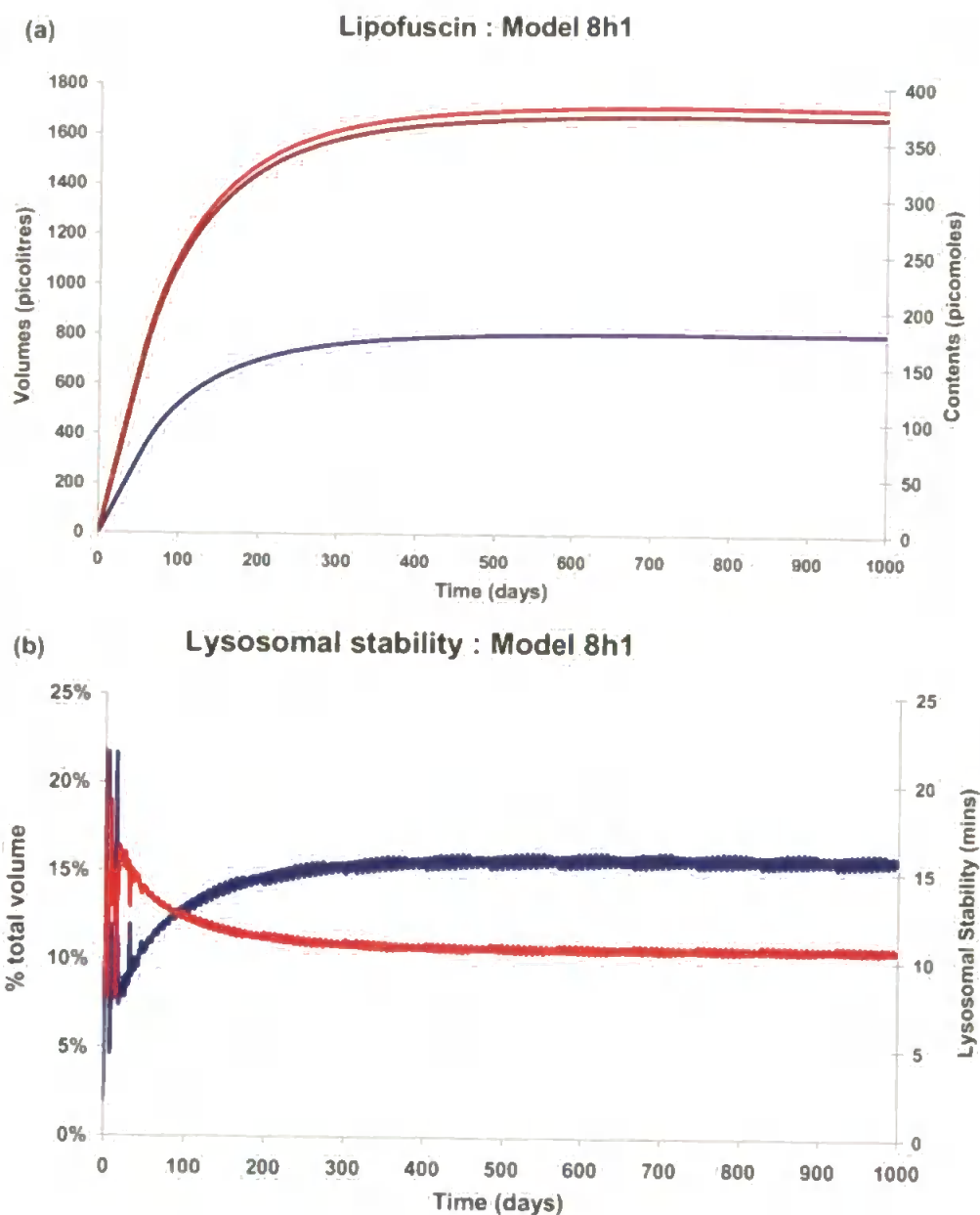


*Fig 9.25 as for previous model except extended to 1000 days to show long term behaviour of lipofuscin and lysosomal stability.*



### *9.11 Discussion*

The general problems with attempting to simulate the uptake and deleterious effect of a toxicant included the lack of timely data, the reliance upon the previous unvalidated 'clean' model and the myriad of responses generated by their presence. Even to simulate the concentration of a toxicant within one part of the cell, or indeed the whole cell, required that the rates of entry, release and biotransformation be known and their subsequent effect on the day-to-day cellular routine. Hence, the approach was to start with as simple a heuristic model as possible and to build in any additions as were deemed necessary.

Various adaptations of the model were attempted, which have not been included in this thesis. They include a study of the difference in effect induced by varying the routes of entry of the toxicant into the cell; a toxicant diffusion entry submodel where the digestive tubule was refreshed with fresh toxicant in line with the feeding cyclic activity; a long term exposure study; and a sub-model to reflect lysosomal stability not as a function of lysosomal volume to cell volume but as the ratio of non-target lysosomal lipid volume to lysosomal volume.

Instead, the toxicity model was developed in an attempt to explain how the counter-intuitive result of dual stress, both toxic and nutritional deprivation, promoted a greater recovery rate than a singular toxic stress. The premise behind the explanation was that with less food available to the

cell, there would be a surfeit of lysosomal capacity and the starvation induced autophagy would more rapidly clear the cell of harmful toxicants, thus decreasing the amount of damage done to the cellular constituents.

However, increasing the autophagic rate necessitated the uptake of undamaged cellular components. Since the lysosomal processes cost the cell in energetic terms and were not totally efficient, a balance had to be found whereby these costs do not subsume the beneficial effects of reduction in toxic action within the cytosol.

One significant problem with the model was the lack of smooth change between a healthy and a moribund final state over certain parameter spaces (e.g., the increase in lysosomal damage due to the presence of contaminants). It would appear that the formulation of the model was such as to preclude any intermediate states for some variables. This instability was contrary to the robustness exhibited by the mussel in spite of prolonged exposure to toxic and/or nutritional stress. Various attempts to incorporate possible behavioural responses, particularly the feeding functions (e.g. the constraints put on the tubule phases in order to model the surface concentration of the contaminant and to show the decline over the feeding phase), have shown that they can explain some facet of this robustness, but their introduction has inevitably marred the verisimilitude of other parts of the model.

When the model was first conceived, the role of lipofuscin was considered to be of importance due to its persistence in the cell and its

perceived role in toxicokinetics (Moore & Willows, 1998). However, the production and expulsion of lipofuscin is linked to the presence of toxic substances and its role so poorly understood that it represented another, higher level of complexity, which was reluctantly deemed too complex to model.

Simulating the ability of lipofuscin to bind contaminants was abandoned due to poor understanding of its dynamics and how this might affect the lysosome. If the lipofuscin accretes more material around its surface, then deleterious contaminants will presumably become inert as they are incarcerated away from the cellular constituents. However, the greater the surface of the lipofuscin the more contaminants can be bound and exposed to the cellular components for longer, due to the reduced capability of the cell to rid itself of lipofuscin (Brunk & Terman, 2002). Consequently, without greater knowledge of the processes governing lipofuscin production and discharge, attempts at modelling its effects at this juncture have limited value.



## 10 General Discussion

This thesis sought to develop a model of the hepatopancreatic digestive cell of the blue mussel, *Mytilus sp.* The general aim was to produce a model which could reproduce the stress responses observed under toxic insult. However, the majority of the effort was consumed by the development of a model for an unstressed cell. The lack of data of adequate frequency or resolution (data was chiefly for the entire gland) for even the regular functioning of the cell naturally hindered this development.

To conclude this work the major hypotheses of the model (Section 1.13) are now reviewed.

**Hypothesis 1.1:** The 3 compartment system was broadly adhered to throughout the model evolution. Generally, there was little evidence to suggest that this approach was defective. It may have borne closer scrutiny if time had allowed a more comprehensive the study of the toxicity induced interactions. However, as with all models, the trade-off between complexity and results had to be considered. Overall, the clarity/simplicity of this idea enabled the model development to proceed quite smoothly, with the following caveats.

The work on the lipid metabolism led to the consideration of the benefit of the addition of peroxisomes as a further compartment. The time

constraint on the work meant that this was never truly scrutinised and the issue remains unresolved.

The aggregation of all lysosomes into one compartment was possibly the most contentious of all the assumptions, given their centrality to the model. The damage to, or malfunction of, each individual lysosome could lead to their decommissioning. Thus, under stress, it might be expected to see heightened genesis of lysosomes by the cell. This would then signify a strain on the cellular budget. However, this malfunction and rejection does not occur immediately, as evidenced by the frequent observation of impaired but functioning lysosomes. Hence, the threshold for and pattern of damage, and the cellular decision making processes would have to be taken into account if individual lysosomes were to be modelled.

The latter models sought to mediate this possible deficiency by demanding replenishment of the lysosomal internal components at discrete time intervals. The arbitrary regime imposed for replenishment obviously warranted further investigation. In order to proceed further, a timeframe for a lysosomal life cycle would have had to be found. Unfortunately, no such data could be found.

**Hypothesis 1.2:** Increased autophagy alone was never shown by the model to satisfactorily reproduce the responses to stress observed. By enhancing the autophagic rate, the response of the model was unequivocal, a more rapid decrease in cell volume, due to the inherent inefficiency in the degradative process.

The swollen lysosomes observed during toxic stress do not necessarily imply increased autophagy, impairment to the time taken to degrade material coupled with a continued rate of autophagy would produce similar results (Moore *et al.*, 2006a). Impairments to the degradative processes could be caused by a number of ways, e.g., decreasing the concentration of enzymes or altering the optimal environmental conditions within the lysosome. Lipofuscin is now believed to bind iron, thus increasing radical production and exacerbating oxidative damage within the lysosome; and to also sequester proteases, thus inhibiting lysosomal degradation (Moore, 2008). Given that there was extra damage observed under toxic stress, then extra degradation of material would be necessary. Hence, it was decided to model the toxic stress as a twofold impairment: increased damage in the cytosol causing enhanced autophagy and impairment to the lysosomal degradative efficiency.

Hypothesis 1.2 should be qualified, as autophagy alone in the model was shown to be inadequate to replicate the observed results.

**Hypothesis 1.3:** Endocytosis was quickly recognised as the major factor in the behaviour of an unstressed cell. Therefore, it is necessary to model this rate as accurately as possible. The feeding pattern of the animal as a whole has to be considered to replicate the food signal presented to an individual cell. Once a food signal is established then the capacity of the cell to ingest the material has to be taken into account. If the apical surface area of the cell changes with volume then the capacity to endocytose would

presumably alter simultaneously. The model has been parameterised to one specific set of environmental conditions, should these change then all rates would necessarily have to be re-parameterised. Notably this would affect this model when changes in salinity induce changes in cell volume. The internal capacity of the cell to manage material would also affect this rate.

Should the composition of the food affect this rate? Food quality below a certain threshold was used in the model as a switch for increased autophagy. It was shown that in the simpler models that continued endocytosis with poor carbon and nitrogen ratios led to increased rates of cell expiry. However, the concepts of hypothesis 1.4 led to better control of the model, so this became less of an issue. The final model based on protein, carbohydrate and lipid flows attempted to be able to resolve internally the relative composition of the food. Hence, it was concluded that hypothesis 3 was sufficient for the model; however, the modelling of the signal of food arriving at the cell surface required more validation.

**Hypothesis 1.4:** The conceptual analogy of the endosome/lysosome as processing plants was implemented. Execution of this hypothesis revealed that a number of possible schemes were possible. The decision was made to take a sequential approach to the degradative process. It would have been beneficial to explore queuing theory to see if this was applicable in the model. Generally, this concept allowed for a more detailed simulation of lysosomal efficiency.



In general, proteolytic capability declines with age which has been linked to decreased autophagic efficiency (Cuervo & Dice, 2000). Cells which are subject to caloric restrictions, which require the switching on and off of autophagy, are proposed to have increased lifespan. The environmental conditions the blue mussel is subject to equally induce the switching on and off of the autophagic processes (Moore *et al.*, 2007). This may be a partial explanation for their robustness to toxic insult. Hence, the model required that the endosome/lysosome be imbued with some 'history' in order to be able to simulate these responses.

Lipofuscin was considered in the final model, but its implementation proved highly suspect. In part this was due to the lack of data about its function and behaviour. Exploration of the role this age/stress pigment plays in toxicity induced dysfunction could prove a significant advance in the model's ability to replicate observed pathologies.

**Hypothesis 1.5:** Attempts at annual simulation of protein, lipid and carbohydrate dry weights were made. The data it was compared with was taken from entire gland measurements. This revealed that a varying control signal would account for the majority of the behaviour seen. This was interpreted at the time as a signal from the rest of the animal demanding reserves at various ratios over the annual cycle. These were imposed by making the cell's control ratios of these components subject to an annual pattern. If the function of these cells were to change over the annual cycle, perhaps some state of hibernation during the winter, then they could be

providing the stimulus for this signal themselves. There is no data to support either argument so this issue remains unresolved.



## Appendix A Revised System of ODEs

For model 2 the following system of ODEs was used.

$$\frac{dEL_v}{dt} = k_{endL} - k_{recL} - k_{lysL}$$

$$\frac{dEN_v}{dt} = k_{endN} - k_{recN} - k_{lysN}$$

$$\frac{dE_v}{dt} = k_{end} - k_{rec} - k_{lys}$$

$$\frac{dLL_v}{dt} = k_{lysL} + k_{autL} - k_{degL} - k_{exol}$$

$$\frac{dLN_v}{dt} = k_{lysN} + k_{autN} - k_{degN} - k_{exoN}$$

$$\frac{dL_v}{dt} = k_{lys} + k_{aut} - k_{deg} - k_{exo}$$

$$\frac{dCL_v}{dt} = k_{degL} - k_{autL} - k_{expL} - k_{resL} - k_{cat}$$

$$\frac{dCN_v}{dt} = k_{degN} - k_{autN} - k_{expN} - k_{secN} - k_{resN} + k_{sto} + k_{cat} + k_{dif}$$

$$\frac{dG_v}{dt} = -k_{sto}$$

$$\frac{dC_v}{dt} = k_{deg} - k_{aut} - k_{exp} - k_{sec} - k_{res} + k_{dif}$$

$$\frac{dEL_{xc}}{dt} = k_{endL} SL_c - (f_{rL} k_{recL} + k_{lysL}) EL_c$$

$$\frac{dEN_{xc}}{dt} = k_{endN} SN_c - (f_{rN} k_{recN} + k_{lysN}) EN_c$$

$$\frac{dE_{xc}}{dt} = \frac{dEL_{xc}}{dt} + \frac{dEN_{xc}}{dt} \quad c$$

$$\frac{dLL_{xc}}{dt} = k_{lysL} EL_c + k_{autL} CL_c - (k_{degL} + k_{exol}) LL_c$$

$$\frac{dLN_{xc}}{dt} = k_{lysN}EN_c + k_{aut}CN_c - (k_{degN} + k_{exoN})LN_c$$

$$\frac{dL_{xc}}{dt} = \frac{dLN_{xc}}{dt} + \frac{dLL_{xc}}{dt}$$

$$\frac{dCL_{xc}}{dt} = k_{degL}LL_c - (k_{autL} + k_{expL} + k_{catL} + k_{resL})CL_c$$

$$\frac{dCN_{xc}}{dt} = k_{degN}LN_c + k_{catL}CL_c + k_{sto}G_c - (k_{autN} + k_{expN} + k_{secN} + k_{resN})CN_c$$

$$\frac{dG_{xc}}{dt} = -k_{sto}G_c$$

$$\frac{dC_{xc}}{dt} = \frac{dCL_{xc}}{dt} + \frac{dCN_{xc}}{dt} + \frac{dG_{xc}}{dt}$$

For model 7 the following system of ODEs was used.

$$\frac{dEL_v}{dt} = k_{Erepl} - k_{EdamL}$$

$$\frac{dEL_{xc}}{dt} = k_{Erepl}EVL_c - k_{EdamL}EL_c$$

$$\frac{dEP_v}{dt} = k_{EsynP} - k_{EdamP}$$

$$\frac{dEP_{xc}}{dt} = k_{EsynP}EWP_c - k_{EdamP}EP_c$$

$$\frac{dEP_{xn}}{dt} = k_{EsynP}EWP_n - k_{EdamP}EP_n$$

$$\frac{dETP_v}{dt} = k_{endP} + k_{EdamP} - k_{recP} - k_{lysP}$$

$$\frac{dETP_{xc}}{dt} = k_{endP}SP_c + k_{EdamP}EP_c - k_{recP}EYP_c - k_{lysP}EXP_c$$

$$\frac{dETP_{xn}}{dt} = k_{endP}SP_n + k_{EdamP}EP_n - k_{recP}EYP_n - k_{lysP}EXP_n$$

$$\frac{dETL_v}{dt} = k_{endL} + k_{EdamL} - k_{recL} - k_{lysL}$$

$$\frac{dETL_{xc}}{dt} = k_{endL}SL_c + k_{EdamL}EL_c - k_{recL}EYL_c - k_{lysL}EXL_c$$

$$\frac{dETS_v}{dt} = k_{endS} - k_{recS} - k_{lysS}$$

$$\frac{dETS_{xc}}{dt} = k_{endS}SS_c - k_{recS}EYS_c - k_{lysS}EXS_c$$

$$\frac{dE_v}{dt} = k_{end} + k_{Erep} + k_{Esyn} - k_{rec} - k_{lys}$$

$$\frac{dE_{xc}}{dt} = k_{end}S_c + k_{Erep}EVL_c + k_{Esyn}EWP_c - k_{rec}EY_c - k_{lys}EX_c$$

$$\frac{dE_{xn}}{dt} = k_{end}S_n + k_{Esyn}EWP_n - k_{rec}EY_n - k_{lys}EX_n$$

$$\frac{dLL_v}{dt} = k_{LrepL} - k_{LdamL}$$

$$\frac{dLL_{xc}}{dt} = k_{LrepL}LVL_c - k_{LdamL}LL_c$$

$$\frac{dLP_v}{dt} = k_{LSynP} - k_{LdamP}$$

$$\frac{dLP_{xc}}{dt} = k_{LSynP}LWP_c - k_{LdamP}LP_c$$

$$\frac{dLP_{xn}}{dt} = k_{LSynP}LWP_n - k_{LdamP}LP_n$$

$$\frac{dLTP_v}{dt} = k_{lysP} + k_{LdamP} + k_{autP} + k_{DautP} - k_{TgenP} - k_{RBP} - k_{degP} - k_{LTdijP}$$

$$\begin{aligned} \frac{dLTP_{xc}}{dt} = & k_{lysP}EXP_c + k_{LdamP}LP_c + k_{autP}CP_c + k_{DautP}CDP_c - k_{TgenP}LTP_c \\ & - k_{RBP}LYP_c - k_{degP}LXP_c - k_{LTdijP}LUTP_c \end{aligned}$$

$$\begin{aligned} \frac{dLTP_{xn}}{dt} = & k_{lysP}EXP_n + k_{LdamP}LP_n + k_{autP}CP_n + k_{DautP}CDP_n - k_{TgenP}LTP_n \\ & - k_{RBP}LYP_n - k_{degP}LXP_n - k_{LTdijP}LUTP_n \end{aligned}$$

$$\frac{dLTL_v}{dt} = k_{lysL} + k_{LdamL} + k_{autL} + k_{DautL} - k_{degL} - k_{RBL} - k_{TgenL} - k_{LTdijL}$$

$$\frac{dLTL_{xc}}{dt} = k_{hysL} EXL_c + k_{LdamL} LL_c + k_{autL} CL_c + k_{DautL} CDL_c - k_{degL} LXL_c \\ - k_{RBL} LYL_c - k_{TgenL} LTL_c + k_{LTdifL} LUTL_c$$

$$\frac{dLTS_v}{dt} = k_{hysS} + k_{autS} + k_{DautS} - k_{degS} - k_{RBS} - k_{TgenS} - k_{LTdifS}$$

$$\frac{dLTS_{xc}}{dt} = k_{hysS} EXS_c + k_{autS} CS_c + k_{DautS} CDS_c - k_{degS} LXS_c - k_{RBS} LYS_c \\ - k_{TgenS} LTS_c - k_{LTdifS} LUTS_c$$

$$\frac{dL_v}{dt} = k_{hys} + k_{aut} + k_{Daut} + k_{Lrep} + k_{Lsyn} - k_{deg} - k_{RB} - k_{Ldif} - k_{LTdif} - k_{LFRB}$$

$$\frac{dL_{xc}}{dt} = k_{hys} EX_c + k_{Lrep} LVL_c + k_{Lsyn} LWP_c - k_{deg} LX_c - k_{RB} LY_c - k_{LFRB} LF_c \\ - k_{LdifP} LP_c - k_{LdifL} LL_c - k_{LTdifP} LTP_c - k_{LTdifL} LTL_c - k_{LTdifS} LTS_c$$

$$\frac{dL_{xn}}{dt} = k_{hys} EX_n + k_{Lsyn} LWP_n - k_{deg} LX_n - k_{RB} LY_n - k_{LFRB} LF_n - k_{LdifP} LP_n - k_{LTdifP} LTP_n$$

$$\frac{dCL_v}{dt} = k_{degL} - k_{resL} - k_{Erepl} - k_{Lrepl} - k_{CdamL} - k_{autL} - k_{TstoL} + k_{Trell} - k_{stodifL}$$

$$\frac{dCL_{xc}}{dt} = k_{degL} LXL_c - k_{Erepl} EVL_c - k_{Lrepl} LVL_c - (k_{resL} + k_{CdamL} + k_{autL}) CL_c \\ + (k_{Trell} - k_{TstoL}) TL_c$$

$$\frac{dTL_v}{dt} = k_{TstoL} - k_{Trell} - k_{GTdamL} - k_{expL}$$

$$\frac{dTL_{xc}}{dt} = (k_{TstoL} - k_{Trell} - k_{GTdamL} - k_{expL}) TL_c$$

$$\frac{dCDL_v}{dt} = k_{CdamL} + k_{GTdamL} + k_{LdifL} + k_{LTdifL} - k_{DautL}$$

$$\frac{dCDL_{xc}}{dt} = k_{CdamL} CL_c + k_{GTdamL} TL_c + k_{LdifL} LUL_c + k_{LTdifL} LUTL_c - k_{DautL} CDL_c$$

$$\frac{dAA_v}{dt} = k_{degP} - k_{excP} - k_{deanimP} - k_{excif} - k_{CtranP} - k_{expP}$$

$$\frac{dAA_{xc}}{dt} = k_{degP} LXP_c - k_{deanimP} CXP_c - (k_{CtranP} + k_{expP}) AA_c$$

$$\frac{dAA_{xn}}{dt} = k_{degP}LXP_n - k_{excP}CXP_n - (k_{CtranP} + k_{expP})AA_n$$

$$\frac{dCP_v}{dt} = k_{CtranP} - k_{EsynP} - k_{LsynP} - k_{CdamP} - k_{autP} - k_{secP}$$

$$\frac{dCP_{xc}}{dt} = k_{CtranP}AA_c - k_{EsynP}EWP_c - k_{LsynP}LWP_c - (k_{CdamP} + k_{autP} + k_{secP})CP_c$$

$$\frac{dCP_{xn}}{dt} = k_{CtranP}AA_n - k_{EsynP}EWP_n - k_{LsynP}LWP_n - (k_{CdamP} + k_{autP} + k_{secP})CP_n$$

$$\frac{dCDP_v}{dt} = k_{CdamP} + k_{LdijP} + k_{LTdijP} - k_{DautP}$$

$$\frac{dCDP_{xc}}{dt} = k_{CdamP}CP_c + k_{LdijP}LUP_c + k_{LTdijP}LUTP_c - k_{DautP}CDP_c$$

$$\frac{dCDP_{xn}}{dt} = k_{CdamP}CP_n + k_{LdijP}LUP_n + k_{LTdijP}LUTP_n - k_{DautP}CDP_n$$

$$\frac{dCS_v}{dt} = k_{degS} + k_{deanimP} - k_{resS} - k_{CdamS} - k_{autS} - k_{GstoS} + k_{GrelS} - k_{stodijS}$$

$$\frac{dCS_{xc}}{dt} = k_{degS}LXS_c + k_{deanimP}CXP_c - (k_{resS} + k_{CdamS} + k_{autS})CS_c + (k_{GrelS} - k_{GstoS})G_c$$

$$\frac{dCDS_v}{dt} = k_{CdamS} + k_{GTdamS} + k_{LTdijS} - k_{DautS}$$

$$\frac{dCDS_{xc}}{dt} = k_{CdamS}CS_c + k_{GTdamS}G_c + k_{LTdijS}LUTS_c - k_{DautS}CDS_c$$

$$\frac{dG_v}{dt} = k_{GstoS} - k_{GrelS} - k_{GTdamS} - k_{expS}$$

$$\frac{dG_{xc}}{dt} = (k_{GstoS} - k_{GrelS} - k_{GTdamS} - k_{expS})G_c$$

$$\frac{dRB_v}{dt} = k_{RB} + k_{LFRB} - k_{exo}$$

$$\frac{dRB_{xc}}{dt} = k_{RBP}LYP_c + k_{RBL}LYL_c + k_{RBS}LYS_c + k_{LFRB}LF_c - k_{exo}RB_c$$

$$\frac{dRB_{xn}}{dt} = k_{RBP}LYP_n + k_{LFRB}LF_n - k_{exo}RB_n$$



$$\frac{dC_v}{dt} = k_{deg} + k_{RB} + k_{LFRB} + k_{Ldif} + k_{LTdif} + k_{Mrel} - k_{exo} - k_{exp} - k_{aut} - k_{Daut} \\ - k_{res} - k_{exc} - k_{sec} - k_{stodif} - k_{excdif} - k_{Erep} - k_{Lrep} - k_{Esyn} - k_{Lsyn}$$

$$\frac{dC_{xc}}{dt} = k_{deg} LX_c + k_{RB} LY_c + k_{LFRB} LF_c + k_{Ldif} LU_c + k_{LTdif} LUT_c - k_{exo} RB_c + k_{expS} G_c \\ - k_{resS} CS_c - k_{resL} CL_c - k_{sec} CP_c - k_{Erep} EVL_c - k_{Lrep} LVL_c - k_{Esyn} EWL_c - k_{Lsyn} LWL_c \\ - k_{expL} TL_c - k_{autP} CP_c - k_{DautP} CDP_c - k_{autS} CS_c - k_{DautS} CDS_c - k_{autL} CL_c \\ - k_{DautL} CDL_c - k_{expP} AA_c$$

$$\frac{dC_{xn}}{dt} = k_{deg} LX_n + k_{RB} LY_n - k_{exo} RB_n - k_{sec} CP_n - k_{Esyn} EWL_n - k_{Lsyn} LWL_n \\ - k_{exc} CXP_n - k_{autP} CP_n - k_{DautP} CDP_n - k_{expP} AA_n$$

$$\frac{dCell_v}{dt} = k_{end} - k_{rec} - k_{exo} - k_{exp} - k_{res} - k_{exc} - k_{sec} - k_{stodif} - k_{excdif}$$

$$\frac{dCell_{xc}}{dt} = k_{end} S_c - k_{expS} G_c - k_{expL} TL_c - k_{expP} AA_c \\ - k_{rec} EY_c - k_{exo} RB_c - k_{resS} CS_c - k_{resL} CL_c - k_{sec} CP_c$$

$$\frac{dCell_{xn}}{dt} = k_{end} S_n - k_{expP} AA_n - k_{rec} EY_n - k_{exo} RB_n - k_{sec} CP_n - k_{exc} CP_n$$

## Appendix B Analytical solutions to decay equations

With the delay models there are various analytical solutions available for endosomal volumes and contents for simple endocytotic rate functions.

The volume of the endosome was given by

$$\frac{dE_v}{dt} = k_{end}(t) - k_{lys}(t) - k_{rec}(t) = k_{end}(t) - k_{end}(t - \tau)$$

The endocytotic rate was modelled by the following simple functions:

$$k_{end1}(t) = \begin{cases} 0 & t < t_0 \\ A & \text{when } t_0 \leq t \leq t_1 \\ 0 & t > t_1 \end{cases} \quad k_{end2}(t) = \begin{cases} 0 & t < t_0 \\ A \cos\left(\frac{\pi(t-t_0)}{2(t_1-t_0)}\right) & \text{when } t_0 \leq t \leq t_1 \\ 0 & t > t_1 \end{cases}$$

$$k_{end3}(t) = \begin{cases} 0 & t < t_0 \\ A \frac{t_1-t}{t_1-t_0} & \text{when } t_0 \leq t \leq t_1 \\ 0 & t > t_1 \end{cases} \quad k_{end4}(t) = \begin{cases} 0 & t < t_0 \\ A \left(\frac{t_1-t}{t_1-t_0}\right)^2 & \text{when } t_0 \leq t \leq t_1 \\ 0 & t > t_1 \end{cases}$$

with  $A$  constant. Then the following analytical solutions were available,

where  $\tau$  is the endosomal sortation period.

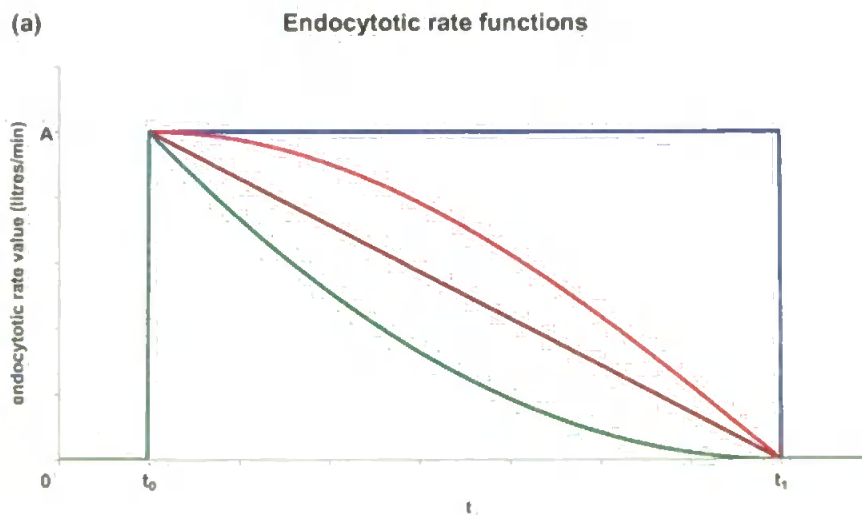
$$E_{v1}(t) = \begin{cases} E_v(t_0) + A(t-t_0) & t_0 \leq t \leq t_0 + \tau \\ E_v(t_0) + A\tau & t_0 + \tau \leq t \leq t_1 \\ E_v(t_0) + A(\tau + t_1 - t) & t_1 \leq t \leq t_1 + \tau \\ E_v(t_0) & t > t_1 + \tau \end{cases}$$

$$E_{v2}(t) = \begin{cases} E_v(t_0) + \frac{2(t_1-t_0)A}{\pi} \sin\left(\frac{\pi(t-t_0)}{2(t_1-t_0)}\right) & t_0 \leq t \leq t_0 + \tau \\ E_v(t_0) + \frac{2(t_1-t_0)A}{\pi} \left( \sin\left(\frac{\pi(t-t_0)}{2(t_1-t_0)}\right) - \sin\left(\frac{\pi(t-\tau-t_0)}{2(t_1-t_0)}\right) \right) & t_0 + \tau \leq t \leq t_1 \\ E_v(t_0) + \frac{2(t_1-t_0)A}{\pi} \left( 1 - \sin\left(\frac{\pi(t-\tau-t_0)}{2(t_1-t_0)}\right) \right) & t_1 \leq t \leq t_1 + \tau \\ E_v(t_0) & t > t_1 + \tau \end{cases}$$

$$E_{v3}(t) = \begin{cases} E_v(t_0) + \frac{A}{t_1 - t_0} \left( t_1(t - t_0) + \frac{t_0^2 - t^2}{2} \right) & t_0 \leq t \leq t_0 + \tau \\ E_v(t_0) + \frac{A\tau \left( t_1 + \frac{\tau}{2} - t \right)}{t_1 - t_0} & t_0 + \tau \leq t \leq t_1 \\ E_v(t_0) + \frac{A}{t_1 - t_0} \left( \frac{t_1^2 + \tau^2 + t^2}{2} + t_1\tau - t(t_1 + \tau) \right) & t_1 \leq t \leq t_1 + \tau \\ E_v(t_0) & t > t_1 + \tau \end{cases}$$

$$E_{v4}(t) = \begin{cases} E_v(t_0) + A \frac{(t_1 - t_0)^3 - (t_1 - t)^3}{3(t_1 - t_0)^2} & t_0 \leq t \leq t_0 + \tau \\ E_v(t_0) + A \frac{3\tau(t_1 - t)^2 + \tau^2(\tau + 3t_1 - 3t)}{3(t_1 - t_0)^2} & t_0 + \tau \leq t \leq t_1 \\ E_v(t_0) + \frac{A(t_1 + \tau - t)^3}{3(t_1 - t_0)^2} & t_1 \leq t \leq t_1 + \tau \\ E_v(t_0) & t > t_1 + \tau \end{cases}$$

If the surface concentration remains constant then carbon content and concentration solutions were equally easily derived. The results are shown in Figure B1.



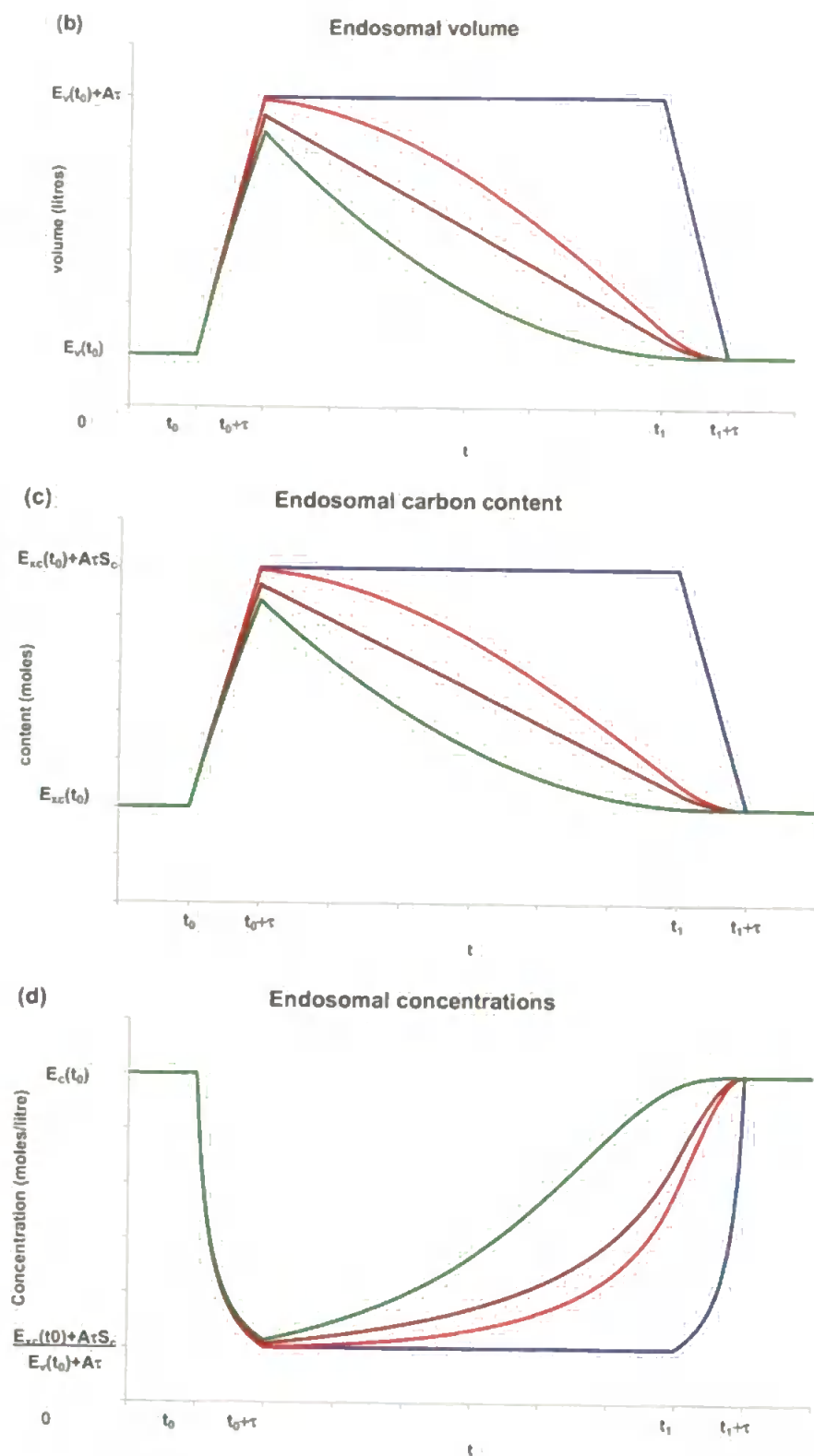


Fig B1 Analytical solutions (a) endocytic rate (b) endosomal volume (c) endosomal carbon content (d) carbon concentrations. Key: —  $k_{end1}$ , —  $k_{end2}$ , —  $k_{end3}$ , —  $k_{end4}$

For these simple functions and under these very constrained conditions analytical solution for endosomal volume, carbon content and concentrations were readily obtainable. Attempts to extend these analytical solutions to the lysosome variables were hampered by the dependence of the autophagic rates on cytosolic volume and the non-linearity this preserves in the remaining system of ODEs.

## Appendix C Numerical solutions to PDE exact solution

This appendix details an examination conducted on approximations to the Bessel functions of the first kind order 0, which were necessary for the solution to the PDE for endocytosis. A similar examination was conducted on the order 1 function  $J_1(x)$  and the results concurred with those presented here. MAPLE was used to evaluate the various approximations and compared against the built in Bessel function.

Since the model was required to be tested under various nutritional regimes it had to be able to be adaptable in FORTRAN, hence a subroutine was sought for calculating these eigenvalues and the concentration in general.

Bessel functions of first kind order  $n$ ,  $J_n(x)$  satisfy the initial condition ODEs

$$x^2 y'' + xy' + (x^2 - n^2)y = 0 \quad y(0) = \begin{cases} 1 & n = 0 \\ 0 & n \neq 0 \end{cases} \quad \text{for } n = 0, 1, 2, \dots$$

The series expansions are

$$J_n(x) = \sum_{m=0}^{\infty} \frac{(-1)^m}{m!(m+n)!} \left(\frac{x}{2}\right)^{2m+n}$$

A number of approximation methods for  $J_0(x)$  were utilised.

Definition Method 1: Derived from the series expansion, calculated each term in order and was limited by the factorial calculation. The curtailment of this series at the  $N$ th term was denoted approximation  $R'_N(x)$ .

The results showed good agreement in the range  $0 < x < 8$ , with maximum absolute error  $< 10^{-14}$ . However, thereafter, it became increasingly unstable as the  $x$  term dominated over the limited ability of the program to calculate large factorials.

Definition Method 2: The series was truncated at step  $N$ , denoted as  $R^2_N$ , and rearranged from a sum into a multiple, so that the factorial no longer needed to be calculated explicitly.

$$R^2_N = \sum_{m=0}^N \frac{(-1)^m}{m!^2} \left( \frac{x}{2} \right)^{2m}$$

$$= 1 - \frac{x^2}{4} \prod_{i=0}^{N-2} 1 - \left( \frac{x}{2(N-i)} \right)^2$$

The results for  $N = 10$  were used. Unfortunately, the accuracy was poor compared with Method 1. However a rearrangement of the calculation as an iterative process produced better results.

Definition Method 3:

- (i) Temp = 1 , m = 1
- (ii) Temp = Temp  $\times$   $x^2 / (4 \times (61 - m))^2 + (-1)^m$
- (iii) m = m + 1
- (iv) IF m = 61 THEN End ELSE Goto (ii)

This method was denoted  $R^3_N$  and the improvement on both previous methods was apparent. Almost 6 full oscillations were completed compared to  $< 3$  for Method 1. The initial range  $x < 8$  had absolute errors of the same order as  $R^1_N$ ; but, thereafter the absolute error increased at an approximate

rate of  $0.25 \times 10^{-9} e^{0.5x}$  which was a vast improvement on the first approximation.

The NAG library recommended a Chebyshev approximation for  $0 < x < 8$ .

Definition Method 4: A basic Chebyshev approximation was implemented, i.e. it was supposed that the Bessel function could be expressed as an infinite sum of Chebyshev polynomials,  $T_n(x) = \cos(n \cos^{-1}(x))$  so that:

$$J_0(x) = \sum_{n=0}^{\infty} a_n T_n(x)$$

Where

$$a_n = \begin{cases} \frac{2}{\pi} \int_{-1}^1 \frac{J_0(x) T_n(x)}{\sqrt{1-x^2}} dx & n \neq 0 \\ \frac{1}{\pi} \int_{-1}^1 \frac{J_0(x) T_n(x)}{\sqrt{1-x^2}} dx & n = 0 \end{cases}$$

This method was denoted  $R_N^4$  and was given by:

$$R_N^4 = \sum_{n=0}^N a_n T_n$$

The substitution  $x = \cos(\theta)$  was used to circumvent the discontinuity at  $x = \pm 1$ . Then it was necessary to solve the integral:

$$a_n = \frac{2}{\pi} \int_0^{\pi} J_0(\cos(\theta)) \cos(n\theta) d\theta = \frac{2}{\pi} \int_{\frac{\pi}{2}}^{\frac{\pi}{2}} J_0\left(\cos\left(\frac{\pi}{2} + \phi\right)\right) \cos\left(\frac{n\pi}{2} + n\phi\right) d\phi$$



In the latter definition for  $n = 2k$ , the integrand was a product of two even functions, about the point  $\frac{\pi}{2}$ , and must therefore have been even itself.

Whereas, for  $n = 2k + 1$  the integrand was a product of an even and an odd function, and hence must be odd and the integral equal to zero. Thus

$$a_n = (-1)^{\frac{n}{2}} \frac{2}{\pi} \int_{-\frac{\pi}{2}}^{\frac{\pi}{2}} J_0(\sin(\phi)) \cos(n\phi) d\phi \quad \text{for } n = 2k, k=0,1,2,\dots$$

Which gave

$$a_0 = J_0^2\left(\frac{1}{2}\right),$$

$$a_2 = -2J_1^2\left(\frac{1}{2}\right),$$

$$a_4 = 2J_0^2\left(\frac{1}{2}\right) + 32J_1^2\left(\frac{1}{2}\right) - 16J_0\left(\frac{1}{2}\right)J_1\left(\frac{1}{2}\right), \text{ etc...}$$

Hence, it was necessary to find approximate values for the Bessel function of the first kind with orders 0 and 1 at the point  $x = 0.5$ . From the definition (approximate method  $R'_N$ ) the following were calculated.

$$J_0\left(\frac{1}{2}\right) = 0.9384698072408129 \quad \text{and} \quad J_0^2\left(\frac{1}{2}\right) = 0.8807255791026085$$

$$J_1\left(\frac{1}{2}\right) = 0.2422684576748739 \quad \text{and} \quad J_1^2\left(\frac{1}{2}\right) = 0.05869400558416216$$

$$J_0\left(\frac{1}{2}\right)J_1\left(\frac{1}{2}\right) = 0.2273616327746679$$

Then it was necessary to numerically calculate the coefficients, an. The

NAG routine suggested using the transformation  $t = 2\left(\frac{x}{8}\right)^2 - 1$ . Maple was then used to calculate the necessary Chebyshev coefficients for  $J_0(t)$ . From which the results were derived. Note the NAG routine was only intended for the domain  $x < 8$ .

Definition Method 5: The NAG routine suggests using a decaying cosine wave for large  $x$ .

$$R^5 = \sqrt{\frac{2}{\pi x}} \cos\left(x - \frac{\pi}{4}\right)$$

The results obviously were poor for small  $x$ , but became increasingly sound. However, for large  $x$  the amplitude was not a problem, but the phase of oscillation became increasingly indeterminable.

Definition Method 6: A polynomial approximation from Abramowitz and Stegun (1964) gave a polynomial approximation.

$$R^6 = \begin{cases} 1 - 2.2499997\left(\frac{x}{3}\right)^2 + 1.2656208\left(\frac{x}{3}\right)^4 - .3163866\left(\frac{x}{3}\right)^6 \\ + .04444479\left(\frac{x}{3}\right)^8 - .0039444\left(\frac{x}{3}\right)^{10} + .00021\left(\frac{x}{3}\right)^{12} & x \leq 3 \\ \frac{1}{\sqrt{x}} \left( 0.79788456 - 7.7 \times 10^{-7}\left(\frac{3}{x}\right) - .0055274\left(\frac{3}{x}\right)^2 - 9.512 \times 10^{-5}\left(\frac{3}{x}\right)^3 \right. \\ \left. + .00137237\left(\frac{3}{x}\right) - .00072805\left(\frac{3}{x}\right)^5 + .00014476\left(\frac{3}{x}\right)^6 \right) \cos(\phi) & x > 3 \end{cases}$$

Where

$$\phi = x - .78539816 - .04166397\left(\frac{3}{x}\right) - 3.954 \times 10^{-5}\left(\frac{3}{x}\right)^2 \\ + .00262573\left(\frac{3}{x}\right)^3 - .00054125\left(\frac{3}{x}\right)^4 - .00029333\left(\frac{3}{x}\right)^5 + .00013558\left(\frac{3}{x}\right)^6$$

Definition Method 7: Finally, a further rational approximation in Abramowitz and Stegun (1964) was utilised.

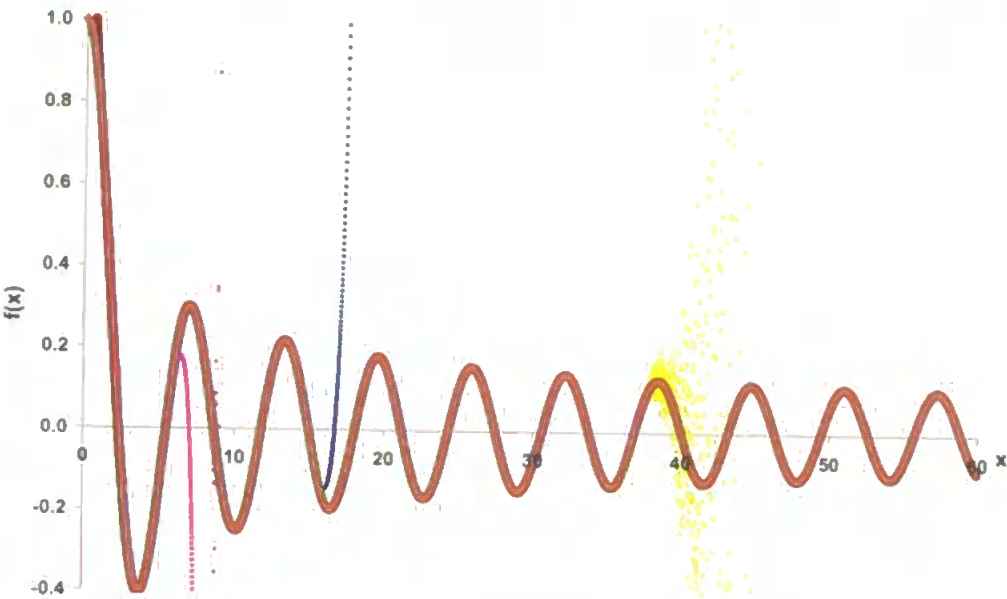
$$R^7 = \begin{cases} p_1(x)/q_1(x) & 0 < x \leq 8 \\ \sqrt{\frac{2}{\pi x}} \left( \cos\left(x - \frac{\pi}{4}\right) p_2(x) - \frac{8}{x} \sin\left(x - \frac{\pi}{4}\right) q_2(x) \right) & x > 8 \end{cases}$$

Where

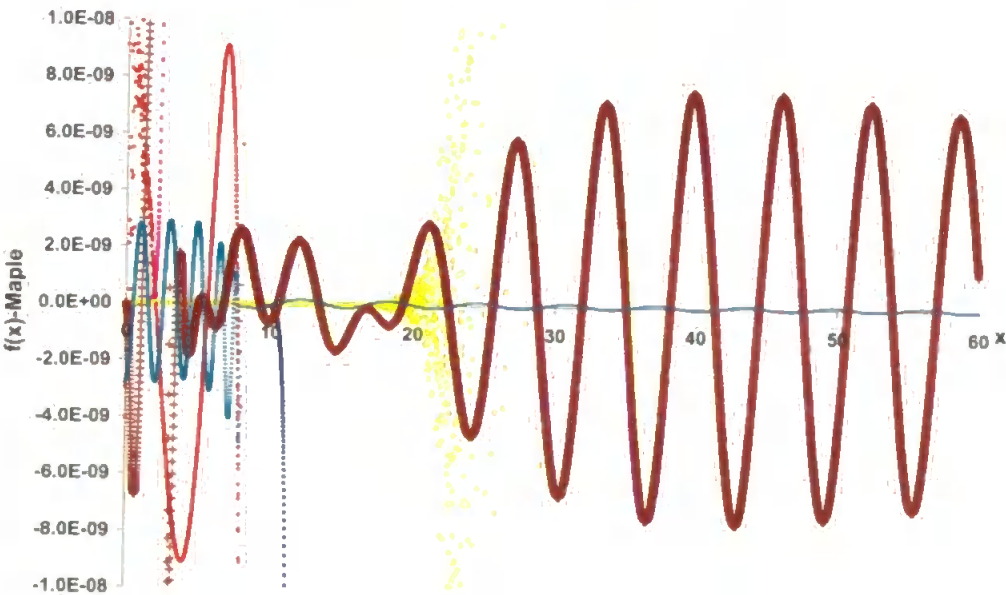
$$p_1(x) = 57568490574 - x^2 \left( \begin{aligned} &13362590354 \\ &-x^2 \left( \begin{aligned} &651619640.7 \\ &+ x^2 (-11214424.18 + x^2 (77392.3301 - 184.9052456x^2)) \end{aligned} \right) \end{aligned} \right) \\ q_1(x) = 57568490411 + x^2 \left( \begin{aligned} &1029532985 \\ &+ x^2 (9494680.718 + x^2 (59272.64853 + x^2 (267.8532712 + x^2))) \end{aligned} \right) \\ p_2(x) = 1 - \left(\frac{8}{x}\right)^2 \left( \begin{aligned} &.001098628627 \\ &- \left(\frac{8}{x}\right)^2 \left( \begin{aligned} &2.734510407 \times 10^{-5} \\ &+ \left(\frac{8}{x}\right)^2 \left( \begin{aligned} &2.073370639 \times 10^{-6} + 2.093887211 \times 10^{-7} \left(\frac{8}{x}\right)^2 \end{aligned} \right) \end{aligned} \right) \end{aligned} \right) \\ q_2(x) = -0.01562499995 + \left(\frac{8}{x}\right)^2 \left( \begin{aligned} &1.430488765 \times 10^{-4} \\ &+ \left(\frac{8}{x}\right)^2 \left( \begin{aligned} &6.911147651 \times 10^{-6} \\ &+ \left(\frac{8}{x}\right)^2 \left( \begin{aligned} &7.621095161 \times 10^{-7} - 9.34945152 \times 10^{-8} \left(\frac{8}{x}\right)^2 \end{aligned} \right) \end{aligned} \right) \end{aligned} \right) \end{aligned}$$

Results were compared to the 32 digit Maple solutions and are shown in Figure C1.

(a) Approximations to Bessel Function of the first kind order 0



(b) Approximations Errors



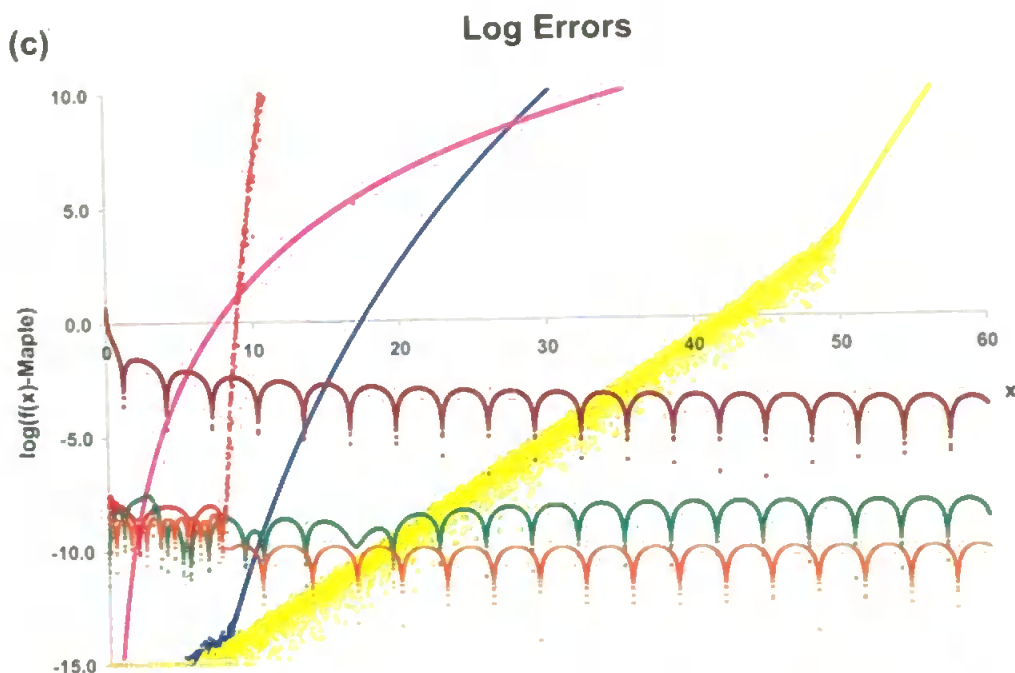


Fig C1 Comparison of approximations.  $R^1_N$ —,  $R^2_N$ —,  $R^3_N$ —,  $R^4_N$ —,  $R^5_N$ —,  $R^6_N$ —,  $R^7_N$ —, Maple —. (a) Actual results (b) actual errors (c) log of absolute error.

For small  $x$  the series approaches produced the best results. However, the factorials in the summation series,  $R1N$ , made the first approximation unstable. The iterative product series approximation,  $R3N$ , remained the most successful until  $x \approx 20$ . Thereafter it was the rational series approximation which became the most accurate approximation.

Finally, to implement the PDE solution only a few of the first occurring eigenvalues could be used in the FORTRAN. A comparison of the initial condition for differing precision and number of eigenvalues,  $n$ , showed that it was the number of eigenvalues which generally governed the ability of the series to replicate the initial conditions. 50 digit precision was used for the comparison in Figure A2. It was deemed sufficient to use the first 100 eigenvalues in the approximation.

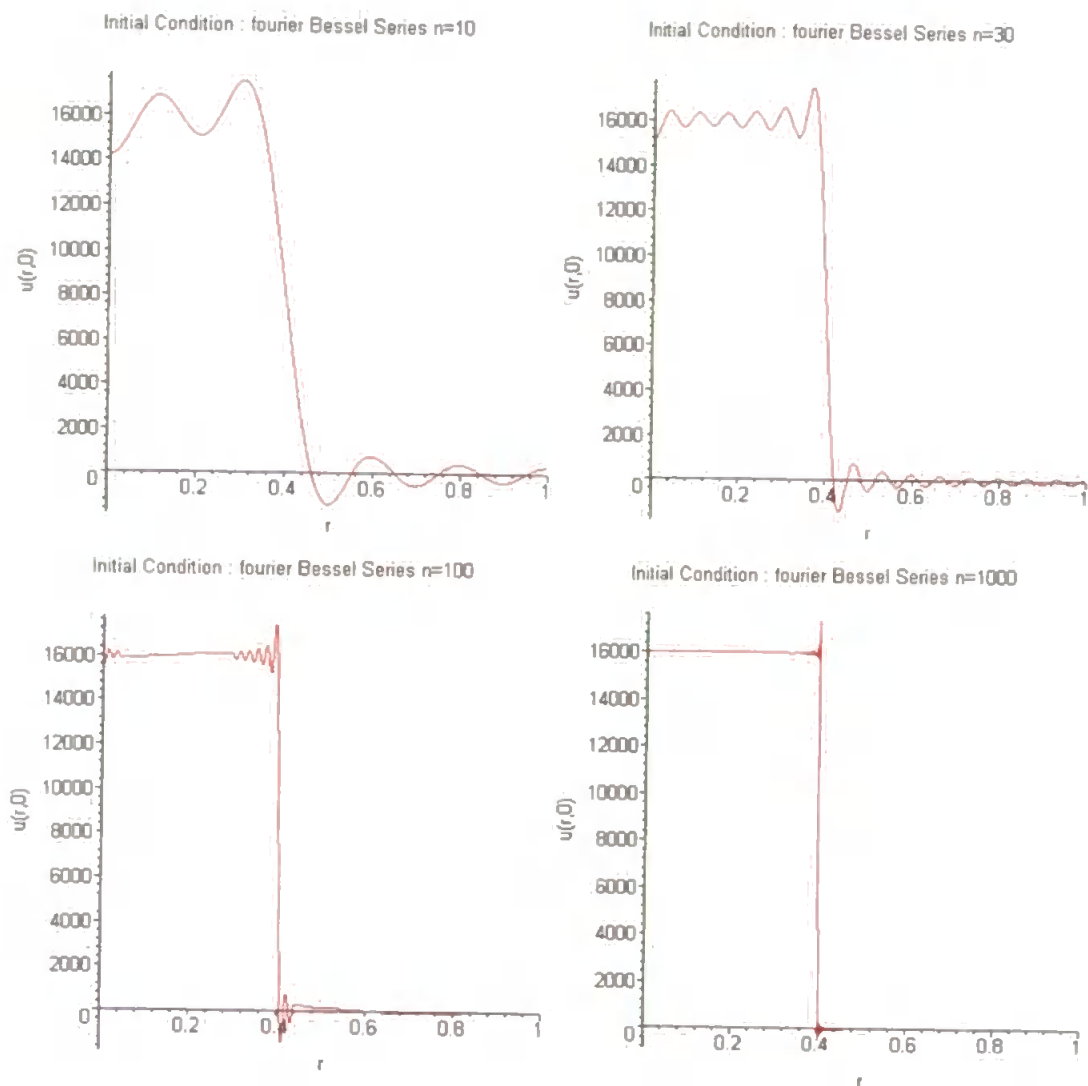


Fig C2 approximations to the initial conditions using various numbers of eigenvalues and  $A = 16000$ ,  $L1 = 0.4$ ,  $L = 1$  and  $B = 1$ .

## Appendix D Vesicle sizes

Origin	Vesicle Type	Diameter nm	Radius nm	Length nm	Membrane Depth nm	Total Volume nm <sup>3</sup>	Membrane Volume nm <sup>3</sup>	Lumen Volume nm <sup>3</sup>	Membrane /Total Volume	Lumen /Total Volume
Owen	Macrovesicle Minimum	2000	1000	N/A	8	4.19E+09	9.97E+07	4.09E+09	2.38%	97.62%
Owen	Macrovesicle Average	3000	1500	N/A	8	1.41E+10	2.25E+08	1.39E+10	1.59%	98.41%
Owen	Macrovesicle Maximum	4000	2000	N/A	8	3.35E+10	4.01E+08	3.31E+10	1.20%	98.80%
Owen	Type 1 Microvesicle	150	75	N/A	8	1.77E+06	5.07E+05	1.26E+06	28.71%	71.29%
Owen	Type 2 Microvesicle	300	150	N/A	6	1.41E+07	1.63E+06	1.25E+07	11.53%	88.47%
Pal	Apical spherical microvesicles	150	75	N/A	8	1.77E+06	5.07E+05	1.26E+06	28.71%	71.29%
Pal	Apical vermiform microvesicles	100	50	400	8	3.14E+06	1.01E+06	2.13E+06	32.26%	67.74%
Pal	Apical Macrovesicle Minimum	1000	500	N/A	8	5.24E+08	2.47E+07	4.99E+08	4.72%	95.28%
Pal	Apical Macrovesicle Average	2000	1000	N/A	8	4.19E+09	9.97E+07	4.09E+09	2.38%	97.62%
Pal	Apical Macrovesicle Maximum	3000	1500	N/A	8	1.41E+10	2.25E+08	1.39E+10	1.59%	98.41%
Pal	Cytosolic microvesicles type a	40	20	N/A	8	3.35E+04	2.63E+04	7.24E+03	78.40%	21.60%
Pal	Cytosolic microvesicles type b minimum	120	60	N/A	8	9.05E+05	3.16E+05	5.89E+05	34.90%	65.10%
Pal	Cytosolic microvesicles type b average	160	80	N/A	8	2.14E+06	5.81E+05	1.56E+06	27.10%	72.90%
Pal	Cytosolic microvesicles type b maximum	200	100	N/A	8	4.19E+06	9.27E+05	3.26E+06	22.13%	77.87%
	Microvesicle Average Excluding Pal type A					4.59E+06	8.48E+05	3.74E+06	18.46%	81.54%
	Microvesicle Average Excluding Pal type A & vermiform	190	95		7.5	4.95E+06	8.06E+05	4.15E+06	16.28%	83.72%

Table D Various results given for size of vesicles from Owen (1970) and Pal (1972).

## References

- Abramowitz, M. & Stegun, I.A., 1964, Handbook of Mathematical Functions with Formulas, Graphs, and Mathematical Tables. Dover, New York, Ninth Dover printing, Tenth GPO printing.
- Aksenova, M.V., Aksenov, M.Y., Carney, J.M. & Butterfield, D.A., 1998, Protein oxidation and enzyme activity decline in old brown Norway rats are reduced by dietary restriction. *Mechanisms of Ageing Development*, 100, 157-168.
- Alarcón, T., Byrne, H.M. & Maini, P.K., 2004, Towards whole organ modelling of tumour growth. *Progress in Biophysics & Molecular Biology*, 85, 451-472.
- Allen, J.I., & Moore, M.N., 2004, Environmental prognostics: Is the current use of biomarkers appropriate for environmental risk evaluation? *Marine Environmental Research*, 58, 227-232.
- Baba, M., Osumi, M., Scott, S.V., Klionsky, D.J., & Ohsumi, Y., 1997, Two distinct pathways for targeting proteins from the cytoplasm to the vacuole/lysosome. *The Journal of Cell Biology*, 139, 1687-1695.



Baba, M., Takeshige, K., Baba, N. & Ohsumi, Y., 1994, Ultrastructural analysis of the autophagic process in yeast: Detection of autophagosomes and their characterization. *The Journal of Cell Biology*, 124, 903-913.

Bassingthwaighte J.B., 2001, The modelling of a primitive 'sustainable' conservative cell. *Philosophical Transactions of the Royal Society of London A*, 359, 1055-1072.

Bayne, B.L., 1973a, Physiological changes in *Mytilus edulis* L. induced by temperature and nutritive stress. *Journal of the Marine Biological Association of the U.K.*, 53, 39-58.

Bayne, B.L., 1973b, Aspects of the metabolism of *Mytilus edulis* during starvation. *Netherlands Journal of Sea Research*, 7, 399-410.

Bayne, B.L., & Scullard, C., 1977a, Rates of nitrogen excretion by species of *Mytilus* (Bivalvia: Mollusca). *Journal of the Marine Biological Association of the U.K.*, 57, 355-369.

Bayne, B.L., & Scullard, C., 1977b, An apparent specific dynamic action in *Mytilus edulis* L. *Journal of the Marine Biological Association of the U.K.*, 57, 371-378

Bayne, B.L., Holland, D.L, Moore, M.N., Lowe, D.M. & Widdows, J., 1978, Further studies on the effect of stress in the adult on the eggs of *Mytilus edulis*. Journal of the Marine Biological Association of the U.K., 58, 825-841.

Bishop SH ,1976, Nitrogen metabolism and excretion: regulation of intracellular amino acid concentrations. In: Witey M (ed) Estuarine processes, Vol 1. Academic Press, New York, p 414-431

Brunk, U.T. & Terman, A., 2002, Lipofuscin: mechanisms of age-related accumulation and influence on cell function. Free Radical Biology & Medicine, 33, 611-619.

Cajaraville, M.P., Bebianno, M.J., Blasco, J., Porte, C., Sarasquete, C. & Viarengo, A., 2000, The use of biomarkers to assess the impact of pollution in coastal environments of the Iberian peninsula: a practical approach. The Science of the Total Environment, 247, 295-311.

Cajaraville, M.P., Marigómez, J.A., Diez, G. & Angulo, E., 1992, Comparative effects of the water accommodated fraction of three oils on mussels – 2. Quantitative alterations in the structure of the digestive tubules. Comparative Biochemistry & Physiology C, 102, 113-123

Cajaraville, M.P., Orbea, A., Marigomez, I. & Cancio, I., 1997, Peroxisome proliferation in the digestive epithelium of mussels exposed to the water accommodated fraction of three oils. *Comparative Biochemistry & Physiology*, 117C, 233-242.

Cavallini, G., Donati, A., Gori, Z., Pollera, M. & Bergamini, E., 2001, The protection of rat liver autophagic proteolysis from the age-related decline co-varies with the duration of anti-ageing food restriction. *Experimental Gerontology*, 36, 497-506.

Chiang, H.L., Schekman, R. & Hamamoto S., 1996, Selective uptake of cytosolic, peroxisomal, and plasma membrane proteins into the yeast lysosome for degradation. *The Journal of Biological Chemistry*, 271, 9934-9941.

Cranford, P.J. & Hill, P.S., 1999, Seasonal variation in food utilization by the suspension-feeding bivalve molluscs *Mytilus edulis* and *Placopecten magellanicus*. *Marine Ecology Progress Series*, 190, 223-239.

Cuervo, A.M., 2004, Autophagy: in sickness and health. *Trends in Cell Biology*, 14, 70-77.

Cuervo, A.M. & Dice, J.F., 2000, Age-related decline in chaperone-mediated autophagy. *Journal of Biological Chemistry*, 275, 31505-31513.

de Duve, C., 1983, Lysosomes revisited. *European Journal of Biochemistry*, 137, 391-397.

de Duve, C. & Wattiaux, R., 1966, functions of lysosomes. *Annual Review of Physiology*, 28, 435-492.

Depledge, M.H. & Galloway, T.S., 2005, Healthy animals, healthy ecosystems. *Frontiers in Ecology and the Environment*, 3, 251-258.

Depledge, M.H., Amaral-Mendes, J.J., Daniel, B., Halbrook, R.S., Kloepper-Sams, P., Moore, M.N. & Peakall, D.P., 1993, The conceptual basis of the biomarker approach. In: *Biomarkers - research and application in the assessment of environmental health*, (Eds. D.G. Peakall, and L.R. Shugart), pp. 15-29. Springer, Berlin, Heidelberg.

Desjardins, M. & Griffiths, G., 2003, Phagocytosis: latex leads the way. *Current Opinion in Cell Biology*, 15, 498-503.

Di Giulio, R.T. & Benson, W.H., 2002, Interconnections between human health and ecological integrity. Society of Environmental Toxicology and Chemistry (SETAC), Pensacola, Florida, 110p.

Djomo, J.E., Garrigues, P. & Narbonne J.F., 1996, Uptake and depuration of polycyclic aromatic hydrocarbons from sediment by the zebrafish (*Brachydanio rerio*). Environmental Toxicology and Chemistry, 15, 1177-1181.

Doherty, F.J. & Mayer, R.J., 1992, Intracellular Protein Degradation, Oxford University Press.

Dunlop, R.A., Rodgers, K.J. & Dean, R.T., 2002, Recent developments in the intracellular degradation of oxidized proteins. Free Radical Biology & Medicine, 33, 894-906.

Dunn, W.A., 1990. Studies on the mechanisms of autophagy: maturation of the autophagic vacuole. Journal of Cell Biology, 110, 1935-1945.

Edinger, A.L. & Thompson, C.B., 2004, death by design: apoptosis, necrosis and autophagy. Current Opinion in Cell Biology, 16, 663-669.

Eskelinen, E.L., Tanaka, Y. & Saftig, P., 2003, At the acidic edge: emerging functions for lysosomal membrane proteins. *Trends in Cell Biology*, 13, 137-145.

Fengsrud, M., Sneve, M.L., Overbye, A. & Seglen, P.O., 2004, structural aspects of mammalian autophagy. In: *Autophagy*, ed. D.J. Klionsky, Landes Bioscience, Georgetown, USA, pp11-25.

Finkel, T. & Holbrook, N.J., 2000, Oxidants, oxidative stress and the biology of ageing. *Nature*, 408, 239-247.

Fowler, S. & de Duve, C., 1969, Digestive activity of lysosomes. III. The digestion of lipids by rat liver lysosomes. *Journal of Biological Chemistry*, 244, 471-481.

Gabbott, P.A. & Bayne, B.L., 1973, Biochemical effects of temperature and nutritive stress on *Mytilus edulis* L. *Journal of the Marine Biological Association of the U.K.*, 53, 269-286.

Gabbot, P.A. & Peek, K., 1991, Cellular biochemistry of the mantle tissue of mussel *Mytilus edulis* L. *Aquaculture*, 94, 165-176

Gardner, J.P.A. & Thompson, R.J., 2001, The effects of coastal and estuarine conditions on the physiology and survivorship of the mussels *Mytilus edulis*, *M. trossulus* and their hybrids. *Journal of Experimental Marine Biology and Ecology*, 265, 119-140.

Hawkins, A.J.S. & Bayne, B.L., 1985, Seasonal variation in the relative utilisation of carbon and nitrogen by the mussel *Mytilus edulis*: budgets, conversion efficiencies and maintenance requirements. *Marine Ecology Progress Series*, 25, 181-188.

Hawkins, A.J.S. & Bayne, B.L., 1991, Nutrition of marine mussels: factors influencing the relative utilizations of protein and energy. *Aquaculture*, 94, 177-196.

Hawkins, A.J.S. & Bayne, B.L., 1992, Physiological interrelations, and the regulation of production. In: *The mussel Mytilus: Ecology, Physiology, Genetics and Culture*, E. Gosling ed. Elsevier, Amsterdam, pp171-222.

Hawkins, A.J.S. & Day, A.J., 1996, The metabolic basis of genetic differences in growth efficiency among marine animals. *Journal of Experimental marine Biology & Ecology*, 203, 93-115.

Hawkins, A.J.S., Salkeld, P.N., Bayne, B.L., Gnaiger, E. & Lowe, D.M., 1985, Feeding and resource allocation in the mussel *Mytilus edulis*: evidence for time-averaged optimization. Marine Ecology Progress Series, 20, 273-287.

Huang, P.H. & Chiang, H.L., 1997, Identification of novel vesicles in the cytosol to vacuole protein degradation pathway. The Journal of Cell Biology, 136, 803-810.

Ishihara, N., Hamasaki, M., Yokota, S., Suzuki, K., Kamada, Y., Kihara, A., Yoshimori, T., Noda, T. & Ohsumi, Y., 2001, Autophagosome requires specific early Sec proteins for its formation and NSF/SNARE for vacuolar fusion. Molecular Biology of the Cell, 12, 3690-3702.

Klionsky, D.J. & Emr, S.D, 2000, Autophagy as a regulated pathway of cellular degradation. Science, 290, 171-1721.

Klionsky, D.J., 2005, Autophagy. Current Biology, 15, 282-283.

Köhler, A., Wahl, E. & Söffker, K., 2002, Functional and morphological changes of lysosomes as prognostic biomarkers of toxic liver injury in a marine flatfish (*Platichthys flesus* (L.)). Environmental Toxicology and Chemistry, 21, 2434-2444.



Krishnakumar, P.K., Casillas, E. & Varanasi, U., 1994, Effect of environmental contaminants on the health of *Mytilus edulis* from Puget Sound, Washington, USA. I. Cytochemical measures of lysosomal responses in the digestive cells using automatic image analysis. Marine Ecology Progress Series, 106, 249-261.

Krishnakumar, P.K., Casillas, E. & Varanasi, U., 1997, Cytochemical responses in the digestive tissue of *Mytilus edulis* complex exposed to microencapsulated PAHs or PCBs. Comparative Biochemistry and Physiology, 118C, 11-18.

Langton, R.W., 1975, Synchrony in the digestive diverticula of *Mytilus edulis* L. Journal of the Marine Biological Association of the U.K., 55, 221-229.

Langton, R.W., 1977, Digestive rhythms in the mussel *Mytilus edulis*. Marine Biology, 41, 53-58.

Langton, R.W. & Gabbott, P.A., 1974, The tidal rhythm of extracellular digestion and the response to feeding in *Ostrea edulis*. Marine Biology, 24, 181-187.

Lauffenburger, D.A. & Linderman, J.J., 1993, Receptors: Models for binding, trafficking and signalling. Oxford University Press, Oxford, New York, 365p.

Levine, B. & Klionsky, D.J., 2004, Development by self-digestion: Molecular mechanisms and biological functions of autophagy. *Developmental Cell*, 6, 463-477.

Livingstone, D.R., 2001, Contaminant-stimulated Reactive Oxygen Species production and oxidative damage in aquatic organisms. *Marine Pollution Bulletin*, 42, 656-666.

Livingstone, D.R. & Pipe, R.K., 1992, Mussels and environmental contaminants: molecular and cellular aspects. In: *The mussel Mytilus: Ecology, Physiology, Genetics and Culture*, E. Gosling ed. Elsevier, Amsterdam, pp 425-464.

Livingstone, D. R., Chipman, J. K., Lowe, D. M., Minier, C., Mitchelmore, C. L., Moore, M. N., Peters, L. D. & Pipe, R. K., 2000a,. Development of biomarkers to detect the effects of organic pollution on aquatic invertebrates: recent molecular, genotoxic, cellular and immunological studies on the common mussel (*Mytilus edulis* L.) and other mytilids. *International Journal of Pollution*, 13, 56-91.

Livingstone, D.R., Garcia-Martinez, P., Michel, X., Narbonne, J.F., O'Hara, S., Ribera, D. & Winston, G.W., 1990, Oxyradical production as a pollution-mediated mechanism of toxicity in the common mussel, *Mytilus edulis* L., and other molluscs. *Functional Ecology*, *4*, 415-424.

Livingstone, D.R., Mitchelmore, C.L., O'Hara, S.C.M., Lemaire, P., Sturve, j. & Forlin, L., 2000b, Increased potential for NAD(P)H-dependent reactive oxygen species production of hepatic subcellular fractions of fish species with in vivo exposure to contaminants. *Marine Environmental Research*, *50*, 57-60.

Lockshin, R.A. & Zakeri, Z., 2004, Apoptosis, autophagy, and more. *The International Journal of Biochemistry and Cell Biology*, *36*, 2405-2419.

Lodish, H., Berk, A., Zipursky, S.L., Matsudaira, P., Baltimore, d. & Darnell, J., 1999, *Molecular Cell Biology*. Freeman, New York.

Lowe, D.M., 1988, Alterations in the cellular structure of *Mytilus edulis* resulting from exposure to environmental contaminants under field and experimental conditions. *Marine Ecology Progress Series*, *46*, 91-100.

Lowe, D.M. & Pipe, R.K., 1986, Hydrocarbon exposure in mussels: A quantitative study of the responses in the reproductive and nutrient storage cell systems. *Aquatic Toxicology*, 8, 265-272.

Lowe, D.M., Moore, M.N. & Clarke, K.R., 1981, effects of oil on digestive cells in mussels: quantitative alterations in cellular and lysosomal structure. *Aquatic Toxicology*, 1, 213-226.

McCarthy, J.F., Jiminez, B.D. & Barbee, T., 1985, Effect of dissolved humic material on accumulation of polycyclic aromatic hydrocarbons: structure-activity relationships. *Aquatic Toxicology*, 7, 15-24.

McVeigh, A, Moore, M.N., Allen, J.I. & Dyke, P., 2006, Lysosomal responses to nutritional and contaminant stress in mussel hepatopancreatic digestive cells: A modelling study. *Marine Environmental Research*, 62, S433-S438.

Mann, K.H. 1982. Ecology of coastal waters. *Studies in Ecology* V.8. University of California Press, Berkeley. 322pp.

Marigómez, I. & Baybay-Villacorta, L., 2003, Pollutant-specific and general lysosomal responses in digestive cells of mussels exposed to model organic chemicals. *Aquatic Toxicology*, 64, 235-257.

Marigómez, I., Izaguirre, U. & Lekube, X., 2005, Lysosomal enlargement in digestive cells of mussels exposed to cadmium, benzo[a]pyrene and their combination. *Comparative Biochemistry and Physiology C*, *141*, 188-193.

Marigómez, I., Lekube, X. & Cancio, I., 1999, Immunochemical localisation of proliferating cells in mussel digestive gland tissue. *The Histochemical Journal*, *31*, 781-788.

Masoro, E.J., 2005, Overview of caloric restriction and ageing. *Mechanisms of Ageing and Development*, *126*, 913-922.

Mathers, N.F., 1972, The tracing of a natural algal food labelled with a carbon 14 isotope through the digestive tract of *Ostrea edulis* L. *Proceedings of the Malacological Society of London*, *40*, 115-124.

Moore, M.N., 1976, Cytochemical demonstration of latency of lysosomal hydrolases in digestive cells of the common mussel, *Mytilus edulis*, and changes induced by thermal stress. *Cell and Tissue Research*, *175*, 279-287.

Moore, M.N., 1985, Cellular responses to pollutants. *Marine Pollution Bulletin*, *16*, 134-139.

Moore, M.N, 1988, Cytochemical responses of the lysosomal system and NADPH-ferrihemoprotein reductase in molluscan digestive cells to environmental and experimental exposure to xenobiotics. *Marine Ecology Progress Series*, 46, 81-89.

Moore, N.M., 2002, Biocomplexity: the post-genome challenge in ecotoxicology. *Aquatic Toxicology*, 59, 1-15.

Moore, M.N., 2004, Diet restriction induce autophagy: a lysosomal protective system against oxidative- and pollutant-stress and cell injury. *Marine Environmental Research*, 58, 603-607.

Moore, M.N., 2008, in press, Autophagy as a second level protective process in conferring resistance to environmentally-induced oxidative stress. *Autophagy*.

Moore, M.N. & Allen, J.I., 2002, A computational model of the digestive gland epithelial cell of marine mussels and its simulated response to oil-derive aromatic hydrocarbons. *Marine Environmental Research*, 54, 579-584.

Moore, M.N & Viarengo, A., 1987, Lysosomal membrane fragility and catabolism of proteins: evidence for a direct relationship. *Experientia*, *43*, 320-323.

Moore, M.N. & Willows, R.I., 1998, A model for cellular uptake and intracellular behaviour of particulate-bound micropollutants. *Marine Environmental Research*, *46*, 509-514.

Moore, M.N., Allen, J.I. & McVeigh, A., 2006a, Environmental prognostics: an integrated model supporting lysosomal stress responses as predictive biomarkers of animal health status. *Marine Environmental Research*, *61*, 278-304.

Moore, M.N., Allen, J.I., McVeigh, A. & Shaw, J., 2006b, Lysosomal and autophagic reactions as predictive indicators of environmental impact in aquatic animals. *Autophagy*, *2*, 217-220.

Moore, M.N., Depledge, M.H., Readman, J.W. & Leonard, P., 2004, An integrated biomarker-based strategy for ecotoxicological evaluation of risk in environmental management. *Mutation Research*, *552*, 247-268.

Moore, N.M., Koehn, R.K. & Bayne, B.L., 1980, Leucine aminopeptidase (aminopeptidase-I), N-acetyl- $\beta$ -hexosaminidase and lysosomes in the

mussel, *Mytilus edulis* L., in response to salinity changes. The Journal of Experimental Zoology, 214, 239-249.

Moore, M.N, Livingstone, D.R., Widdows, J., Lowe, D.M. & Pipe, R.K., 1987, Molecular, cellular and physiological effects of oil-derived hydrocarbons on molluscs and their use in impact assessment.

Philosophical Transactions of the Royal Society of London B, 316, 603-623.

Moore, M.N., Viarengo, A., Donkin, P. & Hawkins, A.J.S., 2007, Autophagic and lysosomal reactions to stress in the hepatopancreas of blue mussels. Aquatic Toxicology, 84, 80-91.

Moore, M.N, Widdows, J., Cleary, J.J., Pipe, R.K., Salkeld, P.N., Donkin, P., Farrar, S.V., Evans, S.V. & Thomson, P.E., 1984, Responses of the mussel *Mytilus edulis* to Copper and Phenanthrene: Interactive Effects. Marine Environmental Research, 14, 167-183.

Müller, O., Sattler, T., Flötenmeyer, H.S., Plattner, H. & Mayer, A., 2000, Autophagic tubes: vacuolar invaginations involved in lateral membrane sorting and inverse vesicle budding. Journal of Cell Biology, 151, 519-528,



Noble, D., 2002, The rise of computational biology. *Nature Reviews in Molecular and Cell Biology*, 3, 460-463.

Nott, J.A. & Nicolaidou, A., 1989, The cytology of heavy metal accumulations in the digestive glands of three gastropods. *Proceedings of the Royal Society London*, 237B, 347-362.

Owen, G., 1970, The fine structure of the digestive tubules of the marine bivalve *Cardium Edule*. *Philosophical Transactions of the Royal Society of London B*, 258, 245-260.

Pacifici, R.E. & Davies, K.J., 1991, Protein, lipid and DNA repair systems in oxidative stress: the free radical theory of aging revisited. *Gerontology*, 37, 166-180.

Pal, S.G., 1972, The fine structure of the digestive tubules of *Mya Arenaria L.*: II digestive cell. *Journal of Molluscan Studies*, 40, 161-170.

Pierce S.K., 1971, Volume regulation and valve movements by marine mussels. *Comparative Biochemistry and Physiology Part A: Physiology*, 103-117.

Pillay, C.S., Elliott, E. & Dennison, C., 2002, Endolysosomal proteolysis and its regulation. *Biochemical Journal*, 363, 417-429.

Pipe, R.K. & Moore, M.N., 1985, Ultrastructural changes in the lysosomal-vacuolar system in digestive cells of *Mytilus edulis* as a response to increased salinity. *Marine Biology*, 87, 157-163.

Ramaiah, S.K., Apte, U. & Mehendale, H.M., 2000, Diet restriction as a protective mechanism in noncancer toxicity outcomes: A review. *International Journal of Toxicology*, 19, 413-424.

Readman, J.W., Mantoura, R.F.C. & Rhead, M.M., 1984, The physico-chemical speciation of polycyclic aromatic hydrocarbons (PAH) in aquatic systems. *Analytical and Bioanalytical Chemistry*, 319, 126-131.

Reggiori, F. & Klionsky, D.J., 2002, Autophagy in the eukaryotic cell. *Eukaryotic Cell*, 1, 11-21.

Regoli, F., 2000, Total oxyradical scavenging capacity (TOSC) in polluted and translocated mussels: a predictive biomarker of oxidative stress. *Aquatic Toxicology*, 50, 351-361.

Reverter-Branchart, G., Cabiscol, E., Tamarit, J. & Ros, J., 2004, Oxidative damage to specific proteins in replicative and chronological-aged

*Saccharomyces cerevisiae*. The Journal of Biological Chemistry, 279, 31983-31989.

Robinson, M.S., Watts, C. & Zerial, M., 1996, Membrane dynamics in endocytosis. Cell, 84, 13-21.

Ryan, T.A., 2003, kiss-and-run, fuse-pinch-and-linger, fuse-and-collapse: The life and times of a neurosecretory granule. Proceedings of the National Academy of Sciences USA, 100, 2171-2173.

J. P. Shaw, A. T. Large, P. Donkin, S. V. Evans, F. J. Staff, D. R.

Livingstone, J. K. Chipman & L. D. Peters ,2004, Seasonal variation in cytochrome P450 immunopositive protein levels, lipid peroxidation and genetic toxicity in digestive gland of the mussel *Mytilus edulis*. Aquatic Toxicology, 67, 325-336.

Stinchcombe, J., Bossi, G. & Griffiths, G.M., 2004, Linking albinism and immunity: the secrets of secretory lysosomes. Science, 305, 55-59.

Szego, C.M., 1975, Lysosomal function in nucleocytoplasmic communication. In: Lysosomes in Biology & Pathology (J.T. Dingle & R.T. Dean, Eds.), vol. 4, 385-477. Elsevier, Amsterdam, Oxford, New York.

Thompson, R.J. & Bayne, B.L., 1972, Active metabolism associated with feeding in the mussel *Mytilus edulis* L. Journal of Experimental Marine Biology and Ecology, 9, 111-124.

Thompson, R.J., Ratcliffe, N.A. & Bayne, B.L., 1974, Effects of starvation on structure and function in digestive gland of the mussel (*Mytilus edulis* L.). Journal of the Marine Biological Association U.K., 54, 699-712.

Tuttle, D.L. & Dunn, W.A. Jr, 1995, Divergent modes of autophagy in the methylotrophic yeast *Pichia pastoris*. Journal of Cell Science, 108, 23-35.

Viarengo, A., Zannicchi, G., Moore, M. N. and Orenusu, M., 1981, Accumulation and detoxication of copper by the mussel *Mytilus galloprovincialis* Lam.: A study of the subcellular distribution in the digestive gland cells. Aquatic Toxicology 1, 147-157

Viarengo, A, 1985, Biochemical effects of trace metals. Marine Pollution Bulletin, 16, 153-158.

Viarengo, A., Moore, M.N., Pertica, M., Mancinelli, G., Zanicchi, G. and Pipe, R.K., 1985, Detoxification of copper in the cells of the digestive gland of mussel: the role of lysosomes and thioneins. The Science of the Total Environment, 44, 135-145.

Widdows, J. & Donkin, P., 1992, Mussels and environmental contaminants: biochemical and physiological aspects. In: The mussel *Mytilus*: Ecology, Physiology, Genetics and Culture, E. Gosling ed. Elsevier, Amsterdam, pp383-424.

Widdows, J., & Hawkins, A.J.S., 1989, Partitioning of rate of heat dissipation by *Mytilus edulis* into maintenance, feeding and growth components. *Physiological Zoology*, 62, 764-784.

Widdows, J., Bakke, T., Bayne, B.L., Donkin, P., Livingstone, D.R., Lowe, D.M., Moore, M.N., Evans, S.V. & Moore, S.L., 1982, Responses of *Mytilus edulis* on exposure to the water-accommodated fraction of North Sea oil. *Marine Biology*, 67, 15-31.

Widdows, J., Donkin, P., Brinsley, M.D., Evans, S.V., Salkeld, P.N., Franklin, A., Law, R.J. & Waldock, M.J., 1992, Scope for growth and contaminant levels in the North sea mussels *Mytilus edulis*. *Marine Ecology Progress Series*, 127, 131-148.

Winkler, B. S., Boulton, M. E., Gottsch, J. D. & Sternberg, P., 1999, Oxidative damage and age-related macular degeneration. *Molecular Vision*, 5, 3.

Yamamoto, A., Maskai, R. & Tashiro, Y., 1990, Absence of cytochrome P450 and the presence of autolysosomal membrane antigens on the isolation membranes and autophagosomal membranes in rat hepatocytes. *Journal of Histochemistry and Cytochemistry*, 38, 1571-1581.

## Towards computational models of cells for environmental toxicology

J Icarus Allen<sup>1</sup> & Allan McVeigh<sup>1,2</sup>

<sup>1</sup>*Plymouth Marine Laboratory, Prospect Place, The Hoe, Plymouth, PL1 3DH, UK*

<sup>2</sup>*Department of Mathematics and Statistics, University of Plymouth, Drake Circus, Plymouth, PL4 8AA, UK*

Received 28 January 2004

### Summary

This paper outlines an approach to the development of computational models of cells for marine environmental toxicology. Exposure of cells to pollutants can lead to lysosomal damage and dysfunction, augmented autophagy, cellular dysfunction and atrophy and ultimately tissue pathology and organ damage. The application of carbon and nitrogen based models of intra cellular vesicular traffic for simulating the autophagic and lysosomal response of the hepatopancreatic digestive cells of marine molluscs is described. Two numerical models of the vesicular transport of carbon and nitrogen in the cell are presented. These demonstrate the importance of endocytotic uptake as a driver of lysosomal dynamics and the need to recognize and model it as a discrete process. Conceptual and mathematical models of the toxic impact of polycyclic aromatic hydrocarbons on the digestive gland are presented. The role of experimental research and the need to integrate it with modelling is highlighted.

### Introduction

Environmental toxicology is the study of the impact of contaminants upon biological activity in the environment. This can take place at a range of levels from cells to organism to whole ecosystems. Such environmental disturbances can result in adaptive responses, stress syndromes, disease and changes in functional biodiversity. The vast complexity of the interactions between these processes dictates that we have to think in terms of integrative models to address the problem in a way that our mental computing capability cannot (Noble 2002a, b). A crucial challenge is the development of predictive simulation models of toxic effects on complex cellular and physiological processes. Understanding of the molecular and sub cellular interactions with pollutant chemicals including genomic and proteomic aspects is key to this. Mathematical models can provide insights into the links between molecular properties and cell and organ behaviour.

Biological science has been essentially reductionist for over 50 years. The current challenge is to reassemble this data to unravel how complex systems from sub-cellular processes to organisms work. Systems biology attempts to reconstruct biological systems by developing and evolving series of overlapping conceptual, numerical and statistical models (Hunter 2003), a process involving the interaction of experiment and simulation in an ongoing iterative process. Complex systems require models to understand them. The recent rapid growth of computational power allows this to happen.

The heart of the procedure is the definition and evaluation of models of the system in question. This requires the use of a number of interdependent tools: conceptual, statistical and numerical models, empirical experimental work and bioinformatics. Bioinformatics is the acquisition, archiving and interpretation of biological information. Statistical analysis is a complementary tool to exploit bioinformatics with the objectives of hypothesis testing, estimation and data exploration. Conceptual models arise from the interpretation of biological data. Numerical models rely on conceptual models to define equations, empirical studies to parameterise them, and statistics to evaluate them.

Conceptual models of biological systems are common. They often exist in isolation from one another, and are frequently not formally or explicitly declared. For even the simplest conceptual models the results or outcomes are not always tractable or apparent. Models should be constructed at an appropriate level of complexity to address the hypothesis being tested and the data available to support it. Additionally we should bear in mind that a well constructed model which fails is often more informative than one that succeeds. A good model should be descriptive (represents the available data), integrative (demonstrate how elements interact) and explanatory (provide biological insight).

Currently numerical models for environmental toxicology are in their infancy and used for heuristic purposes (Allen and Moore in press). The great advantage of simulation is that it encourages an understanding of

how processes are linked and how system properties emerge in space and time. Simulations of lysosomal volume in response to toxic impact in molluscan hepatopancreatic or digestive gland cells have already been made (Moore and Allen 2002, McVeigh *et al.* 2004), indicating that prognostic simulations of organism health are possible. The epithelial cells of the mussel digestive gland provide a key interface between the organism and pollutants such as aromatic hydrocarbons. Exposure to such pollutants causes augmented cellular autophagy, the lysosome to swell, accumulate lipid and decrease in stability (e.g. Lowe *et al.* 1981, 1995a,b, Moore *et al.* 1996). The effects upon the lipid and lipofuscin distributions within lysosomes when exposed to polycyclic aromatic hydrocarbons (PAHs) are illustrated in Figure 1. Micrographs from a clean site are shown for comparison. The swelling of the lysosomes can clearly be seen. Lysosomal stability reflects toxicant induced cell pathologies and integrates various classes of pollutants. It is a good indicator of the degree of stress or disease and health status of the animal (see Moore 2002 and references cited therein). Taking the example of the bivalve mollusc *Mytilus edulis* (blue mussel), the energy balance of the organism (scope for growth) is a robust indicator of the health status of the animal. Scope for growth is linearly correlated with the lysosomal stability of digestive gland epithelial cells indicating that lysosomal stability

is also a good indicator of the overall health of the organism (Allen and Moore 2004).

In this paper we describe the application of carbon and nitrogen based models of intra cellular vesicular traffic for simulating the lysosomal response of the digestive cells of molluscs, and develop the conceptual framework for modeling the response of such systems to exposure to PAHs.

### Modelling basic cell function

#### Conceptual model framework

The first stage of any numerical modeling exercise is to establish the conceptual framework that we will construct mathematical equations to represent. For the purpose of this paper we consider the digestive gland epithelial cell of the blue mussel. In our simplified model world, the digestive gland is considered to be represented by a generic single cell. This cell is an average of the 300–400 million cells that make up the epithelial gland and is therefore assumed to be immortal unless exposed to a lethal environmental shock. The model system is conceived to exist in isolation from external influences. Environmental conditions (for example heat and salinity) are assumed to be either stable or unobtrusive, the stage in the organ-

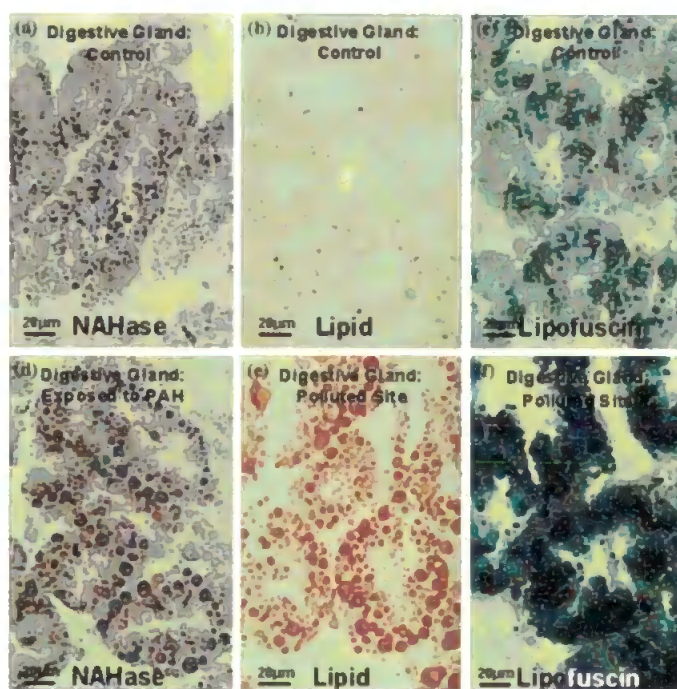


Figure 1. Lysosomal swelling and lipid accumulation in the digestive gland cells of *Mytilus edulis* after exposure to PAH. (a) lysosomal size as indicated by NAHase at a clean site, (b) lipid in cells from a clean site, (c) lipofuscin in cells from a clean (d) lysosomal size as indicated by NAHase at a polluted site, (e) lipid in cells from a polluted site, (f) lipofuscin in cells from a polluted site. NAHase or  $\beta$ -N-acetylhexosaminidase is a lysosomal marker enzyme (Moore 1990).



ism's life cycle is disregarded and the cell cycle is ignored.

Our first major simplification is that the cell is assumed to be made up of three compartments, an endosome, a lysosome and the cytoplasm. Each of these compartments represents the aggregate of all the individual endosomes, lysosomes or organelles and proteins that make up a cell. Only the major physiological pathways relevant to the flow of either carbon or nitrogen or cell volume are considered and are illustrated in Figure 2. The cell takes up particulate carbon and nitrogen via the endocytotic pathway, it is processed via the lysosome, to maintain or grow the cell. Excess carbon is stored as glycogen or exported to the rest of the animal or and waste products are removed. Autophagy (protein and organelle turnover) is considered and lysosomal lipid accumulation is considered when autophagic rates are enhanced.

#### Numerical model

From this premise, and the general assumptions of conservation of mass and exit from compartments at average concentrations, a system of ordinary differential equations (ODE) is easily derived. The model system has progressed through several stages. The original model only described the flow of carbon through the cell, with a glycogen store (Moore & Allen 2002). It successfully simulated observed changes in cell volumes and demonstrated the concept. However the increasing recognition that the autophagic protein turnover was a key process in regulating cell function it became clear that we needed to move towards being

able to represent protein turnover. Consequently, the flow of nitrogen and lipid was added to the system (McVeigh *et al.* 2004). Further details and some validation of the model can be found in McVeigh *et al.* (2004).

The equations for the carbon, nitrogen, lipid model are given below.

#### Volumes (litres)

$$\frac{dE_v}{dt} = k_{\text{end}} - k_{\text{rec}} - k_{\text{lys}} \quad (1)$$

$$\frac{dL_v}{dt} = k_{\text{lys}} + k_{\text{aut}} - k_{\text{deg}} - k_{\text{exo}} \quad (2)$$

$$\frac{dC_v}{dt} = k_{\text{deg}} - k_{\text{aut}} - k_{\text{exp}} - k_{\text{sec}} - k_{\text{res}} - k_{\text{exc}} + k_{\text{diff}} \quad (3)$$

#### Carbon (moles)

$$\frac{dE_{xc}}{dt} = k_{\text{end}}S_c - (f_r k_{\text{rec}} + k_{\text{lys}})E_c \quad (4)$$

$$\frac{dL_{xc}}{dt} = k_{\text{lys}}E_c + k_{\text{aut}}C_c - (k_{\text{deg}} + k_{\text{exo}})L_c \quad (5)$$

$$\frac{dC_{xc}}{dt} = k_{\text{deg}}L_c - (k_{\text{aut}} + k_{\text{exp}} + k_{\text{sec}} + k_{\text{res}})C_c \quad (6)$$

#### Nitrogen (moles)

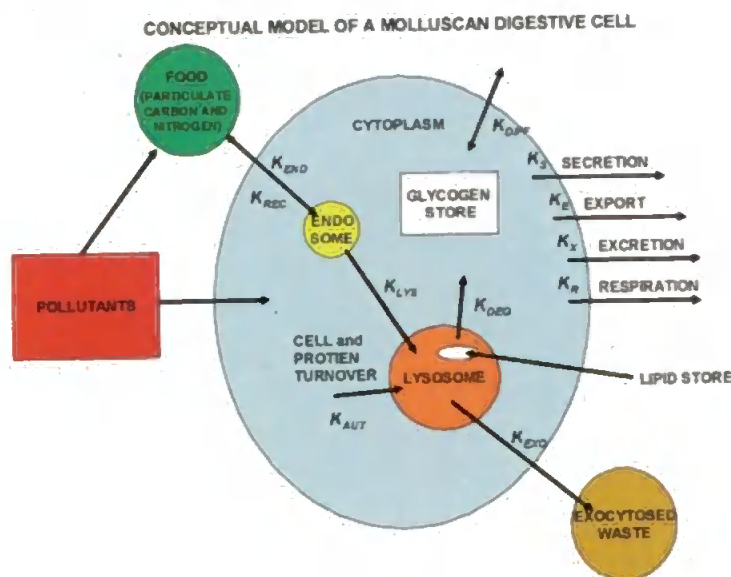


Figure 2. Conceptual model of the vesicular transport of carbon and nitrogen through the digestive gland epithelial cell of a mollusc. The symbols in the diagram are given in Table 1.

$$\frac{dE_{xn}}{dt} = k_{\text{end}}S_n - (f_r k_{\text{rec}} + k_{\text{lys}})E_n \quad (7)$$

$$\frac{dL_{xn}}{dt} = k_{\text{lys}}E_n + k_{\text{aut}}C_n - (k_{\text{deg}} + k_{\text{exo}})L_n \quad (8)$$

$$\frac{dC_{xn}}{dt} = k_{\text{deg}}L_n - (k_{\text{aut}} + k_{\text{exp}} + k_{\text{sec}} + k_{\text{exc}})C_n \quad (9)$$

See Table 1 for glossary of terms

From a numerical and computational point of view solving these sets of parallel ODE's via Eulerian integration is trivial as long as the chosen time step for the integration is small enough to ensure numerical stability and conservation of mass.

A crucial control condition for the system is that the carbon concentration in the cytosol remains constant at a predetermined level given in Table 1. A consequence of this is the inclusion of a diffusion rate constant, whereby mass can be either added or extracted from the cell. This is not intended to model the real process of diffusion. The same approach will not work for nitrogen. However, adding the nitrogen equations is not a redundant exercise. The nitrogen concentration is regulated by the excretion rate constant which may be increased or decreased as applicable.

The real 'work' of modelling is in defining how the rate constants are to be expressed. Endocytosis is described as a discrete process, because it is dependent upon food availability. All of the other transfer rates are assumed to occur continuously. Autophagy is modelled as a percentage of the cell volume per day.

Export, which is indicative of a healthy well-fed cell, relies upon passing a predetermined threshold and then all excess material passing to the rest of the animal. The other rate constants in the earliest version of the model were defined as source compartment volume dependent, as in the example below

$$k_{\text{lys}}(t) = k_{\text{lys min}} + (k_{\text{lys max}} - k_{\text{lys min}}) \left( \frac{E_v(t) - E_{v \text{ min}}}{E_{v \text{ max}} - E_{v \text{ min}}} \right)^{\frac{1}{2}} \quad (10)$$

Where  $k_{\text{lys}}(t)$  is the rate constant for the transfer of material from the endosome to the lysosome.  $k_{\text{lys min}}$  and  $k_{\text{lys max}}$  are, respectively, the minimum and maximum observed rates of this transfer.  $E_v(t)$  is the current volume of the endosome.  $E_{v \text{ min}}$  and  $E_{v \text{ max}}$  are the minimum and maximum allowable volumes of the endosome. The indicial value is there to reflect that this method of transport (vesicular) was dependant on surface area rather than volume.

To illustrate the model, results are presented from a simulation of a mussel being fed at a maintenance level with food being supplied for 6 h, followed by a 6 h rest (Figure 3a). This represents the tidally controlled feeding of inter-tidal molluscs. Maintenance is defined as the amount of food required for the cell to maintain its current state. The initial conditions for the models (volumes, carbon and nitrogen concentrations) are given in Table 1. The simulations are for ten days.

The response of cell volume and cell nitrogen concentration (carbon shows similar trends) are shown in Figure 3a, b. The major features to note are that while the total cell and cytoplasm volumes are increasing,

Table 1.

Symbol	Definition	Value or lower-upper limits
$C_c$	Concentration of C in cell cytoplasm	8.3 mol. $l^{-1}$
$C_n$	Concentration of N in cell cytoplasm	0.5 mol. $l^{-1}$
$E_c$	Concentration of C in endosomes	8.3–12.0 mol
$E_n$	Concentration of N in endosomes	0.5–0.8 mol. $l^{-1}$
$L_c$	Concentration of C in lysosomes	8.3–15.0 mol. $l^{-1}$
$L_n$	Concentration of N in lysosomes	0.5–0.9 mol. $l^{-1}$
$S_c$	Concentration of C at cell surface	2.1 (0–6.0) mol. $l^{-1}$
$S_n$	Concentration of N at cell surface	0.1 (0–0.4) mol. $l^{-1}$
$f_d$	Fraction of N digested in lysosome and passed to cell	0–0.9
$f_r$	Fraction of N recycled from endosome to cell surface	0.01
$k_{\text{aut}}$	Rate constant for autophagy	$1.7 \times 10^{16}$ – $1.2 \times 10^{15}$ $l. \text{ min}^{-1}. \text{ cell}^{-1}$
$k_{\text{deg}}$	Rate constant for intracellular digestion	$1.0 \times 10^{16}$ – $1.0 \times 10^{15}$ $l. \text{ min}^{-1}. \text{ cell}^{-1}$
$k_{\text{end}}$	Rate constant for endocytosis	$6.7 \times 10^{17}$ – $2.0 \times 10^{15}$ $l. \text{ min}^{-1}. \text{ cell}^{-1}$
$k_{\text{exo}}$	Rate constant for exocytosis	$1.0 \times 10^{16}$ – $1.0 \times 10^{15}$ $l. \text{ min}^{-1}. \text{ cell}^{-1}$
$k_{\text{lys}}$	Rate constant for vesic. traffic from endosome to lysosome	$0$ – $3.5 \times 10^{16}$ $l. \text{ min}^{-1}. \text{ cell}^{-1}$
$k_{\text{diff}}$	Rate constant for diffusion to regulate carbon concentration in cytoplasm	
$k_X$	Rate constant for N excretion	$1.25 \times 10^{18}$ – $4.0 \times 10^{18}$ $l. \text{ min}^{-1}. \text{ cell}^{-1}$
$k_S$	Rate constant for secretion	$1.4 \times 10^{19}$ – $2.8 \times 10^{18}$ $l. \text{ min}^{-1}. \text{ cell}^{-1}$
$k_E$	Rate constant for export	$0$ – $6.0 \times 10^{16}$ $l. \text{ min}^{-1}. \text{ cell}^{-1}$
	Cell Volume	$2.4 \times 10^{13}$ – $2.4 \times 10^{12}$ $l$
	Lysosomal volume	1–30% of cell volume
	Endosomal volume	1–5% of cell volume
	Number of digestive cells per mussel	$3.125 \times 10^6$

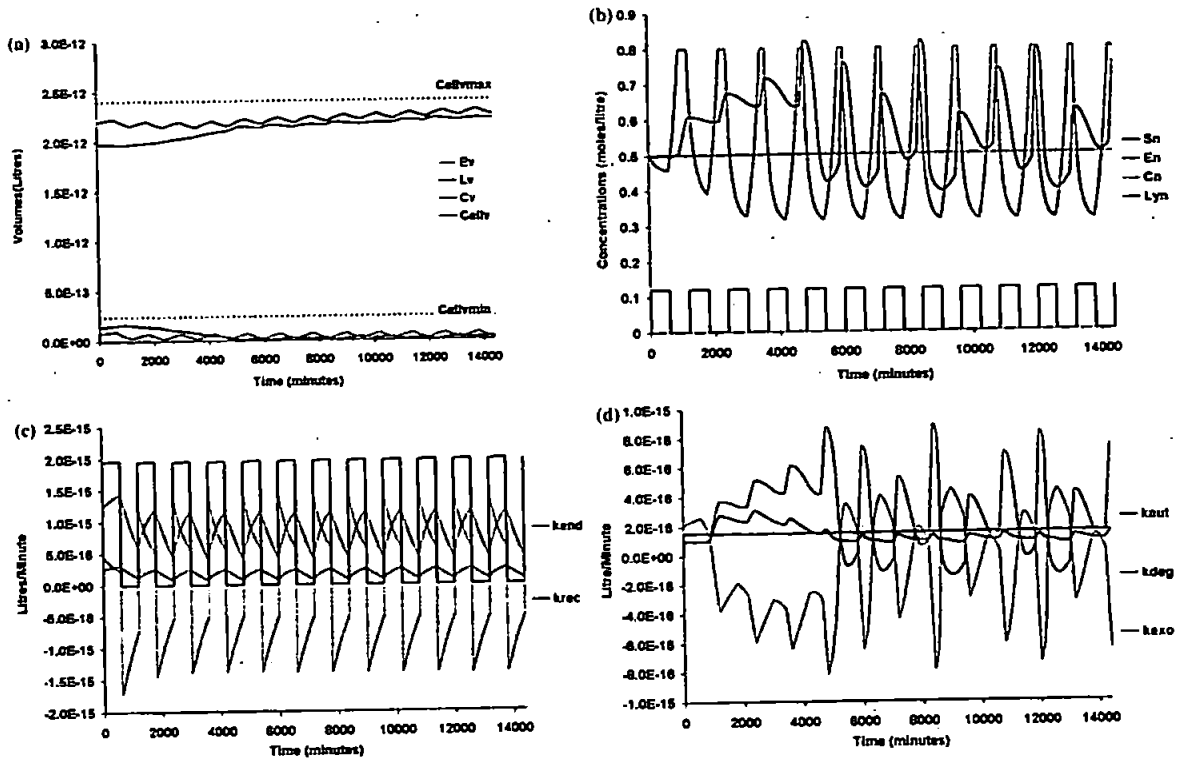


Figure 3. Simulation results from model 1. (a) Volume of the cell and its components, (b) nitrogen concentrations of food, cell, lysosomal and the endosome, (c) endosomal volume fluxes, (d) lysosomal volume fluxes. The nomenclature is as given in Table 1.

the lysosomal volume collapses to be lower than the endosomal volume which is probably unrealistic. Also the nitrogen concentration in the lysosome behaves in an unlikely manner. Figure 3c shows the rate constants for the endosome. The rate of transfers from the endosome to the lysosome has a saw tooth shape, with a minimum when feeding starts and a maxima when it stops, reflecting the changes in endosomal volume. The rates of removal of material are continuous in this model version. Figure 3d illustrates change in transfer rates into and out of the lysosome. The rate constant for vesic traffic between the endosome and lysosome, changes with endosomal volume, while the autophagic rate remains increases slowly over the period of the simulation as the cytoplasm volume increases. The rate constant for intracellular digestion ( $k_{deg}$ ) periodically goes negative, which is unrealistic. In this first model the rate constants and the processes they represent are considered to be continuous. The alternative is to consider them as discrete. For example, logically the two possible routes from the endosome (transfer to the lysosome and recycling of the cell wall) should not be activated unless there had previously been an endocytotic input. Following this approach a conceptual throughput is ascribed to each compartment, i.e. a unit of incoming material is processed in a prescribed

amount of time and then apportioned into the available exit routes at the end of this period. This time delay approach was applied to the activity of the lysosome and endosome was adopted and is described here.

For example the endosomal traffic would be governed by the following restrictions

$$k_{lysV}(t + \tau) + k_{recV}(t + \tau) = k_{endV}(t) \quad (11)$$

$$k_{endV}(t)SN_c(t) = k_{lysV}(t + \tau)EX_c(t + \tau) + k_{recV}(t + \tau)EY_c(t + \tau) \quad (12)$$

$$k_{endV}(t)SN_n(t) = k_{lysV}(t + \tau)EX_n(t + \tau) + k_{recV}(t + \tau)EY_n(t + \tau) \quad (13)$$

where  $EX_c, EX_n$ , respectively, are the carbon and nitrogen concentrations of material leaving for the lysosome and  $EY_c, EY_n$  similarly are the carbon and nitrogen concentrations of material leaving to be recycled to the cell surface and  $\tau$  is the residence time in the endosome. This is taken to be 5 min, the time taken between uptake and material starting to be recycled to the cell wall.

The system of ODEs has to be rewritten and can be

expressed involving delay terms. So for example the endocytosis volume, carbon amounts and concentrations become

$$\begin{aligned}\frac{dE_v}{dt} &= k_{\text{end}N}(t) - k_{\text{rec}N}(t) - k_{\text{lys}N}(t) \\ &= k_{\text{end}N}(t) - k_{\text{end}N}(t - \tau)\end{aligned}\quad (14)$$

$$\begin{aligned}\frac{dEN_{xc}}{dt} &= k_{\text{end}N}(t)SN_c(t) \\ &\quad - k_{\text{rec}N}(t)EY_c(t) - k_{\text{lys}N}(t)EX_c(t) \\ &= k_{\text{end}N}(t)SN_c(t) - \left(\frac{x-1+f_{rN}}{x}\right)k_{\text{end}N}(t-\tau)EY_c(t) \\ &\quad - \left(\frac{1-f_{rN}}{x}\right)k_{\text{end}N}(t-\tau)EX_c(t) \\ &= k_{\text{end}N}(t)SN_c(t) - k_{\text{end}N}(t-\tau) \\ &\quad \times \left(\left(\frac{x-1+f_{rN}}{x}\right)\frac{x f_{rN}}{x-1+f_{rN}}SN_c(t-\tau) \right. \\ &\quad \left. + \left(\frac{1-f_{rN}}{x}\right)xSN_c(t-\tau)\right) \\ &= k_{\text{end}N}(t)SN_c(t) - k_{\text{end}N}(t-\tau)SN_c(t-\tau)\end{aligned}\quad (15)$$

where  $x$  is a dimensionless constant with a fitted value of 3.

Once again to illustrate the model, results are presented from a simulation of a mussel being fed at a maintenance level with food being supplied for 6 h, followed by a 6 h rest (Figure 4a). The initial conditions and parameters are identical to those used in the first simulation so a direct comparison is possible. The cell is more efficient than the previous version, the maximum cell volume is achieved after 5 days and lysosomal volume is maintained (Figure 4a). The cell is storing excess carbon and nitrogen in the cytosol and lysosomal concentrations are stable. The effect of the delay imposed on the rates on endosomal dynamics can be seen in Figure 4c by comparing  $k_{\text{end}}$  with  $k_{\text{rec}}$  and  $k_{\text{lys}}$ . Similar effects can be seen for the lysosomal rate constants (Figure 4c) and in particular  $k_{\text{deg}}$  no longer has negative values. The lysosomal digestion rate  $k_{\text{deg}}$  increases in response to material being transferred from the endosome, and returns to a base rate which is the difference between autophagy and excretion.

The models presented indicate the importance of endocytosis, as the driving force for vesicular carbon and nitrogen transport and that better understanding of this process is crucial to further model development. The crucial point is that endocytotic uptake is a dis-

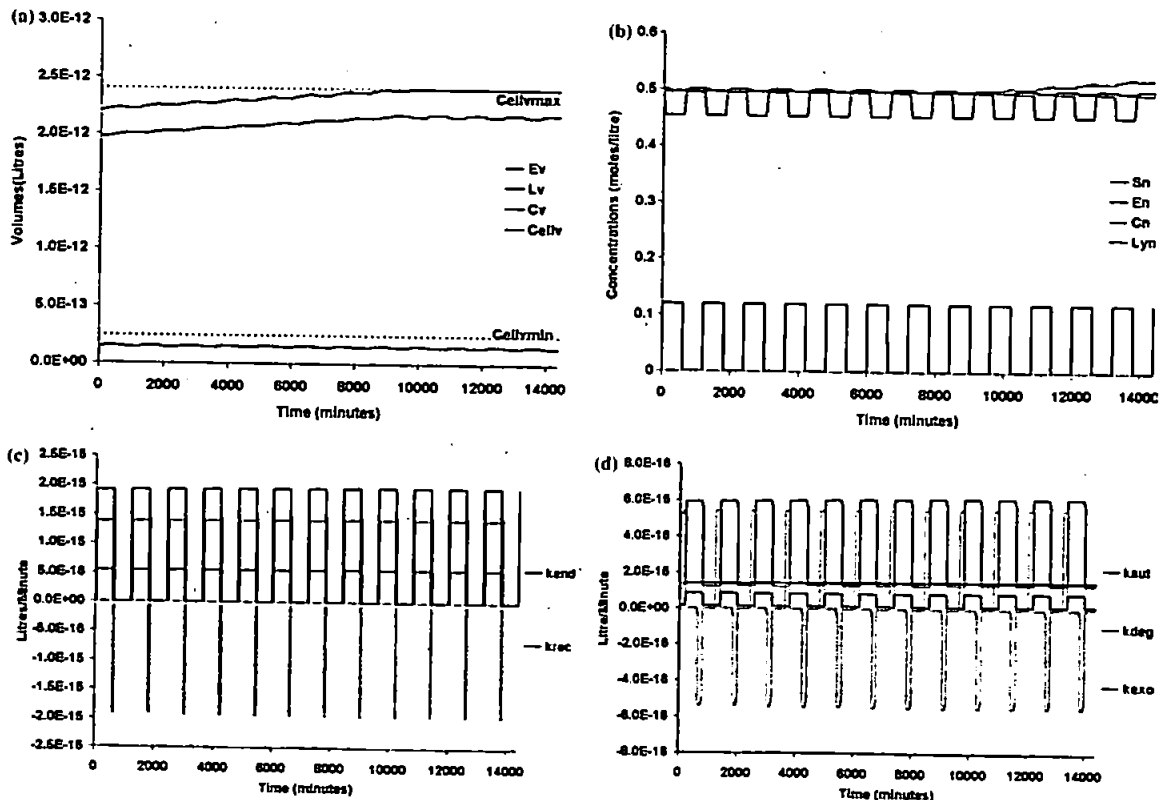


Figure 4. Simulation results from model 2. (a) Volume of the cell and its components, (b) nitrogen concentrations of food, cell, lysosomal and the endosome, (c) endosomal volume fluxes, (d) lysosomal volume fluxes. The nomenclature is as given in Table 1.

crete, not a continuous process. When we modeled the system as continuous we failed to simulate plausible lysosomal dynamics. By modeling the response of the endosome in a discrete manner we begin to simulate phasic activity of intracellular digestion. There is evidence of environmentally driven (e.g. tidal cycles) phasic activity of intracellular digestion in the digestive gland of *M. Edulis*. (Langton 1977). In reality endocytosis is a stochastic process dependent on the concentration of particles in the tubules of the digestive gland and the exposed surface area of the cell. These processes may need to be explicitly resolved in future models.

#### Modelling pollutant damage pathways

Many physiological responses (e.g. rates of oxygen consumption, feeding, excretion, and scope for growth), cellular responses (e.g. lysosomal latency and digestive cell size) and biochemical responses (e.g. specific enzyme activities) are influenced by exposure to a PAH (Widdows *et al.* 1982).

In order to move towards a theoretical ecotoxicology, we need to attempt to model a number of key processes. These are mechanisms of pollutant uptake, biotransformation and radical generation, and molecular damage and consequent cell injury (antioxidant protection and repair vesicular transport of proteins, protein turnover and interactions of the nervous and endocrine systems). Figure 5 shows a conceptual diagram of how some of these processes may be represented as a precursor to the development of a numerical model. To model the cell's response to insult we must speculate how the pollutant affects the rate constants and/or fractional parameters. PAH accumulation in the digestive cell indicates a relationship

between PAH concentration in the cell and the level of protein catabolism (Viarengo *et al.* 1992). We will consider two pathways of pollutant uptake and its consequent effects, diffusion and endocytotic uptake. PAHs are considered as the class of pollutant because they are ubiquitous in the marine environment and consequently their effects are well studied. Following the diffusive pathway, PAHs enter the cell via diffusion across the cell wall. The presence of PAHs increases the production of free radical reactive oxygen species (ROS) within the cell (Viarengo *et al.* 1992, Kirchin *et al.* 1992, Livingstone 2001) and may trigger or enhance the cell's anti-oxidant defence (Livingstone 2001). The toxic effects caused by ROS are limited by complex anti-oxidant defence mechanisms, including low molecular weight compounds (such as vitamin E and ascorbic acid) and specially adapted enzymes such as the superoxide dismutases (Manduzio *et al.* 2003). ROS react with the proteins and organelles. Damaged components are targeted for degradation, thus increasing the autophagic rate. We consider the autophagic pathway to be split into two components, basal (including enhancement due to starvation) and ROS-induced. Colloidally-bound PAHs also enter via the endocytotic pathway, passing via the endosome into the lysosome. At this stage, we need to consider the strength of binding of the PAHs to colloids and hence their bioavailability, particularly into context of the changing chemical environments as colloids pass through the cell wall to the lysosome (pH 3–5.5) via the endosome (pH 5.5–7) along a gradient of increasing acidity. PAHs accumulate within the lysosome generating radicals, and triggering antioxidant defences e.g. superoxide dismutases (Winston *et al.* 1991). The accumulation of contaminants in the lysosome is known to lead to membrane damage resulting in the leakage of the con-

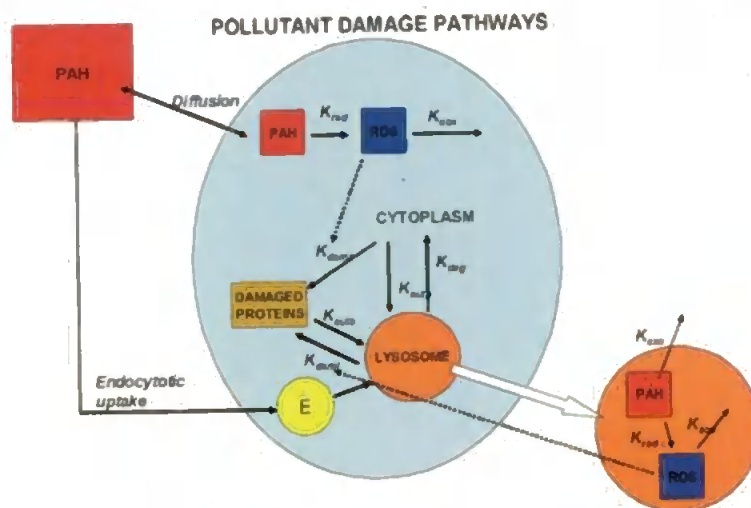


Figure 5. Conceptual model of the pollutant transport pathways and subsequent impact on the digestive gland epithelial cell of a mollusc. The symbols in the diagram are given in Table 1.

tents in to the cytosol and cell damage (Lowe and Fossato 2000). In our model, radical attack damages the structural integrity of the lysosome causing dysfunction and leading to the leakage of enzymes and lysosomal material into the cytosol.

Based on the conceptual model we can formulate the following set of ordinary differential equations to describe these processes.

#### Volumes (litres)

$$\frac{dE_v}{dt} = k_{end} - k_{rec} - k_{lys} \quad (16)$$

$$\frac{dL_v}{dt} = k_{lys} + k_{autb} + k_{auto} - k_{deg} - k_{exo} - k_{damL} \quad (17)$$

$$\frac{dC_v}{dt} = k_{deg} - k_{autb} - k_{exp} - k_{damC} - k_{sec} - k_{res} - k_{exc} + k_{diff} \quad (18)$$

$$\frac{dDP_v}{dt} = k_{damL} + k_{damC} - k_{auto} \quad (19)$$

#### Carbon (moles)

$$\frac{dE_{xc}}{dt} = k_{end}S_c - (f_r k_{rec} + k_{lys})E_c \quad (20)$$

$$\frac{dL_{xc}}{dt} = k_{lys}E_c + k_{autb}C_c - (k_{deg} + k_{exo} + k_{damL})L_c + k_{auto}DP_c \quad (21)$$

$$\frac{dC_{xc}}{dt} = k_{deg}L_c - (k_{autb} + k_{exp} + k_{sec} + k_{res} + k_{damC})C_c \quad (22)$$

$$\frac{dDP_{xc}}{dt} = k_{damL}L_c + k_{damC}C_c - k_{auto}DP_c \quad (23)$$

with the constraint that  $C_c + DP_c =$  cytosol carbon concentration (8.5 moles).

#### PAH (moles)

$$\frac{dE_{xPAH}}{dt} = k_{end}S_{PAH} - (f_r k_{rec} + k_{lys})E_{PAH} \quad (24)$$

$$\frac{dL_{xPAH}}{dt} = k_{lys}E_{PAH} + k_{autb}C_{PAH} - k_{exo}L_{PAH} - [k_{radL}L_{PAH}] \quad (25)$$

$$\frac{dC_{xPAH}}{dt} = (k_{IN}S_{PAH} - k_{OUT}C_{PAH}) - k_{autb}C_{PAH} - [k_{radC}C_{PAH}] \quad (26)$$

#### Radical generation

$$\frac{dL_{xROS}}{dt} = k_{radL} - k_{aoxL} \quad (27)$$

$$\frac{dC_{xROS}}{dt} = k_{radC} - k_{aoxC} \quad (28)$$

Analogous equations can easily be constructed for the nitrogen pathways.

A glossary of extra terms introduced is given in Table 2.

Once these rate constants and toxin entry and treatment have been described a numerical model can be implemented and various scenarios simulated and compared to experimental evidence.

#### Discussion

Recent work by Marigomez and Baybay-Villacorta (2003) has shown that the response of the digestive cells of mussels (*Mytilus Galloprovincialis*) is intricate. Exposure to di(2-ethylhexyl)phthalate (DEHP) rapidly induces the stress response of lysosomal enlargement. However, exposure to the PAH benzo(a)pyrene (B[a]P) and a water-accommodated fraction (WAF) of a lubricant oil exhibit a biphasic response: a transient lysosomal enlargement is observed, followed by shrinkage, which may be followed by lysosomal enlargement after further exposure. Reduction and enlargement of lysosomes can be considered as the result of different levels of toxicity or different mechanisms of toxic action (Cajaraville *et al.* 1995). One thing is clear: individual parameterizations will be required for each toxin, and that further experimental work is required in order to obtain this information.

Augmented autophagy and subsequent lysosomal degradation in response to toxic cell injury is a recurrent theme not just in invertebrates but also in fish and mammals (e.g. Lowe *et al.* 1992, Moore *et al.* 1996, Haliwell 1997). The identification of the crucial molecular, functional and structural changes which trigger autophagy, are key to understanding cell injury and predicting the pathological consequences (Moore 2002 and references cited therein). Recent work focused on yeast as an experimental model for autophagy has identified a number of proteins that function as autophagy factors. The interactions of these factors is beginning to provide a mechanistic molecular basis for the regulation of cellular autophagy (e.g. Hutchins *et al.* 1999, Kim *et al.* 1999). This all points to a requirement to ex-

Table 2.

Symbol	Definition	Units
$DP_p$	Damaged protein pool volume	l
$DP_{xc}$	Amount of C in damaged protein pool	mol
$DP_c$	Concentration of C in damaged protein pool	mol litre <sup>-1</sup>
$E_{PAH}$	Amount of PAH in endosomes	mol
$L_{PAH}$	Amount of PAH in lysosomes	mol
$C_{PAH}$	Amount of PAH in cytosol	mol
$S_{PAH}$	Concentration of PAH at cell surface	mol l <sup>-1</sup>
$E_{PAH}$	Concentration of PAH in endosomes	mol l <sup>-1</sup>
$L_{PAH}$	Concentration of PAH in lysosomes	mol l <sup>-1</sup>
$C_{PAH}$	Concentration of PAH in cytosol	mol l <sup>-1</sup>
$L_{ROS}$	Amount of ROS in lysosome	mol
$C_{ROS}$	Amount of ROS in cytosol	mol
$k_{autb}$	Rate constant for basal autophagy	l min <sup>-1</sup> cell <sup>-1</sup>
$k_{auto}$	Rate constant for oxyradical induced autophagy	l min <sup>-1</sup> cell <sup>-1</sup>
$k_{damL}$	Rate constant for damaged protein generation in lysosome	l min <sup>-1</sup> cell <sup>-1</sup>
$k_{damC}$	Rate constant for damaged protein generation in cytosol	l min <sup>-1</sup> cell <sup>-1</sup>
$k_{radL}$	Rate constant for ROS generation in lysosome	mol min <sup>-1</sup> cell <sup>-1</sup>
$k_{radC}$	Rate constant for ROS generation in cytosol	mol min <sup>-1</sup> cell <sup>-1</sup>
$k_{IN,OUT}$	Rate constant for diffusion of PAH into or out of cytosol	l min <sup>-1</sup> cell <sup>-1</sup>
$k_{oxL}$	Rate constant for antioxidant neutralisation of ROS in lysosome	mol min <sup>-1</sup> cell <sup>-1</sup>
$k_{oxC}$	Rate constant for antioxidant neutralisation of ROS in cytosol	mol min <sup>-1</sup> cell <sup>-1</sup>

where  $k_{damC}$ :  $F(C_{ROS}, C_{pH})$  and  $k_{damL}$ :  $k_{eal} F(L_{ROS}, L_{pH})$  for some function  $F$  given  $k_{eal}$ :  $G(\text{LysosomalStability})$  for some function  $G$ , and  $k_{radC}$ :  $H(C_{PAH}, C_{pH})$  and  $k_{radL}$ :  $H(L_{PAH}, L_{pH})$  for some function  $H$ .

plicity rather than implicitly (as in the current models) model the interactions of protein autophagy factors, and hence a requirement for experimental proteomics. Another aspect of stress response that requires attention is the effect on expression of enzymes of intermediary metabolism. Transcriptomic studies have shown that such enzymes are affected. For instance phenobarbital administration to mice leads to down regulation of enzymes of energy metabolism ( $\beta$ -oxidation and gluconeogenesis) as well as upregulation of xenobiotic-metabolising enzymes (Yamamoto *et al.* 2003). As the existing model relies on carbon and nitrogen fluxes, determining how stressors affect intermediary metabolism is of major importance. This indicates a need for parallel metabolomic investigations to complement protein expression profiles.

To reflect real-life situations, cellular modelling must take into account inter-individual variation of response to stressors. Systematic analysis of gene expression and metabolite profile, in individual animals, may more clearly indicate the important parameters and thus allow a more realistic model to be developed which can factor in individual variation.

## Conclusions

There is a huge amount of data relating to the behaviour and effects of chemical contaminants on physical, chemical and biological processes in aquatic ecosystems. Currently we lack a holistic integrated explanatory framework for evaluating this information, and

predicting harmful effects on biota and the subsequent consequences for ecosystem health. In order to address this issue we have attempted to demonstrate the need for computational simulations and how they clearly show the implications of the initial assumptions and perturbations to the system. Our models describe the main functions of the lysosome as the degradative compartment for vesicular and protein traffic, endocytotic uptake of contaminants bound with particles and the subsequent intracellular behaviour. This includes augmented autophagy and the generation of ROS. They highlight the importance of endocytosis as a driver for the intracellular dynamics. However, it is clear that further investigation of toxic impact and their underlying mechanisms are required to determine their significance in the process of cell injury and pathology. This requires an integrated research program where model development and experimental design are linked in an ongoing iterative manner.

## Acknowledgements

This work is partly funded by the core science research program of the Plymouth Marine Laboratory and in part by PREDICT 2 (DEFRA contract).

## References

- Allen JJ, Moore M (2004) Environmental Prognostics: Is the current use of biomarkers appropriate. *Mar Env Res* 58: 227–232.

- Cajaraville MP, Abascal I, Etxeberria M, Marigomez I (1995) Lysosomes as cellular markers of environmental pollution: time and dose-dependent responses of the digestive lysosomal system of mussels after petroleum hydrocarbon exposure. *Environ Toxicol Water Qual* 10: 1-8.
- Halliwell WH (1997) Cationic amphiphilic drug induced phospholipidosis. *Toxicol Pathol* 25: 53-60.
- Hunter P (2003) *The Scientist*, 17: 20-21.
- Hutchins CV, Veenhuis M, Klionsky D (1999) Peroxisome degradation in *Saccharomyces cerevisiae* is dependent on machinery of macro autophagy and the Cvt pathway. *J Cell Sci* 112: 4079-4087.
- Kim J, Dalton VM, Eggerton, KP, Scott SV, Klionsky DJ (1999) Agp7p/Cvt2p is required for the cytoplasm to vacuole targeting macroautophagy and peroxisome degradation pathways. *Mol Biol Cell* 10: 1337-1351.
- Kirchin MA, Moore MN, Dean RT, Winston GW (1992) The role of oxyradicals in intracellular proteolysis and toxicity in mussels. *Mar Env Res* 34: 315-320.
- Livingstone DR (2001) Contaminant-stimulated Reactive Oxygen Species Production and Oxidative Damage in Aquatic Organisms. *Mar Poll Bull* 42: 656-666.
- Lowe DM, Moore MN, Clarke KR (1981) Effects of oil on digestive cells in mussels: Quantitative alterations in cellular and lysosomal structure. *Aquat Toxicol* 1: 213-226.
- Lowe DM, Moore MN, Evans B (1992) Contaminant impact on interactions of molecular probes with lysosomes in living hepatocytes from Dab. *Mar Ecol Prog Ser* 91: 135-140.
- Lowe DM, Fossato VU, Depledge MH (1995a) Contaminant induced lysosomal membrane damage in blood cells of mussels *M. galloprovincialis* from the Venice Lagoon: an in vitro study. *Mar Ecol Prog Ser* 129: 189-196.
- Lowe DM, Soverchia C, Moore MN (1995b) Lysosomal membrane responses in the blood and digestive cells of mussels experimentally exposed to fluoranthene. *Aquat Toxicol* 33: 105-112.
- Lowe DM, Fossato VU (2000) The influence of environmental contaminants on lysosomal activity in the digestive cells of mussels (*Mytilus galloprovincialis*) from the Venice lagoon. *Aquat Toxicol* 48: 75-85.
- Marigomez I, Baybay-Villacorta L (2003) Pollutant-specific and general lysosomal responses in digestive cells of mussels exposed to model organic chemicals. *Aquat Toxicol* 64: 235-257.
- Manduzio H, Monsinjon T, Rocher B, Le Boulenger F, Galap C (2003) Characterisation of an inducible isoform of the Cu/Zn superoxide dismutase in the blue mussel *Mytilus edulis*. *Aquat Toxicol* 64: 73-83.
- McVeigh A, Moore MN, Allen JI, Dyke P, Noble D (2004) A carbon and nitrogen flux model of mussel digestive epithelial cells and their response to pollutants. *Mar Env Res* 58: 821-827.
- Moore MN (1990) Lysosomal cytochemistry in marine environmental monitoring. *Histochem J* 22: 187-191.
- Moore MN, Soverchia C, Thomas M (1996) Enhanced lysosomal autophagy of intracellular proteins by xenobiotics in living molluscan blood cells. *Acta Histochem Cytochem. (Suppl.)* 29: 947-948.
- Moore MN, Allen JI (2002) A computational model of the digestive gland epithelial cell of marine mussels and its simulated responses to oil-derived aromatic hydrocarbons. *Mar Env Res* 54: 579-584.
- Moore MN (2002) Biocomplexity: the post economic challenge in ecotoxicology. *Aquat Toxicol* 59: 1-15.
- Noble D (2002a) Modelling the heart: insights failures and progress. *BioEssays*, 24: 1155-1163.
- Noble D (2002b) The rise of computational biology. *Nature Rev Mol Cell Biol* 460-463.
- Langton RW (1977) Digestive rhythm in the mussel *Mytilus Edulis*. *Mar Biol* 41: 53-58.
- Viarengo A, Canesi L, Pertica M, Livingstone DR (1992) A simple procedure for evaluating the protein degradation rate in mussel (*M. galloprovincialis* Lam.) tissues and its application in a study of phenanthrene effects on protein catabolism. *Comp Biochem Physiol* 103B: 27-32.
- Widdows J, Bakke T, Bayne BL, Donkin P, Livingstone DR, Lowe DM, Moore MN, Evans SV, Moore SL (1982) Responses of *Mytilus edulis* on exposure to the water accommodated fraction of North Sea oil. *Mar Biol* 67: 15-31.
- Winston GW, Moore MN, Straatsburg I, Kirchin M (1991) Lysosomal stability in *Mytilus edulis* L.: potential as a biomarker of oxidative stress related to environmental contamination. *Arch Environ Contam Toxicol* 21: 401-408.
- Yamamoto Y, Kawamoto T, Negishi M (2003) The role of the nuclear receptor CAR as a coordinate regulator of hepatic gene expression in defence against chemical toxicity. *Arch Biochem Biophys* 409: 207-211.





Available online at [www.sciencedirect.com](http://www.sciencedirect.com)

SCIENCE @ DIRECT®

Marine Environmental Research 58 (2004) 821–827

MARINE  
ENVIRONMENTAL  
RESEARCH

[www.elsevier.com/locate/marenvres](http://www.elsevier.com/locate/marenvres)

## A carbon and nitrogen flux model of mussel digestive gland epithelial cells and their simulated response to pollutants

A. McVeigh <sup>a,\*</sup>, J.I. Allen <sup>a</sup>, M.N. Moore <sup>a</sup>, P. Dyke <sup>b</sup>,  
D. Noble <sup>c</sup>

<sup>a</sup> Plymouth Marine Laboratory, Prospect Place, The Hoe, Plymouth PL1 3DH, UK

<sup>b</sup> Department of Mathematics and Statistics, University of Plymouth, Drake Circus,  
Plymouth PL4 8AA, UK

<sup>c</sup> Department of Physiology, University of Oxford, Parks Road, Oxford OX1 3PT, UK

---

### Abstract

The mussel digestive gland epithelial cells provide a key interface between the organism and pollutants such as aromatic hydrocarbons. The simulation of their uptake and export mechanisms as well as an internal protein degradation pathway, and any subsequent disruption to any of them, has been undertaken. A computational model is described, which simulates the flow of carbon and nitrogen through a mussel's digestive cell. The model uses a compartmentalised view of the cell with inviolate 'pipelines' connecting each of the volume-variable partitions. Only the major physiological pathways relevant to the flow of either carbon or nitrogen or volume are modelled. Simulated response to hydrocarbon exposure is examined. © 2004 Elsevier Ltd. All rights reserved.

**Keywords:** Computational model; Mussel digestive cell; Toxic insult; Autophagy; Lysosomes; Polycyclic aromatic hydrocarbons

---

Conceptual biological systems abound, often in isolation from one another, and often not formally or explicitly declared. Even at their simplest the outcomes or results of such conceptual models are not always tractable or apparent, hence, the need for computational simulations that clearly show the implications of the initial assumptions and perturbations to the system (Hunter, 2003; Noble, 2003). This

---

\* Corresponding author.

model aims initially to provide, by means of a rigorous approach to the conservative properties of matter transfer, a numerical validation by direct simulation of the importance of the endocytotic path in the uptake of and response to contaminants by marine mussels (Moore, 1990; Moore & Willows, 1998). Success in this venture will enable interested parties to use the model as a predictive tool to foresee the consequences to mussel health of contaminant release. This paper provides an example of the problems and successes that the current model has in replicating the effects of long term exposure to low concentrations of PAHs on a marine mussel (Widdows et al., 1982).

A system of differential equations (see below) has been derived from the conceptual model of the cell (see Fig. 1): an enhancement of a previous system (Moore & Allen, 2002). The variables are compartmental volumes and concentrations, whilst the coefficients of the system either describe rate constants for the pathways or, else, fractional proportions. The required inputs to the system are the food quality, quantity and availability. Any perturbation or comparison of the system will, therefore, be constrained to effects or measurements of these variables or coefficients. Different rate constants have been modelled by various approaches, which are reliant on observed parameter values derived from the literature (Moore & Allen, 2002).

$$\frac{dE_v}{dt} = k_{\text{end}} - k_{\text{lys}} - k_{\text{rec}}, \quad (1)$$

$$\frac{dE_c}{dt} = \frac{1}{E_v} (k_{\text{end}}(S_c - E_c) + k_{\text{rec}}(1 - f_r)E_c), \quad (2)$$

$$\frac{dE_n}{dt} = \frac{1}{E_v} (k_{\text{end}}(S_n - E_n) + k_{\text{rec}}(1 - f_r)E_n), \quad (3)$$

$$\frac{dL_v}{dt} = k_{\text{aut}} + k_{\text{lys}} - k_{\text{deg}} - k_{\text{exo}}, \quad (4)$$

$$\frac{dL_c}{dt} = \frac{1}{L_v} (k_{\text{lys}}(E_c - L_c) + k_{\text{deg}}(1 - f_d)L_c + k_{\text{aut}}(C_c - L_c)), \quad (5)$$

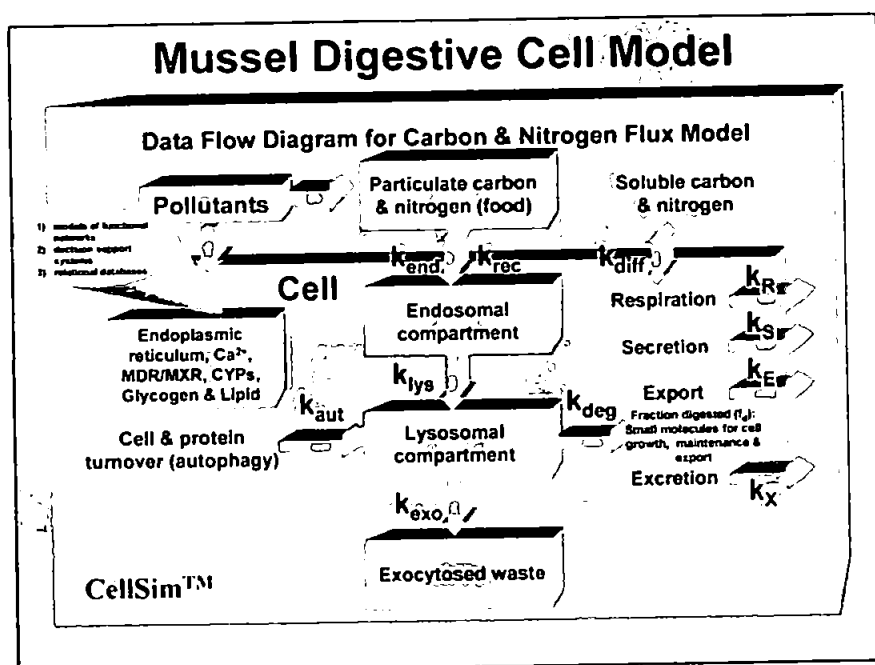
$$\frac{dL_n}{dt} = \frac{1}{L_v} (k_{\text{lys}}(E_n - L_n) + k_{\text{deg}}(1 - f_d)L_n + k_{\text{aut}}(C_n - L_n)), \quad (6)$$

$$\frac{dC_v}{dt} = k_{\text{deg}} - (k_{\text{aut}} + k_{\text{exp}} + k_{\text{sec}} + k_{\text{res}} + k_{\text{exc}}) + k_{\text{dif}}, \quad (7)$$

$$\frac{dC_c}{dt} = \frac{1}{C_v} (k_{\text{deg}}(f_d L_c - C_c) + (k_{\text{exc}} - k_{\text{dif}})C_c), \quad (8)$$

$$\frac{dC_n}{dt} = \frac{1}{C_v} (k_{\text{deg}}(f_d L_n - C_n) + (k_{\text{res}} - k_{\text{dif}})C_n). \quad (9)$$

See Fig. 1 for glossary of terms.

**Symbol Definition**

$C_c$	Concentration of C in cell cytoplasm
$C_n$	Concentration of N in cell cytoplasm
$E_c$	Concentration of C in endosomes
$E_n$	Concentration of N in endosomes
$L_c$	Concentration of C in lysosomes
$L_n$	Concentration of N in lysosomes
$S_c$	Concentration of C at cell surface
$S_n$	Concentration of N at cell surface
$f_d$	Fraction of N digested in lysosome and passed to cell
$f_r$	Fraction of N recycled from endosome to cell surface
$k_{aut}$	Rate constant for autophagy
$k_{deg}$	Rate constant for intracellular digestion
$k_{end}$	Rate constant for endocytosis
$k_{exo}$	Rate constant for exocytosis
$k_{lys}$	Rate constant for vesic. traffic from endosome to lysosome
$k_{diff}$	Rate constant for diffusion to regulate carbon concentration in cytoplasm
$k_x$	Rate constant for N excretion
$k_s$	Rate constant for secretion
$k_e$	Rate constant for export
$V_c$	Cell Volume
$V_{lys}$	Lysosomal Volume
$V_{end}$	Endosomal Volume
$N$	Number of digestive cells per mussel

**Value or lower-upper limits**

$8.3 \text{ mol. l}^{-1}$
$0.5 \text{ mol. l}^{-1}$
$8.3 - 12.0 \text{ mol}$
$0.5 - 0.8 \text{ mol. l}^{-1}$
$8.3 - 15.0 \text{ mol. l}^{-1}$
$0.5 - 0.9 \text{ mol. l}^{-1}$
$*2.1 (0 - 6.0) \text{ mol. l}^{-1}$
$*0.1 (0 - 0.4) \text{ mol. l}^{-1} \text{ (Notes)}$
$0 - 0.9$
$0.01$
$1.7 \times 10^{-16} - 1.2 \times 10^{-13} \text{ l. min}^{-1} \text{ cell}^{-1}$
$1.0 \times 10^{-16} - 1.0 \times 10^{-13} \text{ l. min}^{-1} \text{ cell}^{-1}$
$6.7 \times 10^{-17} - 2.0 \times 10^{-13} \text{ l. min}^{-1} \text{ cell}^{-1}$
$1.0 \times 10^{-16} - 1.0 \times 10^{-13} \text{ l. min}^{-1} \text{ cell}^{-1}$
$0 - 3.5 \times 10^{-16} \text{ l. min}^{-1} \text{ cell}^{-1}$
$1.25 \times 10^{-18} - 4.0 \times 10^{-18} \text{ l. min}^{-1} \text{ cell}^{-1}$
$1.4 \times 10^{-19} - 2.8 \times 10^{-18} \text{ l. min}^{-1} \text{ cell}^{-1}$
$0 - 6.0 \times 10^{-16} \text{ l. min}^{-1} \text{ cell}^{-1}$
$2.4 \times 10^{-13} - 2.4 \times 10^{-12} \text{ l}$
$1 - 30\% \text{ of cell volume}$
$1 - 5\% \text{ of cell volume}$
$3.125 \times 10^4$

(see figure caption on next page)

As a continuation of the exposed surface to the external environment, these cells constitute the main interface and buffer for the whole animal to toxic insult. Lysosomotropic pollutants enter the cell as ligands absorbed with food by the endocytotic pathway or else by diffusion across the plasma membrane (Rashid, Horobin, & Williams, 1991). Endocytosis takes the pollutant to the lysosome, from which its fate is to cause injury or, else, exocytosis without causing damage to the cell. For pollutants entering via this route the question is: how might they affect lysosomal degradative efficiency or stability? Toxins entering by diffusion also have the opportunity to damage the cytoplasmic compartments. Hence, it is necessary to determine the diffusion rates of toxic material into the cell, which is determined by its lipophilicity (Rashid et al., 1991).

To model the cell's response to insult we must speculate how the pollutant affects the systems' parameters. PAH accumulation in the digestive cell indicates a relationship between PAH concentration in the cell and the level of lysosomal autophagic protein catabolism (Nott & Moore, 1987; Viarengo, Moore, Pertica, Mancinelli, & Accomando, 1992). Modelled protein catabolism is regarded as being directly proportional to the autophagocytosed material that is degraded and returned to the cytosol. PAHs can also cause oxyradical damage (Moore, 1990). Damaged components are targeted for degradation, thus increasing the autophagic rate. Furthermore, at higher cellular concentrations the PAH starts to impede the lysosome's degradative ability (Viarengo et al., 1992). Consequently, this effect has been modelled as a threefold process, increased autophagy, decline in lysosomal degradative efficiency and a longer intralysosomal residence time. These are applied as general effects on all cellular material entering the lysosome, which affects the amount of nutrient exported to the rest of the animal.

To validate the model, results are compared with historical experimental data. Mussels were exposed for 180 days to a relatively low constant concentration ( $30 \mu\text{g l}^{-1}$ ) of the water accommodated fraction of North Sea oil (Widdows et al., 1982). In making a comparison, problems included: determination of food availability; hydrocarbon diffusion rates; cell life expectancy and extrapolating modelled to experimental results. In this last case, this has been achieved by constructing a simple model of the structure of the cell and relating volume to cell height. Additionally, cellular volume has been compared with the experimental results. The only other purely cellular result in the experiment was a measurement of lysosomal stability, which is related to lysosomal volume (Widdows et al., 1982).

Fig. 1. Data flow diagram showing the conceptual basis of the simulation model. Notes: If cell volume falls below  $2.4 \times 10^{-13}$  l then the cell dies; \*concentration for maintenance replacement of C and N loss respectively; increased autophagy is used as the toxicological response (i.e., as in reactions to toxic insult by lipophilic organics). Starvation scenario: when food ( $S_c$  and  $S_n$ ) are 0 then autophagy continues at a rate of 10% of cell volume per day; export of carbon and nitrogen is dependant on availability from digestion of particulate food. It will be 0 when ( $S_c$  and  $S_n$ ) are 0, and in this situation, with autophagy at 10% of cell volume per day, there is no food-derived carbon or nitrogen available for export. Therefore, carbon and nitrogen for cell maintenance and export must come from autophagy.

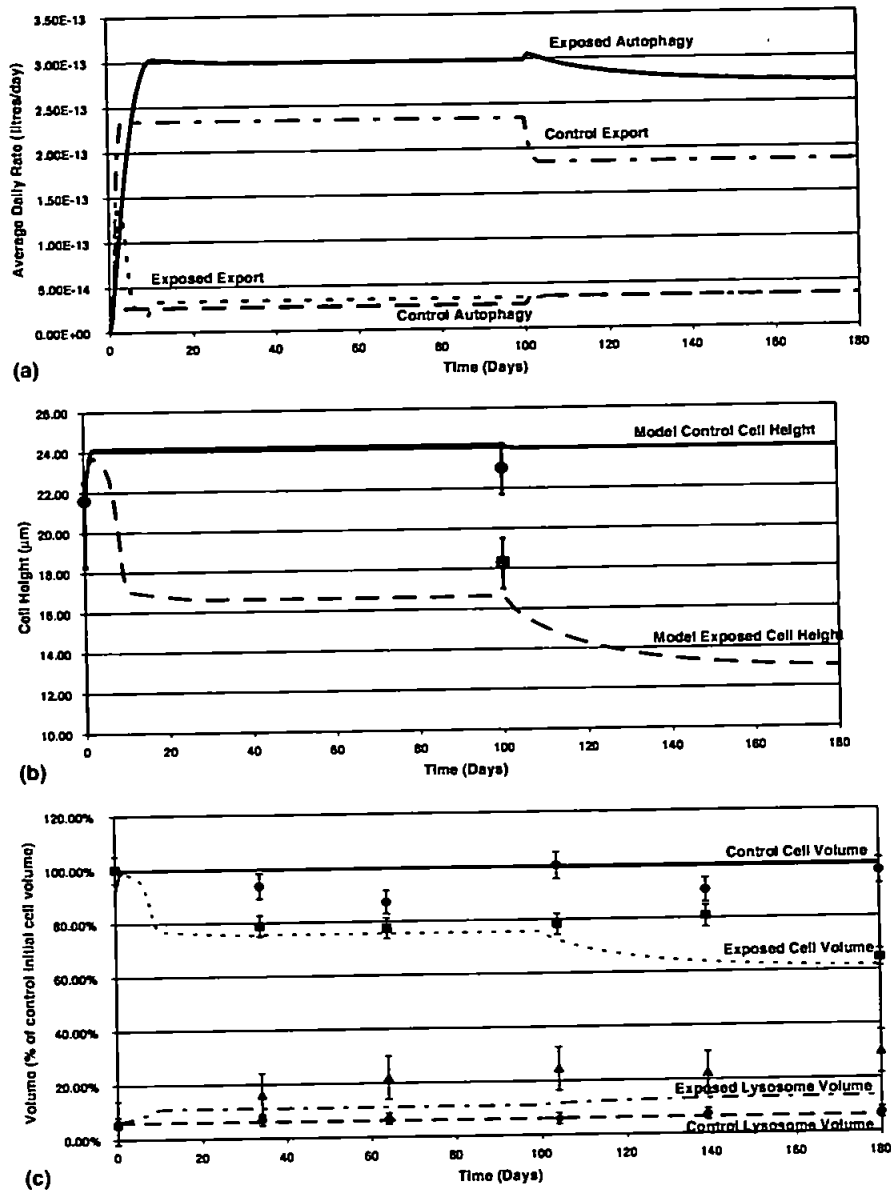


Fig. 2. Comparison of simulation and experimental results. Model results are shown as lines, experimental results as solitary points with error bars ( $\pm 95\%$  CL): (a) daily rates of export and autophagy, (b) cell height: ● control results, ■ exposed results and (c) cellular and lysosomal volume as a percentage of the initial cell volume: ● – control cell, ■ – exposed cell, ◆ – control lysosome, ▲ – exposed lysosome.

A 180 day simulation was run with identical food presented to both a control cell and an exposed cell, where PAH was present at the surface at the relevant concentration. During the course of the experiment, food quality diminished after 100 days, which has been reproduced in the food input to the model. The model shows the effect of increased autophagy (Fig. 2a), due initially to the PAH solely and then in conjunction with the effect of food deprivation, and digestive efficiency decline on the cellular height and the cell volume (Fig. 2b and c, respectively). In the exposed simulation, the cell exports an eighth of the control value (Fig. 2a). This is reflected in the decline in scope for growth in exposed animals (Bayne, Moore, Widdows, Livingstone, & Salkeld, 1979; Widdows et al., 1982). Simulated lysosomal volume also increased and, with the decline in food, enters the range ( $\geq 15$  min) where it is related to lysosomal stability (not shown). The model does not predict the correct magnitude of lysosomal percentage increase but does follow the observed trends. This deficiency appears to be a dual consequence of cellular volume retention and lysosomal inability to accumulate cellular material in the model.

Overall effects of exposure to PAH are readily modelled and bear reasonable resemblance to patterns seen in the experiment. The model demonstrates a robustness to the PAH insult but appears to lack sufficient flexibility to simulate the full range of cellular responses. Either the system's assumptions are incomplete or erroneous, or else the system's parameters require better definition. Problems encountered in comparing modelled with experimental results indicates that improvement needs to be made in modelling the presentation of food to the cell. More detailed or frequent experimental observations of cell and lysosomal volume would enable further validation of the models predictions.

#### Acknowledgements

The work was partly funded by the NERC (UK) core science research programme of the Plymouth Marine Laboratory and partly by the Defra (UK) PREDICT 2 Contract (CSA 6132).

#### References

- Bayne, B. L., Moore, M. N., Widdows, J., Livingstone, D. R., & Salkeld, P. N. (1979). *Philosophical Transactions of the Royal Society of London B*, 286, 563–581.
- Hunter, P. (2003). *The Scientist*, 17, 20–21.
- Moore, M. N. (1990). *Histochemistry Journal*, 22, 187–191.
- Moore, M. N., & Allen, J. I. (2002). *Marine Environment Research*, 54, 579–584.
- Moore, M. N., & Willows, R. I. (1998). *Marine Environment Research*, 46, 509–514.
- Noble, D. (2003). *Biochemical Society Transactions*, 31, 156–158.
- Nott, J. A., & Moore, M. N. (1987). *Histochemistry Journal*, 19, 357–368.
- Rashid, F., Horobin, R. W., & Williams, M. A. (1991). *Histochemistry Journal*, 23, 450–459.

- Viarengo, A., Moore, M. N., Pertica, M., Mancinelli, G., & Accomando, R. (1992). *Comparative Biochemistry and Physiology B*, 103, 27–32.
- Widdows, J., Bakke, T., Bayne, B. L., Donkin, P., Livingstone, D. R., Lowe, D. M., Moore, M. N., Evans, S. V., & Moore, S. L. (1982). *Marine Biology*, 67, 15–31.



Available online at [www.sciencedirect.com](http://www.sciencedirect.com)

SCIENCE @ DIRECT®

Marine Environmental Research 62 (2006) S433–S438

[www.elsevier.com/locate/marenvres](http://www.elsevier.com/locate/marenvres)

MARINE  
ENVIRONMENTAL  
RESEARCH

Short communication

## Lysosomal responses to nutritional and contaminant stress in mussel hepatopancreatic digestive cells: A modelling study

Allan McVeigh<sup>a,b,\*</sup>, Michael Moore<sup>a</sup>, J. Icarus Allen<sup>a</sup>, Phil Dyke<sup>b,c</sup>

<sup>a</sup> Plymouth Marine Laboratory, Prospect Place, The Hoe, Plymouth PL1 3DH, UK

<sup>b</sup> University of Plymouth, School of Mathematics & Statistics, Drake Circus, Plymouth PL4 8AA, UK

<sup>c</sup> University of Plymouth, School of Computing, Communications & Electronics, Drake Circus, Plymouth PL4 8AA, UK

### Abstract

The lysosomal system occupies a central and crucial role in cellular food degradation (intracellular digestion), toxic responses and internal turnover (autophagy) of the hepatopancreatic digestive cell of the blue mussel *Mytilus edulis*. Understanding the dynamic response of this system requires factors affecting performance, conceived as a function of the throughput, degradative efficiency and lysosomal membrane stability, to be defined and quantified. A previous carbon/nitrogen flux model has been augmented by separately identifying lysosomal 'target' material (autophagocytosed or endocytosed proteins, carbohydrates and lipids) and 'internal' material (digestive enzymes and lipid membrane components). Additionally, the whole cell's energetic costs for maintaining lysosomal pH and production of these internal components have been incorporated, as has the potentially harmful effect of generation of lipofuscin on the transitory and semi-permanent lysosomal constituents. Inclusion of the three classes of nutrient organic compounds at the whole cell level allows for greater range in the simulated response, including deamination of amino acids to provide molecules as a source of energy, as well as controlling nitrogen and carbon concentrations in the cytosol. Coupled with a more functional framework of pollutant driven reactive oxygen species (ROS) production and antioxidant defence, the separate and combined effects of three stressors (nutritional quality, nutrient quantity and a polycyclic aromatic hydrocarbon [PAH-phenanthrene]) on the digestive cell are simulated and compare favourably with real data.

© 2006 Elsevier Ltd. All rights reserved.

\* Corresponding author.

E-mail address: [ahmv@pml.ac.uk](mailto:ahmv@pml.ac.uk) (A. McVeigh).



**Keywords:** Cellular model; Lysosomes; Environmental prognostics; Starvation-induced autophagy; Nutritional stress

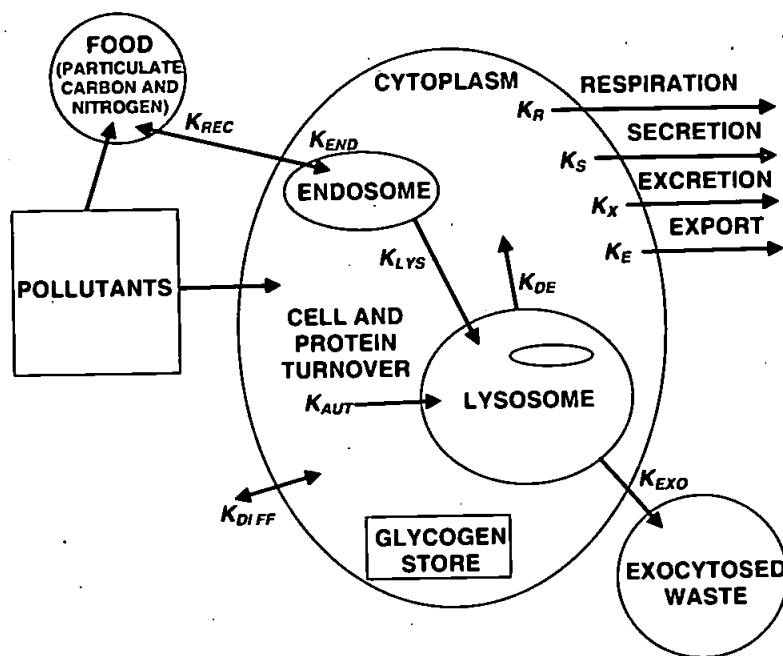
Interactive cellular responses to combinations of stress often give rise to surprising emergent properties. Modelling facilitates the integration of separately observed responses into whole system behaviour. Additionally, the rigour involved in constructing a mathematically conserved system highlights gaps in current knowledge, enabling the focusing of future experimentation. This paper describes recent efforts to simulate the behaviour of a marine mussel (*Mytilus edulis*) hepatopancreatic digestive cell, both throughout an annual cycle, and in a short-term exposure experiment designed to simulate the apparent protective properties of short-term starvation induced autophagy against PAH toxicity.

Previous attempts to simulate digestive cell behaviour by carbon/nitrogen compartment based models (Moore and Allen, 2002; McVeigh et al., 2004) have now been superseded by modelling the pathways of the three classes of nutrient organic compounds (lipid, protein and carbohydrates) and their subunits. The reason for this change was to allow for a more realistic simulation of the lysosomal degradative capability, considered central to the healthy functioning of the cell. The lysosomal compartment is now typified by three features: amount of 'target' (endocytosed and autophagocytosed) material, lysosomal degradative capacity (based on lysosomal digestive enzyme concentration) and membrane lipid content (to reflect lysosomal stability). A throughput of successfully degraded material is then determined based on the state of these three variables.

Further enhancements to the previous model include: (1) an integrated control strategy whereby cellular volume is controlled by the availability of amino acids (for protein synthesis), lipid (for membrane components) and appropriate energy stores together dictating the rates of excretion, deamination, protein synthesis, glycogen storage and release; (2) the respiration rate is now determined by a cellular activity function incorporating processes such as food uptake, endosome and lysosome pH maintenance, protein synthesis and antioxidant defences; (3) damage to internal viable components in all three compartments dependent on reactive oxygen species (ROS) concentrations; from which basal autophagy rates are determined and augmented by nutritional stress; (4) a new toxicity model which provokes enhanced ROS generation linearly according to both concentration and toxicity of pollutant (Allen and McVeigh, 2004); and (5) a three phase digestive tubule temporal system, based on Langton (1975) without the reconstituting phase, and a theoretical-stochastic-physical endocytosis rate incorporated to better simulate daily and tidal cycle dependent nutrient uptake.

The effectiveness of these modifications stimulated further inclusions and considerations such as: a system of endosomal and lysosomal lipid and degradative enzyme replenishment; antioxidant defences with consideration of cost to the cell; loss kinetics of pollutants are taken into account in order to simulate concentrations; and incorporation of residual bodies into cytosol compartment between the beginning of the holding phase through the feeding phase until expulsion during the disintegrating phase. A paper describing the redesigned model in detail is in preparation (see Fig. 1).

The first validation test of the model was a simulation of an annual cycle by providing a seasonal food pattern in terms of availability and quality. The simulation is compared with observed seasonal data for the biochemical composition of the non-mantle tissues (Gabbott and Bayne, 1973) in Fig. 2(a–d). Starting after the spawning period in the spring and early



$k_{end}$	Rate of Endocytosis	$6.7 \times 10^{-17} - 2.0 \times 10^{-15}$ Litres/sec
$k_{rec}$	Rate of Recycling	$0.0 - 1.65 \times 10^{-15}$ Litres/sec
$k_{lys}$	Rate of Traffic to Lysosome	$0.0 - 3.5 \times 10^{-16}$ Litres/sec
$k_{aut}$	Rate of Autophagy	$1.7 \times 10^{-16} - 1.2 \times 10^{-15}$ Litres/sec
$k_{deg}$	Rate of Degradation	$1.0 \times 10^{-18} - 1.0 \times 10^{-15}$ Litres/sec
$k_{exo}$	Rate of Exocytosis	$1.0 \times 10^{-18} - 1.0 \times 10^{-15}$ Litres/sec
$k_{res}$	Rate of Cellular Respiration	$0.0 - 2.0 \times 10^{-17}$ Litres/sec
$k_{sec}$	Rate of Secretion	$1.4 \times 10^{-19} - 2.8 \times 10^{-18}$ Litres/sec
$k_{exc}$	Rate of Excretion	$1.25 \times 10^{-18} - 4.0 \times 10^{-18}$ Litres/sec
$k_{exp}$	Rate of Export	$0.0 - 6.0 \times 10^{-16}$ Litres/sec
$k_{diff}$	Rate of Diffusion	$0.0 - 7.5 \times 10^{-18}$ Litres/sec

Fig. 1. Conceptual model schematic and glossary showing the basic compartmental system and pathways.

summer when the mussel is at its poorest energetic state, there is a period of high food availability and quality resulting in the rapid increase in dry weight and energy stores; with the deterioration in food over the autumn and winter the glycogen reserves are initially utilised until a threshold is met, thereafter protein becomes the main energy reserve. The simulated total cellular, carbon and protein dry weights all show fairly good accordance with the trends observed. Lipid behaviour has however proved more troublesome: the model has an inferior degradative ability for lipid in comparison to protein and carbohydrates,

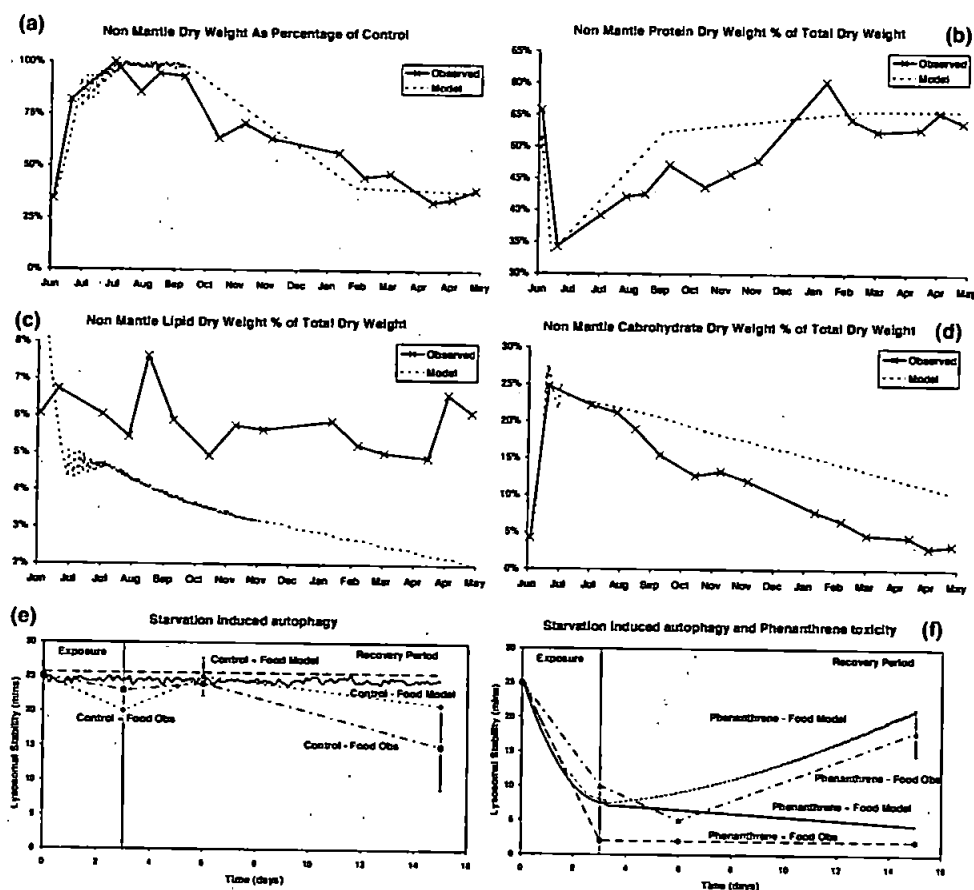


Fig. 2. Simulation results compared to observed biochemical and experimental data. (a) Seasonal non mantle tissue dry weight expressed as a percentage of maximum observation. (b–d) Dry weight of protein, lipid and carbohydrate, respectively, expressed as percentage of total cellular dry weight. (e) Effects of starvation on lysosomal stability. —●— Control + Food observed, —■— Control - Food observed, —●— Control + Food model results, —■— Control - Food model results (f) Effects of starvation coupled with phenanthrene exposure on lysosomal stability. Phenanthrene was dosed at a concentration of  $50 \mu\text{g mus}^{-1} \text{ day}^{-1}$  as a single daily dose (Moore, 2004). —●— Phenanthrene + Food Observed, —■— Phenanthrene - Food observed, —●— Phenanthrene + Food model results, —■— Phenanthrene - Food model results.

coupled with the dual model constraints on lipid (as both a possible energy source and component part of membranes). This has invoked a simulated response whereby total lipid content does have seasonal variation, but the trend against the rest of the cell is decreasing monotonically. Possibly other parts of the non-mantle contribute to the real data as a form of lipid store. Possible future improvements include changing the lipid content of the nutrients and changing the lipid control functions.

The model was also run to simulate an experiment coupling short-term starvation and phenanthrene exposure (Moore, 2004). Phenanthrene and PAH treatment of molluscan digestive cells results in oxidative stress, probably by direct oxidative attack on intra-lysosomal PAH by oxyradicals normally generated in the lysosomal compartment. Such oxi-

ductive attack will generate AH-quinones which will result in redox cycling contributing to oxidative stress (Moore, 1990; Moore et al., 1985; Sjölin and Livingstone, 1997; Winston et al., 1991). It was observed that the starvation-induced autophagy apparently provides a protective mechanism (indicated by recovery in lysosomal stability) when combined with toxic exposure. The lysosomal stability output of the model was calculated by a quadratic function of lysosomal volume density fitted to data. The control fluctuations in the fed control model correspond to the lysosomal swelling under feeding and its replenishment over the holding phase. The starved control model shows no perceptible decline in lysosomal stability, which matches observation (Bayne et al., 1978; Moore, 2004). The starved phenanthrene treated model follows a similar trend to the observed recovery, although the recovery occurs faster in the model and starts immediately after the exposure period (Moore, 2004). The fed phenanthrene treated model cell shows a continual decline in lysosomal stability, rapidly at first during xenobiotic exposure; and then more gradually after exposure has ceased.

Possible interpretations for these results reveal that the starvation means the lysosomal capability is only moderately impaired as the cell volume shrinks; hence the lysosome of the starved cell has only to deal with autophagocytosed food and toxic effects of phenanthrene; while the fed cell with only a slightly increased lysosomal capability has to degrade ingested food and the basal autophagocytosed material as well as the toxicity of phenanthrene. Furthermore, the increased autophagy for the nutrient deprived cell may facilitate non-specific detoxification of cytosolic phenanthrene at a greater rate than in the fed PAH treated cell. Starvation augmented autophagy will remove oxidatively damaged proteins more effectively from the cytoplasm, while the fed cell will tend to accumulate damaged proteins leading to molecular and cellular pathology and an increased burden on the already overstretched lysosome. Lipofuscin generation is initially more pronounced in the starved model but the removal of lipofuscin is possible due to the relatively small workload of the lysosome by a gross strategy of removal of lysosomal compartment reflecting exocytosis and apocrine secretion or apical pinching-off of the cytoplasm (Moore, 2004; Moore et al., 2006). Within the fed cell, lipofuscin generation continues unabated due to its first order kinetics and the lack of opportunity for removal (as the lysosome is overburdened and in continual demand) resulting in the continual decline in lysosomal stability.

This simulation has prompted the following possible considerations for the model: (1) since the integrated physiological function of the cell depends upon the interactions of proteins, an increase in the amount of damaged proteins should lead to a less efficient cell, hence some cost needs to be added to the model for damaged proteins; (2) and it should be possible to determine the critical space within the parameter space where recovery occurs and this should be possible to validate by direct experimentation.

In conclusion, this new model provides a fairly robust simulation of both an annual cycle and the role of starvation induced autophagy as a protective measure. Further work is required on lipid metabolism and the detrimental effect of the presence of damaged proteins on the functional state of the digestive cell.

#### Acknowledgement

The work forms part of the PREDICT 2 Project supported by the Department for Environment, Food and Rural Affairs (Defra, UK), Contract No. AE1136.

## References

- Allen, J.I., McVeigh, A., 2004. Towards computational models of cells for environmental toxicology. *Journal of Molecular Histology* 35, 697–706.
- Bayne, B.L., Holland, D.L., Moore, M.N., Lowe, D.M., Widdows, J., 1978. Further studies on the effects of stress in the adult on the eggs of *Mytilus edulis*. *Journal of the Marine Biological Association UK* 58, 825–841.
- Gabbott, P.A., Bayne, B.L., 1973. Biochemical effects of temperature and nutritive stress on *Mytilus edulis* L.. *Journal of the Marine Biological Association UK* 53, 269–286.
- Langton, R.W., 1975. Synchrony in the digestive diverticula of *Mytilus edulis* L. *Journal of the Marine Biological Association UK* 55, 221–229.
- McVeigh, A., Allen, J.I., Moore, M.N., Dyke, P., Noble, D., 2004. A carbon and nitrogen flux model of mussel digestive gland epithelial cells and their simulated response to pollutants. *Marine Environmental Research* 58, 821–827.
- Moore, M.N., 1990. Lysosomal cytochemistry in marine environmental monitoring. *Histochemical Journal* 22, 187–191.
- Moore, M.N., 2004. Diet restriction induced autophagy: a lysosomal protective system against oxidative- and pollutant-stress and cell injury. *Marine Environmental Research* 58, 603–607.
- Moore, M.N., Allen, J.I., 2002. A computational model of the digestive gland epithelial cell of the marine mussel and its simulated responses to aromatic hydrocarbons. *Marine Environmental Research* 54, 579–584.
- Moore, M.N., Allen, J.I., McVeigh, 2006. Environmental prognostics: an integrated model supporting lysosomal stress responses as predictive biomarkers of animal health status. *Marine Environmental Research* 61, 278–304.
- Moore, M.N., Mayernick, J.A., Giam, C.S., 1985. Lysosomal responses to a polynuclear aromatic hydrocarbon in a marine snail: effects of exposure to phenanthrene and recovery. *Marine Environmental Research* 17, 230–233.
- Sjölin, A.M., Livingstone, D.R., 1997. Redox cycling of aromatic hydrocarbon quinones catalysed by digestive gland microsomes of the common mussel (*Mytilus edulis* L.). *Aquatic Toxicology* 38, 83–99.
- Winston, G.W., Moore, M.N., Straatsburg, I., Kirchin, M., 1991. Lysosomal stability in *Mytilus edulis* L.: potential as a biomarker of oxidative stress related to environmental contamination. *Archives of Environmental Contamination and Toxicology* 21, 401–408.



Available online at [www.sciencedirect.com](http://www.sciencedirect.com)

SCIENCE @ DIRECT®

Marine Environmental Research 62 (2006) S433–S438

[www.elsevier.com/locate/marenvres](http://www.elsevier.com/locate/marenvres)

MARINE  
ENVIRONMENTAL  
RESEARCH

Short communication

## Lysosomal responses to nutritional and contaminant stress in mussel hepatopancreatic digestive cells: A modelling study

Allan McVeigh<sup>a,b,\*</sup>, Michael Moore<sup>a</sup>, J. Icarus Allen<sup>a</sup>, Phil Dyke<sup>b,c</sup>

<sup>a</sup> Plymouth Marine Laboratory, Prospect Place, The Hoe, Plymouth PL1 3DH, UK

<sup>b</sup> University of Plymouth, School of Mathematics & Statistics, Drake Circus, Plymouth PL4 8AA, UK

<sup>c</sup> University of Plymouth, School of Computing, Communications & Electronics, Drake Circus, Plymouth PL4 8AA, UK

### Abstract

The lysosomal system occupies a central and crucial role in cellular food degradation (intracellular digestion), toxic responses and internal turnover (autophagy) of the hepatopancreatic digestive cell of the blue mussel *Mytilus edulis*. Understanding the dynamic response of this system requires factors affecting performance, conceived as a function of the throughput, degradative efficiency and lysosomal membrane stability, to be defined and quantified. A previous carbon/nitrogen flux model has been augmented by separately identifying lysosomal 'target' material (autophagocytosed or endocytosed proteins, carbohydrates and lipids) and 'internal' material (digestive enzymes and lipid membrane components). Additionally, the whole cell's energetic costs for maintaining lysosomal pH and production of these internal components have been incorporated, as has the potentially harmful effect of generation of lipofuscin on the transitory and semi-permanent lysosomal constituents. Inclusion of the three classes of nutrient organic compounds at the whole cell level allows for greater range in the simulated response, including deamination of amino acids to provide molecules as a source of energy, as well as controlling nitrogen and carbon concentrations in the cytosol. Coupled with a more functional framework of pollutant driven reactive oxygen species (ROS) production and antioxidant defence, the separate and combined effects of three stressors (nutritional quality, nutrient quantity and a polycyclic aromatic hydrocarbon [PAH-phenanthrene]) on the digestive cell are simulated and compare favourably with real data.

© 2006 Elsevier Ltd. All rights reserved.

\* Corresponding author.

E-mail address: [almv@pml.ac.uk](mailto:almv@pml.ac.uk) (A. McVeigh).

**Keywords:** Cellular model; Lysosomes; Environmental prognostics; Starvation-induced autophagy; Nutritional stress

---

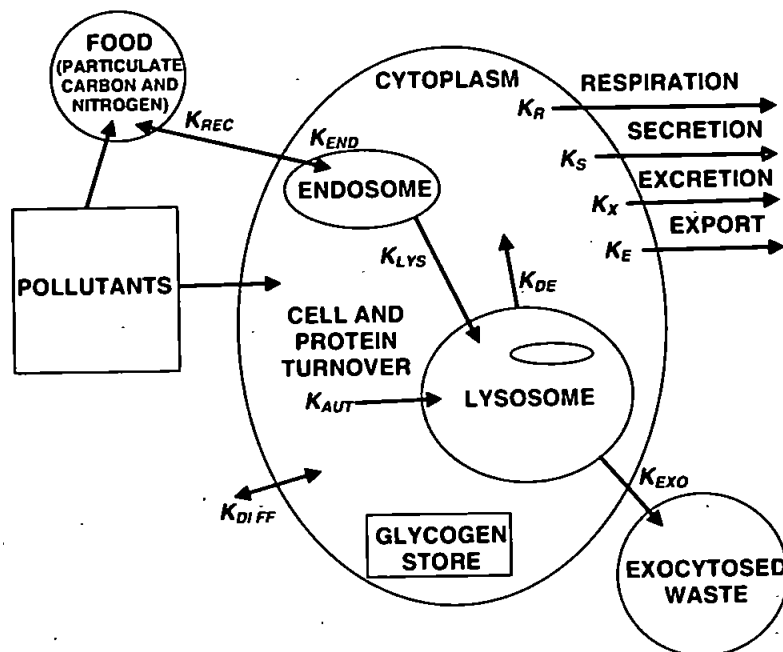
Interactive cellular responses to combinations of stress often give rise to surprising emergent properties. Modelling facilitates the integration of separately observed responses into whole system behaviour. Additionally, the rigour involved in constructing a mathematically conserved system highlights gaps in current knowledge, enabling the focusing of future experimentation. This paper describes recent efforts to simulate the behaviour of a marine mussel (*Mytilus edulis*) hepatopancreatic digestive cell, both throughout an annual cycle, and in a short-term exposure experiment designed to simulate the apparent protective properties of short-term starvation induced autophagy against PAH toxicity.

Previous attempts to simulate digestive cell behaviour by carbon/nitrogen compartment based models (Moore and Allen, 2002; McVeigh et al., 2004) have now been superseded by modelling the pathways of the three classes of nutrient organic compounds (lipid, protein and carbohydrates) and their subunits. The reason for this change was to allow for a more realistic simulation of the lysosomal degradative capability, considered central to the healthy functioning of the cell. The lysosomal compartment is now typified by three features: amount of 'target' (endocytosed and autophagocytosed) material, lysosomal degradative capacity (based on lysosomal digestive enzyme concentration) and membrane lipid content (to reflect lysosomal stability). A throughput of successfully degraded material is then determined based on the state of these three variables.

Further enhancements to the previous model include: (1) an integrated control strategy whereby cellular volume is controlled by the availability of amino acids (for protein synthesis), lipid (for membrane components) and appropriate energy stores together dictating the rates of excretion, deamination, protein synthesis, glycogen storage and release; (2) the respiration rate is now determined by a cellular activity function incorporating processes such as food uptake, endosome and lysosome pH maintenance, protein synthesis and antioxidant defences; (3) damage to internal viable components in all three compartments dependent on reactive oxygen species (ROS) concentrations; from which basal autophagy rates are determined and augmented by nutritional stress; (4) a new toxicity model which provokes enhanced ROS generation linearly according to both concentration and toxicity of pollutant (Allen and McVeigh, 2004); and (5) a three phase digestive tubule temporal system, based on Langton (1975) without the reconstituting phase, and a theoretical-stochastic-physical endocytosis rate incorporated to better simulate daily and tidal cycle dependent nutrient uptake.

The effectiveness of these modifications stimulated further inclusions and considerations such as: a system of endosomal and lysosomal lipid and degradative enzyme replenishment; antioxidant defences with consideration of cost to the cell; loss kinetics of pollutants are taken into account in order to simulate concentrations; and incorporation of residual bodies into cytosol compartment between the beginning of the holding phase through the feeding phase until expulsion during the disintegrating phase. A paper describing the redesigned model in detail is in preparation (see Fig. 1).

The first validation test of the model was a simulation of an annual cycle by providing a seasonal food pattern in terms of availability and quality. The simulation is compared with observed seasonal data for the biochemical composition of the non-mantle tissues (Gabbott and Bayne, 1973) in Fig. 2(a–d). Starting after the spawning period in the spring and early



$k_{end}$	Rate of Endocytosis	$6.7 \times 10^{-17} - 2.0 \times 10^{-15}$ Litres/sec
$k_{rec}$	Rate of Recycling	$0.0 - 1.65 \times 10^{-15}$ Litres/sec
$k_{lys}$	Rate of Traffic to Lysosome	$0.0 - 3.5 \times 10^{-16}$ Litres/sec
$k_{aut}$	Rate of Autophagy	$1.7 \times 10^{-16} - 1.2 \times 10^{-15}$ Litres/sec
$k_{deg}$	Rate of Degradation	$1.0 \times 10^{-16} - 1.0 \times 10^{-15}$ Litres/sec
$k_{exo}$	Rate of Exocytosis	$1.0 \times 10^{-16} - 1.0 \times 10^{-15}$ Litres/sec
$k_{res}$	Rate of Cellular Respiration	$0.0 - 2.0 \times 10^{-17}$ Litres/sec
$k_{sec}$	Rate of Secretion	$1.4 \times 10^{-19} - 2.8 \times 10^{-18}$ Litres/sec
$k_{exc}$	Rate of Excretion	$1.25 \times 10^{-18} - 4.0 \times 10^{-18}$ Litres/sec
$k_{exp}$	Rate of Export	$0.0 - 6.0 \times 10^{-18}$ Litres/sec
$k_{diff}$	Rate of Diffusion	$0.0 - 7.5 \times 10^{-18}$ Litres/sec

Fig. 1. Conceptual model schematic and glossary showing the basic compartmental system and pathways.

summer when the mussel is at its poorest energetic state, there is a period of high food availability and quality resulting in the rapid increase in dry weight and energy stores; with the deterioration in food over the autumn and winter the glycogen reserves are initially utilised until a threshold is met, thereafter protein becomes the main energy reserve. The simulated total cellular, carbon and protein dry weights all show fairly good accordance with the trends observed. Lipid behaviour has however proved more troublesome: the model has an inferior degradative ability for lipid in comparison to protein and carbohydrates,



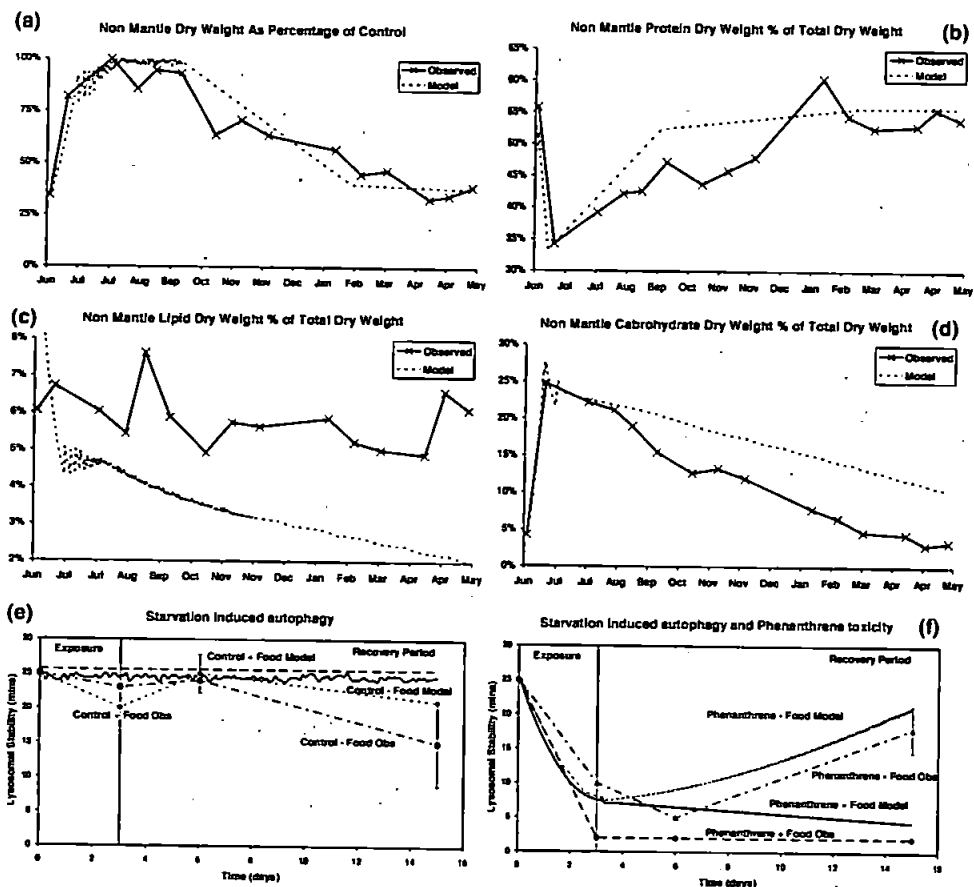


Fig. 2. Simulation results compared to observed biochemical and experimental data. (a) Seasonal non mantle tissue dry weight expressed as a percentage of maximum observation. (b–d) Dry weight of protein, lipid and carbohydrate, respectively, expressed as percentage of total cellular dry weight. (e) Effects of starvation on lysosomal stability. —●— Control + Food observed, —■— Control – Food observed, — Control + Food model results, — Control – Food model results (f) Effects of starvation coupled with phenanthrene exposure on lysosomal stability. Phenanthrene was dosed at a concentration of  $50 \mu\text{g mus}^{-1} \text{day}^{-1}$  as a single daily dose (Moore, 2004). —●— Phenanthrene + Food Observed, —▲— Phenanthrene – Food observed, — Phenanthrene + Food model results, — Phenanthrene – Food model results.

coupled with the dual model constraints on lipid (as both a possible energy source and component part of membranes). This has invoked a simulated response whereby total lipid content does have seasonal variation, but the trend against the rest of the cell is decreasing monotonically. Possibly other parts of the non-mantle contribute to the real data as a form of lipid store. Possible future improvements include changing the lipid content of the nutrients and changing the lipid control functions.

The model was also run to simulate an experiment coupling short-term starvation and phenanthrene exposure (Moore, 2004). Phenanthrene and PAH treatment of molluscan digestive cells results in oxidative stress, probably by direct oxidative attack on intra-lysosomal PAH by oxyradicals normally generated in the lysosomal compartment. Such oxi-

dative attack will generate AH-quinones which will result in redox cycling contributing to oxidative stress (Moore, 1990; Moore et al., 1985; Sjölin and Livingstone, 1997; Winston et al., 1991). It was observed that the starvation-induced autophagy apparently provides a protective mechanism (indicated by recovery in lysosomal stability) when combined with toxic exposure. The lysosomal stability output of the model was calculated by a quadratic function of lysosomal volume density fitted to data. The control fluctuations in the fed control model correspond to the lysosomal swelling under feeding and its replenishment over the holding phase. The starved control model shows no perceptible decline in lysosomal stability, which matches observation (Bayne et al., 1978; Moore, 2004). The starved phenanthrene treated model follows a similar trend to the observed recovery, although the recovery occurs faster in the model and starts immediately after the exposure period (Moore, 2004). The fed phenanthrene treated model cell shows a continual decline in lysosomal stability, rapidly at first during xenobiotic exposure; and then more gradually after exposure has ceased.

Possible interpretations for these results reveal that the starvation means the lysosomal capability is only moderately impaired as the cell volume shrinks; hence the lysosome of the starved cell has only to deal with autophagocytosed food and toxic effects of phenanthrene; while the fed cell with only a slightly increased lysosomal capability has to degrade ingested food and the basal autophagocytosed material as well as the toxicity of phenanthrene. Furthermore, the increased autophagy for the nutrient deprived cell may facilitate non-specific detoxification of cytosolic phenanthrene at a greater rate than in the fed PAH treated cell. Starvation augmented autophagy will remove oxidatively damaged proteins more effectively from the cytoplasm, while the fed cell will tend to accumulate damaged proteins leading to molecular and cellular pathology and an increased burden on the already overstretched lysosome. Lipofuscin generation is initially more pronounced in the starved model but the removal of lipofuscin is possible due to the relatively small workload of the lysosome by a gross strategy of removal of lysosomal compartment reflecting exocytosis and apocrine secretion or apical pinching-off of the cytoplasm (Moore, 2004; Moore et al., 2006). Within the fed cell, lipofuscin generation continues unabated due to its first order kinetics and the lack of opportunity for removal (as the lysosome is overburdened and in continual demand) resulting in the continual decline in lysosomal stability.

This simulation has prompted the following possible considerations for the model: (1) since the integrated physiological function of the cell depends upon the interactions of proteins, an increase in the amount of damaged proteins should lead to a less efficient cell, hence some cost needs to be added to the model for damaged proteins; (2) and it should be possible to determine the critical space within the parameter space where recovery occurs and this should be possible to validate by direct experimentation.

In conclusion, this new model provides a fairly robust simulation of both an annual cycle and the role of starvation induced autophagy as a protective measure. Further work is required on lipid metabolism and the detrimental effect of the presence of damaged proteins on the functional state of the digestive cell.

#### Acknowledgement

The work forms part of the PREDICT 2 Project supported by the Department for Environment, Food and Rural Affairs (Defra, UK), Contract No. AE1136.

## References

- Allen, J.I., McVeigh, A., 2004. Towards computational models of cells for environmental toxicology. *Journal of Molecular Histology* 35, 697–706.
- Bayne, B.L., Holland, D.L., Moore, M.N., Lowe, D.M., Widdows, J., 1978. Further studies on the effects of stress in the adult on the eggs of *Mytilus edulis*. *Journal of the Marine Biological Association UK* 58, 825–841.
- Gabbott, P.A., Bayne, B.L., 1973. Biochemical effects of temperature and nutritive stress on *Mytilus edulis* L.. *Journal of the Marine Biological Association UK* 53, 269–286.
- Langton, R.W., 1975. Synchrony in the digestive diverticula of *Mytilus edulis* L. *Journal of the Marine Biological Association UK* 55, 221–229.
- McVeigh, A., Allen, J.I., Moore, M.N., Dyke, P., Noble, D., 2004. A carbon and nitrogen flux model of mussel digestive gland epithelial cells and their simulated response to pollutants. *Marine Environmental Research* 58, 821–827.
- Moore, M.N., 1990. Lysosomal cytochemistry in marine environmental monitoring. *Histochemical Journal* 22, 187–191.
- Moore, M.N., 2004. Diet restriction induced autophagy: a lysosomal protective system against oxidative- and pollutant-stress and cell injury. *Marine Environmental Research* 58, 603–607.
- Moore, M.N., Allen, J.I., 2002. A computational model of the digestive gland epithelial cell of the marine mussel and its simulated responses to aromatic hydrocarbons. *Marine Environmental Research* 54, 579–584.
- Moore, M.N., Allen, J.I., McVeigh, 2006. Environmental prognostics: an integrated model supporting lysosomal stress responses as predictive biomarkers of animal health status. *Marine Environmental Research* 61, 278–304.
- Moore, M.N., Mayernick, J.A., Giam, C.S., 1985. Lysosomal responses to a polynuclear aromatic hydrocarbon in a marine snail: effects of exposure to phenanthrene and recovery. *Marine Environmental Research* 17, 230–233.
- Sjölin, A.M., Livingstone, D.R., 1997. Redox cycling of aromatic hydrocarbon quinones catalysed by digestive gland microsomes of the common mussel (*Mytilus edulis* L.). *Aquatic Toxicology* 38, 83–99.
- Winston, G.W., Moore, M.N., Straatsburg, I., Kirchin, M., 1991. Lysosomal stability in *Mytilus edulis* L.: potential as a biomarker of oxidative stress related to environmental contamination. *Archives of Environmental Contamination and Toxicology* 21, 401–408.



Available online at [www.sciencedirect.com](http://www.sciencedirect.com)

SCIENCE @ DIRECT®

Marine Environmental Research 62 (2006) S433–S438

[www.elsevier.com/locate/marenvres](http://www.elsevier.com/locate/marenvres)

MARINE  
ENVIRONMENTAL  
RESEARCH

Short communication

## Lysosomal responses to nutritional and contaminant stress in mussel hepatopancreatic digestive cells: A modelling study

Allan McVeigh <sup>a,b,\*</sup>, Michael Moore <sup>a</sup>, J. Icarus Allen <sup>a</sup>, Phil Dyke <sup>b,c</sup>

<sup>a</sup> Plymouth Marine Laboratory, Prospect Place, The Hoe, Plymouth PL1 3DH, UK

<sup>b</sup> University of Plymouth, School of Mathematics & Statistics, Drake Circus, Plymouth PL4 8AA, UK

<sup>c</sup> University of Plymouth, School of Computing, Communications & Electronics, Drake Circus, Plymouth PL4 8AA, UK

### Abstract

The lysosomal system occupies a central and crucial role in cellular food degradation (intracellular digestion), toxic responses and internal turnover (autophagy) of the hepatopancreatic digestive cell of the blue mussel *Mytilus edulis*. Understanding the dynamic response of this system requires factors affecting performance, conceived as a function of the throughput, degradative efficiency and lysosomal membrane stability, to be defined and quantified. A previous carbon/nitrogen flux model has been augmented by separately identifying lysosomal 'target' material (autophagocytosed or endocytosed proteins, carbohydrates and lipids) and 'internal' material (digestive enzymes and lipid membrane components). Additionally, the whole cell's energetic costs for maintaining lysosomal pH and production of these internal components have been incorporated, as has the potentially harmful effect of generation of lipofuscin on the transitory and semi-permanent lysosomal constituents. Inclusion of the three classes of nutrient organic compounds at the whole cell level allows for greater range in the simulated response, including deamination of amino acids to provide molecules as a source of energy, as well as controlling nitrogen and carbon concentrations in the cytosol. Coupled with a more functional framework of pollutant driven reactive oxygen species (ROS) production and antioxidant defence, the separate and combined effects of three stressors (nutritional quality, nutrient quantity and a polycyclic aromatic hydrocarbon [PAH-phenanthrene]) on the digestive cell are simulated and compared favourably with real data.

© 2006 Elsevier Ltd. All rights reserved.

\* Corresponding author.

E-mail address: [almv@pml.ac.uk](mailto:almv@pml.ac.uk) (A. McVeigh).

**Keywords:** Cellular model; Lysosomes; Environmental prognostics; Starvation-induced autophagy; Nutritional stress

---

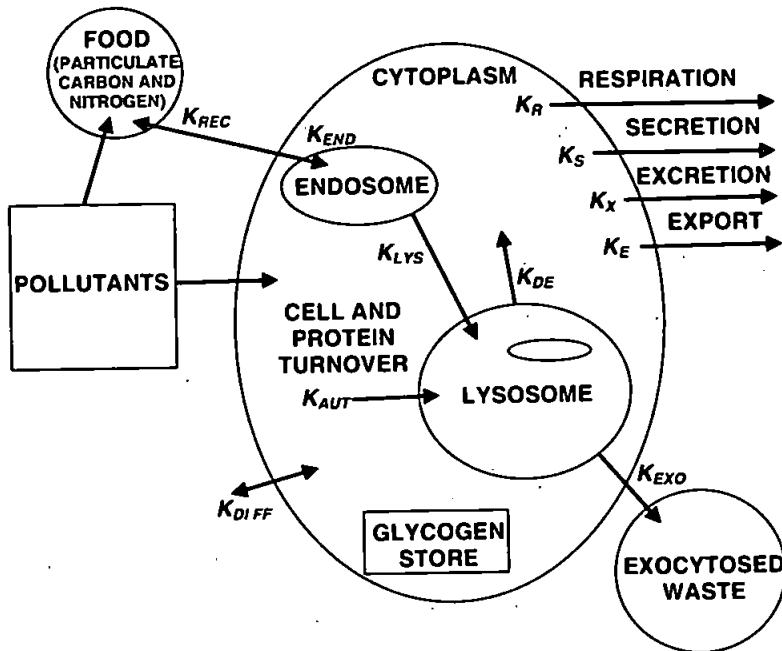
Interactive cellular responses to combinations of stress often give rise to surprising emergent properties. Modelling facilitates the integration of separately observed responses into whole system behaviour. Additionally, the rigour involved in constructing a mathematically conserved system highlights gaps in current knowledge, enabling the focusing of future experimentation. This paper describes recent efforts to simulate the behaviour of a marine mussel (*Mytilus edulis*) hepatopancreatic digestive cell, both throughout an annual cycle, and in a short-term exposure experiment designed to simulate the apparent protective properties of short-term starvation induced autophagy against PAH toxicity.

Previous attempts to simulate digestive cell behaviour by carbon/nitrogen compartment based models (Moore and Allen, 2002; McVeigh et al., 2004) have now been superseded by modelling the pathways of the three classes of nutrient organic compounds (lipid, protein and carbohydrates) and their subunits. The reason for this change was to allow for a more realistic simulation of the lysosomal degradative capability, considered central to the healthy functioning of the cell. The lysosomal compartment is now typified by three features: amount of 'target' (endocytosed and autophagocytosed) material, lysosomal degradative capacity (based on lysosomal digestive enzyme concentration) and membrane lipid content (to reflect lysosomal stability). A throughput of successfully degraded material is then determined based on the state of these three variables.

Further enhancements to the previous model include: (1) an integrated control strategy whereby cellular volume is controlled by the availability of amino acids (for protein synthesis), lipid (for membrane components) and appropriate energy stores together dictating the rates of excretion, deamination, protein synthesis, glycogen storage and release; (2) the respiration rate is now determined by a cellular activity function incorporating processes such as food uptake, endosome and lysosome pH maintenance, protein synthesis and antioxidant defences; (3) damage to internal viable components in all three compartments dependent on reactive oxygen species (ROS) concentrations; from which basal autophagy rates are determined and augmented by nutritional stress; (4) a new toxicity model which provokes enhanced ROS generation linearly according to both concentration and toxicity of pollutant (Allen and McVeigh, 2004); and (5) a three phase digestive tubule temporal system, based on Langton (1975) without the reconstituting phase, and a theoretical–stochastic–physical endocytosis rate incorporated to better simulate daily and tidal cycle dependent nutrient uptake.

The effectiveness of these modifications stimulated further inclusions and considerations such as: a system of endosomal and lysosomal lipid and degradative enzyme replenishment; antioxidant defences with consideration of cost to the cell; loss kinetics of pollutants are taken into account in order to simulate concentrations; and incorporation of residual bodies into cytosol compartment between the beginning of the holding phase through the feeding phase until expulsion during the disintegrating phase. A paper describing the redesigned model in detail is in preparation (see Fig. 1).

The first validation test of the model was a simulation of an annual cycle by providing a seasonal food pattern in terms of availability and quality. The simulation is compared with observed seasonal data for the biochemical composition of the non-mantle tissues (Gabbott and Bayne, 1973) in Fig. 2(a–d). Starting after the spawning period in the spring and early



$k_{end}$	Rate of Endocytosis	$6.7 \times 10^{-17} - 2.0 \times 10^{-15}$ Litres/sec
$k_{rec}$	Rate of Recycling	$0.0 - 1.65 \times 10^{-15}$ Litres/sec
$k_{lys}$	Rate of Traffic to Lysosome	$0.0 - 3.5 \times 10^{-15}$ Litres/sec
$k_{aut}$	Rate of Autophagy	$1.7 \times 10^{-18} - 1.2 \times 10^{-15}$ Litres/sec
$k_{deg}$	Rate of Degradation	$1.0 \times 10^{-16} - 1.0 \times 10^{-15}$ Litres/sec
$k_{exo}$	Rate of Exocytosis	$1.0 \times 10^{-18} - 1.0 \times 10^{-15}$ Litres/sec
$k_{res}$	Rate of Cellular Respiration	$0.0 - 2.0 \times 10^{-17}$ Litres/sec
$k_{sec}$	Rate of Secretion	$1.4 \times 10^{-19} - 2.8 \times 10^{-18}$ Litres/sec
$k_{exr}$	Rate of Excretion	$1.25 \times 10^{-18} - 4.0 \times 10^{-18}$ Litres/sec
$k_{exp}$	Rate of Export	$0.0 - 6.0 \times 10^{-18}$ Litres/sec
$k_{diff}$	Rate of Diffusion	$0.0 - 7.5 \times 10^{-18}$ Litres/sec

Fig. 1. Conceptual model schematic and glossary showing the basic compartmental system and pathways.

summer when the mussel is at its poorest energetic state, there is a period of high food availability and quality resulting in the rapid increase in dry weight and energy stores; with the deterioration in food over the autumn and winter the glycogen reserves are initially utilised until a threshold is met, thereafter protein becomes the main energy reserve. The simulated total cellular, carbon and protein dry weights all show fairly good accordance with the trends observed. Lipid behaviour has however proved more troublesome: the model has an inferior degradative ability for lipid in comparison to protein and carbohydrates,

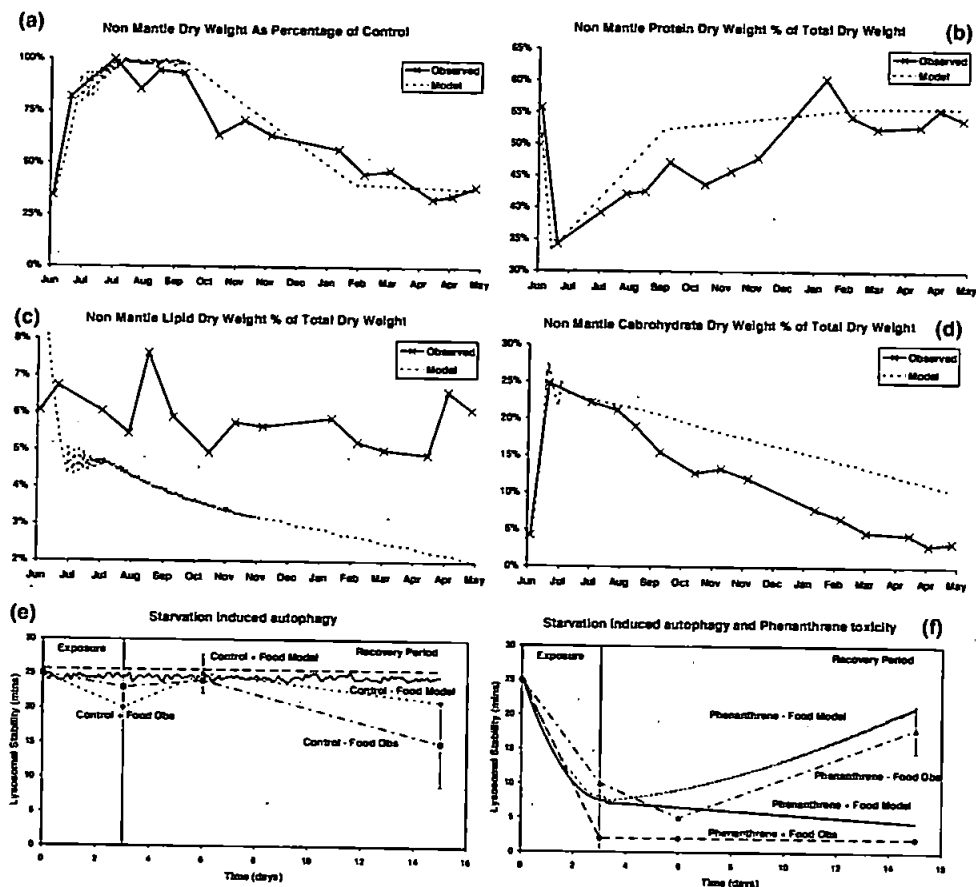


Fig. 2. Simulation results compared to observed biochemical and experimental data. (a) Seasonal non mantle tissue dry weight expressed as a percentage of maximum observation. (b-d) Dry weight of protein, lipid and carbohydrate, respectively, expressed as percentage of total cellular dry weight. (e) Effects of starvation on lysosomal stability. —◆— Control + Food observed, —■— Control – Food observed, — Control + Food model results, — Control – Food model results (f) Effects of starvation coupled with phenanthrene exposure on lysosomal stability. Phenanthrene was dosed at a concentration of  $50 \mu\text{g mus}^{-1} \text{ day}^{-1}$  as a single daily dose (Moore, 2004). —●— Phenanthrene + Food Observed, —▲— Phenanthrene – Food observed, — Phenanthrene + Food model results, — Phenanthrene – Food model results.

coupled with the dual model constraints on lipid (as both a possible energy source and component part of membranes). This has invoked a simulated response whereby total lipid content does have seasonal variation, but the trend against the rest of the cell is decreasing monotonically. Possibly other parts of the non-mantle contribute to the real data as a form of lipid store. Possible future improvements include changing the lipid content of the nutrients and changing the lipid control functions.

The model was also run to simulate an experiment coupling short-term starvation and phenanthrene exposure (Moore, 2004). Phenanthrene and PAH treatment of molluscan digestive cells results in oxidative stress, probably by direct oxidative attack on intra-lysosomal PAH by oxyradicals normally generated in the lysosomal compartment. Such oxi-

ductive attack will generate AH-quinones which will result in redox cycling contributing to oxidative stress (Moore, 1990; Moore et al., 1985; Sjölin and Livingstone, 1997; Winston et al., 1991). It was observed that the starvation-induced autophagy apparently provides a protective mechanism (indicated by recovery in lysosomal stability) when combined with toxic exposure. The lysosomal stability output of the model was calculated by a quadratic function of lysosomal volume density fitted to data. The control fluctuations in the fed control model correspond to the lysosomal swelling under feeding and its replenishment over the holding phase. The starved control model shows no perceptible decline in lysosomal stability, which matches observation (Bayne et al., 1978; Moore, 2004). The starved phenanthrene treated model follows a similar trend to the observed recovery, although the recovery occurs faster in the model and starts immediately after the exposure period (Moore, 2004). The fed phenanthrene treated model cell shows a continual decline in lysosomal stability, rapidly at first during xenobiotic exposure; and then more gradually after exposure has ceased.

Possible interpretations for these results reveal that the starvation means the lysosomal capability is only moderately impaired as the cell volume shrinks; hence the lysosome of the starved cell has only to deal with autophagocytosed food and toxic effects of phenanthrene; while the fed cell with only a slightly increased lysosomal capability has to degrade ingested food and the basal autophagocytosed material as well as the toxicity of phenanthrene. Furthermore, the increased autophagy for the nutrient deprived cell may facilitate non-specific detoxification of cytosolic phenanthrene at a greater rate than in the fed PAH treated cell. Starvation augmented autophagy will remove oxidatively damaged proteins more effectively from the cytoplasm, while the fed cell will tend to accumulate damaged proteins leading to molecular and cellular pathology and an increased burden on the already overstretched lysosome. Lipofuscin generation is initially more pronounced in the starved model but the removal of lipofuscin is possible due to the relatively small workload of the lysosome by a gross strategy of removal of lysosomal compartment reflecting exocytosis and apocrine secretion or apical pinching-off of the cytoplasm (Moore, 2004; Moore et al., 2006). Within the fed cell, lipofuscin generation continues unabated due to its first order kinetics and the lack of opportunity for removal (as the lysosome is overburdened and in continual demand) resulting in the continual decline in lysosomal stability.

This simulation has prompted the following possible considerations for the model: (1) since the integrated physiological function of the cell depends upon the interactions of proteins, an increase in the amount of damaged proteins should lead to a less efficient cell, hence some cost needs to be added to the model for damaged proteins; (2) and it should be possible to determine the critical space within the parameter space where recovery occurs and this should be possible to validate by direct experimentation.

In conclusion, this new model provides a fairly robust simulation of both an annual cycle and the role of starvation induced autophagy as a protective measure. Further work is required on lipid metabolism and the detrimental effect of the presence of damaged proteins on the functional state of the digestive cell.

#### Acknowledgement

The work forms part of the PREDICT 2 Project supported by the Department for Environment, Food and Rural Affairs (Defra, UK), Contract No. AE1136.



## References

- Allen, J.I., McVeigh, A., 2004. Towards computational models of cells for environmental toxicology. *Journal of Molecular Histology* 35, 697–706.
- Bayne, B.L., Holland, D.L., Moore, M.N., Lowe, D.M., Widdows, J., 1978. Further studies on the effects of stress in the adult on the eggs of *Mytilus edulis*. *Journal of the Marine Biological Association UK* 58, 825–841.
- Gabbott, P.A., Bayne, B.L., 1973. Biochemical effects of temperature and nutritive stress on *Mytilus edulis* L.. *Journal of the Marine Biological Association UK* 53, 269–286.
- Langton, R.W., 1975. Synchrony in the digestive diverticula of *Mytilus edulis* L. *Journal of the Marine Biological Association UK* 55, 221–229.
- McVeigh, A., Allen, J.I., Moore, M.N., Dyke, P., Noble, D., 2004. A carbon and nitrogen flux model of mussel digestive gland epithelial cells and their simulated response to pollutants. *Marine Environmental Research* 58, 821–827.
- Moore, M.N., 1990. Lysosomal cytochemistry in marine environmental monitoring. *Histochemical Journal* 22, 187–191.
- Moore, M.N., 2004. Diet restriction induced autophagy: a lysosomal protective system against oxidative- and pollutant-stress and cell injury. *Marine Environmental Research* 58, 603–607.
- Moore, M.N., Allen, J.I., 2002. A computational model of the digestive gland epithelial cell of the marine mussel and its simulated responses to aromatic hydrocarbons. *Marine Environmental Research* 54, 579–584.
- Moore, M.N., Allen, J.I., McVeigh, 2006. Environmental prognostics: an integrated model supporting lysosomal stress responses as predictive biomarkers of animal health status. *Marine Environmental Research* 61, 278–304.
- Moore, M.N., Mayernick, J.A., Giam, C.S., 1985. Lysosomal responses to a polynuclear aromatic hydrocarbon in a marine snail: effects of exposure to phenanthrene and recovery. *Marine Environmental Research* 17, 230–233.
- Sjölin, A.M., Livingstone, D.R., 1997. Redox cycling of aromatic hydrocarbon quinones catalysed by digestive gland microsomes of the common mussel (*Mytilus edulis* L.). *Aquatic Toxicology* 38, 83–99.
- Winston, G.W., Moore, M.N., Straatsburg, I., Kirchin, M., 1991. Lysosomal stability in *Mytilus edulis* L.: potential as a biomarker of oxidative stress related to environmental contamination. *Archives of Environmental Contamination and Toxicology* 21, 401–408.



Available online at [www.sciencedirect.com](http://www.sciencedirect.com)

SCIENCE @ DIRECT®

MARINE  
ENVIRONMENTAL  
RESEARCH

Marine Environmental Research 61 (2006) 278–304

[www.elsevier.com/locate/marenvres](http://www.elsevier.com/locate/marenvres)

## Environmental prognostics: An integrated model supporting lysosomal stress responses as predictive biomarkers of animal health status

Michael N. Moore <sup>a,\*</sup>, J. Icarus Allen <sup>a</sup>, Allan McVeigh <sup>a,b</sup>

<sup>a</sup> Plymouth Marine Laboratory, Prospect Place, The Hoe, Plymouth PL1 3DH, United Kingdom

<sup>b</sup> University of Plymouth, Department of Mathematics and Statistics,  
Drake's Circus, Plymouth PL4 8AA, United Kingdom

Received 28 November 2004; received in revised form 21 October 2005; accepted 26 October 2005

### Abstract

The potential prognostic use of lysosomal reactions to environmental pollutants is explored in relation to predicting animal health in marine mussels, based on diagnostic biomarker data. Cellular lysosomes are already known to accumulate many metals and organic xenobiotics and the lysosomal accumulation of the carcinogenic polycyclic aromatic hydrocarbon 3-methylcholanthrene (3-MC) is demonstrated here in the hepatopancreatic digestive cells and ovarian oocytes of the blue mussel. Lysosomal membrane integrity or stability appears to be a generic indicator of cellular well-being in eukaryotes; and in bivalve molluscs it is correlated with total oxygen and nitrogen radical scavenging capacity (TOSC), protein synthesis, scope for growth and larval viability; and inversely correlated with DNA damage (micronuclei), as well as lysosomal swelling (volume density), lipidosis and lipofuscinosis, which are all characteristic of failed or incomplete autophagy. Integration of multiple biomarker data is achieved using multivariate statistics and then mapped onto “health status space” by using lysosomal membrane stability as a measure of cellular well-being. This is viewed as a crucial step towards the derivation of explanatory frameworks for prediction of pollutant impact on animal health; and has facilitated the development of a conceptual mechanistic model linking lysosomal damage and autophagic dysfunction with injury to cells, tissues and the whole animal. This model has also complemented the creation and use of a cell-based bioenergetic computational model of molluscan hepatopancreatic cells that simulates lysosomal and cellular reactions to pollutants. More speculatively, the use of coupled empirical measurements of biomarker reactions

\* Corresponding author.

E-mail address: [mnmm@pml.ac.uk](mailto:mnmm@pml.ac.uk) (M.N. Moore).

and modelling is proposed as a practical approach to the development of an operational toolbox for predicting the health of the environment.

© 2005 Elsevier Ltd. All rights reserved.

**Keywords:** Autophagy; Environmental risk; Eukaryotes; Health status; Lipofuscin; Lysosomes; 3-methylcholanthrene; Mussels; Oxyradicals; PAHs; Pollutants; Prognostic biomarkers; Simulation modelling

## 1. Introduction

Biomarkers include a variety of measures of specific molecular, cellular and physiological responses of key species to contaminant exposure (Depledge, 1994, 1999; Depledge et al., 1993; Moore, Depledge, Readman, & Leonard, 2004). A response is generally indicative of either contaminant exposure or compromised physiological fitness. The challenge is to integrate individual biomarker responses into a set of tools and indices capable of detecting and monitoring the degradation in health of a particular type of sentinel organism.

However, what we are currently lacking are integrated explanatory frameworks for evaluating complex environmental information and predicting harmful biological effects and their subsequent consequences for environmental health. And while it is clearly recognised that stress-induced changes at the population/assembly/ecosystem/human health levels of biological organisation are the ultimate concern; they are generally too complex and far removed from the causative events to be of much use in developing tools for the early detection and prediction of the consequences of environmental stress (Depledge et al., 1993; Moore et al., 2004).

Consequently, it is only at the lower levels of biological organisation that we will have the reasonable expectation of developing a basis of mechanistic understanding of how different environmental conditions can modulate organismal function, which in turn will ultimately help in linking causality with predictability of response (Livingstone et al., 2000; Marigómez & Baybay-Villacorta, 2003; Moore, Köhler, Lowe, & Simpson, 1994). This is in part due to our ability to make certain generalisations about biological organisation and function at the molecular and cellular level; which rapidly disappears as we ascend the hierarchical ladder. Hence, distress signals at the molecular, cellular and physiological levels of organisation should be capable of providing “early warning biomarkers” (molecular, cellular, physiological and behavioural) indicating reduced performance; some of which may be prognostic for impending pathology and severe damage to health of the animal (Depledge, 1994; Depledge et al., 1993; Galloway et al., 2002, 2004; Moore, 2002).

Responses of the lysosomal-vacuolar system may provide a solution to the question of prognostic biomarkers, since injurious lysosomal reactions frequently precede cell and tissue pathology. Lysosomal perturbations have been widely used as early indicators of adverse effect to various factors, including pollutant exposure (Galloway et al., 2004; Moore, 2002; Moore et al., 2004). Consequently, lysosomal function can be used across a range of animals, including annelids, molluscs, crustaceans and fish to detect responses to environmental stress (Cajaraville et al., 2000; Galloway et al., 2004; Hankard et al., 2004; Hwang, Wade, & Sericano, 2002; Köhler, Deisemann, & Lauritzen, 1992; Köhler, Wahl, & Söffker, 2002; Lekube, Cajaraville, & Marigomez, 2000; Lowe, Moore, & Evans, 1992; Lowe, Fossato, & Depledge, 1995; Svendsen & Weeks, 1995; Wedderburn, Cheung, Bamber, Bloxham, & Depledge, 1998).

Lysosomes are highly conserved multi-functional cellular organelles present in almost all cells of eukaryotic organisms from yeast to humans. Their function in the cellular economy includes the degradation of redundant or damaged organelles (e.g., mitochondria and endoplasmic reticulum) and longer lived proteins as part of autophagic cellular turnover (Klionsky & Emr, 2000). Lysosomes are also involved in the digestion of materials ingested by endocytosis and phagocytosis (i.e., intracellular digestion).

Lysosomal reactions are involved in normal physiological responses as well as many cell injury and disease processes; these include augmented sequestration and autophagy of organelles and proteins (Cuervo, 2004; Klionsky & Emr, 2000; Moore, 1990, 2002). Stress-induced macroautophagy, such as that triggered by nutrient deprivation, is regulated by the mTOR kinase (mammalian target of rapamycin) in eukaryotic cells from yeast to mammals (Klionsky & Emr, 2000). Such reactions have been widely documented for many adaptive and developmental physiological and disease processes; and lysosomal responses have been shown to be involved in generalised reactions to environmental stress (Cajaraville, Abascal, Etxeberria, & Marigómez, 1995; Köhler et al., 2002; Moore, 1985, 1990, 2002). The functional stability of the lysosomal membrane is a good indicator of lysosomal integrity and has been used widely to measure responses to environmental perturbation in fish and molluscs (Hwang et al., 2002; Köhler et al., 2002; Lowe, Soverchia, & Moore, 1995; Moore, 2002; Allen & Moore, 2004; Moore et al., 2004).

Lysosomes are also remarkable for the vast and diverse array of chemicals and pharmaceuticals that they can sequester and accumulate (De Duve et al., 1974; Moore, 1990, 2002; Moore et al., 2004; Rashid, Horobin, & Williams, 1991). These range from metal ions such as iron, copper and mercury, transuranics, asbestos, polycyclic aromatic hydrocarbons (PAHs), heterocyclics, anti-psychotic drugs to nanoparticles, to name but a few (De Duve et al., 1974; Gould, 2004; Howard, 2004; Moore, 1985; Moore, Mayernick, & Giam, 1985; Moore, Lowe, Soverchia, Haigh, & Hales, 1997; Nott & Moore, 1987; Panyam & Labhasetwar, 2003; Rashid et al., 1991).

Understandably, however, the concerns of environmental managers and regulators are largely focused on the ecosystem level and not individual animals (Rice, 2003; Xu, Dawson, Li, & Cao, 2002). Unfortunately, the necessary epidemiological data for pollutant impact on sentinel animals that should permit a more comprehensive understanding of possible causal links between animal and ecosystem health is often limited or fragmentary, both spatially and temporally (Rice, 2003; Xu et al., 2002). Consequently, alternative interdisciplinary approaches will be required to identify such links and we are proposing that the health status of representative sentinel species (e.g., blue and green mussels, oysters, clams, periwinkles, crabs, flatfish) be used in evaluating health of the environment (Allen & Moore, 2004; Depledge, 1994, 1999; Depledge et al., 1993).

In this paper, our aim is to explore the utility of lysosomal responses as prognostic biomarkers for putative pathophysiology that will permit prediction of animal health status; and the development of a realistic integrated conceptual model for lysosomal reactions in cell injury and pathology. In attaining this goal we have three objectives.

Our first objective is to determine whether molluscan lysosomes actually accumulate ubiquitous pollutants like polycyclic aromatic hydrocarbons as has been demonstrated for mammalian cells (Allison & Young, 1969). The second objective is statistical analysis and modelling of lysosomal and other biomarker data, using lysosomal membrane stability as a reference measurement for cellular “well-being” (Allen & Moore, 2004). In order to minimise any bias in our interpretations, we have largely used already published and

independently derived data for this study. This data has been subjected to reanalysis using univariate and multivariate statistical routines, in order to develop an appropriate conceptual framework and statistical models for the role of lysosomal function and responses to environmental variables, particularly chemical pollutants. One very comprehensive data set produced by Krishnakumar, Casillas, and Varanasi (1994) for lysosomal responses to pollutants in Puget Sound has been used as the main statistical test-bed for developing our conceptual model of lysosomal reactions as both diagnostic and prognostic biomarkers for health status.

Our third objective is to derive a relational framework that can be used to integrate disparate data sets and for testing a numerical model used to produce computational simulations of digestive gland function in blue mussels (McVeigh, Allen, Moore, Dyke, & Noble, 2004). Consequently, this paper supports the development of simulation models (i.e., “virtual” cells, organs and possibly even whole animals), based on integrated functional processes of whole systems (the “physiome” and the “ecophysiome”). We propose that these will provide the necessary basis for explanatory frameworks that will facilitate the development of a predictive capacity for estimating risk to the health of sentinel animals associated with the possibility of future environmental events.

## 2. Materials and methods

### 2.1. 3-Methylcholanthrene as a fluorescent marker for cellular and lysosomal PAH uptake

Mussels collected from Exmouth in Devon (UK) were exposed to three separate concentration regimes of 3-methylcholanthrene (3-MC) in static tanks (1 mussel per litre of seawater controlled to field-ambient temperature), with no daylight or artificial light, except during dosing and sampling when the fluorescent strip lighting was turned on (negligible measured UV output). Mussels were exposed to daily single doses of 3-MC (dissolved in dimethylformamide) injected into the seawater, giving nominal water concentrations of 75, 150 or 1500  $\mu\text{g l}^{-1}$  respectively; the exposure period was 7 days (see Livingstone, Farrar, Fossi, Kirchin, & Moore, 1988). Controls were exposed to the equivalent amount of dimethylformamide only and mussels were not fed during the exposure period.

Hepatopancreatic (digestive gland) and gonadal tissues were excised from the mussels, placed on cryostat microtome chucks and quenched in *n*-hexane at  $-70^\circ\text{C}$ . Frozen tissue sections (10  $\mu\text{m}$  in thickness) were prepared as previously described, using a Bright motorised cryostat microtome (Bright Instruments Ltd., UK) and reacted for the lysosomal marker enzymes  $\beta$ -*N*-acetylhexosaminidase (NAH) and arylsulphatase (Moore, 1976, 1988; Moore, Pipe, & Farrar, 1982; Pipe & Moore, 1986). Cover slips were also mounted on fresh tissue sections in aqueous mounting medium for UV-epifluorescent photomicroscopy of 3-MC fluorescence.

Tissue concentrations of 3-MC were determined in duplicate pooled samples of the excised tissues by UV-spectrofluorimetry following steam distillation as described by Donkin and Evans (1984).

### 2.2. Univariate statistical analysis

Published data from a number of sources has been reanalysed in order to investigate possible correlations between lysosomal stability and other biological and chemical

variables. Regressions and trendlines were derived using Microsoft EXCEL (Office 2000 version) and Statgraphics 4.1.

### 2.3. Multivariate analysis

A single published data set produced by Krishnakumar et al. (1994) on the effects of pollutants on blue mussels (described as *Mytilus edulis*) from Puget Sound (Washington State, USA) were reanalysed using non-parametric multivariate analysis software, PRIMER v 6 (PRIMER-E Ltd, Plymouth, UK; Clarke, 1999). Principal component analysis (PCA), cluster analysis and non-metric multi-dimensional scaling analysis (MDS), derived from Euclidean distance similarity matrices was used to visualise dissimilarities between sample groups. All data was log-transformed and normalised prior to analysis. The results were further tested for significance using analysis of similarity (ANOSIM), which is analogous to a univariate ANOVA and reflects on differences between treatment groups in contrast to differences among replicates within samples (the  $R$  statistic). Under the null hypothesis  $H_0$  ("no difference between samples"),  $R = 0$  and this was tested by a non-parametric permutations approach; there should be little or no effect on the average  $R$  value if the labels identifying which replicates belong to which samples are randomly rearranged (Clarke, 1999).

Comparative Mantel-type tests on similarity matrices (PRIMER v6 – RELATE procedure) were used to compare biomarker and biological data with the chemical data. Under the null hypothesis there is no relationship between the two similarity matrices and the statistic  $Rho$  ( $\rho$ ) will be approximately zero.

The PRIMER v6 – BIO-ENV routine linking multivariate biomarker response patterns was used to identify "influential biomarkers" – small subsets of biomarkers capturing the full MDS biomarker response pattern.

Finally, in order to map integrated biomarker data onto "health status space" by using lysosomal membrane stability; first principal components (PC1) for the Puget Sound biomarker data (Krishnakumar et al., 1994) were derived using PRIMER v6 and then plotted against the lysosomal stability (as a measure of cellular well-being) values for each sample station.

## 3. Results and discussion

### 3.1. Lysosomal accumulation of PAH

The purpose of this exposure study was to test whether lysosomes in molluscan cells accumulated the polycyclic aromatic hydrocarbon as has been reported for mammalian cells by Allison and Young (1969). The exposure experiments demonstrated clearly that the polycyclic aromatic hydrocarbon 3-MC was readily taken up into the digestive gland, largely in the lysosomes, giving mean tissue concentrations up to a maximum of  $155 \mu\text{g g}^{-1}$  wet weight depending on the exposure concentration (Livingstone et al., 1988). Fluorescence for 3-MC was present at all three exposure concentrations in enlarged lysosomes in the hepatopancreatic digestive cells Fig. 1A and B; while in the female gonad, 3-MC was also taken up by yolk granules in the oocytes, which are pro-lysosomes (i.e., inactive lysosomes poised for autophagic breakdown of bound protein following fertilisation; Bayne, Holland, Moore, Lowe, & Widdows, 1978; Pipe & Moore, 1985; Fig. 1C and D).

There was no fluorescence or enlargement of digestive cell lysosomes in the sections from control animals. Lysosomal localisation of 3-MC was confirmed in corresponding structures in serial sections by their reactivity for the lysosomal-marker enzymes  $\beta$ -*N*-acetylhexosaminidase (NAH) and arylsulphatase (Fig. 1A and C).

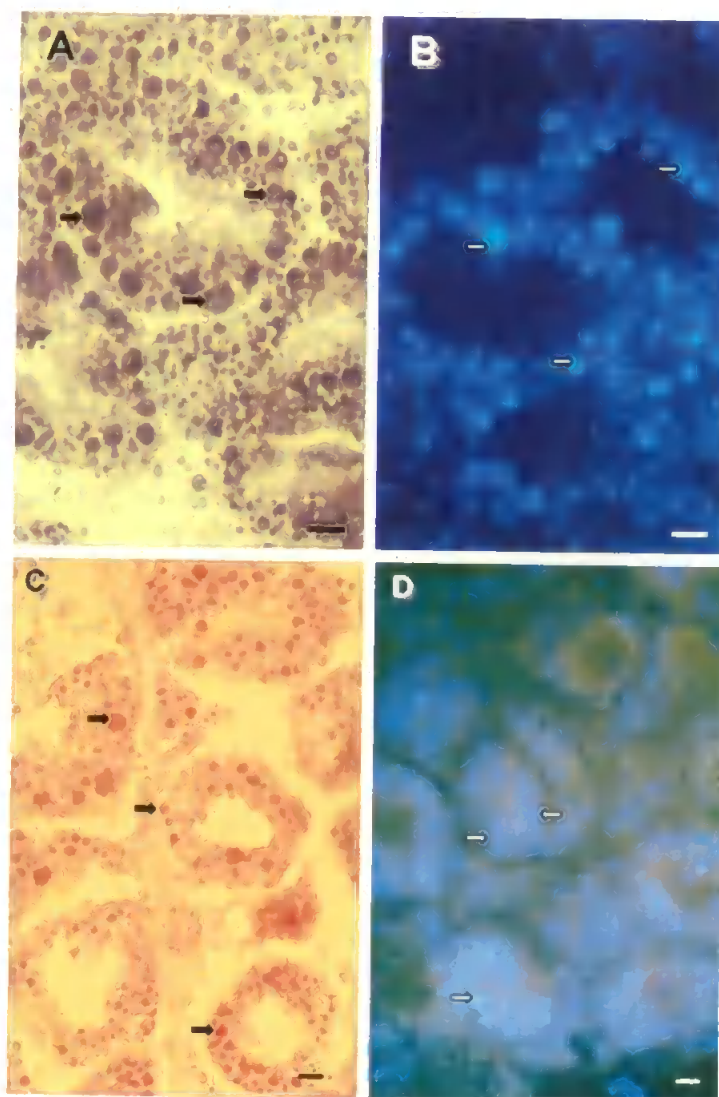


Fig. 1. Frozen tissue sections of digestive gland and gonad from mussels exposed to 3-MC at a daily dose of  $150 \mu\text{g l}^{-1}$  for 7 days. (A) Digestive tubules reacted for the lysosomal marker enzyme  $\beta$ -*N*-acetylhexosaminidase and showing enlarged lysosomes in the digestive cells. (B) 3-MC fluorescence in the enlarged lysosomes as in (A). (C) Gonadal oocytes reacted for arylsulphatase showing the prolysosomal yolk granules. (D) 3-MC fluorescence in the yolk granules; the red fluorescence is believed to be produced by carotenoid pigments in the developing eggs. Arrows indicate representative lysosomes and yolk granules; scale bars =  $10 \mu\text{m}$ .

The swelling of digestive cell lysosomes in 3-MC exposed mussel hepatopancreas is indicative of an autophagic response to the contaminant (Marigómez, Izaguirre, & Lekube, 2005; Moore, 1988; Fig. 1A and B). Similar responses have been observed in blue mussels (*Mytilus edulis* and *Mytilus galloprovincialis*) from laboratory experiments and field studies (Krishnakumar et al., 1994; Lowe, Moore, & Clarke, 1981; Marigómez & Baybay-Villacorta, 2003; Moore & Clarke, 1982; Moore, 1988).

The accumulation of 3-MC in lysosomally related organelles in the ovarian oocytes indicates that these cells are also a target for lipophilic xenobiotics such as polycyclic aromatic hydrocarbons. Their presence in the yolk granules is likely to have detrimental consequences for the development of gametes from such contaminated oocytes due to functional impairment of the lysosomal-yolk granule system. It may also predispose the gametes to damage by solar radiation (UV and blue light) due to the photosensitising effect of certain PAHs or else exacerbate the effects of UV-radiation (Allison & Young, 1969; Lyons, Pascoe, & McFadzen, 2002).

### 3.2. Lysosomal reactions to chemical pollutants

Adverse lysosomal reactions appear to provide useful biomarkers that are diagnostic for cell injury and putative indicators for further pathology (Moore, 1990). Exposure to many contaminants, both metals and organic xenobiotics, can result in increased radical generation and the intralysosomal environment is already a site of oxyradical production (Livingstone, 2001; Winston, Moore, Straatsburg, & Kirchin, 1991; Winston, Moore, Kirchin, & Soverchia, 1996). The resulting oxidative damage to membranes, proteins (e.g., carbonyls) and DNA will undoubtedly contribute to decreased protein synthesis, cell injury and patho-physiological dysfunction (Figs. 2, 3; Dailianis, Domouhtsidou, Raftopoulou, Kaloyianni, & Dimitriadis, 2003; Domouhtsidou & Dimitriadis, 2001; Kalpaxis et al., 2004; Kirchin, Moore, Dean, & Winston, 1992; Krishnakumar et al., 1994; Livingstone, 2001; Regoli, 2000; Winston et al., 1991; Winston et al., 1996). Lysosomal membrane stability in blue mussels is directly correlated with total oxyradical scavenging capacity (TOSC against hydroxyl, peroxyxynitrite and peroxy radicals); and inversely proportional to DNA damage (micronucleus formation), polyribosome formation (translational efficiency in initiation of protein synthesis), lipofuscin (age/stress pigment, ceroid lipofuscin) formation and lysosomal autophagic accumulation of lipid (Figs. 2, 3A–C; Dailianis et al., 2003; Kalpaxis et al., 2004; Krishnakumar et al., 1994; Regoli, 2000).

### 3.3. Lysosomal biomarkers

Multi-dimensional scaling (MDS) and cluster analysis of the biological responses (i.e., lysosomal stability, NAH activity, NAH latency, lipid, lipofuscin and somatic tissue index – measured as somatic tissue weight/shell length) for blue mussels from Puget Sound shows that the data fall within two clusters (Krishnakumar et al., 1994; Figs. 4, 5), designated as “impacted” and “healthy” corresponding to mussel populations with high contaminant body burdens (Sites S1–S4; urban sites) and relatively low body burdens (Sites S6–S9; reference sites and one urban site, S5) respectively. Analysis of similarity shows that these clusters are significantly different (ANOSIM,  $R = 0.938$ ,  $P \leq 0.008$ ).

Multidimensional scaling and cluster analysis for the chemical data (PAHs, PCBs, DDTs, Ag, As, Cd, Cu, Hg, Pb, Se, and Zn) shows a similar grouping with two distinct



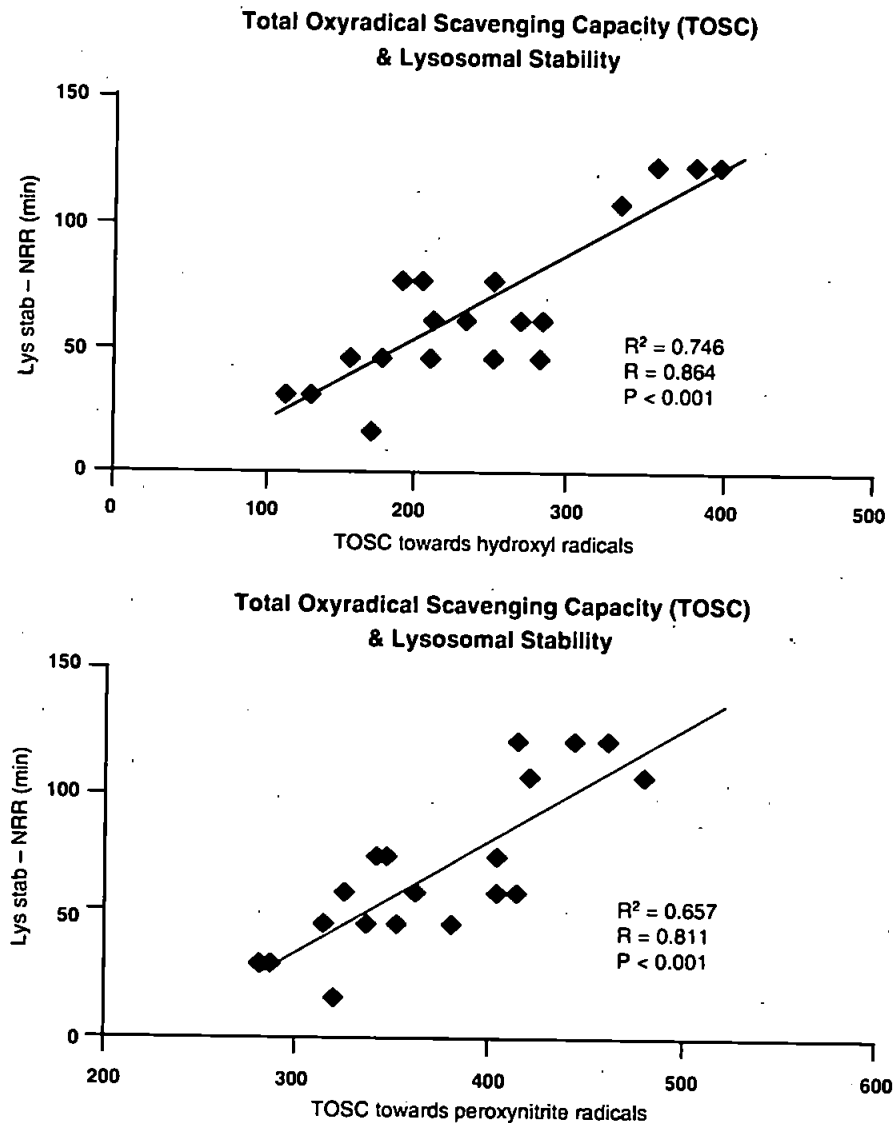


Fig. 2. Correlations between lysosomal stability, as a prognostic “health status” biomarker, and total oxyradical scavenging capacity (TOSC) for hydroxyl and peroxynitrite radicals measured in blue mussels. Data adapted from Regoli (2000).

clusters and a separate single site from within the reference samples (ANOSIM,  $R = 0.675$ ,  $P \leq 0.008$ ; Fig. 4). Bubble plots for selected contaminants measured are shown superimposed onto MDS plots for the biological responses (Fig. 6), illustrating clearly the contaminant differences between the clusters.

Testing of the (dis)similarity matrices generated by PRIMER 6 using the BIO-ENV routine for the biological and chemical data sets shows strong correlations between the

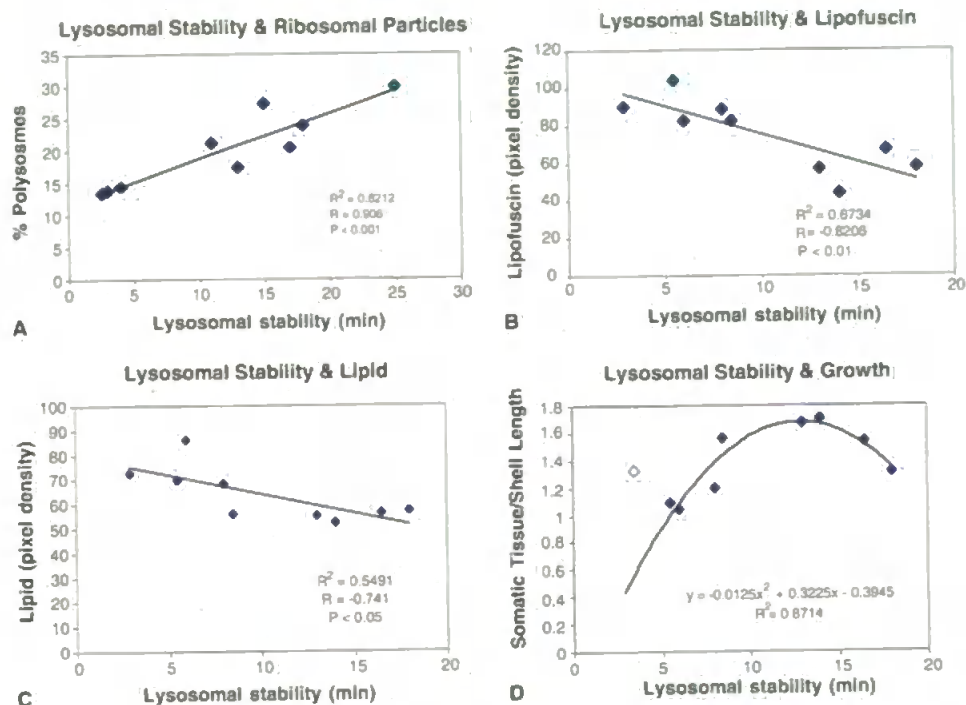


Fig. 3. Correlations between lysosomal stability and (A) – ribosomal translational efficiency (% polysomes), (B) – lipofuscin, (C) – lipid measured in hepatopancreatic digestive cells of blue mussels; and (D) – correlation between lysosomal stability and a morphometric measure of growth (somatic tissue dry weight/shell length). In (D) the most contaminated site (Eagle Harbor, Puget Sound, USA) has been excluded as an outlier ( $\diamond$ ): at this concentration of PAHs protein catabolism will have been inhibited and there may also be selection for more tolerant forms from the planktonic larval gene pool. Original data derived from Kalpaxis et al. (2004) (A) and Krishnakumar et al. (2004) (B–D).

biological parameters and PAHs, PCBs and DDTs (Table 1); but not for the metals. The RELATE routine showed significant Spearman rank correlations between the biological parameters and the organic xenobiotics (Table 2).

Similar analysis of the biological data indicated that many of the biological parameters are correlated (Fig. 7; Table 3). The lysosomal biomarkers themselves, both individually and grouped are strongly correlated (Fig. 7; Table 3).

These findings indicate that the lysosomal parameters are all strongly correlated, which supports the hypothesis that stress or pollution induced lysosomal injury is mechanistically linked with increased autophagy and lysosomal hydrolase activity and consequent cell degradation and organ atrophy (Krishnakumar et al., 1994; Lowe et al., 1981).

A morphometric indicator of growth for blue mussels, based on a somatic tissue index derived from the data of Krishnakumar et al. (1994) has been used as an indicator of tissue growth. This is strongly correlated with lysosomal stability, which provides support for the hypothesis that autophagy is linked with reduced lysosomal membrane stability (Fig. 3D). The somatic tissue index is also strongly inversely correlated with lysosomal lipid, lipofuscin and the activity of the lysosomal marker enzyme  $\beta$ -N-acetylhexosaminidase (Fig. 7).

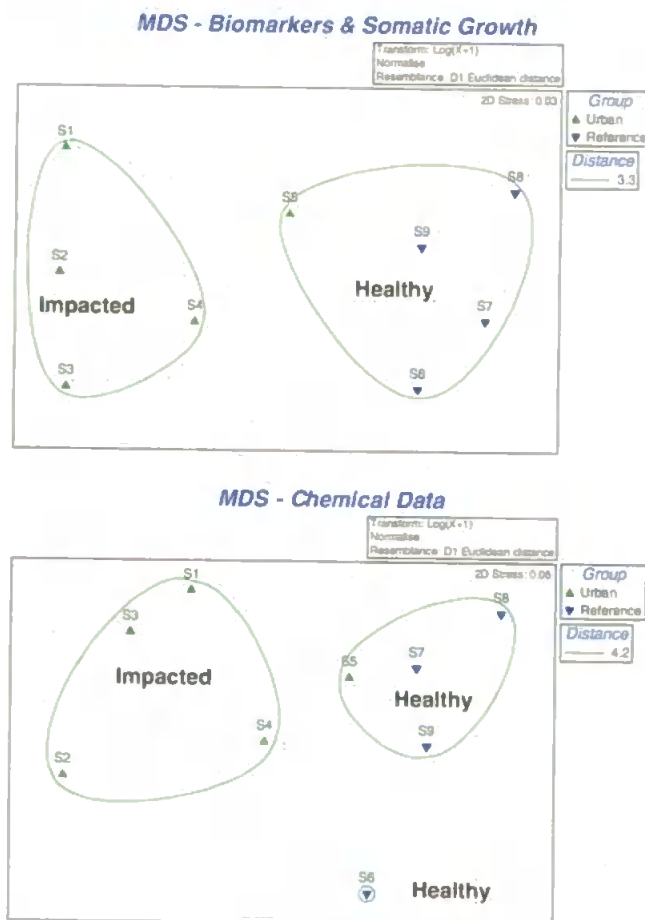


Fig. 4. Multi-dimensional scaling analysis of the biological responses (lysosomal stability, NAH activity, NAH latency, lipid, lipofuscin and somatic tissue index – measured as somatic tissue weight/shell length) and chemical body burden for blue mussels from sample sites in Puget Sound. For the biological responses, the stress is 0.03; and for the chemical data, the stress is 0.06. Samples are grouped as urban (S1–S5) or reference sites (S6–S9) and cluster analysis has been overlaid. Original data derived from Krishnakumar et al. (1994).

Further support comes from evidence of a strong inverse correlation between lysosomal stability and lysosomal volume density (Fig. 8A). The growth indicator is also significantly inversely correlated with total  $\beta$ -N-acetylhexosaminidase (NAH), as well as lysosomal lipid and lipofuscin (Fig. 7). We already know that increases in lysosomal volume are functionally related to autophagy in molluscs and fish (Lowe, 1988; Lowe et al., 1981, 1992; Moore, 1988, 1990; Moore & Halton, 1973; Moore, Pipe, Farrar, Thomson, & Donkin, 1986).

Consequently, we can state with reasonable confidence that lysosomal stability appears to be a good index of integrated lysosomal system integrity in blue mussels and flatfish (Köhler et al., 1992, 2002; Moore, 1990, 2002; Okay, Donkin, Peters, & Livingstone, 2000); and this is supported by strong correlations between measures of lysosomal stability determined in tissue sections and live cells (Fig. 8B). Hence, we can now use this knowledge

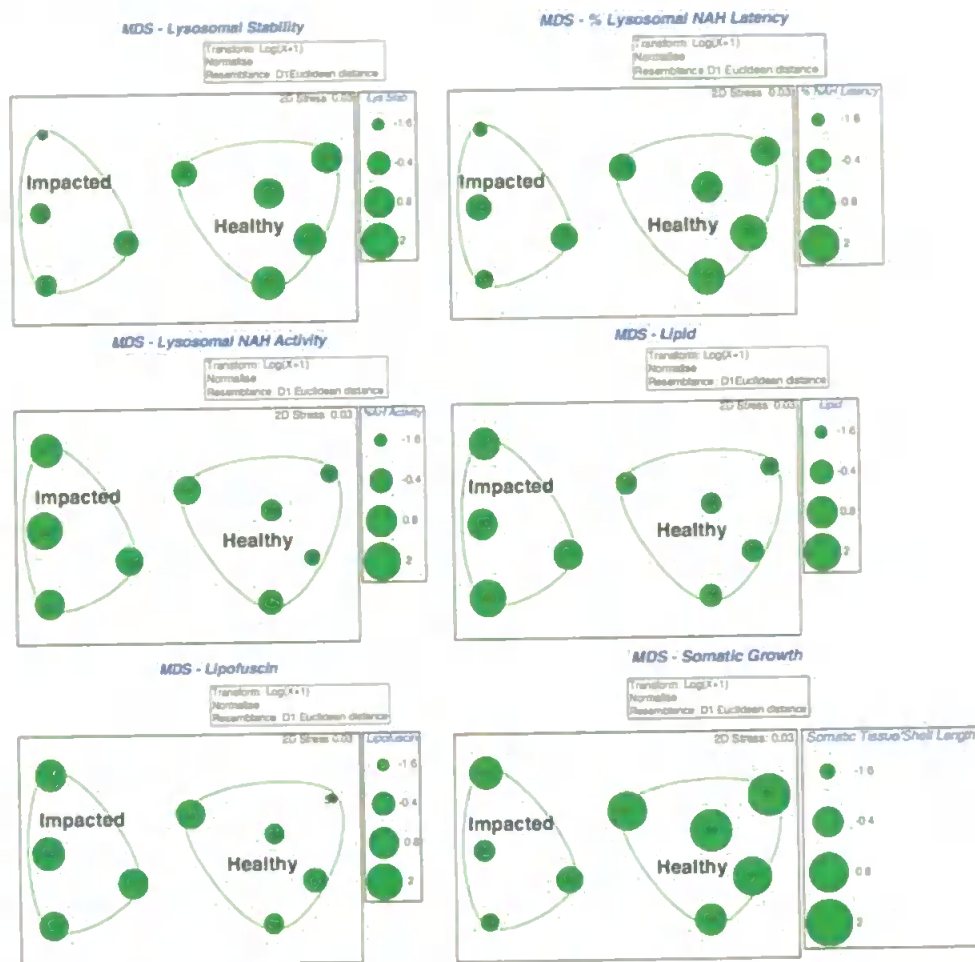


Fig. 5. Multi-dimensional scaling (MDS) analysis of the biological responses (lysosomal stability, NAH activity, NAH latency, lipid, lipofuscin and somatic tissue index – measured as somatic tissue weight/shell length) for blue mussels from nine sample sites in Puget Sound. Bubble plots for the individual biological responses have been serially superimposed. Samples are grouped as urban or reference sites and cluster analysis has been overlaid. Original data derived from Krishnakumar et al. (1994).

of lysosomal integrity as an indicator of cellular well-being that appears to translate between different species (e.g., protozoans, coelenterates, annelids, molluscs, fish, mammals) to interpret more complex information related to pollutant exposure (Galloway et al., 2004; Dayeh, Chow, Schirmer, Lynn, & Bols, 2004; Köhler et al., 1992, 2002; Hankard et al., 2004; Martinez-Vicente, Sovak, & Cuervo, 2005; Moore, 1990, 2002; Moore & Stebbing, 1976; Servais et al., 2005; Svendsen & Weeks, 1995; Svendsen, Spurgeon, Hankard, & Weeks, 2004).

Exposure to PAHs results in a decline in membrane stability; and oxidative derivatives of PAHs such as anthroquinones facilitate redox cycling and increased radical flux (Fig. 8C; Hwang et al., 2002; Krishnakumar et al., 1994; Livingstone, 2001; Okay et al.,

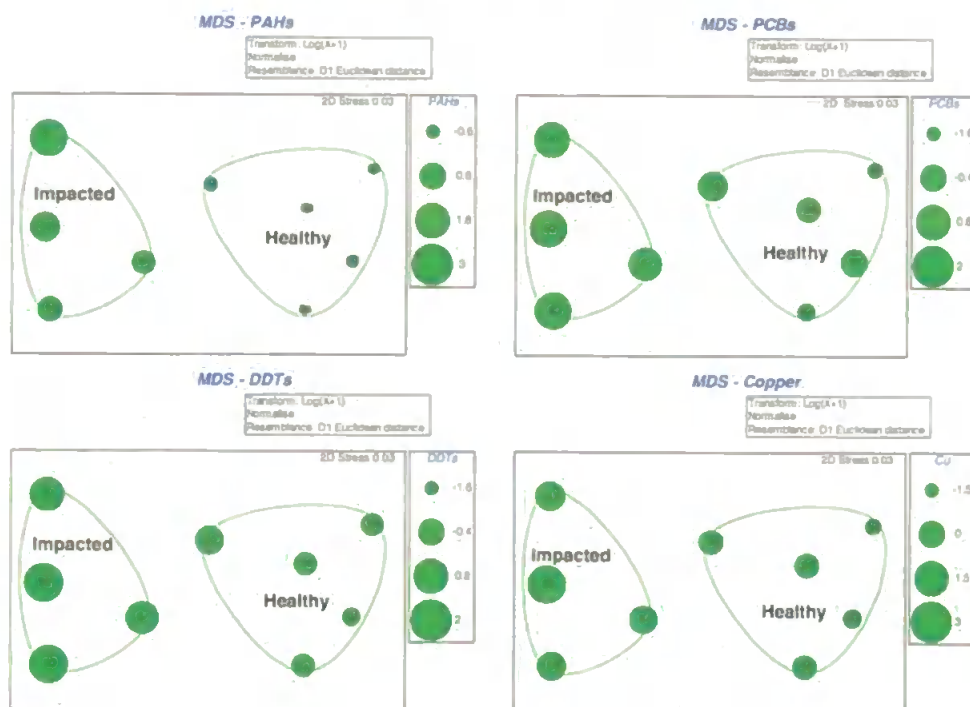


Fig. 6. Multi-dimensional scaling (MDS) analysis of the biological responses (lysosomal stability, NAH activity, NAH latency, lipid, lipofuscin and somatic tissue index – measured as somatic tissue weight/shell length) for blue mussels from Puget Sound. Bubble plots for selected individual chemical contaminants (PAHs, PCBs, DDTs & copper) determined have been serially superimposed. Samples are grouped as urban or reference sites and cluster analysis has been overlaid. Original data derived from Krishnakumar et al. (1994).

Table 1

Spearman rank correlations for all of the biological parameters for mussels from Puget Sound versus pollutant chemicals (PRIMER 6 – Bio-Env procedure)

No. variables	Correlation	Selections
3	0.916	1–3
4	0.915	1–3,11
4	0.891	1–3,7
2	0.880	2,3
5	0.877	1–4,11
3	0.874	1,3,11
5	0.873	1–3,6,11
4	0.872	1–3,10
4	0.870	1–4
3	0.865	2–4

Variables: 1. PAHs; 2. PCBs; 3. DDTs; 4. Ag; 5. As; 6. Cd; 7. Cu; 8. Hg; 9. Pb; 10. Se; 11. Zn.

2000, 2003; Winston et al., 1996). Encouragingly, the results of Hwang et al. (2002) show a very similar relationship between lysosomal stability in oyster hemocytes (*Crassostrea virginica*) and concentration of PAHs ( $\Sigma$ PAH), to the relationship shown for mussels in

Table 2

Testing matched similarity matrices for all of the biological parameters versus pollutant chemicals for blue mussels from Puget Sound (PRIMER 6 – RELATE procedure)

Biological parameters versus	Rho statistic	Probability
All chemicals	0.746	$P \leq 0.002$
PAHs, PCBs & DDTs	0.916	$P \leq 0.001$
PAHs & PCBs	0.837	$P \leq 0.002$
PCBs & DDTs	0.880	$P \leq 0.001$
PAHs & DDTs	0.859	$P \leq 0.001$
PAHs	0.720	$P \leq 0.001$
PCBs	0.780	$P \leq 0.003$
DDTs	0.863	$P \leq 0.001$

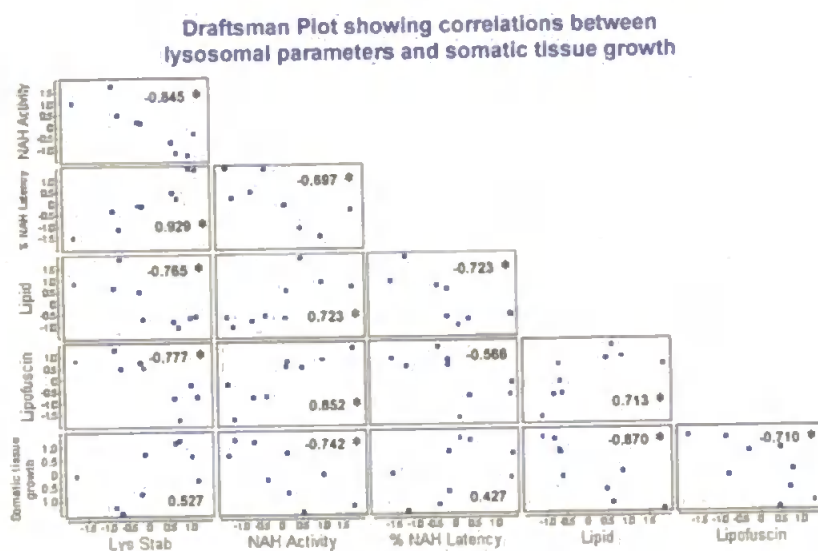


Fig. 7. PRIMER v6 draftsman plot showing the standard product moment correlation coefficient between every pair of biological variables (\* indicates  $P < 0.05$ ).

Fig. 8C, indicating that this reaction may be generic in bivalves. The net consequence is a compensatory increase in lysosomal autophagy resulting initially in increased turnover of (damaged?) proteins and organelles leading to increased production of stress or age pigment (ceroid-lipofuscin) and accumulation of lipid as indicated in Fig. 3B and C (Krishnakumar et al., 1994; Domouhtsidou & Dimitriadis, 2001; Moore, 1988; Moore, Bubel, & Lowe, 1980; Moore et al., 1985; Moore, Soverchia, & Thomas, 1996). Lipofuscin and its associated bound iron is now considered to contribute significantly to radical generation, as well as possibly binding lysosomal proteolytic and other hydrolytic enzymes with a net decrease in degradative capacity (Brunk & Terman, 2002). Moreover, experimental data in mussels indicates that following an initial increase in protein catabolism associated with PAH induced autophagy, that increasing PAH concentration results in an inhibition of protein breakdown (Moore & Viarengo, 1987; Viarengo, Moore, Pertica, Mancinelli, &



Table 3

Spearman rank correlations among the biological parameters for mussels from Puget Sound (PRIMER 6 – Bio-Env procedure)

No. variables	Correlation	Selections
5	1.000	1–5
5	0.981	1,3–6
5	0.979	2–6
4	0.978	1,3–5
4	0.976	2–5
5	0.975	1,2,4–6
4	0.969	1,2,4,5
5	0.967	1–5
4	0.966	2–5
5	0.964	1–3,5,6
4	0.962	1,3,5,6
5	0.960	1–4,6
4	0.958	1,2,4,5
4	0.952	3–6
4	0.952	1–4
3	0.950	1,4,5
3	0.949	3–5
3	0.941	2–4
3	0.937	1,2,4
4	0.937	1–3,5

Variables: 1, Lys Stab; 2, NAH activity; 3, % NAH latency; 4, Lipid; 5, Lipofuscin; 6, Somatic tissue dry weight/shell length.

Accomando, 1992; Fig. 8D). This will in turn result in accumulation of undigested autophagocytosed material within the lysosomal compartment leading to swelling and dysfunction (Marigómez et al., 2005; Moore, 1988; Figs. 1A, 9).

### 3.4. Proposed conceptual model for lysosomal responses to pollutants as indicators of health status

A conceptual model of this system-based network of lysosomally-linked processes is shown in Figs. 9 and 10. This model links the cellular uptake of pollutants such as PAHs (although metals like copper will behave similarly) with damage to lysosomes, radical generation and oxidative injury, through to tissue pathology and harmful physiological consequences. Overall, the predicted consequence of lysosomal injury is cell and tissue dysfunction, tissue and organ atrophy, reduced physiological scope for growth and impaired gamete production (Allen & Moore, 2004; Bayne et al., 1978, Bayne, Moore, Widdows, Livingstone, & Salkeld, 1979; Bayne et al., 1985; Krishnakumar et al., 1994; Moore et al., 2004; Widdows et al., 1982).

It is also essential to be able to link the impact of pollutants on whole biological systems, from subcellular organelles and cells, through to the higher order interactive levels of organisation to animal health (Allen & Moore, 2004). Examples of where this has been possible include: the prognostic use of lysosomal stability in the liver cells of the flatfish flounder (*Platichthys flesus*) to predict the degree of liver degeneration (from cell injury through to hepatocellular carcinoma) as a result of PAH and organochlorine exposure (Köhler et al., 2002); and the direct relationship between lysosomal integrity

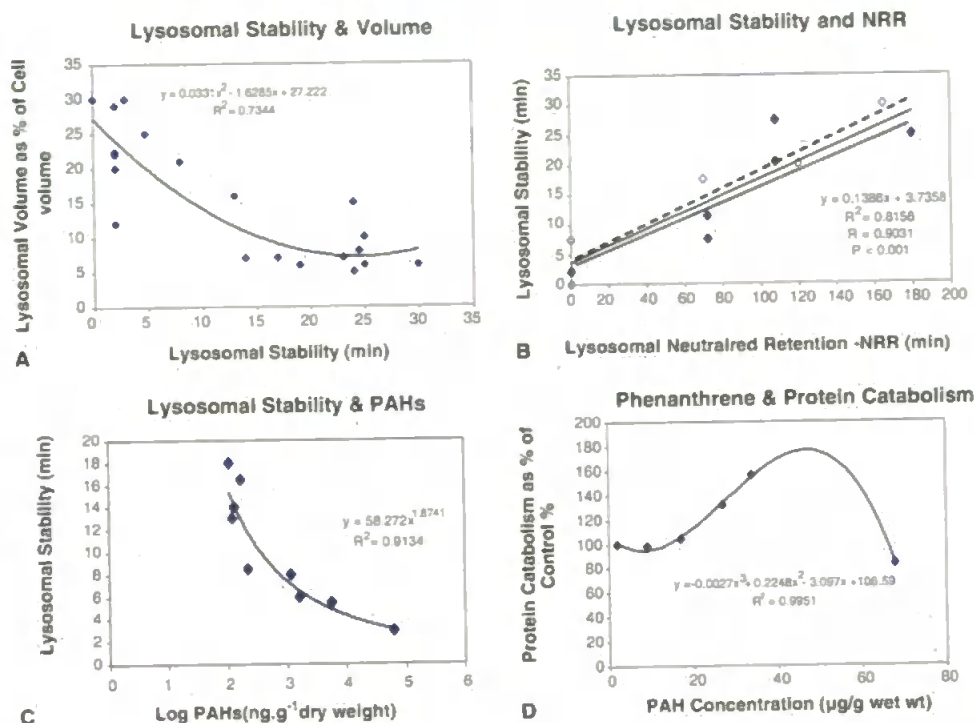


Fig. 8. (A) Relationship between lysosomal stability (determined cytochemically) and lysosomal stability determined as neutral red retention (NRR) (Lowe et al., 1992, 1995; Köhler et al., 1992). The graph shows combined data for the flatfish dab liver cells ( $\diamond$ ) and mussel hepatopancreatic digestive cells ( $\blacklozenge$ ). Separate regressions are shown for mussels (dotted line), dab (dashed line) and combined (solid line). (B) Relationship between lysosomal stability (determined cytochemically) and lysosomal volume in mussel hepatopancreatic digestive. Data from Clarke and Moore (1983), Lowe et al. (1981), Moore and Clarke (1982), Moore – previously unpublished data and Widdows et al. (1982). (C) Correlation between tissue burden of summed low and high molecular weight polycyclic aromatic hydrocarbons and lysosomal stability measured in hepatopancreatic digestive cells of blue mussels from Puget Sound, USA. Original data derived from Krishnakumar et al. (1994) and (D) Relationship between PAH (phenanthrene) concentration in mussel hepatopancreatic tissue and protein catabolism. Data derived from Moore and Viarengo (1987), Nott and Moore (1987) and Viarengo et al. (1992).

in hepatopancreatic digestive cells of mussels and scope for growth; and also, between lysosomal stability in the digestive cells of oysters (*Crassostrea virginica*) and larval viability (Fig. 11; Allen & Moore, 2004; Ringwood, Hoguet, Keppler, & Gielazyn, 2004). The inference here is that measures of lysosomal stability appear to provide potentially powerful prognostic biomarkers for whole animal health and may also have predictive use for larval health status (Köhler et al., 2002; Marigómez & Baybay-Villacorta, 2003; Ringwood et al., 2004). Furthermore, the evidence is steadily accumulating that lysosomal membrane stability is a generic indicator of cellular health in eukaryotic cells, as is indicated by studies with protozoans, coelenterates, annelids, crustaceans, molluscs, fish and mammals (Galloway et al., 2004; Dayeh et al., 2004; Hankard et al., 2004; Moore & Stebbing, 1976; Svendsen et al., 2004; Martinez-Vicente et al., 2005; Servais et al., 2005).



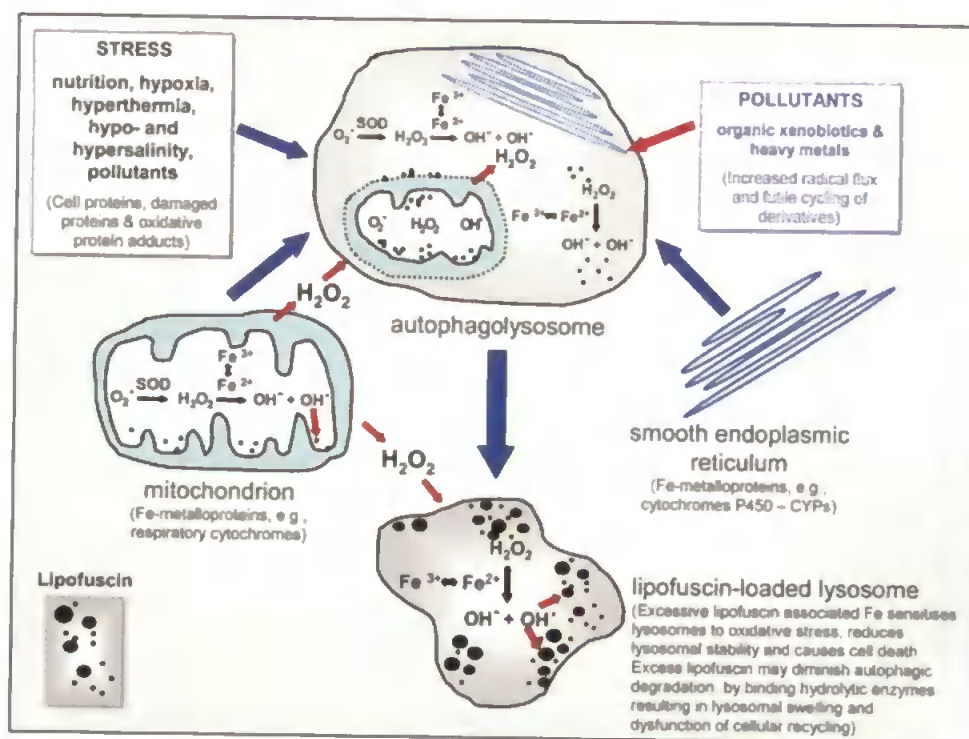


Fig. 9. Conceptual model for the role of oxyradicals and lipofuscin in lysosomal autophagy and oxyradical-mediated cell injury. This model draws on one proposed by Brunk and Terman (2002).

### 3.5. Integration and proposed use of lysosomal biomarkers in “environmental prognostics”

Allen and Moore (2004) have proposed “environmental prognostics” as a putative branch of systems biology. The key enabling concepts of environmental prognostics are:

- (1) Acknowledgement that reductionist science acts to disassemble ecotoxicological impacts into constituent processes.
- (2) Acceptance that biology is a cross-disciplinary science involving mathematics, engineering, information technology and chemistry.
- (3) Moving towards the notion that biology is an information-based rather than a qualitative science.
- (4) The process requires the assembly of systems by modelling followed by disassembly and focused experimentation as an ongoing procedure.

The crux of the procedure is the definition and evaluation of models of the system in question. This requires the use of the following heavily interdependent tools: conceptual, statistical and numerical models, empirical experimental work and bioinformatics (Fig. 12; Allen & Moore, 2004). We suspect that many biomarkers probably only exhibit a response in a part of the “health status space” (Allen & Moore, 2004; Depledge et al., 1993); where they will indicate that a reaction has taken place and may even indicate health status

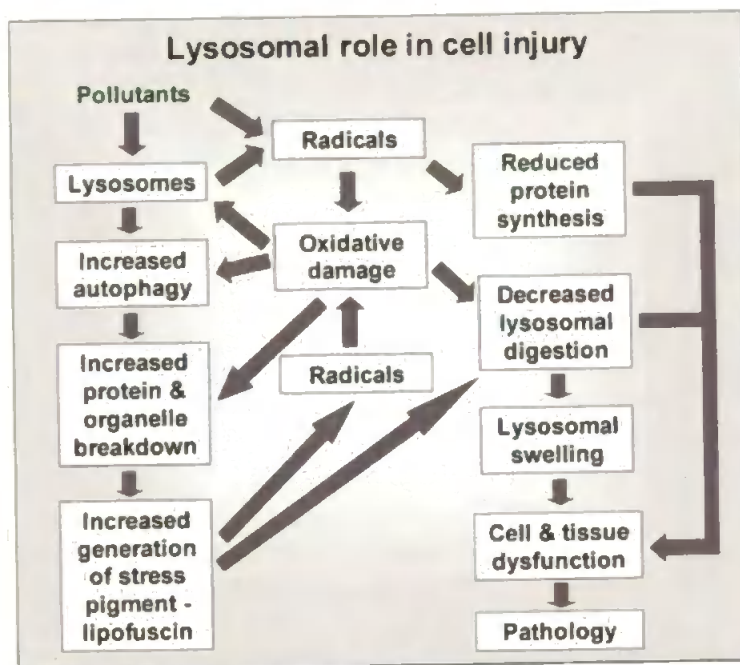


Fig. 10. Conceptual model for pollutant interactions with lysosomal processes of autophagy, cell injury and pathology, based on empirical data where there is a reasonable mechanistic basis for making assumptions about the linkages.

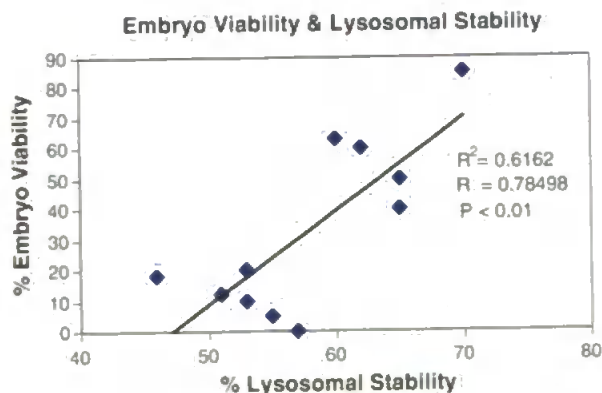


Fig. 11. Linear relationship between lysosomal stability (derived from neutral red retention) in oyster hepatopancreatic digestive cells and the viability of oyster larvae derived from the same adults. Modified from Ringwood et al. (2004).

within a narrow range, or what has induced the response, but they do not generally indicate the health status of the whole range from healthy to irreversible damage in flatfish (Köhler et al., 2002). In terms of environmental prognostics, the first stage is to relate bio-marker responses to health status of individual organisms by mapping the said responses

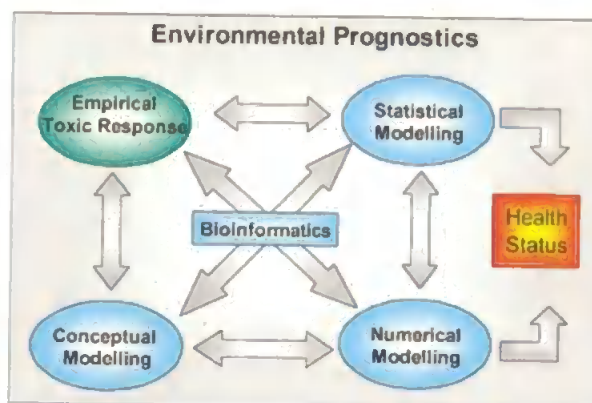


Fig. 12. Diagram showing a schematic of how the disciplines of environmental prognostics relate to each other for the development of explanatory frameworks (adapted from Allen & Moore, 2004).

against an integrated “health status” indicator, such as lysosomal stability; and then to derive explanatory frameworks (Allen & Moore, 2004; Köhler et al., 2002; Moore et al., 2004).

The integration of biomarker data can be achieved using multivariate statistics and then mapped onto a two dimensional representation of “health status space” (see below) by using lysosomal membrane stability as a measure of cellular well-being (Allen & Moore, 2004; Clarke, 1999). This is viewed as a crucial step towards the derivation of explanatory frameworks for prediction of pollutant impact on animal health.

Health status space is analogous to phase space in physics. For a system of  $n$  first-order ordinary differential equations, the  $2n$ -dimensional space consisting of the possible values of  $x$  is known as its phase space. In its simplest form it is a two dimensional graph where any point can be described in terms of two numbers: the  $x$  and  $y$  coordinates. In our case the dimensions of multi-dimensional health status space are multiple contaminant and biomarker data, environmental variability, space and time.

A useful method of integrating biomarker data into a health status index involves the use of principal components analysis (PCA) to reduce the dimensionality of the problem to a simple two dimensional representation (Chatfield & Collins, 1980; Allen & Moore, 2004). PCA is commonly used as a cluster analysis tool and is designed to capture the variance in a dataset in terms of principle components. In effect, one is trying to reduce the dimensionality of the data to summarise the most important (i.e., defining) parts, whilst simultaneously filtering out noise. Principal components analysis replaces the original variables by a much smaller set of derived variables that embody as much as possible of the variance of the data, thereby aiding interpretation. Essentially the PCA takes a set of data points, and rotates it such that the maximum variability is visible, thus identifying the most important gradients. Hence, by plotting the first principal component (PC1) of the cellular biomarkers (i.e., lipid, lipofuscin, NAH activity, lysosomal NAH latency and ratio of somatic tissue to shell length), which effectively integrate the selected biomarker data, against lysosomal stability, as an indicator of the gradient from health to pathology and disease, the resulting graph reflects the health-related significance of the individual biomarkers to the pollutant toxicity (Fig. 13). Lysosomal stability is used as

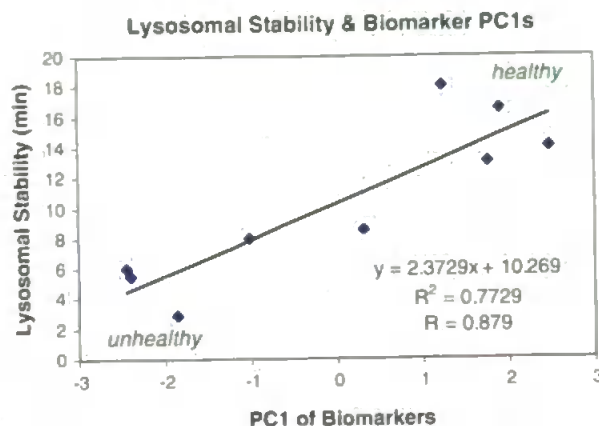


Fig. 13. First principal component (PC1) of mussel tissue biomarkers (eigenvectors for: NAH activity  $-0.470$ , % NAH latency  $0.396$ , Lipid  $-0.473$ , Lipofuscin  $-0.451$ , somatic tissue/shell length  $0.442$ ) from nine urban and reference sites in Puget Sound, USA (Krishnakumar et al., 1994) plotted against lysosomal stability in hepatopancreatic digestive cells. The data has been log transformed and normalised and from principal component analysis, PC1 represents 76.7% of the total variability in the biomarker data, not including lysosomal stability. In the graph, PC1 explains 77% (i.e.,  $R^2 = 0.7729$ ) of the variability in the lysosomal stability data.

the benchmark for cellular health since it is strongly correlated with physiological scope for growth in mussels (Allen & Moore, 2004).

Previous studies increasingly suggest that multivariate statistics are useful in integrating and interpreting multiple biomarker data (Astley, Meigh, Glegg, Braven, & Depledge, 1999; Allen & Moore, 2004; Galloway et al., 2002, 2004; Wedderburn et al., 1998); and we have previously shown that lysosomal stability is a good indicator of physiological fitness in fish liver (Allen & Moore, 2004).

Consequently, by plotting lysosomal stability against the first principal component (PC1) of selected cellular biomarker data (listed in the legend to Fig. 13) from the blue mussel in the Puget Sound (Krishnakumar et al., 1994), we effectively integrate the selected biomarker data and the graph reflects the contaminant gradient between the sampling sites. PC1 is a measure of the contaminant gradient with the left-hand side being the most contaminated and the right-hand side the cleanest (Fig. 13). Lysosomal accumulation of lipid (lipidosis) and lipofuscin (lipofuscinosis) and high NAH activity are indicative of the contaminated sites, with high % lysosomal NAH latency (a measure of lysosomal membrane integrity; Moore, 1976) and somatic tissue index reflecting the clean sites (Moore, 1990; Fig. 13). PC1 explains 77% of the variability in lysosomal stability between the sample sites (Fig. 13).

Hence, by treating cellular responses involving the lysosomal-vacuolar system (i.e., endocytosis, lysosomal function and autophagy) as an integrated system, we have shown that complex and diverse data can be largely interpreted within the framework of the conceptual model described above in Figs. 9 and 10. This is tentatively represented in an idealised diagram where the probable adaptive or dysfunctional significance of physiological and biomarker responses and pathological reactions is mapped against animal health status (Fig. 14), with lysosomal stability used as an indicator of physiological fitness (Allen & Moore, 2004).



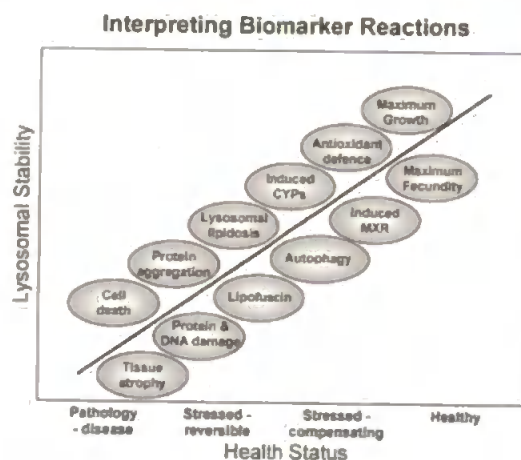


Fig. 14. Idealised diagram of a putative tool for interpreting the probable adaptive or dysfunctional significance of physiological and biomarker responses and pathological reactions in relation to health status. Lysosomal stability is used as an indicator of physiological fitness (Allen & Moore, 2004). CYPs are cytochromes P-450 and MXR is multidrug resistance protein (based on Minier & Moore, 1996).

The second stage of developing environmental prognostics is to use our integrated understanding to derive the conceptual models and then develop numerical simulations in order to derive testable explanatory frameworks.

### 3.6. Simulation model for mussel hepatopancreatic cells

In chemical engineering, physics and epidemiology, for example, it is well understood that complex systems can be accurately understood only by constructing quantitative mathematical models (Maddox, 1998; Noble, Levin, & Scott, 1999). However, this has been largely not the case in ecotoxicology; and will remain so, until realistic models have been built for the process describing how the specificity of the whole system response matches that of the external signal or potentially harmful perturbation it receives (Moore, 2002; Moore & Noble, 2004).

Currently numerical models are in their infancy and used for heuristic purposes (Allen & McVeigh, 2004; McVeigh et al., 2004; Moore, 2002; Moore & Allen, 2002). The great advantage of simulation is that it encourages an understanding of how processes are linked and how system properties emerge in space and time (Hunter, Robbins, & Noble, 2002; Noble, 2002a, 2002b, 2002c).

Simulations have already been made indicating that prognostic simulations of organism health are possible (McVeigh et al., 2004; Moore & Allen, 2002). This computational model simulates the flow of carbon and nitrogen through a mussel's hepatopancreatic digestive cell. The model uses a compartmentalised view of the cell with inviolate pipelines connecting each of the volume-variable partitions. Only the major physiological pathways relevant to the flow of either carbon or nitrogen or volume are modelled. The mussel digestive gland epithelial cells provide a key interface between the organism and pollutants such as polycyclic aromatic hydrocarbons; and the model can simulate pollutant uptake and its effect on cellular energetic physiology, nutrient export processes and lysosomal turnover of intracellular proteins (McVeigh et al., 2004; Moore & Allen, 2002).

Consequently the simulation of key biomarkers related to whole animal health is already achievable within the context of the existing model framework. One current output from this model is simulated cell and tissue pathology, which indicates lysosomal injury and autophagic dysfunction (i.e., lysosomal swelling) leading to digestive cell atrophy (Fig. 15); and lysosomal stability and other related parameters can be predicted from simulated lysosomal volume (Fig. 8A). These simulations parallel those observed in real mussels (Marigómez et al., 2005); and ultimately, this will lead to the development of nowcast/forecast models of environmental health based on “health status” of sentinel animals.

In the longer term context of prediction of environmental risk, a hierarchy of overlapping computational models will be needed, each capable of interacting with the others. Development of these models will be hypothesis-driven and will integrate physical and chemical processes with animal function using a systems biology approach. The aim here is the development of an affordable pre-operational predictive toolbox to aid decision-making in integrated environmental management (IEM) and science-based environmental policy formulation. Achievement of this aim will require a critical interdisciplinary evaluation of the existing physical and chemical parameters, diagnostic and prognostic biomarkers of health status and indices of biodiversity/ecosystem integrity currently used as indicators of biological and ecological damage (Depledge, 1994, 1999; Galloway, 2004; Rice, 2003).

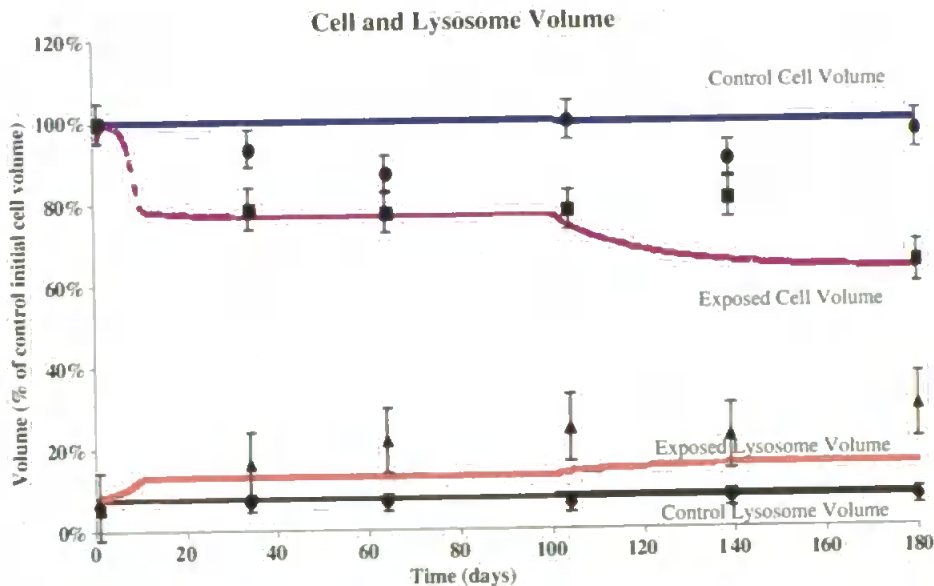


Fig. 15. Comparison of simulated and experimental results for pathological effects of exposure of mussels to oil-derived PAHs on the hepatopancreatic digestive cell and lysosomal volumes. Model results are shown as lines and experimental results as solitary points with error bars (95% CL). Cellular and lysosomal volume are given as a percentage of the initial cell volume: ● – control cell, ■ – exposed cell, ◆ – control lysosome, ▲ – exposed lysosome (adapted from McVeigh et al., 2004).

#### 4. Conclusions and prospectus

We have clearly demonstrated lysosomal accumulation of the polycyclic aromatic hydrocarbon 3-methylcholanthrene (3-MC) by hepatopancreatic cells and ovarian oocytes in mussel. We have also shown that lysosomal membrane stability is a predictive indicator for cell injury and pathology; and supporting evidence indicates that this parameter is generic in the eukaryotes. We have also addressed the complex problem of evaluating and predicting health of environmental sentinel animals, such as blue mussels, through a coupled biomarker testing and modelling approach in the wider context of forecasting risk. The approach described here will facilitate the validation, and further the essential new development of robust diagnostic and prognostic tools that can be used along with other chemical, biological and ecological tools as indices of sustainability (Fig. 16). Efforts must also focus on an integrated approach to the validation of biomarkers and relating these to indices of ecological functional integrity that are prognostic for population, community and possibly human endpoints (Moore et al., 2004; Rice, 2003; Xu et al., 2002; Figs. 3D and 11).

A major challenge for the future is the development of computational models to bridge the gap between individual organism “health-status” and ecosystem-level functional properties; and how they affect and are quantifiably connected to health of the environment (Moore, Allen, & Somerfield, 2006; Rees, Setiapermana, Sharp, Weeks, & Williams, 1999).

We can perhaps begin to bridge this gap by identifying “common targets” in the biota. Essentially, lysosomal functional integrity is one such generic common target in all eukaryotic organisms, that is evolutionarily highly conserved, and is a good diagnostic biomarker of individual health status (see Fig. 8B; Allen & Moore, 2004; Bayne & Moore, 1998; Galloway et al., 2002; Köhler et al., 1992, 2002; Lekube et al., 2000; Moore, 2002; Winston

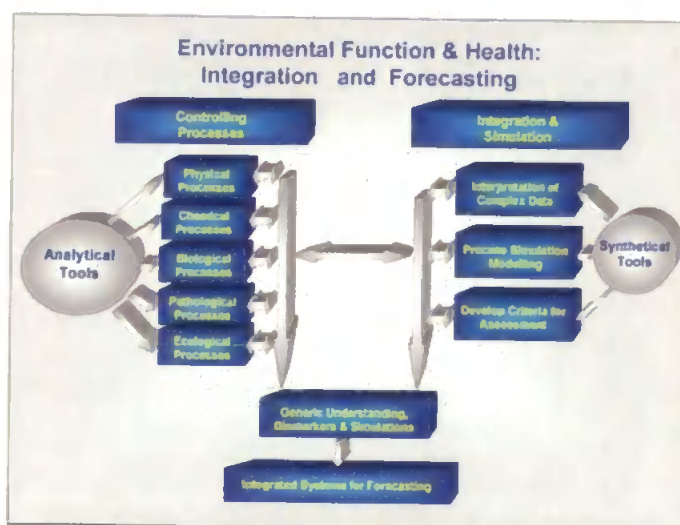


Fig. 16. Process based synthesis for the evaluation of “health” of the environment and predicting the consequences of future change.

et al., 2002). This biomarker can also be used to predict liver damage and tumour progression in fish liver, as well as enhanced protein turnover (i.e., lysosomal autophagy), as a result of radical attack on proteins, and energetic status (i.e., scope for growth) as a predictive indicator of fitness of individuals within a population (Figs. 10, 13 and 14; Allen & Moore, 2004; Kirchin et al., 1992; Moore et al., 2004).

In the future, we may be able to embed bioenergetic models in ecosystem and/or contaminant models (e.g., oil-spill models), and force the bioenergetic models with food from ecosystem models or PAHs for oil spill models. For example, one can perhaps envisage bioenergetic models being used to predict the harmful effects of contaminant exposure on properties of individuals, populations, communities, and ecosystems (Allen & Moore, 2004; Beyers, Rice, & Clements, 1999; Beyers, Rice, Clements, & Henry, 1999; Bevelhimer & Bennett, 2000; Di Giulio & Benson, 2002; McVeigh et al., 2004; Moore et al., 2006; Rees et al., 1999; Winston et al., 2002). Inputs such as contaminant dose (e.g., PAHs as shown in Fig. 8C), which affects physiological parameters, could be used to force these models to predict organism-level responses (for example, energy metabolism and storage, reproductive functions, pathology and growth dynamics).

Speculating into the more distant future, outputs from biomarker-linked bioenergetic models may possibly be used as inputs into an individual-based population model to predict emergent properties of populations, such as abundance, reproductive fitness, and life-stage dynamics. In turn, outputs from population models may possibly be used as inputs into ecosystem models to predict certain ecosystem properties such as productivity of various trophic levels or nutrient dynamics.

### Acknowledgements

Invited versions of the major content of this paper were presented at the 12th International Congress of Histochemistry and Cytochemistry at the University of California at San Diego, La Jolla, USA; and at the UNEP-GEF Scientific and Technical Assessment Panel (STAP) Workshop on the use of bioindicators, biomarkers and analytical methods for the analysis of POPs in developing countries, Tsukuba, Japan, December 2003. M. Moore attended the GEF meeting as the representative of the United Nations Industrial Development Organisation UNIDO. The work forms part of the PREDICT 2 Project supported by the Department for Environment, Food and Rural Affairs (Defra, UK), Contract No. AE1136.

### References

- Allen, J. I., & Moore, M. N. (2004). Environmental prognostics: is the current use of biomarkers appropriate for environmental risk evaluation. *Marine Environmental Research*, 58, 227–232.
- Allen, J. I., & McVeigh, A. (2004). Towards computational models of cells for environmental toxicology. *Journal of Molecular Histology*, 35, 697–706.
- Allison, A. C., & Young, M. R. (1969). Vital staining and fluorescence microscopy of lysosomes. In J. T. Dingle & H. B. Fell (Eds.), *Lysosomes in biology and pathology* (pp. 600–628). Amsterdam, Oxford, New York: Elsevier.
- Astley, K. N., Meigh, H. C., Glegg, G. A., Braven, J., & Depledge, M. H. (1999). Multi-variate analysis of biomarker responses in *Mytilus edulis* and *Carcinus maenas* from the Tees Estuary, (UK). *Marine Pollution Bulletin*, 39, 145–154.
- Bayne, B. L., Brown, D. W., Burns, K., Dixon, D. R., Ivanovici, A., Livingstone, D. R., et al. (1985). *The effects of stress and pollution on marine animals*. New York, Philadelphia, Eastbourne U.K., Toronto: Praeger, 384 p.



- Bayne, B. L., Holland, D. L., Moore, M. N., Lowe, D. M., & Widdows, J. (1978). Further studies on the effects of stress in the adult on the eggs of *Mytilus edulis*. *Journal of the Marine Biological Association of the United Kingdom*, 58, 825–841.
- Bayne, B. L., Moore, M. N., Widdows, J., Livingstone, D. R., & Salkeld, P. N. (1979). Measurement of the responses of individuals to environmental stress and pollution: studies with bivalve molluscs. *Philosophical Transactions of the Royal Society of London Series*, 286B, 563–581.
- Bayne, C. J., & Moore, M. N. (1998). Non-lymphoid immunologic defenses in aquatic invertebrates and their value as indicators of aquatic pollution. In J. T. Zelikoff (Ed.), *Ecotoxicology: responses, biomarkers and risk assessment* (pp. 243–261). Fair Haven, New Jersey: Published for OECD by SOS Publications.
- Bevelhimer, M. S., & Bennett, W. A. (2000). Assessing cumulative thermal stress in fish during chronic intermittent exposure to high temperatures. *Environmental Science Policy*, 3, 211–216.
- Beyers, D. W., Rice, A., & Clements, W. H. (1999). Evaluating biological significance of chemical exposure to fish using a bioenergetics-based stressor–response model. *Canadian Journal of Fisheries and Aquatic Science*, 56, 823–829.
- Beyers, D. W., Rice, A., Clements, W. H., & Henry, C. J. (1999). Estimating physiological cost of chemical exposure: Integrating energetics and stress to quantify toxic effects in fish. *Canadian Journal of Fisheries and Aquatic Science*, 56, 814–822.
- Brunk, U. T., & Terman, A. (2002). Lipofuscin: mechanisms of age-related accumulation and influence on cell function. *Free Radical Biology and Medicine*, 33, 611–619.
- Cajaraville, M. P., Bebianno, M. J., Blasco, J., Porte, C., Sarasquete, C., & Viarengo, A. (2000). The use of biomarkers to assess the impact of pollution in coastal environments of the Iberian peninsula: a practical approach. *Science of the Total Environment*, 247, 295–311.
- Cajaraville, M. P., Abascal, I., Etcheberria, M., & Marigómez, I. (1995). Lysosomes as cellular markers of environmental pollution: time- and dose-dependent responses of the digestive lysosomal system of mussels after petroleum hydrocarbon exposure. *Environmental Toxicology and Water Quality*, 10, 1–8.
- Chatfield, C., & Collins, A. J. (1980). *Introduction to multivariate analysis*. London: Chapman and Hall.
- Clarke, K. R. (1999). Non-metric multivariate analysis in community-level ecotoxicology. *Environmental Toxicology and Chemistry*, 18, 117–127.
- Clarke, K. R., & Moore, M. N. (1983). Unbiased linear property estimation for spheres, from sections exhibiting over projection and truncation. *Journal of Microscopy*, 131, 311–322.
- Cuervo, A. M. (2004). Autophagy: in sickness and in health. *Trends in cell biology*, 14, 70–77.
- Dailianis, S., Domouhtsidou, G. P., Raftopoulou, E., Kaloyianni, M., & Dimitriadis, V. K. (2003). Evaluation of neutral red retention assay, micronucleus test, acetylcholinesterase activity and a signal transduction molecule (cAMP) in tissues of *Mytilus galloprovincialis* (L.), in pollution monitoring. *Marine Environmental Research*, 56, 443–470.
- Dayeh, V. R., Chow, S. L., Schirmer, K., Lynn, D. H., & Bols, N. C. (2004). Evaluating the toxicity of Triton X-100 to protozoan, fish, and mammalian cells using fluorescent dyes as indicators of cell viability. *Ecotoxicology and Environmental Safety*, 57, 357–382.
- De Duve, C., De Barse, T., Poole, B., Trouet, P., Tulkens, P., & Van Hoof, F. (1974). Lysosomotropic agents. *Biochemical Pharmacology*, 23, 2495–2531.
- Depledge, M. H. (1994). Genotype toxicity: Implications for individuals and populations. *Environmental Health Perspectives*, 102, 101–104.
- Depledge, M. H. (1999). Recovery of ecosystems and their components following exposure to pollution. *Journal of Aquatic Ecosystem Health*, 6, 199–206.
- Depledge, M. H., Amaral-Mendes, J. J., Daniel, B., Halbrook, R. S., Kloepper-Sams, P., Moore, M. N., et al. (1993). The conceptual basis of the biomarker approach. In D. G. Peakall & L. R. Shugart (Eds.), *Biomarkers – research and application in the assessment of environmental health* (pp. 15–29). Berlin, Heidelberg: Springer.
- Di Giulio, R. T., & Benson, W. B. (Eds.). (2002). *Interconnections between Human Health and Ecological Integrity* (pp. 110). Pensacola, Florida: Society of Environmental Toxicology and Chemistry (SETAC).
- Domouhtsidou, G. P., & Dimitriadis, V. K. (2001). Lysosomal and lipid alterations in the digestive gland of mussels, *Mytilus galloprovincialis* (L.) as biomarkers of environmental stress. *Environmental Pollution*, 115, 123–137.
- Donkin, P., & Evans, S. V. (1984). Application of steam distillation in the determination of petroleum hydrocarbons in water and mussels (*Mytilus edulis*) from dosing experiments with crude oil. *Analytica Chimica Acta*, 156, 207–219.

- Galloway, T. S., Sanger, R. C., Smith, K. L., Fillmann, G., Readman, J. W., Ford, T. E., et al. (2002). Rapid assessment of marine pollution using multiple biomarkers and chemical immunoassays. *Environmental Science and Technology*, 36, 2219–2226.
- Galloway, T. S., Brown, R. J., Browne, M. A., Dissanayake, A., Lowe, D., Jones, M. B., et al. (2004). A multibiomarker approach to environmental assessment. *Environmental Science and Technology*, 38, 1723–1731.
- Gould, P. (2004). Nanoparticles probe biosystems. *Materials Today*, 7, 36–43.
- Hankard, P. K., Svendsen, C., Wright, J., Wienberg, C., Fishwick, S. K., Spurgeon, D. J., et al. (2004). Biological assessment of contaminated land using earthworm biomarkers in support of chemical analysis. *Science of the Total Environment*, 330, 9–20.
- Howard, V. (2004). Small particles – big problems. *International Laboratory News*, 34(2), 28–29.
- Hunter, P. J., Robbins, P., & Noble, D. (2002). The IUPS human physiome project. *Pflügers Archives – European Journal of Physiology*, 445, 1–9.
- Hwang, H.-M., Wade, T. L., & Sericano, J. L. (2002). Relationship between lysosomal membrane destabilization and chemical body burden in eastern oysters (*Crassostrea virginica*) from Galveston Bay, Texas, USA. *Environmental Toxicology and Chemistry*, 21, 1268–1271.
- Kalpaxis, D. L., Theos, C., Xaplanteri, M. A., Dinos, G. P., Catsiki, A. V., & Leotsinidis, M. (2004). Biomonitoring of Gulf of Patras N. Peloponnese, Greece. Application of a biomarker suite including evaluation of translation efficiency in *Mytilus galloprovincialis* cells. *Environmental Research*, 94, 211–220.
- Kirchin, M. A., Moore, M. N., Dean, R. T., & Winston, G. W. (1992). The role of oxyradicals in intracellular proteolysis and toxicity in mussels. *Marine Environmental Research*, 34, 315–320.
- Klionsky, D. J., & Emr, S. D. (2000). Autophagy as a regulated pathway of cellular degradation. *Science*, 290, 1717–1721.
- Köhler, A., Deisemann, H., & Lauritzen, B. (1992). Ultrastructural and cytochemical indices of toxic injury in dab liver. *Marine Ecology Progress Series*, 91, 141–153.
- Köhler, A., Wahl, E., & Söfker, K. (2002). Functional and morphological changes of lysosomes as prognostic biomarkers of toxic liver injury in a marine flatfish (*Platichthys flesus* (L)). *Environmental Toxicology and Chemistry*, 21, 2434–2444.
- Krishnakumar, P. K., Casillas, E., & Varanasi, U. (1994). Effect of environmental contaminants on the health of *Mytilus edulis* from Puget Sound, Washington, USA. I. Cytochemical measures of lysosomal responses in the digestive cells using automatic image analysis. *Marine Ecology Progress Series*, 106, 249–261.
- Lekube, X., Cajaraville, M. P., & Marigomez, I. (2000). Use of polyclonal antibodies for the detection of changes induced by cadmium in lysosomes of aquatic organisms. *Science of the Total Environment*, 247, 201–212.
- Livingstone, D. R. (2001). Contaminant-stimulated reactive oxygen species production and oxidative damage in aquatic organisms. *Marine Pollution Bulletin*, 42, 656–666.
- Livingstone, D. R., Chipman, J. K., Lowe, D. M., Minier, C., Mitchelmore, C. L., Moore, M. N., et al. (2000). Development of biomarkers to detect the effects of organic pollution on aquatic invertebrates: recent molecular, genotoxic, cellular and immunological studies on the common mussel (*Mytilus edulis* L.) and other mytilids. *International Journal of Environmental Pollution*, 13(1–6), 56–91.
- Livingstone, D. R., Farrar, S. V., Fossi, C., Kirchin, M. A., & Moore, M. N. (1988). Responses of the digestive gland cytochrome P-450 monooxygenase system of the common mussel (*Mytilus edulis*) to 3-methylcholanthrene and sodium phenobarbital. *Marine Environmental Research*, 24, 118–119.
- Lowe, D. M. (1988). Alterations in the cellular structure of *Mytilus edulis* resulting from exposure to environmental contaminants under field and experimental conditions. *Marine Ecology Progress Series*, 46, 91–100.
- Lowe, D. M., Fossato, V. U., & Depledge, M. H. (1995). Contaminant induced lysosomal membrane damage in blood cells of mussels *M. galloprovincialis* from the Venice Lagoon: an in vitro study. *Marine Ecology Progress Series*, 129, 189–196.
- Lowe, D. M., Moore, M. N., & Clarke, K. R. (1981). Effects of oil on digestive cells in mussels: quantitative alterations in cellular and lysosomal structure. *Aquatic Toxicology*, 1, 213–226.
- Lowe, D. M., Moore, M. N., & Evans, B. M. (1992). Contaminant impact on interactions of molecular probes with lysosomes in living hepatocytes from dab *Limanda limanda*. *Marine Ecology Progress Series*, 91, 135–140.
- Lowe, D. M., Soverchia, C., & Moore, M. N. (1995). Lysosomal membrane responses in mussels to experimental contaminant exposure. *Aquatic Toxicology*, 33, 105–112.
- Lyons, B. P., Pascoe, C. K., & McFadzen, I. R. B. (2002). Phototoxicity of pyrene and benzo[a]pyrene to embryonic larval stages of the pacific oyster *Crassostrea gigas*. *Marine Environmental Research*, 54, 627–631.

- McVeigh, A., Allen, J. I., Moore, M. N., Dyke, P., & Noble, D. (2004). A carbon and nitrogen flux model of mussel digestive gland epithelial cells and their simulated response to pollutants. *Marine Environmental Research*, 58, 821–827.
- Maddox, J. (1998). *What remains to be discovered*. New York: The Free Press, 434p.
- Marigómez, I., & Baybay-Villacorta, L. (2003). Pollutant-specific and general lysosomal responses in digestive cells of mussels exposed to model organic chemicals. *Aquatic Toxicology*, 64, 235–257.
- Marigómez, I., Izaguirre, U., & Lekube, X. (2005). Lysosomal enlargement in digestive cells of mussels exposed to cadmium benzo[a]pyrene and their combination. *Comparative Biochemistry and Physiology*, C141, 188–193.
- Martinez-Vicente, M., Sovak, G., & Cuervo, A. M. (2005). Protein degradation and ageing. *Experimental Gerontology*, 40, 622–633.
- Minier, C., & Moore, M. N. (1996). Multixenobiotic resistance in mussel blood cells. *Marine Environmental Research*, 42, 389–392.
- Moore, M. N. (1976). Cytochemical demonstration of latency of lysosomal hydrolases in digestive cells of the common mussel, *Mytilus edulis* and changes induced by thermal stress. *Cell Tissue Research*, 175, 279–287.
- Moore, M. N. (1988). Cytochemical responses of the lysosomal system and NADPH-ferrihemoprotein reductase in molluscs to environmental and experimental exposure to xenobiotics. *Marine Ecology Progress Series*, 46, 81–89.
- Moore, M. N. (1985). Cellular responses to pollutants. *Marine Pollution Bulletin*, 16, 134–139.
- Moore, M. N. (1990). Lysosomal cytochemistry in marine environmental monitoring. *Histochemical Journal*, 22, 187–191.
- Moore, M. N. (2002). Biocomplexity: the post-genome challenge in ecotoxicology. *Aquatic Toxicology*, 59, 1–15.
- Moore, M. N., & Allen, J. I. (2002). A computational model of the digestive gland epithelial cell of the marine mussel and its simulated responses to aromatic hydrocarbons. *Marine Environmental Research*, 54, 579–584.
- Moore, M. N., & Clarke, K. R. (1982). Use of microstereology and cytochemical staining to determine the effects of crude oil-derived aromatic hydrocarbons on lysosomal structure and function in a marine bivalve mollusc, *Mytilus edulis*. *Histochemical Journal*, 14, 713–718.
- Moore, M. N., & Halton, D. W. (1973). Histochemical changes in the digestive gland of *Lymnaea truncatula* infected with *Fasciola hepatica*. *Z. Parasitkde.*, 43, 1–16.
- Moore, M. N., & Noble, D. (2004). Computational modelling of cell and tissue processes and function. *Journal of Molecular Histology*, 35, 655–658.
- Moore, M. N., & Stebbing, A. R. D. (1976). The quantitative cytochemical effects of three metal ions on a lysosomal hydrolase of a hydroid. *Journal of Marine Biological Association of the United Kingdom*, 56, 995–1005.
- Moore, M. N., Allen, J. I., & Somerfield, P. J. (2006). Autophagy: role in surviving environmental stress. *Marine Environmental Research*, in press.
- Moore, M. N., Bubel, A., & Lowe, D. M. (1980). Cytology and cytochemistry of the pericardial gland cells of *Mytilus edulis* and their lysosomal responses to injected horseradish peroxidase and anthracene. *Journal of Marine Biological Association of the United Kingdom*, 60, 135–149.
- Moore, M. N., Depledge, M. H., Readman, J. W., & Leonard, D. R. P. (2004). An integrated biomarker-based strategy for ecotoxicological evaluation of risk in environmental management. *Mutation Research*, 552, 247–268.
- Moore, M. N., Köhler, A., Lowe, D. M., & Simpson, M. G. (1994). An integrated approach to cellular biomarkers in fish. In M. C. Fossi & C. Leonzio (Eds.), *Non-destructive biomarkers in vertebrates* (pp. 171–197). Boca Raton: Lewis/CRC.
- Moore, M. N., Lowe, D. M., Soverchia, C., Haigh, S. D., & Hales, S. G. (1997). Uptake of a non-calorific, edible sucrose polyester oil and olive oil by marine mussels and their influence on uptake and effects of anthracene. *Aquatic Toxicology*, 39, 307–320.
- Moore, M. N., Mayernick, J. A., & Giam, C. S. (1985). Lysosomal responses to a polynuclear aromatic hydrocarbon in a marine snail: effects of exposure to phenanthrene and recovery. *Marine Environmental Research*, 17, 230–233.
- Moore, M. N., Pipe, R. K., & Farrar, S. V. (1982). Lysosomal and microsomal responses to environmental factors in *Littorina littorea* from Sullom Voe. *Marine Pollution Bulletin*, 13, 340–345.
- Moore, M. N., Pipe, R. K., Farrar, S. V., Thomson, S., & Donkin, P. (1986). Lysosomal and microsomal responses to oil-derived hydrocarbons in *Littorina littorea*. In J. M. Capuzzo & D. R. Kester (Eds.), *Oceanic processes in marine pollution – biological processes and waste in the ocean* (Vol. 1, pp. 89–96). Melbourne (Florida): Krieger Publishing.
- Moore, M. N., Soverchia, C., & Thomas, M. (1996). Enhanced lysosomal autophagy of intracellular proteins by xenobiotics in living molluscan blood cells. *Cytochem., Acta Histochem. Cytochem.*, 29(Supplement), 947–948.

- Moore, M. N., & Viarengo, A. (1987). Lysosomal membrane fragility and catabolism of cytosolic proteins: evidence for a direct relationship. *Experientia*, 43, 320–323.
- Noble, D. (2002a). Modelling the heart: insights, failures and progress. *Bioessays*, 24, 1155–1163.
- Noble, D. (2002b). The rise of computational biology. *Nature Reviews Molecular Cell Biology*, 460–463.
- Noble, D. (2002c). Unraveling the genetics and mechanisms of cardiac arrhythmia. *Proceedings of National Academy of Sciences of the United States of America*, 99, 5755–5756.
- Noble, D., Levin, J., & Scott, W. (1999). Biological simulations in drug discovery. *Drug Discovery Today*, 4, 10–16.
- Nott, J. A., & Moore, M. N. (1987). Effects of polycyclic aromatic hydrocarbons on molluscan lysosomes and endoplasmic reticulum. *Histochemical Journal*, 19, 357–368.
- Okay, O. S., Donkin, P., Peters, L. D., & Livingstone, D. R. (2000). The role of algae (*Isochrysis galbana*) enrichment on the bioaccumulation of benzo[a]pyrene and its effects on the blue mussel *Mytilus edulis*. *Environmental Pollution*, 110, 103–113.
- Okay, O. S., Tolun, L., Telli-Karakoc, F., Tufekci, V., Tufekci, H., Olgun, A., & Morkoc, E. (2003). The changes of T-PAH levels and health status of mussels in Izmit bay (Turkey) after Marmara earthquake and subsequent refinery fire. *Environment International*, 28, 671–675.
- Panyam, J., & Labhasetwar, V. (2003). Biodegradable nanoparticles for drug and gene delivery to cells and tissues. *Advanced Drug Delivery Reviews*, 55, 329–347.
- Pipe, R. K., & Moore, M. N. (1985). The ultrastructural localization of acid hydrolases in developing oocytes of *Mytilus edulis*. *Histochemical Journal*, 17, 939–949.
- Pipe, R. K., & Moore, M. N. (1986). Arylsulphatase activity associated with phenanthrene induced digestive cell deletion in the marine mussel *Mytilus edulis*. *Histochemical Journal*, 18, 557–564.
- Rashid, F., Horobin, R. W., & Williams, M. A. (1991). Predicting the behaviour and selectivity of fluorescent probes for lysosomes and related structures by means of structure-activity models. *Histochemical Journal*, 23, 450–459.
- Rees, J. G., Setiapermana, D., Sharp, V. A., Weeks, J. M., & Williams, T. M. (1999). Evaluation of the impacts of land-based contaminants on the benthic faunas of Jakarta bay, Indonesia. *Oceanologica Acta*, 22, 627–640.
- Regoli, F. (2000). Total oxyradical scavenging capacity (TOSC) in polluted and translocated mussels: a predictive biomarker of oxidative stress. *Aquatic Toxicology*, 50, 351–361.
- Rice, J. (2003). Environmental health indicators. *Ocean and Coastal Management*, 46, 235–259.
- Ringwood, A. H., Hoguet, J., Keppler, C., & Gielazyn, M. (2004). Linkages between cellular biomarker responses and reproductive success in oysters *Crassostrea virginica*. *Marine Environmental Research*, 58, 151–155.
- Servais, H., Van der Smitten, P., Thirion, G., Van der Essen, G., Van Bambeke, F., Tulkens, P. M., et al. (2005). Gentamicin-induced apoptosis in LLC-PK1 cells: involvement of lysosomes and mitochondria. *Toxicology and Applied Pharmacology*, 206, 321–333.
- Svendsen, C., & Weeks, J. M. (1995). The use of a lysosome assay for the rapid assessment of cellular stress from copper to the freshwater snail *Viviparus costectus* (Millet). *Marine Pollution Bulletin*, 31, 139–142.
- Svendsen, C., Spurgeon, D. J., Hankard, P. K., & Weeks, J. M. (2004). A review of lysosomal membrane stability measured by neutral red retention: is it a workable earthworm biomarker. *Ecotoxicology and Environmental Safety*, 57, 20–29.
- Viarengo, A., Moore, M. N., Pertica, M., Mancinelli, G., & Accomando, R. (1992). A simple procedure for evaluating the protein degradation rate in mussel (*Mytilus galloprovincialis* Lam.) tissues and its application in a study of phenanthrene effects on protein catabolism. *Comparative Biochemistry and Physiology*, 103B, 27–32.
- Wedderburn, J., Cheung, V., Bamber, S., Bloxham, M., & Depledge, M. H. (1998). Biomarkers of histochemical and cellular stress in *Carcinus maenas*: an in situ field study. *Marine Environmental Research*, 46, 321–324.
- Widdows, J., Bakke, T., Bayne, B. L., Donkin, P., Livingstone, D. R., Lowe, D. M., et al. (1982). Responses of *Mytilus edulis* L. on exposure to the water accommodated fraction of North Sea oil. *Marine Biology*, 67, 15–31.
- Winston, G. W., Adams, S. M., Benson, W. H., Gray, L. E., Matthews, H. S., Moore, M. N., et al. (2002). Biological bases of similarities and differences. In R. T. Di Giulio & W. B. Benson (Eds.), *Interconnections between human health and ecological integrity* (pp. 43–65). Pensacola, Florida: Society of Environmental Toxicology and Chemistry (SETAC).
- Winston, G. W., Moore, M. N., Kirchin, M. A., & Soverchia, C. (1996). Production of reactive oxygen species (ROS) by hemocytes from the marine mussel, *Mytilus edulis*. *Comparative Biochemistry and Physiology*, 113C, 221–229.
- Winston, G. W., Moore, M. N., Straatsburg, I., & Kirchin, M. (1991). Lysosomal stability in *Mytilus edulis* L.: potential as a biomarker of oxidative stress related to environmental contamination. *Archives of Environmental Contamination and Toxicology*, 21, 401–408.
- Xu, F.-L., Dawson, R. W. S., Li, B.-G., & Cao, J. (2002). System-level responses of lake ecosystems to chemical stresses using exergy and structural exergy as ecological indicators. *Chemosphere*, 46, 173–185.

Addenda

# Lysosomal and Autophagic Reactions as Predictive Indicators of Environmental Impact in Aquatic Animals

Michael N. Moore<sup>1,\*</sup>

J. Icarus Allen<sup>1</sup>

Allan McVeigh<sup>1,2</sup>

Jenny Shaw<sup>1</sup>

<sup>1</sup>Plymouth Marine Laboratory, Prospect Place, The Hoe, Plymouth, UK

<sup>2</sup>University of Plymouth, Department of Mathematics & Statistics, Drake's Circus, Plymouth, UK

\*Correspondence to: Michael N. Moore; Plymouth Marine Laboratory, Prospect Place, The Hoe, Plymouth, PL1 3DH, UK; Tel.: +00.44.1752.633100; Fax: +00.44.1752.633101; Email: mnm@pml.ac.uk

Received 03/07/06; Accepted 03/07/06

Previously published online as an Autophagy E-publication:  
<http://www.landesbioscience.com/journals/autophagy/abstract.php?id=2663>

## KEY WORDS

autophagy, environmental risk, health status, lipofuscin, lysosomes, mussels, reactive oxygen species, pollutants, prognostic indicators, simulation modeling.

## ACKNOWLEDGEMENTS

The research described is part of the PREDICT 2 Project supported by the UK Department for Environment, Food and Rural Affairs (Defra, UK), Contract No. AE1136.

## Addendum to:

*Environmental Prognostics: An Integrated Model Supporting Lysosomal Stress Responses as Predictive Biomarkers of Animal Health Status*

M.N. Moore, J.I. Allen and A. McVeigh

Mar Environ Res 2006; 61:278-304

## ABSTRACT

The lysosomal-autophagic system appears to be a common target for many environmental pollutants as lysosomes accumulate many toxic metals and organic xenobiotics, which perturb normal function and damage the lysosomal membrane. In fact, lysosomal membrane integrity or stability appears to be an effective generic indicator of cellular well-being in eukaryotes: in bivalve molluscs and fish, stability is correlated with many toxicological responses and pathological reactions. Prognostic use of adverse lysosomal and autophagic reactions to environmental pollutants has been explored in relation to predicting cellular dysfunction and health in marine mussels, which are extensively used as sensitive bioindicators in monitoring ecosystem health. Derivation of explanatory frameworks for prediction of pollutant impact on health is a major goal; and we have developed a conceptual mechanistic model linking lysosomal damage and autophagic dysfunction with injury to cells and tissues. This model has also complemented the creation of a cell-based computational model for molluscan hepatopancreatic cells that simulates lysosomal, autophagic and other cellular reactions to pollutants. Experimental and simulated results have also indicated that nutritional deprivation-induced autophagy has a protective function against toxic effects mediated by reactive oxygen species (ROS). Finally, coupled measurement of lysosomal-autophagic reactions and modelling is proposed as a practical toolbox for predicting toxic environmental risk.

Lysosomal and autophagic reactions to pollutant stress are widely used as indicators of cell injury in bioindicator species, such as molluscs, earthworms and fish, for monitoring toxic impact of environmental contamination on the health of aquatic and terrestrial ecosystems.<sup>1-6</sup> This information is critical in ensuring the maintenance of sustainable agricultural land and aquatic food supply, as well as for the prevention of unintentional species extinction that may result from human activities that cause soil and water pollution. Many toxic chemicals accumulate in lysosomes, including pollutants such as metal ions, heterocyclics and polycyclic aromatic hydrocarbons, where they can perturb function, and damage the lysosomal membrane.<sup>5,7-9</sup> Lysosomal membrane integrity or stability appears to be a generic common target for stressors and provides an indicator of cellular well-being in eukaryotes.<sup>3,10-13</sup> In bivalve molluscs, such as mussels (*Mytilus* sp.) and oysters, lysosomal stability is positively correlated with total oxygen and nitrogen radical scavenging capacity (TOSC), protein synthesis, energetic status (scope for growth) and larval viability; and inversely correlated with efficiency of protein synthesis, autophagic protein turnover, DNA damage (formation of micronuclei), as well as lysosomal swelling (volume density), lipidoses and lipofuscinosis.<sup>7,10-12,14-17</sup> Lysosomal membrane stability can also be used to predict liver damage and tumor progression in fish liver.<sup>12</sup>

Multivariate and univariate statistical analysis and modelling of adverse lysosomal and other responses to pollutants, together with lysosomal membrane stability as an index of cell viability, provides a reference measurement for cellular "well-being".<sup>10,11,14</sup> We have derived a conceptual framework that can be used to integrate disparate data sets, and for constructing a computational model used to produce functional simulations of hepatopancreas (digestive gland - liver analogue) in blue mussels, including lysosomal and autophagic responses to environmental variables and toxic chemicals.<sup>18</sup> This model has also been used to simulate the protective effects of augmented autophagy induced by nutritional deprivation (Fig. 1).<sup>15,19</sup> We further proposed that computational models will provide the necessary basis for explanatory frameworks that will facilitate the development of predictive tools that can be used in environmental management for estimating risk to the health of ecosystems from chemical pollution.<sup>7</sup> Coupled application of the computational model together with environmental biomonitoring, using key target animals like

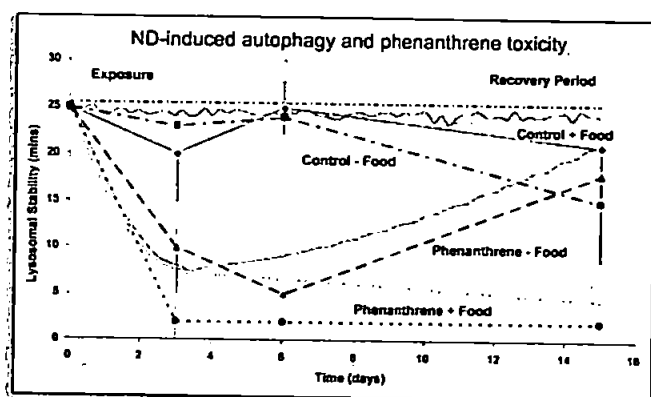


Figure 1. Simulation results from computational model of molluscan hepatopancreatic digestive cell compared to experimental data, showing effects of nutritional deprivation coupled with phenanthrene exposure on lysosomal stability. Nutritionally deprived (ND) animals show reduced toxicity after three days and recover after a further 12 days, while fed animals do not recover. Phenanthrene was administered at 50  $\mu\text{g}/\text{mussel}/\text{day}$  as a single daily dose in filtered seawater (Moore, 2004). Treatments ( $n = 5$ ,  $\pm 95\%$  confidence limit): —●— Control + Food; - -■- Control - Food; . .▲. Phenanthrene + Food; - -▲- Phenanthrene - Food. Lighter lines are simulated results and darker lines are experimental results. Data modified from Moore and McVeigh et al.<sup>15,19</sup>

mussels and oysters as bioindicators, will be of practical value in evaluating larger scale ecosystem health risks from environmental changes.

Pollutant exposure often causes oxidative attack on the protein machinery and organelles of the cell.<sup>20</sup> Protein carbonyls and age pigment (lipofuscin) are products of oxidative attack on proteins.<sup>21-23</sup> Lipofuscin accumulates in lysosomes as a result of peroxidation of autophagocytosed proteins associated with protein aggregates and oxidatively damaged organelles, and was previously considered to be just cellular junk.<sup>23-25</sup> However, new evidence indicates that lipofuscin binds iron, which generates reactive oxygen species (ROS), resulting in exacerbation of oxidative damage.<sup>21</sup> Brunk and Terman also hypothesize that lipofuscin binds lysosomal hydrolases, thereby inhibiting protein degradation.<sup>21</sup> The probable outcome is incomplete digestion or "failed autophagy" with autophagic accumulation of essentially undegradable damaged organelles, proteins, phospholipids and lipids contributing to further lipofuscin formation.<sup>7,21,25,26</sup>

Incomplete or "failed autophagy" has been described in molluscs, fish and mammals exposed to pollutants and xenobiotics.<sup>3,4,7,10,15,25,27</sup> Reports on other animals tend to be largely descriptive, so systematic observations of other phyletic groups would be beneficial to the development of a generic understanding of the role of autophagy in toxic stress.

Recent evidence indicates that autophagy is much more than just a survival process in response to stress and is intimately involved in cell physiology.<sup>7,15,25,28,29,30</sup> In molluscan models, as in mammals, augmented autophagy is induced by nutrient deprivation and hypoxia.<sup>14,15,31,32</sup> Autophagic removal of oxidatively damaged organelles and proteins may perhaps provide a second tier of defense against oxidative stress.<sup>28,31</sup> Nutritional deprivation is an established inducer of autophagy in hepatopancreatic digestive cells of mussels; and new data are shown in (Fig. 2) indicating that augmented autophagy induced by nutrient deprivation reduces the formation of lipofuscin in oxidatively stressed mussels (Shaw, Moore, Lowe & Beesley, in preparation).<sup>14,15,31</sup>

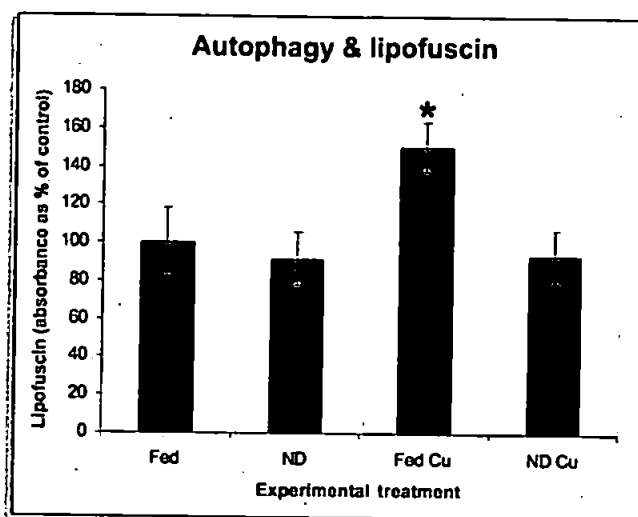


Figure 2. Lipofuscin formation in mussels as a result of copper induced oxidative stress: relative absorbance of lipofuscin (Schmorl reaction in 10  $\mu\text{m}$  frozen tissue sections; mean  $\pm 95\%$  confidence limit,  $n = 10$ ; \* $p < 0.05$ , Mann-Whitney) in hepatopancreatic digestive cells of fed and nutritionally deprived (ND) mussels after three days  $\pm$  copper (10  $\mu\text{g Cu}^{2+}/\text{mussel}/\text{day}$  as a single daily dose in filtered seawater). See Moore (1988 and 2004) for experimental protocols: fed mussels were provided with  $\geq 30$  mg dry weight of algal food (*Isochrysis galbana*) per mussel per day at 15°C. Nutritional deprivation treatments were initiated four days prior to starting the copper treatments in order to induce augmented autophagy. Data are adapted from Shaw, Moore, Lowe and Beesley, in preparation.

An effective ability to upregulate the autophagic process is probably advantageous to organisms exposed to toxic chemicals, since this will facilitate the removal of damaged cellular constituents and conserve cell function; and may also reduce the amount of lipofuscin produced.<sup>22,24,30,33</sup> Perhaps repeated triggering of augmented autophagy can protectively minimize oxidative damage and lipofuscin generation.<sup>33</sup> If so, then animals such as mussels, living in highly fluctuating environments such as estuaries, where autophagy is repeatedly stimulated by natural variables like salinity increase, hypoxia and nutrient levels, may be generically more tolerant of pollutant stress than those from more stable environments.<sup>34</sup> In fact, marine mussels are generally very tolerant of environmental fluctuations, but are nonetheless highly responsive to measurable environmental changes; and this property makes them eminently suitable for long-term biomonitoring, since their extinction from an ecosystem will only occur under extreme conditions.<sup>2,11,14,23,31</sup> Lipofuscin accumulation and other lysosomally-related reactions in the digestive cells of mussels are generally related to the environmental concentration of pollutants, and can be effectively measured, whereas a less resistant species would probably be eliminated.<sup>2,7,34</sup>

A simplified conceptual model of some of the probable interactions of lysosomal-autophagic processes in oxidative stress is shown in (Fig. 3). This model links the cellular uptake of pollutants with radical generation and oxidative injury, through to tissue pathology and harmful physiological consequences.<sup>22,35</sup> Overall, the predicted consequence of lysosomal injury is cell and tissue dysfunction, tissue and organ atrophy, reduced physiological scope for growth and impaired gamete production.<sup>5,10,11,14,26</sup>

The further coevolutionary development of computational cellular physiological models coupled with empirical studies will help to

# Autophagy and oxidative cell injury

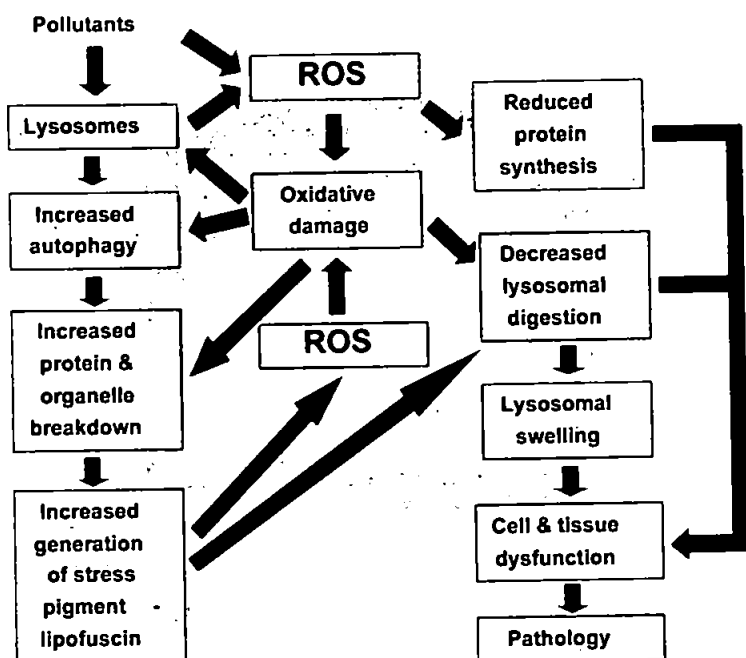


Figure 3. Simplified conceptual model for interactions of pollutant induced oxidative stress with lysosomal and autophagic processes leading to cell injury and pathology, based on empirical data where there is a reasonable mechanistic basis for making assumptions about the linkages. Reactive oxygen species (ROS) are produced by normal metabolism and enhanced by the action of many chemical toxins. ROS attack proteins and essential cellular organelles, such as mitochondria, contributing to lipid peroxidation and the formation of protein carbonyls, protein aggregates and stress or age pigment (lipofuscin), which is currently thought to produce further free-radicals and may also inhibit autophagic breakdown of cell constituents. It is hypothesized that repeated stimulation of augmented autophagy by various environmental factors that induce mild stress, will result in a more effective recycling of cellular proteins and organelles, before major oxidative damage occurs, consequently reducing lipofuscin formation and thus protecting the cell from further injury. Adapted from Moore et al.<sup>7</sup>

bridge the gap in understanding between cellular reactions involving autophagy and lysosomes, and pathological effects on "health-status"; and this will facilitate derivation of new tools for environmental risk prediction.<sup>5,7,13</sup>

In summary, our findings indicate that cellular changes, such as reduced lysosomal membrane stability, lipofuscin accumulation and other lysosomally related assays, are good indicators of cell injury; and in a situation where exposure to environmental stressors is likely to be sustained, they can be used to predict that further pathological changes will occur.<sup>3,5,10,23</sup> Lysosomal and autophagic functional perturbations also appear to have potential as a measure of damage to ecological health; although caution is required in interpretation of data in respect of possible selection for tolerant phenotypes.<sup>26,23,34</sup>

## References

1. Cajaraville MP, Abascal I, Etxebarria M, Marigómez I. Lysosomes as cellular markers of environmental pollution: Time- and dose-dependent responses of the digestive lysosomal system of mussels after petroleum hydrocarbon exposure. *Environ Toxicol Water Qual* 1995; 10:1-8.
2. Cajaraville MP, Bebianno MJ, Blasco J, Porte C, Sarasquete C, Viarengo A. The use of biomarkers to assess the impact of pollution in coastal environments of the Iberian peninsula: A practical approach. *Sci Tot Environ* 2000; 247:295-311.
3. Köhler A, Deisemann H, Lauritzen B. Ultrastructural and cytochemical indices of toxic injury in dab liver. *Mar Ecol Prog Ser* 1992; 91:141-53.
4. Marigómez I, Baybay-Villacorta L. Pollutant-specific and general lysosomal responses in digestive cells of mussels exposed to model organic chemicals. *Aquatic Toxicol* 2003; 64:235-57.
5. Moore MN, Depledge MH, Readman JW, Leonard P. An integrated biomarker-based strategy for ecotoxicological evaluation of risk in environmental management. *Mutat Res* 2004; 552:247-68.
6. Svendsen C, Spurgeon DJ, Hankard PK, Weeks JM. A review of lysosomal membrane stability measured by neutral red retention: Is it a workable earthworm biomarker. *Ecotox Environ Safety* 2004; 57:20-9.
7. Moore MN, Allen JJ, McVeigh A. Environmental prognostics: An integrated model supporting lysosomal stress responses as predictive biomarkers of animal health status. *Mar Environ Res* 2006; 61:278-304.
8. Rashid F, Horobin RW, Williams MA. Predicting the behaviour and selectivity of fluorescent probes for lysosomes and related structures by means of structure-activity models. *Histochem J* 1991; 23:450-9.
9. Viarengo A, Nott JA. Mini-review: Mechanisms of heavy metal cation homeostasis in marine invertebrates. *Comp Biochem Physiol* 1993; 104C:355-72.
10. Allen JJ, Moore MN. Environmental prognostics: Is the current use of biomarkers appropriate for environmental risk evaluation? *Mar Environ Res* 2004; 58:227-32.
11. Bayne BL, Moore MN, Widdows J, Livingstone DR, Salkeld PN. Measurement of the responses of individuals to environmental stress and pollution: Studies with bivalve molluscs. *Phil Trans R Soc (Lond)* 1979; 286B:563-81.
12. Köhler A, Wähl E, Söffker K. Functional and morphological changes of lysosomes as prognostic biomarkers of toxic liver injury in a marine flatfish (*Platichthys flesus* (L)). *Environ Toxicol Chem* 2002; 21:2434-44.
13. Winston GW, Adams SM, Benson WH, Gray LE, Matthews HS, Moore MN, Safe S. Biological bases of similarities and differences. In: Di Giulio RT, Benson WB, eds. *Interconnections between Human Health and Ecological Integrity*. Pensacola, FL: Society of Environmental Toxicology and Chemistry (SETAC), 2002:43-65.
14. Bayne BL, Holland DL, Moore MN, Lowe DM, Widdows J. Further studies on the effects of stress in the adult on the eggs of *Mytilus edulis*. *J mar biol Ass UK* 1978; 58:825-41.
15. Moore MN. Diet restriction induced autophagy: A protective system against oxidative- and pollutant-stress and cell injury. *Mar Environ Res* 2004; 58:603-7.
16. Regoli F. Total oxyradical scavenging capacity (TOSC) in polluted and translocated mussels: A predictive biomarker of oxidative stress. *Aquatic Toxicol* 2000; 50:351-61.
17. Viarengo A, Moore MN, Perica M, Mancinelli G, Accomando R. A simple procedure for evaluating the protein degradation rate in mussel (*Mytilus galloprovincialis* Lam.) tissues and its application in a study of phenanthrene effects on protein catabolism. *Comp Biochem Physiol* 1992; 103B:27-32.
18. McVeigh A, Allen JJ, Moore MN, Dyke P, Noble D. A carbon and nitrogen flux model of mussel digestive gland epithelial cells and their simulated response to pollutants. *Mar Environ Res* 2004; 58:821-7.
19. McVeigh A, Moore MN, Allen JJ, Dyke P. Lysosomal responses to nutritional and contaminant stress in mussel hepatopancreatic digestive cells: A modelling study. *Mar Environ Res* 2006; In press.
20. Livingstone DR. Contaminant-stimulated reactive oxygen species production and oxidative damage in aquatic organisms. *Mar Pollut Bull* 2001; 42:656-66.
21. Brunk UT, Terman A. Lipofuscin: Mechanisms of age-related accumulation and influence on cell function. *Free Rad Biol Med* 2002; 33:611-9.
22. Kirchin MA, Moore MN, Dean RT, Winston GW. The role of oxyradicals in intracellular proteolysis and toxicity in mussels. *Mar Environ Res* 1992; 34:315-20.
23. Moore MN. Lysosomal cytochemistry in marine environmental monitoring. *Histochem J* 1990; 22:187-91.
24. Grune T, Jung T, Merker K, Davies KJA. Decreased proteolysis caused by protein aggregates, inclusion bodies, plaques, lipofuscin, ceroid, and "aggregates" during oxidative stress, ageing and disease. *Internat J Biochem Cell Biol* 2004; 36:2519-30.

25. Moore MN. Cytochemical responses of the lysosomal system and NADPH-ferrihemoprotein reductase in molluscs to environmental and experimental exposure to xenobiotics. *Mar Ecol Prog Ser* 1988; 46:81-9.
26. Krishnakumar PK, Casillas E, Varanasi U. Effect of environmental contaminants on the health of *Mytilus edulis* from Puget Sound, Washington, USA. I. Cytochemical measures of lysosomal responses in the digestive cells using automatic image analysis. *Mar Ecol Prog Ser* 1994; 106:249-61.
27. Lüllmann-Rauch R. Drug-induced lysosomal storage disorders. In: Dingle JT, Jacques PJ, Shaw IH, eds. *Lysosomes in Applied Biology and Therapeutics*, vol 6. Amsterdam: Elsevier, 1979:49-130.
28. Cuervo AM. Autophagy: In sickness and in health. *TRENDS Cell Biol* 2004; 14:70-7.
29. Klionsky DJ, Emr SD. Autophagy as a regulated pathway of cellular degradation. *Science* 2000; 290:1717-21.
30. Lockshin RA, Zakeri Z. Apoptosis, autophagy, and more. *Internat J Biochem Cell Biol* 2004; 36:2405-19.
31. Hawkins AJS, Day AJ. The metabolic basis of genetic differences in growth efficiency among marine animals. *J Exp Mar Biol Ecol* 1996; 203:93-115.
32. Moore MN, Lowe DM, Moore SL. Induction of lysosomal destabilisation in marine bivalve molluscs exposed to air. *Mar Biol Letters* 1979; 1:47-57.
33. Bergamini E, Cavallini G, Donati A, Gori Z. The anti-ageing effects of caloric restriction may involve stimulation of macroautophagy and lysosomal degradation, and can be intensified pharmacologically. *Biomed Pharmacother* 2003; 57:203-8.
34. Moore MN, Allen JL, Somerfield PJ. Autophagy: Role in surviving environmental stress. *Mar Environ Res* 2006; In press.
35. Winston GW, Moore MN, Strauszburg I, Kirchin M. Lysosomal stability in *Mytilus edulis* L.: Potential as a biomarker of oxidative stress related to environmental contamination. *Arch Environ Contam Toxicol* 1991; 21:401-8.



# A Simple Computational Model of digestion in the Marine Mussel

by

Allan McVeigh <sup>1,2</sup> and Phil Dyke <sup>1</sup>

<sup>1</sup> School of Mathematics and Statistics,

University of Plymouth,

Drake Circus,

Plymouth PL4 8AA, UK

<sup>2</sup> BMT Cordah,

Grove House,

7 Oceans Way,

Meridians Cross

Southampton SO14 3TJ, UK

## Abstract

A simplified model of a marine mussel is proposed. We model the digestive system as a cellular analogue, physically partitioned into a lysosome and endosome, with the flow of particulate carbon to represent energy. The parameters in the rate equations that govern the interactions between compartments are assumed to be a simple linear form but are consistent with experiment and observation. The model is tested first by using continuous feeding and then by using a periodic feeding representative of tidal input. The responses in both cases produce interesting results compatible with observations of the biology of the animal. We define a "health function" which indicates whether or not the animal survives. It is found that survival is critically dependent on lysosomal efficiency.

## 1 Introduction

We propose a mathematical model of a simple animal, and we choose the marine mussel. In recent years there have at last emerged a few successful working marine ecosystems models (e.g. Allen et al (2001)). These have been incorporated into hydrodynamic models and the resulting software is becoming a tool that can be used by a diverse community of interested scientists and engineers. A good example is the POLCOMS model (Proudman Oceanographic Laboratory Coastal Ocean Modelling System - see Allen et al (2001)) that has an ecosystem model built into it. We now feel that we are ready to move to the next stage; instead of modelling communities of animals, the animal itself is modelled, and the effects outside influences have on an animal population modelled (eventually) by summing all the individual influences (individuals to be separately characterised by deviations in initial conditions and rate constant parameters), see comments in Chapter 7 of Dyke (2007). At the moment we are not quite at that stage, but this paper presents a model of a simple creature the marine mussel and this model is shown to mimic well its interaction with its environment.

The starting point for the model is to formulate the essential biology through a system of rate equations that contain some non linear dynamics.

This non-linearity shows that a system of exclusively stable components need not necessarily lead to a stable system. Instability may arise from the interactions between the stable components: such counter-intuitive results are encountered often enough to show that identifying individual components and mechanisms should not be the endpoint of scientific investigation. The reductionist history of biology has achieved a wonderful cornucopia of results, insights and data by identifying individual components and their responses, right down to the level of individual proteins. The current challenge facing the biological sciences is to take this myriad of concepts and models and integrate them across all levels to produce a functional model of entire systems. In order to do so a new integrative multidisciplinary systems biology approach has been proposed. This work is conceived to be part of such an approach within the field of marine environmental toxicology. Environmental toxicology studies the impact of contaminants upon biological systems of all levels in the environment. So complex and subtle are system responses to combinations of environmental stressors that in the past the mantra has been that it is impossible for the human mind to calculate or predict them. With increasing computational power available this is no longer the case as we can simulate aspects of nature and compute the various known interactions. Furthermore the complexity of the responses can arise from the interaction of simple rules (Wolfram, 2002). Past efforts to control negative effects of man's interference with ecological systems have only been partially successful; as the direct and indirect consequences of urbanisation, industrial processes and pest control were either unable to be predicted to an effective degree or else were simply not understood or known to the requisite level. What is required is a system which picks up the early warning signals of possible deleterious effects on human and ecological health by means of bioindicators. Under the auspices of 'environmental prognostics' it is proposed that this be implemented by a two prong strategy, Moore, Allen and McVeigh (2006). Initially suitable biomarkers are identified which are sensitive enough to identify appropriate levels of ecological damage to environmental stressors. Second collectively to relate these biomarker responses to ecological consequences. In order to achieve the second of these aims various computational techniques are required to integrate, both horizontally and vertically, these responses. These techniques include multivariate statistics and simulation models of sentinel species, which is the *raison d'être* of this paper, explicitly the development of a first numerical model of a marine mussel digestive cell.

## 2 The Mussel Model

Marine ecotoxicology has long recognised the utility of the marine mussel as an indicative organism of entire ecological health. The mussel is widely used as an environmental sentinel due to a number of characteristics (Widdows and Donkin, 1992). They have a wide geographic distribution and are usually abundant where they do colonise. They are quite robust having relatively high tolerances to contaminants and environmental conditions. As sessile filter feeders a large proportion of their aqueous environment

passes through them, thus exposing them to a high proportion of any associated contaminant. The digestive cell has been chosen as the initial development of the mussel for a number of reasons. It forms part of the continuous interface between the animal and its environment. It is also the destination for food particles, previously sorted and roughly degraded along their passage through the gills and stomach, and a number of toxins are introduced to the organic mass through speciation with colloidal matter ingested as a perceived source of nutrition. In addition it acts as one of the buffers against toxic stress, having well developed defence mechanisms against such attacks.

Cellular modelling has been around for at least 40 years, previous successes range in scope from supercomputer simulations of human hearts and lungs (Hunter et al., 2001), to models of cellular signalling pathways (Bunk, 2003), all the way down to models of genetic regulatory networks (Kauffman, 1969) showing that simple interactions between members in a network would give complicated system behaviour. Counter intuitive effects of drug responses have been predicted in the heart model which has helped to strengthen the confidence in such models and raise their profile. The first step in the process of cellular modelling is a conceptual model; the premise behind an observation is speculated and reduced to its most significant parts. Once such a model is available it is necessary to translate it mathematically and generate appropriate computer code in order to test the hypothesis under scrutiny. The rigorous nature of a mathematical model often provides impetus into directing experimental study into areas where the behaviour of the process under discussion is not fully known. This is then translated back into a revised model and the process is expected to iterate until a successful simulation is achieved. Then the model can be tested against another data set in order to determine its capabilities.

Turning now to modelling the cell, certain physical characteristics of the cell can be used as early indicators of reduction in animal fitness. First of all we need to define a lysosome. This denotes a section of a cell in its own membrane that is responsible for digesting various matter such as bacteria, viruses and other foreign bodies for example worn out bits of cell wall. One good indicator of fitness reduction is how well the lysosomal volume is maintained, the proportion of lysosomal volume to cell volume is termed lysosomal stability. A cautionary approach must be adopted when utilising this as a measure of health as a high lysosomal volume ratio could be the result of a large number of small, functional lysosomes or through a small number of swollen, inefficient lysosomes; until the lysosomal life cycle is implemented the second of these variants is assumed. Thus if we can accurately model both of these variables under stressful conditions the result will be an indication of what conditions the mussel is susceptible to. Lysosomal stability correlates well with other biomarker responses both at the same cellular level and upwards to tissue and animal responses; hence it can act as an integrated biological stress indicator. If the mussel cell model can accurately predict lysosomal and cellular volume then by using this correlation, by direct extension the health of entire animals can be confidently predicted. It will of course be necessary to ensure that these correlations exist and are positive enough

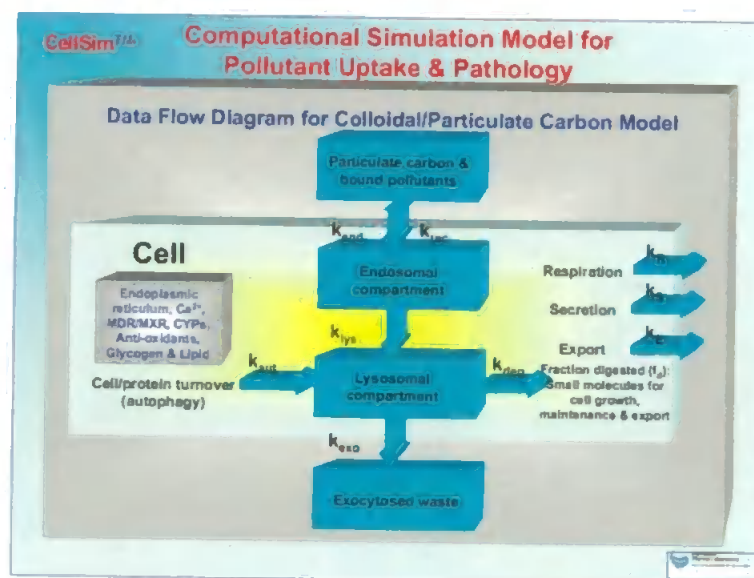


Figure 1: Initial Conceptual Aggregated Discrete compartment model of mussel digestive cell with relevant pathways.

for all stressful conditions tested.

Attempts have been made previously to describe a mathematical model of pollutant uptake, one such precursor to the marine mussel model which this project develops is detailed in Moore and Willows (1998), where both MDR as a defence mechanism and the importance of the chemical speciation of the pollutant are stressed. The model (Moore and Allen, 2002), from which the current work evolved, illustrates the possibilities that a fully developed model could have. The assumptions driving this model are that the cell can be modelled as three discrete amalgamated compartments; the energy balance of the cell can be simulated by the flow of carbon between these compartments, thus only pathways which carry either appreciable amounts of volume or carbon need be considered; flow of material between compartments is considered to be at the average source compartmental concentration; and the control condition is that the concentration of cytosol carbon remains constant throughout - thus providing regulation on cell volume. These assumptions ensure the simplicity of the

model. Indeed, initially a model that had all rates as constant was tried but this turned out to not to work. The eventual model we hope obeys a version of the maxim due to Albert Einstein that models should be as simple as possible, but no simpler.

We are now ready to set up the first simple model. The flow of carbon through the mussel is indicated in the flow chart displayed in Figure 1. In setting up the model, the system of ordinary differential or rate equations usually relies upon the assumption of advective flow between the cellular compartments. A more detailed inspection reveals that this will not in general be the case due to the finite volumes of the compartments. A stricter approach gives the set of equations detailed below. The proportion of absorbed material which is digested and passed on to the cytosol can be accounted for by the ratio between the digestion and exocytosis rates. Each equation represents the rate of change of a particular variable with time, and this is displayed on the left. The terms on the right denote input and output terms. Some but not all of these will be constant. For example, the total rate of exocytosis which is the process by which material migrates across the cell membrane is assumed to be a linear interpolation of the measured minimum and maximum rates. It is realised that this is a gross simplification of complex cell biology. For some processes, for example endocytosis, the absorption of material by the cell it proves necessary to make this process dependent on initial cell volume. The compartmental volume equations are thus:

$$\frac{dE_V}{dt} = k_{end} - k_{rec} - k_{lys} \quad (1)$$

$$\frac{dL_V}{dt} = k_{lys} + k_{aut} - k_{deg} - k_{exo} \quad (2)$$

$$\frac{dC_V}{dt} = k_{deg} - k_{aut} - k_{exp} - k_{sec} - k_{res} \quad (3)$$

The first equation tells how the total endosomal volume  $E_V$  changes with time. The process of endocytosis (the absorption of external material through the cell wall) is a complex one and this equation is a cartoon version of reality. The right hand side comprises the first term that lumps together all the different inputs to the cell. The second term denotes that which is recycled and the third pulls out that which is taken in by the lysosome, necessary as the lysosome is treated separately next. In a later model the transfer of lipid (fat soluble) and non-lipid matter will be distinguished. The second equation tells how the total lysosomal volume ( $L_V$ ) changes. The first two terms increase  $L_V$  through ordinary input (the term  $k_{lys}$ ) and through autophagy  $k_{aut}$  which is the absorption of the mussel's own cell material a natural catabolic process. The lysosomal volume decreases through digestion and through exocytosis (secretion of material from the cell). The third equation denotes the rate of change of the cytosol  $C_V$  or cell fluid. This time the right hand side has five terms. The input is total digestion, and the output is the four term: autophagy  $k_{aut}$  (to the lysosome) export of material ( $k_{exp}$ ) from the cell, secretion of material out of the cell  $k_{sec}$ , and the rate of cellular respiration  $k_{res}$ . All of these are straightforward rate equations.

The compartmental carbon content equations are:

$$\frac{dE_{xc}}{dt} = k_{end}S_c - (f_r k_{rec} + k_{lys})E_c \quad (4)$$

$$\frac{dL_{xc}}{dt} = k_{lys}E_c + k_{aut}C_c - (k_{deg} + k_{exo})L_c \quad (5)$$

$$\frac{dC_{xc}}{dt} = k_{deg}L_c - (k_{aut} + k_{exp} + k_{sec} + k_{res})C_c \quad (6)$$

These equations dictate how the flow of carbon takes place in the cell. We focus on the three carbon reservoirs,  $E_{xc}$  that represents the endosomal carbon content,  $L_{xc}$  that represents the lysosomal carbon content and finally  $C_{xc}$  that represents the cytosolic carbon content. The rate equations obeyed by these three variables take a slightly different form than the three above. The first equation states that the endosomal carbon content increases due to transport of carbon through the surface  $S_c$  and decreases due to changes in the endosomal carbon  $E_c$  brought about by the fraction of recycled carbon  $f_r k_{rec}$  and the traffic to the lysosome  $k_{lys}$ . The next two equations are of similar type: the increase of lysosomal carbon content is due to the rate constant  $k_{lys}$  by definition, and the increase of cytosolic carbon is due to digestion. Decreases are due to defined transports out. Finally, the compartmental carbon concentration equations are:

$$\frac{dE_c}{dt} = \frac{1}{E_v} (k_{end}(S_c - E_c) + k_{rec}(1 - f_r)E_c) \quad (7)$$

$$\frac{dL_c}{dt} = \frac{1}{L_v} (k_{lys}(E_c - L_c) + k_{aut}(C_c - L_c)) \quad (8)$$

$$\frac{dC_c}{dt} = \frac{1}{C_v} k_{deg}(L_c - C_c) \quad (9)$$

The form of these equations follows from considering the ratio in each of the three cases of the change in the volume due to processes divided by the volume. So, for example for the lysosome, it is the change due to traffic into the difference of the endosomal and lysosomal carbon concentrations plus the change due to autophagy divided by the lysosomal volume. To reiterate, the rate constants have the following definitions:

Rate Constant	Description	Range in Litres per second
$k_{end}$	rate of total endocytosis	$6.7 \times 10^{-17} - 2.0 \times 10^{-15}$
$k_{rec}$	rate of total recycling	$0 - 1.65 \times 10^{-15}$
$k_{lys}$	rate of total traffic to lysosome	$0 - 3.5 \times 10^{-16}$
$k_{aut}$	rate of total autophagy	$1.7 \times 10^{-16} - 1.2 \times 10^{-15}$
$k_{deg}$	rate of total digestion	$10^{-16} - 10^{-15}$
$k_{exp}$	rate of export	$0 - 6.0 \times 10^{-16}$
$k_{exo}$	rate of total exocytosis	$10^{-16} - 10^{-15}$
$k_{sec}$	rate of secretion	$1.4 \times 10^{-19} - 2.8 \times 10^{-18}$
$k_{res}$	rate of cellular respiration	$0 - 2 \times 10^{-17}$

The best values of these rate constants have been obtained by experiment, the ranges given are from the microbiological literature. It is recognised that under ideal circumstances sensitivity tests would be done on all these rate constants, however those that have been done indicate that the results are insensitive to the precise values chosen. This is however something that would benefit from further research. The principle of conservation of matter and a preliminary look at this system reveals that the control condition of constant cytosolic carbon cannot be achieved without leaving the prescribed parameter space. To compensate a new 'fictional' rate has been invoked which introduces or removes solvent to the cytosol to keep the concentration constant. It is recognized that this is a makeshift quick fix, and a better alternative is being developed for a modified model which is the next step. For now we introduce an artificial diffusion rate, ( $k_{dif}$ ). The affected ODEs are

$$\frac{dC_v}{dt} = k_{deg} - k_{aut} - k_{exp} - k_{sec} - k_{res} - k_{dif}$$

and

$$\frac{dC_c}{dt} = \frac{1}{C_v} (k_{deg}(L_c - C_c) + k_{dif}C_c)$$

From which this new rate is calculated as

$$k_{dif} = k_{deg} \left( \frac{L_c}{C_c} - 1 \right)$$

The variables have the following meaning:

$E_v$  - total endosomal volume,

$L_v$  - total lysosomal volume,

$C_v$  - total cytosol volume,

$E_c$  - total endosomal carbon concentration,

$L_c$  - total lysosomal carbon concentration,

$C_c$  - total cytosolic carbon concentration,

$E_{xc}$  - total endosome content,

$L_{xc}$  - total lysosomal content,

$C_{xc}$  - total cytosol content,

$f_r$  - the fraction of all material endocytosed that is recycled,

$S_c$  - surface carbon concentration (strictly the carbon concentration of the ingested food vesicles which are delivered to the endosome).

### 3 Results using constant feeding

These nine equations are non-linear, coupled ordinary differential equations which must be solved numerically. Initial attempts at solving these equations using rates that were constant gave spurious results. Constants rates are inconsistent with the complexity of the cell. Various numerical methods were also tried including Runge-Kutta and predictor corrector

methods. Comparing all of these with the simplest possible method (Euler's method) it was found that there was no difference in the answers. Therefore we used Euler's method with a time step of 0.01 minutes. This choice of time step provides a compromise between retaining a small truncation error and computational convenience.

A number of systems to model the rates have been proposed and implemented, however as the system was due eventually to be further developed and incorporate more complexities; only the simplest linear models were used. Generally the rates were modelled as being linearly dependent on the volume of their source compartment. For example the rate of traffic between endosome and lysosome would be modelled as

$$k_{lys}(t) = k_{lysmin} + (k_{lysmax} - k_{lysmin}) \left( \frac{E_v(t) - E_{vmin}}{E_{vmax} - E_{vmin}} \right)$$

Exceptions to this rule were: endocytosis, which was initially made dependent on cell volume; the total rate of exocytosis and degradation was calculated as above and then split in a ratio to correspond to lysosomal efficiency denoted by  $f_d$  and export, which was to take excess volume once the cell had attained its maximum volume. There are a number of problems with such a system, e.g. endocytosis acting as a driver for the whole system will decrease as the cell shrinks which reduces the capability of the cell to grow, which is self defeating in terms of cellular growth. Additionally factors such as stressed cells enhancing their autophagic rate to provide the necessary energy to cope with starvation or to deal with toxic effects damaging cellular components had to be factored in at a later stage. With this initial methodology in place the simplest numerical method was chosen to solve the system and produce results. A mass balance check indicated that the code has to be double precision in order to cope with some of the algorithms invoked. The time-step used had to be determined in order to generate consistent results, eventually settling on a time-step of 0.01 minutes as a fair medium between computation time and precision (for individual simulations the computational time is relatively insignificant but when multiple runs to identify effects across the parameter space are made; computation time did become an issue). Once these issues had been taken care of the first model was subjected to varying nutritional scenarios and initial conditions to observe the general behavioural patterns exhibited. With a surfeit of food made available the cell eventually reaches its maximum attainable level and starts to export carbon to the rest of the animal. There are four observable phases, Figure 2 - (i) an initial decline of cytosolic volume concurrent with a rapid expansion of endosomal and lysosomal volume; (ii) as the lysosome swells its contribution to the cytosol, through the digestive rate, exceeds the flow out of the metabolic and autophagic rates, causing the cytosol to increase in volume; (iii) upon achieving the maximal cell volume for the first time the cell starts to export and there is a long period of slight increase in lysosome volume and concomitant decrease in cytosolic volume, the endosome quickly reaches an equilibrium level; (iv) the system settles into an equilibrium state, exporting material and the individual compartmental volumes remaining constant.



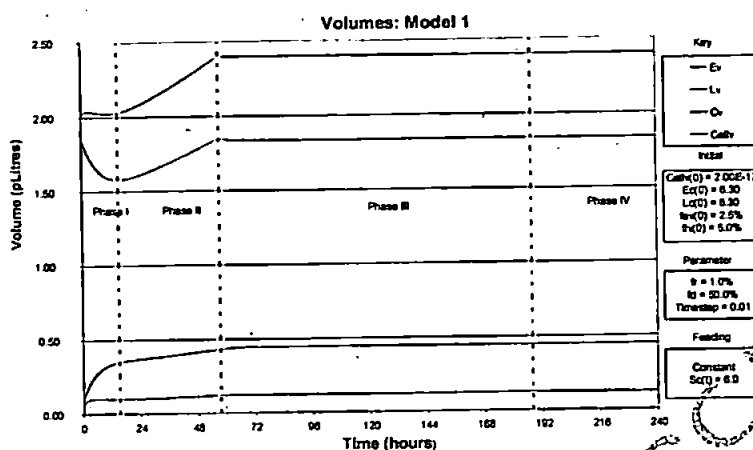


Figure 2: Model 1: Starvation scenario showing effect on compartmental volumes, death at 116.5 hours.

The results are not all within the acceptable parameter limits set as the endosomal carbon concentration far exceeds the set upper limit, see Figure 3. This problem was addressed once the complete system had been implemented. In addition the lysosome swells to a large proportion of the cell volume, whilst within the set bounds (1-30%) this appears high for a 'healthy' cell.

A second behavioural pattern is observed when the food available is not sufficient to stop the cells inexorable descent to minimal volume.

The endosome concentration is seen to rapidly drop as endocytosis brings in no carbon and initial carbon is taken to the lysosome or lost in recycling. This fall is expounded by the increase in volume in this initial phase. As the endosome loses carbon concentration the material entering the lysosome is also of less than minimum concentration reducing the lysosome concentration and invoking negative diffusion. However as the endosome decreases the cytosol becomes the lysosomes main tributary of carbon so it starts to increase in concentration and would eventually if allowed to run for long enough tend to the cytosolic carbon concentration. The lysosome swells to a maximum of 19% of cellular volume which in a stressed cell is not considered unfeasible. The carbon content of the cell shows a monotonic decrease. The nutritionally deprived scenario provokes a number of concerns with the rate constant modelling. Endocytosis based purely on cell size does not seem advantageous to the cell as this simply decreases the lysosomal carbon concentration. Equally, adjusting endocytosis to be factored for food below maintenance level creates problems with endocytotic behaviour. Thus the recycling and lysosomal traffic rates were also subjected to changes. Furthermore boosting the autophagy to take into account the lack of energetic material entering the cell only increase the cellular volume decline. The major concern of the results is that the lysosome swells to 60% of cellular volume which is

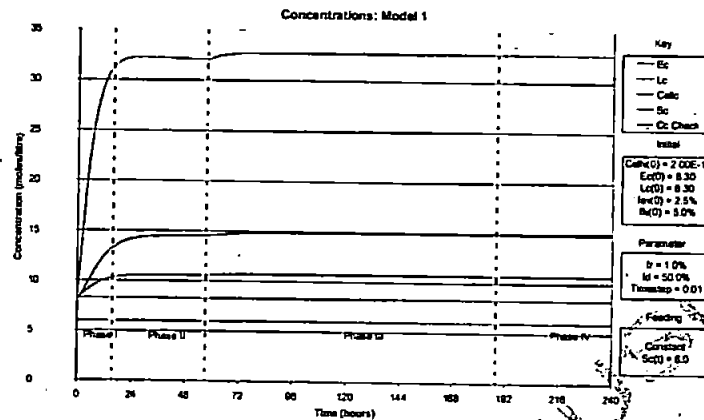


Figure 3: Model 1: 10 day food at constant maximum concentration: Showing behaviour of compartmental carbon concentrations split according to observed volume phases

clearly unacceptable, but can be addressed in a revised model.

A grid in a cross section of the parameter space was constructed and the model run to see which of the behavioural patterns was exhibited. To express this concept a "health function"  $H$  was defined as:

$$H = \begin{cases} \frac{t_n - \text{max time of death}}{\text{max time of death}} & \text{when cell dies at time } t_n \\ \frac{\text{cell}_v(t_n) - \text{cell}_{v \min}}{\text{cell}_{v \max} - \text{cell}_{v \min}} & \text{when a cell achieves equilibrium} \\ \frac{\text{cumulative export (100days)}}{\text{maximum export}} & \text{when cell exports} \end{cases}$$

Cellular death does not equate to animal death as there are grosser strategies such as programmed cell death, which enables the animal to utilise extant cells as sources of nutrition (Jamal et al, 2008), or release of material from storage cells within the mantle to enable enhanced survival times.

Then the results were plotted as a contour plot in order to see how one cross section of the parameter space was divided. From Figure 6 it can be observed that there is only a small area in the parameter space for which the system survives. Since the mussel is considered to be a robust animal it is unlikely that this is the case. Increasing the lysosomal efficiency to 75% and high initial carbon gives a far more robust animal, see Figure 7. There is evidence that animals exist just the right side of the critical line

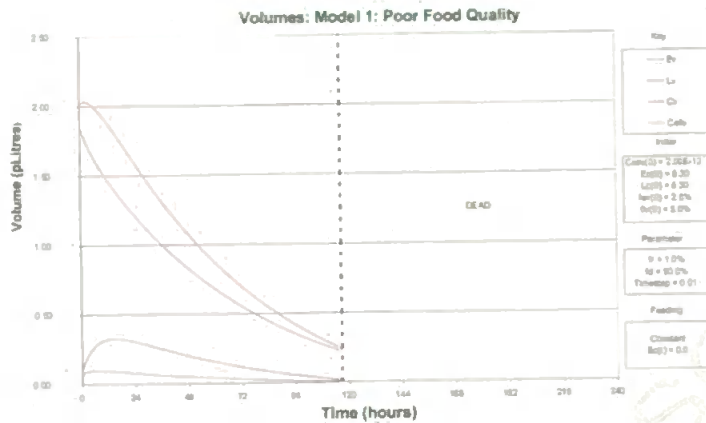


Figure 4: Model 1: Starvation scenario showing effect on compartmental volumes, death at 116.5 hours.

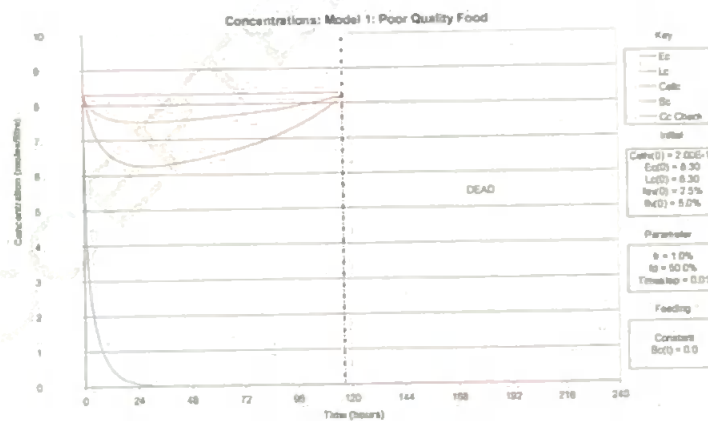


Figure 5: Model 1: Starvation scenario showing effect on compartmental concentrations, death at 116.5 hours.

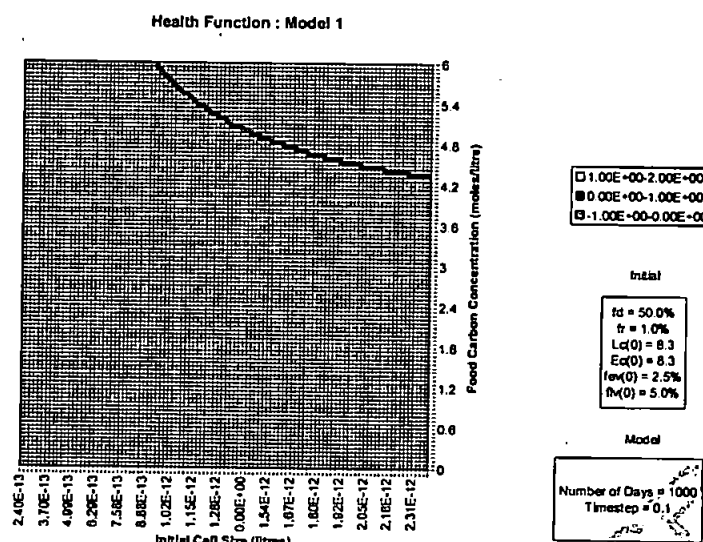


Figure 6: Health function for constant feeding model showing effect of food concentration and initial cell size on cellular fate.

that divides survival and extinction (Moore (personal communication)), so the model results fit well with this function of the lysosome.

#### 4 Results simulating a tidal feeding Pattern

Due to their relatively immobile lifestyle mussels which are in the littoral zone do not have food continuously available to them. Instead they will be subjected to a rhythmic pattern of food availability, dependent on the tidal cycle and their position. To simulate this oscillation the model is driven by food concentration modelled as a square wave function. Initially the food is double the maximum food concentration so that over the day the mussel has the same amount of food available to it as in the previous well fed example. For propriety the same model with the food available at maximum concentration when available gives a system which inevitably decreases in volume. This provoked the determination of the crest and trough period for a mussel half submerged which would lead to a healthy animal. This proved to be more than a tidal cycle so this model version is considered inadequate at representing a mussel situated in such an environment. Additionally the concentration required for a cell, subject to half a day feeding and half a day resting, to export was determined and shown to be outside the parameter space. The square wave food pattern revealed several problems with the rate constant modelling. The autophagic rate as defined with a boost for poor food would automatically switch on as soon as the mussel was no longer submerged. This needed to be revised to include a daily cumulative food history which determined whether or not the autophagy should be so boosted. Various other scenarios were appraised, such as sinusoidal food concentration and hyperbolic sine rate constants. Additionally a more accurate second order numerical scheme based on a predictor corrector method was created

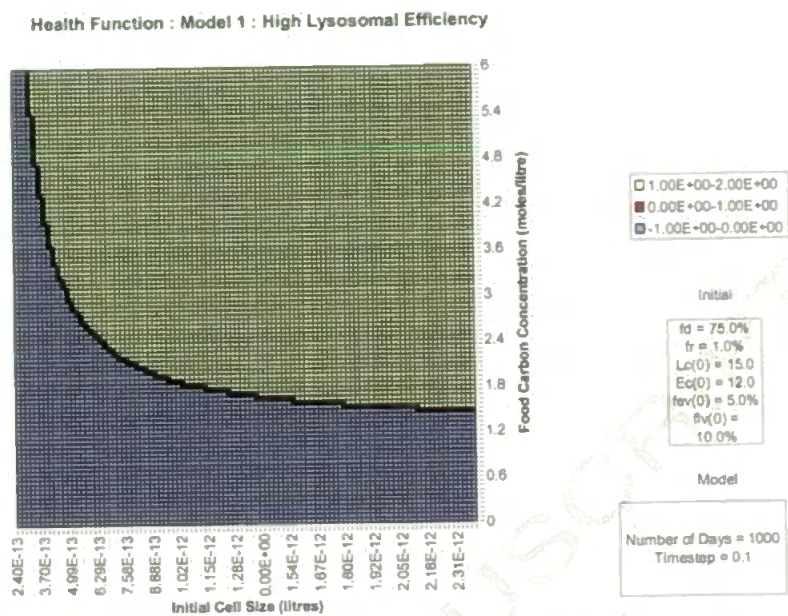


Figure 7: Health function for constant feeding model showing effect of food concentration and initial cell size on cellular fate, with increased lysosomal efficiency  $f_d = 0.75$ .

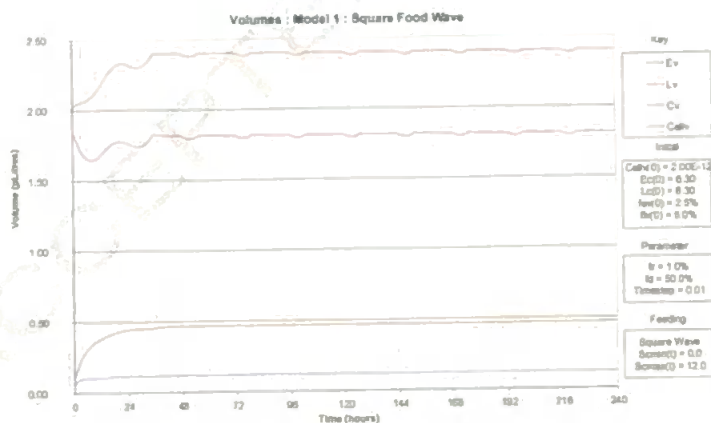


Figure 8: 10 day compartmental volumes for a median intertidal cell with approximately same 24 hour food as an exporting cell.

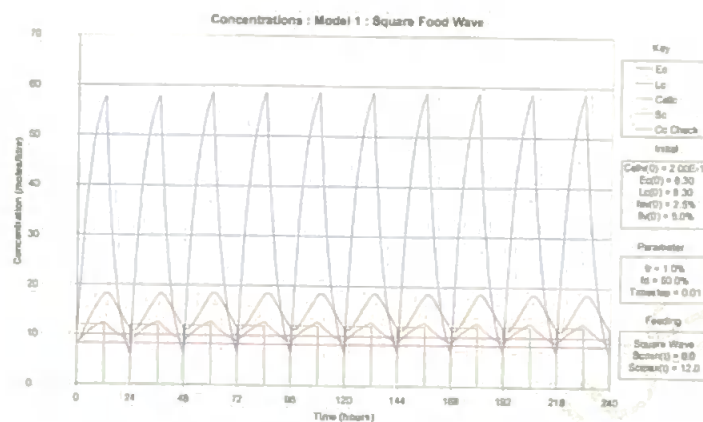


Figure 9: 10 day compartmental concentrations for a median intertidal cell with approximately same 24 hour food as an exporting cell.

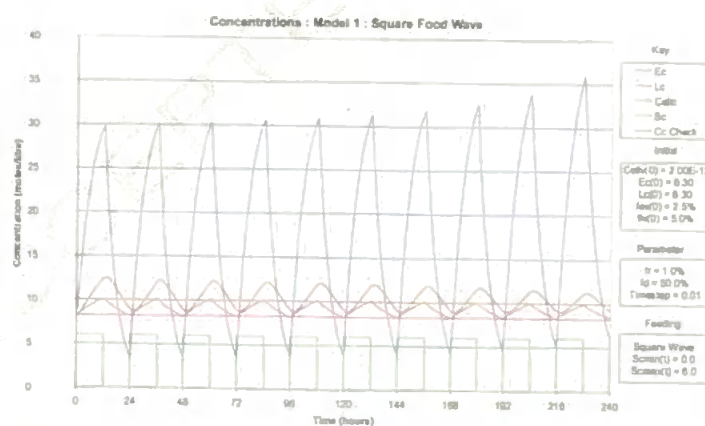


Figure 10: 10 day compartmental concentrations for a median intertidal cell with maximum food concentration when available.

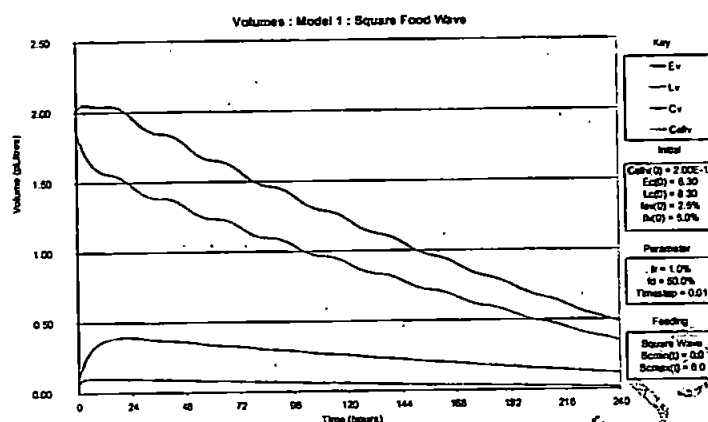


Figure 11: 10 day compartmental volumes for a median intertidal cell with maximum food concentration when available.

and compared with the results from the Euler model. These two results were close enough to indicate that changing from the Euler method to this more accurate method would have no advantages at this early stage; when the final model is being built, then using this more accurate scheme would probably be more appropriate. A final attempt was made to rid the model of the introduced diffusion rate, whereby carbon being released from the lysosome was done so at the cytosolic carbon concentration. However the model volume inevitably declined to the minimum level for all initial conditions and acceptable feeding regimes.

## 5 Conclusions and Further Work

What has been presented above is a simple model of the digestive cell of a marine mussel tested with both continuous feeding and periodic feeding the latter to simulate tides. The mussel model responds in a way that is mostly consistent with observations. The time taken for the mussel to respond to its food intake are right, and the introduction of periodic feeding has been done successfully.

There are many modifications and refinements that can now be added. First of all we can add a glycogen store and lipid subsystem. The lipid subsystem will model the flow of lipid through the cell, initially only as an energy source. Secondly the flow of nitrogen through the cell can also be modelled, as an attempt to replicate the fuller constraints on the cell of biochemical dependence such as the requirement of source material for protein synthesis. At the moment quantity of carbon in the cell can increase indefinitely. Realistically this needs to be capped and the

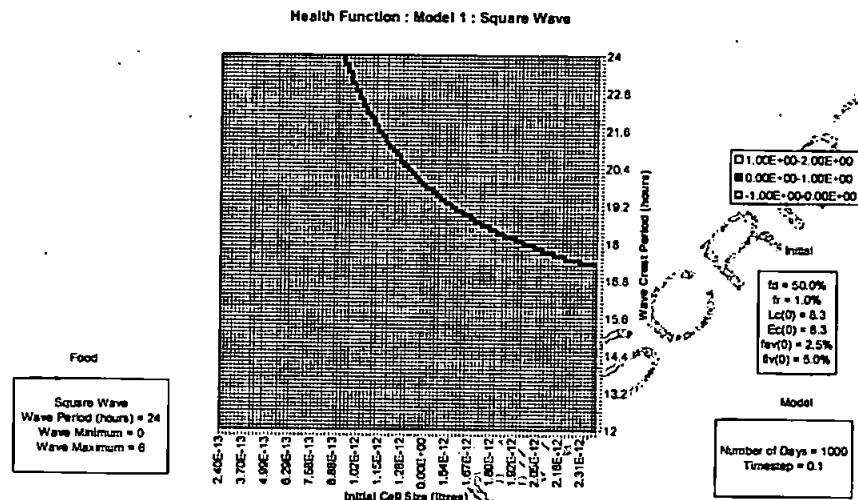


Figure 12: Health function for intertidal model showing effect of wave crest period and initial cell size on cellular fate for median intertidal mussel with maximum food concentration when available.

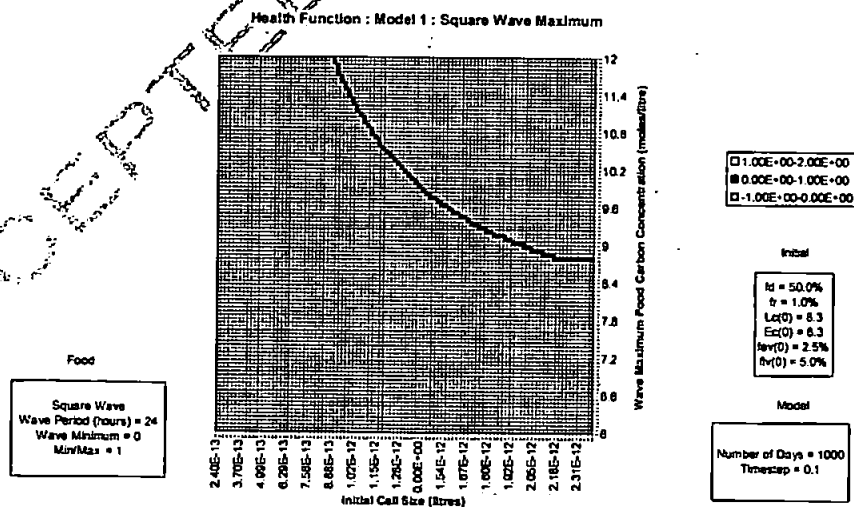


Figure 13: Health function for halfway intertidal model showing effect of food quality when available for half a day and initial cell size on cellular fate.



excess sent either to the cytosol or else expelled by exocytosis. Another modification is to build in a delay in response to input. In this way the robustness of the model will be improved through imposition of internal constraints, considering the endosomal and lysosomal compartments as processing plants. Finally, the food intake is a discrete rather than a continuous process, and the model needs to reflect this (Allen and McVeigh (2005)).

We have here the start of a very useful model. The goal is to produce a working model that will simulate accurately the response of a marine mussel to changes in its environment, and hence provide a tool for assessing the impact of various pollutants on the marine ecosystem. We are some way from achieving this, but this paper presents the first step.

## 6 Acknowledgements

The authors wish to thank Mike Moore and Icarus Allen of Plymouth Marine Laboratory for very helpful discussions and input. One of us (AM) was in receipt of a PML studentship throughout the period of this investigation. Thanks also to anonymous referees whose comments were used to improve the paper.

## References

- [1] Allen J. I., Blackford J. C., Holt J. T., Proctor R., Ashworth M. and Siddorn J., (2001) A highly spatially resolved ecosystem model for the North West European Continental Shelf, *Sarsia*, 86, 423 - 440.
- [2] Allen, J I and McVeigh, A (2004) Towards computational models of cells for environmental toxicology. *Journal of Molecular Histology*, 35, 697 - 706.
- [3] Bunk, S. (2003) The Alpha Project, *The Scientist*, 29, 24-25
- [4] Dyke, P. P. G. (2007) *Modelling Offshore and Coastal Processes*, Imperial College Press, 400pp.
- [5] Hunter, P. J., Kohl, P. and Noble, D. (2001) Integrative models of the heart: achievements and limitations, *Philosophical Transactions of the Royal Society of London A*, 359, 1049-1054.
- [6] Jamal N., Allen J. I., Moore M. N., Dyke P. and Davies, S (2008) A Conceptual Model of Fish Liver Cell Involving Cellular Pathways. *Marine Ecology Progress* (submitted)
- [7] Kauffman, S. A. (1969) Metabolic stability and epigenesis in randomly constructed genetic nets. *Journal of Theoretical Biology*, 22, 437-467.
- [8] McVeigh, A., Allen, J. I., Moore, M. N., Dyke, P. and Noble, D. (2004) A carbon and nitrogen flux model of mussel digestive gland epithelial cells and their simulated response to pollutants, *Marine Environmental Research*, 58, 821-827.

- [9] Moore, M. N. and Allen, J. I. (2002) A computational model of the digestive gland epithelial cell of the marine mussel and its simulated responses to aromatic hydrocarbons, *Marine Environmental Research*, 54, 579-584.
- [10] Moore, M. N., Allen, J. I. and McVeigh, A (2006) Environmental prognosis: An integrated model supporting lysosomal stress responses as predictive biomarkers of animal health status, *Marine Environmental Research*, 61, 278-304.
- [11] Moore, M. N. and Willows, R. I. (1998) A Model for Cellular Uptake and Intracellular Behaviour of Particulate-Bound Micropollutants, *Marine Environmental Research*, 46, 509-514
- [12] Widdows, J. and Donkin, P. (1992) Mussels and Environmental Contaminants: Bioaccumulation and Physiological Aspects. In: *The Mussel Mytilus: Ecology, Physiology, Genetics and Culture*, Ed. by E. Gosling, pp 383-424. Amsterdam: Elsevier
- [13] Wolfram, S. (2002) *A New Kind of Science*, pp 363-369. Champaign: Wolfram Media